(12)

POR-2028-V3(EX)
(WT-2028-V3)(EX)
EXTRACTED VERSION

OPERATION DOMINIC

FISH BOWL SERIES

PROJECT OFFICER'S REPORT - PROJECT 6.9

Radar Clutter Measurements - UHF

R. L. Leadabrand, Project Officer
J. J. Baron — W. E. Jaye
W. G. Chesnut — R. S. Leonard
L. T. Dolphin, Jr. — R. A. Long
J. C. Hodges — R. I. Presnell
Stanford Research Institute
Menlo Park, California

28 August 1964

Extracted version prepared for
Director
DEFENSE NUCLEAR AGENCY
Washington, DC 20305-1000

1 September 1985

Destroy this report when it is no longer needed. Do not return to sender.

PLEASE NOTIFY THE DEFENSE NUCLEAR AGENCY ATTN: TITL, WASHINGTON, DC 20305-1000, IF YOUR ADDRESS IS INCORRECT, IF YOU WISH IT DELETED FROM THE DISTRIBUTION LIST, OR IF THE ADDRESSEE IS NO LONGER EMPLOYED BY YOUR ORGANIZATION.

DNA PRINTING PLANT

UNCLASSIFIED
SECURITY CLASSIFICATION OF THIS PAGE

AD-A995-496

REPORT DOCUMENTATION PAGE

1a. REPORT SECURITY CLASSIFICATION UNCLASSIFIED	1b. RESTRICTIVE MARKINGS
2a. SECURITY CLASSIFICATION AUTHORITY	3 DISTRIBUTION/AVAILABILITY OF REPORT Approved for public release; distribution is unlimited.
2b. DECLASSIFICATION/DOWNGRADING SCHEDULE	
4. PERFORMING ORGANIZATION REPORT NUMBER(S)	5. MONITORING ORGANIZATION REPORT NUMBER(S) POR-2028-V3 (EX) (WT-2028-V3) (EX)
6a NAME OF PERFORMING ORGANIZATION Stanford Research Institute 6b. OFFICE SYMBOL (If applicable)	7a. NAME OF MONITORING ORGANIZATION Defense Atomic Support Agency
6c. ADDRESS (City, State, and ZIP Code) Menlo Park, CA	7b. ADDRESS (City, State, and ZIP Code) Washington, DC
8a. NAME OF FUNDING/SPONSORING ORGANIZATION 8b. OFFICE SYMBOL (If applicable)	9. PROCUREMENT INSTRUMENT IDENTIFICATION NUMBER
8c. ADDRESS (City, State, and ZIP Code)	10. SOURCE OF FUNDING NUMBERS PROGRAM ELEMENT NO. / PROJECT NO. / TASK NO. / WORK UNIT ACCESSION NO.

11 TITLE (Include Security Classification) OPERATION DOMINIC, FISH BOWL SERIES, PROJECT OFFICER'S REPORT; PROJECT 6.9 - Radar Clutter Measurements - UHF, Extracted Version

12. PERSONAL AUTHOR(S) R. L. Leadabrand, M. J. Baron, W. G. Chesnut, L. T. Dolphin, Jr., J. C. Hodges, W. E. Jaye, R. S. Leonard, R. A. Long, R. I. Presnell

13a. TYPE OF REPORT	13b. TIME COVERED FROM ____ TO ____	14. DATE OF REPORT (Year, Month, Day)	15. PAGE COUNT
		640828	346

16 SUPPLEMENTARY NOTATION This report has had sensitive military information removed in order to provide an unclassified version for unlimited distribution. The work was performed by the Defense Nuclear Agency in support of the DoD Nuclear Test Personnel Review Program.

17. COSATI CODES			18. SUBJECT TERMS (Continue on reverse if necessary and identify by block number)		
FIELD	GROUP	SUB-GROUP	Dominic	Tight Rope	Check Mate
18	3		Fish Bowl	Blue Gill	Star Fish
17	9		Radar Clutter	King Fish	

19. ABSTRACT (Continue on reverse if necessary and identify by block number)

The objectives of this project were to (1) determine, as a function of frequency, the time history of the position in space and the strength of all radar echoes associated with these high-altitude bursts, (2) interpret military significance of these results, and (3) use these results to contribute to the overall development of a phenomenological model of high altitude nuclear bursts.

Generally speaking, the quality of the results were satisfactory. With the exception of some interference from neighboring RF radiating experiments on some of the HF equipment at Johnston Island, most records appear to be quite clean, revealing many new and interesting phenomena.

20. DISTRIBUTION/AVAILABILITY OF ABSTRACT	21. ABSTRACT SECURITY CLASSIFICATION
☒ UNCLASSIFIED/UNLIMITED ☐ SAME AS RPT. ☐ DTIC USERS	UNCLASSIFIED
22a. NAME OF RESPONSIBLE INDIVIDUAL MARK D. FLOHR	22b. TELEPHONE (Include Area Code) 202-325-7559 / 22c. OFFICE SYMBOL DNA/ISCM

DD FORM 1473, 84 MAR 83 APR edition may be used until exhausted. All other editions are obsolete.

SECURITY CLASSIFICATION OF THIS PAGE
UNCLASSIFIED

FOREWORD

Classified material has been removed in order to make the information available on an unclassified, open publication basis, to any interested parties. The effort to declassify this report has been accomplished specifically to support the Department of Defense Nuclear Test Personnel Review (NTPR) Program. The objective is to facilitate studies of the low levels of radiation received by some individuals during the atmospheric nuclear test program by making as much information as possible available to all interested parties.

The material which has been deleted is either currently classified as Restricted Data or Formerly Restricted Data under the provisions of the Atomic Energy Act of 1954 (as amended), or is National Security Information, or has been determined to be critical military information which could reveal system or equipment vulnerabilities and is, therefore, not appropriate for open publication.

The Defense Nuclear Agency (DNA) believes that though all classified material has been deleted, the report accurately portrays the contents of the original. DNA also believes that the deleted material is of little or no significance to studies into the amounts, or types, of radiation received by any individuals during the atmospheric nuclear test program.

OPERATION DOMINIC

FISH BOWL SERIES

PROJECT OFFICERS REPORT—PROJECT 6.9

RADAR CLUTTER MEASUREMENTS—UHF

Ray L. Leadabrand, Project Officer
Murray J. Baron
Walter G. Chesnut
Lambert T. Dolphin, Jr.
James C. Hodges
Walter E. Jaye
Robert S. Leonard
Roy A. Long
Ronald L. Presnell

Stanford Research Institute
Menlo Park, California

ABSTRACT

Project 6.9 participation in the Tight Rope, Blue Gill, King Fish, Check Mate, and Star Fish events was quite successful. The objectives of this project were to: (1) determine, as a function of frequency, the time history, position in space, and the strength of all radar echoes associated with these high-altitude bursts, (2) interpret military significance of these results, and (3) use these results to contribute to the overall development of a phenomenological model of high-altitude nuclear detonations.

The UHF instrumentation for this project consisted of the following: ground-based radars at 398, 850, and 1210 Mc were used at Johnston Island. Shipborne radars at 140 and 370 Mc were used in the magnetic conjugate area. A total of six 425-Mc AEW radar aircraft were used in the detonation area and in the magnetic conjugate area.

In the detonation area, the radars located at Johnston Island obtained echoes from the fireball/debris for each of the tests; these echoes are summarized in the table below.

UHF FIREBALL/DEBRIS ECHOES

Test	Maximum Amplitude	Maximum Duration
Star Fish	20 db	1 to 2 seconds
Check Mate	> 50 db	6 minutes
King Fish	> 50 db	10 minutes
Blue Gill	> 50 db	25 minutes
Tight Rope	40 db	5 minutes

In addition, detonation-area auroral clutter was observed north of Johnston Island on Star Fish, Check Mate, and King Fish. These echoes were generally weak and sporadic, but persisted for quite long periods of time. The reflections generally occurred at heights between 80 and 500 km. The table below summarizes these measurements.

DETONATION-AREA AURORAL CLUTTER

Test	Maximum Duration
Star Fish	5 hours
Check Mate	2 hours 39 minutes
King Fish	> 2 hours 55 minutes

Increases in radio noise were detected on the Johnston Island UHF radars on Check Mate, King Fish, and Blue Gill. The maximum temperatures and durations are shown below.

RADIO NOISE

Test	Maximum Temperature	Maximum Duration
Check Mate	10,000° K	> 140 seconds
King Fish	7,000° K	> 20 seconds
Blue Gill	3,000° K	100 seconds

Observations of the radar effects made in the magnetic conjugate area obtained positive results on all except Blue Gill at 140 Mc, and on some shots at 370 Mc. The durations are shown in the following table.

CONJUGATE-AREA AURORAL CLUTTER

Test	140 Mc Maximum Duration	370 Mc Maximum Duration
Star Fish	240 seconds	170 seconds
Check Mate	360 seconds	None
King Fish	740 seconds	110 seconds
Tight Rope	54 to 110 minutes	None

These echoes were similar to the detonation-area auroral clutter in that they were weak and sporadic in nature. Early-time conjugate echoes were used to determine the actual magnetic conjugate point for comparison with the calculated magnetic point, using Finch and Leaton coefficients.

The echoes and increases in background noise levels could have deleterious effects on ballistic missile defense system radars. The increased sensitivity of such missile system radars (as much as 44 db greater) over the Johnston Island radars would make the detonation-area clutter seen on such a radar extremely intense and longer lasting than indicated above.

CONTENTS

TABLES

FIGURES

CHAPTER 1

INTRODUCTION

The detonation of nuclear devices at high altitudes in the atmosphere produces complex and interrelated phenomena dependent not only on yield, altitude, and ratio of fission-to-fusion yield, but also upon geometry with respect to the earth's magnetic field and time of day.

The ionizing radiations from the bomb itself produce wide-scale effects which at high altitudes are constrained only by the earth's curvature, the earth's magnetic field and the denser air below. In addition, the lingering fission products are a significant continuing source of ionization effective for many hours. Thirdly, the deposition of large amounts of energy in the atmosphere produces large-scale motions in the atmosphere; shocks, waves, and turbulence, which in the absence of the other two direct ionization effects, would alone be very important in rearranging the natural existing ionization.

There are two separate viewpoints from which radar measurements during high-altitude detonations are important. Radar studies of bomb-produced clutter are vitally needed to answer the immediate needs of systems designers, and to fill in gaps in present knowledge. From the second viewpoint, diagnostic studies are very much in order to improve our understanding of the phenomenon itself. Only through this latter approach can a good body of detailed knowledge evolve which can be drawn upon in the future for systems as yet unconceived.

1.1 OBJECTIVES

The main objective of Project 6.9 was the development of an improved understanding of the radar reflection phenomena of high-altitude nuclear detonations so that the military significance of such phenomena on AICBM systems can be assessed. In addition, the experimental radars assembled for Fish Bowl Project 6.9 have been specifically designed to yield as much information concerning the phenomenology of high-altitude nuclear bursts as is possible.

More specifically, the objectives of Project 6.9 are listed below:

1. To determine as a function of time the strength, position in space and variation as a function of radar frequency the radar reflections associated with:

    (a) the fireball/debris

    (b) the auroral clutter in the detonation area

    (c) the auroral clutter in the magnetic conjugate area

    (d) the tube of ionization passing overhead at the magnetic equator.

2. To correlate the radar reflection results with visual phenomena seen looking at:

    (a) the fireball/debris

    (b) the auroral effects in the detonation area

    (c) the auroral effects in magnetic conjugate area

    (d) the tube of visual effects passing overhead at the magnetic equator.

3. To provide information concerning the earth's magnetic field by observing magnetic conjugate effects.

4. To contribute information which will allow the assessment of the effects of high-altitude nuclear detonations upon advanced radars presently in use and contemplated for use with ballistic missile systems.

5. To contribute as much information as possible to the development of an overall phenomenological model of high-altitude nuclear detonations so that all effects of such detonations at any other yield and altitude may be predicted as accurately as possible.

1.2 APPENDED INFORMATION

Appendixes A and B contain information on radar performance and data reduction. Appendix C contains a recommendation for radar measurements during Operation Blue Rock. Appendix D presents recommendations for data acquisition and processing.

CHAPTER 2

TIGHT ROPE

2.1 INTRODUCTION

This detonation was expected to produce a well-contained fireball which would expand gradually and rise slowly.[1] The size of the fireball at 1 second was estimated to be in diameter. It was expected to rise at a rate of less than 100 m/sec.

As the fireball should be of high electron density, extensive radar returns were expected from it.

No auroral clutter was expected to be observed in the burst area. Virtually no auroral conjugate effects were expected unless the debris rose to an altitude Some effects in the conjugate area were expected as a result of gamma-produced Compton electrons, though these effects were not expected to be seen by UHF radars.

2.2 PROCEDURE

2.2.1 Johnston Island Radars.

Instrumentation. The Johnston Island instrumentation for Project 6.9 consisted primarily of three UHF radars and a seven-frequency HF pulse radar (sounder). These radars were housed in three portable vans. Figure 2.1 shows one van being unloaded at Johnston Island. The field site layout is shown in Figure 2.1 of Volume 1, which is an aerial photograph of part of

[1] See Volume 1 for a more complete discussion of the expected results.

Johnston Island.

Each UHF radar was composed of a pulsed klystron transmitter, gas tube duplexer, parametric amplifier receiver system, and synchronizing and display equipment. All three UHF radars operated into a common antenna, the 86-foot dish. Figure 2.2 is a block diagram of the 398-Mc radar system; the 850-Mc and 1210-Mc systems were essentially identical. Figure 2.3 shows the interior of the van containing the 398-Mc and 850-Mc transmitters.

Each of the radars was calibrated by first measuring the transmitter power output following the duplexer with a calibrated directional coupler and a microwave power meter using a thermistor mount, then by inserting a calibrated RF pulse from a signal generator back into the receiver through a directional coupler in front of the duplexer. In this way, the radar sensitivity could be monitored continuously at all times.

The antenna was a parabolic dish type with an elevation-azimuth mount, steerable in all directions and continuously rotatable in azimuth. The dish was composed of an aluminum radial truss-and-ring assembly, constructed around a steel-barrel truss-and-tripod support. The dish was mounted on a surplus naval 5-inch gun mount. The dish and mount were supported by a steel tower and base frame. Figure 2.4 shows the mount being lifted onto the tower. Expanded aluminum mesh tied onto the ring assembly formed the reflecting parabolic surface, the measured rms deviation of

which was approximately 1/2 inch. The limited deviation and the mesh size, 5/8 inch by 5/8 inch, ensured that the dish would perform properly up to a maximum frequency of 3 Gc. Figure 2.5 shows the dish being lifted for attachment to the mount.

The mount was driven in azimuth and elevation by 50-hp and 25-hp wound-rotor induction motors, respectively. The motors were controlled from the control van. The dish drives, controls, and position indicators allowed manual positioning to an accuracy ±1/4 degree in azimuth or elevation. The azimuth speed control allowed a continuous speed variation of 2-1/2 to 5 rpm (15 to 30 degrees per second). The elevation speed control allowed a continuous speed variation of 0 to 2 degrees per second. In addition to the manual controls, an automatic programmer could control the dish in a scan mode, wherein the dish revolved continuously in azimuth and moved successively to preselected elevation angles. Any number of 36 elevation angles could be selected to which the dish would move and pause at for one azimuth revolution before proceeding to the next selected angle. This process continued until a lower limit was reached and the elevation scan direction was reversed. The dish would then proceed upward, pausing at the selected elevation angles until an upper limit was reached and the scan direction was again reversed.

A vidicon TV camera with its field of view co-linear with the dish axis was mounted on the lower rim of the dish. A closed-circuit

monitor in the van allowed the dish to be boresighted on any visual object with an accuracy of ±1/4 degree. A parallel monitor was recorded by a movie camera.

The RF system for the dish consisted of a three-frequency feed, two three-channel rotary joints, and three coax lines, each 120 feet long. Figure 2.6 is a view of the completed antenna.

Each of the three transmitters was composed of a pulse-modulated klystron amplifier with power supply, pulse modulator, driver, and cooling system. In order to produce a pulse-modulated RF output from the klystron amplifier without jamming the receiver, both the RF drive and the klystron beam current were pulsed. The RF drive was pulsed by gating all stages of the driver multipliers and amplifiers except the oscillator stage. The klystron beam current was pulsed by switching the klystron modulating anode between ground and the beam voltage. This was accomplished by a pair of switching units in the klystron modulator unit. The high peak-output power was achieved by using a -28-kv operating-beam voltage.

Each of the receiver systems was composed of a parametric amplifier followed by a low-noise converter, blanker, and a Collins 51J4 communications receiver. The parametric amplifier used an Adler tube, had a double-channel noise figure of 1.5 db, and operated very stably without adjustments. The bandwidth of the system, determined by the communications receiver, was 6 kc. The dynamic range of the receiver system without the tape recorder was

in excess of 50 db; the tape recorder limited the dynamic range of the recorded data to approximately 30 db. The frequency stability of the radar system was determined by the driver oscillator, the converter local oscillator, and the communications receiver. The critical oscillators were controlled by crystals in high quality ovens, and the resultant stability was ±500 cps after warmup.

Each transmitter was separated from its receiver by a gas tube. The TR-ATR duplexer system was designed for prompt recovery time.

The data-recording equipment was composed of two magnetic-tape recorders and three 35-mm cameras. The two tape recorders were connected in parallel for backup purposes. The tape recorded A-scans for the 398-, 850-, and 1210-Mc radars; sync; 398-Mc Doppler channel, voice countdown; digital time; and antenna position.

In addition to the A-scan scope displays, there was a PPI system composed of a sawtooth generator, sine-cosine potentiometer, and three display scopes. Each of the scopes was z-axis-modulated with the A-scan video signal from each of the UHF radars. In addition, each scope had a 35-mm camera system, which photographed one frame for each complete revolution of the antenna.

Accurate timing was provided by an Itek digital clock, which was calibrated against WWVH daily. The output from the clock was recorded on tape in digital form.

Echo Doppler information was provided by a separate receiver channel in parallel with the Collins 51J4 receiver, which had an IF

output of approximately 10 kc.

Radar timing was provided by a synchronizer that provided start-and-stop trigger pulses for the transmitters, key pulses for the drivers, scope sync, and range marks for the A-scan video signals. The timing of the synchronizer was controlled by a 150-kc crystal oscillator whose output was divided to produce various PRFs and range marks. Figure 2.7 shows the interior of the receiving-recording van, which also housed the 1210-Mc transmitter.

The equipment operating characteristics are shown in Table 2.1.

Operating Technique. The mode of operation of the UHF radar will be described as the radar results are presented. It is believed that better clarity of understanding will result from this method of data presentation. In general, the UHF radar was operated for several hours prior to an event so that the equipment would have stabilized by detonation time. For the Tight Rope event, the radar was directed at the detonation point prior to detonation. However, due to an interference problem, the transmitters were not turned on until after the detonation. For the Thor launches, Blue Gill, King Fish, and Star Fish, the UHF radar program tracked the Thor missile from launch until just a few minutes before detonation. Then the antenna was oriented at the expected detonation point. For the XM-33-launched Check Mate event, the radar was oriented at the detonation point at missile launch time. Because of an interference problem, the 398-Mc transmitter was not turned on until

after the detonation.

For about the first two minutes following most detonations, the UHF antenna would remain oriented in the detonation area. Usually, this was followed by azimuth-elevation scans through the visible phenomena in the detonation region as viewed on the boresight TV system. Finally, at about H + 10 minutes, the antenna would be put through a variety of scans, including the automatic programmed scan, to search out all possible e· areas.

2.2.2 AEW Aircraft Radars

Instrumentation. Six RC-121-D aircraft participated in the Fish Bowl series. These aircraft belong to the 552nd Aircraft Early Warning and Control (AEW and C) Wing at McClellan Air Force Base. This element was under the command of Lt Col H. T. Wagnon. Four of the aircraft were directly assigned to Project 6.9 under TG 8.1.3 while two aircraft were assigned to TG 8.4 as airborne array control aircraft. Support data, radar as well as other data, were gathered.

The RC-121-D aircraft are modified Lockheed Super Constellations (C-121). Their normal function is the patrolling of the U. S. coast line in order to detect any penetration of the Air Defense Identification Zone (ADIZ) by unidentified aircraft. They operationally report to the Air Defense Command. In order to perform their normal mission they are equipped as shown in Figure 2.6 of Volume 1 with the APS-45 X-band height-finder radar and the APS-95 UHF search radar. In addition to their normal navigational equipment, these aircraft carry five ARC-27 UHF transceivers, one 618-S1 high-frequency AM transceiver, and one 618-T high-

frequency SSB transceiver. Stanford Research Institute (SRI) installed a Collins 75-S1 SSB receiver in the aircraft operating in the conjugate area. The aircraft is capable of up to 17 hours in the air and carries between 14 and 18 crew members on a normal mission. For the purposes of Operation Dominic, only the APS-95 UHF radar was used. The nominal parameters of the APS-95 are shown in Table 2.2.

These aircraft are normally equipped with PPI-scope cameras taking pictures at the rate of one frame per antenna revolution. A heading marker appears on the oscilloscope each time the beam sweeps past the nose of the aircraft. The scopes are north-magnetic stabilized. For the purposes of Operation Dominic, SRI equipped five aircraft with A-scope cameras which were mounted on the 5-inch A-scope normally used to monitor various functions of the radar. The A-scope also took pictures at the rate of one frame per antenna revolution, thus integrating the amplitude-versus-range information over the full 360-degree sweep.

Operating Technique. For Tight Rope, only two aircraft flew in the detonation area. One was a scientific aircraft and the other a control aircraft. They flew in patterns shown in Figure 2.8 at locations given in Table 2.3. Lambkin 1 was located at magnetic north looking at the detonation. Abusive 1 was located at magnetic east looking at the detonation.

The actual radar operating parameters are shown in Table 2.4.

2.2.3 M/V ACANIA Radars

Instrumentation. The M/V ACANIA, shown in Figure 2.4

Volume 1, which housed all of the Project 6.9 equipment in the conjugate area during Fish Bowl, was originally outfitted for participation in Hardtack in 1958. The 140- and 370-Mc radars (the records of which are reported in this volume) were a part of this equipment. Both radars operated simultaneously into a steerable 30-foot parabolic-reflector antenna and are very similar in design and complexity to the Johnston Island radars described in Section 2.2.1. The operating characteristics of the two radars are shown in Table 2.5.

Operating Technique. The ACANIA was located according to the following criteria: "go directly above the detonation to H = 50 km, follow this field line to H = 80 km in the magnetic conjugate area and locate directly under this point." The exact location of the radar equipment is shown in Table 2.3.

Due to a failure of the azimuth drive on the 30-foot dish, the ACANIA operational procedure was somewhat altered, with no resulting loss of data. The ship maintained a constant heading with all movable antennas pointing magnetically south. The ship then changed heading from time to time, to give azimuth coverage. All movable antennas were pointed up at an elevation of about 60 degrees so that the line-of-sight from the radar intersected the E-region at right angles to the magnetic field lines.

2.3 RESULTS

2.3.1 Johnston Island Radars

Fireball/Debris Clutter. Prior to the detonation, the antenna was positioned in the direction of 83-degree elevation and 204-degree azimuth. All three radars were turned off until detonation and were turned on and up to power by H + 1 second. The actual detonation location was about 2 degrees in elevation below the radar beam. The visual fireball expansion and rise was sufficient to move the edge of the fireball into the radar beam at about H + 9 seconds. The fireball stayed partially in the radar beam until H + 95 seconds, when the antenna was scanned about in elevation and azimuth. Excellent correlation between radar echoes and the visual fireball/debris was noted the entire time fireball/debris echoes were observed. An example of this correlation is shown in Figure 2.9. After H + 15 minutes the antenna was scanned either manually or with the automatic programmer for five hours following the Tight Rope detonation.

Starting abruptly at H + 9 seconds as the fireball edge moved into the radar beam, echoes at 398, 850, and 1210 Mc reached an amplitude of 40 db signal-to-noise ratio (S/N). These echoes persisted at decreasing amplitude until H + 95 seconds when antenna scanning was started. The range-versus-time records of the echoes for the first ten minutes are shown in Figures 2.10 and 2.11. The echo amplitude-versus-time records for the first five minutes are shown in Figures 2.12 through 2.14. The echo amplitudes versus time, with antenna-direction-caused fluctuations removed, are shown in Figure 2.15. At H + 90

seconds, an elevation scan was made which showed that the echoes were limited to 80 to 87 degrees in elevation at that time. At H + 180 seconds an azimuth scan was made which showed that the echoes were limited to 175 to 260 degrees in azimuth at that time. No detonation area echoes were observed after H + 6 minutes.

Figures 2.16 through 2.18 show the Doppler records for the first five minutes following the detonation at each frequency. All three records show no shifts or spreads. The 6-kc Doppler width corresponds to the 3-db frequency spectrum of the 150-μsec pulse length used during that test.

Auroral Clutter in the Detonation Area. No auroral clutter was observed in the detonation area by the Johnston Island radars.

Fireball/Debris Noise. No noise emission was observed in the detonation area.

2.3.2 AEW Aircraft Radars.

Fireball/Debris Clutter. Lambkin 1, located north of the detonation area, was not operational until H + 25 seconds. No detonation-induced echoes were observed.

Abusive 1, located east of the burst area, observed weak echoes from the fireball/debris from H = 0 until H + 28 minutes, with an equivalent radar cross section of 0.2 m^2 (based upon a point target).

Auroral Clutter in the Detonation Area. No auroral clutter was observed in the detonation area by the AEW aircraft radars.

2.3.3 M/V ACANIA Radars.

Auroral Clutter in the Conjugate Area. The M/V ACANIA operated its 140-and 370-Mc radars during the burst and for several hours afterwards. The antenna was positioned magnetically south in azimuth and 60 degrees in elevation, with periodic elevation scans being made. No echoes were observed at 370 Mc. The range-versus-time records for the first 141 minutes are shown in Figures 2.19 through 2.27. Echoes were observed at 140 Mc, at 120-km range, and at late times of H + 54 to H + 110 minutes. The spatial location of these echoes is shown in Figure 2.28.

2.4 DISCUSSION

The somewhat unique features of Shot Tight Rope as observed in the conjugate area were a complete lack of test-associated echoes at the time of the event, and the onset of auroral clutter echoes which occurred not at early times, but at relatively late times—the 140-Mc echoes first occurred at H + 54 minutes. (Auroral-type echoes were also observed on the 32-Mc ACANIA radar, starting at about H + 40 minutes. See Volume 2 of this report for details.) These echoes were at ranges of 120 km in the magnetic south direction. The 140-Mc echoes lasted until H + 110 minutes.

The direction (elevation, azimuth) and range to these echoes indicates that they were due to reflections from magnetic field-aligned ionization at about E-region heights. The fact that this ionization was about 60 km farther south than the ACANIA (as it was

have to be in order to be seen, due to the geometry of having to look at right angles to the earth's magnetic field lines) indicates that the source of the ionization was at least 40 km higher than the 50-km point above the burst which was used to position the ACANIA in the first place. This result might imply that the source of the ionization was 90 km over ground zero.

Optical data presented in Volume 4 of this report indicates that the Tight Rope debris reached altitudes of the order of 40 to 50 km by H + 55 minutes. At these altitudes, the fission-product-decay beta rays could escape to the southern conjugate region. The debris had also blown to the north so that the field lines intersecting the debris would have passed over the detonation point at an altitude greater than the debris height. The combination of these two motions, coupled with the fact that, despite careful calculations and an empirical relocation for this event (see Appendix, Volume 1 of this report), we do not know the magnetic field geometry to better than a few tens of kilometers, may possibly explain the unique appearance of auroral echoes in this tropical region.

Considerable skepticism has been expressed concerning the existence of these aurora-like echoes. The echoes were received from the magnetic meridian of the Tight Rope event, not from all meridians satisfying the perpendicularity requirement.

The echoes were observed independently on two rather different frequencies (32 Mc and 140 Mc). Their time-and-intensity behavior on the two frequencies was consistent with our knowledge of auroral activity in arctic regions and on previous events of the Fish Bowl series. Their observed geometry (range, elevation and azimuth) tends to agree with the optical evidence acquired in the detonation area.

We have concluded that these echoes were associated with the Tight Rope event.

2.5 CONCLUSIONS

A Tight Rope event would have a seriously degrading effect on the performance of a ballistic missile defense (BMD) radar system. To evaluate this effect, a comparison has been made between the radars used during Fish Bowl and the planned BMD radar systems.

The radars used during these tests were, in general, somewhat less sensitive than those being planned for use in BMD activities. The advantage that a particular system radar would have over the test radars is shown for various scattering models in Table 2.6. The comparisons were developed by scaling the system radar to its nearest frequency counterpart used during Fish Bowl. For example, the Ballistic Missile Early Warning System (BMEWS) radars were compared with the 398-Mc Johnston Island radar, and the Nike-Zeus TTR radar was compared to the DAMP FPQ-4 C-band radars.

In order to give the reader a better understanding of the degrading

effects of the Tight Rope event, an estimate of the effect on the BMEWS tracking radar has been made, ignoring the fact that the operating pulse length of the BMEWS radar is too long to observe Tight Rope clutter at that range. If the BMEWS radar were located at a range of greater than about 300 km (pulse-length resolution), however, the Tight Rope fireball clutter would be seen. It would be observed by BMEWS out to ranges for which the Tight Rope detonation would be over the radar horizon (approximately 650 km).

The BMEWS system was picked as an example, not to deprecate that particular system, but because that system is operational, field-deployed, and its characteristics are well known. Table 2.7 shows the comparison between the BMEWS tracking radar characteristics and the Johnston Island 398-Mc radar. The comparison was made assuming the scattering was from a beam-filling target of range depth of at least one pulse width (300 μsec).

From the comparison, estimates of the strength and time duration of the clutter and noise effects are given below:

Fireball/Debris Clutter.

H + 0 to H + 10 sec	S/N = 0 to 80 db	Main Beam
	S/N = 0 to 30 db	Side Lobes
H + 10 to H + 30 sec	S/N = 80 db	Main Beam
	S/N = 30 db	Side Lobes
H + 60 to H + 240 sec	S/N = > 44 db	Main Beam
	S/N = > 0 db	Side Lobes
H + 240 sec to ?	S/N = 44 db	Main Beam
	S/N = 0 db	Side Lobes

Angular Diameter of Affected Region.

200 sec 10 degrees

Detonation-Area Auroral Clutter.

None was observed from Johnston Island. However, inasmuch as auroral clutter was seen by radars in the conjugate region at late times, one must surmise that if the Johnston Island Tight Rope geometry had been different, then detonation-area auroral clutter might have been seen and might generate a problem for BMEWS.

Fireball/Debris Noise.

None

Conjugate-Area Auroral Clutter.

Some might be seen.

From the above it is apparent that an area of 100 square degrees would be obscured for a depth of at least one pulse length plus 10 km by the fireball/debris clutter for a period of about five minutes. Although the Doppler spread of the echoes is not severe, the limited bandwidth of the 20-kc Doppler channel used in the Johnston Island radar does not rule out the possibility of there being Doppler components at a velocity comparable to the radial velocity of an approaching ICBM.

The relatively limited volume of intense clutter produced by Tight Rope leads one to think of using spaced radars in a BMD system, but that could be effectively countered by multiple Tight Rope's detonated simultaneously or spaced up to a minute apart.

TABLE 2.1 OPERATING CHARACTERISTICS OF THE JOHNSTON ISLAND RADARS

Frequency	398 Mc	850 Mc	1210 Mc
Peak Power	30 kw	30 kw	25 kw
Pulse Width	300 μs	300 μs	300 μs
Pulse Width (Tight Rope only)	150 μs	150 μs	150 μs
PRF	60 cps	60 cps	60 cps
System Noise Level	600°K	1000°K	600°K
Receiver Bandwidth	6 kc	6 kc	6 kc
Minimum Detectable Signal	-130 dbm	-128 dbm.	-130 dbm
Antenna Gain	38 db	45 db	48 db
Antenna Beamwidth	2°	1°	0.7°
Minimum Detectable σ at 500-km range	0.2 m^2	0.06 m^2	0.02 m^2

TABLE 2.2 NOMINAL CHARACTERISTICS OF THE AEW AIRCRAFT RADARS

Frequency	420 to 450 Mc
Peak power	1.5 Mw
Pulse width	6 to 9 μsec
PRF	250 cps
IF bandwidth	200 kc
Noise figure	8 db
MDS	-115 dbm
σmin at 200 nm	10 m^2
Beamwidth	10 degrees--E plane 18 degrees--H plane
Antenna rotation	6 rpm
Dynamic range	20 db

TABLE 2.3 LOCATIONS OF AEW AIRCRAFT AND M/V ACANIA DURING TIGHT ROPE

	Longitude	Latitude
Lambkin 1	169°12'W	18°11'N
Abusive 1	168°08'20"W	16°05'00"N
ACANIA	175°W	13°S

TABLE 2.4 OPERATING CHARACTERISTICS OF THE AEW AIRCRAFT RADARS DURING TIGHT ROPE

L = Lambkin, A = Abusive.

	L1	A1
Frequency, Mc	428	435
Peak Power, watts x 10^6	1.25	1.6
Pulse Width, μsec	8.5	8.9
PRF, cps	280	280
MDS, -dbm	114	115
Dynamic Range, db	15	21
σmin at 500 km, m^2	20	13

TABLE 2.5 OPERATING CHARACTERISTICS OF THE M/V ACANIA RADARS DURING TIGHT ROPE

Frequency	140 Mc	370 Mc
Peak Power	50 kw	20 kw
Pulse Width	300 μsec	300 μsec
PRF	30 cps	30 cps
Receiver Noise Figure	3 db	3 db
Receiver Bandwidth	6 kc	6 kc
Antenna Gain	21 db	30 db
Antenna Beamwidth	13.5°	5°
Minimum Detectable σ at 150-km range	0.2 m^2	0.2 m^2

TABLE 2.6 RADAR CHARACTERISTICS OF VARIOUS SYSTEMS

	Frequency	Advantage For a Point Target	Advantage For Beam-Filling Target	Advantage For Volume-Scattering Target
	Mc			
BMEWS-DR	425	+51 db	+44 db	+44 db
BMEWS-TR	425	+40 db	+40 db	+40 db
N-Z AR	915	+13 db	+17 db	+17 db
N-Z DDR	1335	+ 4 db	+16 db	+ 8 db
N-Z TTR	5500	+21 db	+26 db	+23 db
ZMAR SEARCH	1300	- 2 db	+ 9 db	+ 9 db
ZMAR DISCRIMINATION	1300	-28 db	-14 db	-22 db
ZMAR TRACK	1300	-32 db	-22 db	-44 db

TABLE 2.7 .RADAR SENSITIVITY COMPARISON

	Experimental Radar, Johnston Island	Operational BMEWS Tracking Radar
Frequency	398 Mc	425 Mc
Peak power	30 kw	10,000 kw
Average power	0.54 kw	540 kw
Pulse width	300 usec	2000 usec
Bandwidth	6 kc	0.2 kc
PRF	60 cps	27 cps
Antenna Size	86'	84'
Antenna Gain	38 db	39 db
System Noise Fig.	5 db	5 db

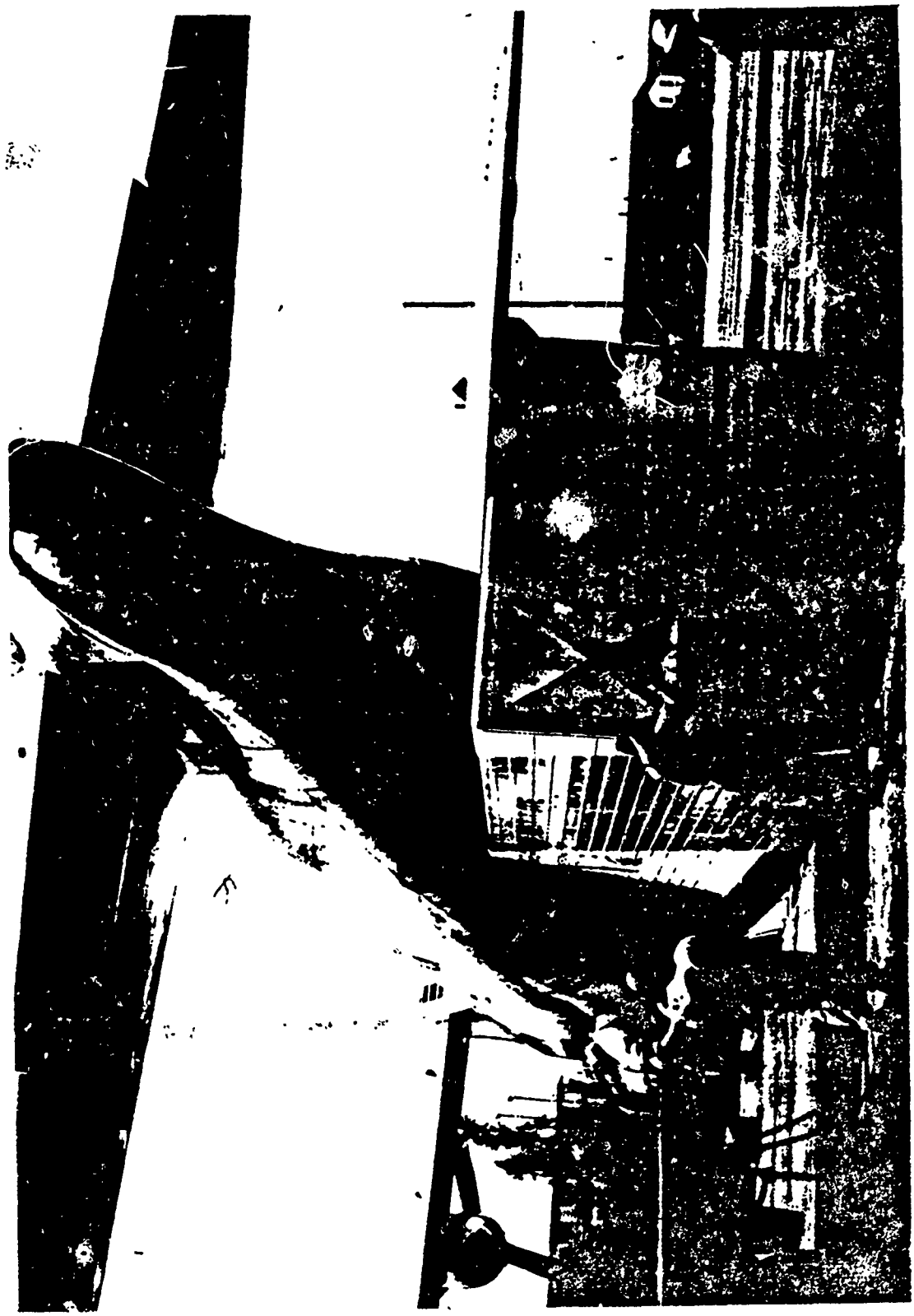

Figure 2.1 Unloading radar van from aircraft.

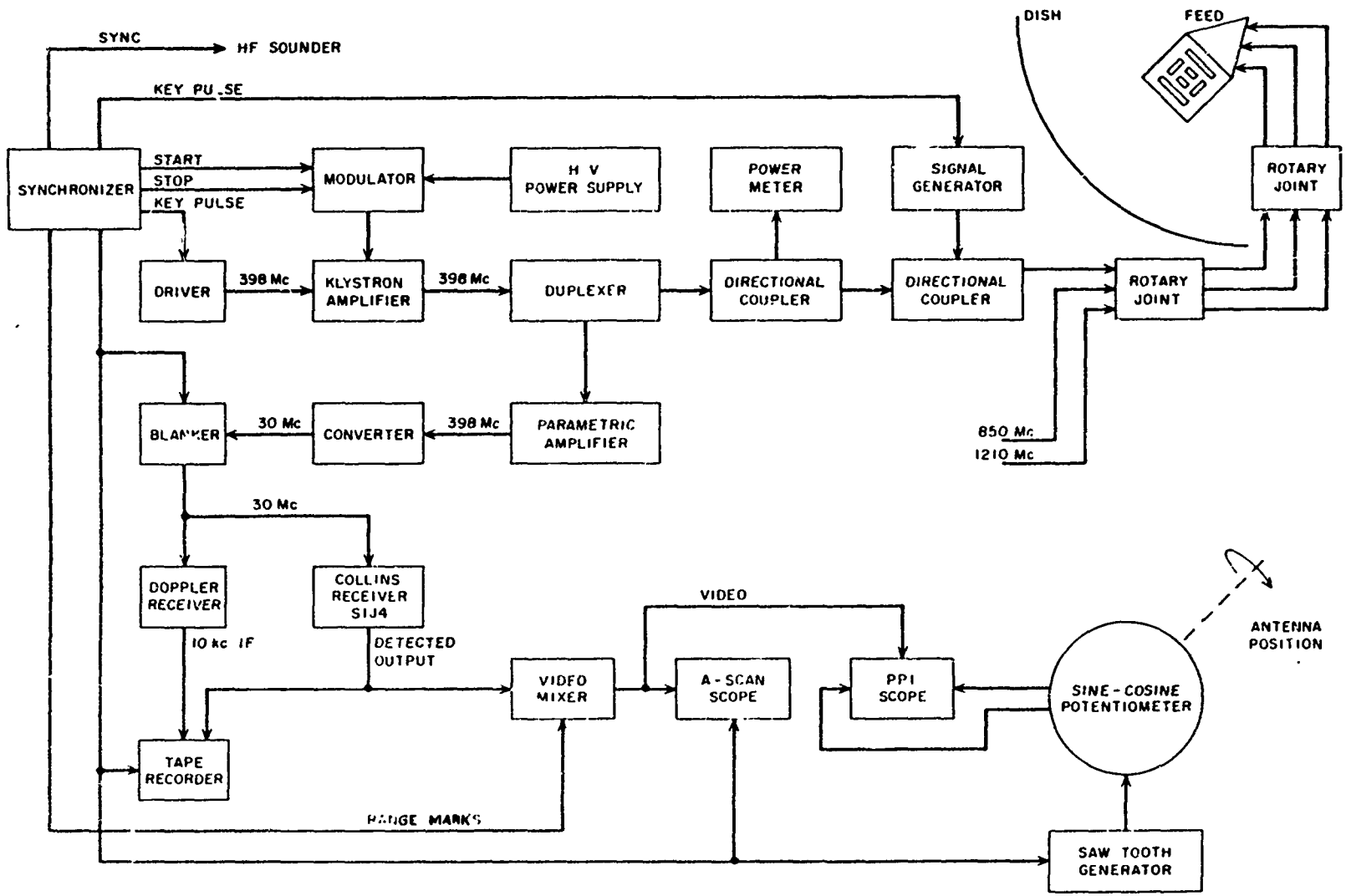

Figure 2.2 Block diagram of 398-Mc radar system.

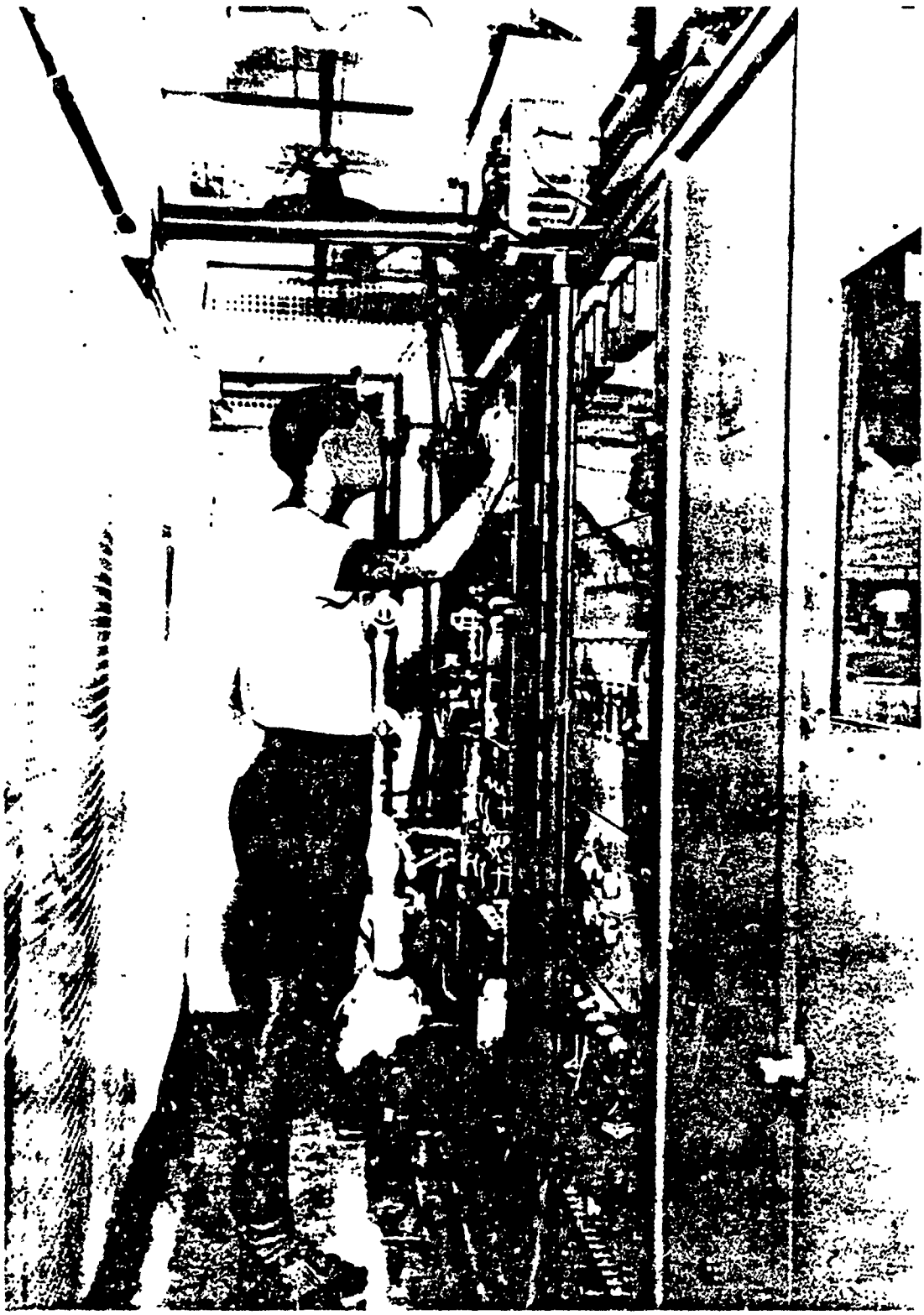

Figure 2.3 Interior of transmitter van.

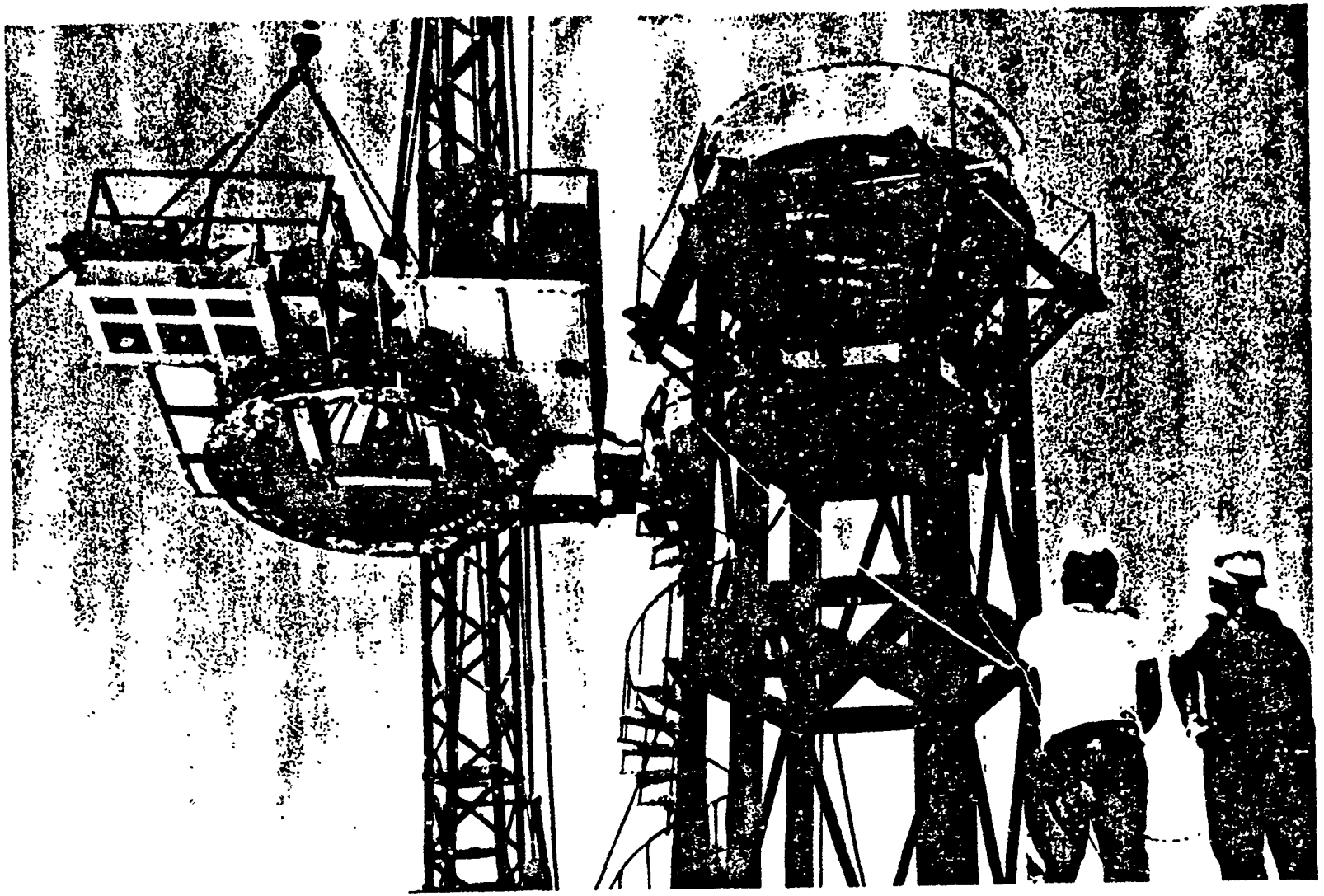

Figure 2.4 Placing antenna mount on tower.

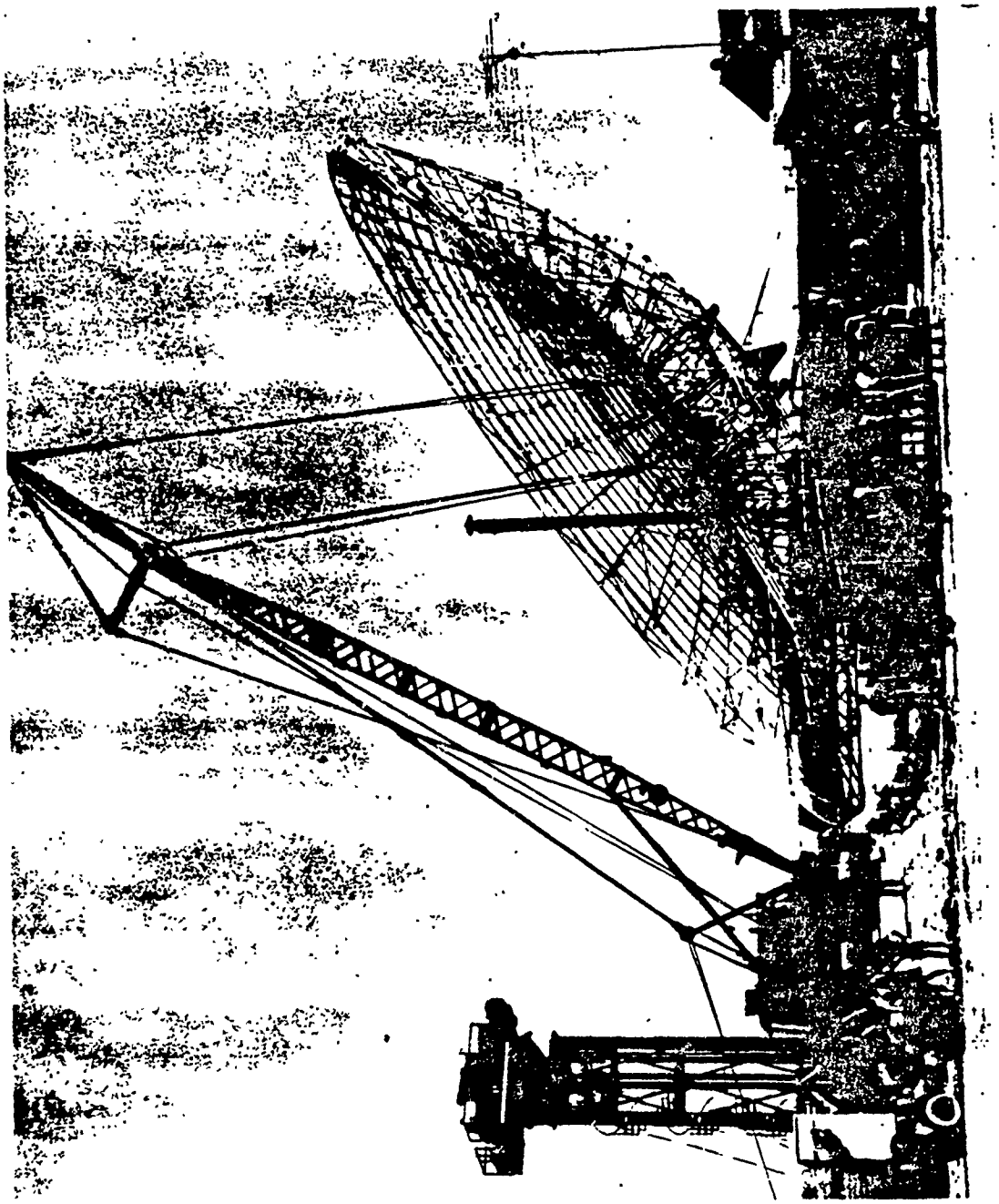

Figure 2.5 Placing antenna dish on mount.

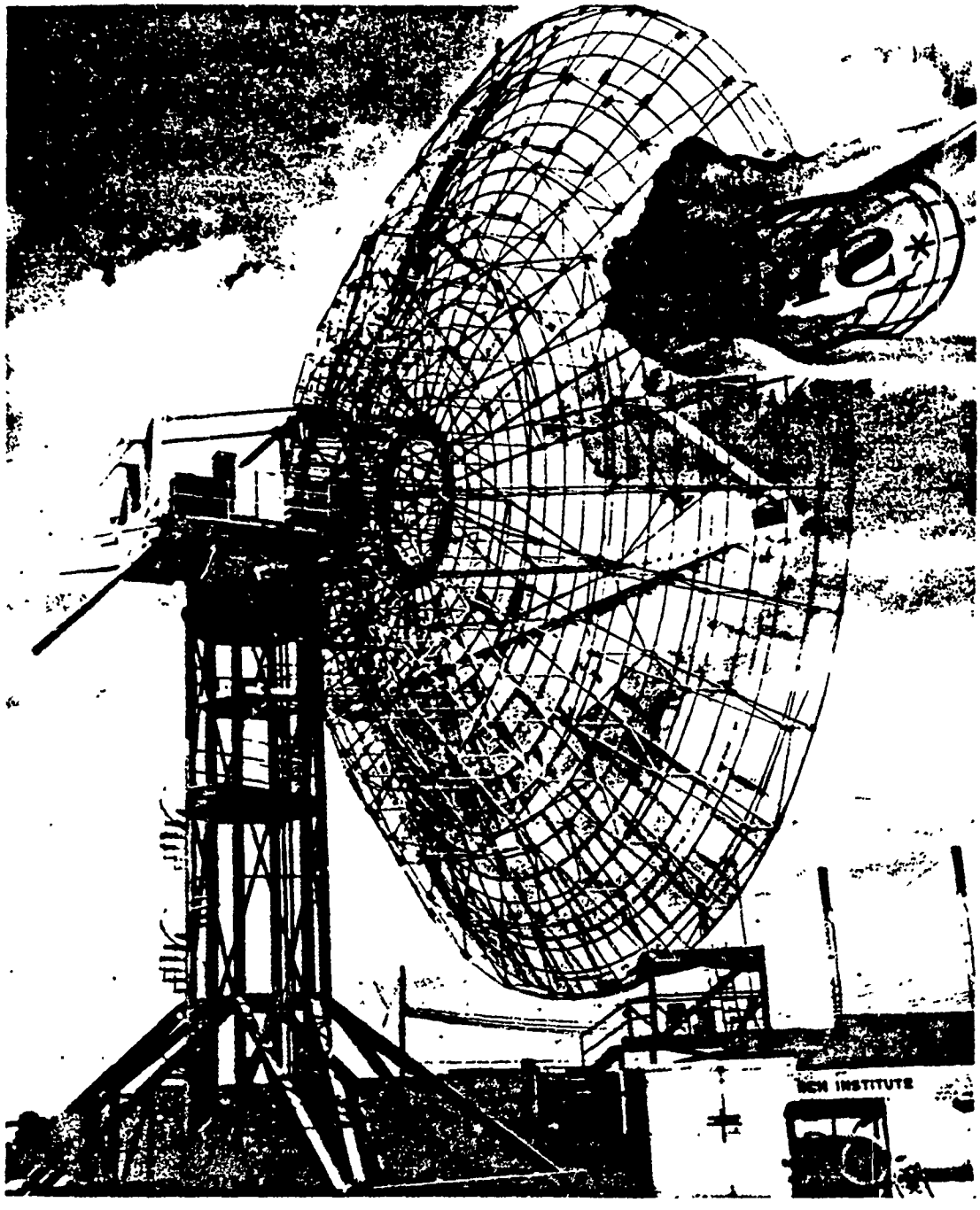

Figure 2.6 View of completed antenna.

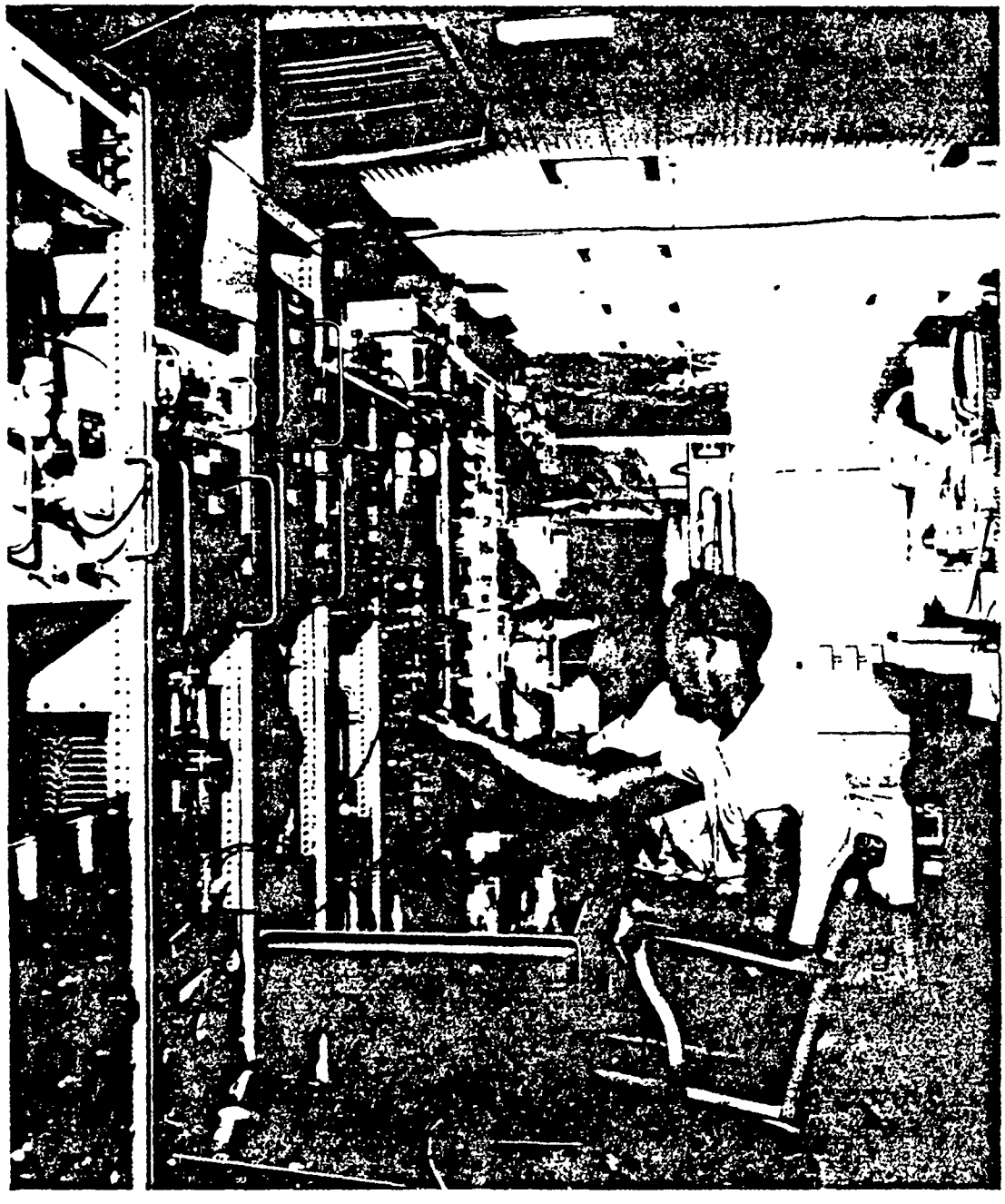

Figure 2.7 Interior of the control van.

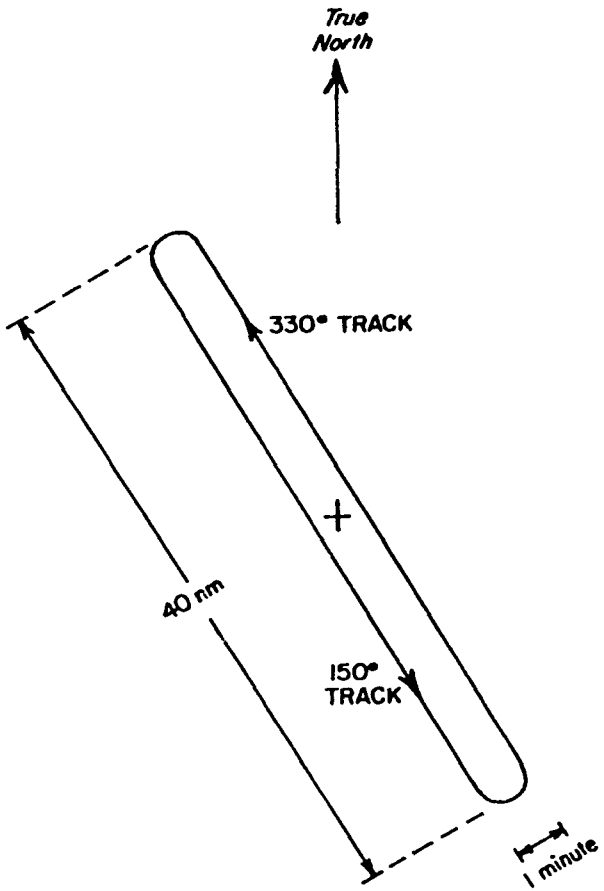

ABUSIVE I PATTERN

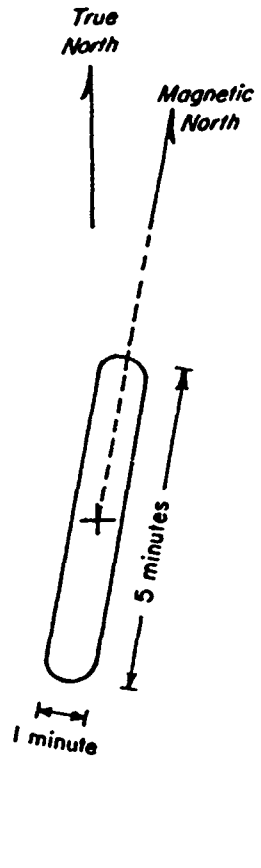

LAMBKIN 1-4 PATTERN

Figure 2.8 Flight pattern for the AEW aircraft.

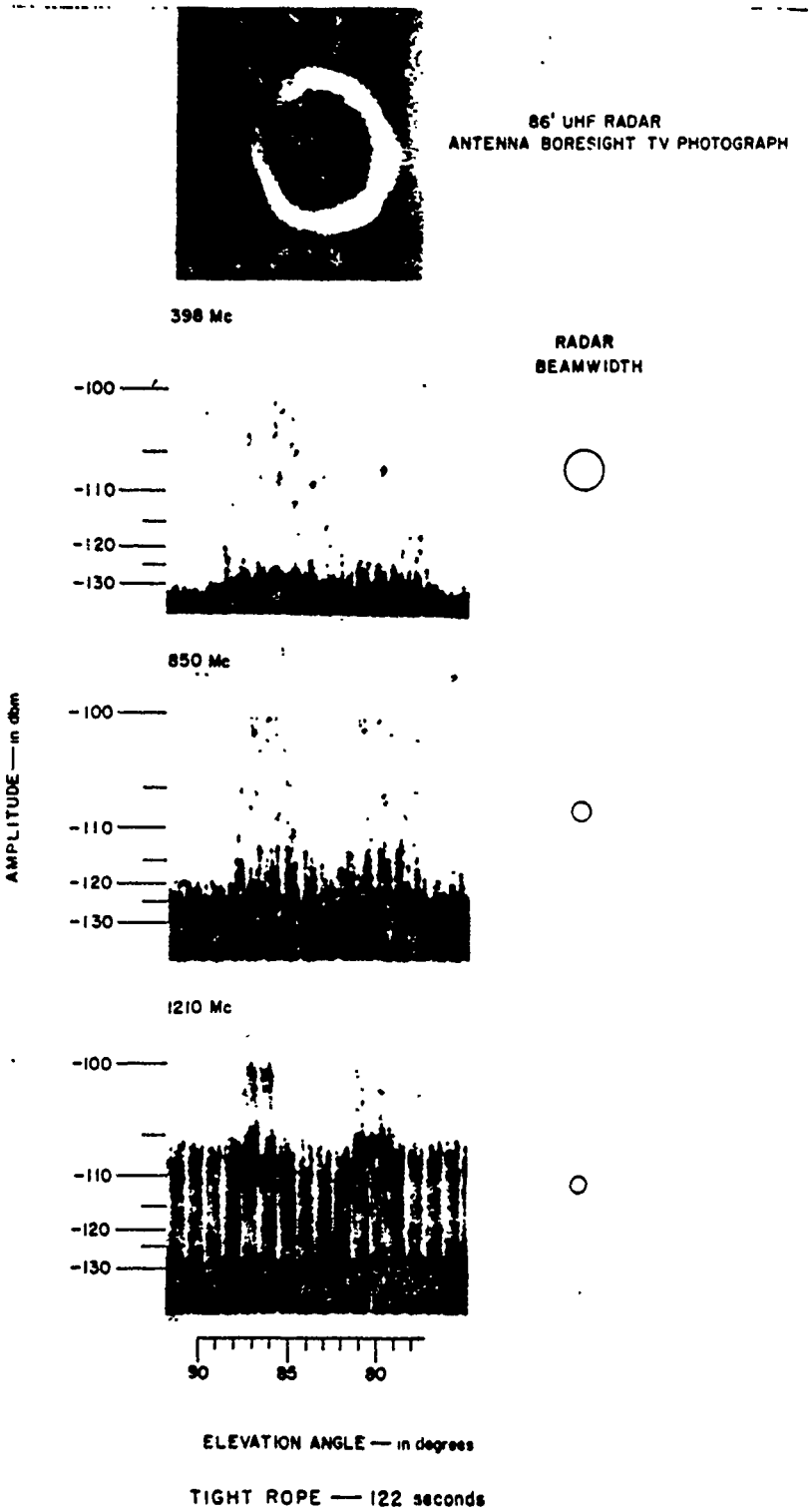

Figure 2.9 Johnston Island radar amplitude and visual comparison for Tight Rope.

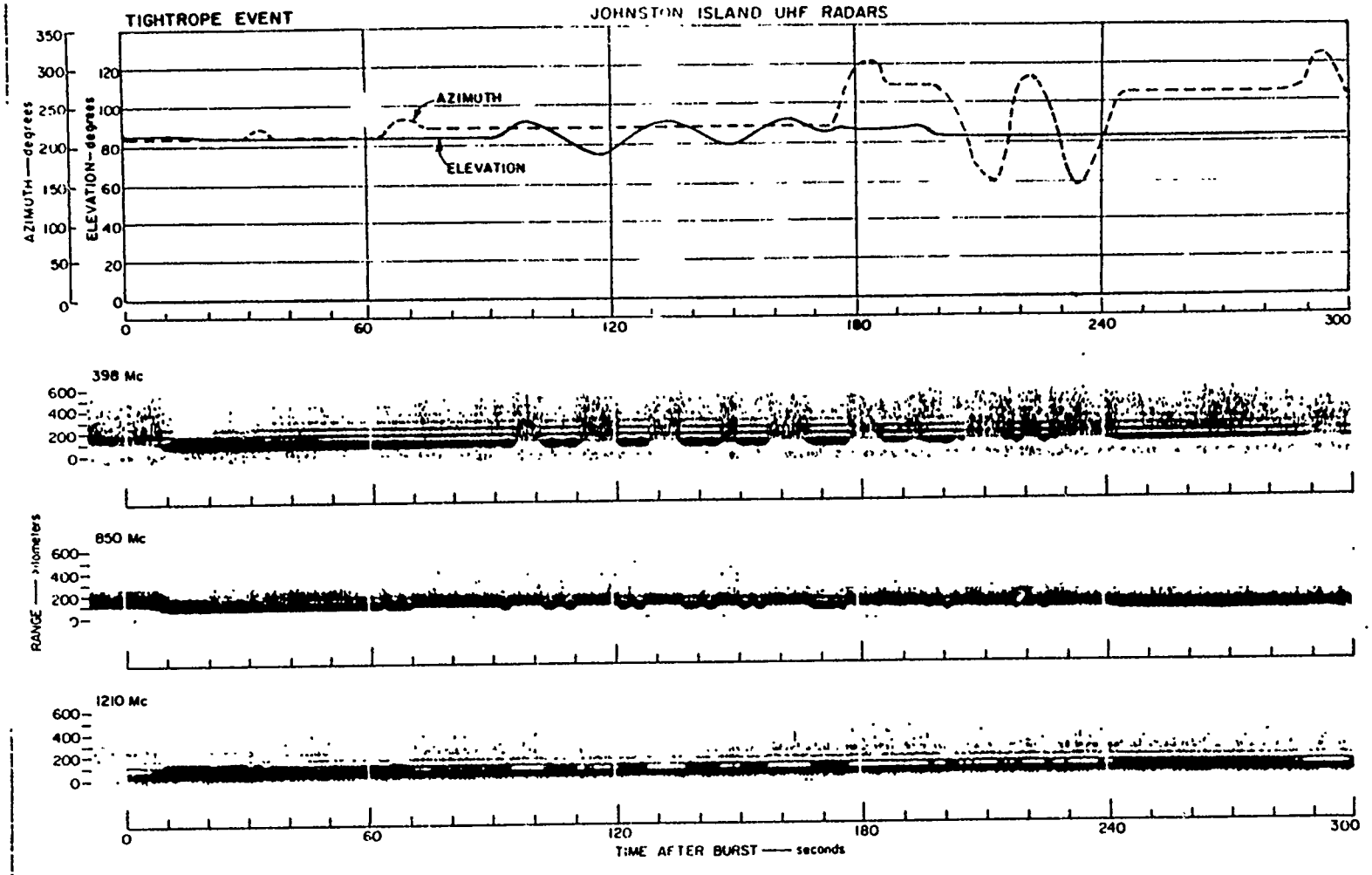

Figure 2.10 Johnston Island radar range versus time for Tight Rope; 0 to 600 km, 0 to 300 seconds.

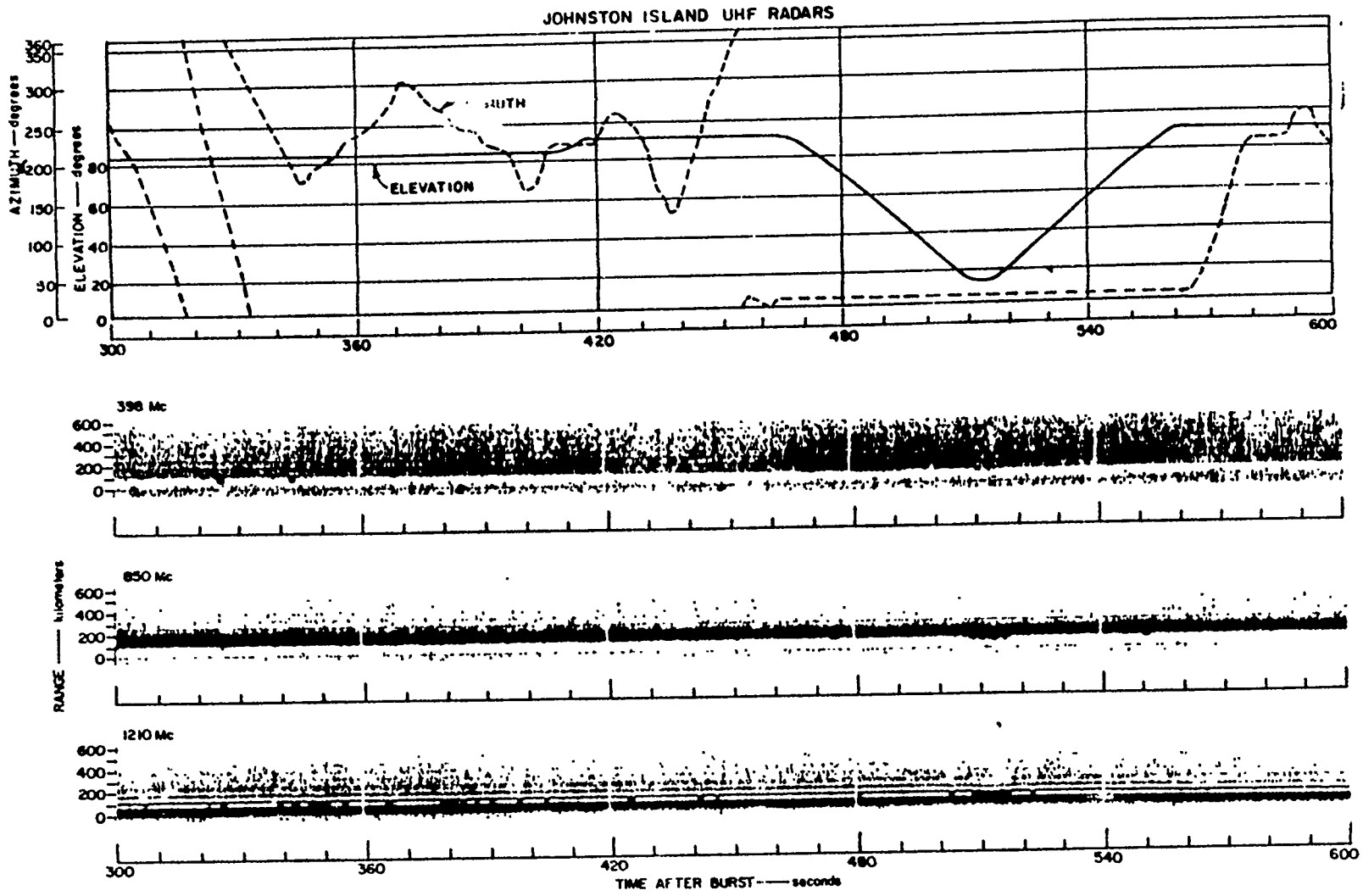

Figure 2.11 Johnston Island radar range versus time for Tight Rope; 0 to 600 km, 300 to 600 seconds.

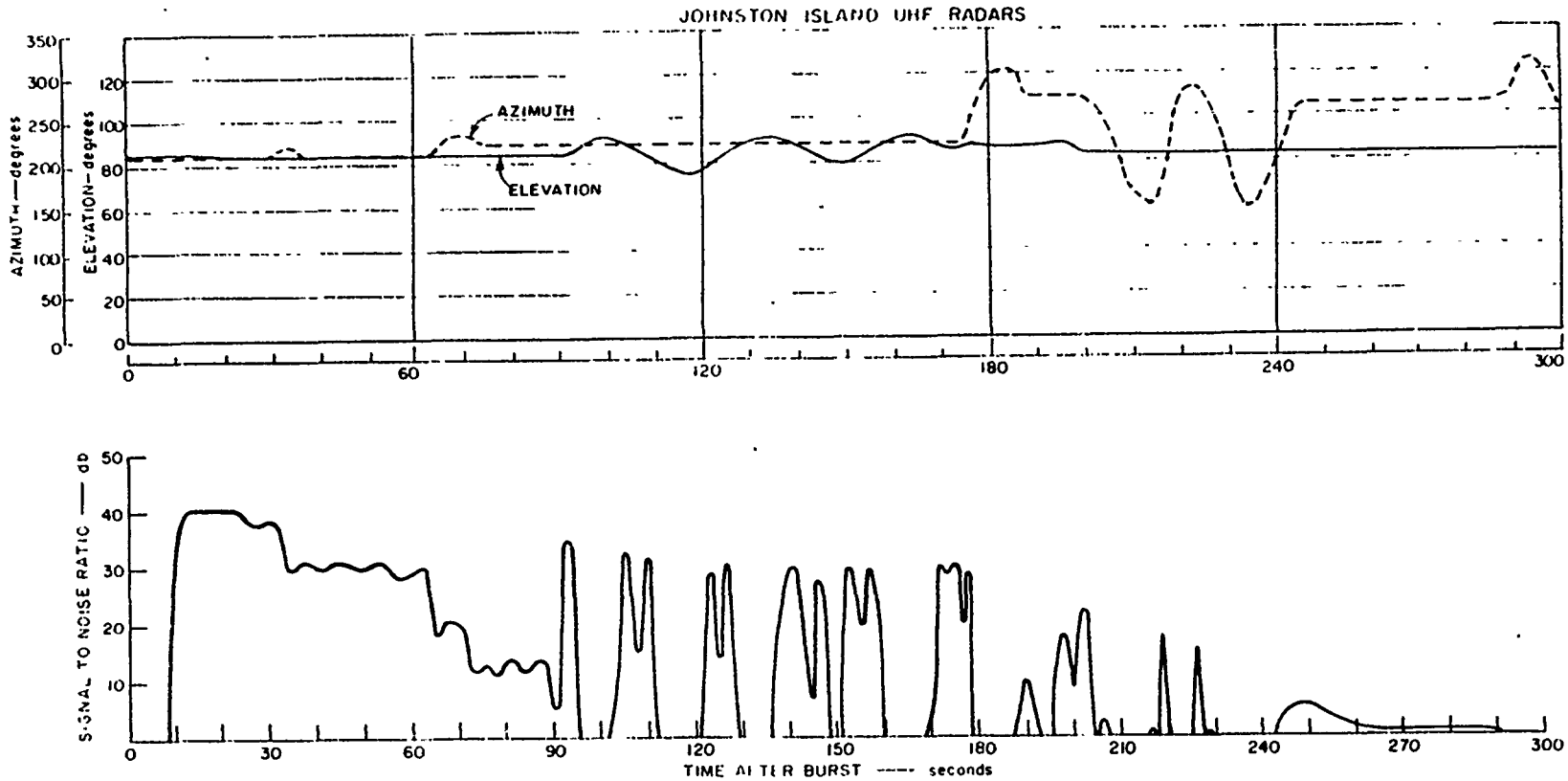

Figure 2.12 Johnston Island radar echo amplitude versus time for Tight Rope; 398 Mc, 0 to 300 seconds.

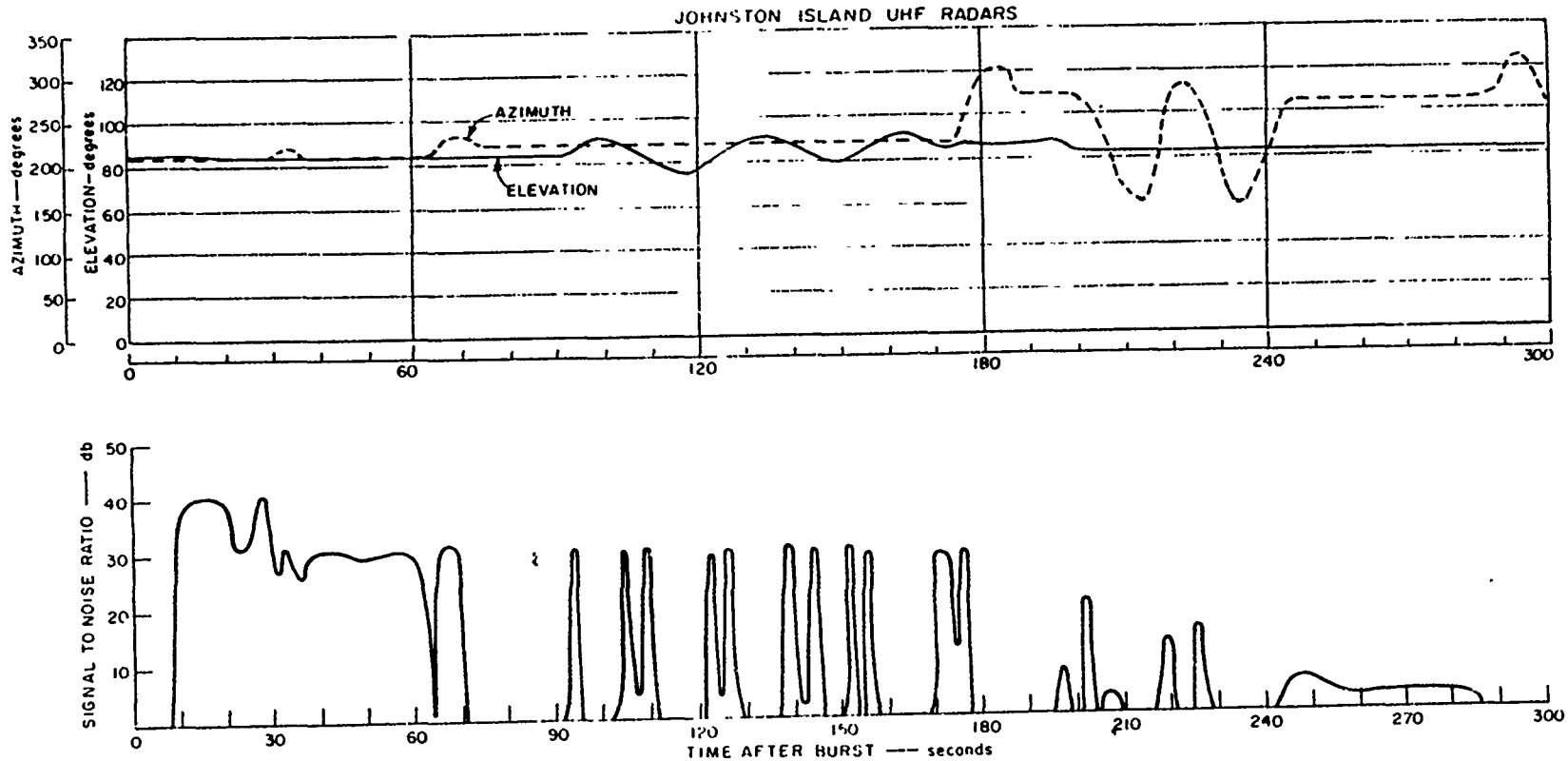

Figure 2.13 Johnston Island radar echo amplitude versus time for Tight Rope; 850 Mc, 0 to 300 seconds.

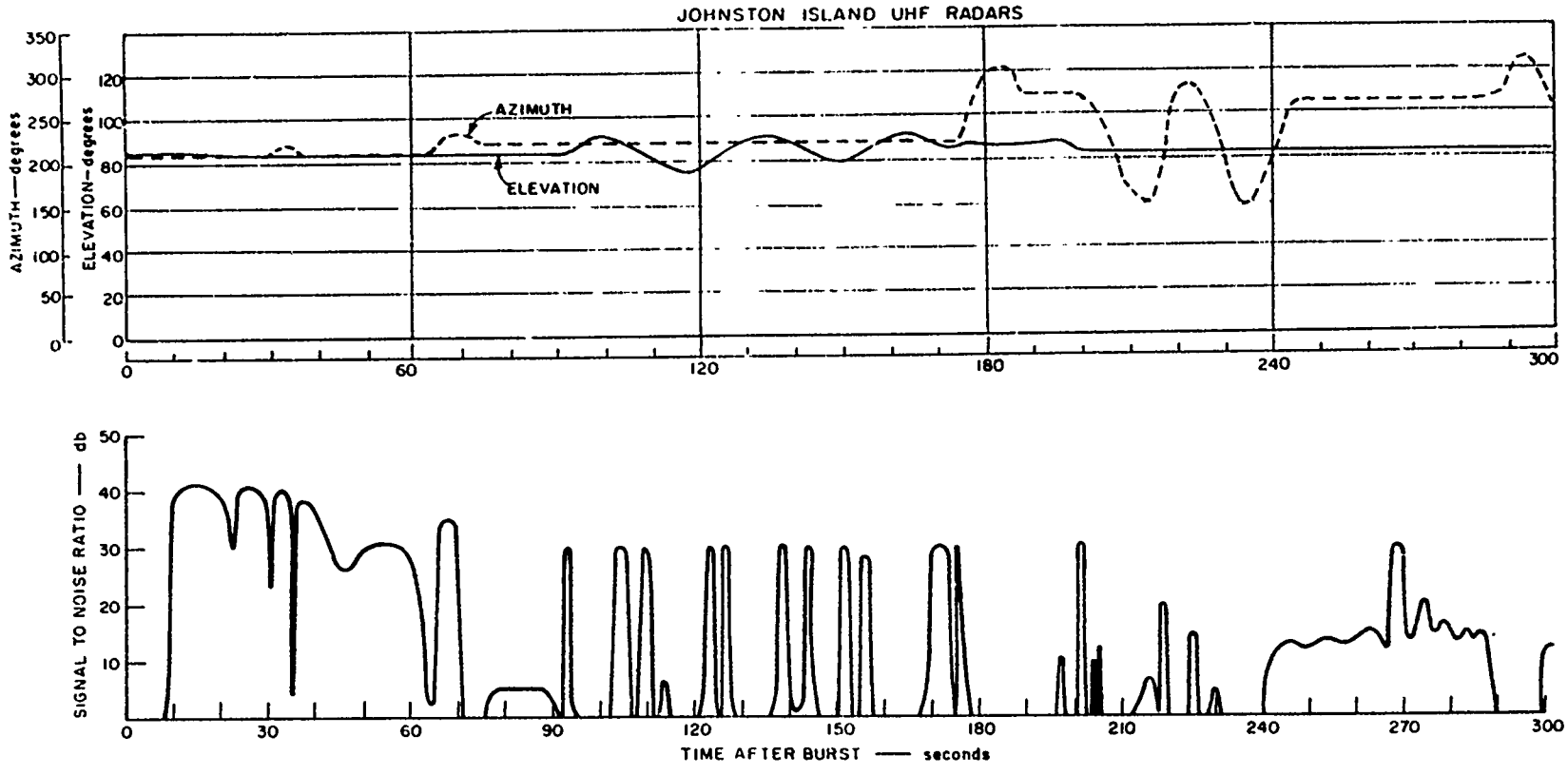

Figure 2.14 Johnston Island radar echo amplitude versus time for Tight Rope; 1210 Mc, 0 to 300 seconds.

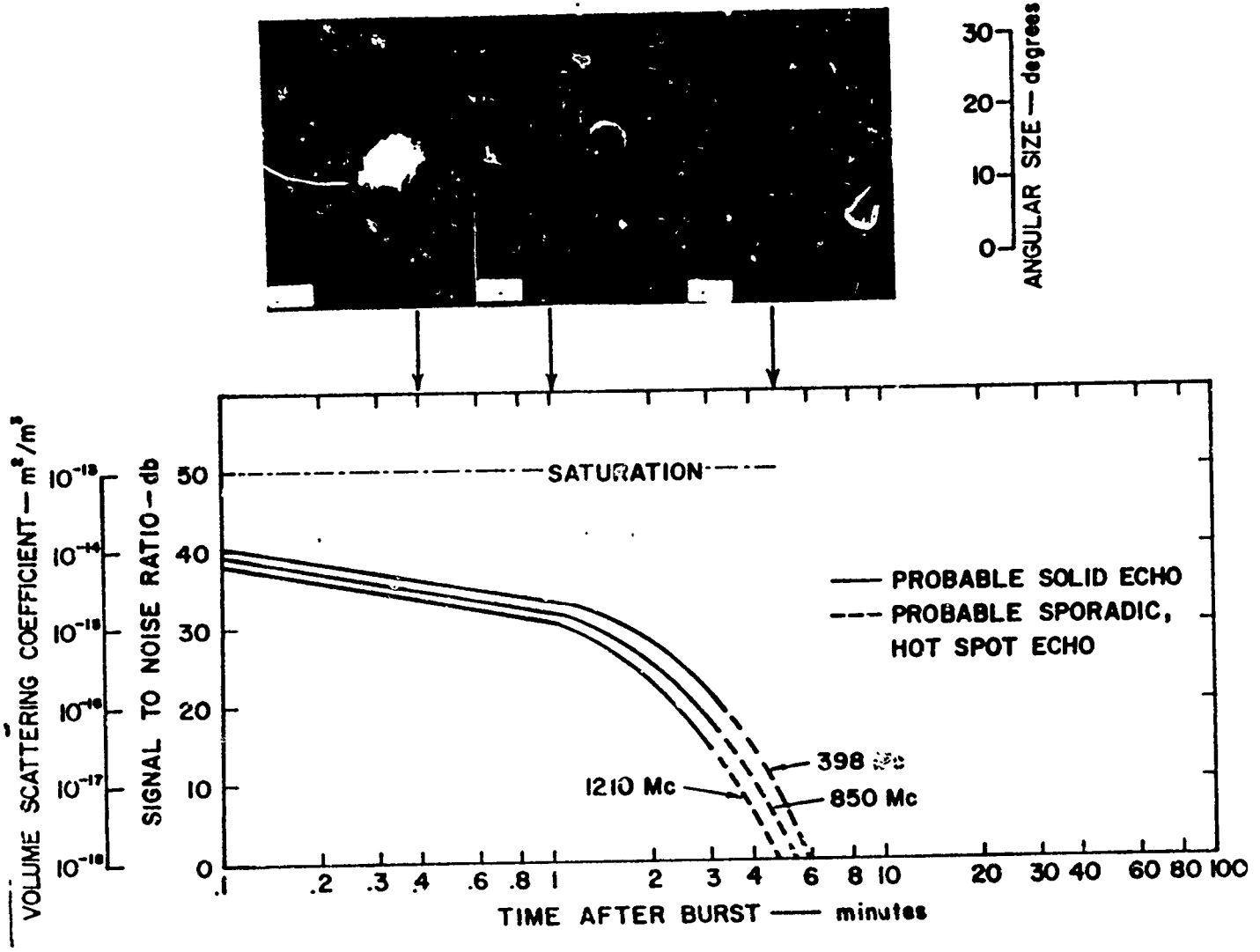

Figure 2.15 Johnston Island radar echo amplitude versus time for Tight Rope; 398, 850, and 1210 Mc.

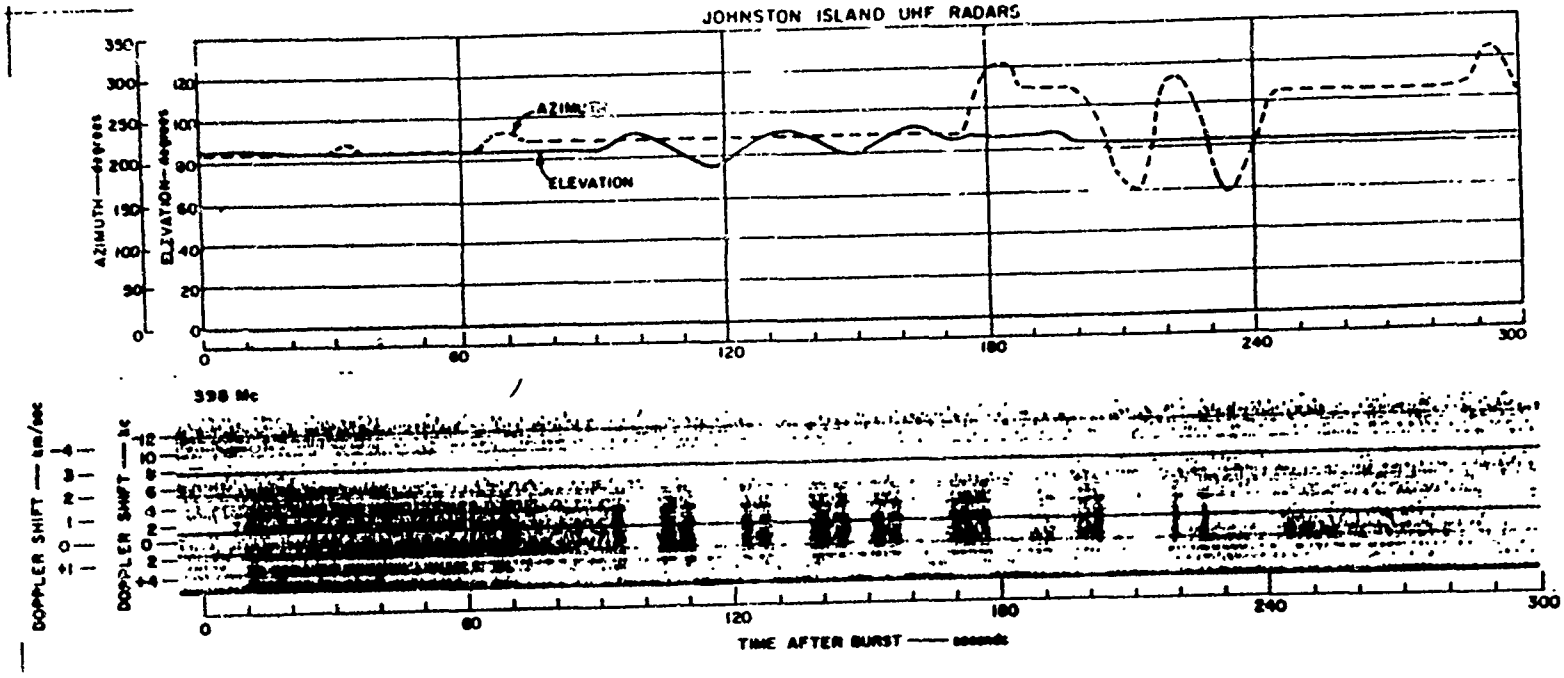

Figure 2.16 Johnston Island radar Doppler versus time for Tight Rope; 398 Mc, 0 to 300 seconds.

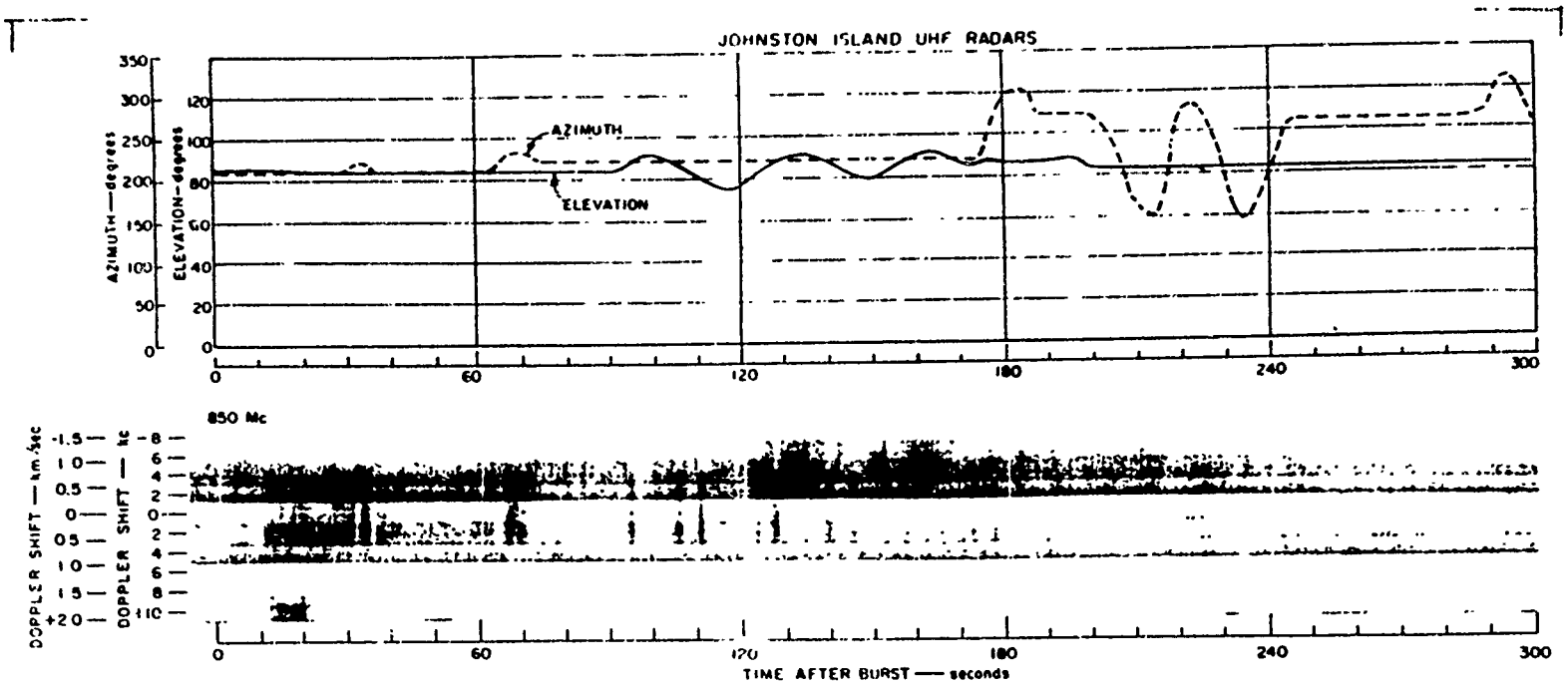

Figure 2.17 Johnston Island radar Doppler versus time for Tight Rope; 850 Mc, 0 to 300 seconds.

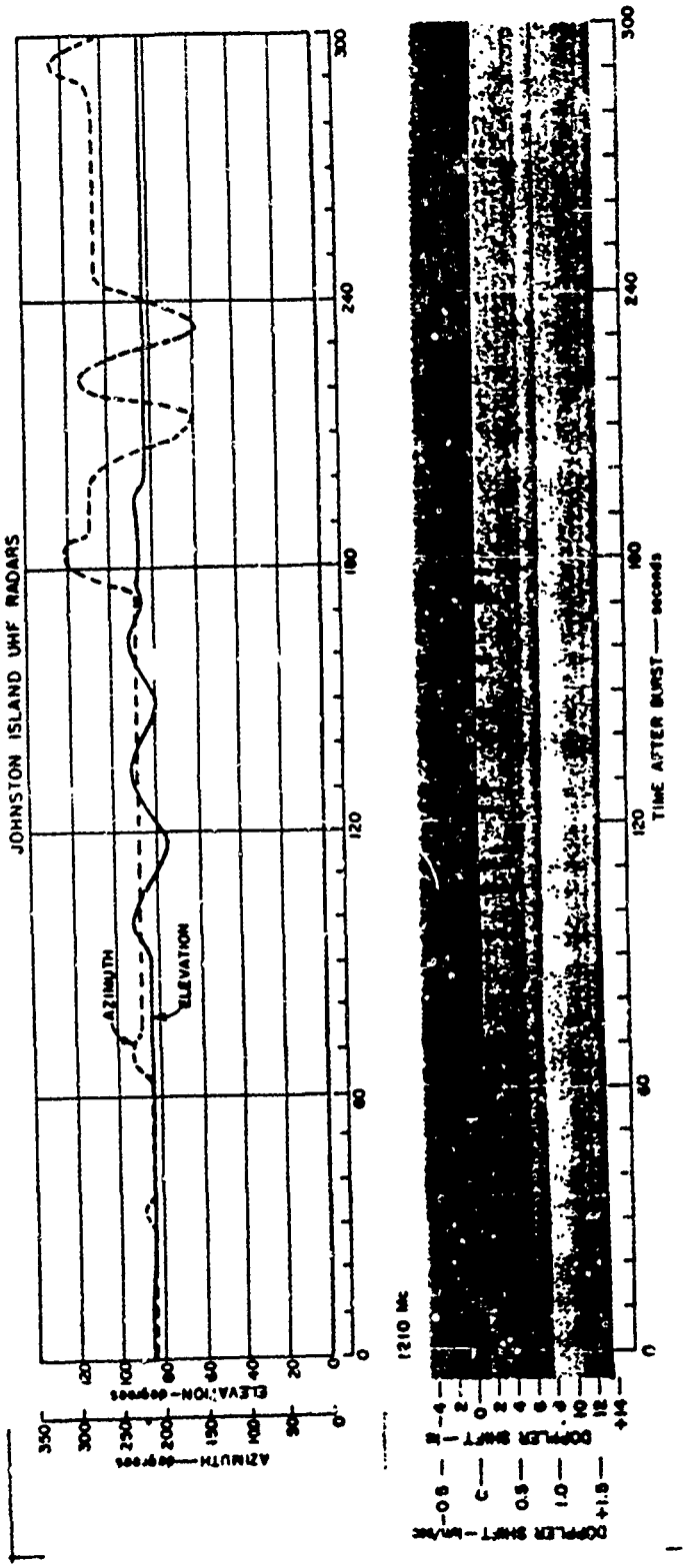

Figure 2.18 Johnston Island radar Doppler versus time for Tight Rope; 1210 Mc, 0 to 300 seconds.

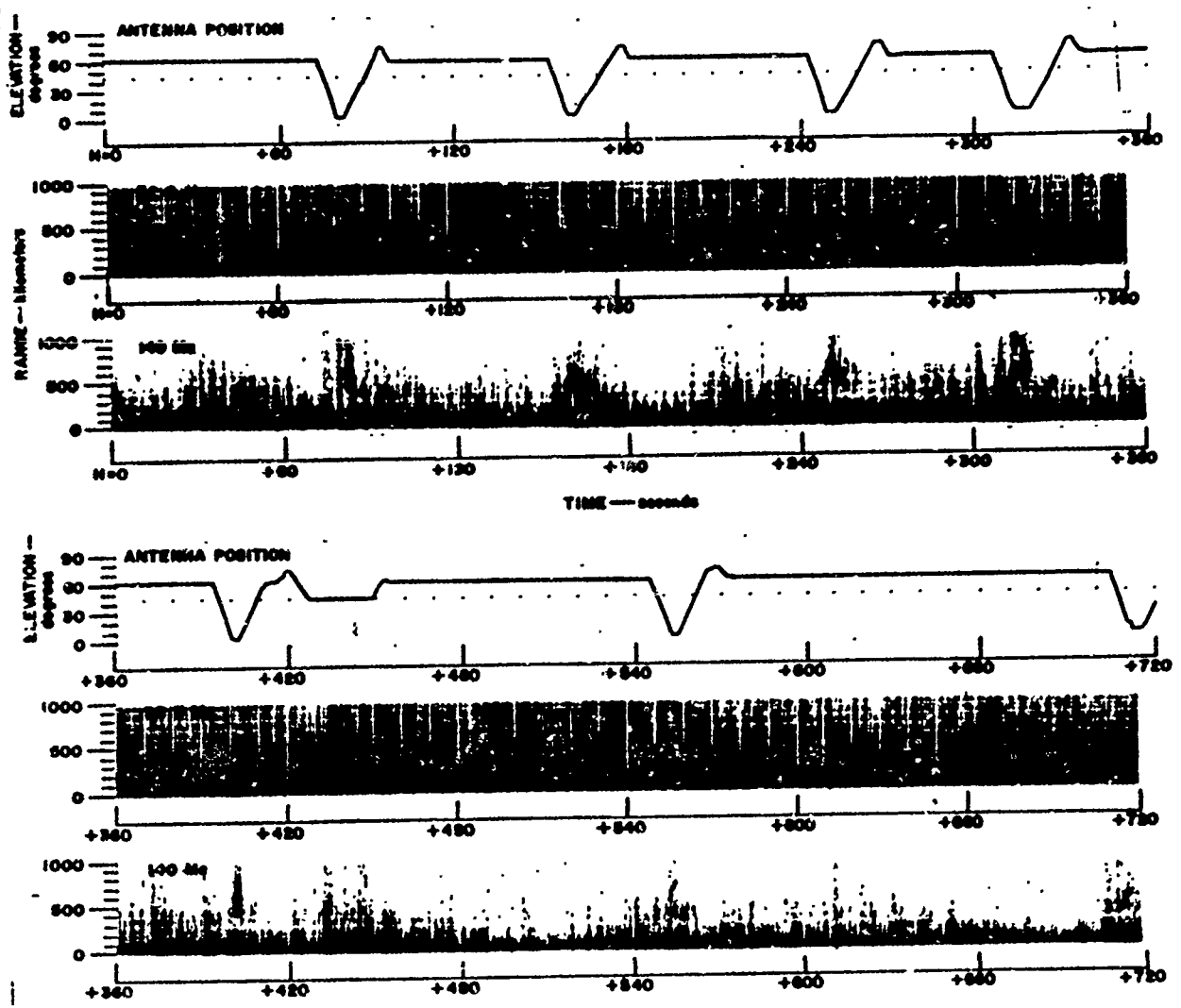

Figure 2.19 M/V ACANIA radar range versus time for Tight Rope, 0 to 720 seconds.

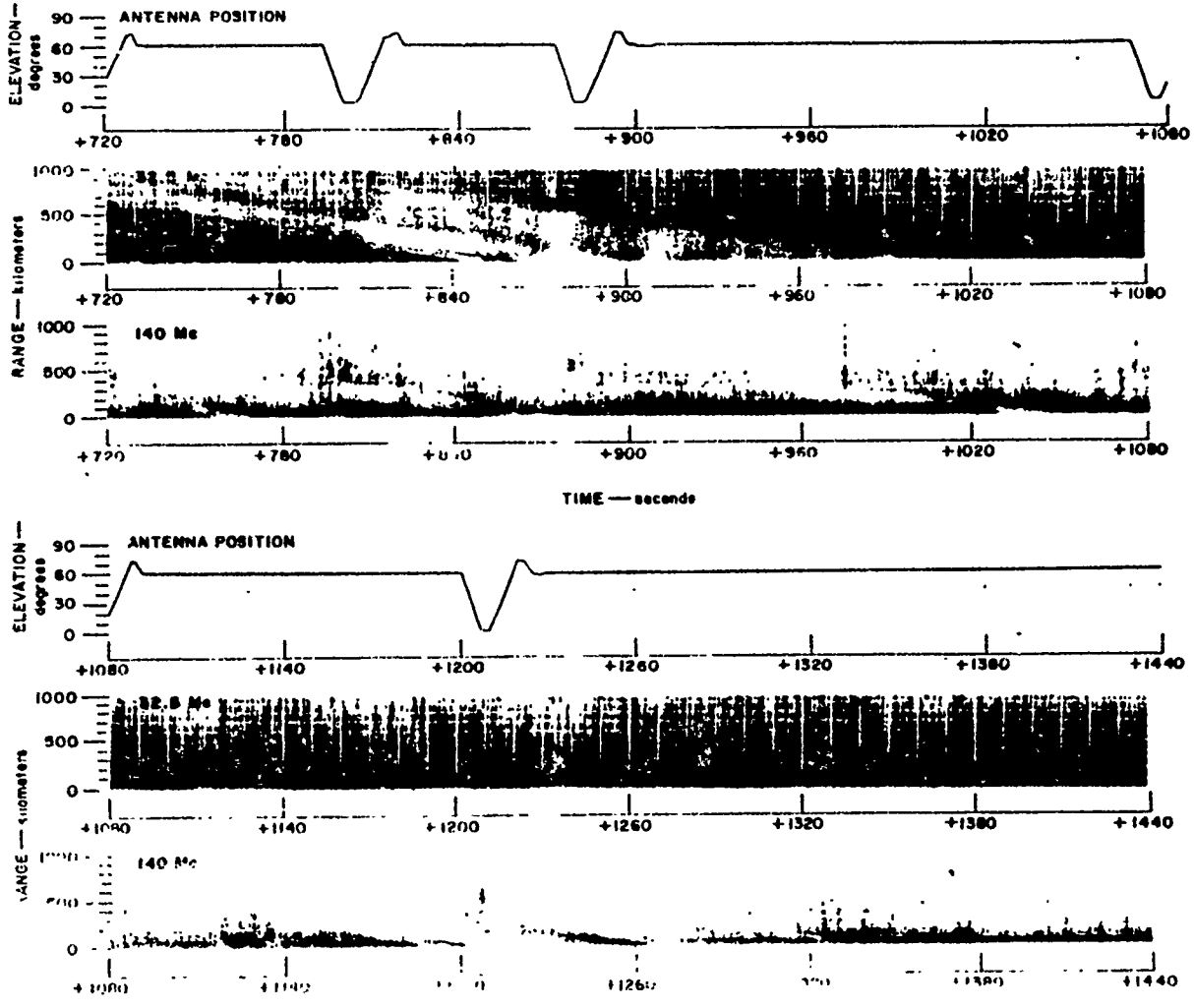

Figure 2.29 M. V ACANIA radar range versus time for Light Reps. 720 to 1,440 seconds.

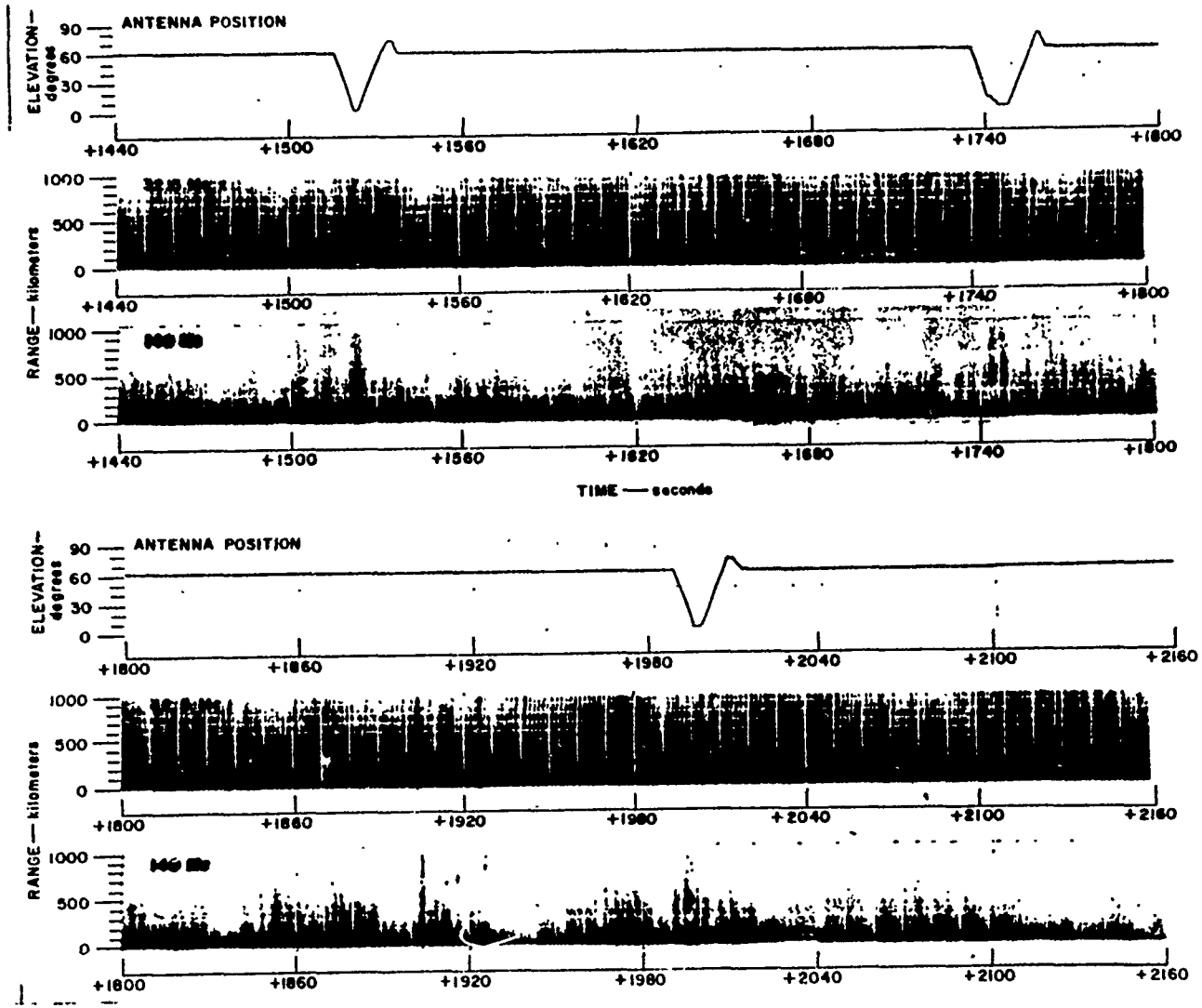

Figure 2.21 M/V ACANIA radar and [illegible] for Flight Rec[illegible] 1410 to 2160 seconds.

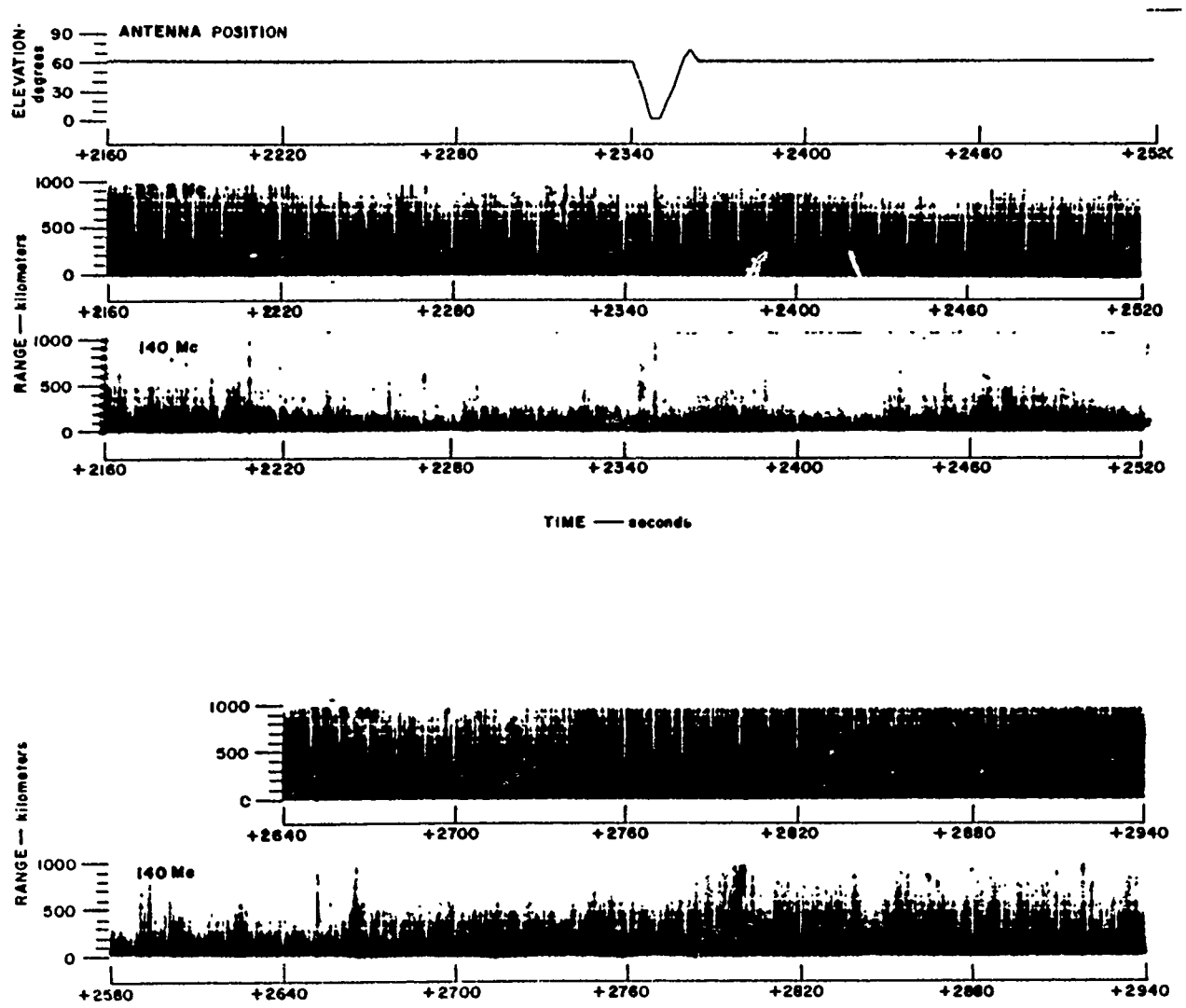

Figure 2.22 M/V ACANIA radar range versus time for Tight Rope, 2,160 to 2,940 seconds.

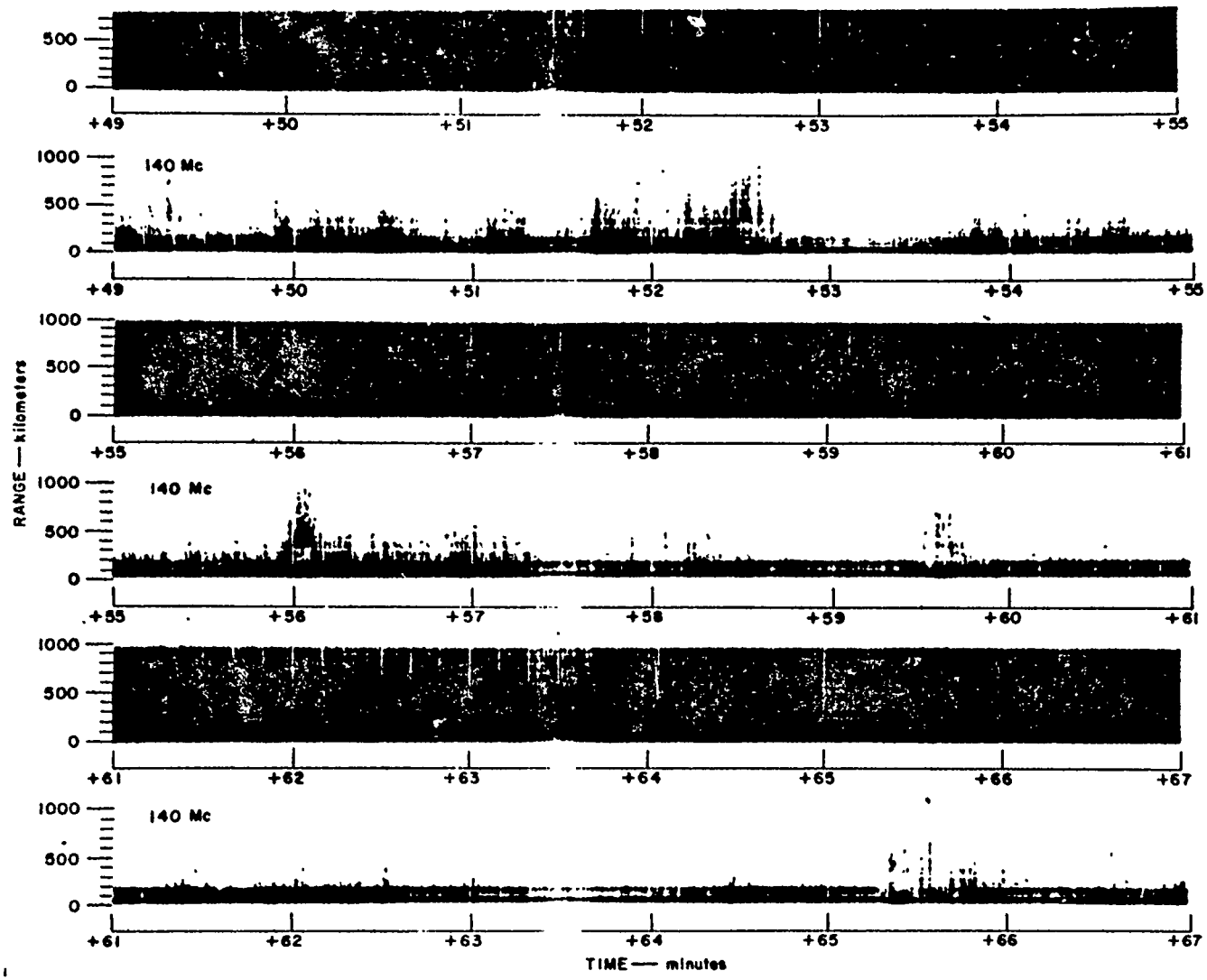

Figure 2.23 M/V ACANIA radar range versus time for Tight Rope, 49 to 67 minutes.

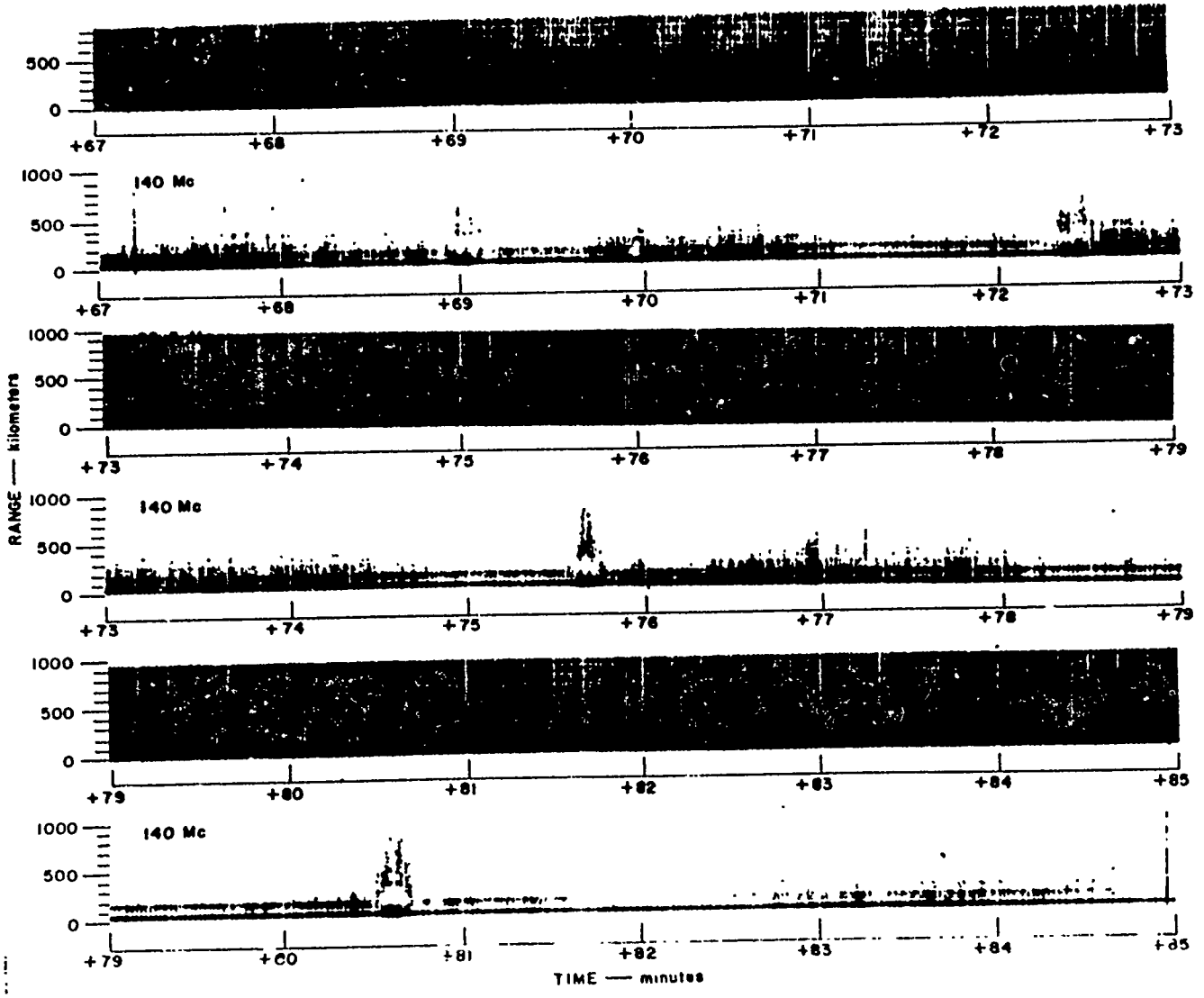

Figure 2.24 M/V ACANIA radar range versus time for Tight Rope, 67 to 85 minutes.

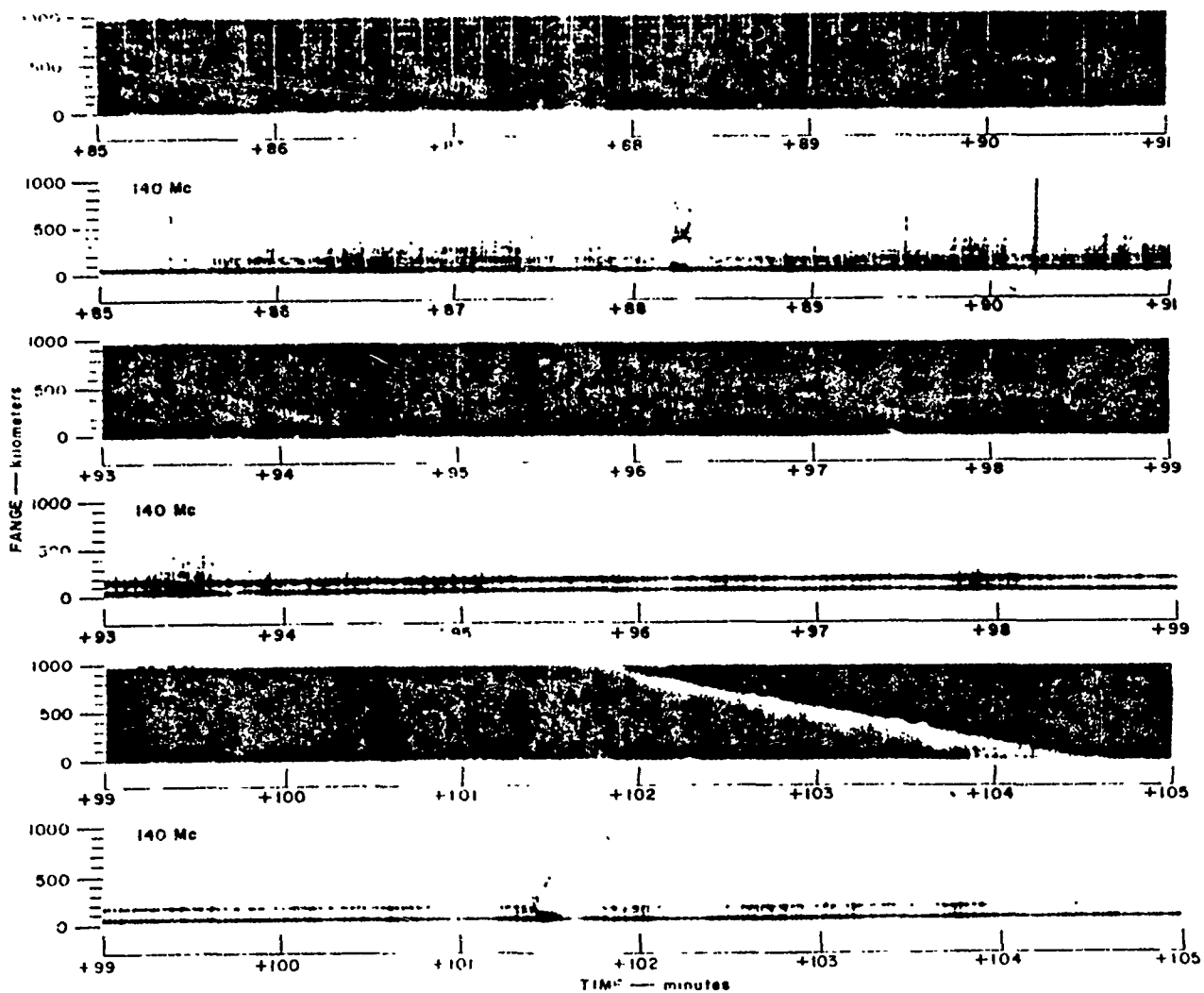

Figure 2.25 M/V ACANIA radar range versus time for Tight Rope, 85 to 105 minutes.

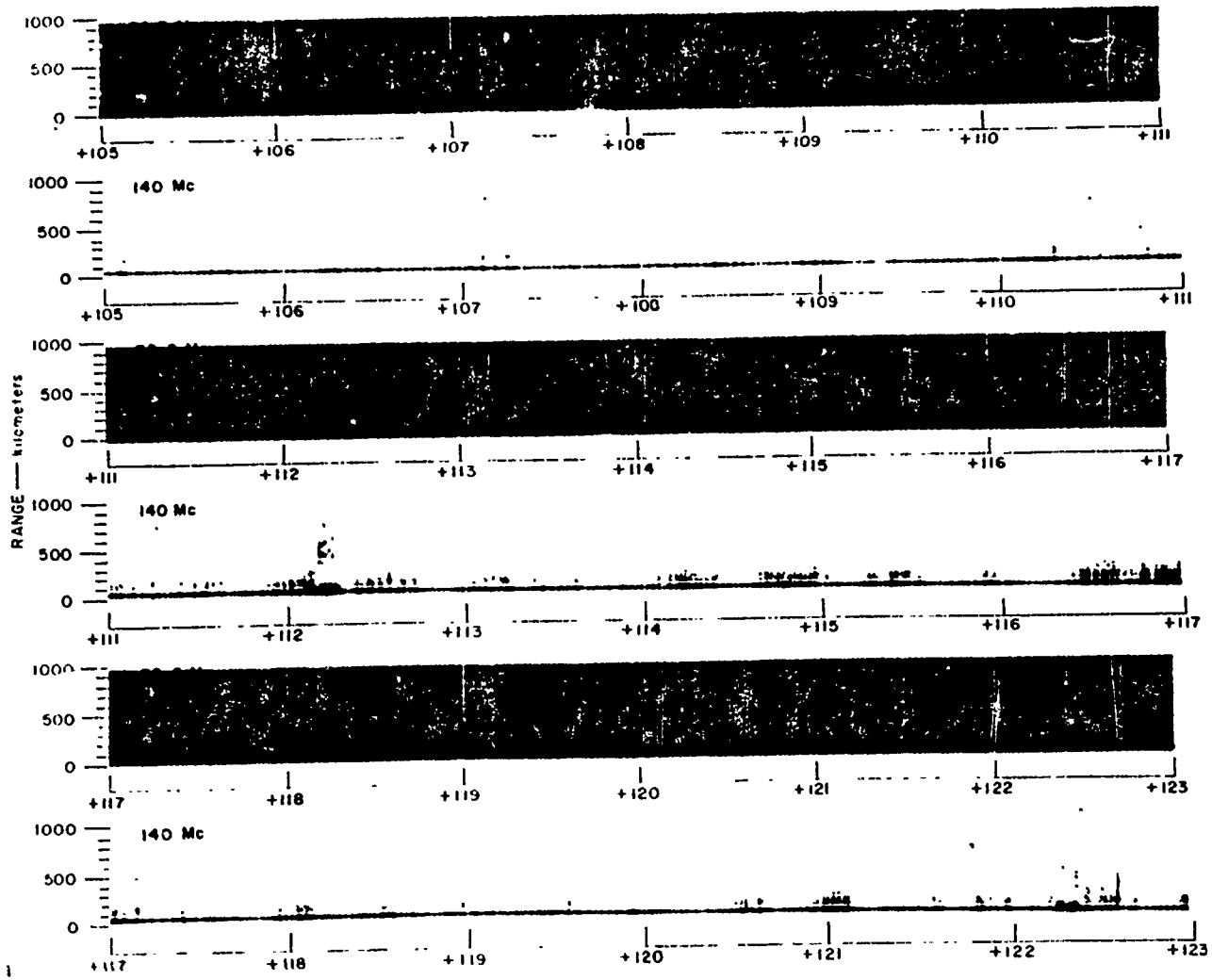

Figure 2.26 M/V ACANIA radar range versus time for Tight Rope, 105 to 123 minutes.

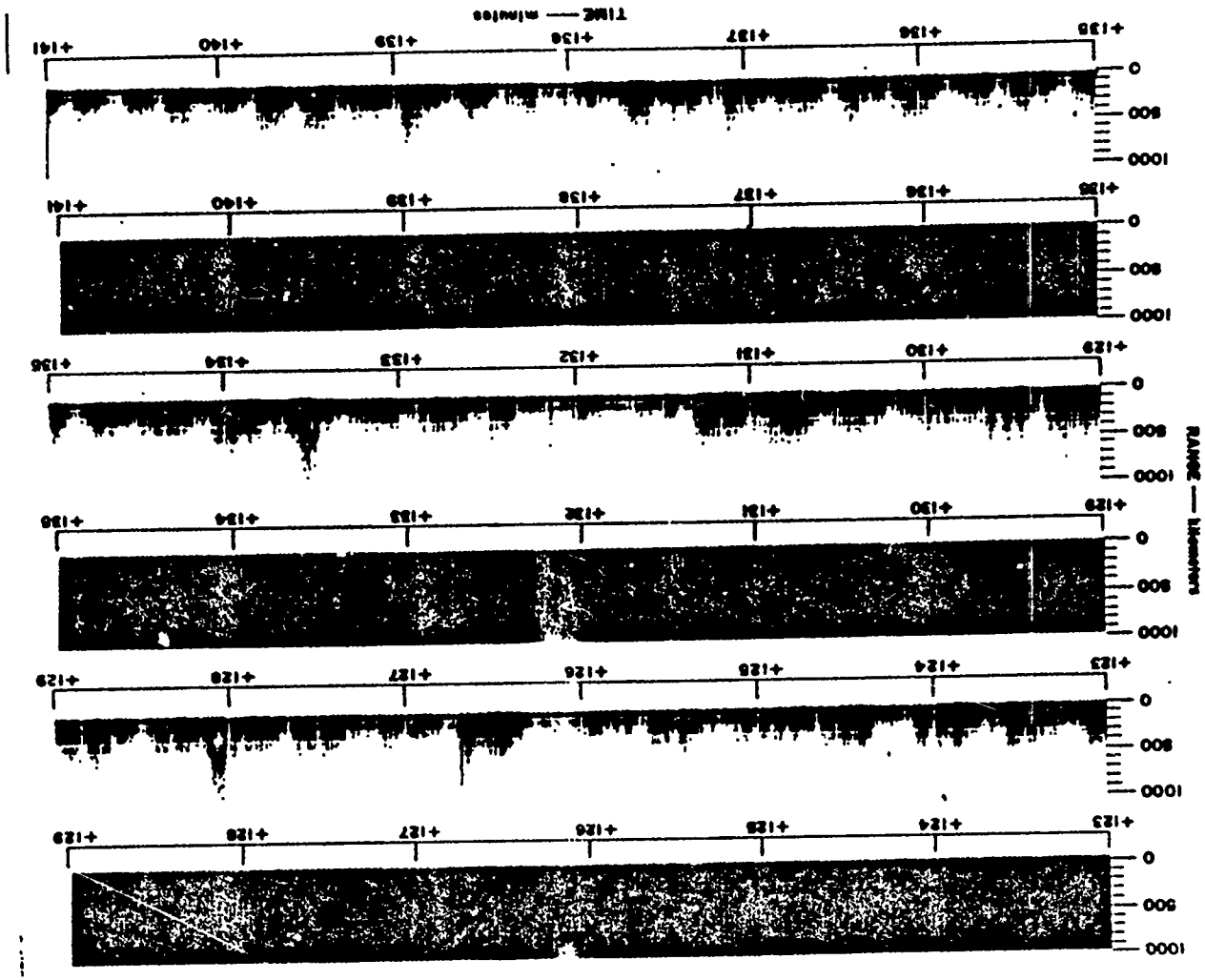

Figure 2.27 M/V ACANIA radar range versus time for Tight Rope, 123 to 141 minutes.

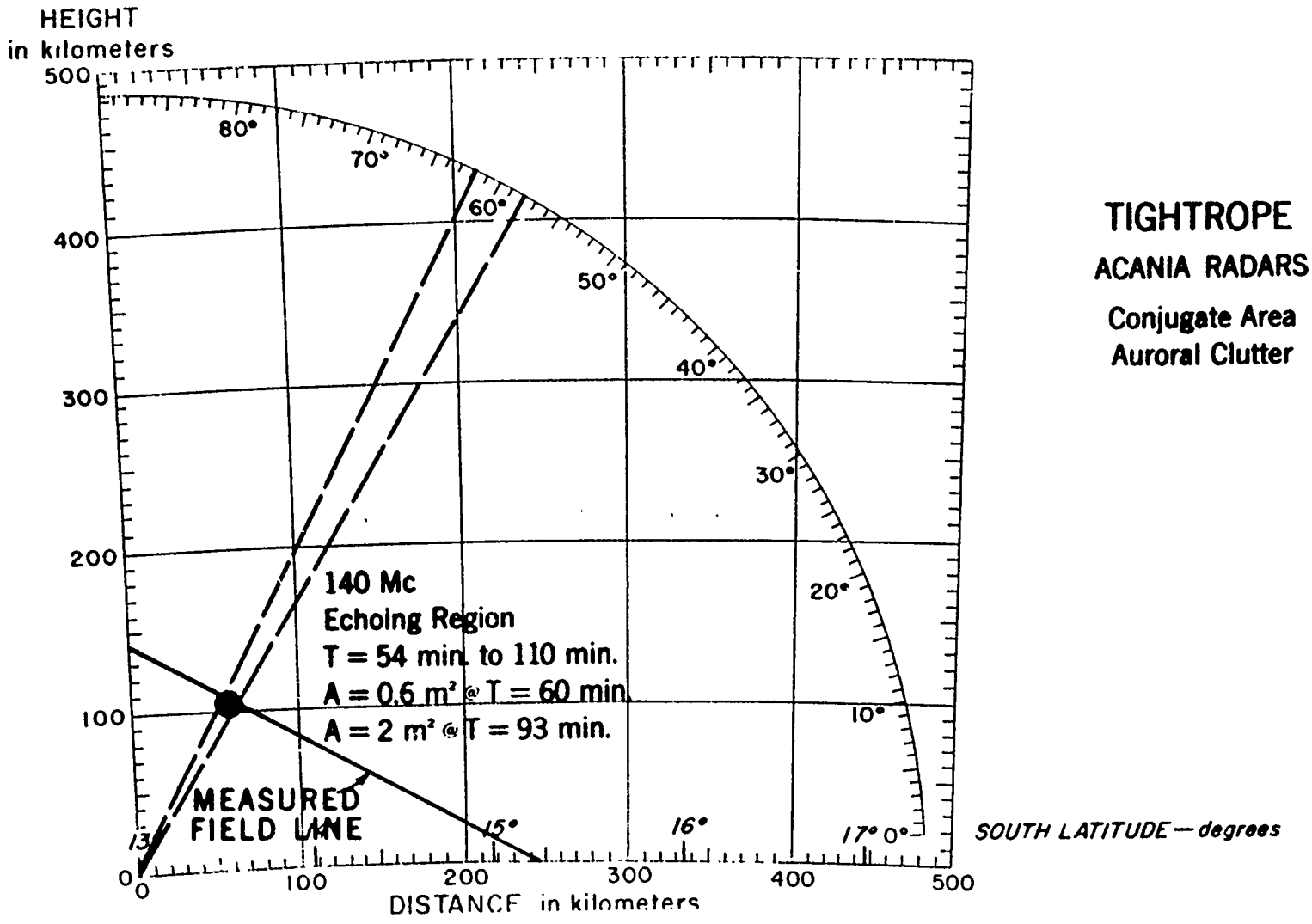

Figure 2.28 M/V ACANIA radar height versus distance for Tight Rope, 140 Mc.

CHAPTER 3

BLUE GILL

3.1 INTRODUCTION

In general, this event was expected to be very similar to Shot Orange of Operation Hardtack.[1] That is, a well-contained fireball was expected to occur, having an initial diameter of the order of 2 km. The temperature in the fireball was expected to be of the order of 10,000 degrees K. The fireball was expected to expand gradually and to rise due to the buoyancy of the atmosphere. The rate of rise was, in general, estimated to be of the order of 0.25 to 0.5 km/sec, and the maximum altitude of the fireball was expected to be less than 100 km. As the fireball expanded, a torus shape was expected to appear, as was seen in Orange.

Because of the geometry of the detonation with respect to the Johnston Island radars, auroral-type radar returns were not expected during the Blue Gill event. At the expected detonation altitude a fraction of the prompt beta rays were expected to reach the conjugate area, giving rise to auroral-type radar activity in that region. Rise of the fireball was expected to rapidly reduce attenuation effects of the atmosphere for these beta particles, so that by H plus a minute or so all betas could escape to the magnetic conjugate region. Compton-converted gamma rays in the detonation area were expected to produce radio and possibly radar effects in the magnetic conjugate area.

---

[1] See Volume 1 for a more complete discussion of the expected results.

Radar echoes from the dense, well-contained fireball and debris were expected, as well as noise emissions due to its very high temperature.

3.2 PROCEDURE

3.2.1 Johnston Island Radars.

Instrumentation. See Section 2.2.1.

Operating Technique. See Section 2.2.1.

3.2.2 AEW Aircraft Radars.

Instrumentation. See Section 2.2.2.

Operating Technique. Based upon the expected results, the radar instrumentation was arranged to maximize the detonation-area results. For this test, four project AEW aircraft radars were available as well as two control aircraft. Two of the project AEW aircraft radars were located in the detonation area and two in the magnetic conjugate area. Lambkin 1 was located so that it was looking at H = 100 km above detonation point. Lambkin 2 was located so that it was looking at H = 100 km perpendicular to the magnetic field line passing through detonation point, as shown in Figure 3.1. Lambkins 3 and 4 were located as conjugates to Lambkins 1 and 2 respectively, as shown in Figure 3.2. All of the AEW aircraft flew in patterns shown in Figure 2.8 at locations given in Table 3.1. The actual radar operating parameters are shown in Table 3.2.

3.2.3 M/V ACANIA Radars.

Instrumentation. See Section 2.2.3.

Operating Technique. The ACANIA was located at the calculated magnetic conjugate point of Johnston Island. Thus, one-to-one comparison of the results from the conjugate and detonation area could be made. The exact location of the ACANIA is shown in Table 3.1. The radar operating technique is given in Section 2.2.3.

3.3 RESULTS

3.3.1 Johnston Island Radars.

Fireball/Debris Clutter. Prior to the detonation, the antenna executed a programmed track of the Thor launch, and the 850-and 1210-Mc radars obtained skin echoes during a portion of the trajectory. The 398-Mc radar was off until detonation. Shortly before the detonation, the antenna was positioned in the direction of 55-degree elevation and 193-degree azimuth. Just prior to detonation, skin echoes from the R/V or the tankage were obtained at 850 and 1210 Mc. The detonation occurred about 1 degree in elevation below the radar beam. The fireball expansion and rise was sufficient to move the edge of the fireball into the radar beam at about H + 2 seconds. The fireball stayed partially in the radar beam until H + 105 seconds when the antenna was scanned about in elevation and azimuth. Excellent correlation between radar echoes and the visual fireball/debris was noted during the first five minutes following the bomb burst. An example of this

correlation is shown in Figure 3.3. The Johnston Island radars were operated for eight hours following the bomb detonation.

Starting abruptly at H + 2 seconds, as the fireball edge moved into the radar beam, echoes at 1210 Mc first appeared at an amplitude of 40 to 50 db S/N. At H + 5 seconds, 850-Mc echoes appeared at an amplitude of 40 to 50 db S/N. At H + 8 seconds, 398-Mc echoes appeared at an amplitude of 10 db S/N. These echoes persisted at fluctuating amplitudes until H + 105 seconds when the antenna was scanned. The range-versus-time records of the echoes for the first 30 minutes are shown in Figures 3.4 through 3.9. The spatial distribution of all the detonation-area echoes as well as the visual fireball/debris is shown in Figures 3.10 through 3.35. The echo amplitude-versus-time records for the first five minutes are shown in Figures 3.36 through 3.38. The echo amplitudes versus time (with antenna-direction-caused fluctuations removed) are shown in Figure 3.39. At H + 120 seconds an elevation scan was made which showed that the echoes were limited to ±5 degrees about the detonation point and were well correlated with the visual fireball. At H + 180 seconds an azimuth scan was made which showed that the echoes were limited to the detonation point ±30 degrees in azimuth at that time. At H + 5 minutes an elevation scan was made. Echoes at 398 Mc occurred from 90 degrees down to 45 degrees elevation, and 850- and 1210-Mc echoes occurred from 78 degrees down to 50-degree elevation. From H + 6 minutes the antenna executed a programmed scan or was manually scanned. Sporadic echoes were seen on all frequencies

from the fireball/debris until about H + 20 minutes. From H + 23 to H + 26 minutes an echo was found at each frequency at 83-degree elevation and 159-degree azimuth which moved out in range from 120 km to 230 km and had a negative Doppler shift which corresponded to a receding velocity of approximately 1 km/sec.

Figures 3.40 through 3.42 show the Doppler records for the first five minutes following the bomb burst at each frequency. The 398-Mc record shows no spread beyond the 3-db frequency spectrum of the transmitted 300-μsec pulse length, and very little shift. Both the 850-and 1210-Mc records show a positive shift corresponding to a 0.5 km/sec velocity for the first 10 seconds. Following that, the records show a negative shift corresponding to a 0.25 km/sec velocity for the next 60 seconds. Figures 3.43 through 3.45 show the Doppler records of the rising echo observed at each frequency at about H + 23 minutes.

Auroral Clutter in the Detonation Area. No auroral clutter was observed in the detonation area by the Johnston Island radars.

Fireball/Debris Noise. Radio-noise emission was observed by the 398-, 850-, and 1210-Mc radars looking at the fireball/debris. The noise level built up in amplitude slowly and lasted until about H + 1-1/2 minutes. The maximum noise temperature indicated was at 1210 Mc and was about 3000 degrees K. This amounted to a noise-level increase of about 7 db. The noise-level increases are shown in Figure 3.46.

3.3.2 AEW Aircraft Radars.

Fireball/Debris Clutter.

Lambkin 1. The first echo ppeared at H + 25 seconds around air zero (281 degrees magnetic (M) at 380 km). The echo was 15 km wide and extended five degrees on either side of air zero. By H + 40 seconds. the diameter of the echo around air zero had grown to 35 km, extending 10 degrees on either side. By H + 60 seconds the most intense center was still located around air zero with the same diameter and bearing spread as at H + 40 seconds but with an extension of the echo to a bearing of 325 degrees M. By H + 80 seconds the echo extended from 240 degrees M to 325 degrees M with the most intense center still around air zero with a width of 30 km. By H + 125 seconds the echo had shrunk to the approximate same dimensions as it had at H + 40 seconds, with the most intense center still around air zero. A weak echo, rapidly shifting in size and intensity, remained until H + 180 seconds around air zero, at which time all echoes disappeared.

Lambkin 2. The electromagnetic pulse at H = 0 was observed on the radar. A weak echo appeared at H + 8 seconds at a bearing and slant range of air zero (291.5 degrees M at 414 km). The echo grew in size and intensity until H + 38 seconds when it remained strong until H + 88 seconds, as shown in Figure 3.47. It then faded rapidly and was completely gone by H + 150 seconds.

Abusive 1. A weak echo appeared shortly after H = 0 at 255 km and a bearing of 78 degrees M. Air zero was calculated to be as 78 degrees M at 184 km at H = 0. The discrepancy in range cannot be explained at this time. This echo remained the same until about H + 40 seconds at which time it became more intense, and its bearing spread increased, as shown in Figure 3.48. By H + 60 seconds the most intense center was at a range of 260 km and a bearing of 85 degrees M extending from a bearing of 60 degrees M to a bearing of 150 degrees M. It began to fade, and by H + 90 seconds it was as it appeared in the first 30 seconds. This echo remained for nearly thirty minutes and is assumed to be Thor tankage debris.

Abusive 2. The electromagnetic pulse was observed at H = 0. An echo appeared at H + 2 seconds at a bearing and range of air zero (229 degrees M at 172 km). This echo grew slightly in intensity for 40 seconds. By H + 52 seconds it was saturated, as shown in Figure 3.49. It reached its greatest spread in azimuth by H + 72 seconds, when it extended from 185 degrees M to 265 degrees M centered around air zero. By H + 120 seconds it was back to the size and intensity it had at H + 12 seconds. This echo remained for nearly 30 minutes, and it is also associated with Thor tankage debris. At H + 98 seconds an echo was observed at a bearing of 75 degrees M at a range of 320 km. This echo became more intense, moving rapidly in a south-easterly direction, disappearing at H + 80 seconds at the edge of the scope at a bearing of 118 degrees M and a

slant range of 530 km. The average rate of motion of this echo is approximately 2.5 km per second. The origin or mechanism producing this echo has not been explained at this time.

The radar cross sections of the fireball/debris clutter observed by the AEW aircraft radars are tabulated in Table 3.3.

Auroral Clutter in the Detonation Area. No auroral clutter was observed in the detonation area by the AEW aircraft radars.

Auroral Clutter in the Conjugate Area. No auroral clutter was observed in the conjugate area by the AEW aircraft radars.

3.3.3 M/V ACANIA Radars,

Auroral Clutter in the Conjugate Area. No auroral clutter was observed in the conjugate area by the M/V ACANIA radars.

3.4 DISCUSSION

The lack of 398-Mc echoes at early time was probably due to lens action of the fireball as well as absorption.

If it is assumed that the reflections are due to a volume scattering, the S/N of 50 db is equivalent to about 10^{-12} m^2/m^3. Interpreted in terms of a point target (very unlikely), this S/N ratio of 50 db is equivalent to about 0.1 m^2. If one computes the electron density in the fireball necessary to give rise to incoherent scattering of this magnitude (50 db S/N) then the electron density is between 10^{10} and 10^{11} electrons/cc. This corresponds to a

plasma frequency between 1000 and 3500 Mc. Since this plasma frequency is greater than that of the UHF radars, incoherent electron scatter would not seem to be the cause of these echoes.

Critically overdense reflections, coupled with absorption on the propagation path, is a likely explanation of these echoes.

3.5 CONCLUSIONS

The performance of a ballistic missile defense radar system would be seriously degraded by the effects of a Blue Gill event. To evaluate this effect, a comparison has been made between the radars used during Fish Bowl and the planned BMD radar systems.

The radars used during these tests were, in general, somewhat less sensitive than those being planned for use in BMD activities. The advantage that a particular system radar would have over the test radars is shown for various scattering models in Table 2.6 of Chapter 2 of this volume. The comparisons were developed by scaling the system radar to its nearest frequency counterpart used during Fish Bowl. For example, the BMEWS radars were compared with the 398-Mc Johnston Island radar and the Nike-Zeus TTR radar was compared to the DAMP FPQ-4 C-band radars.

In order to give the reader a better understanding of the degrading effect of a Blue Gill event, an estimate of the effect on the BMEWS tracking radar has been made. The positioning of a Blue Gill event as close to a BMEWS site as it was to the Johnston Island radars would mean that the clutter would actually be obscured by the long operating pulse.

We again stress that the BMEWS system was picked as an example not to deprecate that particular system, but because that system is operational, field-deployed, and its characteristics are well known.

Table 2.7 of Chapter 2 of this volume shows the comparison between the BMEWS tracking radar characteristics and the Johnston Island 398-Mc radar. The comparison was made assuming the scattering was from a beam-filling target of range depth of at least one pulse width (300 μsec).

From the comparison, estimates of the strength and time duration of the clutter and noise effects are given below:

Fireball/Debris Clutter.

H + 0 to H + 1 min	S/N = 0 to 90 db	Main Beam
	S/N = 0 to 40 db	Side Lobes
H + 1 to H + 5 min	S/N = 90 db	Main Beam
	S/N = 40 db	Side Lobes
H + 5 to H + 10 min	S/N = > 44 db	Main Beam
	S/N = > 0 db	Side Lobes
H + 10 min to H + ?	S/N = 44 db	Main Beam
	S/N = 0	Side Lobes

Angular Diameter of Affected Region.

60 sec	14 degrees
120 sec	18 degrees
240 sec	38 degrees

Detonation-Area Auroral Clutter.

Virtually none would be seen for the Johnston Island Blue Gill

geometry. However, other geometries would allow auroral clutter to be observed.

Fireball/Debris Noise.

Maximum 3000 degrees K for 100 seconds duration,

5 db increase.

From the above it is apparent that as much as 1500 square degrees of area would be obscured for a depth of at least one pulse length plus 20 km by the fireball/debris clutter for a period of as much as 10 minutes. In addition, the 1500 square degrees of area would be observed at a 5-db reduction in sensitivity at all ranges at a 50-percent bandwidth for up to two minutes because of the fireball/debris noise. Although the Doppler spread of the echoes is not severe, the limited bandwidth of the 20-kc Doppler channel used with the Johnston Island radars does not rule out the possibility of there being Doppler components at the velocity of an approaching ICBM.

The extended volume of clutter and noise produced by Blue Gill would make it difficult to avoid the clutter problem by using spaced radars in a BMD system, and impossible in the case where multiple Blue Gill events occurred.

TABLE 3.1 LOCATIONS OF AEW AIRCRAFT AND M/V ACANIA DURING BLUE GILL

	Longitude	Latitude
Lambkin 1	166°18'W	15°08'N
Lambkin 2	166°24'W	14°25'N
Lambkin 3	178°08'W	10°32'S
Lambkin 4	178°28'W	12°00'S
Abusive 1	171°15'45"W	16°20'30"N
Abusive 2	168°16'30"W	17°09'45"N
ACANIA	175°W	13°01'S

TABLE 3.2 OPERATING CHARACTERISTICS OF THE AEW AIRCRAFT RADARS DURING BLUE GILL

L = Lambkin, A = Abusive.

	L1	L2	L3	L4	A1	A2
Frequency, Mc.	425	428	426	443	447	435
Peak Power, watts x 10^6	1.25	1.2	1.6	1.4	1.4*	1.4
Pulse Width, μsec	8.4	8.4	8.0	8.0	8.0*	8.9
PRF, cps	240	240	222	24[illegible]	280	280
MDS, -dbm	114	113	113	114	114*	115
Dynamic Range, db	18	21	24	24	18*	21
σmin at 500 km, m^2	20	26	19	19	20*	15

* approximate values

TABLE 3.3 AEW AIRCRAFT RADAR FIREBALL/DEBRIS CLUTTER FOR BLUE GILL

	Time from Burst (sec)	Radar Cross Section (m^2)
Lambkin 1	80	6.6×10^4
Lambkin 2	50	1.3×10^4
Abusive 1	55	5×10^4
Abusive 2	72	2.3×10^3

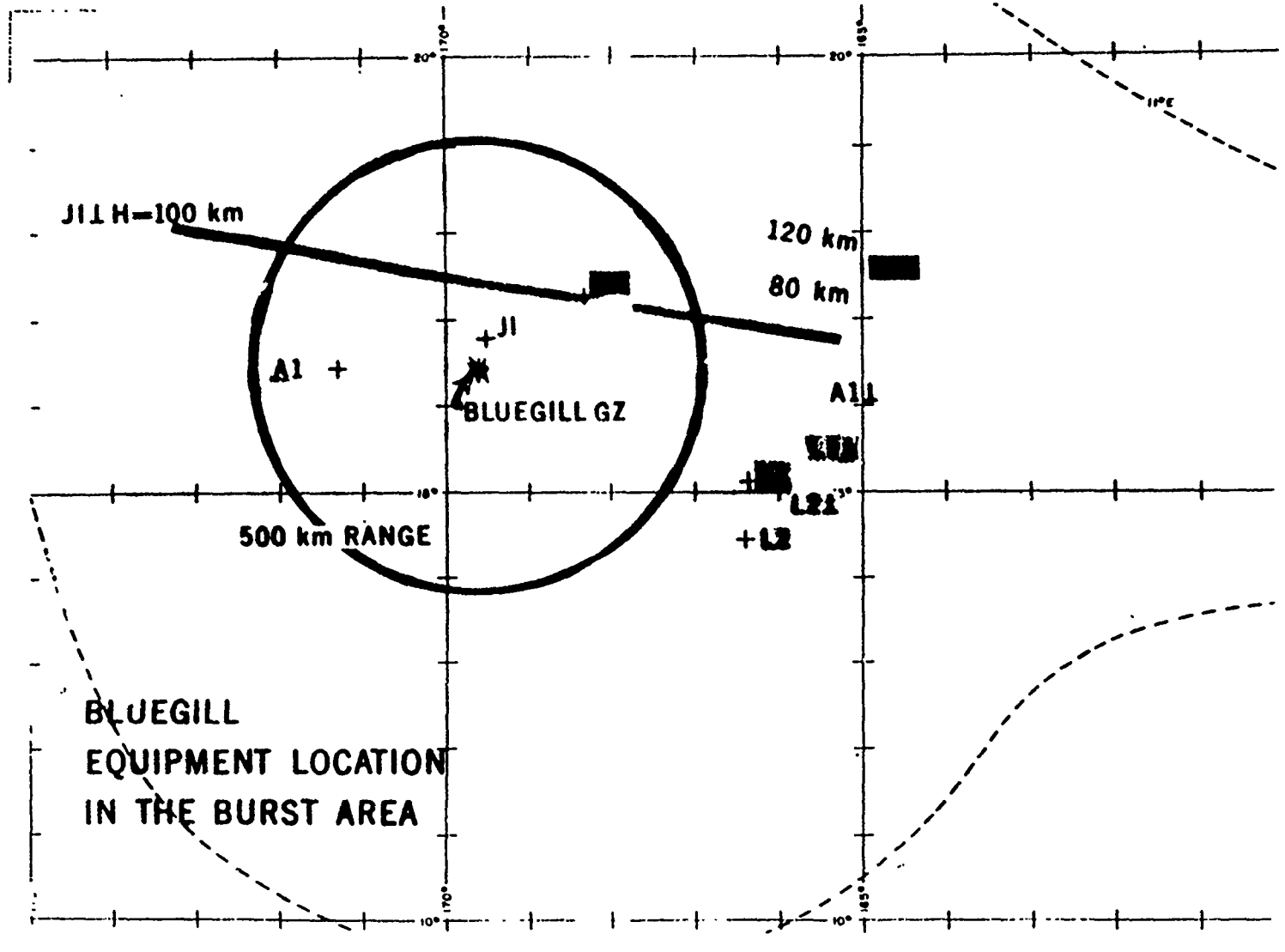

Figure 3.1 Equipment location in the detonation area for Blue Gill.

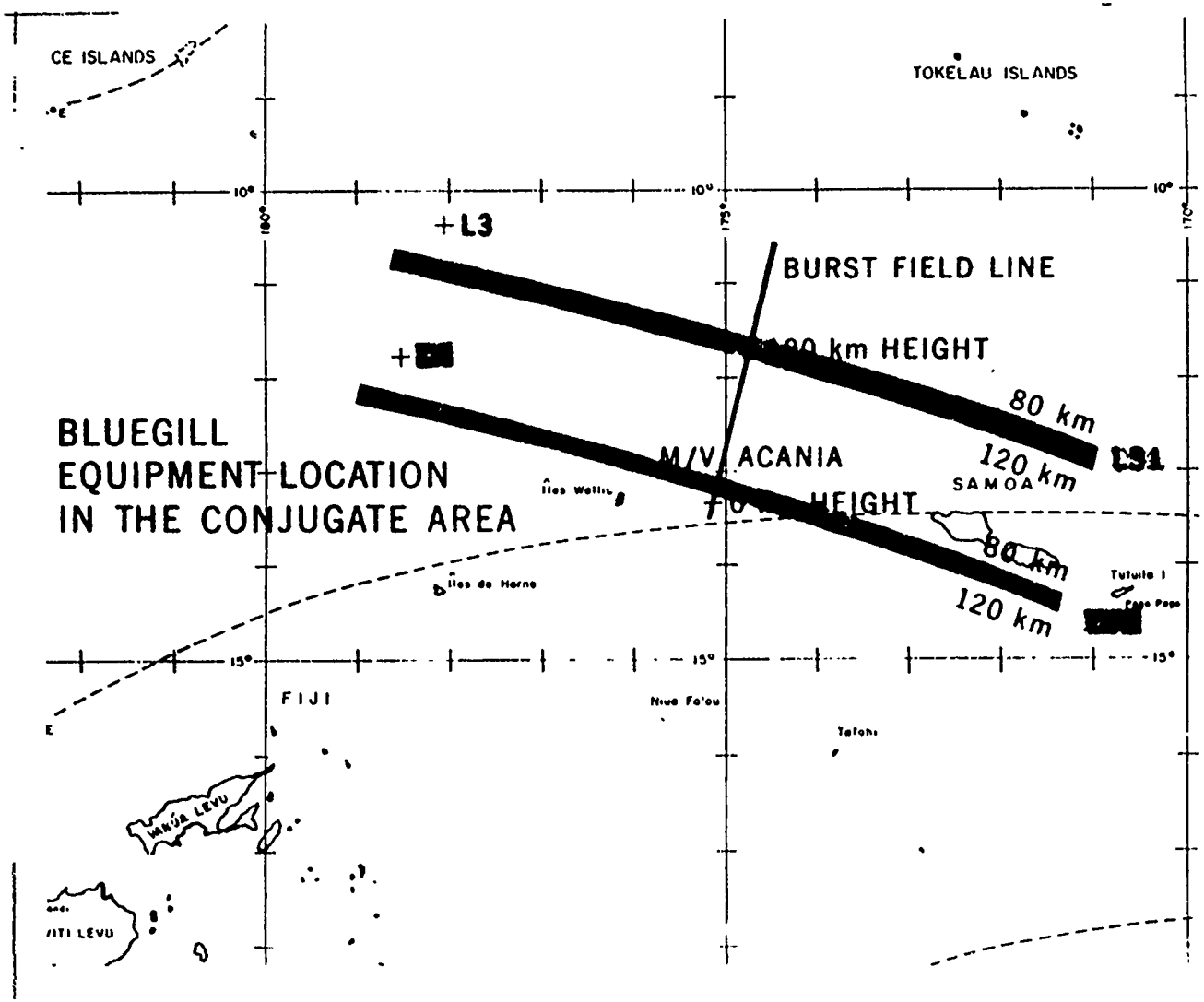

Figure 3.2 Equipment location in the conjugate area for Blue Gill.

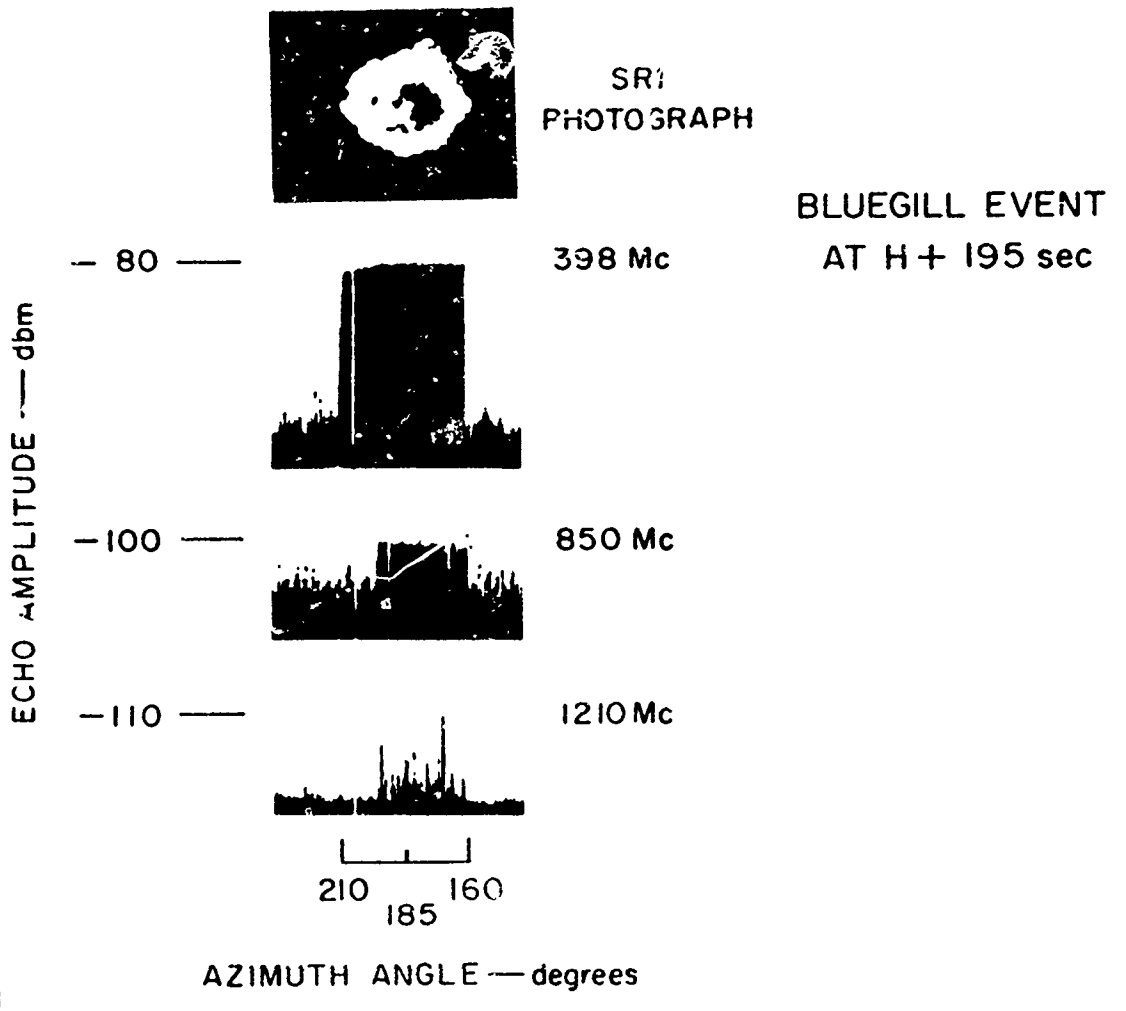

Figure 3.3 Johnston Island radar amplitude and visual comparison for Blue Gill.

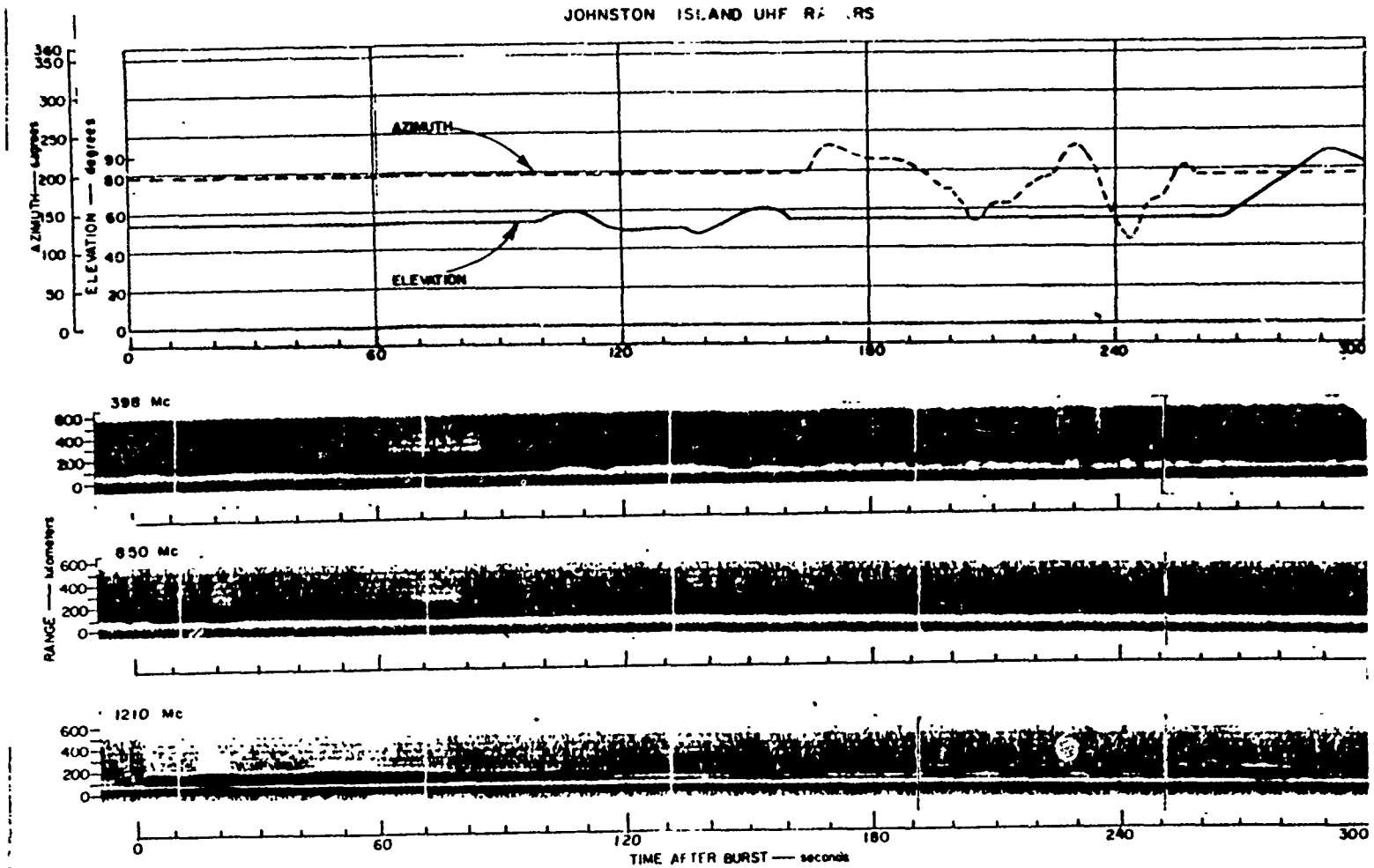

Figure 3.4 Johnston Island radar range versus time for Blue Gill; 0 to 600 km, 0 to 300 seconds.

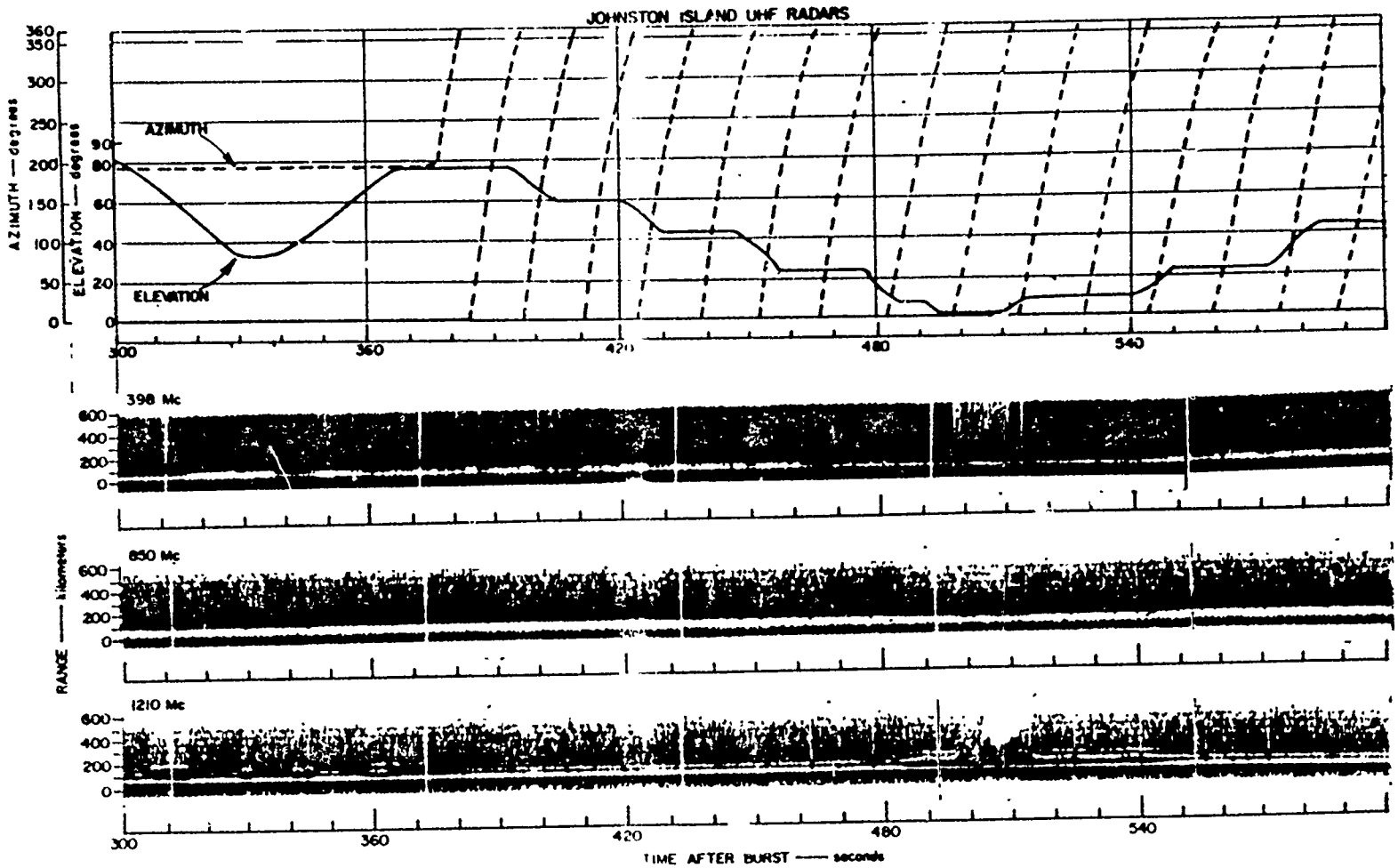

Figure 3.5 Johnston Island radar range versus time for Blue Gill; 0 to 600 km, 300 to 600 seconds.

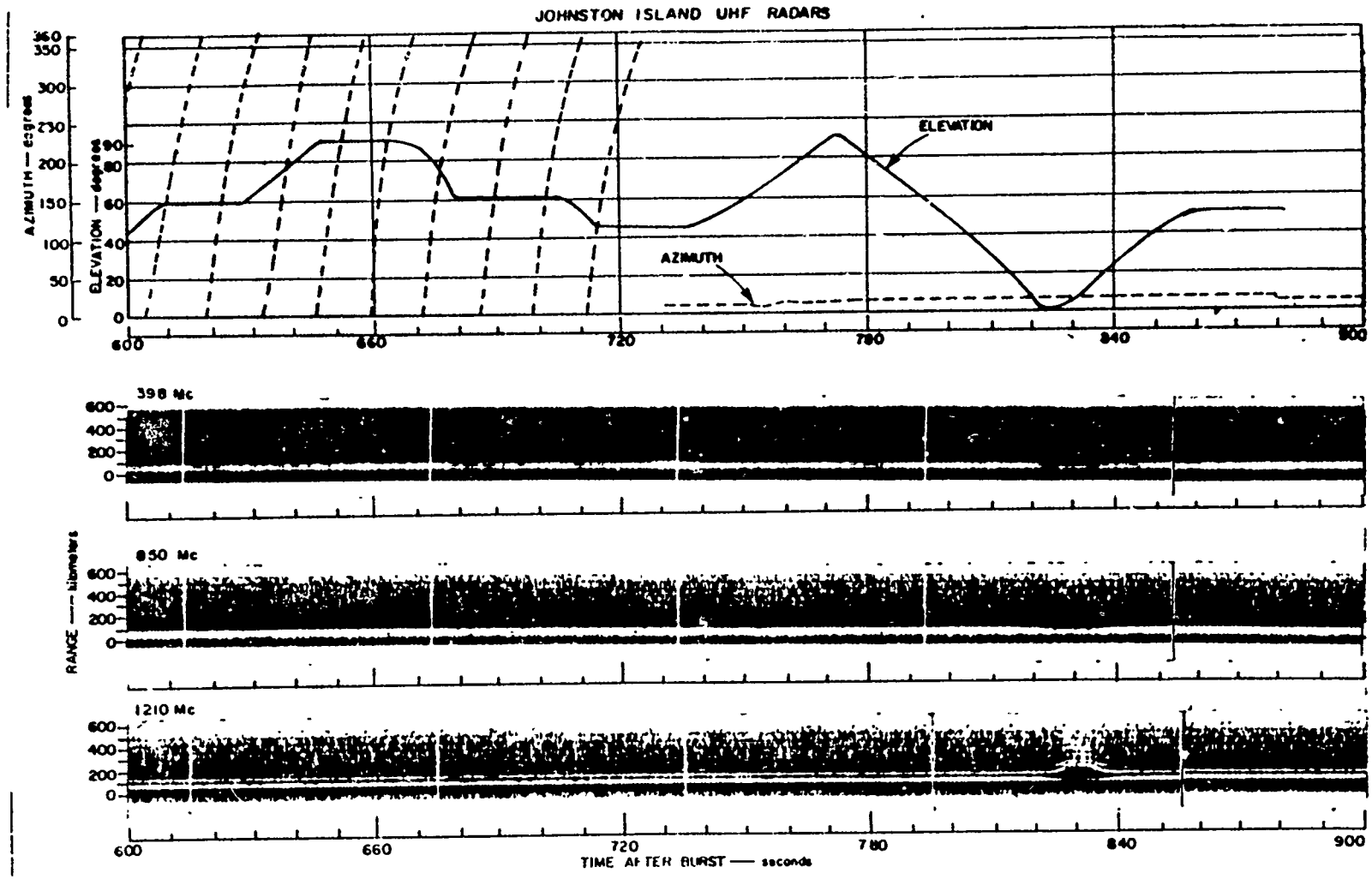

Figure 3.6 Johnston Island radar range versus time for Blue Gill; 0 to 600 km, 600 to 900 seconds.

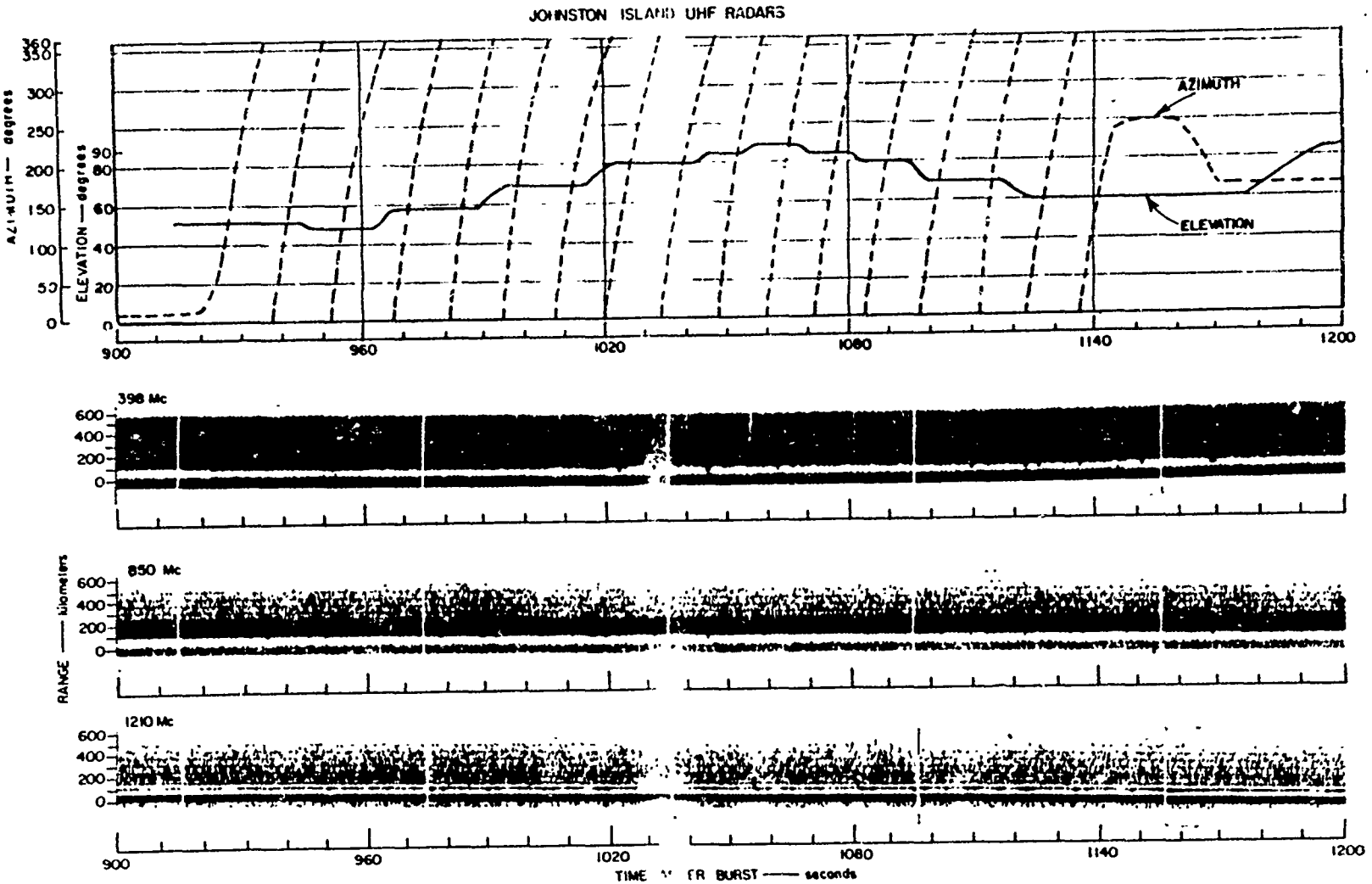

Figure 3.7 Johnston Island radar range versus time for Blue Gill; 0 to 600 km, 900 to 1,200 seconds.

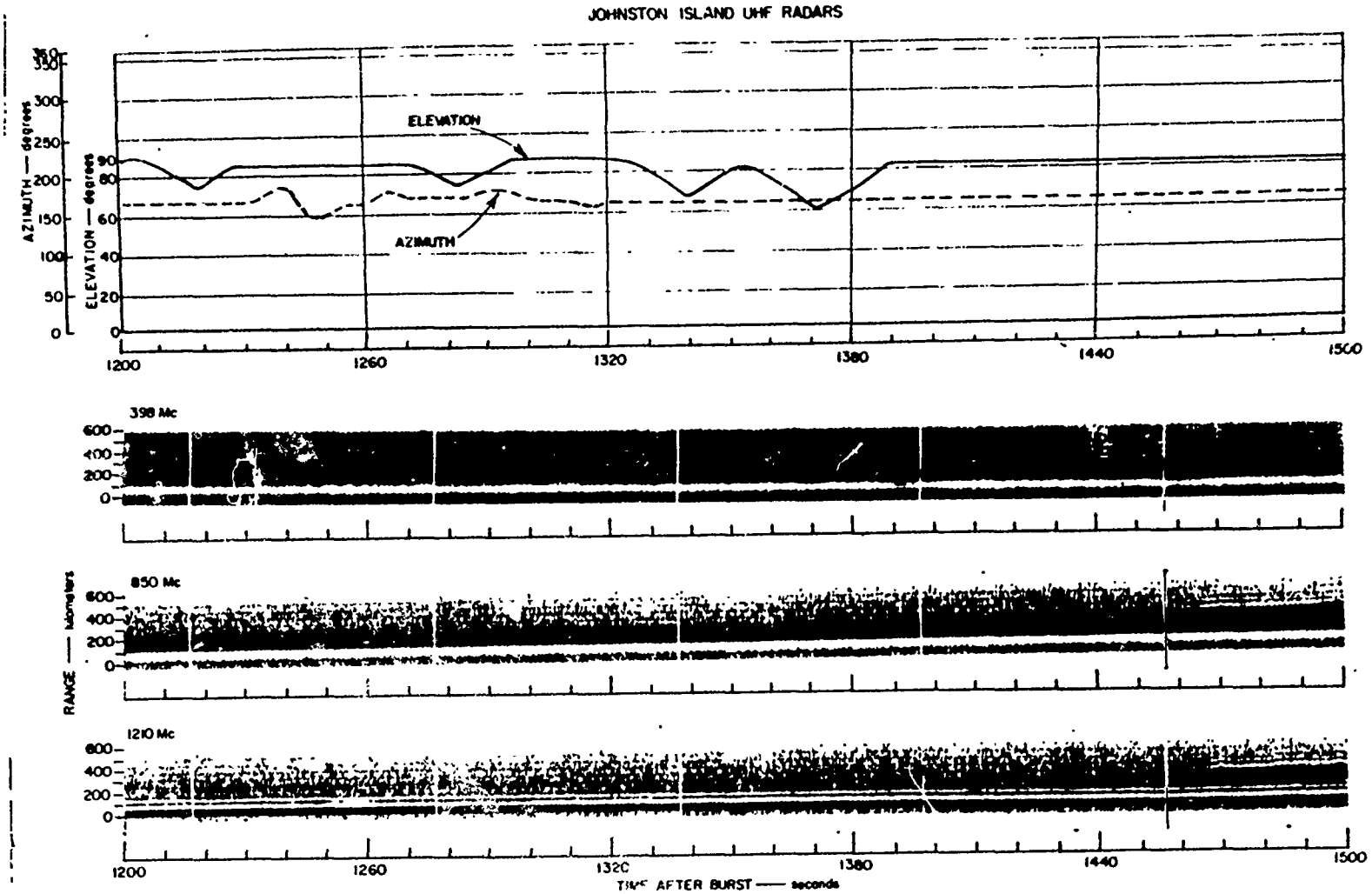

Figure 3.8 Johnston Island radar range versus time for Blue Gill; 0 to 600 km, 1,200 to 1,500 seconds.

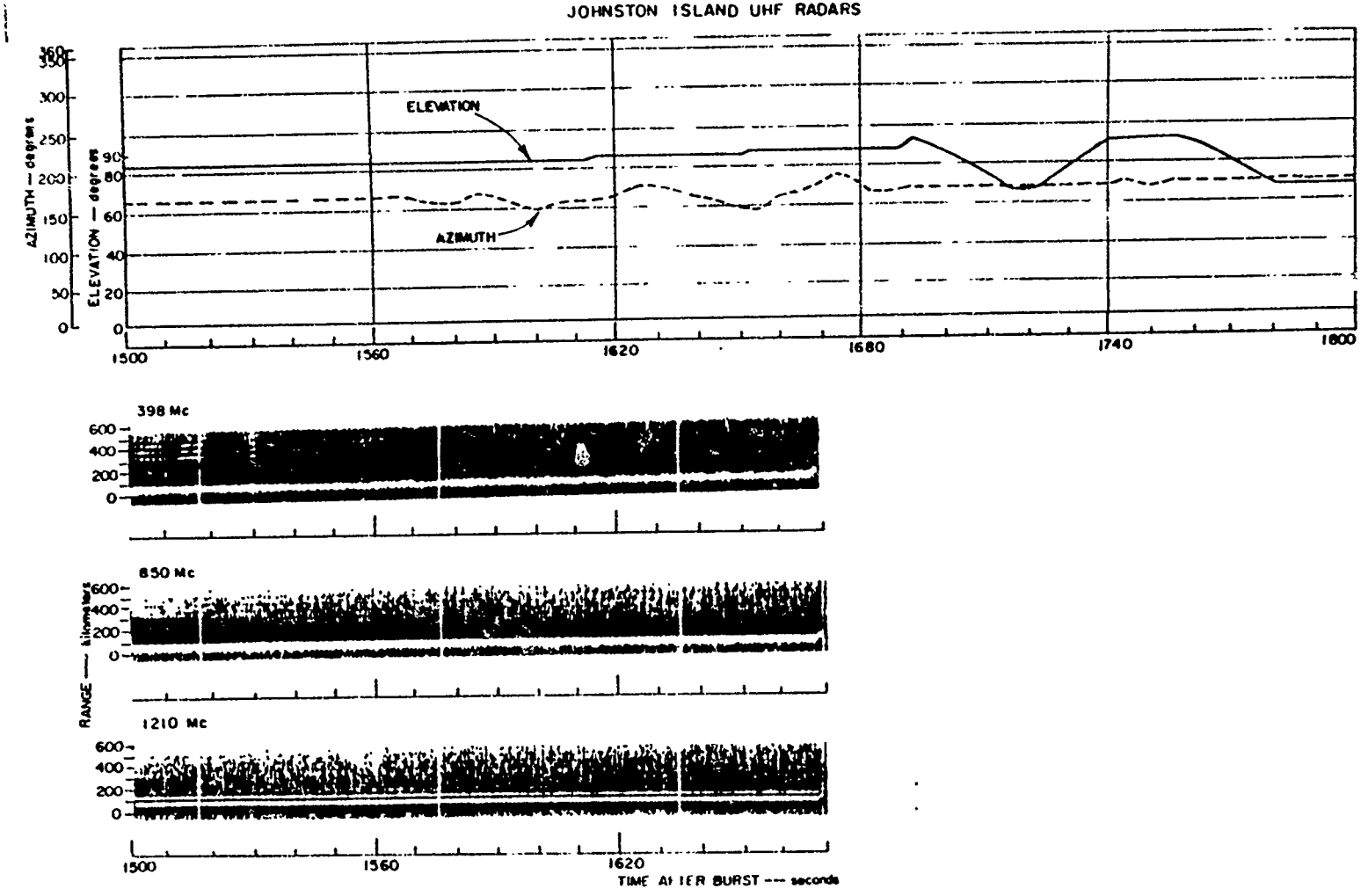

Figure 3.9 Johnston Island radar range versus time for Blue Gill; 0 to 600 km, 1,500 to 1,800 seconds.

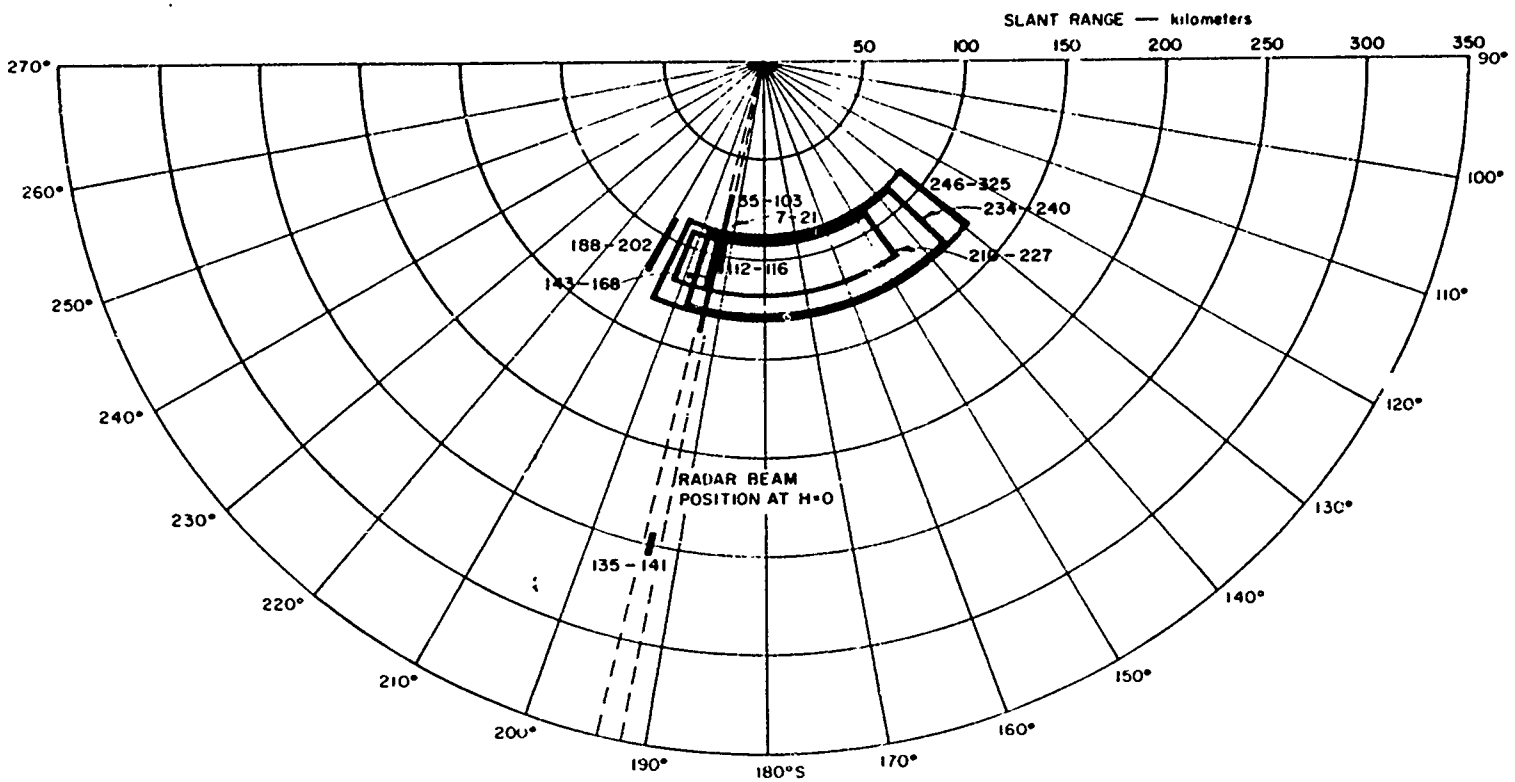

Figure 3.11 Johnston Island radar range versus azimuth for Blue Gill; 398-Mc southern echoes, 0 to 300 seconds.

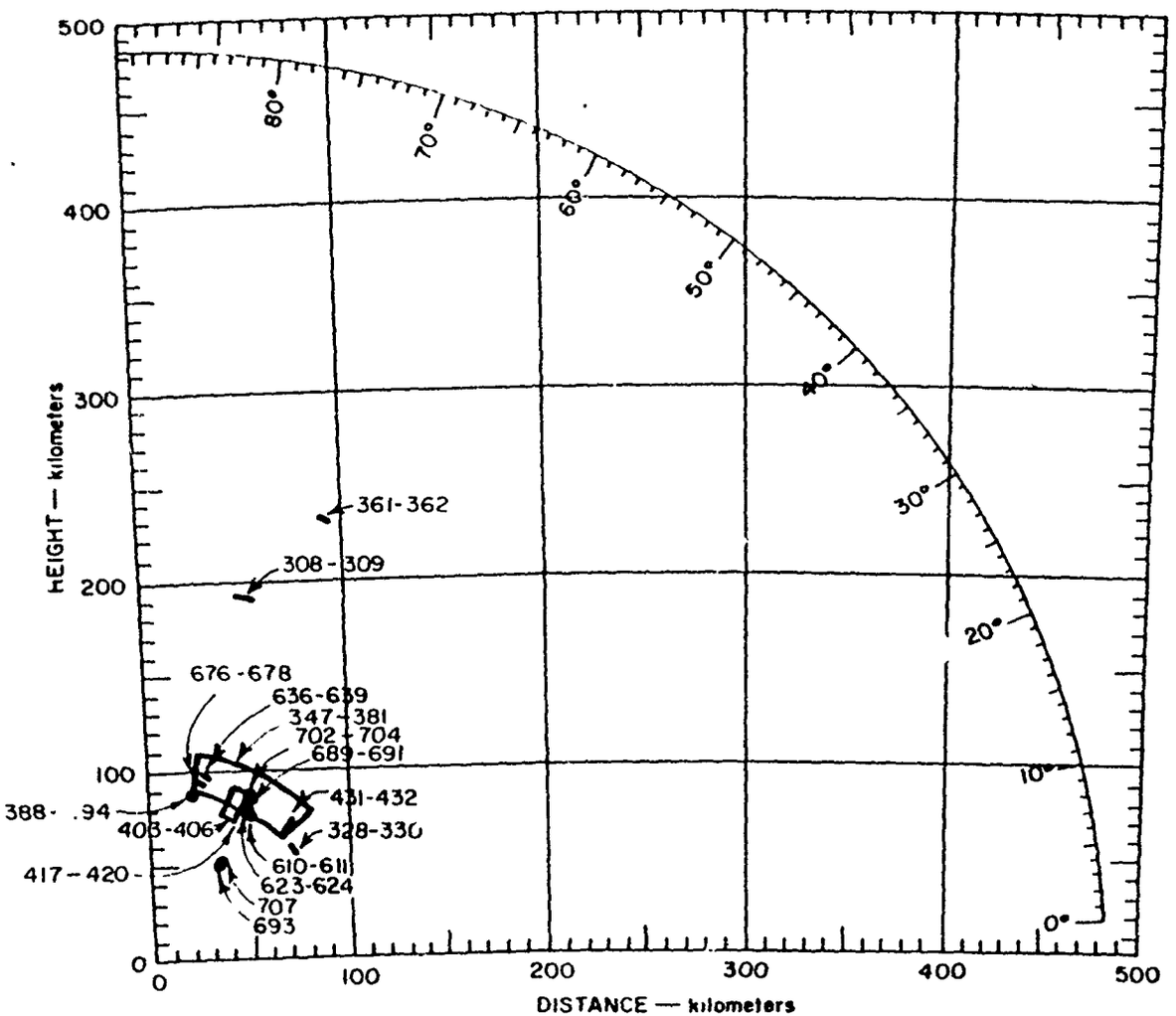

Figure 3.12 Johnston Island radar height versus distance for Blue Gill; 398-Mc southern echoes, 300 to 900 seconds.

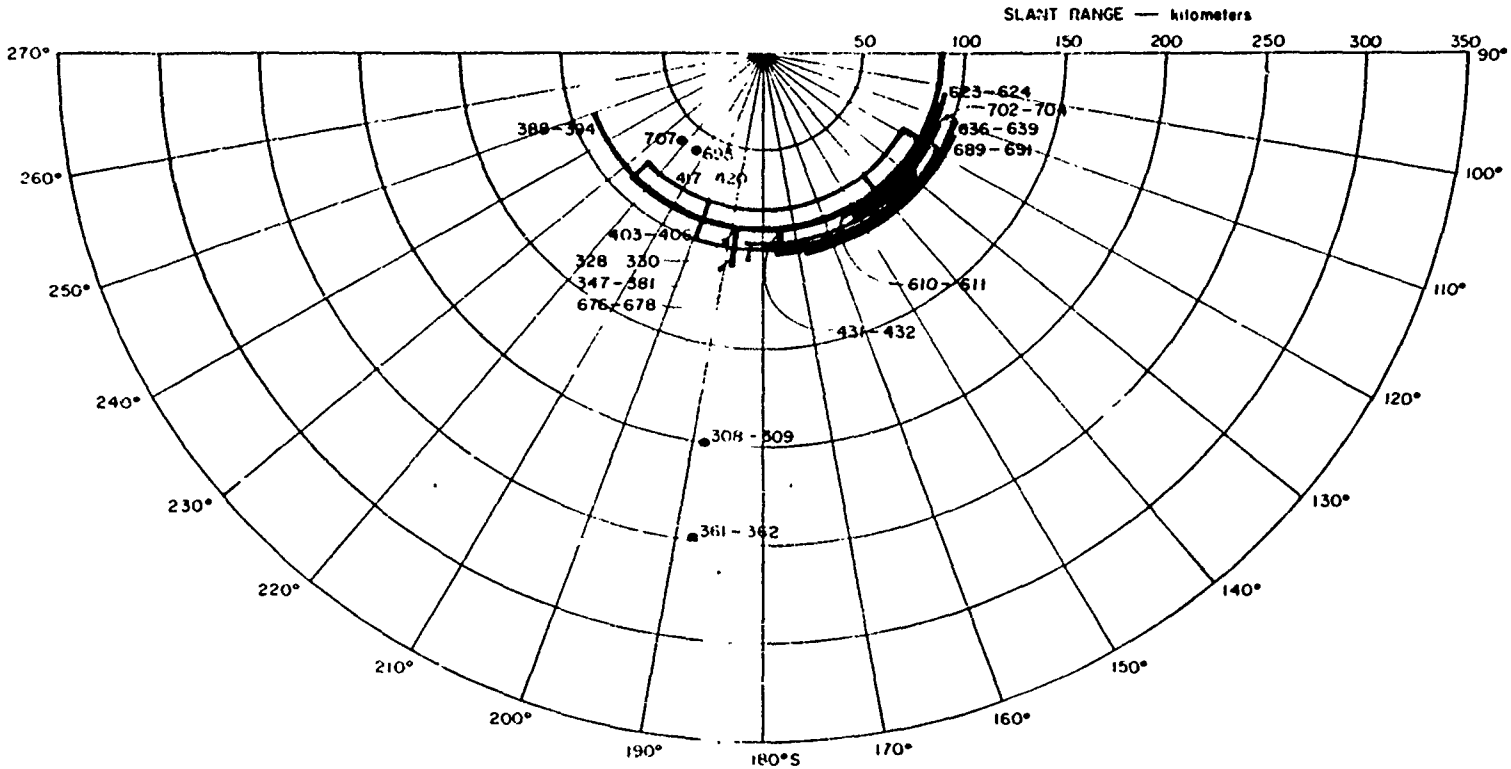

Figure 3.13 Johnston Island radar range versus azimuth for Blue Gill; 398-Mc southern echoes, 300 to 900 seconds.

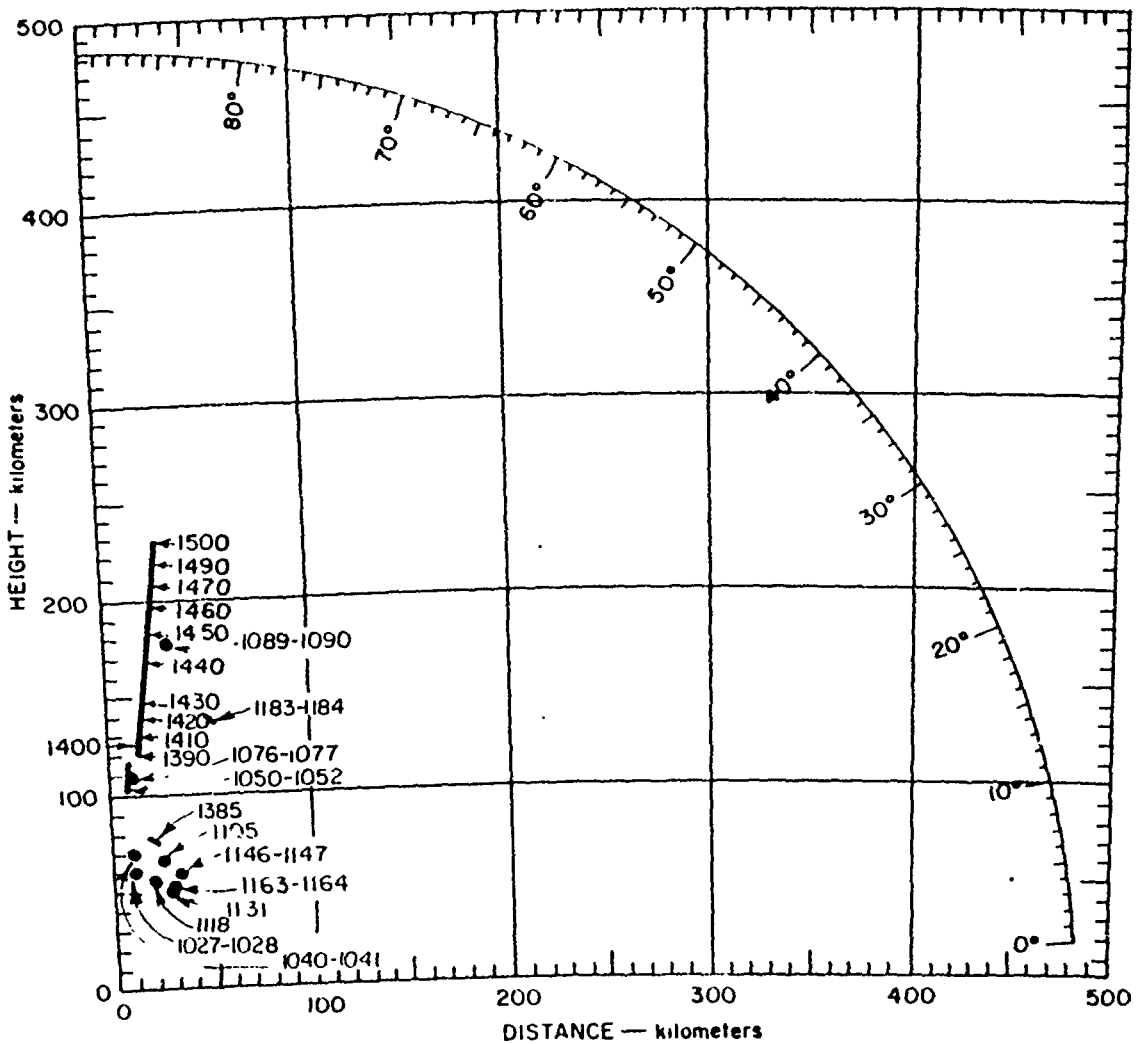

Figure 3.14 Johnston Island radar height versus dist for Blue Gill; 398-Mc southern echoes, 900 to 1,500 seconds.

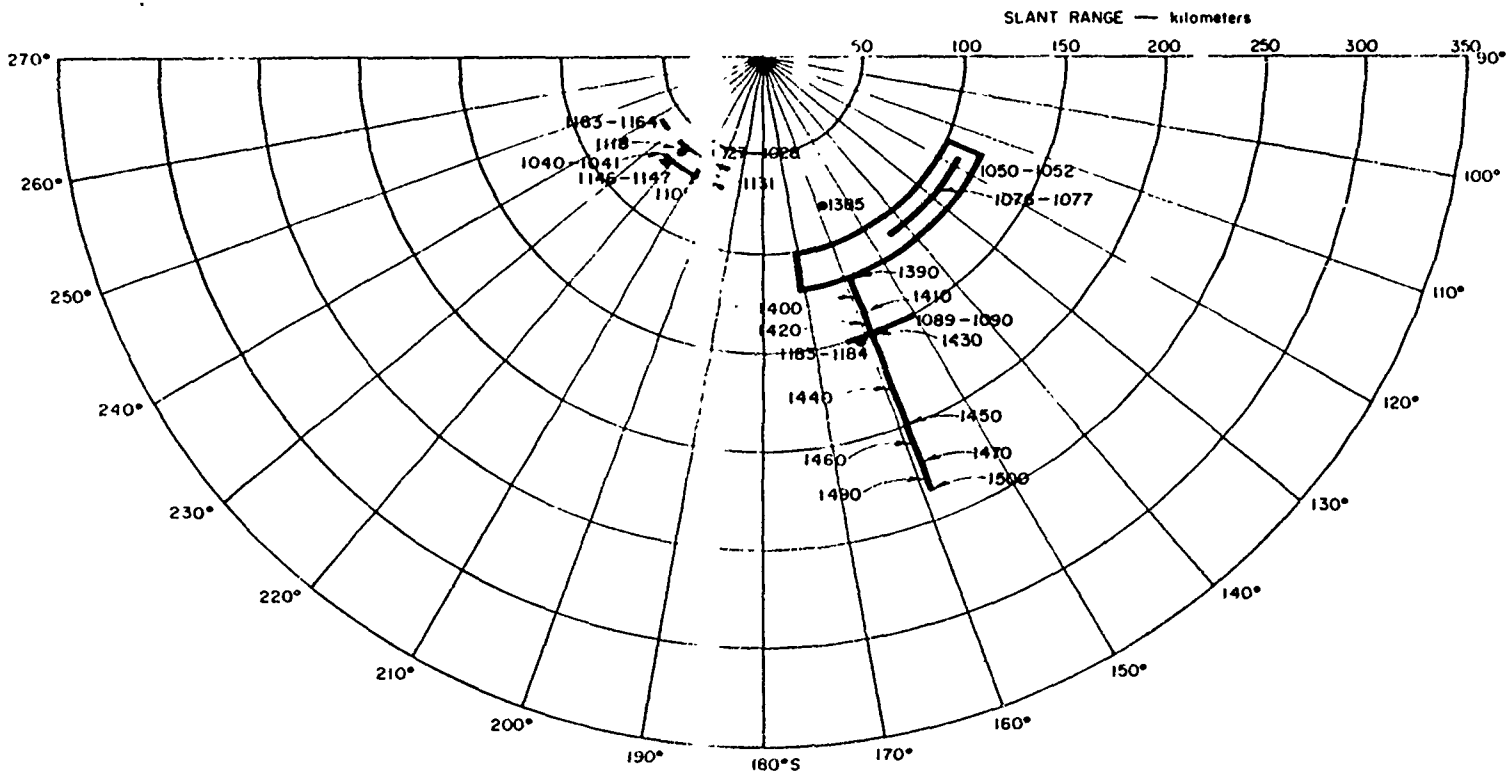

Figure 3.15 Johnston Island radar range versus azimuth for Blue Gill; 398-Mc southern echoes, 900 to 1,500 seconds.

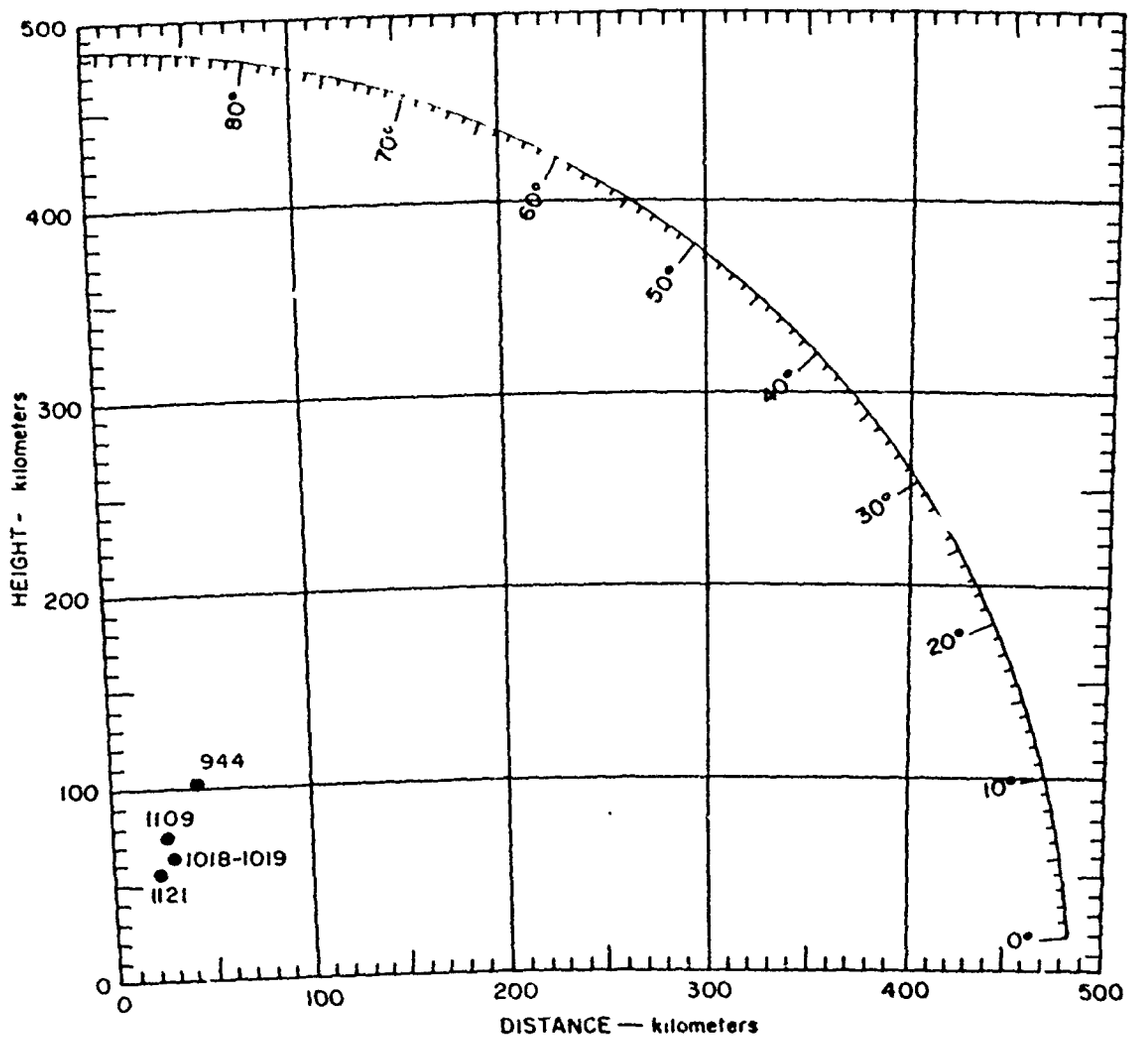

Figure 3.16 Johnston Island radar height versus distance for Blue Gill; 398-Mc northern echoes, 900 to 1,500 seconds.

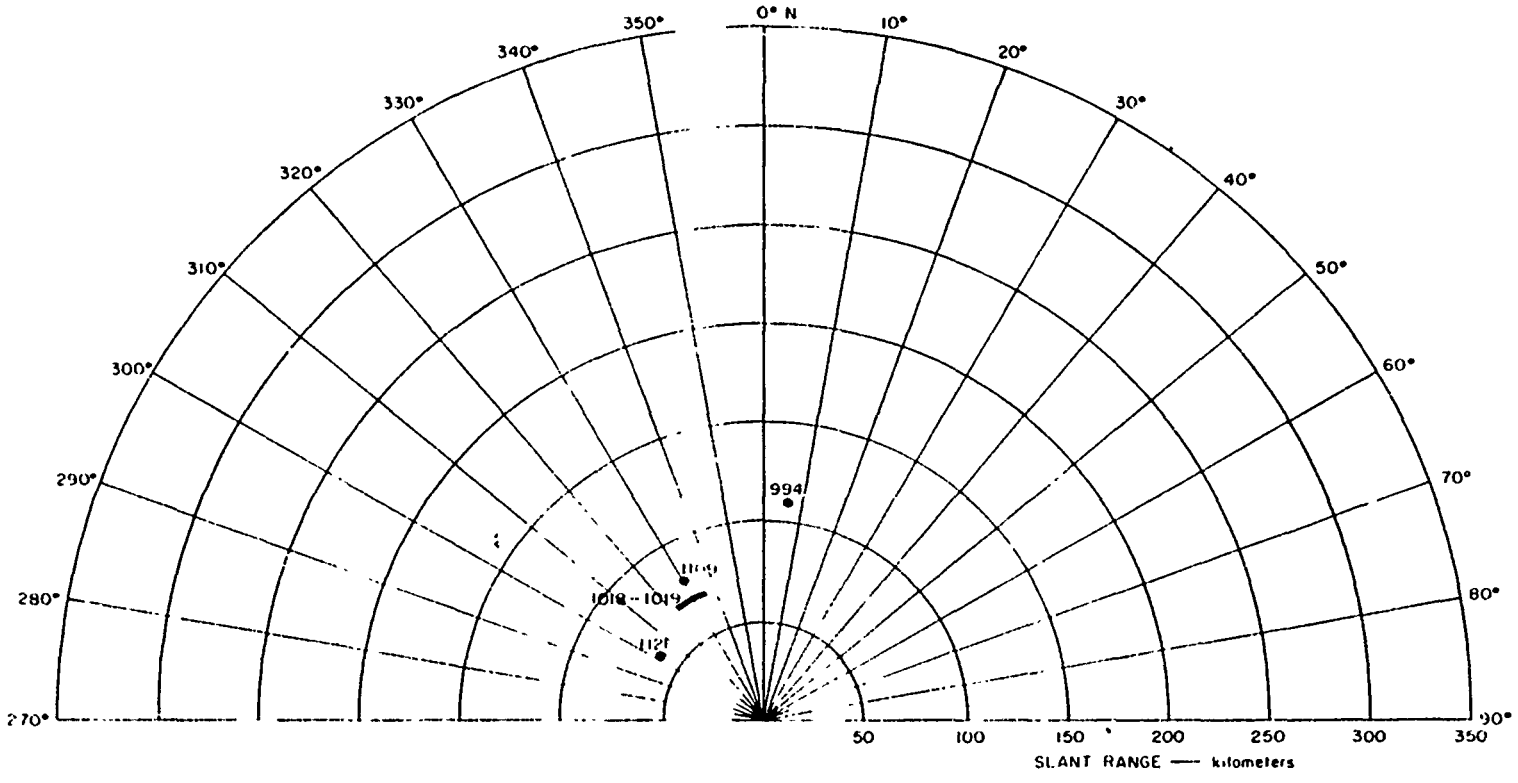

Figure 3.17 Johnston Island radar range versus azimuth for Blue Gill; 398-Mc northern echoes, 900 to 1,500 seconds.

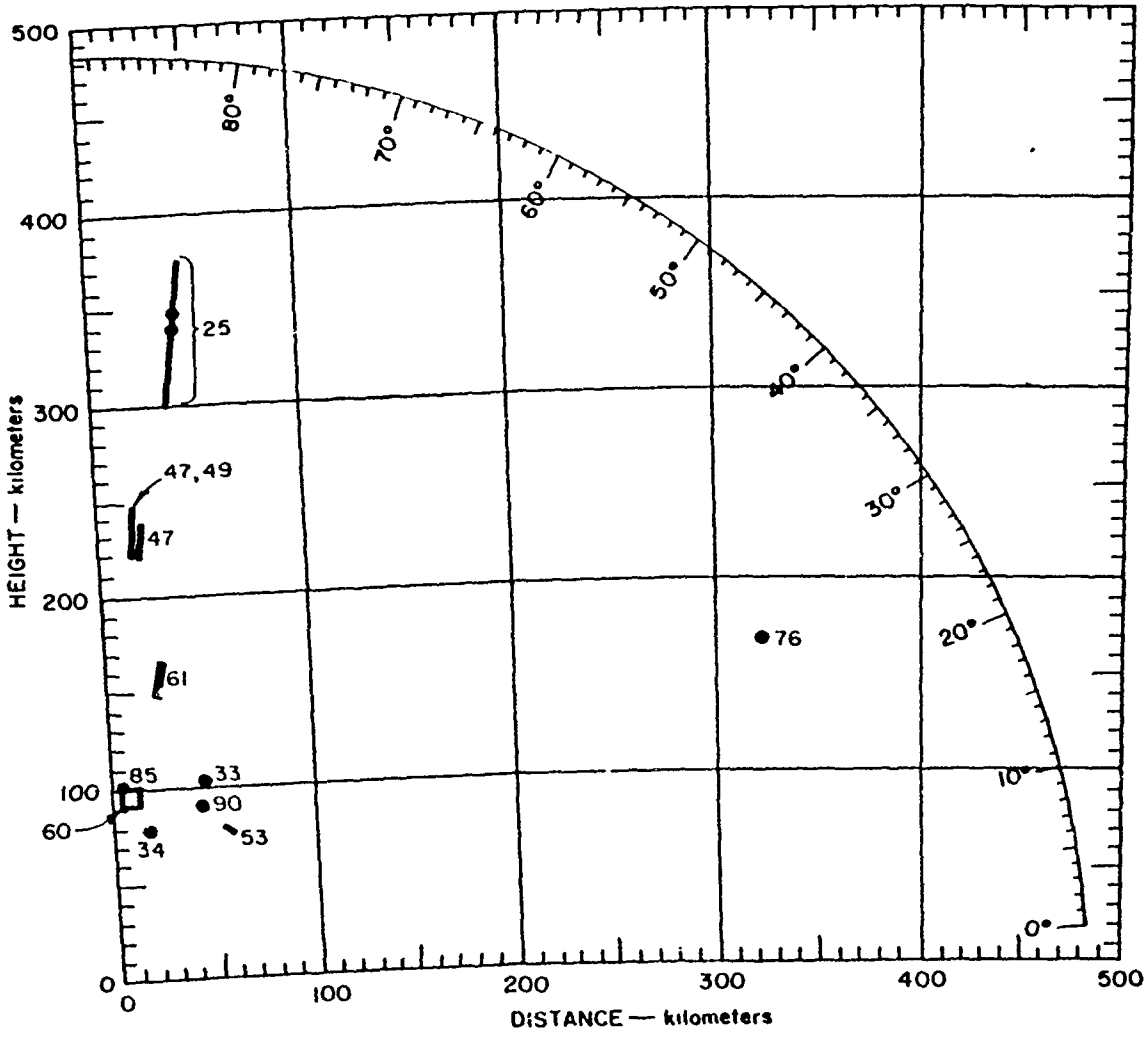

Figure 3.18 Johnston Island radar height versus distance for Blue Gill; 398-Mc southern echoes, 25 to 97 minutes.

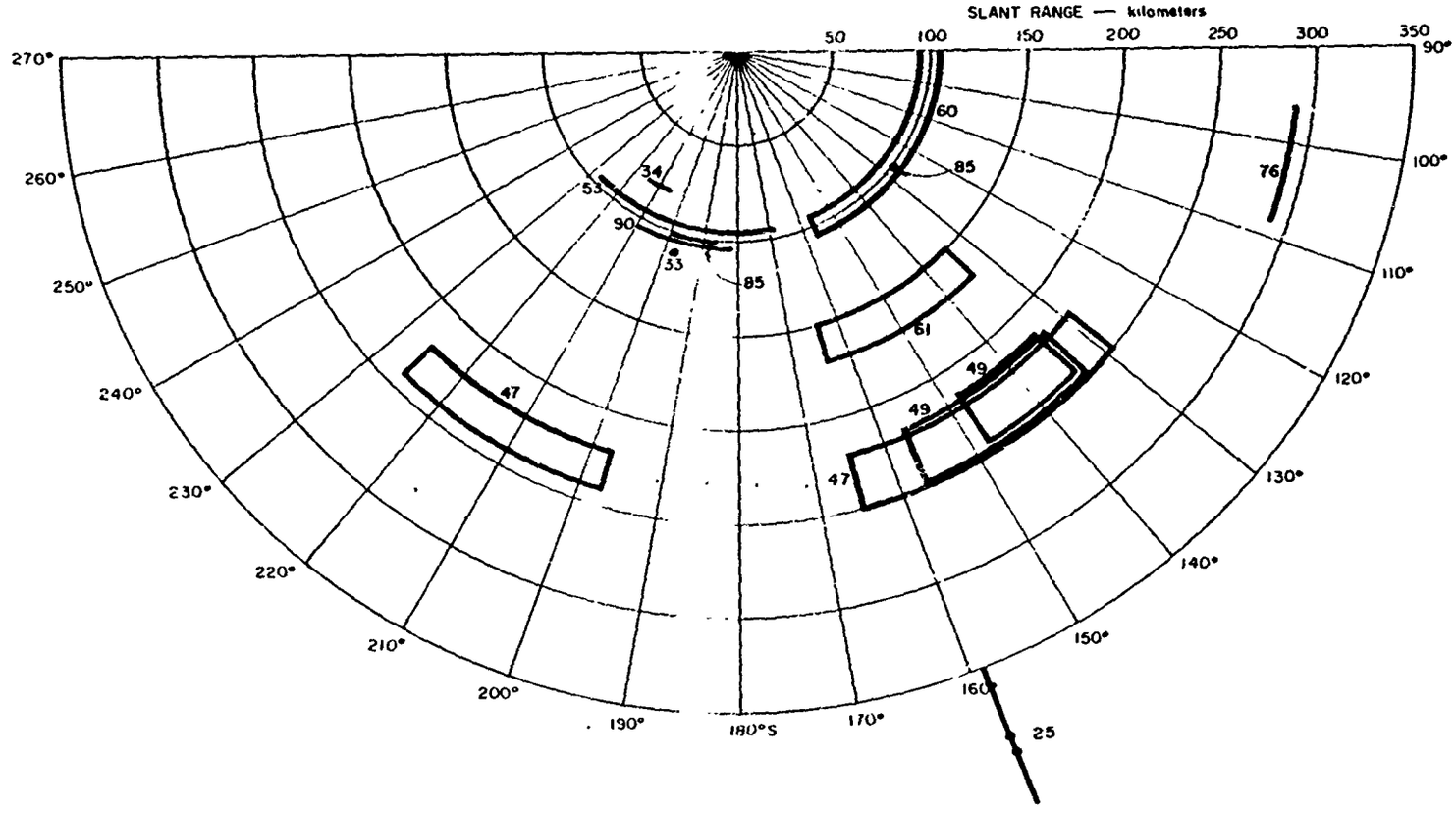

Figure 3.19 Johnston Island radar range versus azimuth for Blue Gill; 398-Mc southern echoes, 25 to 97 minutes.

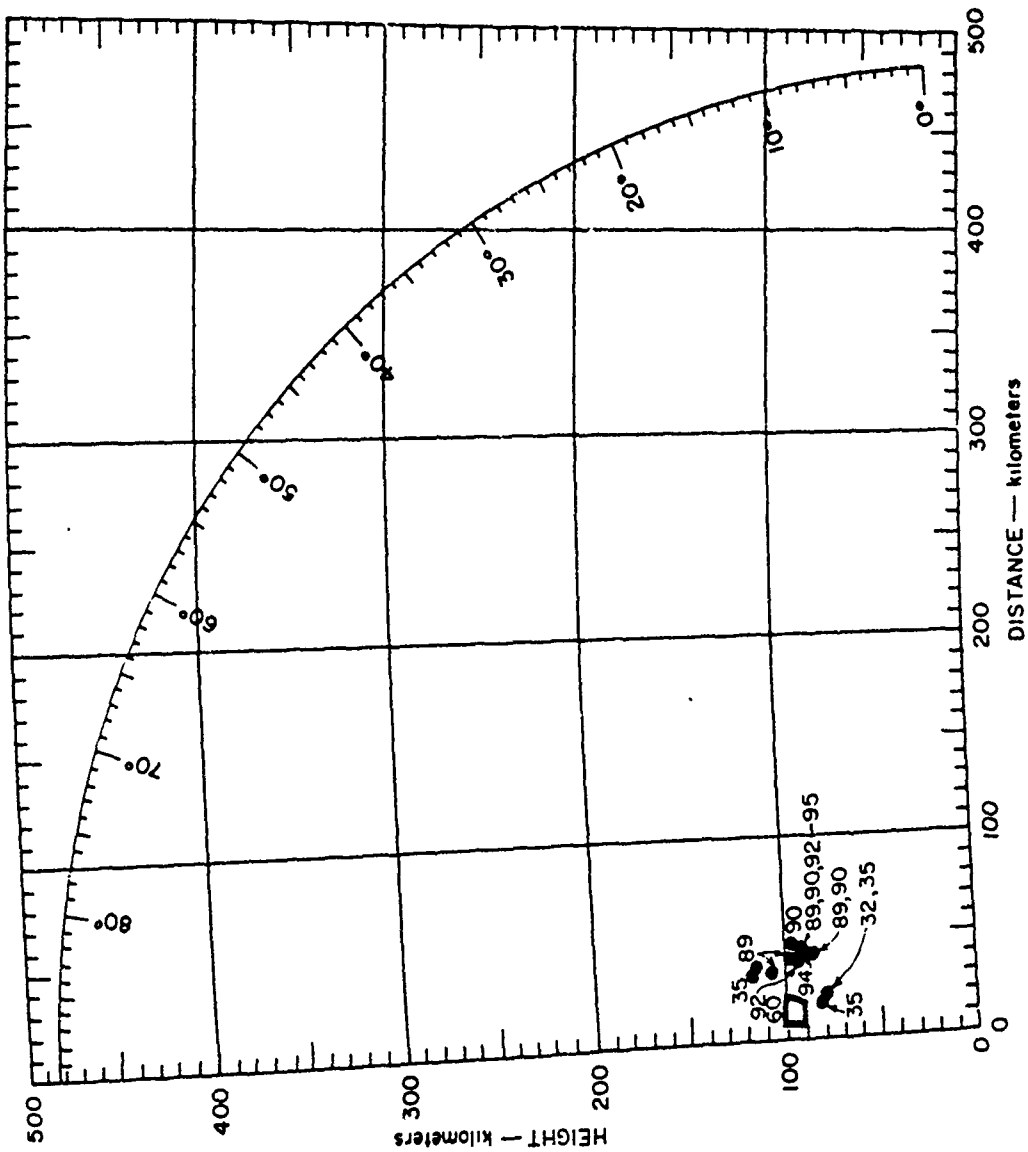

Figure 3.20 Johnston Island radar height versus distance for Blue Gill; 398-Mc northern echoes, 25 to 97 minutes.

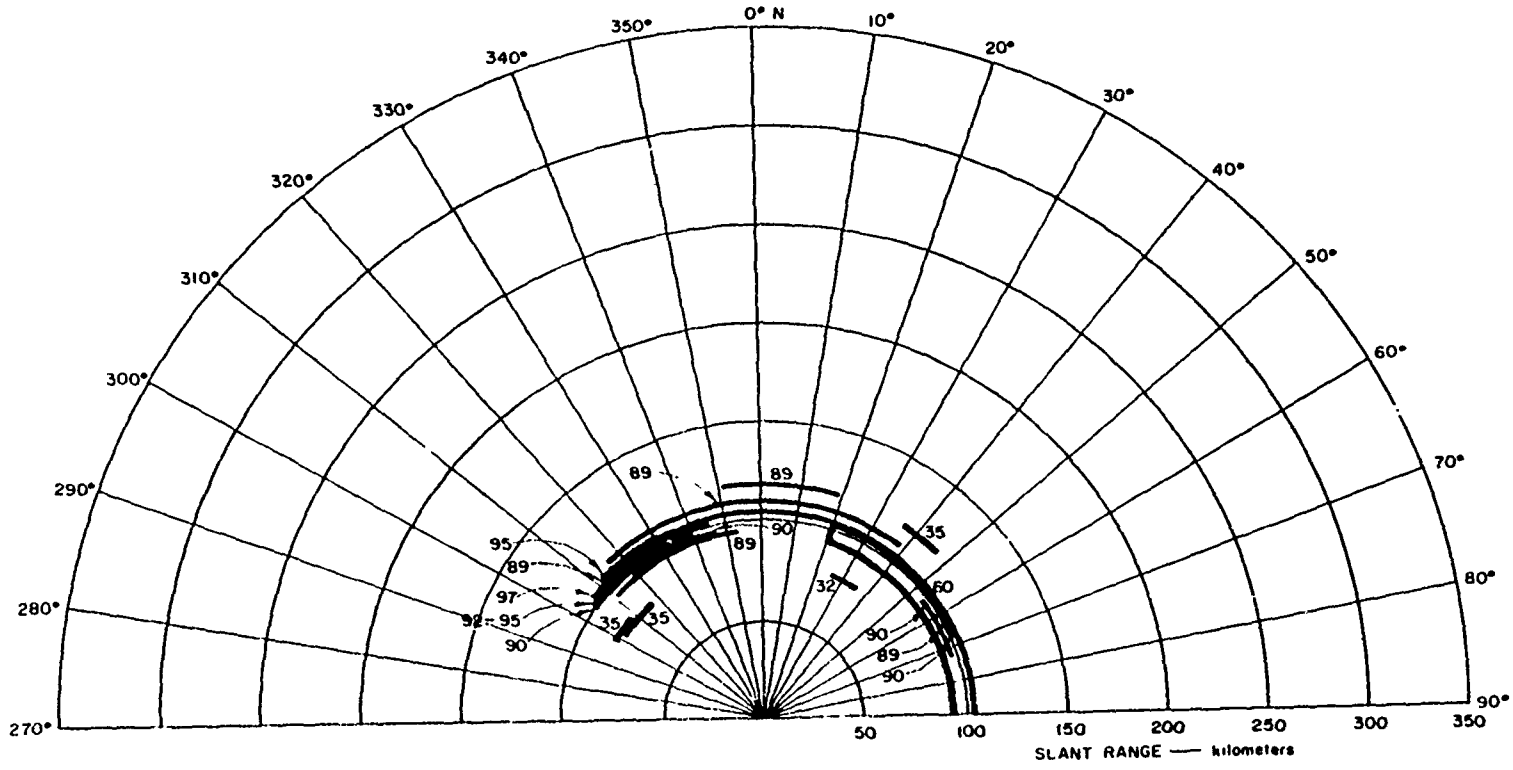

Figure 3.21 Johnston Island radar range versus azimuth for Blue Gill; 398-Mc northern echoes, 25 to 97 minutes.

101 (page 102 deleted)

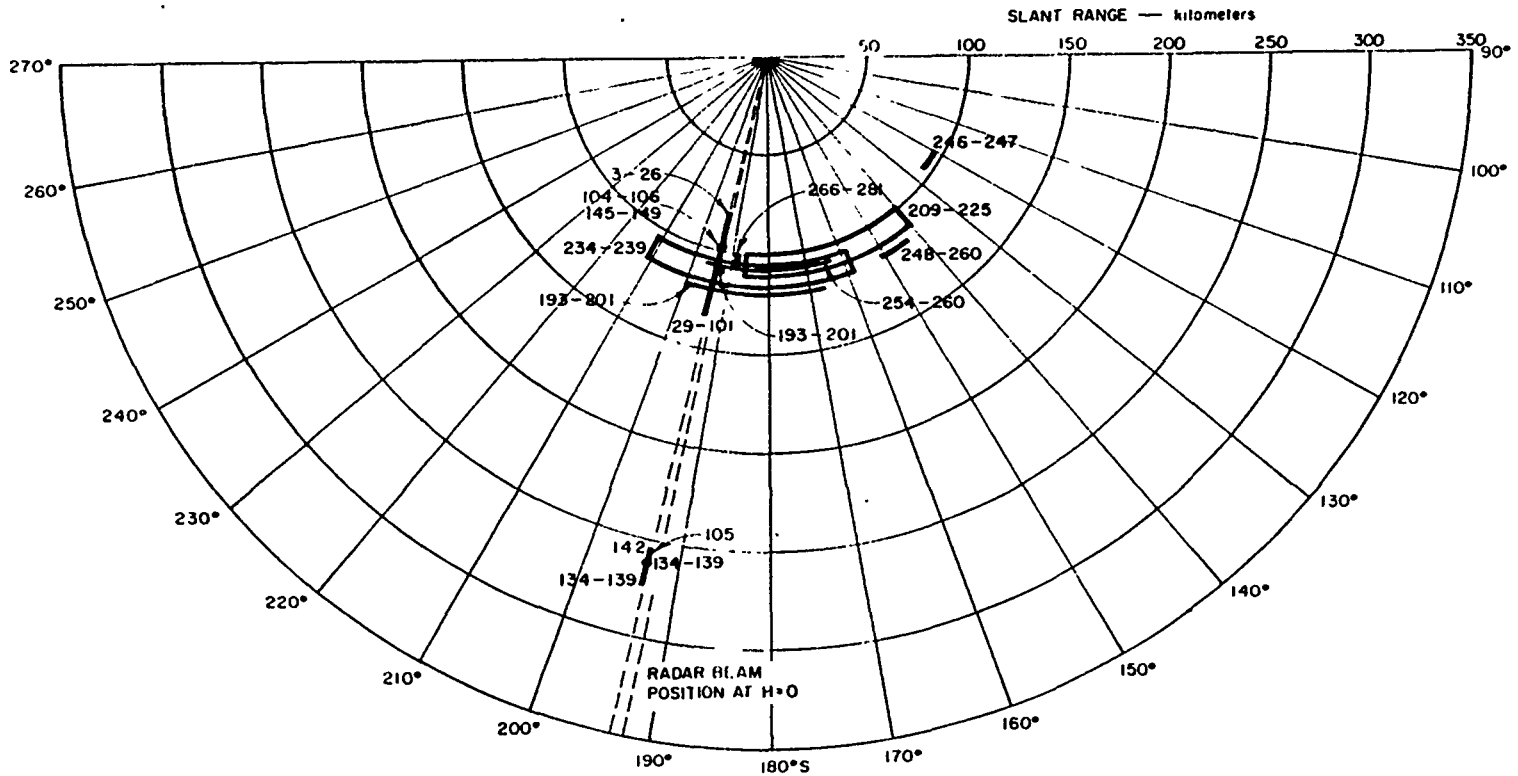

Figure 3.23 Johnston Island radar range versus azimuth for Blue Gill; 850-Mc southern echoes, 0 to 300 seconds.

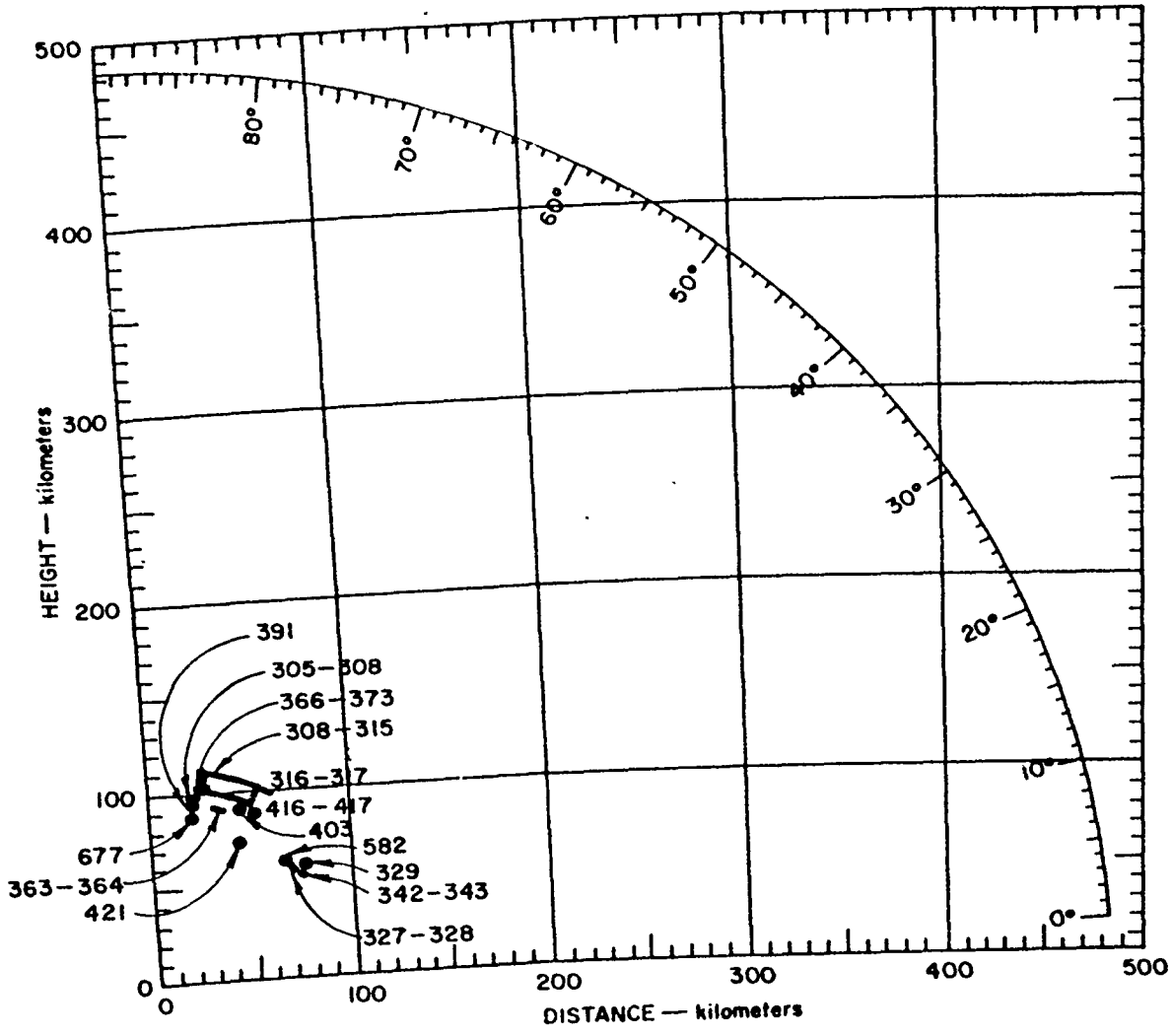

Figure 3.24 Johnston Island radar height versus distance for Blue Gill; 850-Mc southern echoes, 300 to 900 seconds.

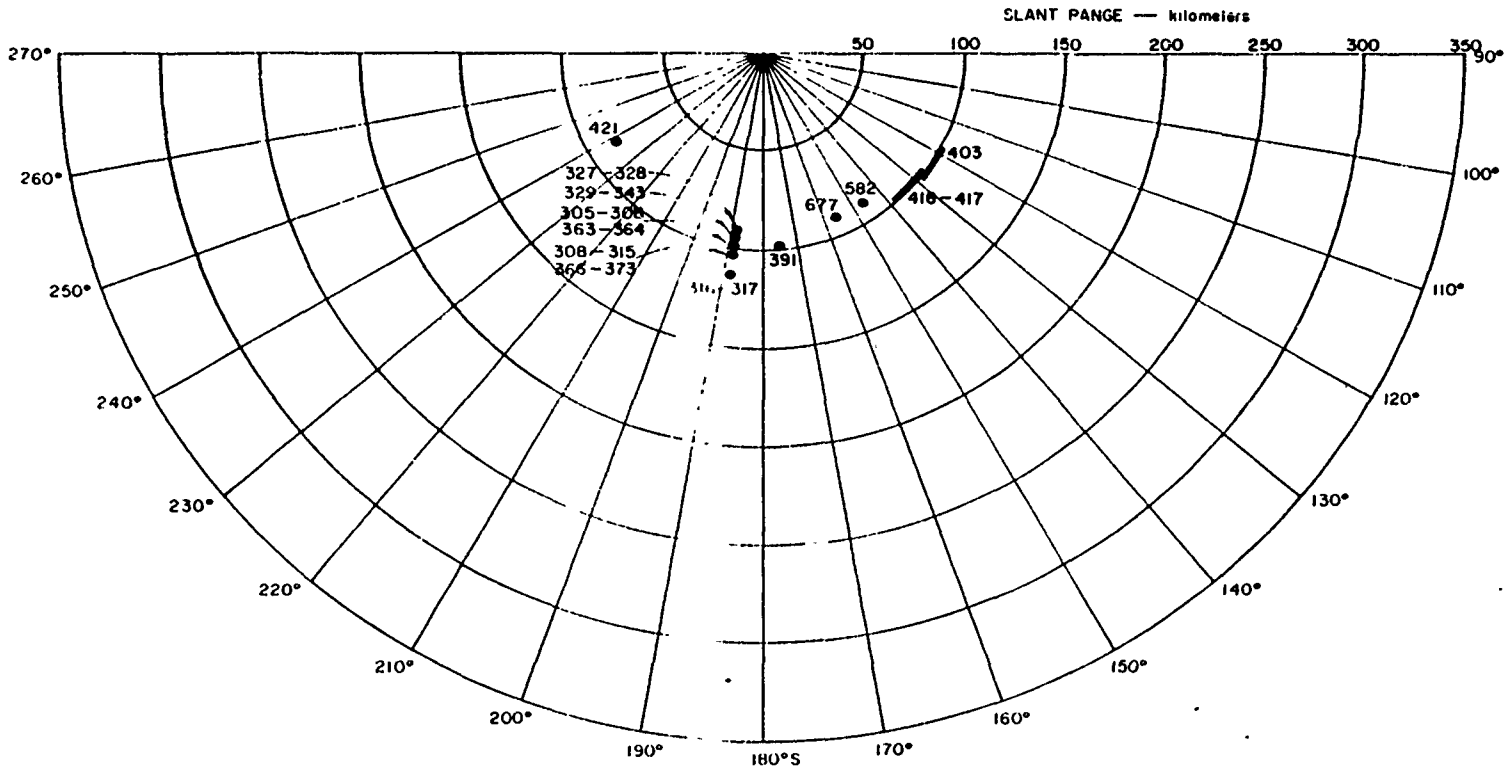

Figure 3.25 Johnston Island radar range versus azimuth for Blue Gill; 850-Mc southern echoes, 300 to 900 seconds.

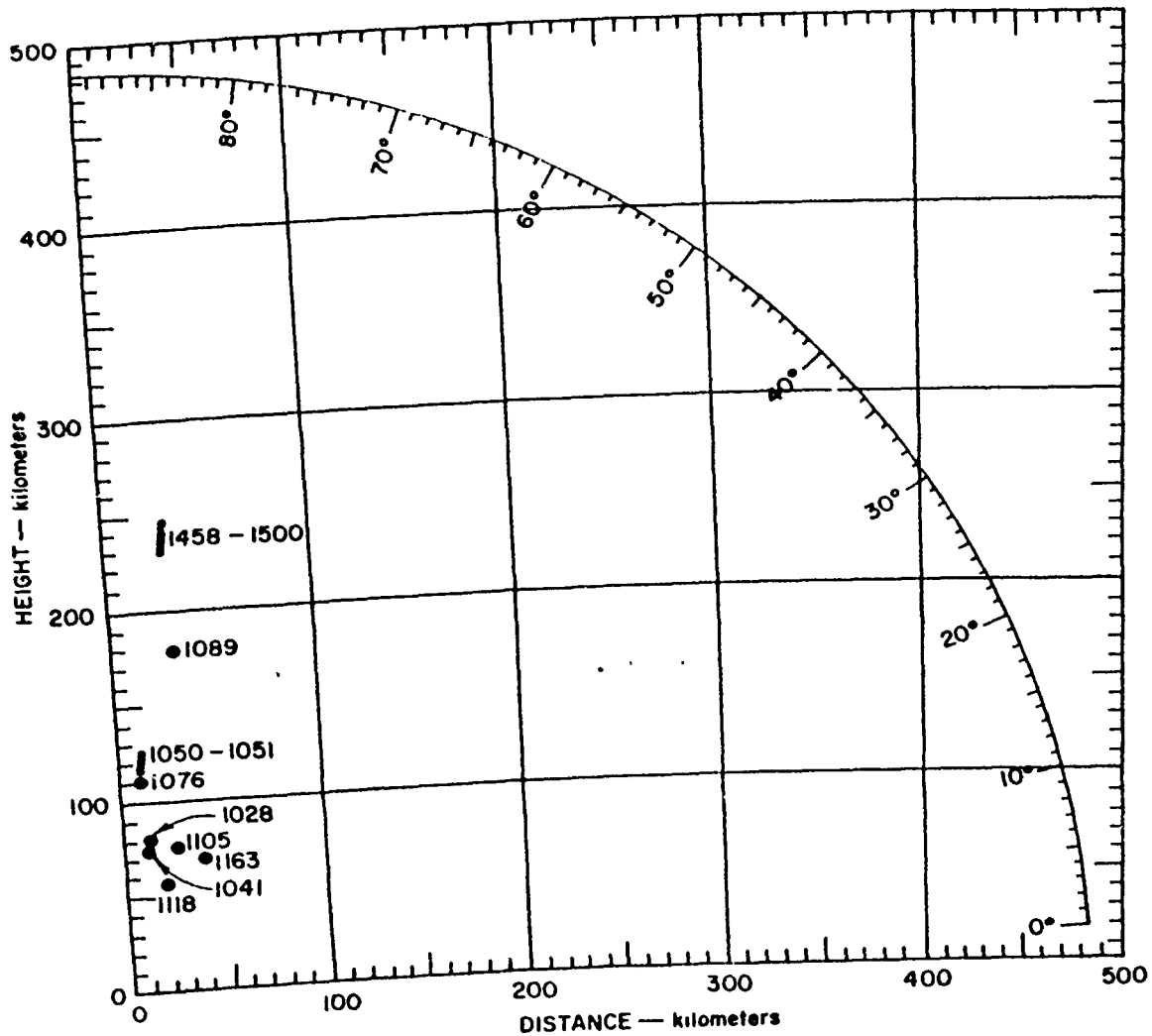

Figure 3.26 Johnston Island radar height versus distance for Blue Gill; 850-Mc southern echoes, 900 to 1,500 seconds.

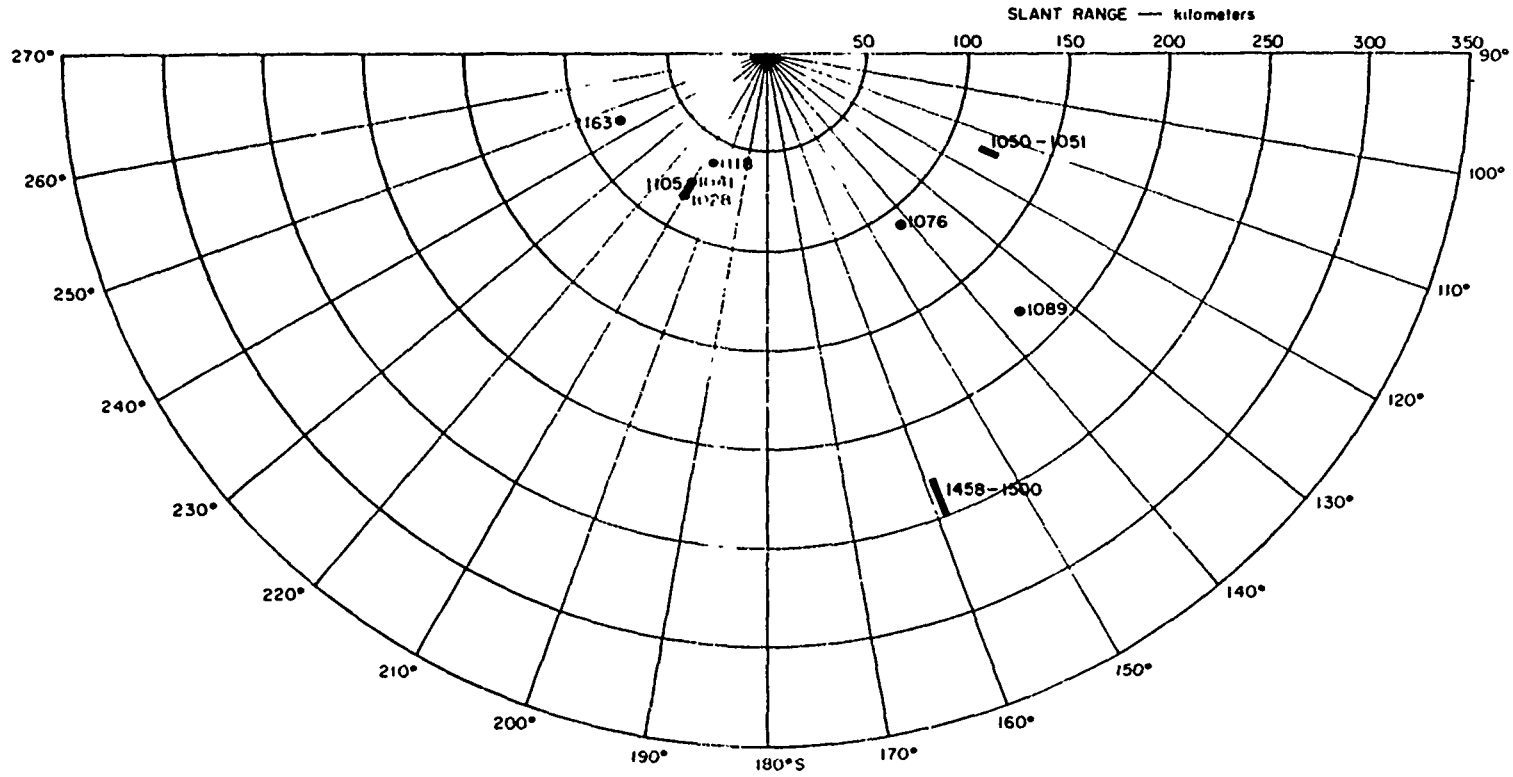

Figure 3.27 Johnston Island radar range versus azimuth for Blue Gill; 850-Mc southern echoes, 900 to 1,500 seconds.

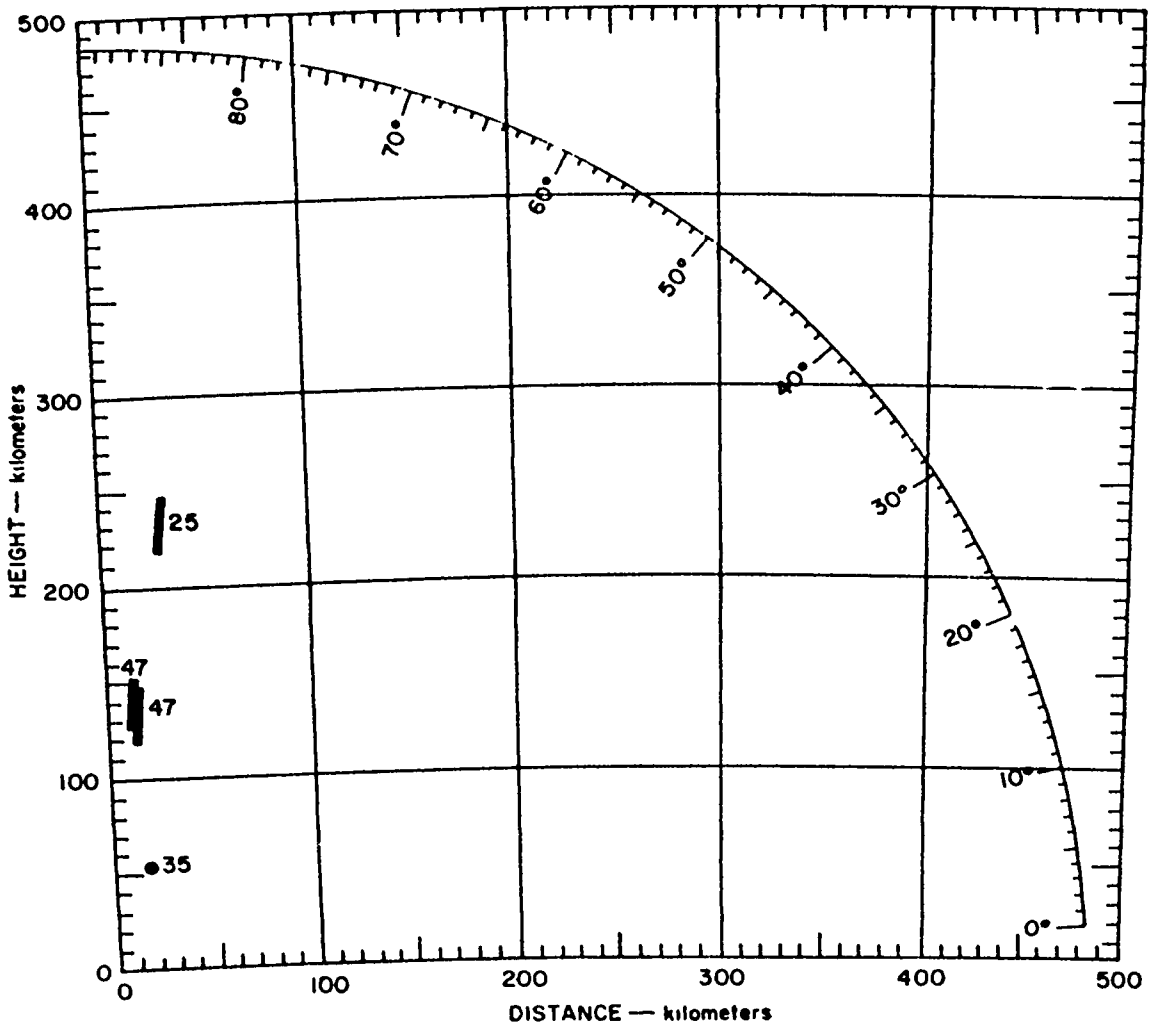

Figure 3.28 Johnston Island radar height versus distance for Blue Gill; 850-Mc southern echoes, 25 to 97 minutes.

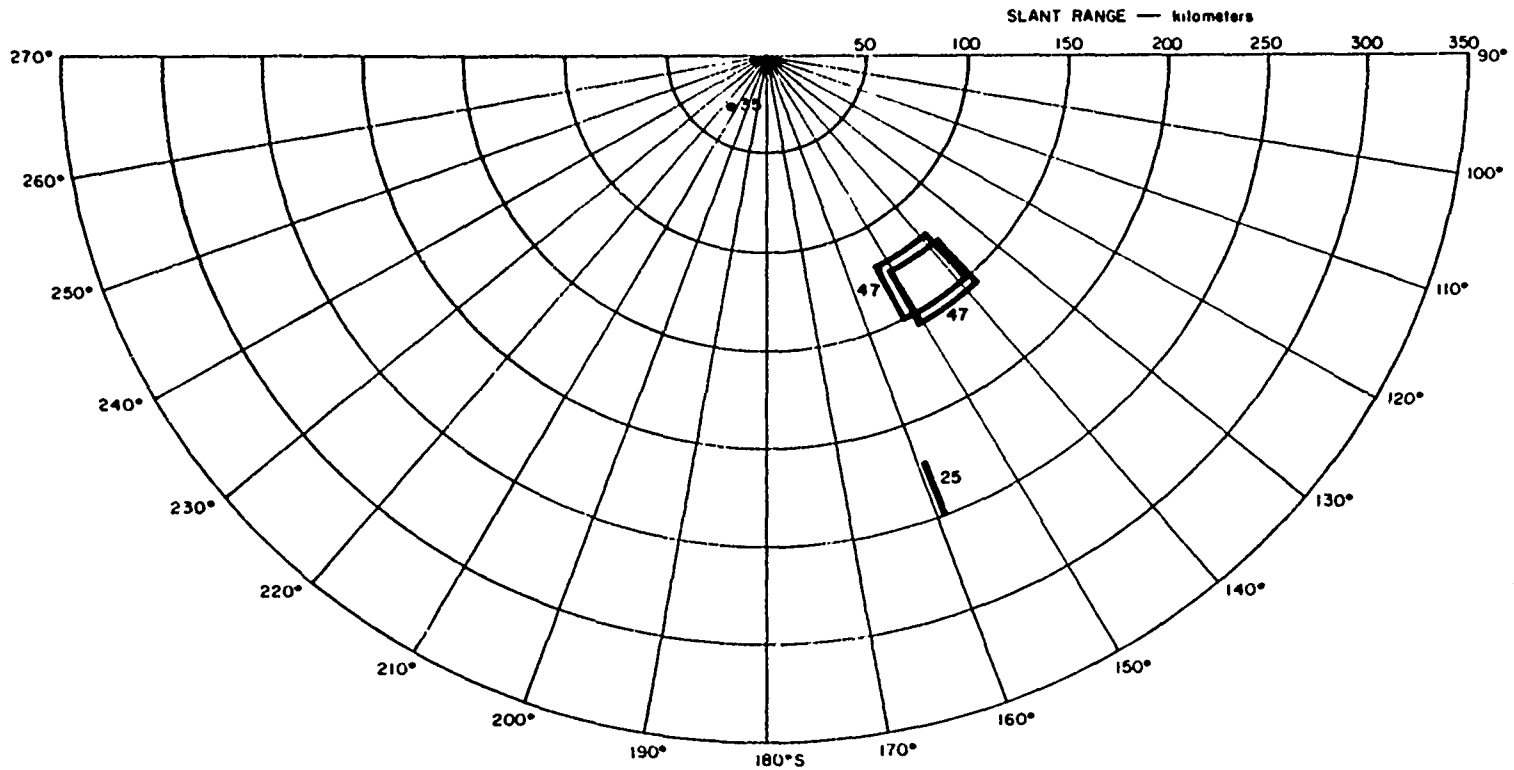

Figure 3.29 Johnston Island radar range versus azimuth for Blue Gill; 850-Mc southern echoes, 25 to 97 minutes.

(nage 110 deleted)

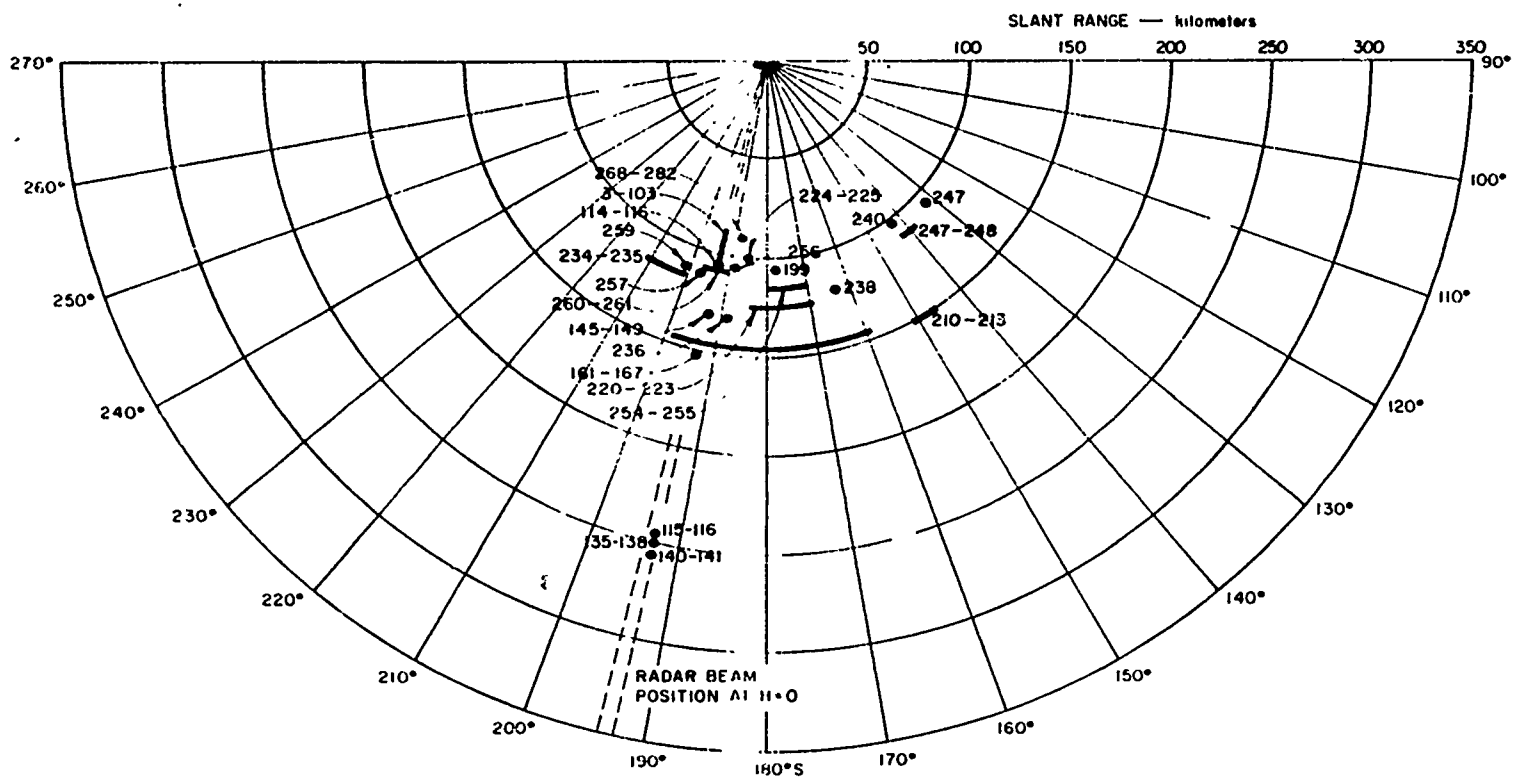

Figure 3.31 Johnston Island radar range versus azimuth for Blue Gill; 1210-Mc southern echoes, 0 to 300 seconds.

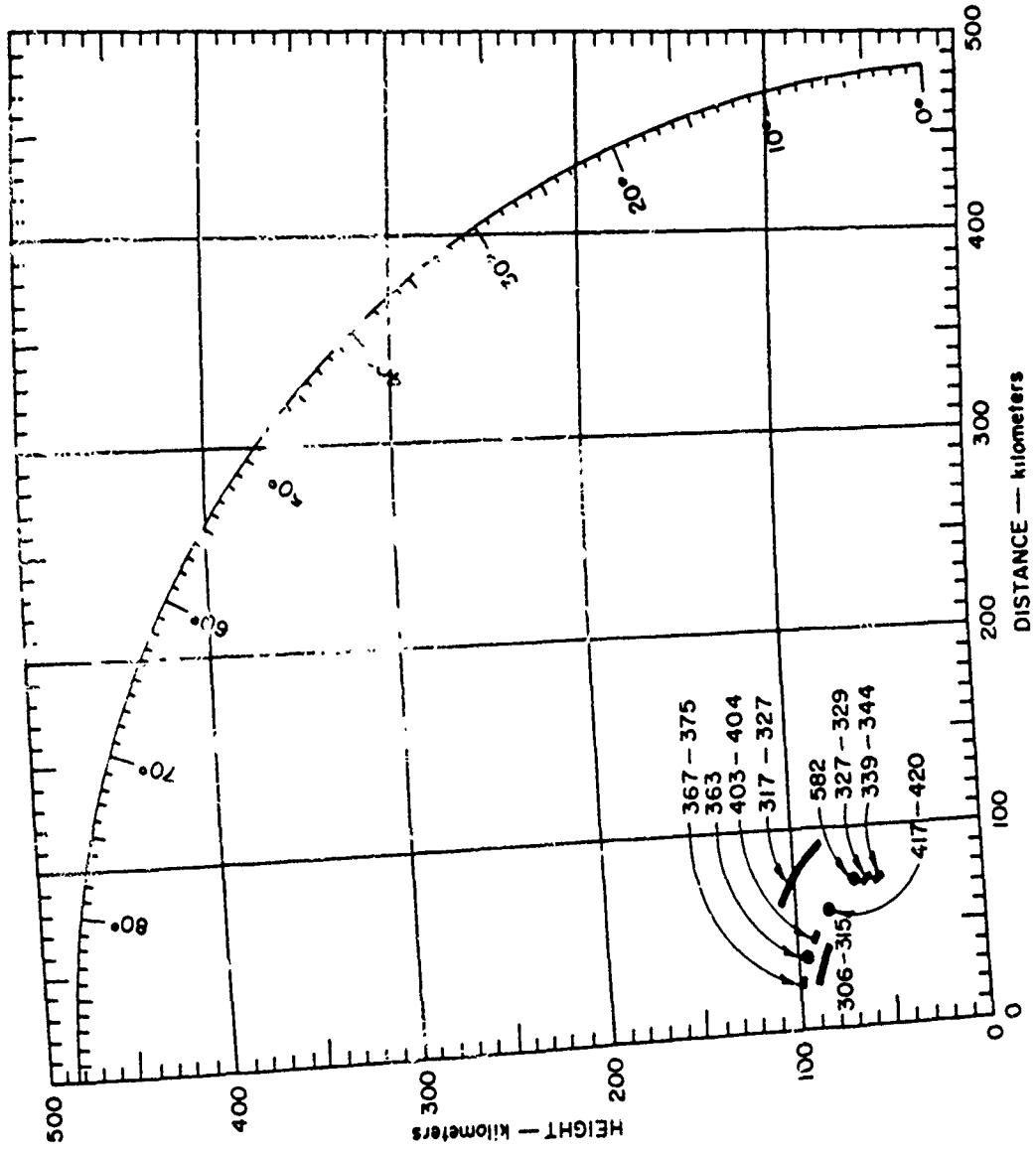

Figure 3.32 Johnston Island radar height versus distance for Blue Gill; 1210-Mc southern echoes, 300 to 900 seconds.

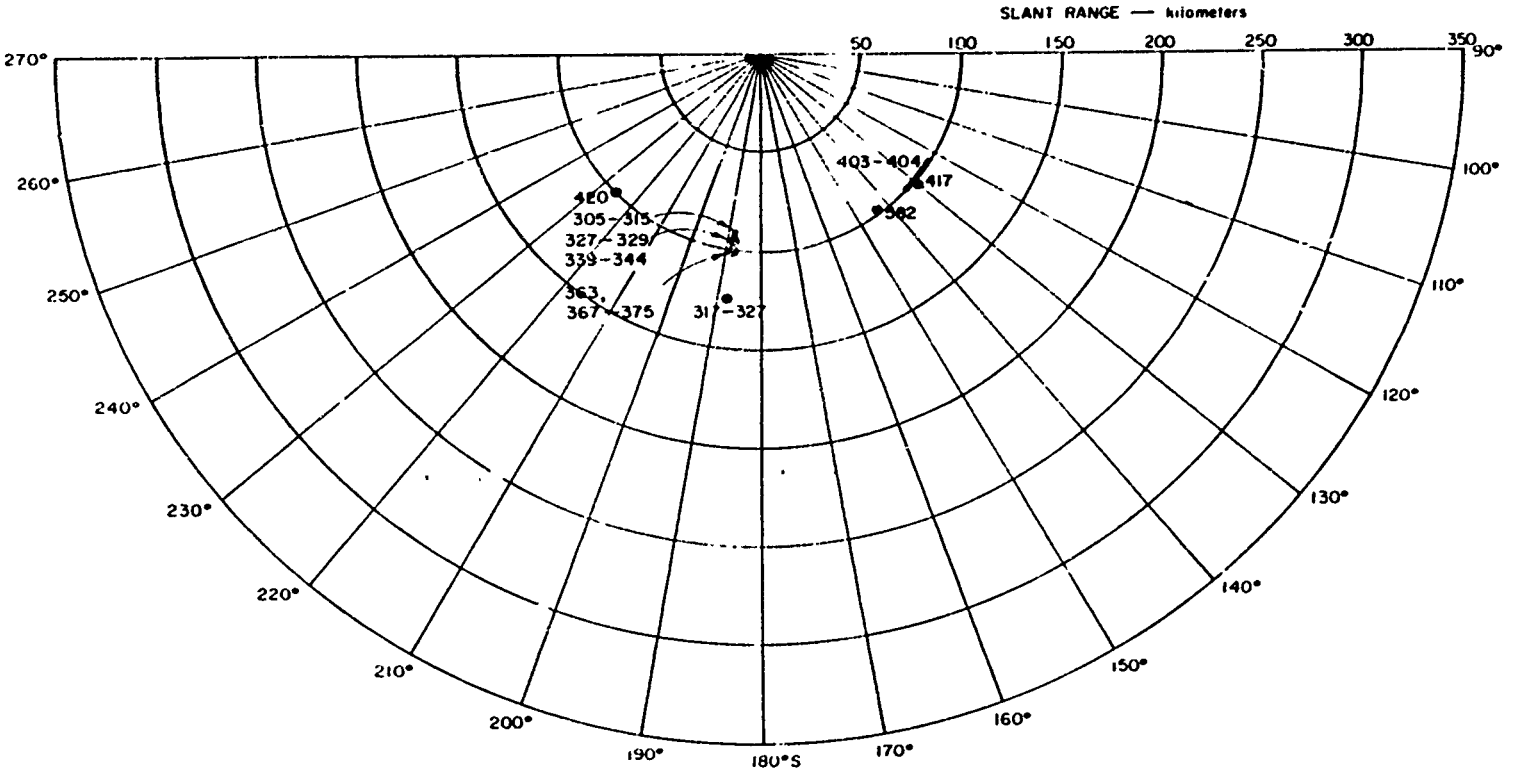

Figure 3.33 Johnston Island radar range versus azimuth for Blue Gill; 1210-Mc southern echoes, 300 to 900 seconds.

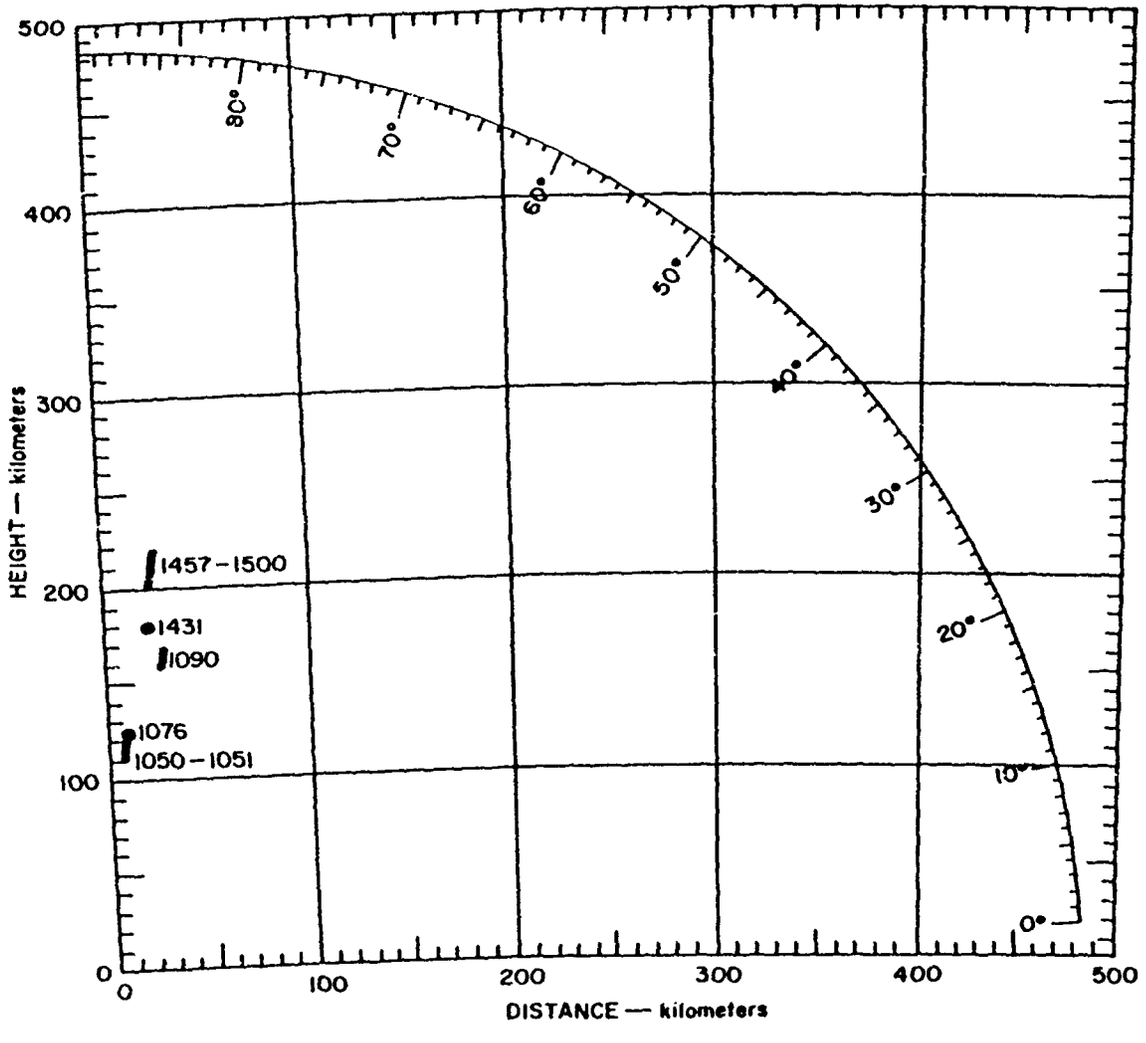

Figure 3.34 Johnston Island radar height versus distance for Blue Gill; 1210-Mc southern echoes, 900 to 1,500 seconds.

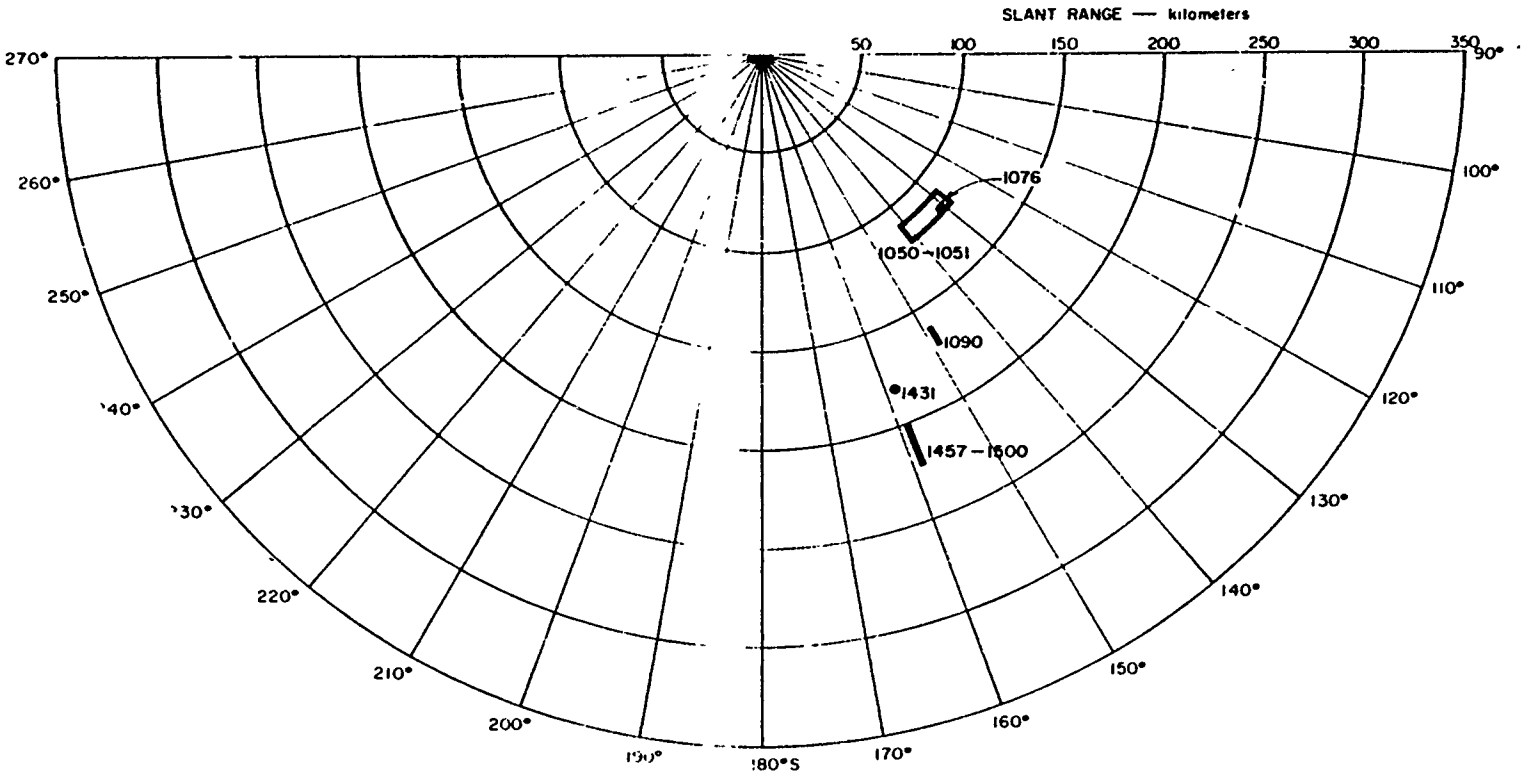

Figure 3.35 Johnston Island radar range versus azimuth for Blue Gill; 1210-Mc southern echoes, 900 to 1,500 seconds.

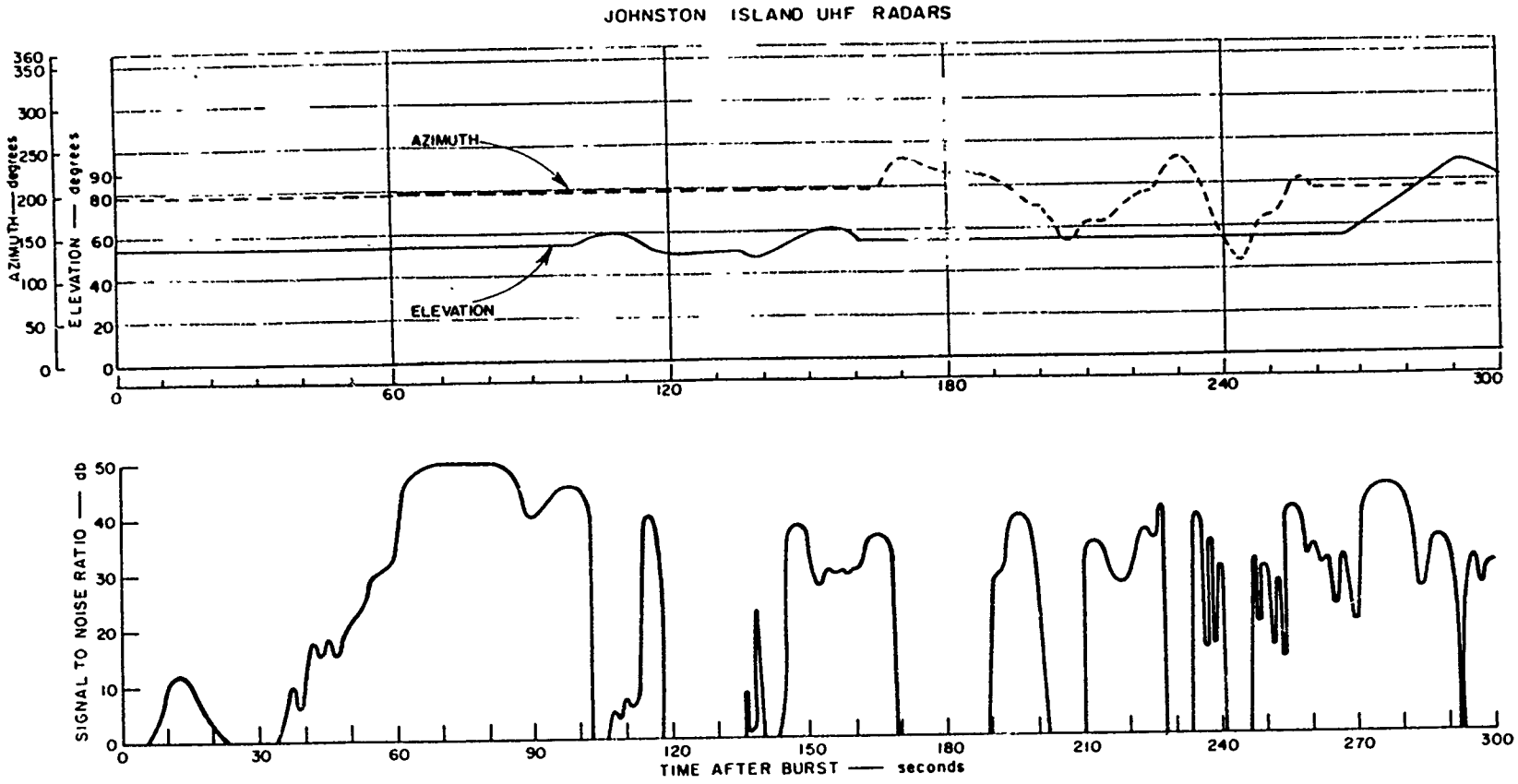

Figure 3.36 Johnston Island radar echo amplitude versus time for Blue Gill; 398 Mc, 0 to 300 seconds.

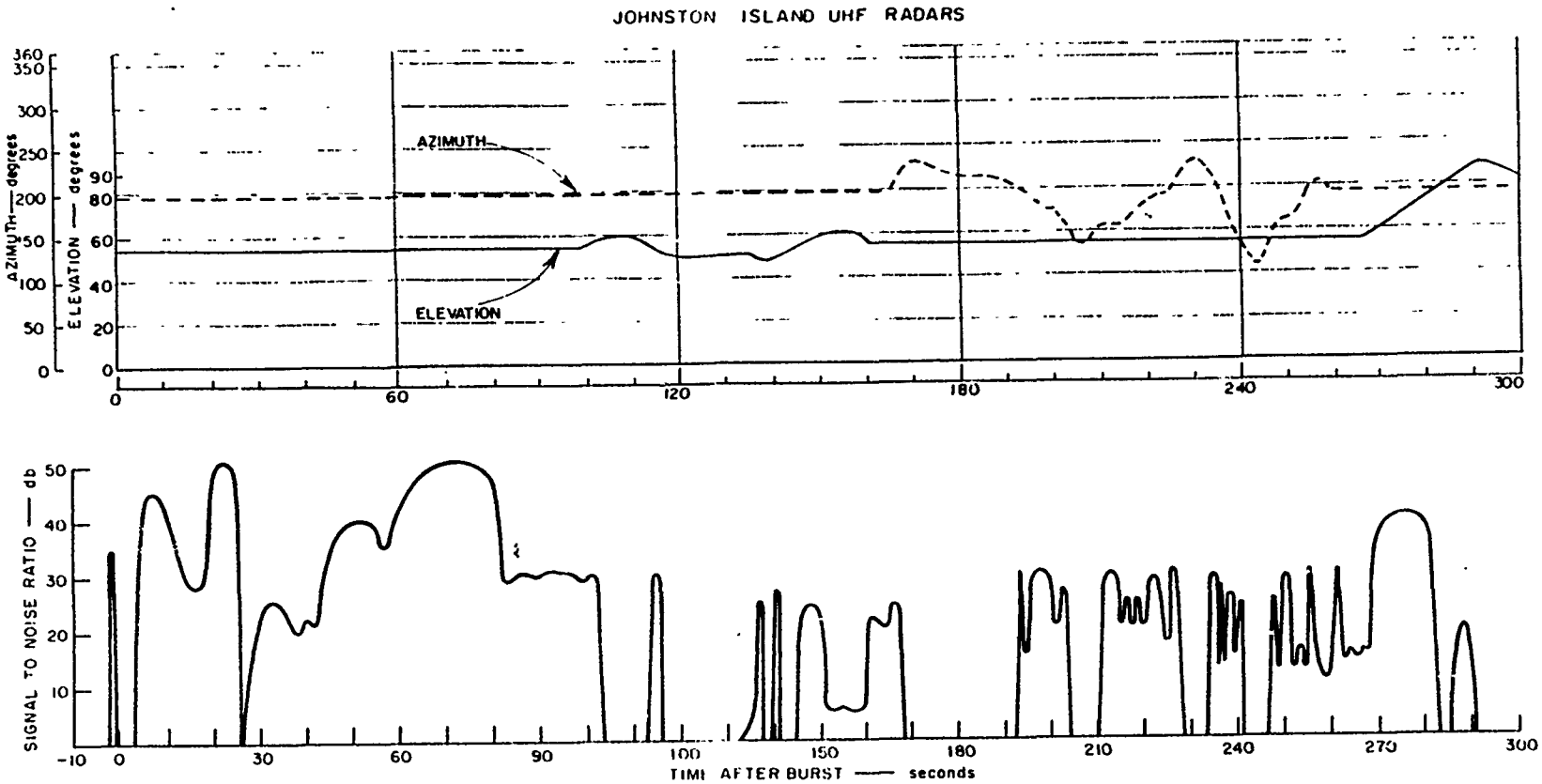

Figure 3.37 Johnston Island radar echo amplitude versus time for Blue Gill; 850 Mc, 0 to 300 seconds.

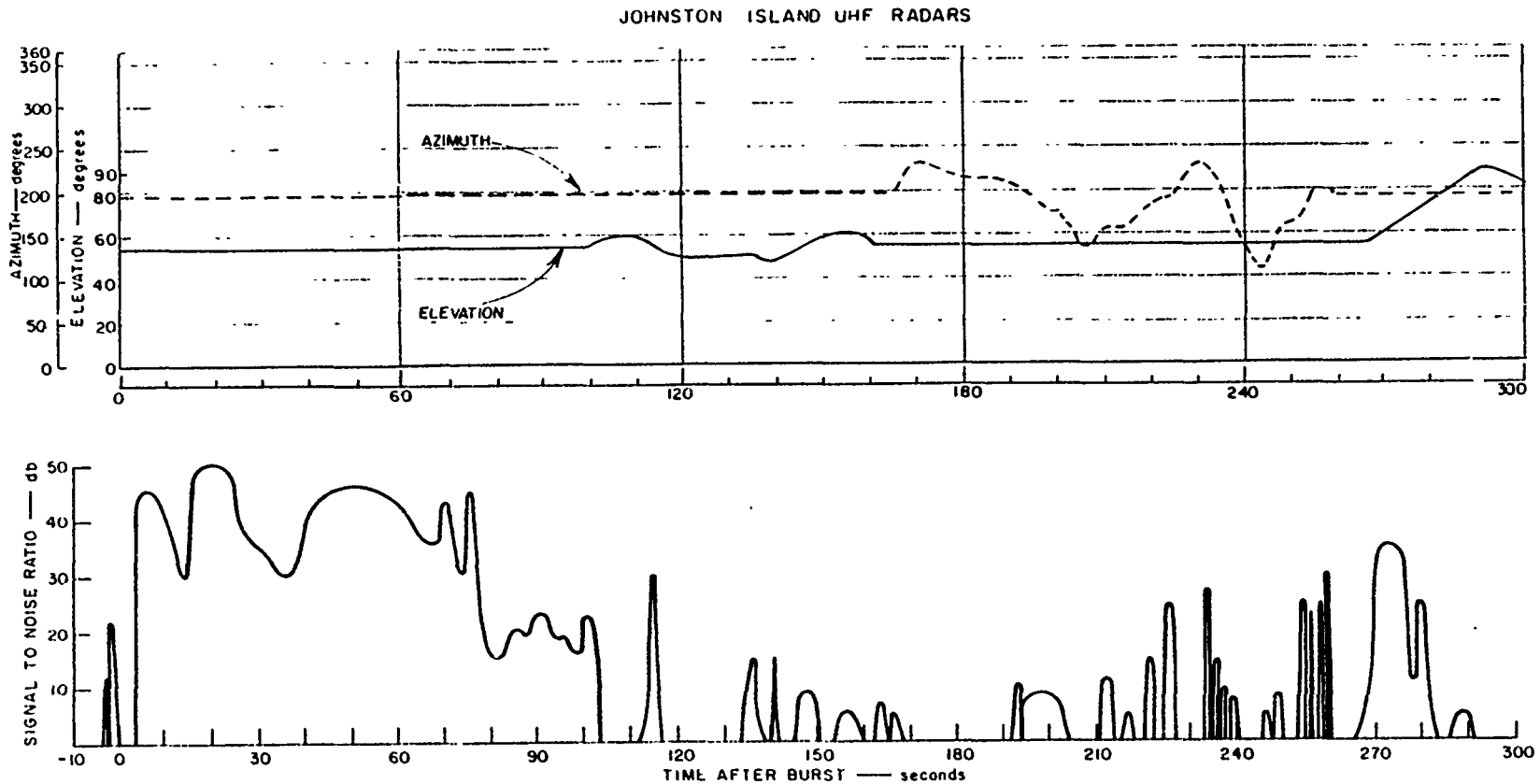

Figure 3.38 Johnston Island radar echo amplitude versus time for Blue Gill; 1210 Mc, 0 to 300 seconds.

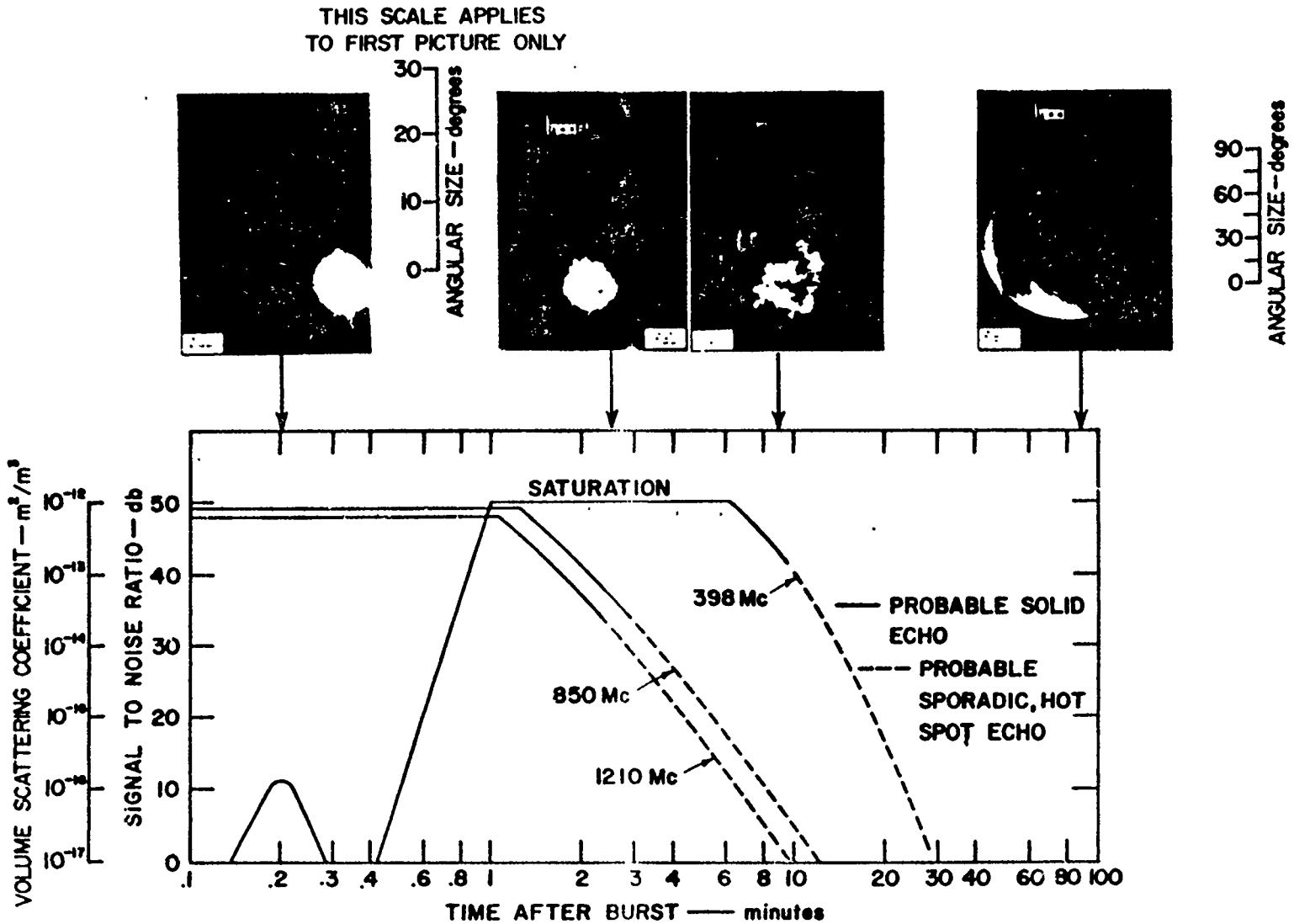

Figure 3.39 Johnston Island radar echo amplitude versus time for Blue Gill; 398, 850, and 1210 Mc.

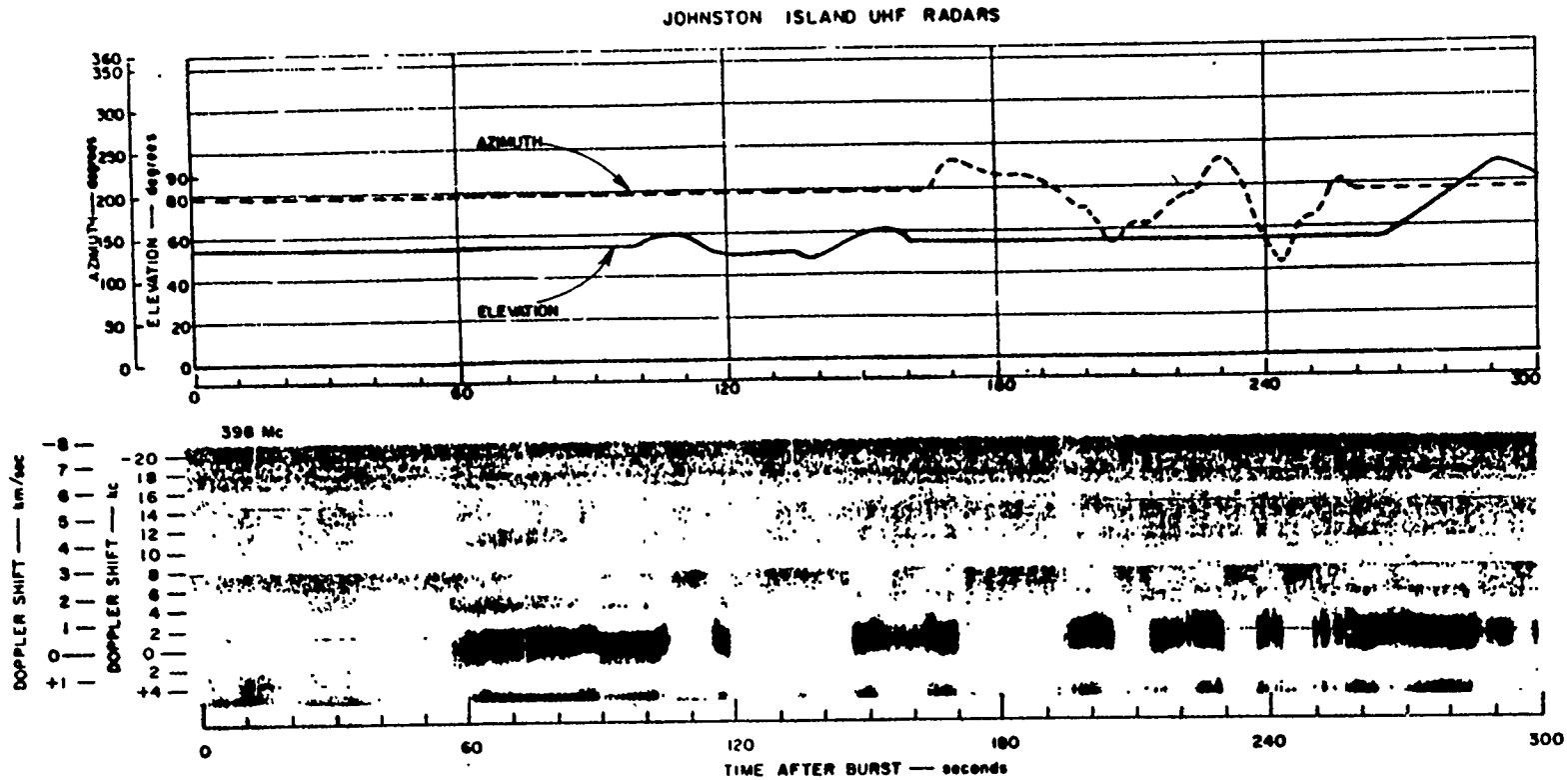

Figure 3.40 Johnston Island radar Doppler versus time for Blue Gill; 398 Mc, 0 to 300 seconds.

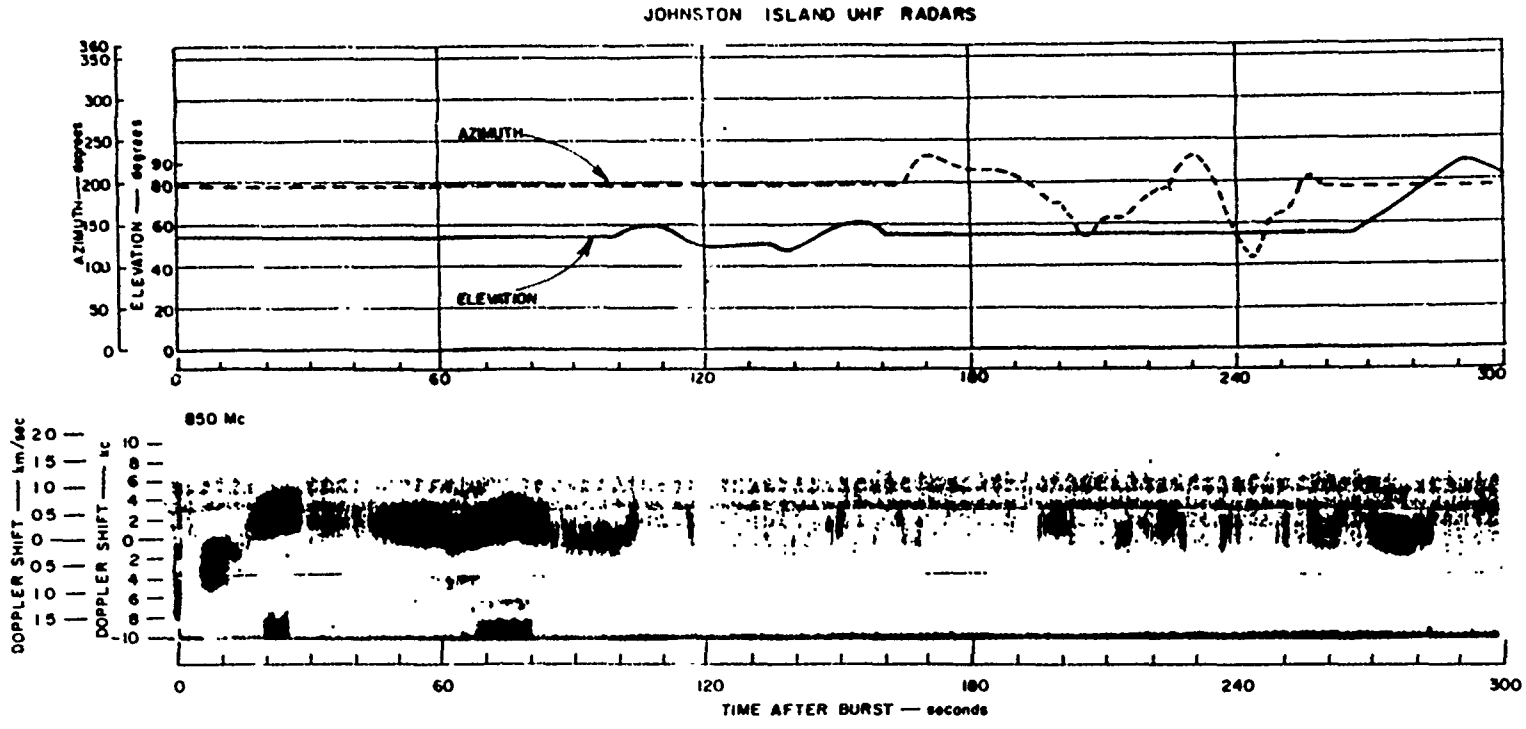

Figure 3.41 Johnston Island radar Doppler versus time for Blue Gill; 850 Mc, 0 to 300 seconds.

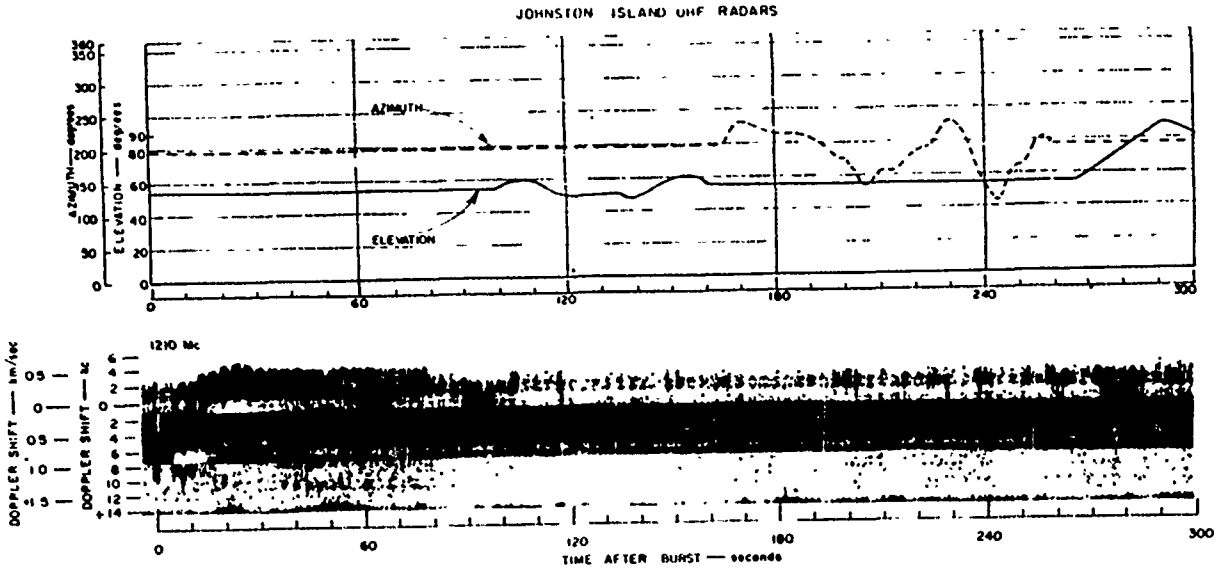

Figure 3.42 Johnston Island radar Doppler versus time for Blue Gill; 1210 Mc, 0 to 300 seconds.

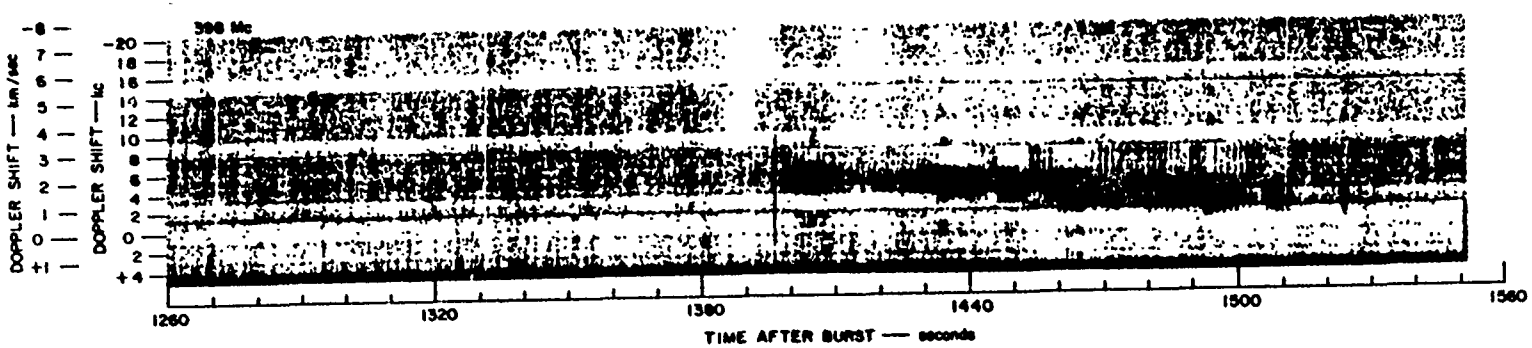

Figure 3.43 Johnston Island radar Doppler versus time for Blue Gill; 398 Mc, 1,260 to 1,560 seconds.

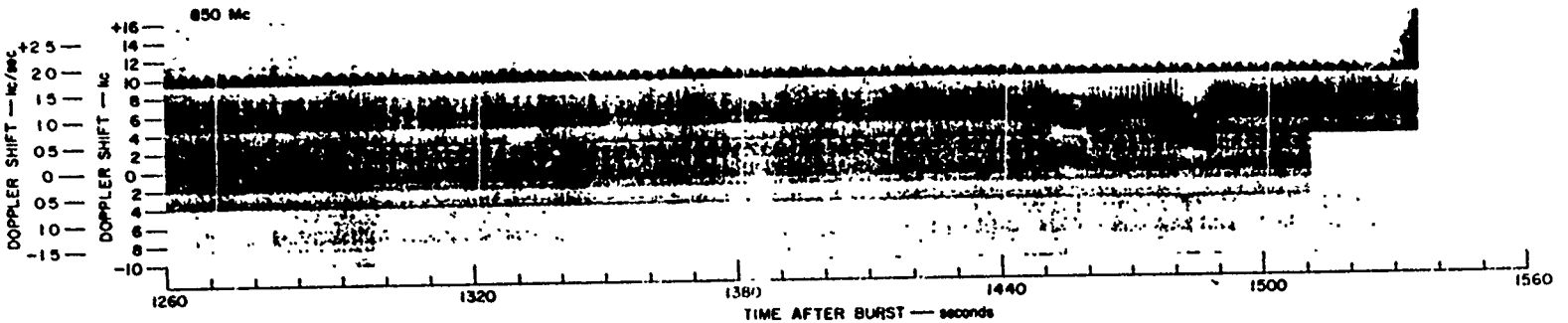

Figure 3.44 Johnston Island radar Doppler versus time for Blue Gill; 850 Mc, 1,260 to 1,560 seconds.

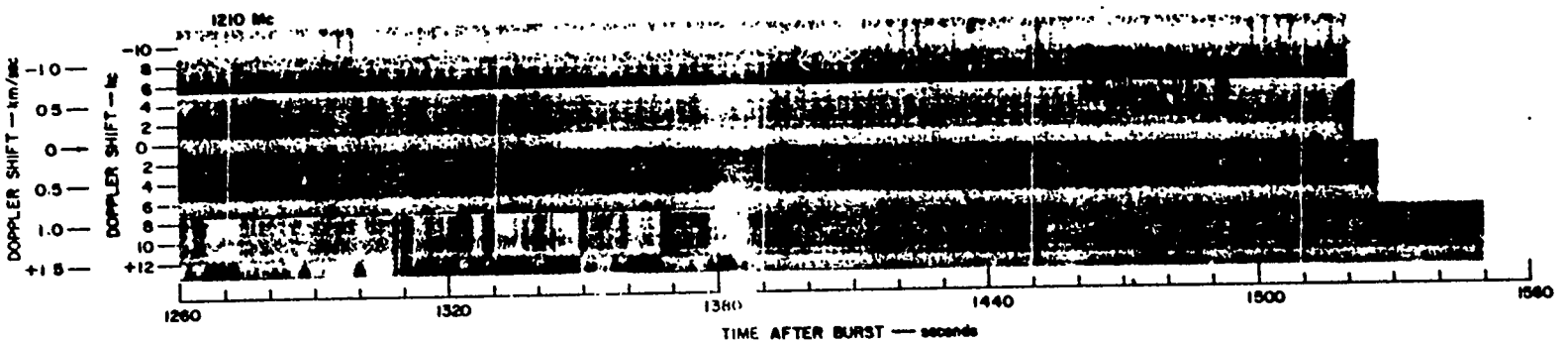

Figure 3.45 Johnston Island radar Doppler versus time for Blue Gill; 1210 Mc, 1,260 to 1,560 seconds.

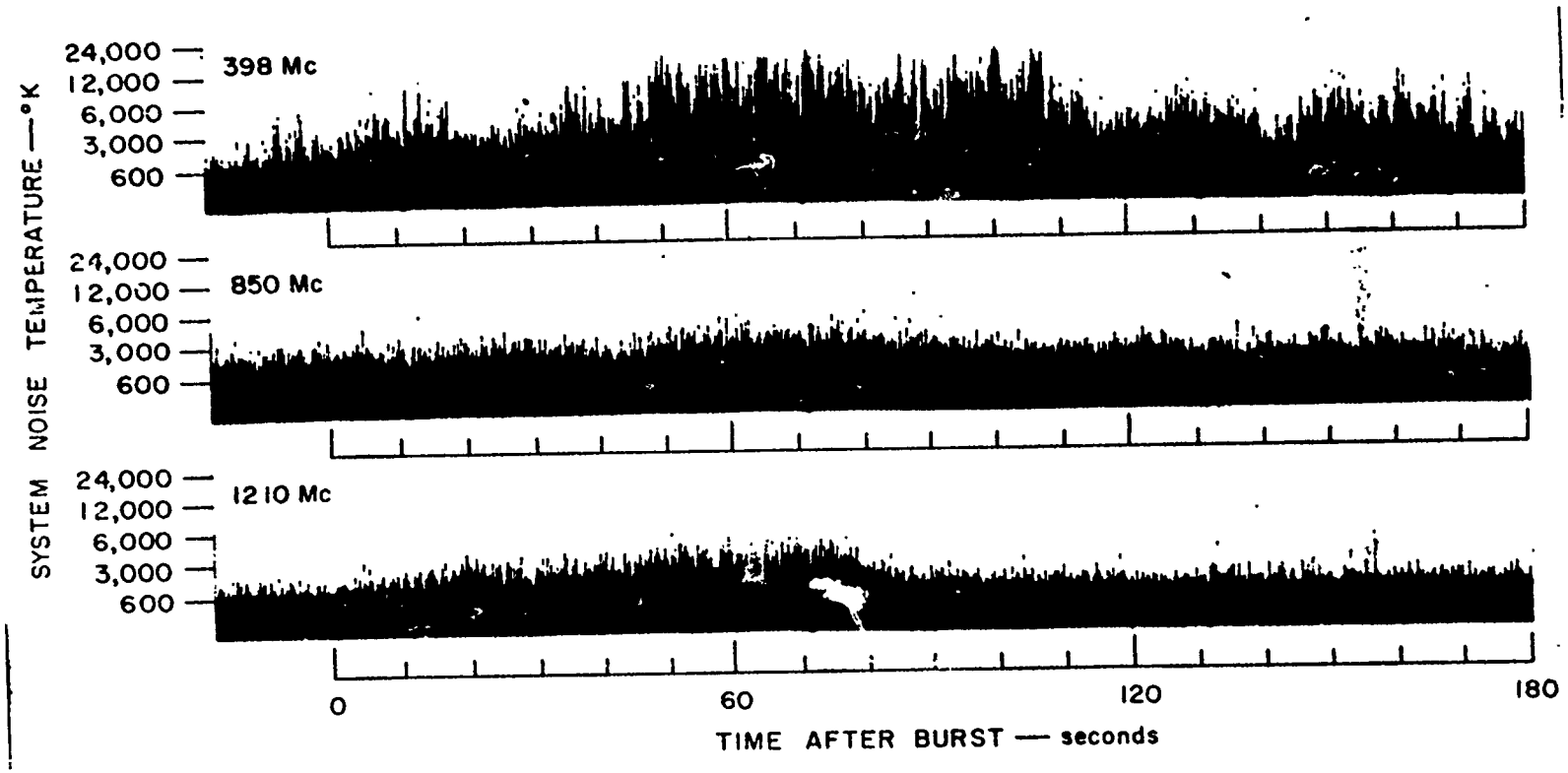

Figure 3.46 Johnston Island radar noise levels for Blue Gill.

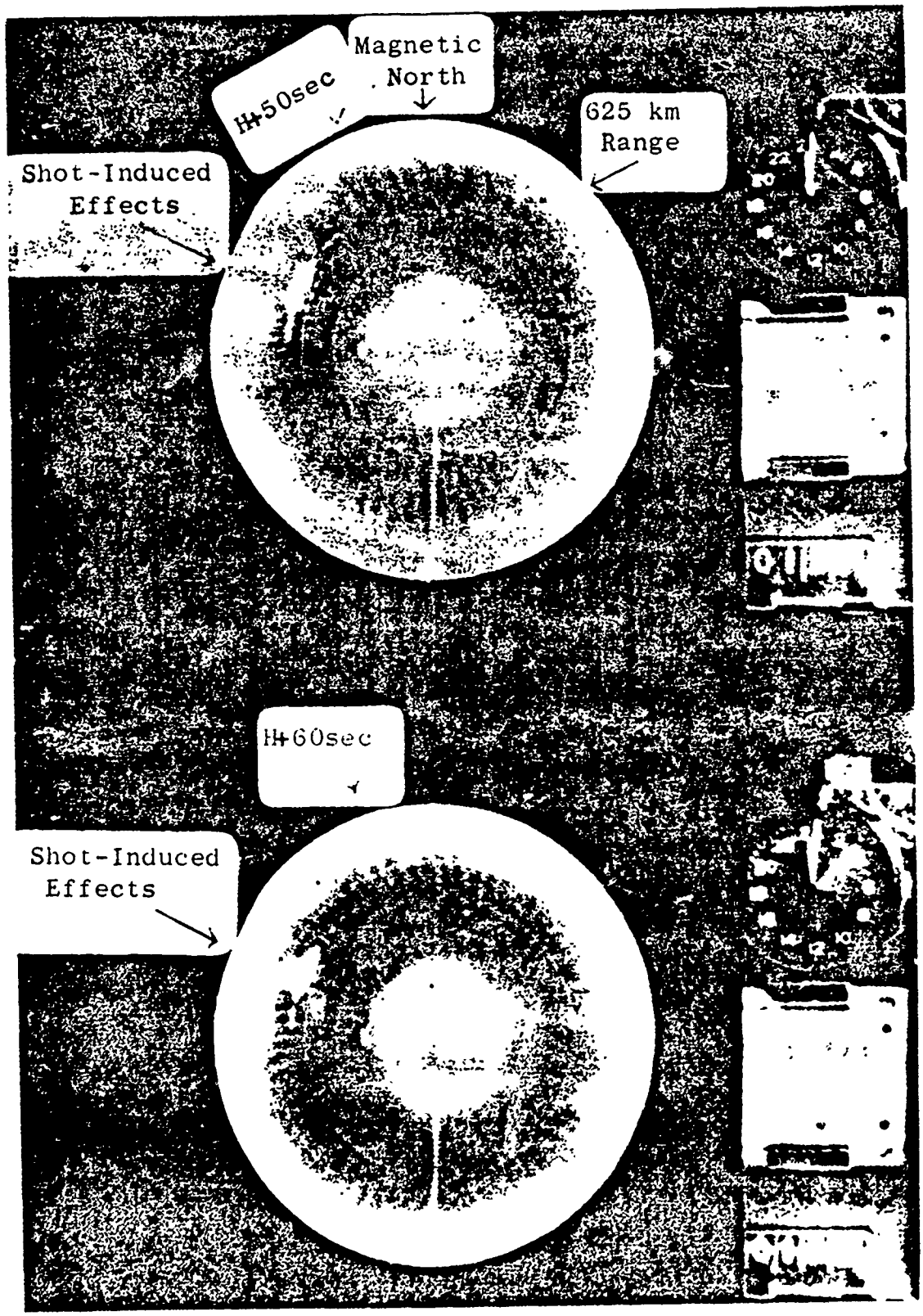

Figure 3.47 AEW aircraft radar and PPI for Blue Gill; Lambkin 2, 50 to 60 seconds.

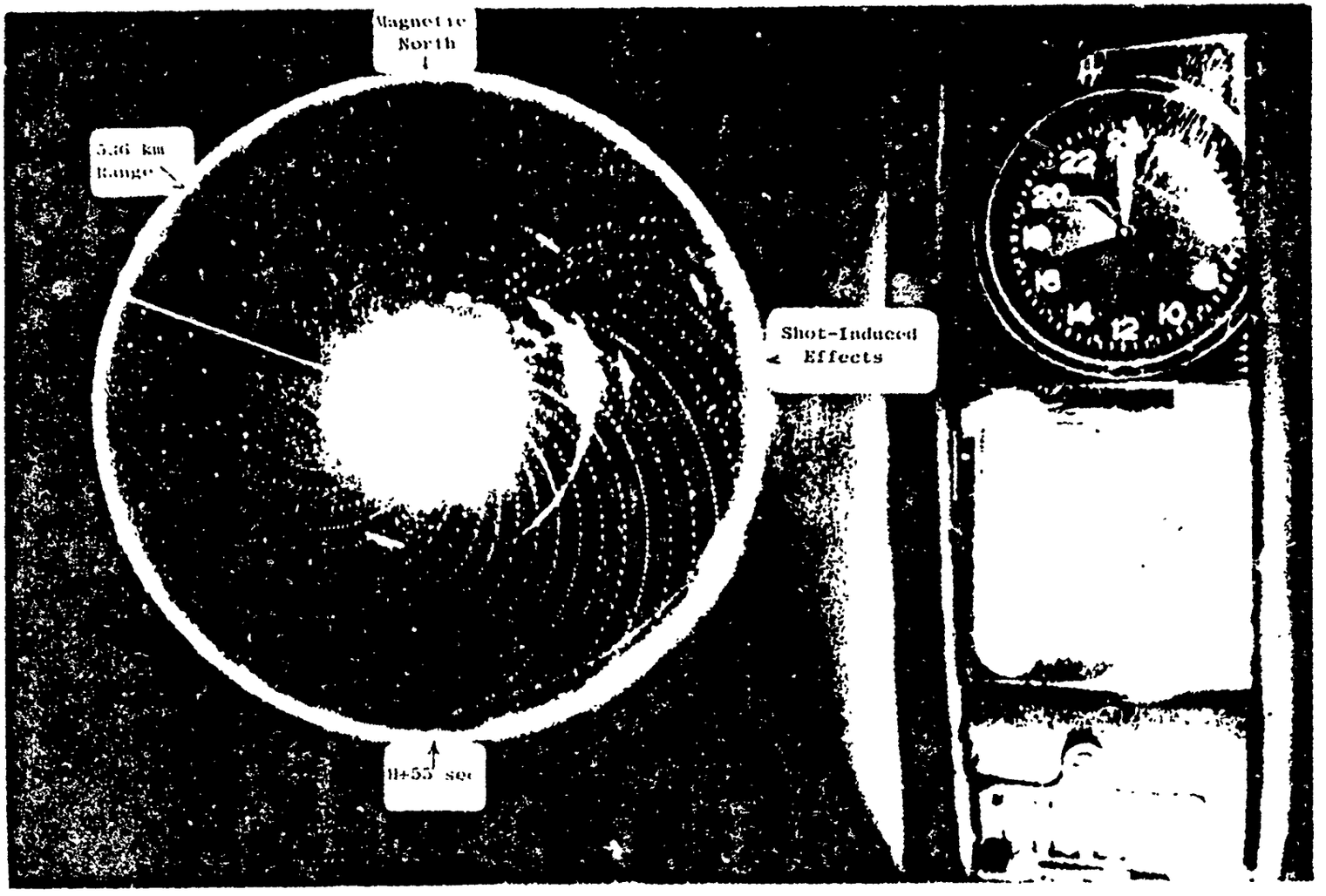

Figure 3.48 AEW aircraft radar and PPI for Blue Gill; Abusive I, 55 seconds.

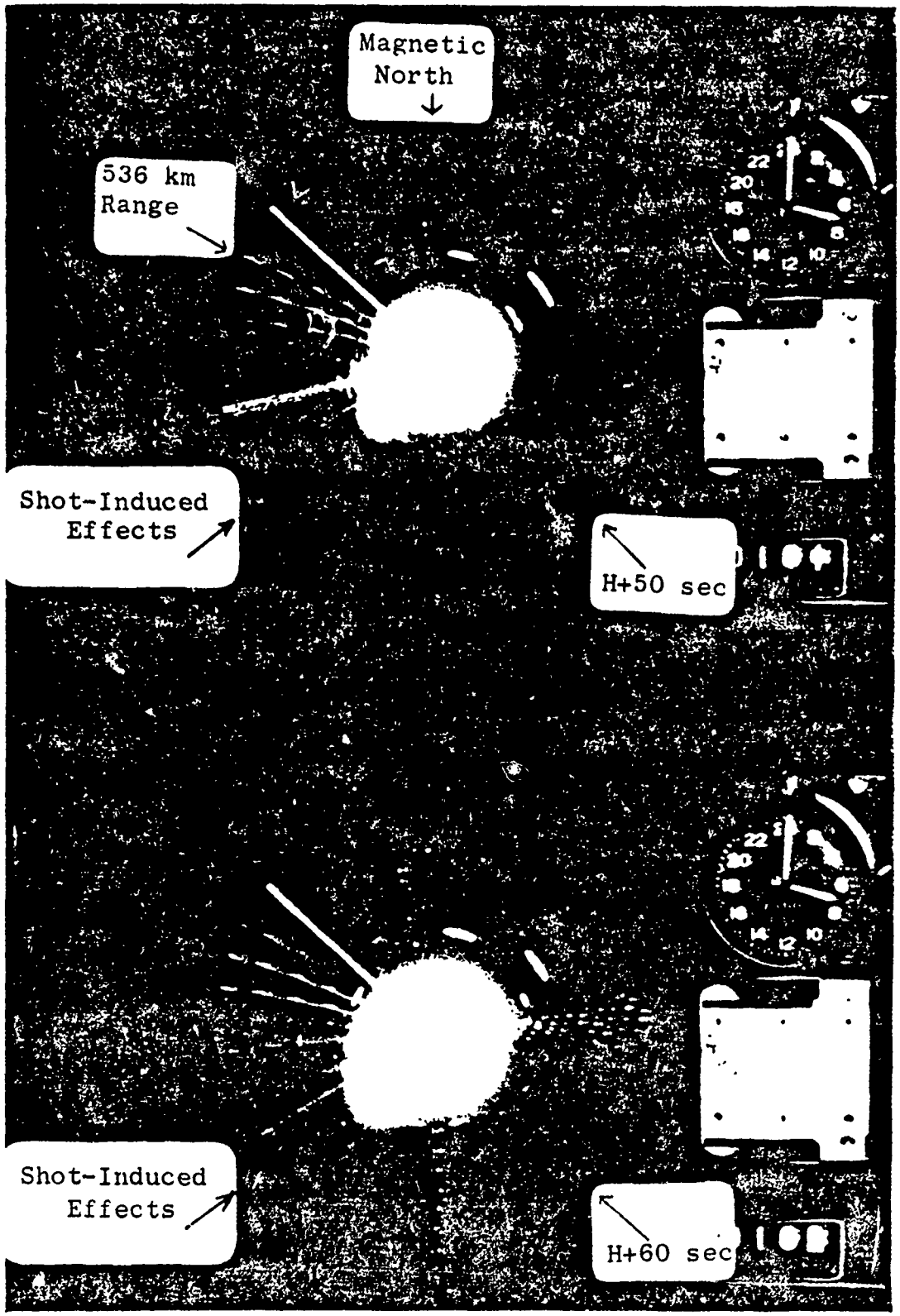

Figure 3.49 AEW aircraft radar and PPI for Blue Gill; Abusive 2, 50 to 60 seconds.

CHAPTER 4

KING FISH

4.1 INTRODUCTION

In many qualitative ways, King Fish was expected to have a behavior similar to Shot Teak of Operation Hardtack.[1] That is, a rapidly expanding fireball was expected to occur, and, due to the buoyancy of the atmosphere, the fireball was expected to rise quite rapidly.

The initial size of the fireball was estimated to be about

The rise rate of the fireball was expected to be between 2.5 and 7 km/sec. The rising fireball was expected to reach a maximum altitude of about 500 km in a period of time of about 6 minutes.

The electron density in the fireball region was expected to be great enough to give rise to UHF echoes. It was not certain as to how long such echoes could be seen, due to the rapidly growing size of the fireball which would decrease the overall electron density.

The initial height of the King Fish burst was such that prompt beta auroral effects were expected in the area north of the detonation and in the magnetic conjugate area. It was believed that these beta auroral regions would expand and move north in the detonation area and south in the magnetic conjugate area. Thus, prompt burst-area auroral clutter and conjugate-area auroral-clutter echoes were expected to occur.

---

[1] See Volume 1 for a more complete discussion of the expected results.

As the rising fireball containing debris reached maximum altitude, the spreading debris was expected to produce long-lasting auroral clutter in the area north of Johnston Island and in the magnetic conjugate area.

4.2 PROCEDURE

4.2.1 Johnston Island Radars.

Instrumentation. See Section 2.2.1.

Operating Technique. See Section 2.2.1.

4.2.2 AEW Aircraft Radars.

Instrumentation. See Section 2.2.2.

Operating Technique. Based upon the expected results, the four AEW aircraft radars[2] were located as shown in Figure 4.1 so that the expanding and northward-moving beta-produced auroral area could best be observed. The two control aircraft, Abusive 1 and Abusive 2, were located by control criteria. The project aircraft, Lambkin 1 and Lambkin 2, were located so as to provide information on the rising fireball by observing the beta aurora. Lambkin 1 was located looking at H = 100 km perpendicular to the magnetic field line above the detonation. Lambkin 2 was located looking at H = 100 km perpendicular to the magnetic field line passing through H = 300 km directly above the detonation.

---

[2] Due to operational decisions not connected with these tests, all AEW aircraft were located in the northern area and none were in the magnetic conjugate area.

All of the aircraft flew in patterns shown in Figure 2.8 at locations given in Table 4.1. The actual radar operating parameters are shown in Table 4.2.

4.2.3 M/V ACANIA Radars.

Instrumentation. See Section 2.2.3.

Operating Technique. The ACANIA was located to look perpendicular to the H = 100 km point on the field line that passed through the detonation as shown in Figure 4.2. The ACANIA location was adjusted to take into account the difference between the measured magnetic conjugate point and the computed conjugate point that was determined from the previous tests.

The exact location of the ACANIA is shown in Table 4.1. The radar operating technique is given in Section 2.2.3.

4.3 RESULTS

4.3.1 Johnston Island Radars.

Fireball/Debris Clutter. Prior to the detonation, the radar executed a programmed track of the Thor launch, and the 850- and 1210-Mc radars obtained skin echoes during the entire trajectory. The 398-Mc radar was off until detonation. Shortly before the detonation the antenna was positioned at 53° elevation and 192° azimuth. The detonation occurred in the radar beam. However, no echoes were observed until H + 2 seconds when echoes appeared at all three frequencies simultaneously. At about H + 20 seconds all the echoes faded out as the fireball moved out of the beam of the

stationary antenna. At H + 60 seconds the antenna was scanned up in elevation to catch up with the fireball. At that time echoes were observed at all frequencies from 60 to 90° elevation. Echoes were observed on all frequencies overhead until about H + 200 seconds. During the first five minutes following the detonation there was good correlation between the visual bright areas and the UHF radar echoes. After H + 15 minutes the antenna was scanned either manually or with the automatic programmer eight hours following the detonation.

Starting abruptly at H + 2 seconds, echoes at 120-km range saturated all three receivers at 50 db S/N. The 398-Mc echo persisted until H + 30 seconds. The 850- and 1210-Mc echoes persisted until H + 15 seconds as the fireball moved out of the radar beam. The range-versus-time records of the echoes for the first thirty minutes are shown in Figures 4.3 through 4.9. The spatial distribution of all the detonation-area echoes as well as the visual fireball/debris is shown in Figures 4.10 through 4.15. The echo amplitude-versus-time records for the first five minutes are shown in Figures 4.16 through 4.18. The echo amplitudes versus time, with antenna-direction-caused fluctuations removed, are shown in Figure 4.19. Starting abruptly at H + 3 seconds, echoes at 250-km range reached amplitudes of 40 to 50 db at each frequency. These echoes corresponded to a one-hop sea-reflection mode and persisted only for 10 to 15 seconds. During the elevation scan from 60 to 90° elevation following H + 60 seconds, several 40 db S/N

echoes were observed at various ranges. The echoes observed until H + 200 seconds comprised about 90 percent of the total number of echoes seen in the detonation area. No detonation-area echoes were observed later than H + 20 minutes.

Figures 4.20 through 4.22 show the Doppler records for the first five minutes following the detonation at each frequency. The 398-Mc record shows both positive and negative shifts and a broad spread during the first 20 seconds. Following that time the echoes are much less disturbed. The 850- and 1210-Mc records show smaller positive and negative shifts and a more narrow spread during the first 20 seconds.

Auroral Clutter in the Detonation Area. The Johnston Island 398- and 850-Mc radar saw extensive beta-produced auroral clutter to the north of Johnston Island. The spatial distribution of these echoes is shown in Figures 4.23 through 4.34, and are limited to height of 200 to 750 km. The 398-Mc auroral clutter lasted until H + 2 hours 55 minutes. The 850-Mc auroral clutter lasted until H + 96 minutes. No auroral clutter was observed at 1210 Mc. The echo amplitude versus time, with antenna-direction-caused fluctuations removed, is shown in Figure 4.35.

Figure 4.36 shows the Doppler record of a strong auroral clutter echo on the 398-Mc radar at H + 660 seconds. The record shows that the frequency shift is 1 kc or less, and the spread does not exceed the 3-db frequency spread of a normal 300-μsec RF pulse. Thus, the characteristics of the detonation-produced auroral echoes are identical with naturally produced auroral echoes.

Fireball/Debris Noise. Radio noise emission was observed by the 398-, 850-, and 1210-Mc radars looking at the fireball/debris. The noise was most intense on the 1210-Mc radar and was equivalent to about 7000°K. This amounted to about a 10-db increase in background noise. The noise as seen on these radars lasted until about H + 20 seconds, when the fireball rose out of the beam of the antenna. The noise-level increases are shown in Figure 4.37 for each of the frequencies.

4.3.2 AEW Aircraft Radars.

Fireball/Debris Clutter. Each of the detonation-area AEW aircraft (Lambkin 1 and 2, Abusive 1 and 2) observed echoes from air zero in the burst area as shown in Figures 4.38 through 4.43. The detonation-area echoes started at about H + 5 seconds and lasted until about H + 50 seconds. Table 4.3 gives the duration of these detonation-area echoes and the equivalent radar cross section in m^2 (based upon a point target) and, when applicable, in m^2/m^3 (based upon a volume scatterer).

Auroral Clutter in the Detonation Area. Each of the detonation-area AEW aircraft observed auroral clutter as shown in Figures 4.38 through 4.43. The auroral clutter began at about H + 65 seconds and lasted until about H + 195 seconds. Table 4.4 tabulates the times and radar cross sections for the echoes observed.

4.3.3 M/V ACANIA Radars.

Auroral Clutter in the Conjugate Area. The M V ACANIA operated its 140- and 370-Mc radars during the detonation and

for several hours afterwards. The antenna was positioned magnetically south in azimuth and 60° elevation, and periodically elevation scans were made. The adjustment in the ACANIA location mentioned earlier was justified by the H + 0, 140-Mc, and 370-Mc echoes observed, as these echoes corresponded quite closely to the magnetic field line based upon previous test results. From H + 30 to H + 110 seconds, 370-Mc echoes were again seen at this position. The range-versus-time records for the first 17 minutes are shown in Figures 4.44 through 4.47. The early-time (H + 0) 140-Mc echoes were equivalent to a radar cross section of 2000 m^2. From H + 20 to H + 160 seconds, the 140-Mc echoes had a radar cross section of about 600 m^2. In addition to the 140-Mc echoes seen on the magnetic field line passing through the burst location, 140-Mc echoes were seen at 250-km height from H + 7 to H + 220 seconds with radar cross sections of 10 m^2, and 300-km height from H + 130 to 740 seconds. From H + 200 to H + 600 seconds 140-Mc echoes were seen at heights above 500 km. The spatial location of these echoes is shown in Figure 4.48.

4.4 DISCUSSION

The Johnston Island radar returns of 50 db S/N correspond to a 2×10^{-12} m^2/m^3 volume-scattering density (beam and pulse length filling target). A point target of 1 m^2 cross section at King Fish range would give a 50 db S/N. If the 50 db S/N scattering were assumed to be due to incoherent electron scattering, then a density of 10^{11} electrons cm^3 would be required. This electron density has

a plasma critical frequency of about 2500 Mc. It is therefore assumed that the observed 50-db S/N returns must be due to some mechanism other than incoherent electron scatter.

Likely candidates to explain the observed debris/fireball clutter are critically overdense reflections with some path absorption, or possibly underdense, coherent reflections from blobs of varying electron density, similar to auroral returns but not field-aligned. When the S/N ratio had dropped to 30 db (about H + 2 seconds), incoherent electron scatter would require an electron density of about 5×10^6 electrons/ cm^3. This density corresponds to a critical frequency of about 200 Mc. In this case incoherent returns are possible at frequencies of 400 through 1200 Mc. However, with a terribly disturbed magnetic field in the debris/fireball, field-aligned clutter is also possible even though the undisturbed radar-magnetic field geometry would seem to have precluded this possibility.

4.5 CONCLUSIONS

To evaluate the seriously degrading effect of King Fish on the performance of a ballistic missile defense radar system, a comparison has been made between the radars used during Fish Bowl and the planned BMD radar systems.

The radars used during these tests were, in general, somewhat less sensitive than those being planned for use in BMD activities. The advantage that a particular system radar would have over the test

radars is shown for various scattering models in Table 2.6 of Chapter 2 of this volume. The comparisons were developed by scaling the system radar to its nearest frequency counterpart used during Fish Bowl. For example, the BMEWS radars were compared with the 398-Mc Johnston Island radar and the Nike-Zeus TTR radar was compared to the DAMP FPQ-4 C-band radars.

In order to give the reader a better understanding of the degrading effects of the King Fish event, an estimate of the effect on the BMEWS tracking radar has been made, ignoring the fact that the operating pulse length of the BMEWS radar is too long to observe King Fish fireball/debris clutter at that range. The BMEWS system was picked as an example not to deprecate that particular system, but because that system is operational, field-deployed, and its characteristics are well known. Table 2.7 of Chapter 2 of this volume shows the comparison between the BMEWS tracking radar characteristics and the Johnston Island 398-Mc radar. The comparison was made assuming the scattering was from a beam-filling target of range depth of at least one pulse width (300 μsec).

From the comparison, estimates of the strength and time duration of the clutter and noise effects are given below:

Fireball/Debris Clutter.

H + 0 .	S/N = 90 db	Main Beam
	S/N = 40 db	Side Lobes

Fireball/Debris Clutter.(Continued)

H + 1 min	S/N = 80 db	Main Beam
	S/N = 30 db	Side Lobes
H + 2 min	S/N = 70 db	Main Beam
	S/N = 20 db	Side Lobes
H + 5 min	S/N = 40 db	Main Beam
	S/N = 0 db	Side Lobe
?	S/N = 0 db	Main Beam
	S/N = 0 db	Side Lobe

Angular Diameter of Affected Region.

5 sec	12^{o}
20 sec	21^{o}
60 sec	24^{o}
120 sec	23^{o}

Penumbra-Area Auroral Clutter.

H + 0 to H + 3 hours S/N= 44 db

H - 3 hours to ?

Fireball Debris Noise.

Maximum 2000^{o} K

20 seconds duration

3-db increase

Conjugate-Area Auroral Clutter.

H + 0 to H + 2 min	S/N > 54 db
H + 2 min to H + ?	S/N = 54 db

From the above it is apparent that as much as 600 square degrees of area would be obscured for a depth of at least one pulse length

plus 50 km by the fireball/debris clutter for a period of as much as 5 minutes. In addition, the 600 square degrees of area would be observed at a 3-db reduction in sensitivity at all ranges at a 50-percent bandwidth for up to 20 seconds, because of the fireball/debris noise. Although the Doppler spread of the echoes is not severe, the limited bandwidth of the 20-kc Doppler channel used with the Johnston Island radars does not rule out the possibility of there being Doppler components at a velocity comparable to the radial velocity of an approaching ICBM.

Detonation-area auroral clutter would obscure considerable area at a variety of ranges from 100 km to 750 km for a depth of at least one pulse length for a period of up to 3 hours. However, the Doppler width would be relatively narrow.

Conjugate-area auroral clutter would obscure a relatively small area at a variety of ranges for a depth of at least one pulse length for a period of up to two minutes. The Doppler width would be relatively narrow.

The extended volume of clutter and noise produced by King Fish would make it difficult to avoid the clutter problem by using spaced radars in a BMD system, and impossible in the case where multiple King Fish type bursts occurred.

TABLE 4.1 LOCATIONS OF AEW AIRCRAFT AND M/V ACANIA DURING KING FISH

Name	Longitude	Latitude
Lambkin 1	166°16'W	14°53'N
Lambkin 2	165°35'W	18°08'N
Abusive 1	167°42'50"W	16°28'10"N
Abusive 2	168°44'00"W	17°48'10"N
ACANIA	174°50'W	12°08'S

TABLE 4.2 OPERATING CHARACTERISTICS OF THE AEW AIRCRAFT RADARS DURING KING FISH

L = Lambkin, A = Abusive.

	L1	L2	A1	A2
Frequency, Mc				
Peak Power, watts x 10^6	1.25	1.5	1.4	1.4
Pulse Width, μsec	8.5	8.4	9.0	8.9
PRF, cps	239	242	280	280
MDS, -dbm	116	113	114	115
Dynamic Range, db	21	21	15	18
σmin at 500 km, m^2	12	20	20	15

TABLE 4.3 AEW AIRCRAFT RADAR FIREBALL/DEBRIS CLUTTER FOR KING FISH

	Time from Burst (Sec)	Radar Cross Section	
		Point Target (m^2)	Volume Scatterer (m^2/m^3)
Lambkin 1	5	4.9×10^{4}	18×10^{-8}
	15 to 45	4.9×10^{6}	18×10^{-6}
	55	4.9×10^{4}	18×10^{-8}
Lambkin 2	15 to 35	6.2×10^{5}	14×10^{-7}
	45	$1.\ldots \times 10^{4}$	0.3×10^{-8}
	55	2×10^{2}	
Abusive 1	5 to 25	1.5×10^{3}	
	35	4.6×10^{2}	
	45	1.9×10^{2}	
Abusive 2	7 to 27	75	
	37	7	

TABLE 4.4 AEW AIRCRAFT BURST AREA AURORAL CLUTTER FOR KING FISH

	Time from Burst (Sec)	Radar Cross Section (m^2)
Lambkin 1	65	8.3×10^{2}
	75	100
	85	50
	95	30
	105	15
Lambkin 2	85	10
	95	25
	105	10
	115	35
	125 - 195	100
Abusive 1	55 - 75	1.3×10^{2}
Abusive 2	80 - 100	2

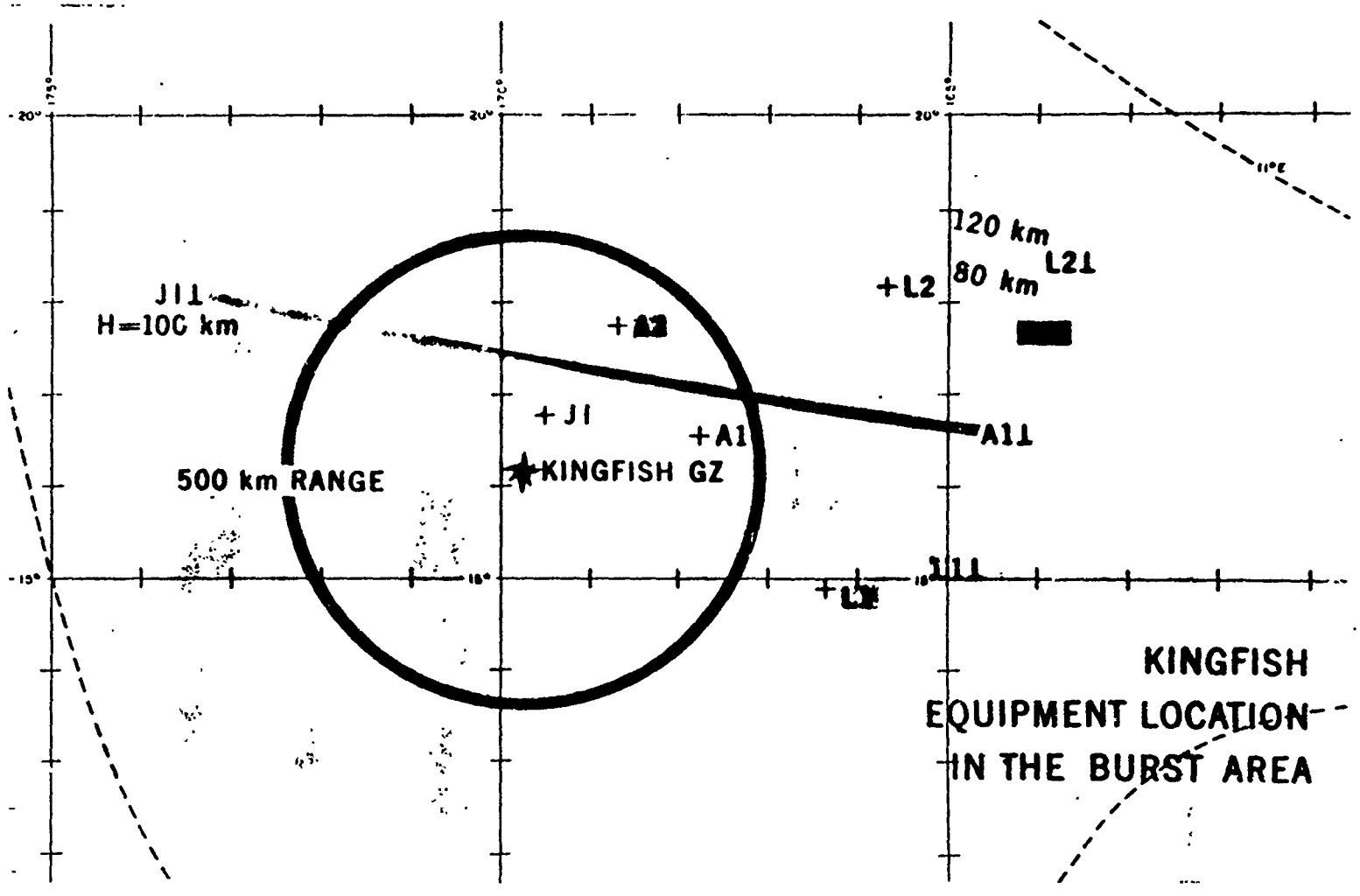

Figure 4.1 Equipment location in the detonation area for King Fish.

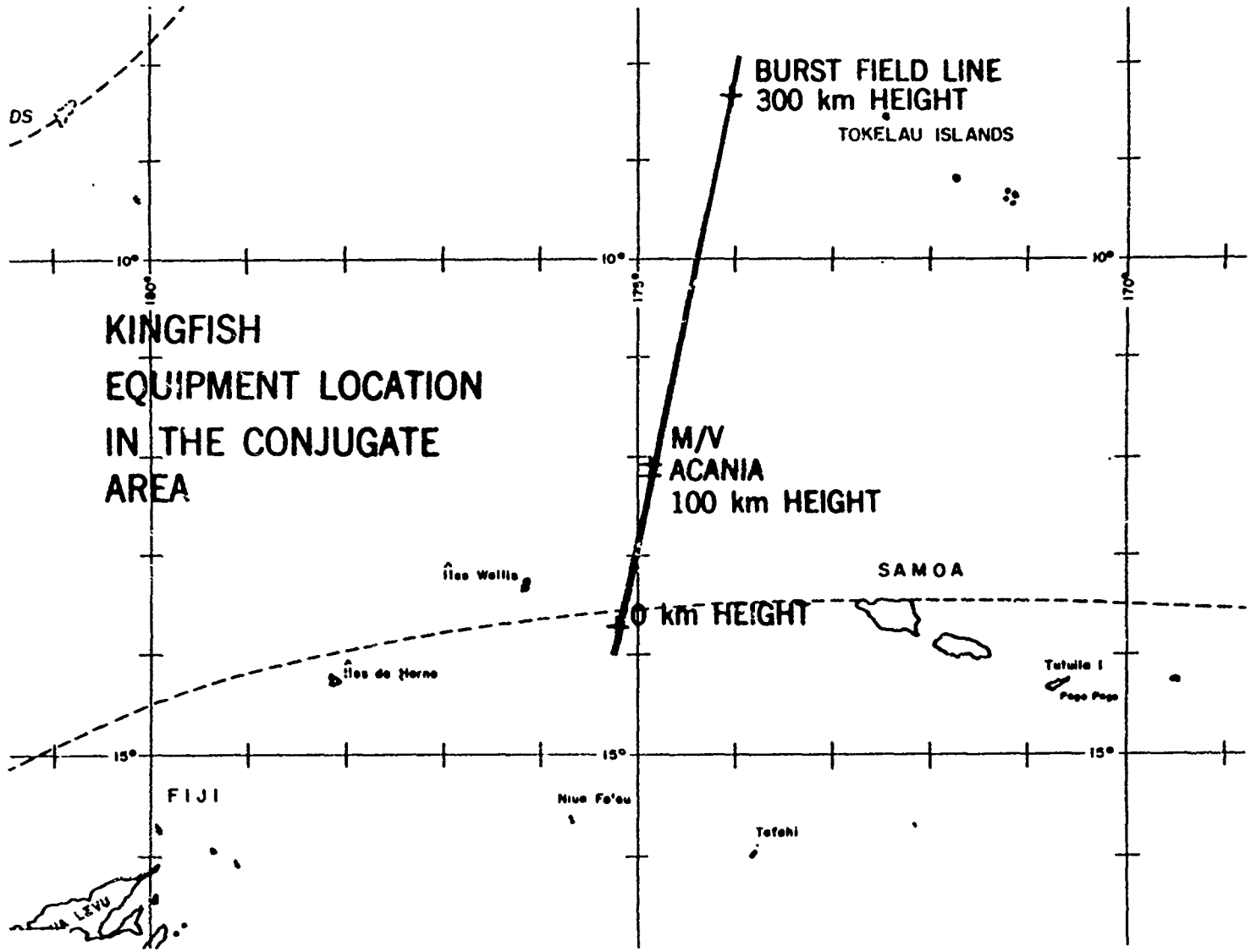

Figure 4.2 Equipment location in the conjugate area for King Fish.

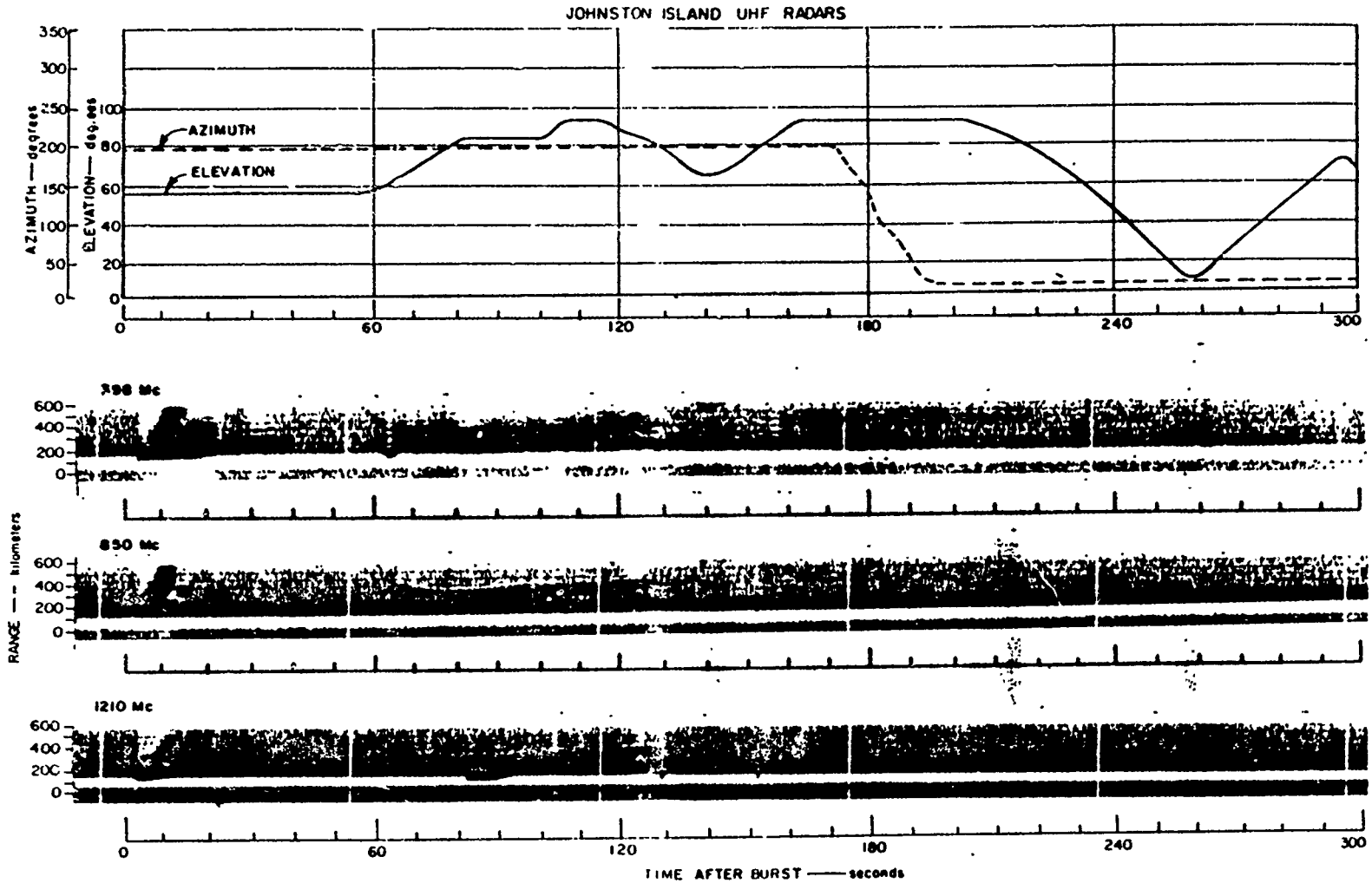

Figure 4.3 Johnston Island radar range versus time for King Fish; 0 to 600 km, 0 to 300 seconds.

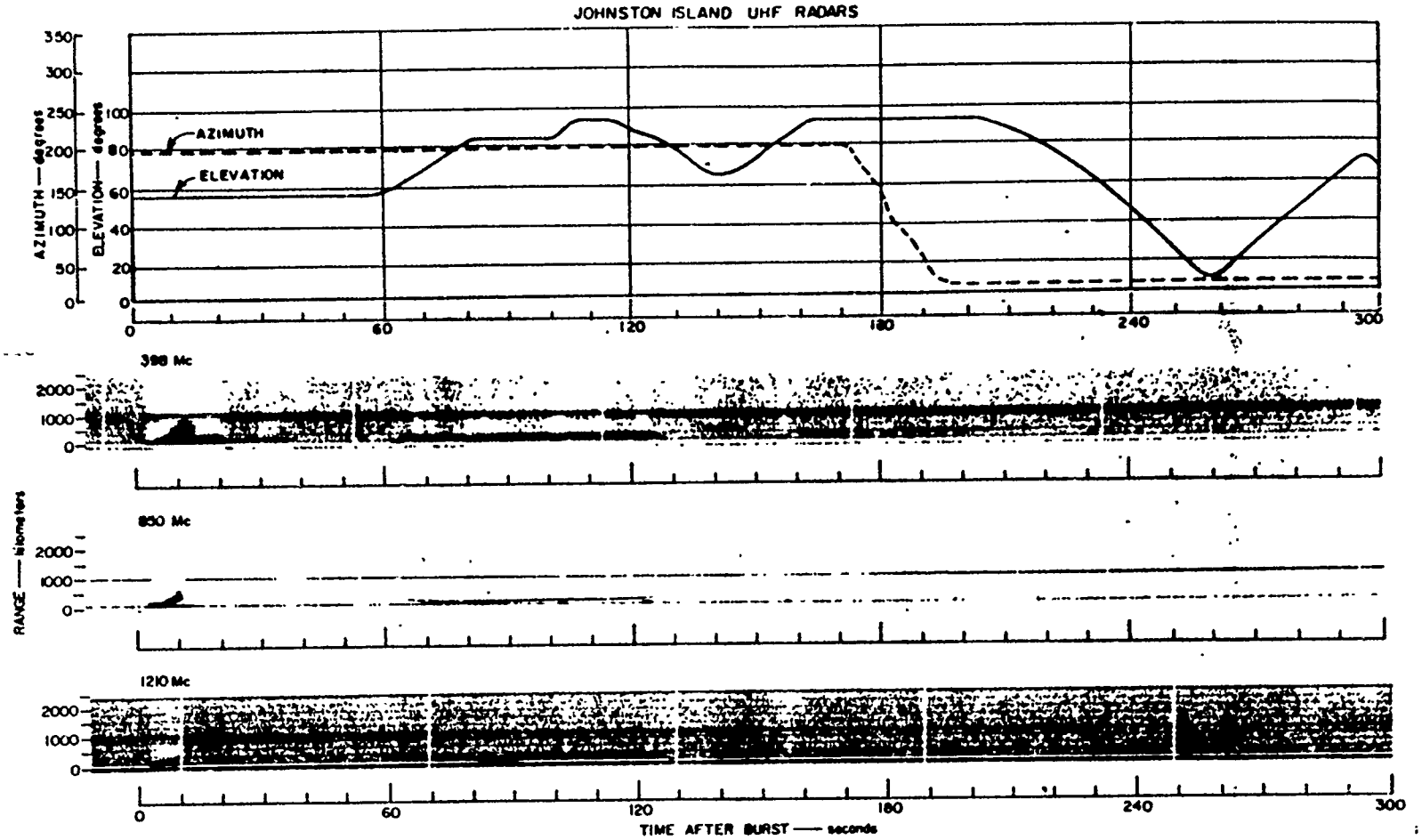

Figure 4.4 Johnston Island radar range versus time for King Fish; 0 to 2,500 km, 0 to 300 seconds.

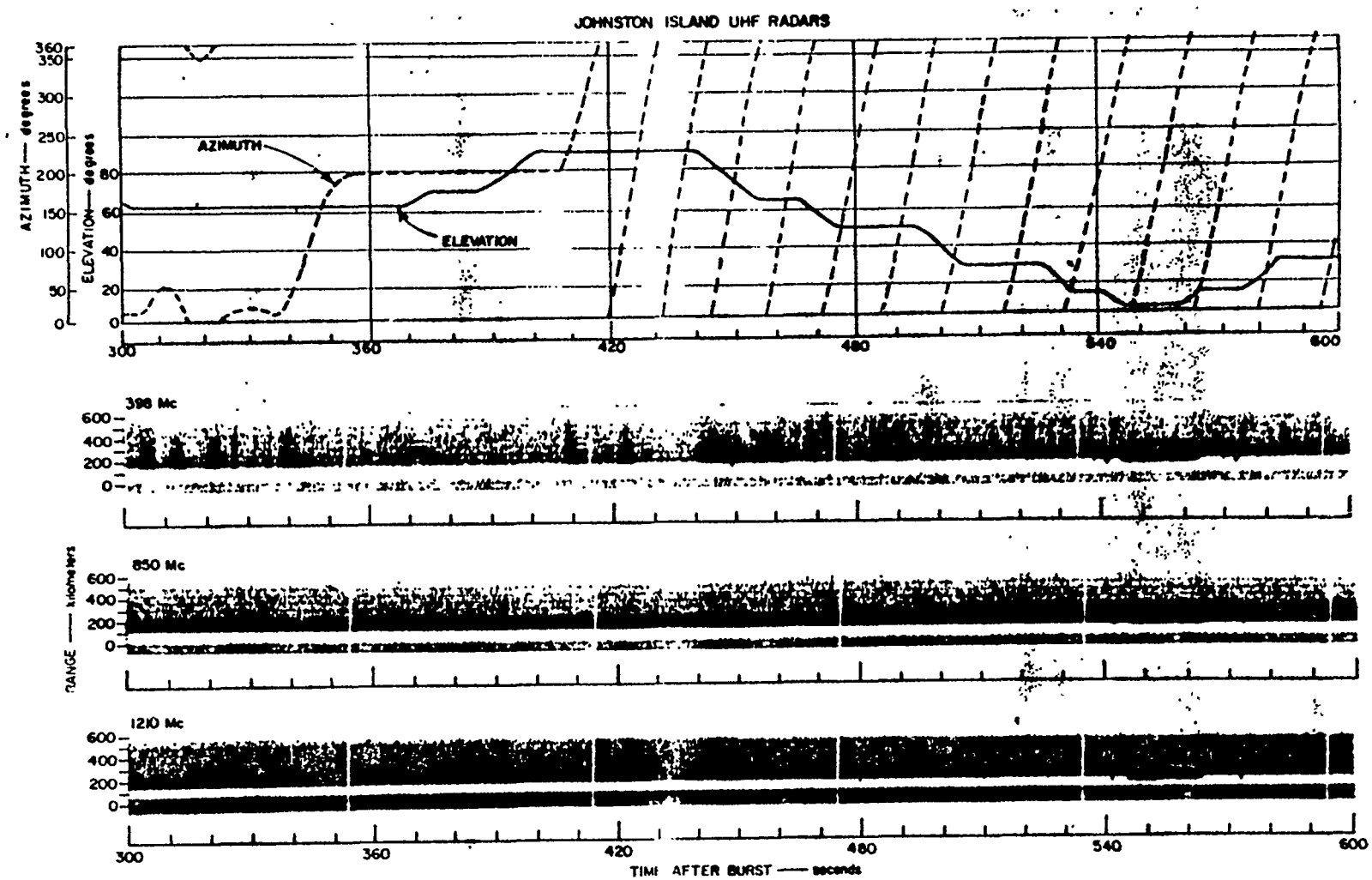

Figure 4.5 Johnston Island radar range versus time for King Fish; 0 to 600 km, 300 to 600 seconds.

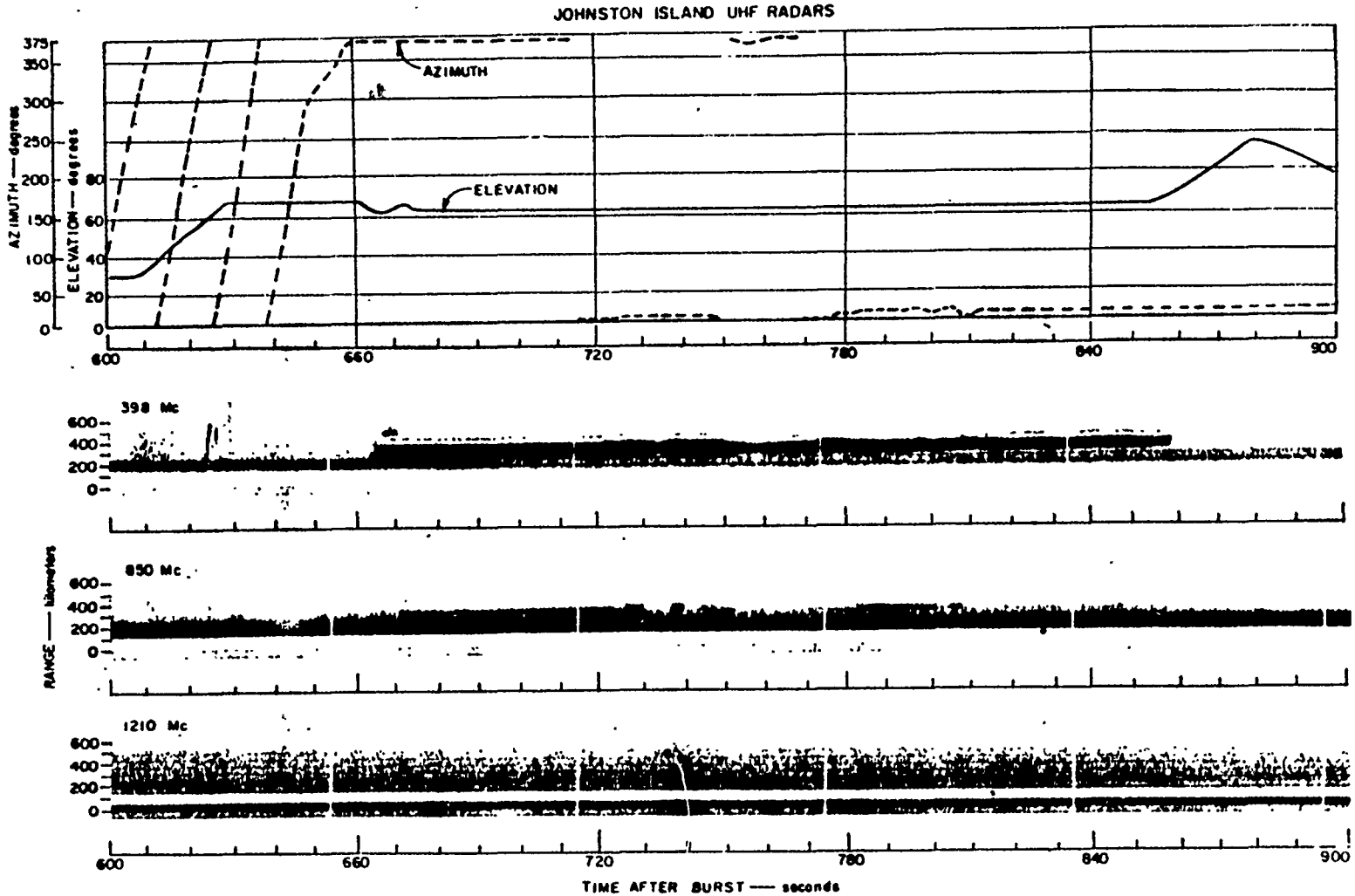

Figure 4.6 Johnston Island radar range versus time for King Fish; 0 to 600 km, 600 to 900 seconds.

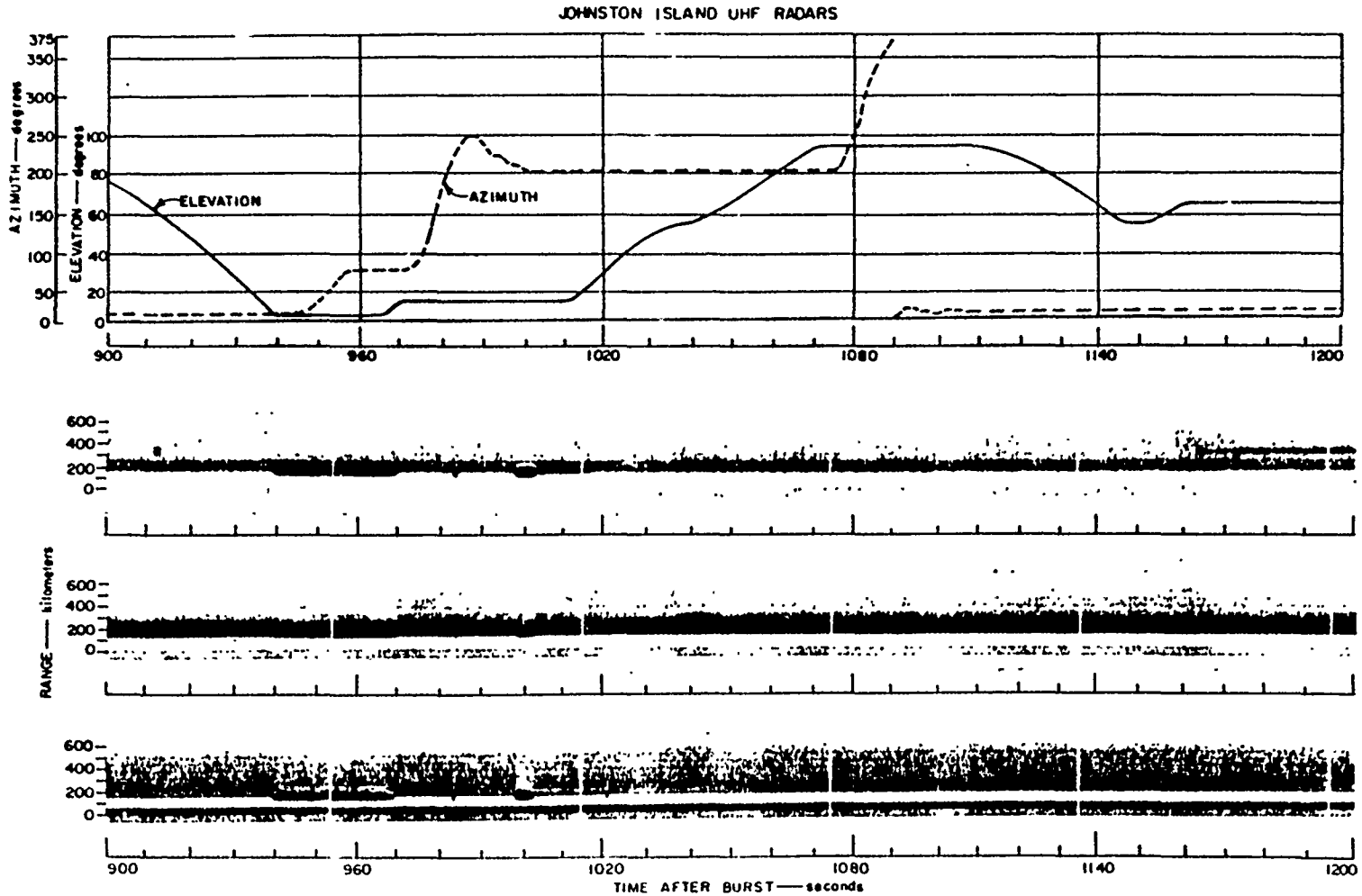

Figure 4.7 Johnston Island radar range versus time for King Fish; 0 to 600 km, 900 to 1,200 seconds.

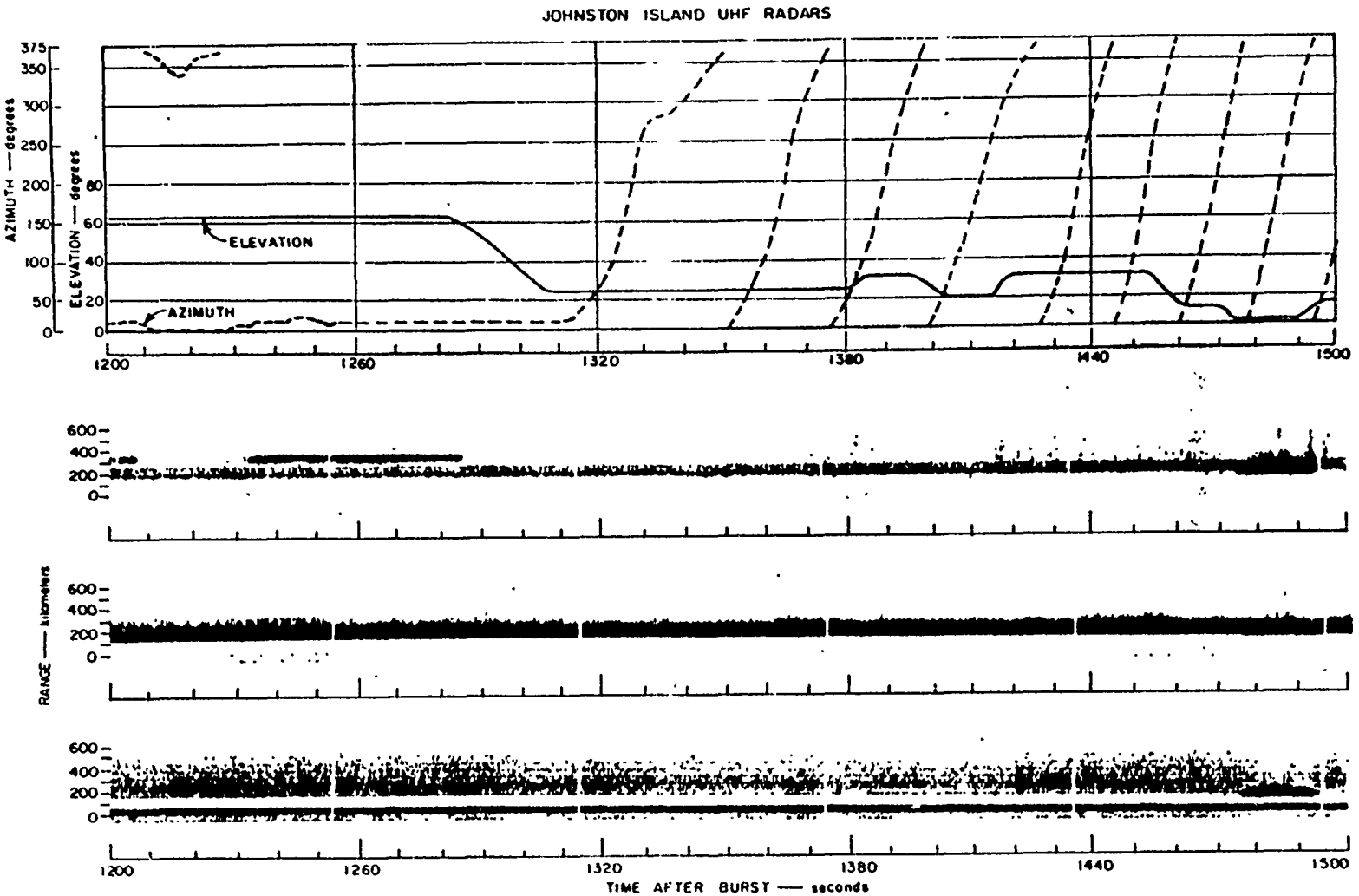

Figure 4.8 Johnston Island radar range versus time for King Fish; 0 to 600 km, 1,200 to 1,500 seconds.

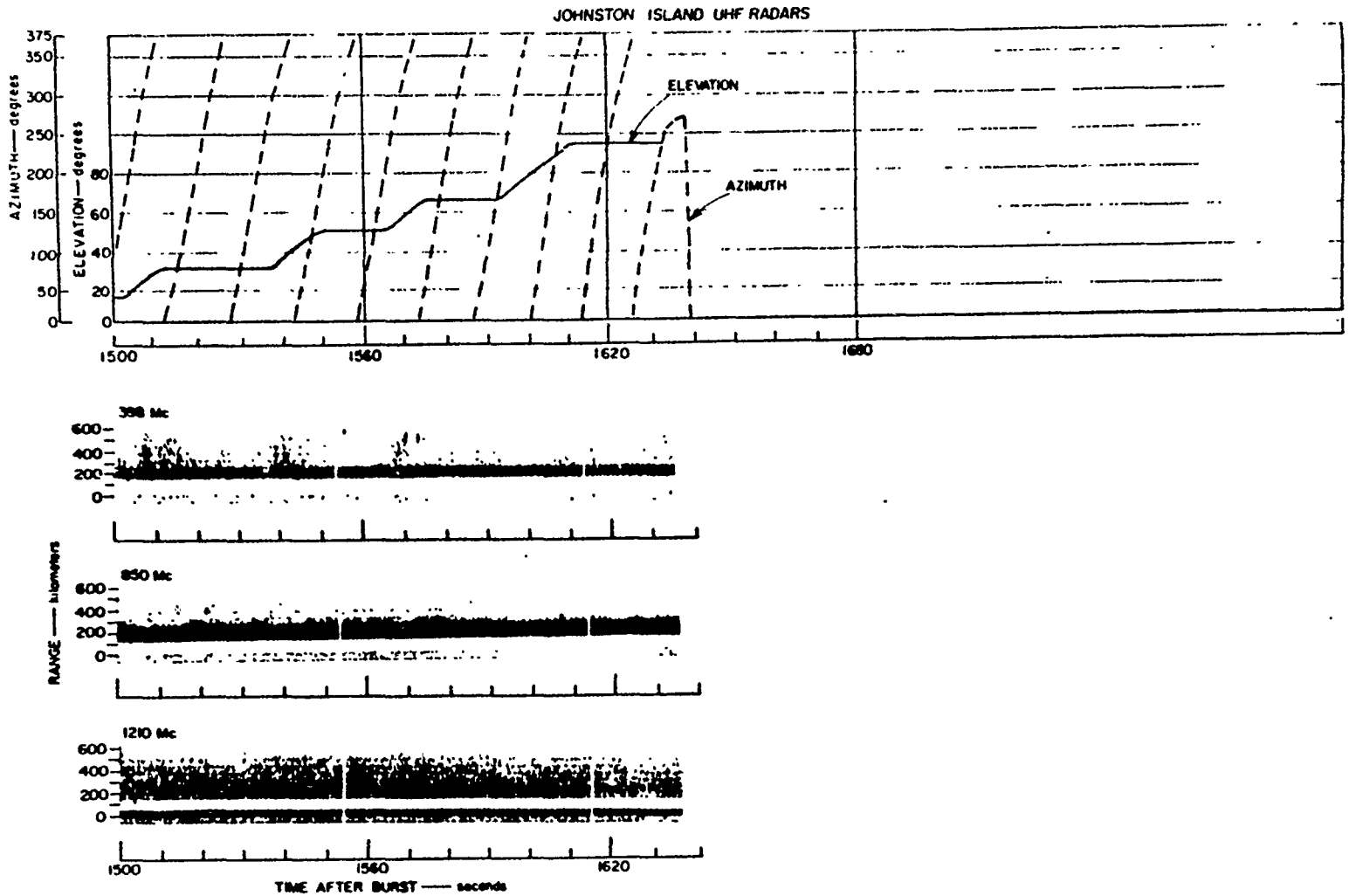

Figure 4.9 Johnston Island radar range versus time for King Fish; 0 to 600 km, 1,500 to 1,640 seconds.

149 (page 150 deleted)

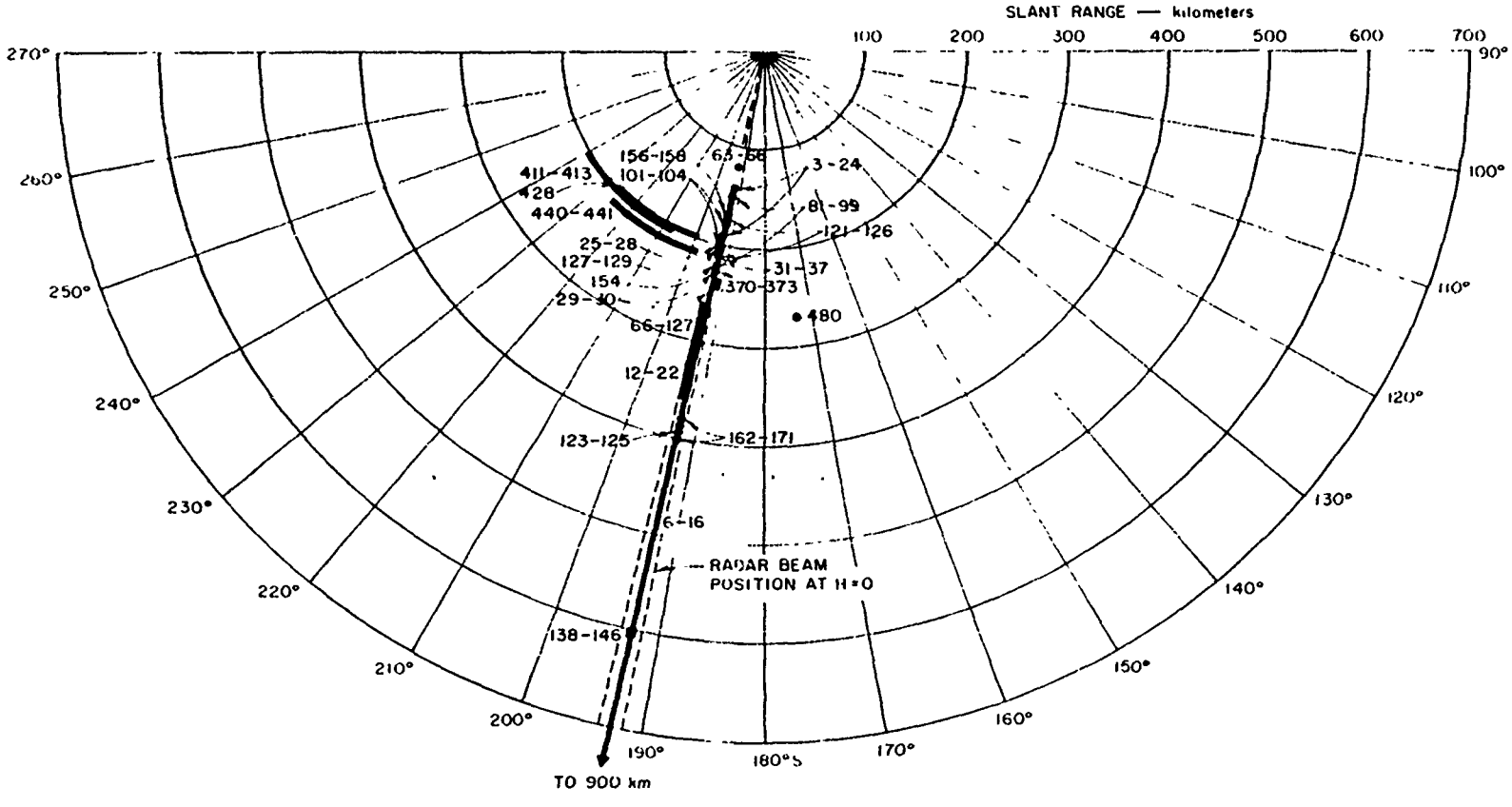

Figure 4.11 Johnston Island radar range versus azimuth for King Fish; 398-Mc southern echoes, 0 to 1,620 seconds.

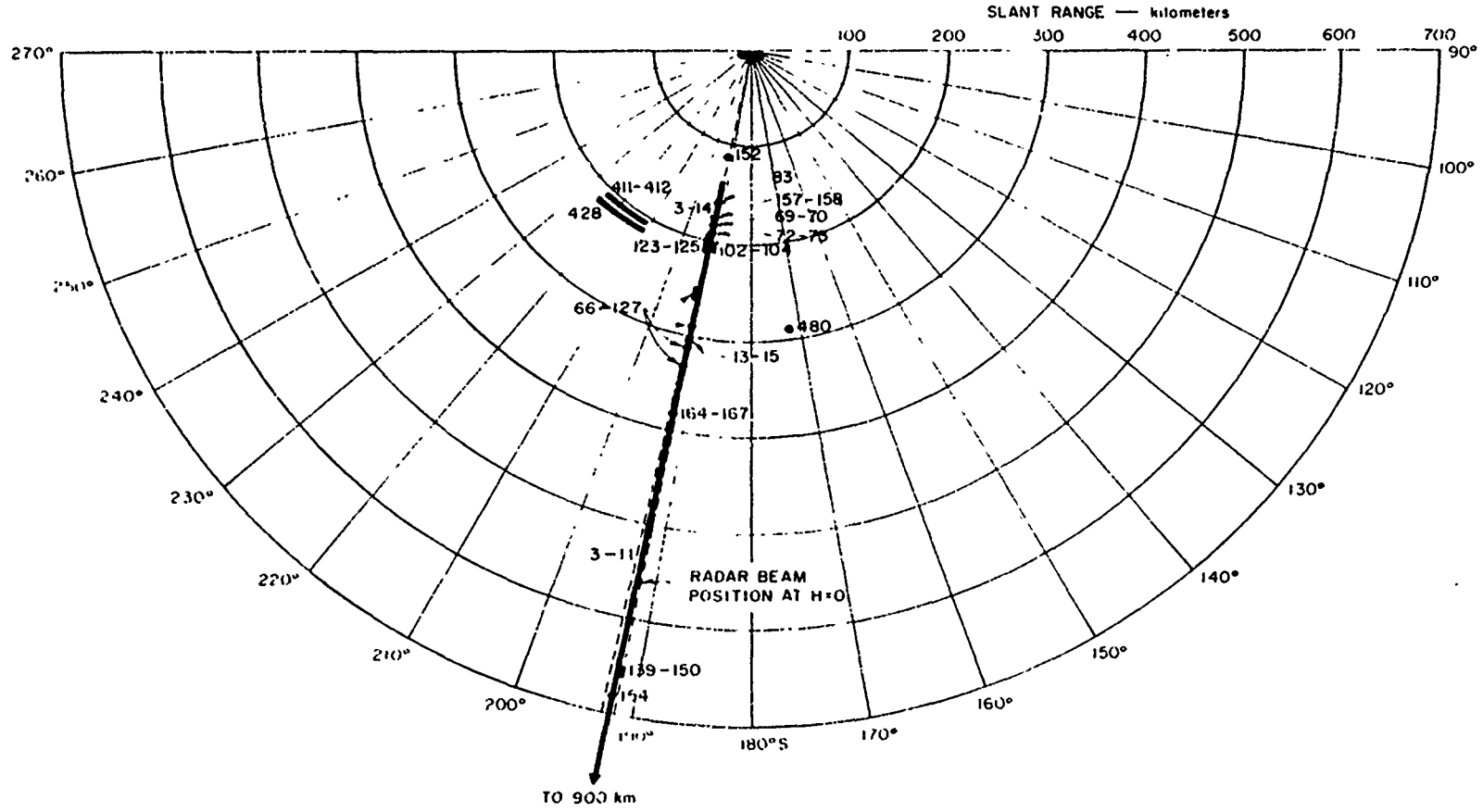

Figure 4.13 Johnston Island radar range versus azimuth for King Fish; 850-Mc southern echoes, 0 to 1,620 seconds.

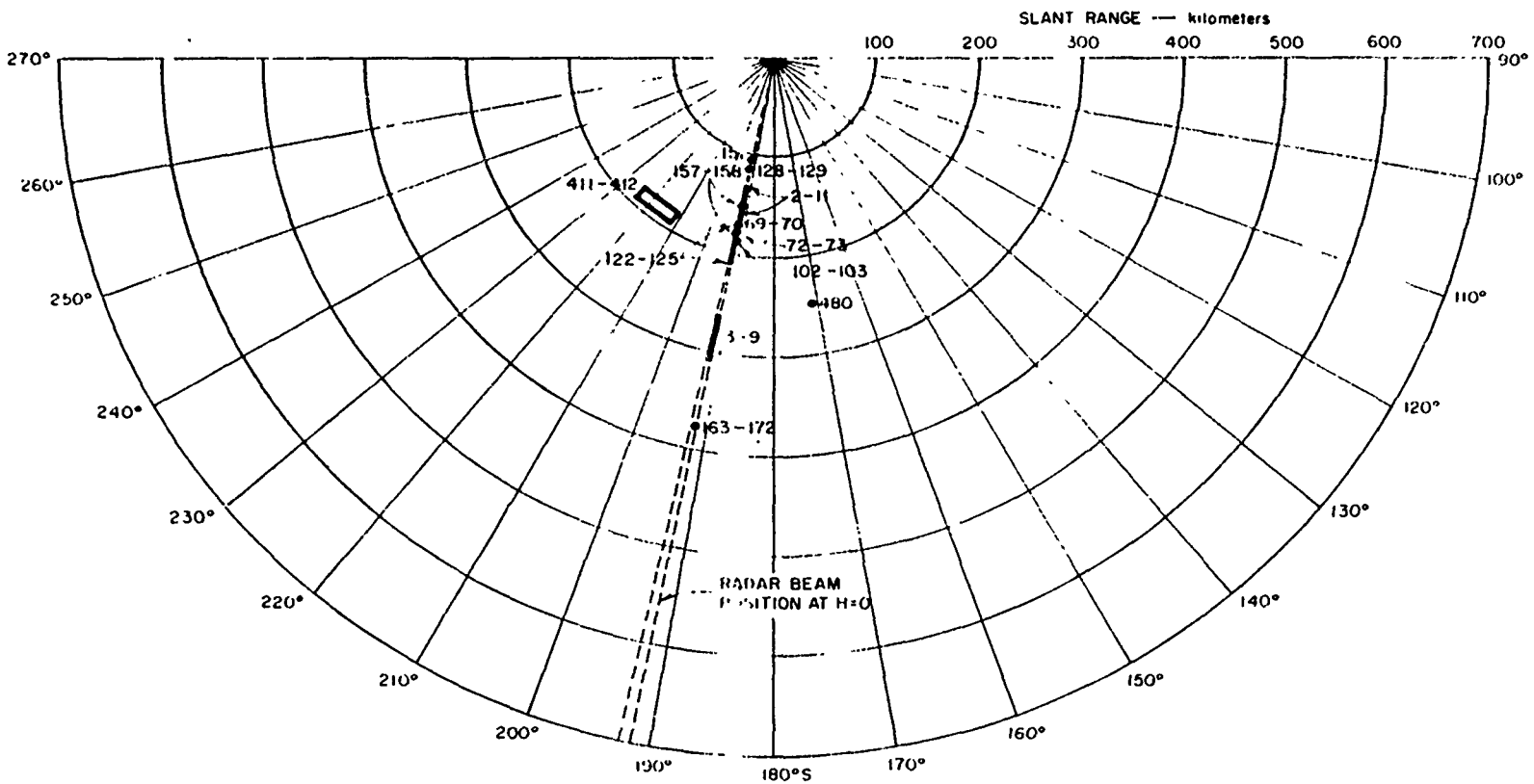

Figure 4.15 Johnston Island radar range versus azimuth for King Fish; 1210-Mc southern echoes, 0 to 1 620 seconds.

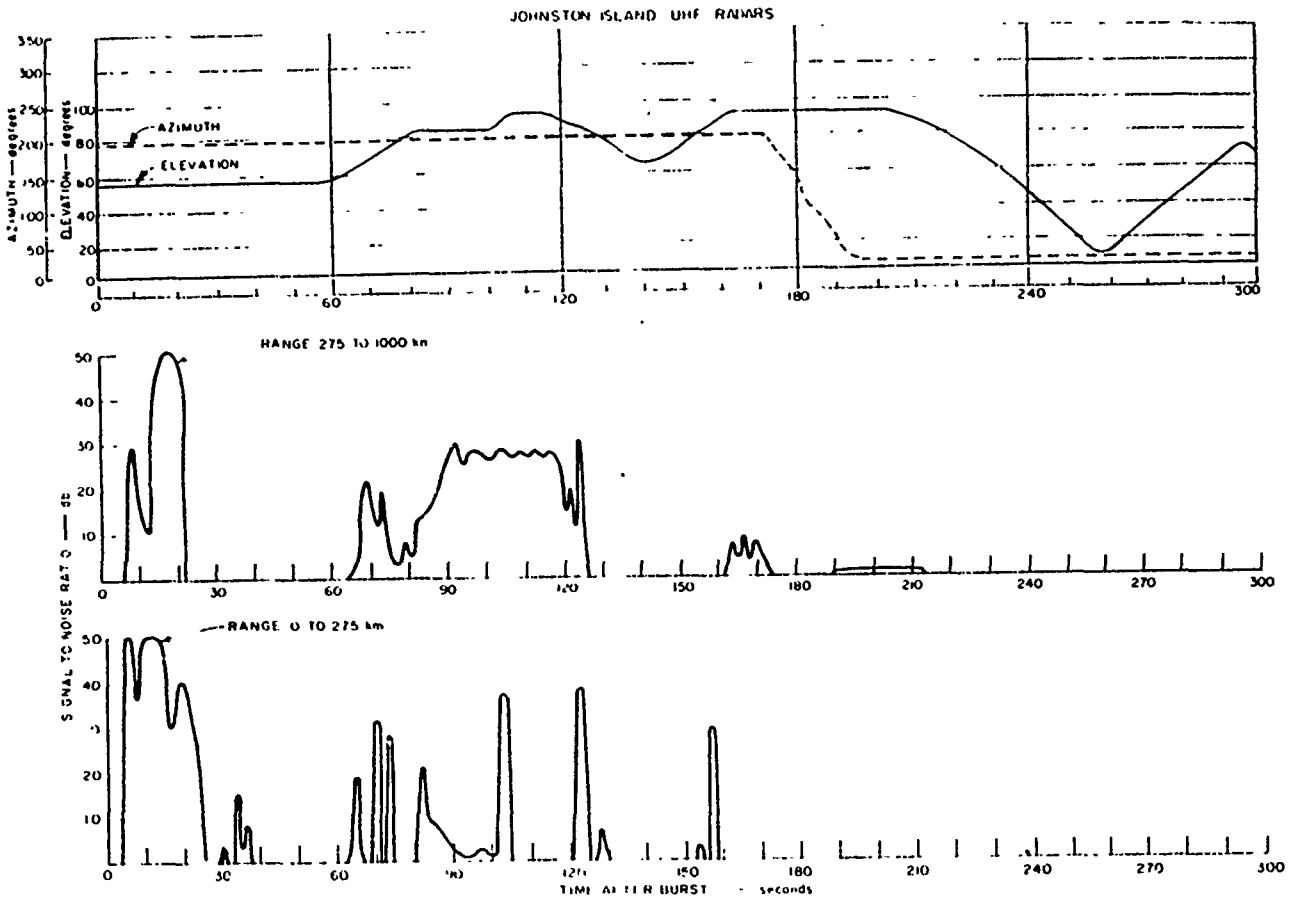

Figure 4.16 Johnston Island radar echo amplitude versus time for King Fish; 398 Mc, 0 to 300 seconds.

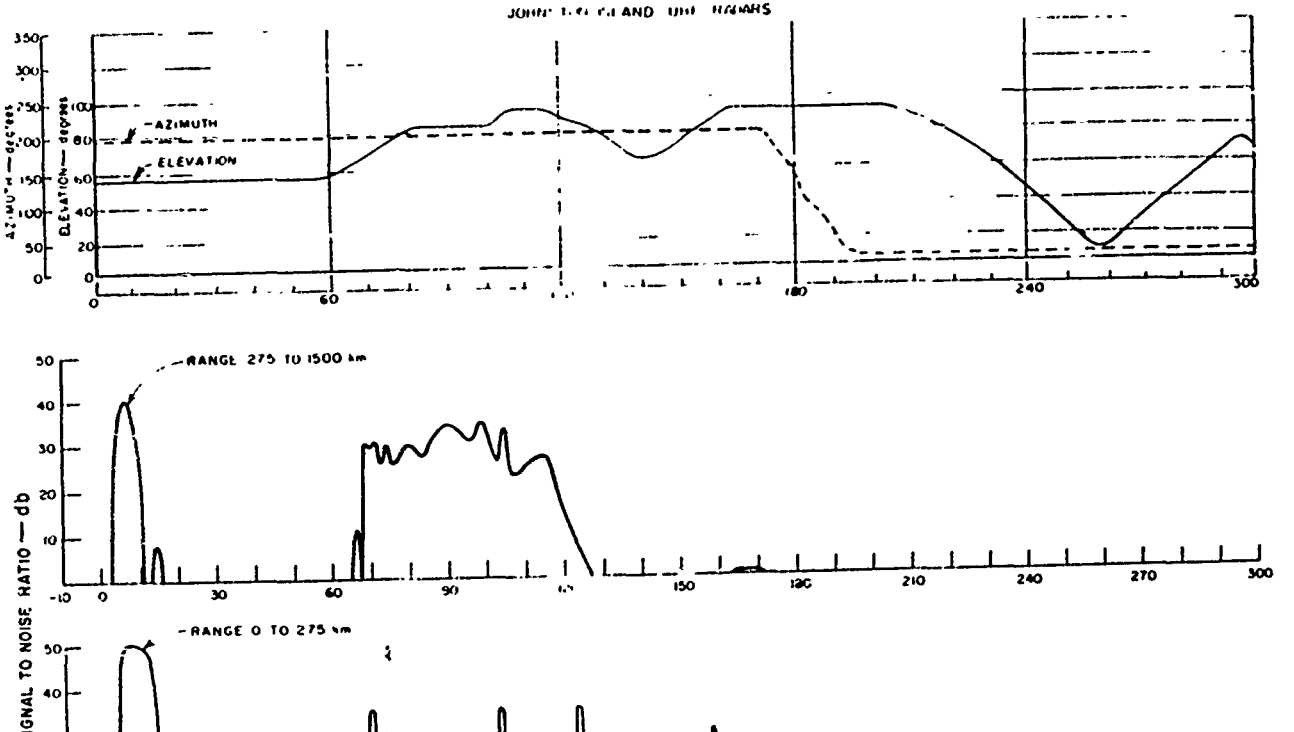

Figure 4.17 Johnston Island radar echo amplitude versus time for King Fish; 850 Mc, 0 to 300 seconds.

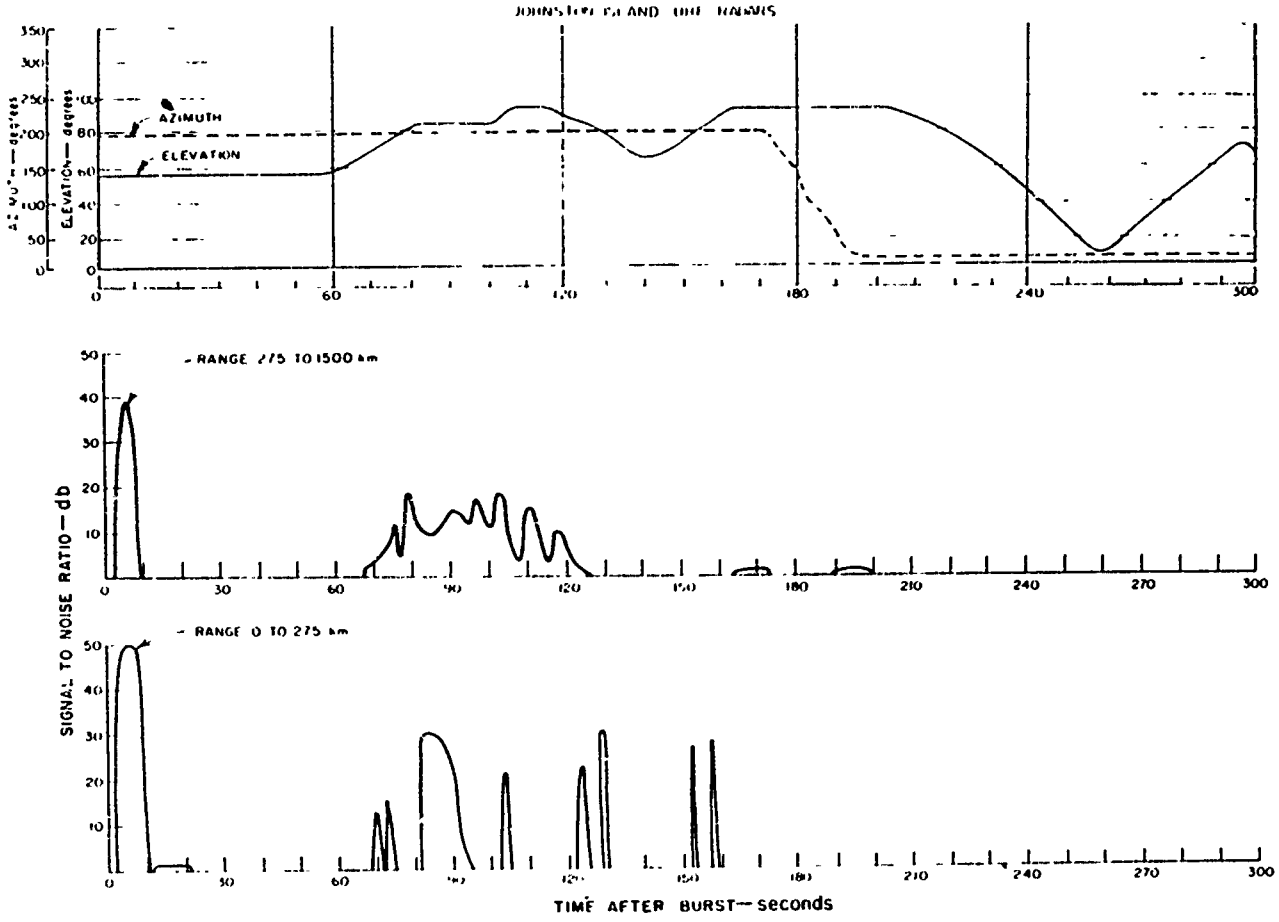

Figure 4.18 Johnston island radar echo amplitude versus time for King Fish; 1210 Mc, 0 to 300 seconds.

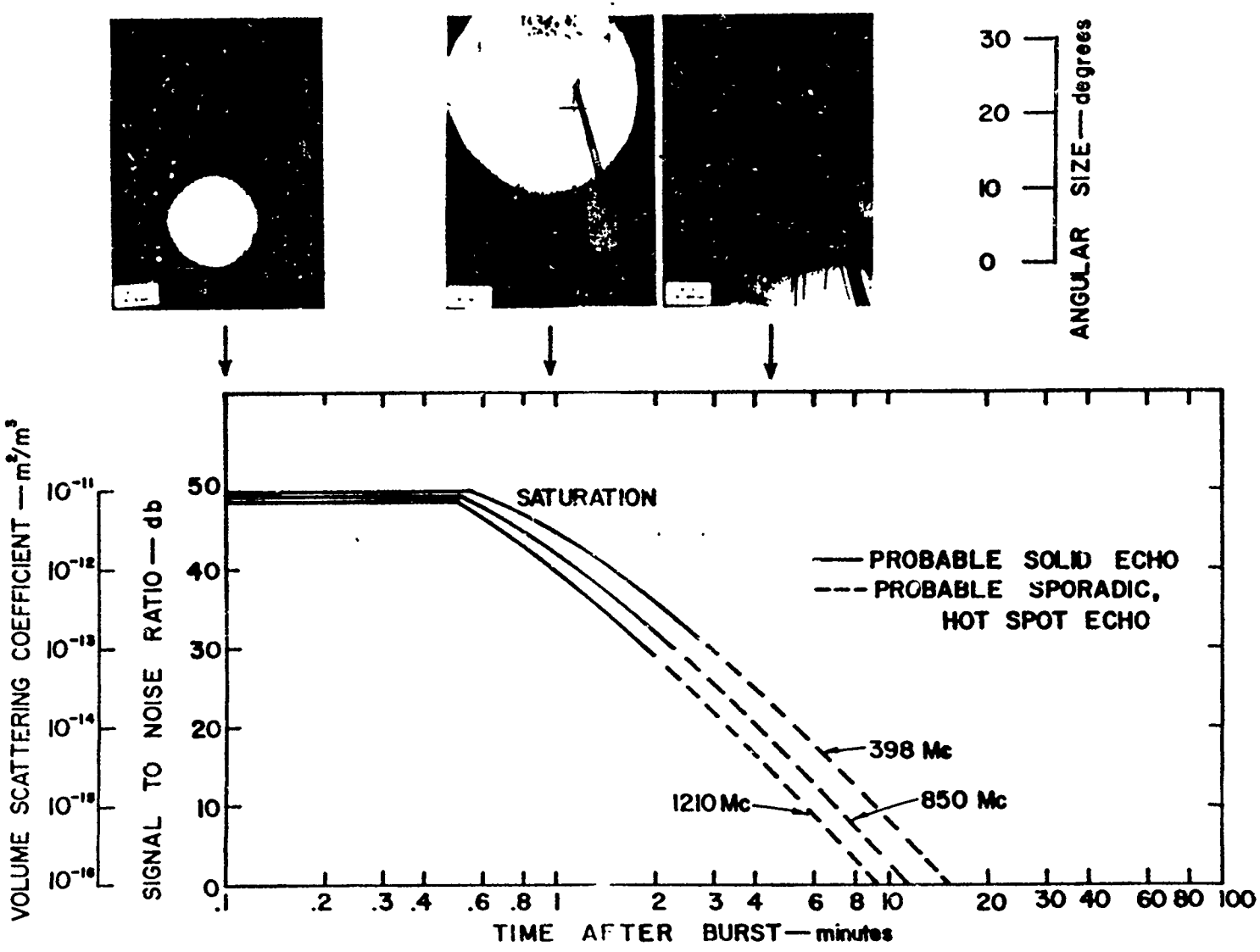

Figure 4.1.5 Johnston Island radar echo amplitude versus time for King Fish; 398, 850, and 1210 Mc.

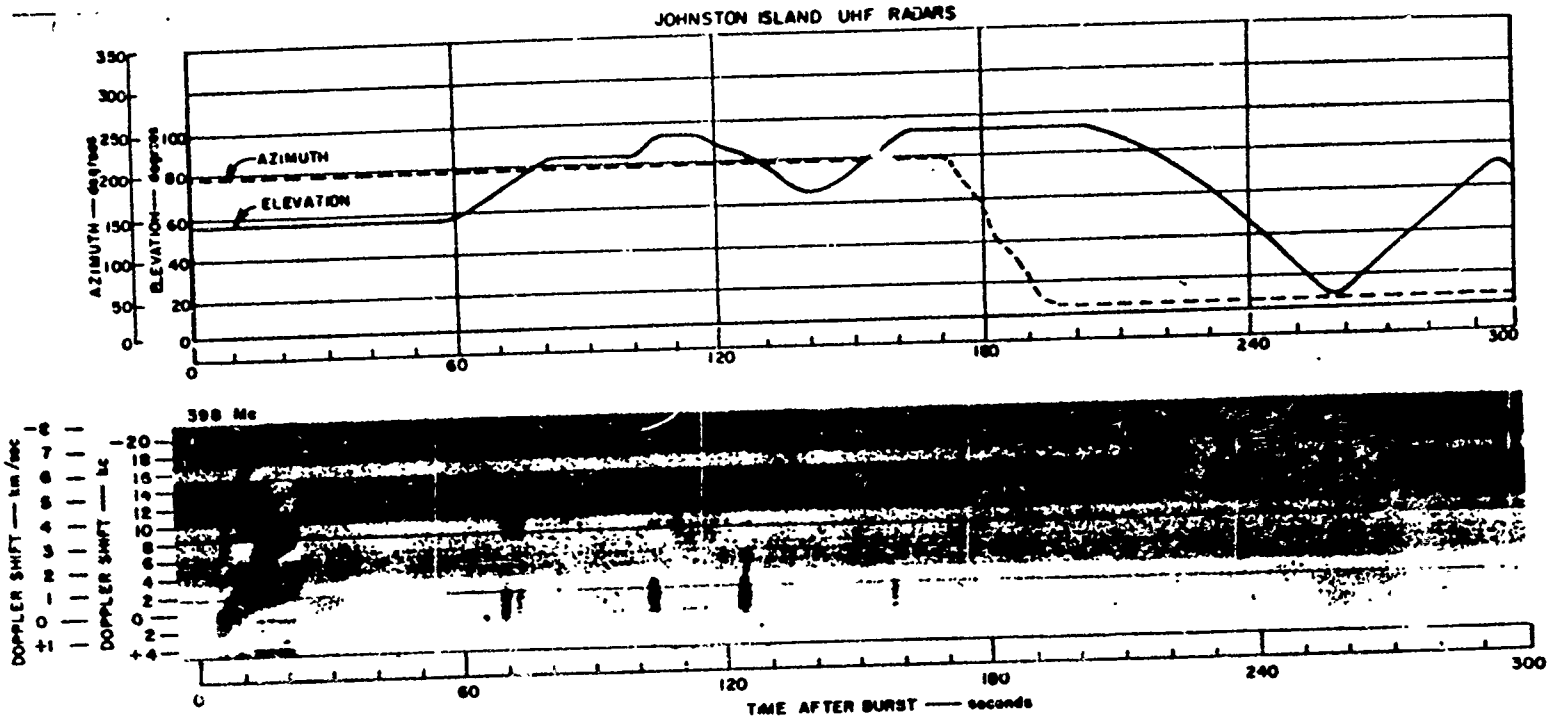

Figure 4.20 Johnston Island radar Doppler versus time for King Fish; 398 Mc, 0 to 300 seconds.

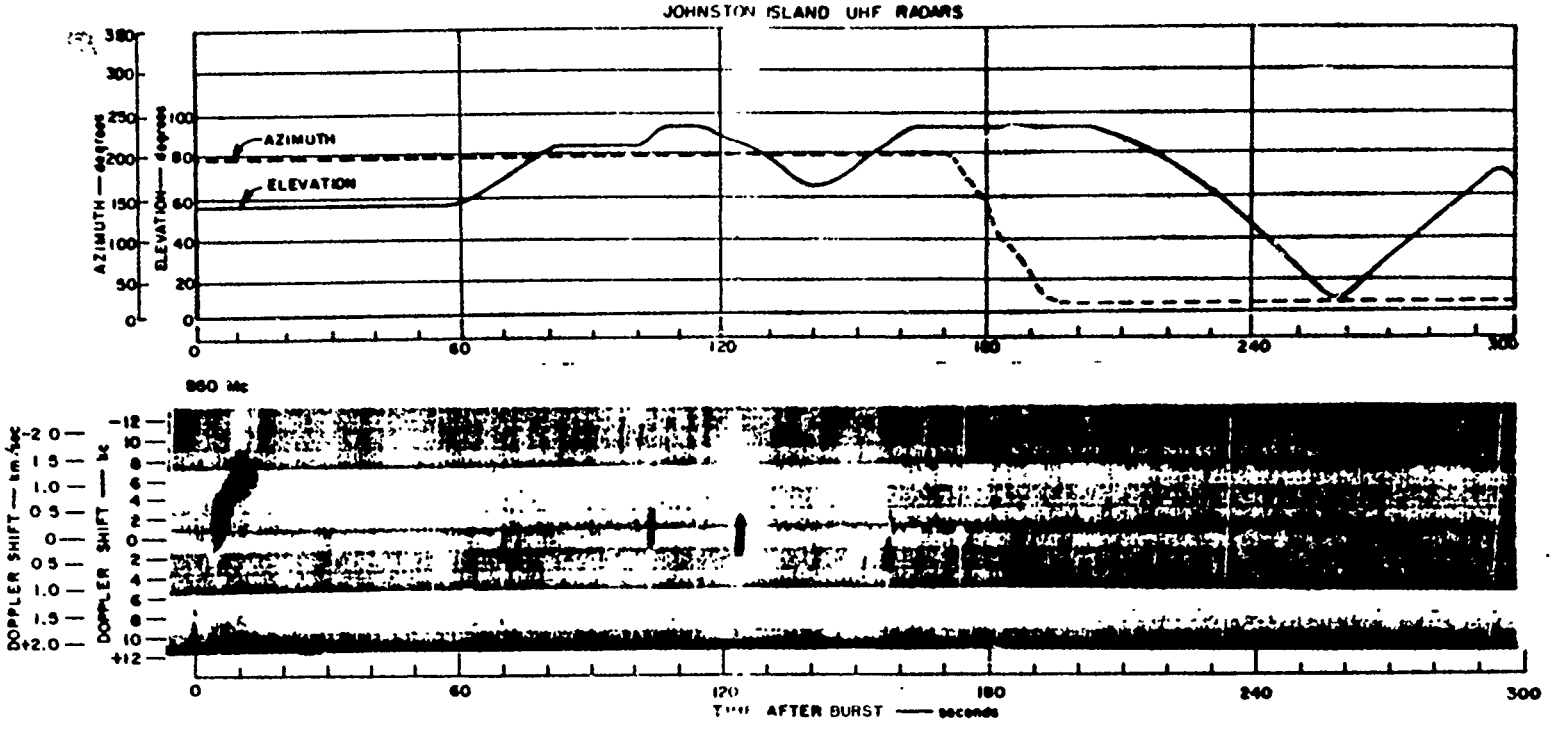

Figure 4.21 Johnston Island radar Doppler versus time for King Fish; 850 Mc, 0 to 300 seconds.

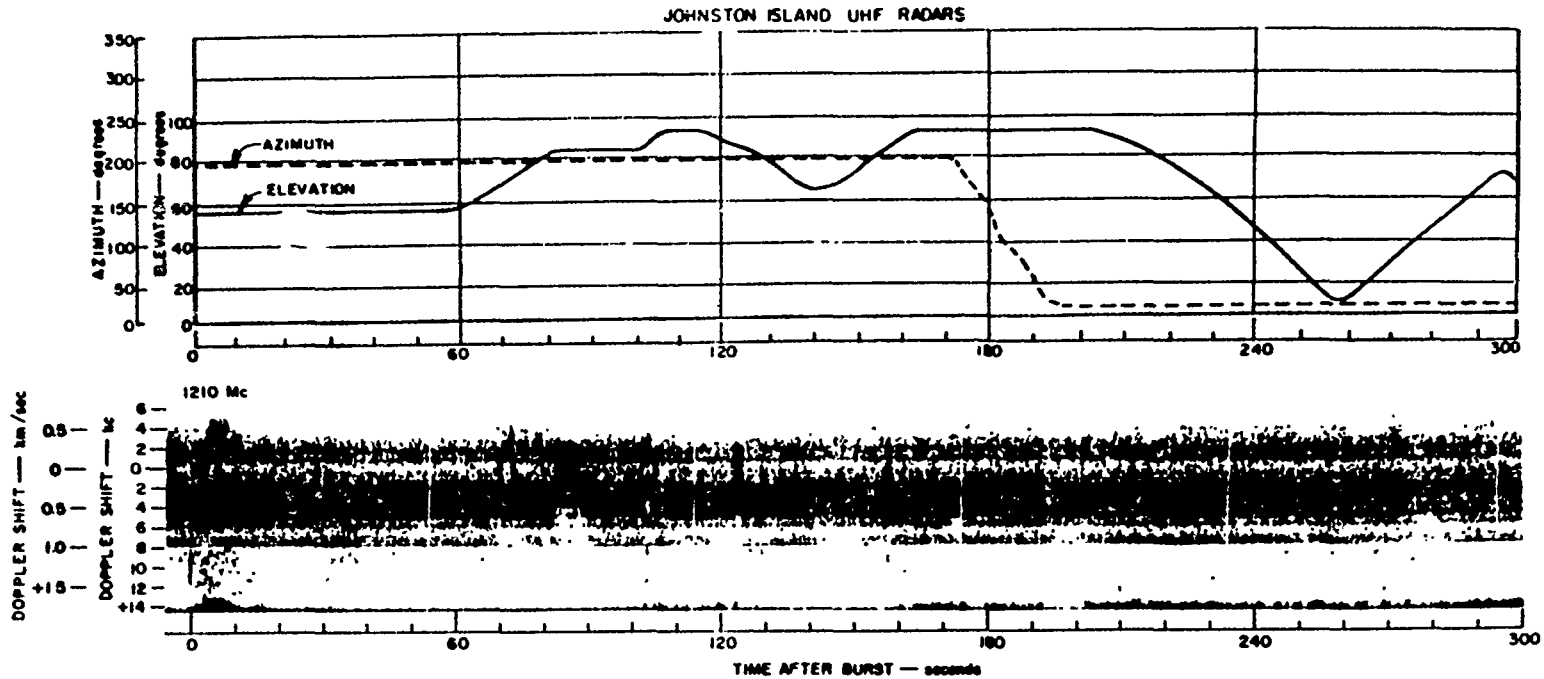

Figure 4.22 Johnston Island radar Doppler versus time for King Fish; 1210 Mc, 0 to 300 seconds.

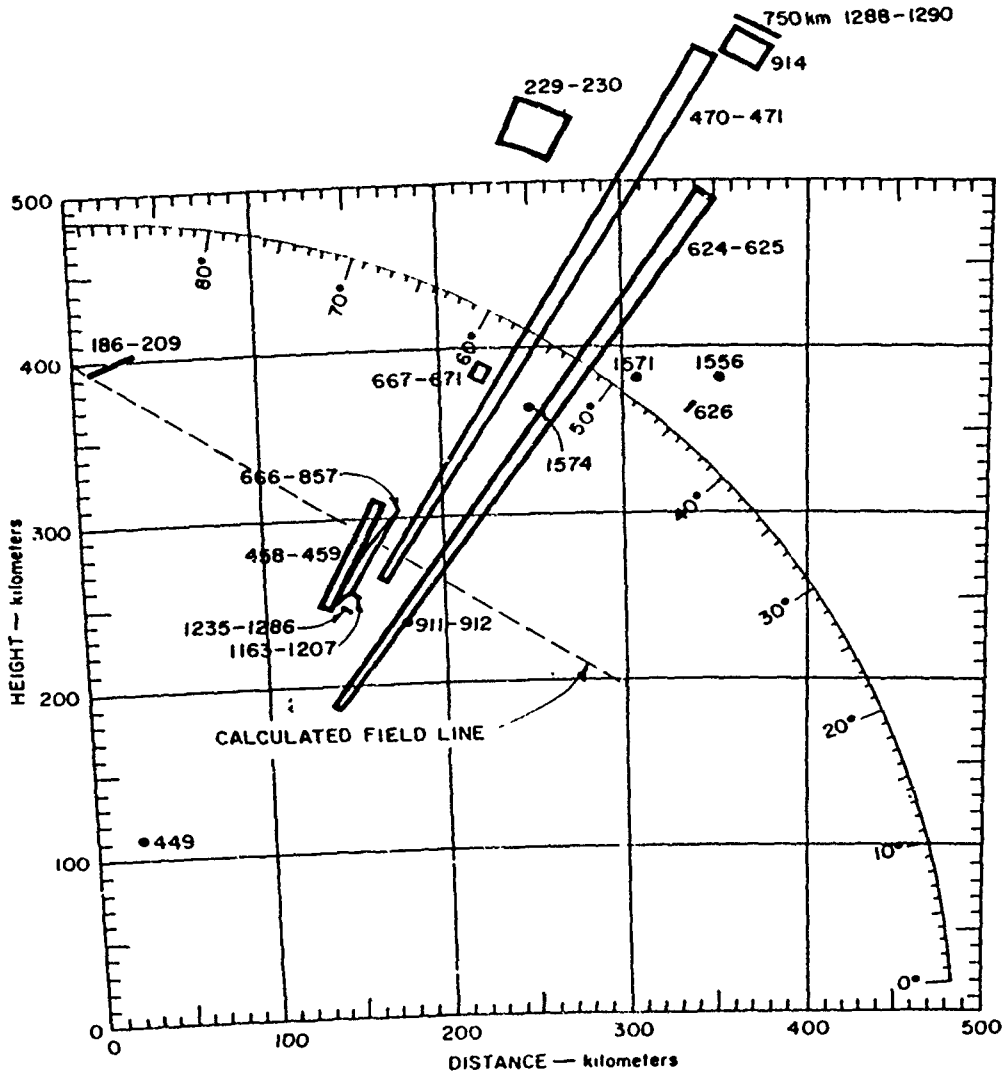

Figure 4.23 Johnston Island radar height versus distance for *King Fish*; 398-Mc northern echoes, 0 to 1,630 seconds.

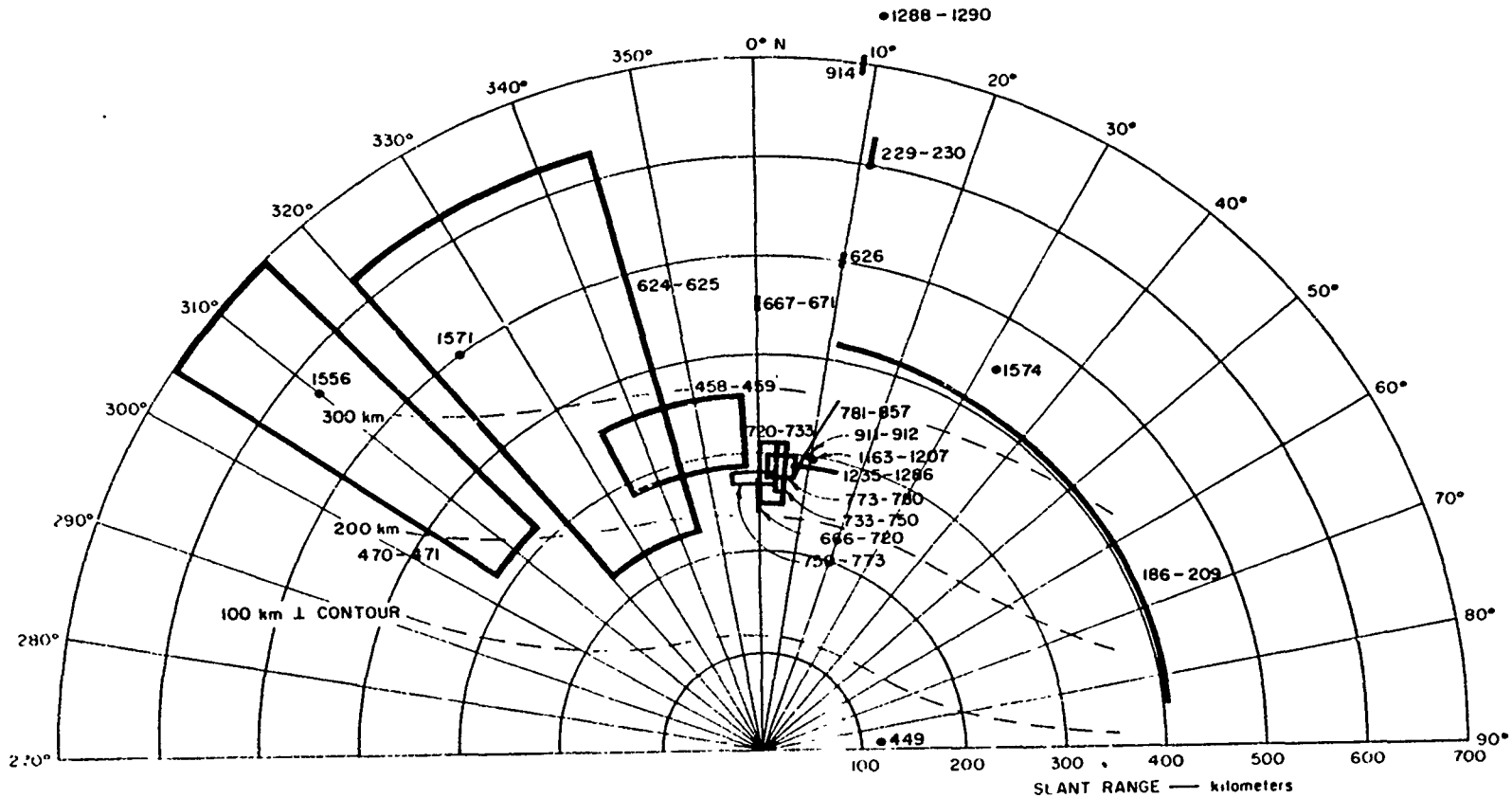

Figure 4.24 Johnston Island radar range versus azimuth for King Fish; 398-Mc northern echoes, 0 to 1,620 seconds.

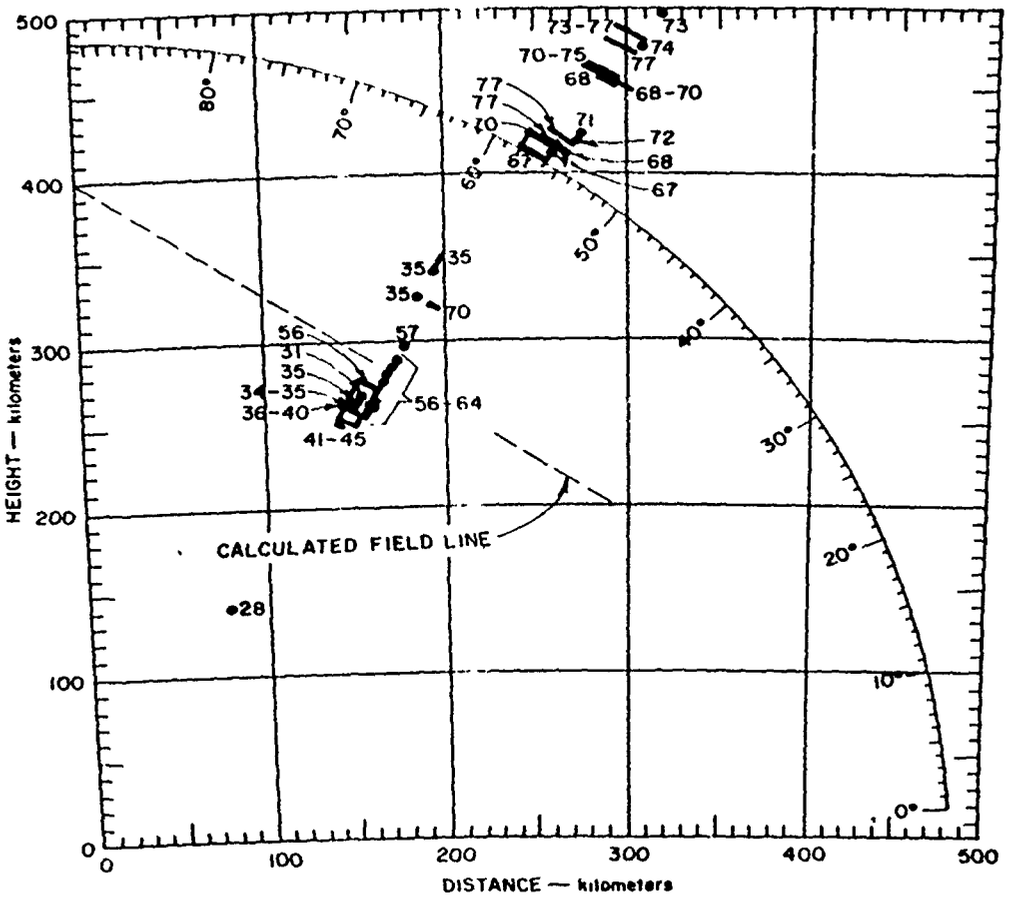

Figure 4.25 Johnston Island radar height versus distance for King Fish; 398-Mc northern echoes, 30 to 80 minutes.

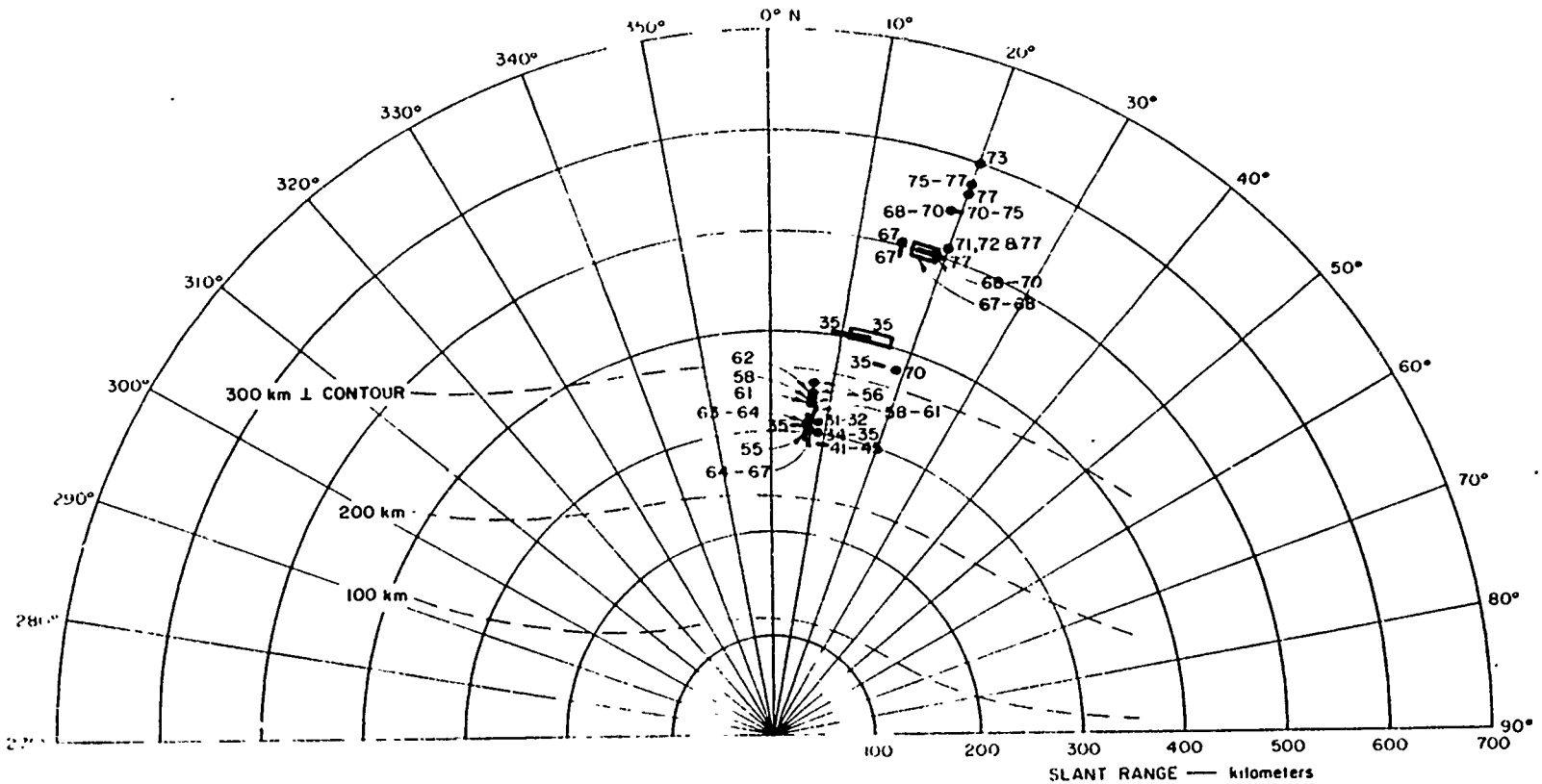

Figure 4.26 Johnston Island radar range versus azimuth for King Fish; 398-Mc northern echoes, 30 to 80 minutes.

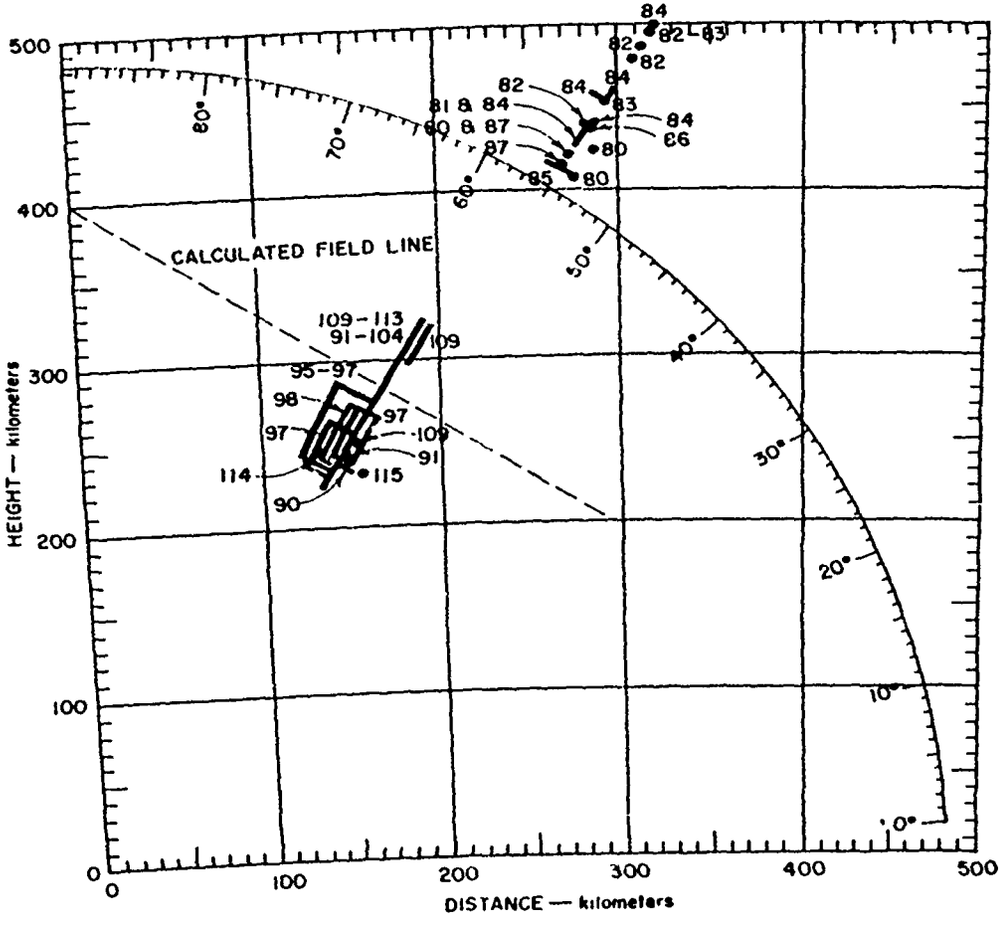

Figure 4.27 Johnston Island radar height versus distance for King Fish; 398-Mc northern echoes, 80 to 125 minutes.

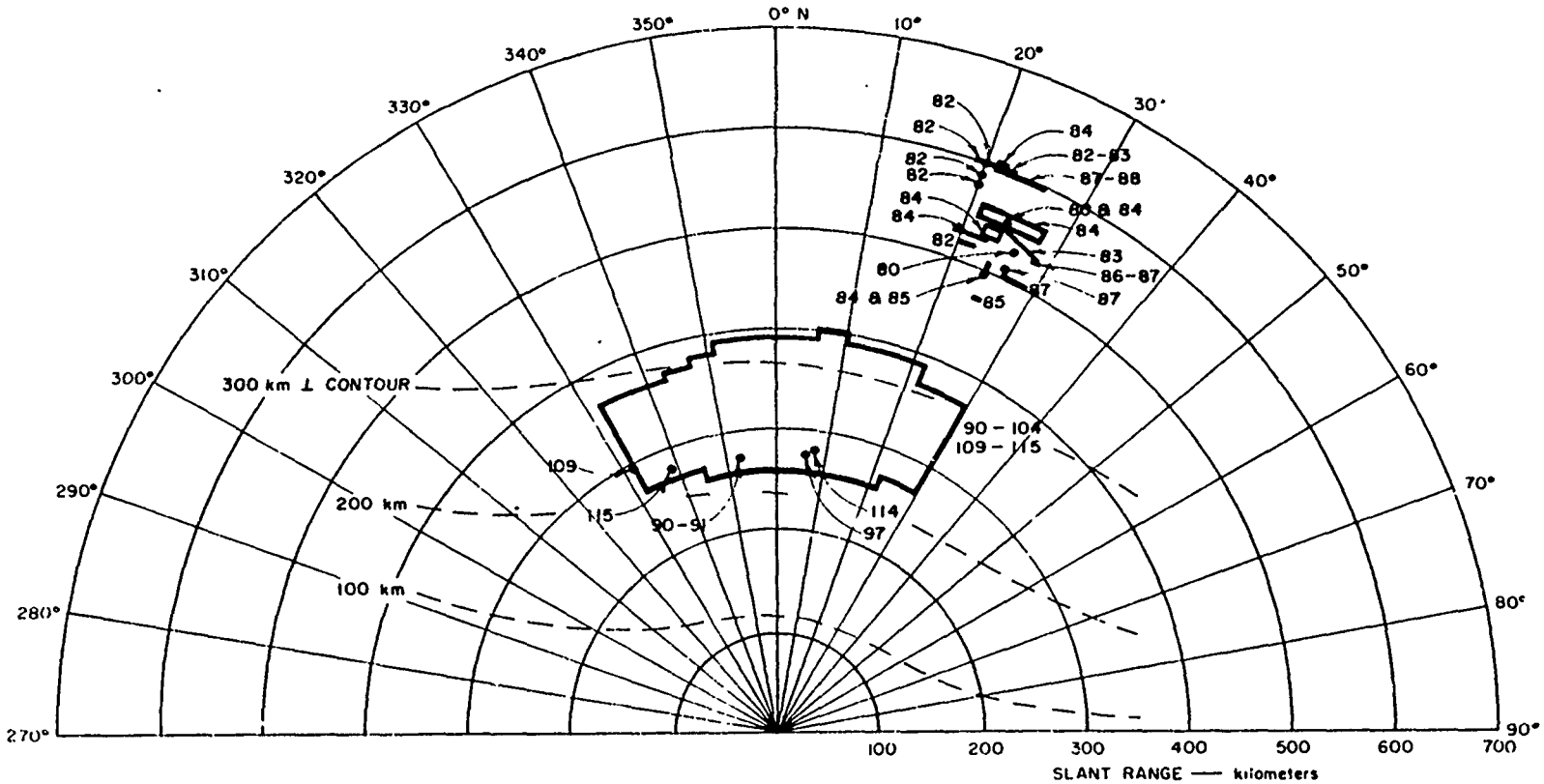

Figure 4.28 Johnston Island radar range versus azimuth for King Fish; 398-Mc northern echoes, 80 to 125 minutes.

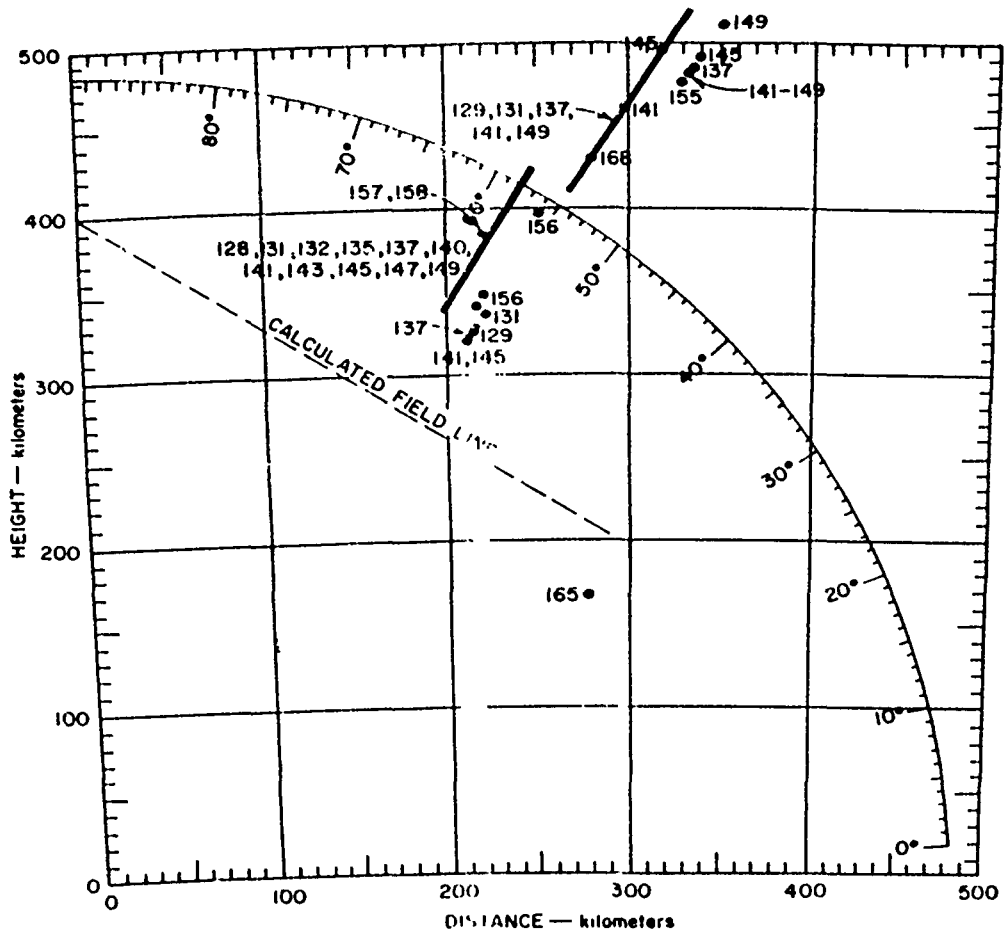

Figure 4.29 Johnston Island radar height versus distance for King Fish; 398-Mc northern echoes, 128 to 173 minutes.

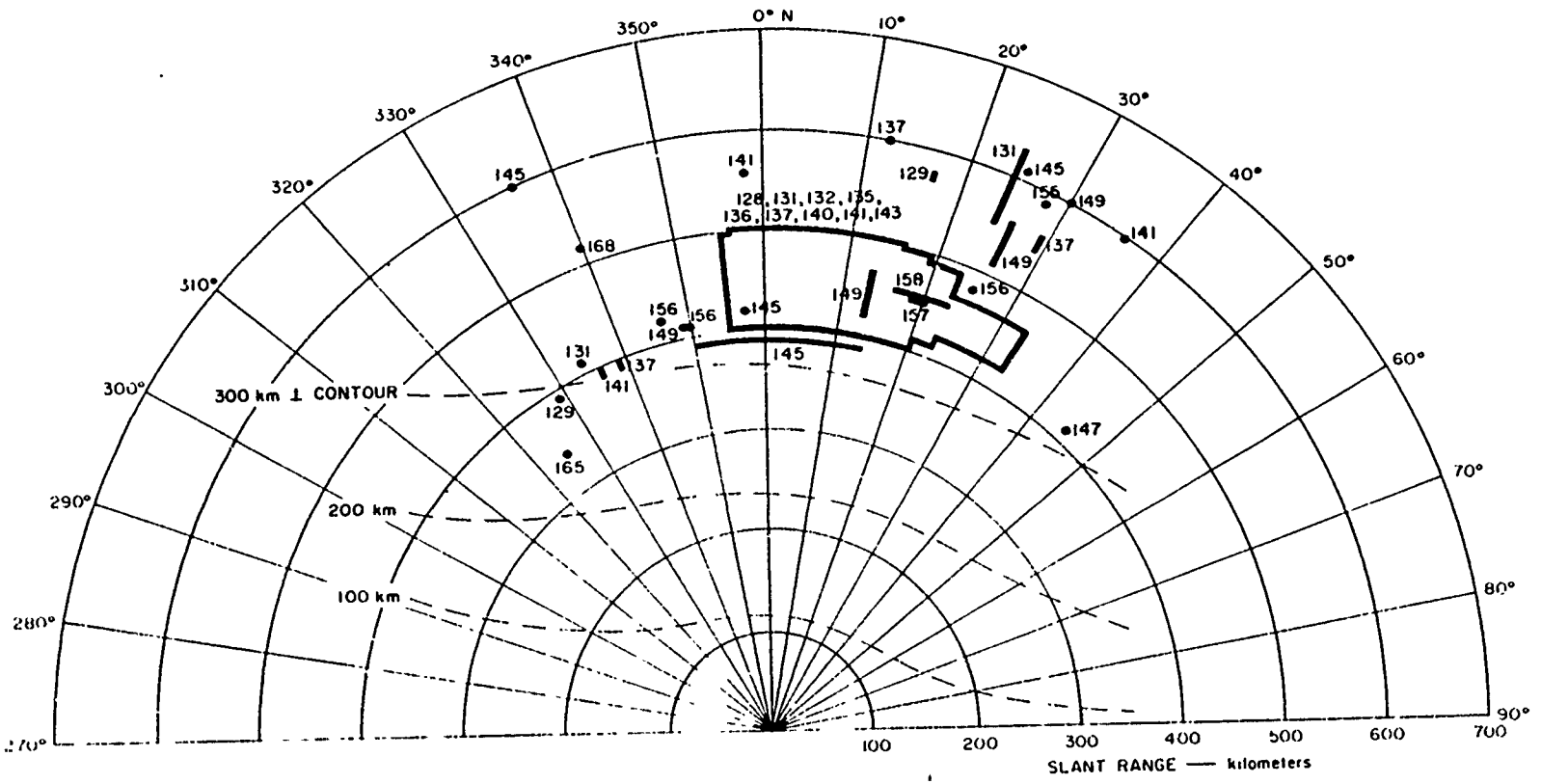

Figure 4.30 Johnston Island radar range versus azimuth for King Fish; 398-Mc northern echoes, 128 to 173 minutes.

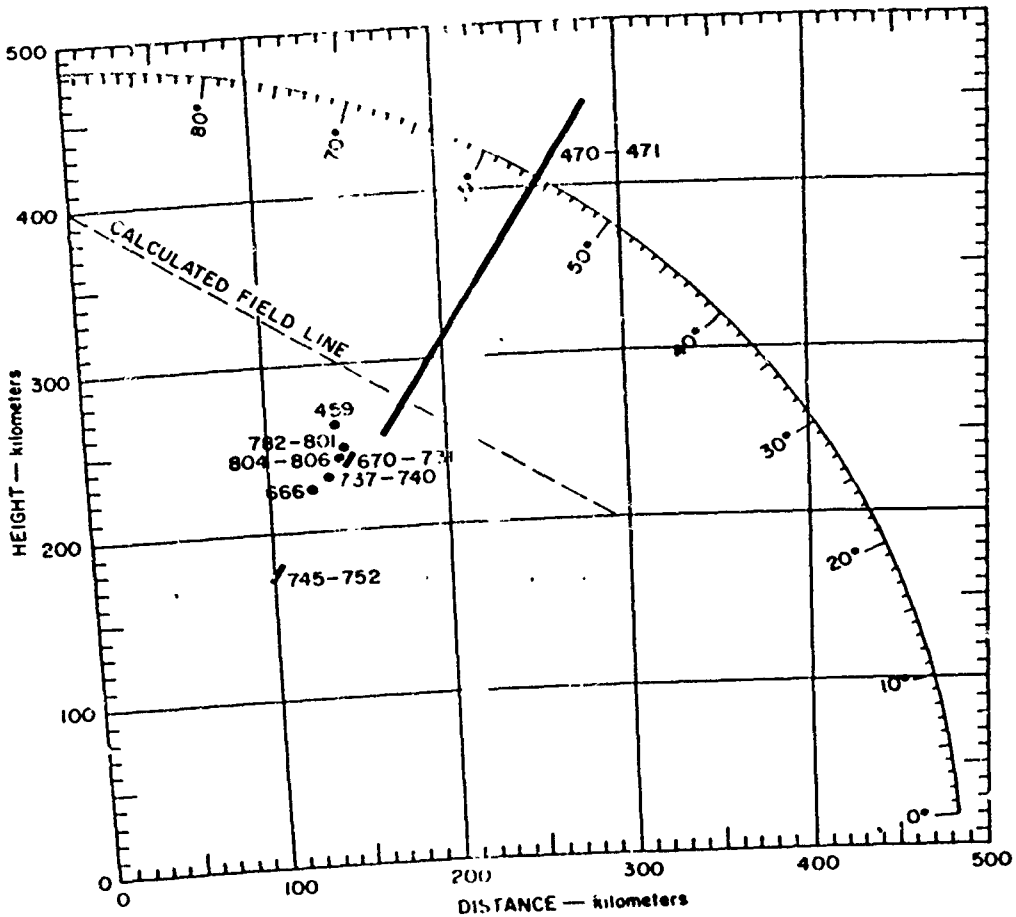

Figure 4.31 Johnston Island radar height versus distance for King Fish; 850-Mc northern echoes, 0 to 1,620 seconds.

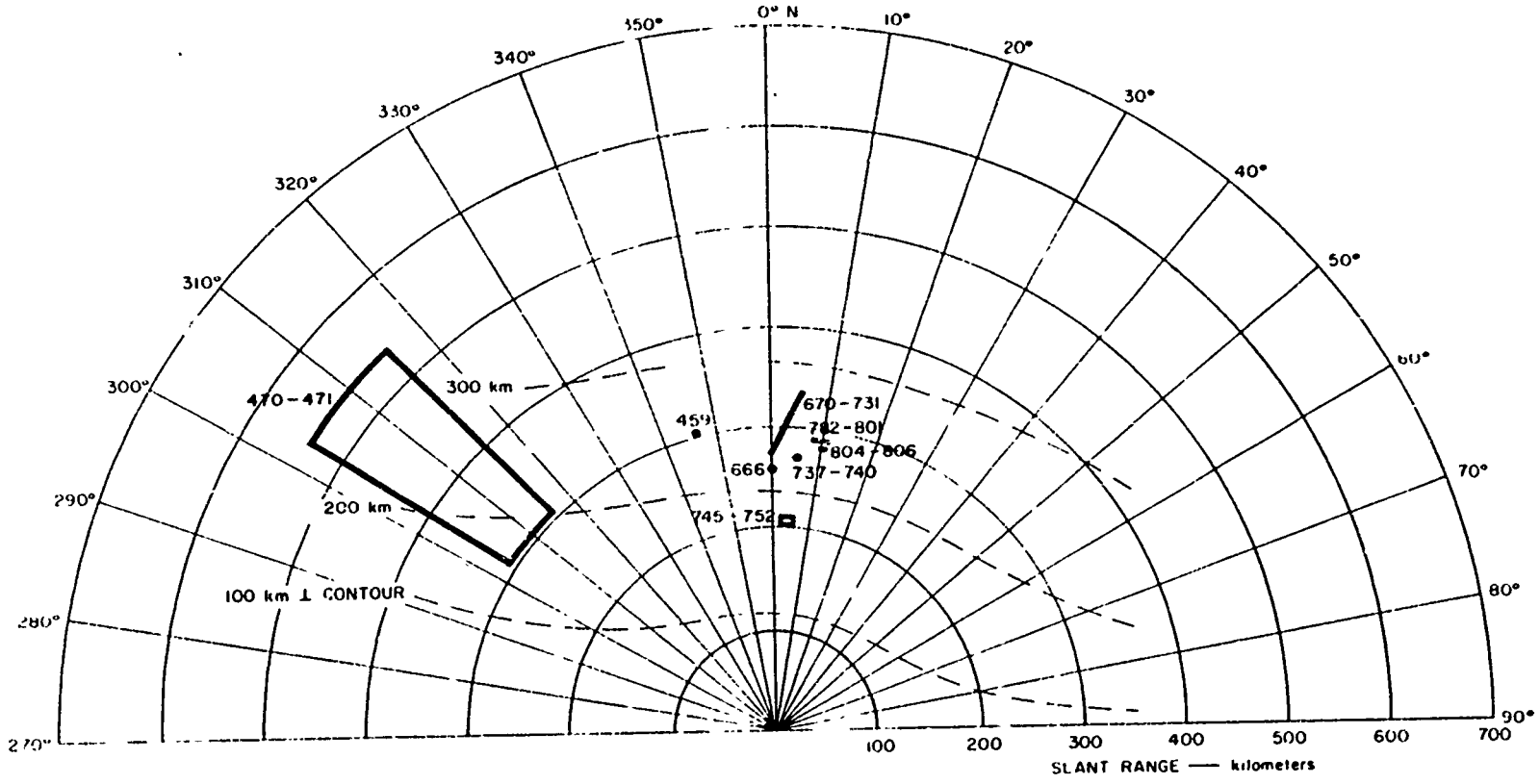

Figure 4.32 Johnston Island radar range versus azimuth for King Fish; 850-Mc northern echoes, 0 to 1,620 seconds.

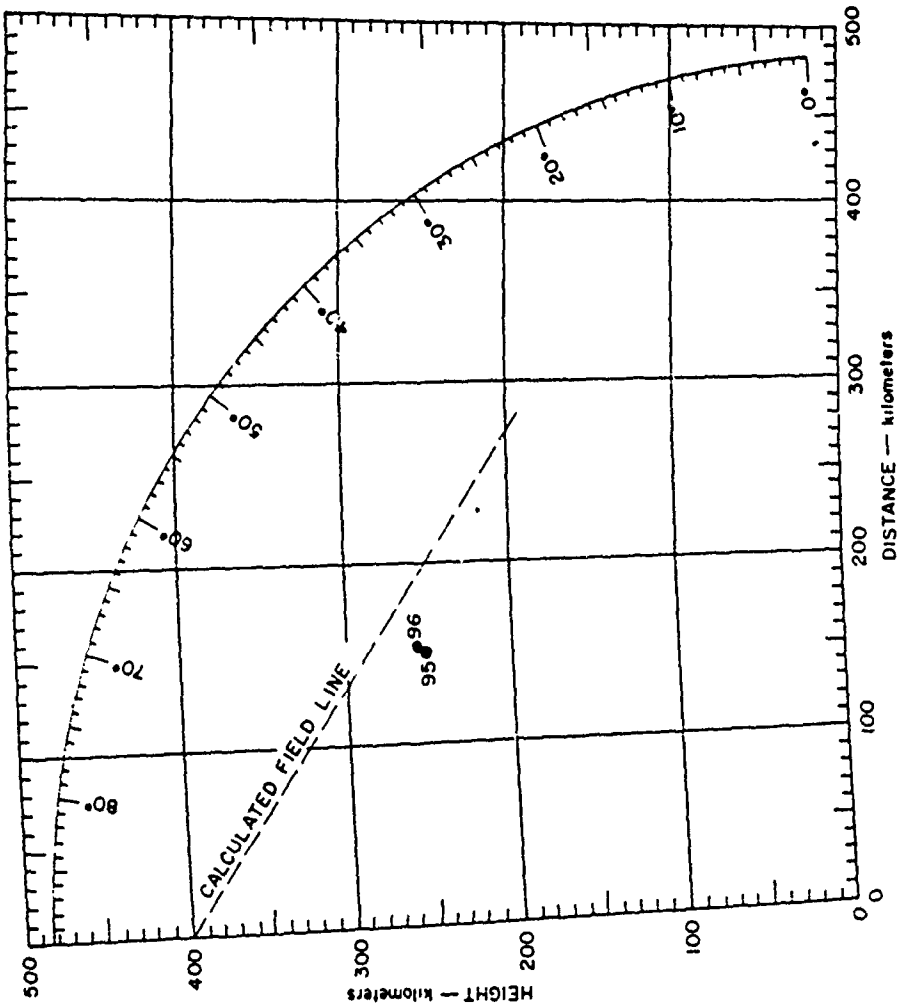

Figure 4.33 Johnston Island radar height versus distance for King Fish; 850-Mc northern echoes, 80 to 125 minutes.

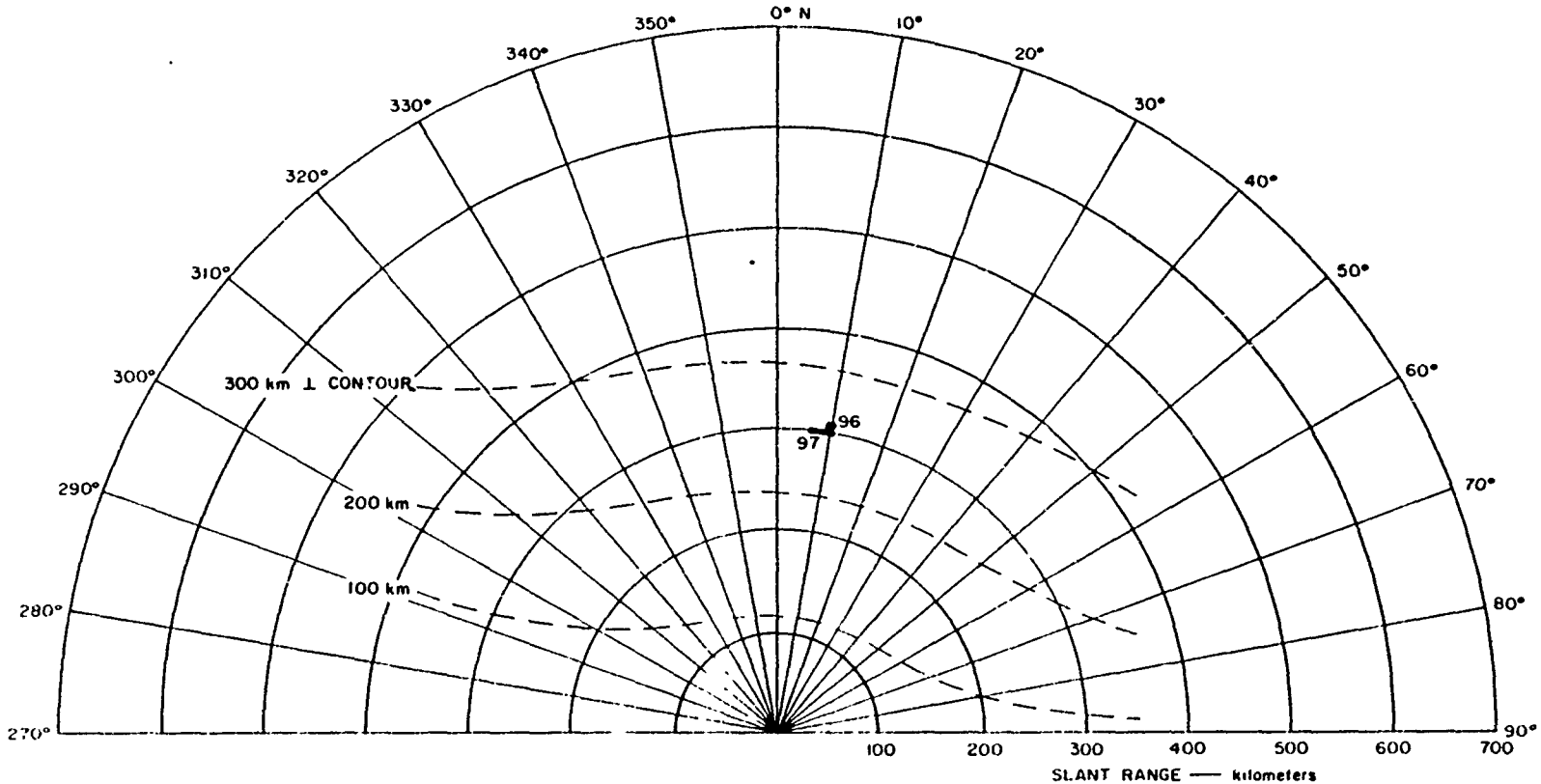

Figure 4.34 Johnston Island radar range versus azimuth for King Fish; 850-Mc northern echoes, 80 to 125 minutes.

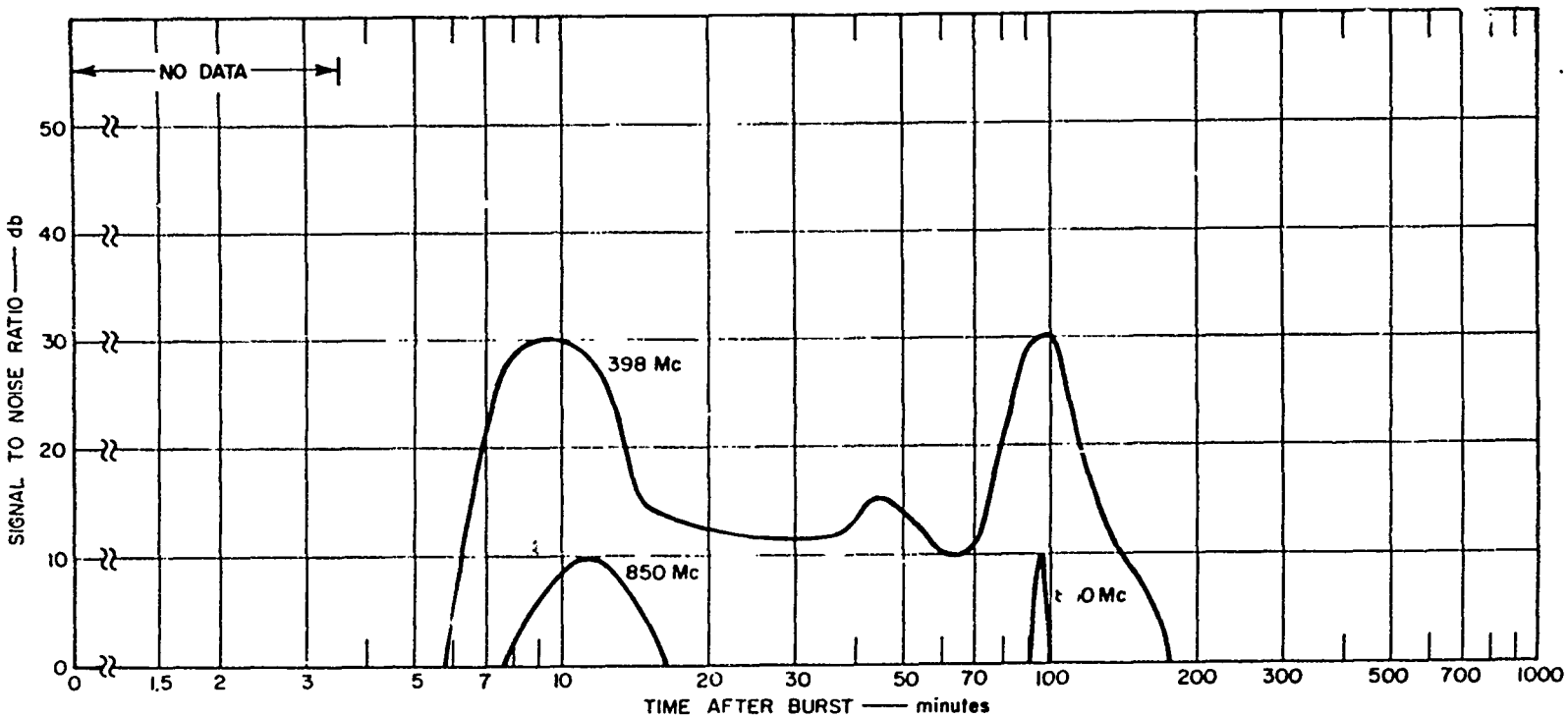

Figure 4.35 Johnston Island radar auroral echo amplitude versus time for King Fish; 398 and 850 Mc.

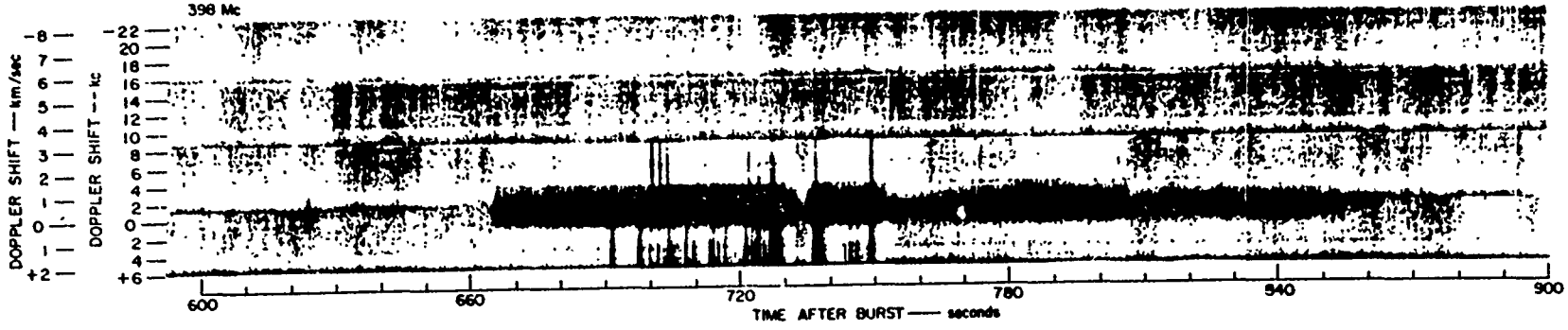

Figure 4.36 Johnston Island radar Doppler versus time for King Fish; 398 Mc, 600 to 900 seconds.

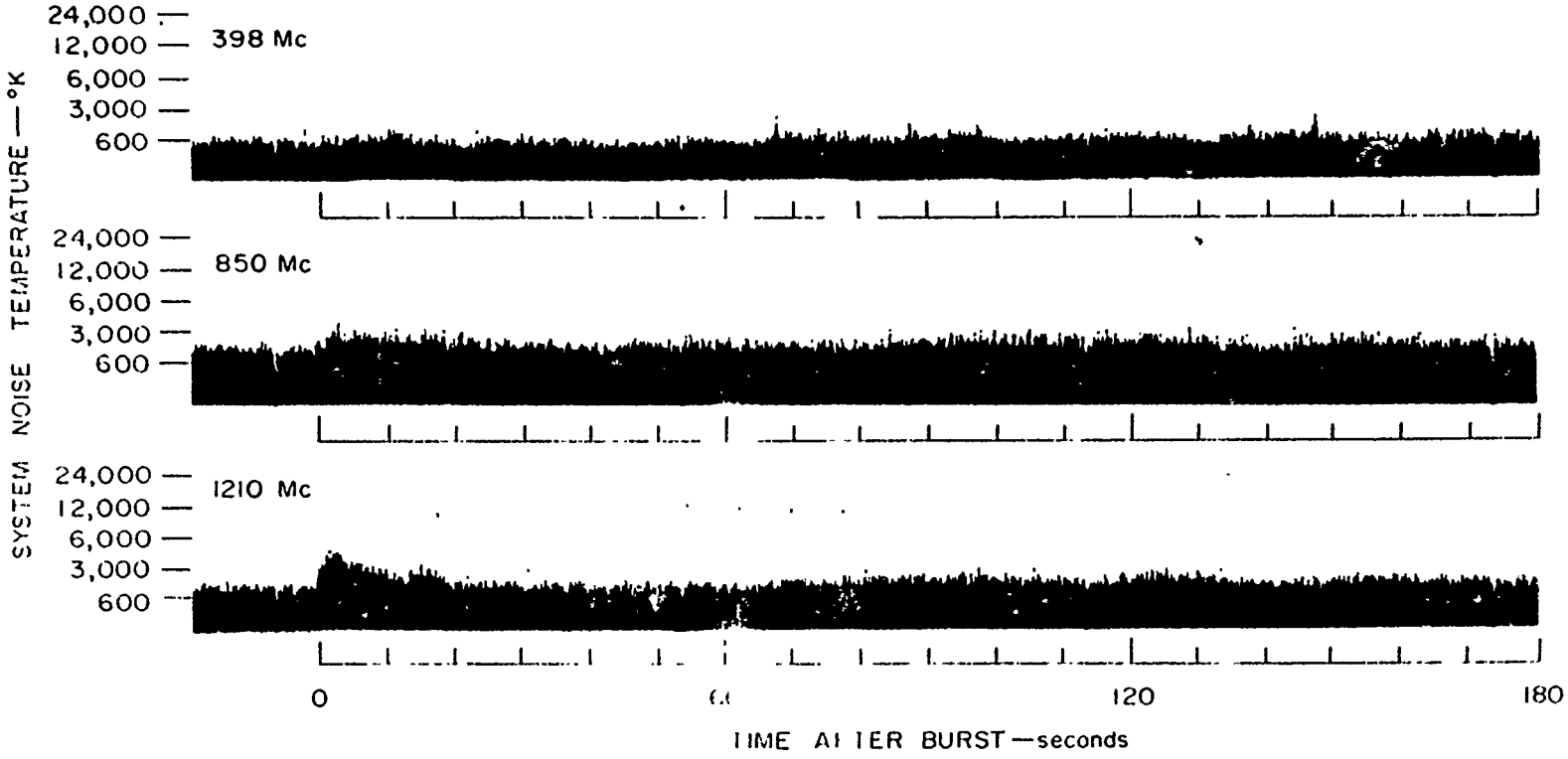

Figure 4.37 Johnston Island radar noise levels for King Fish.

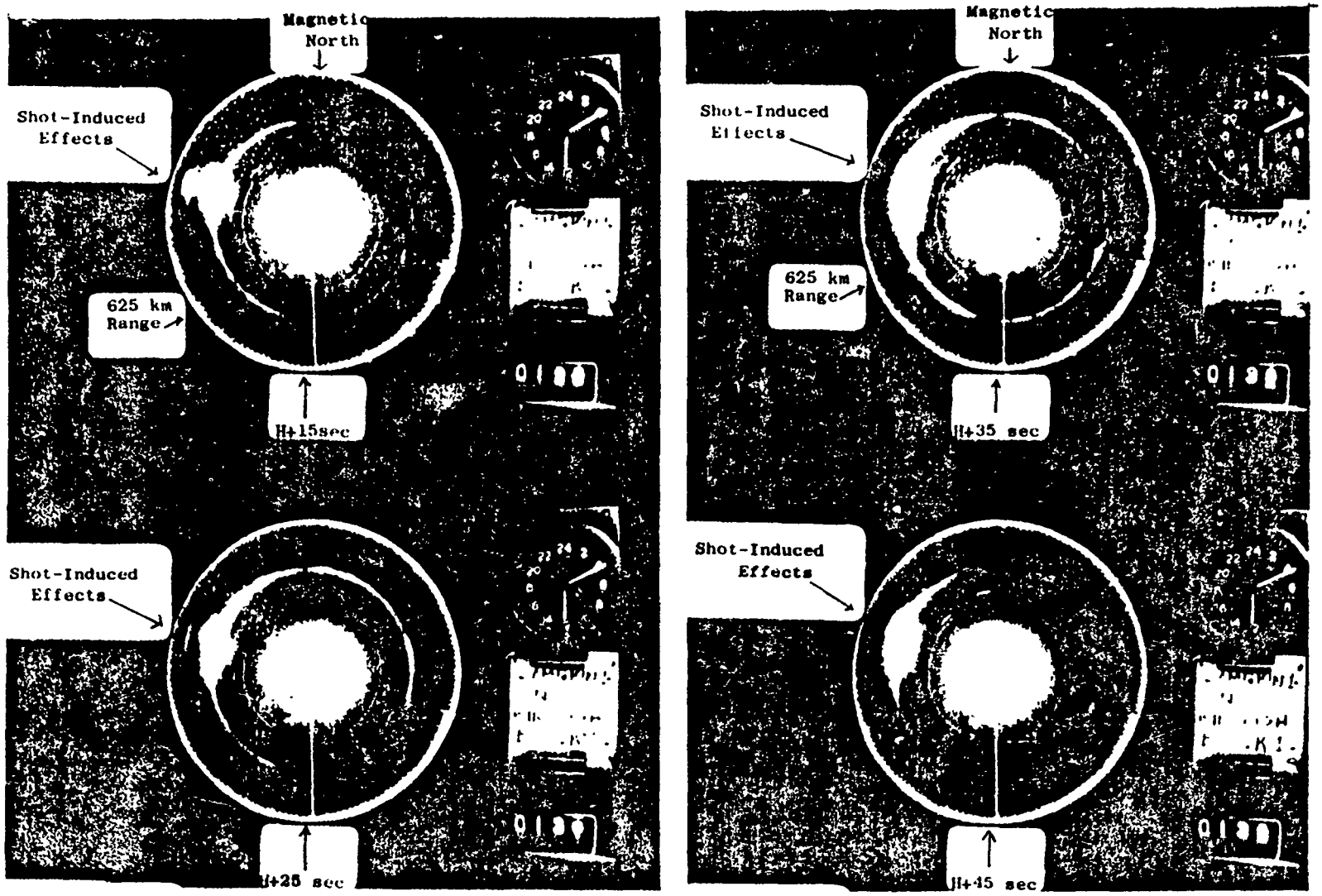

Figure 4.38 AEW aircraft radar PPI for King Fish; Lambkin 1, 15 to 45 seconds.

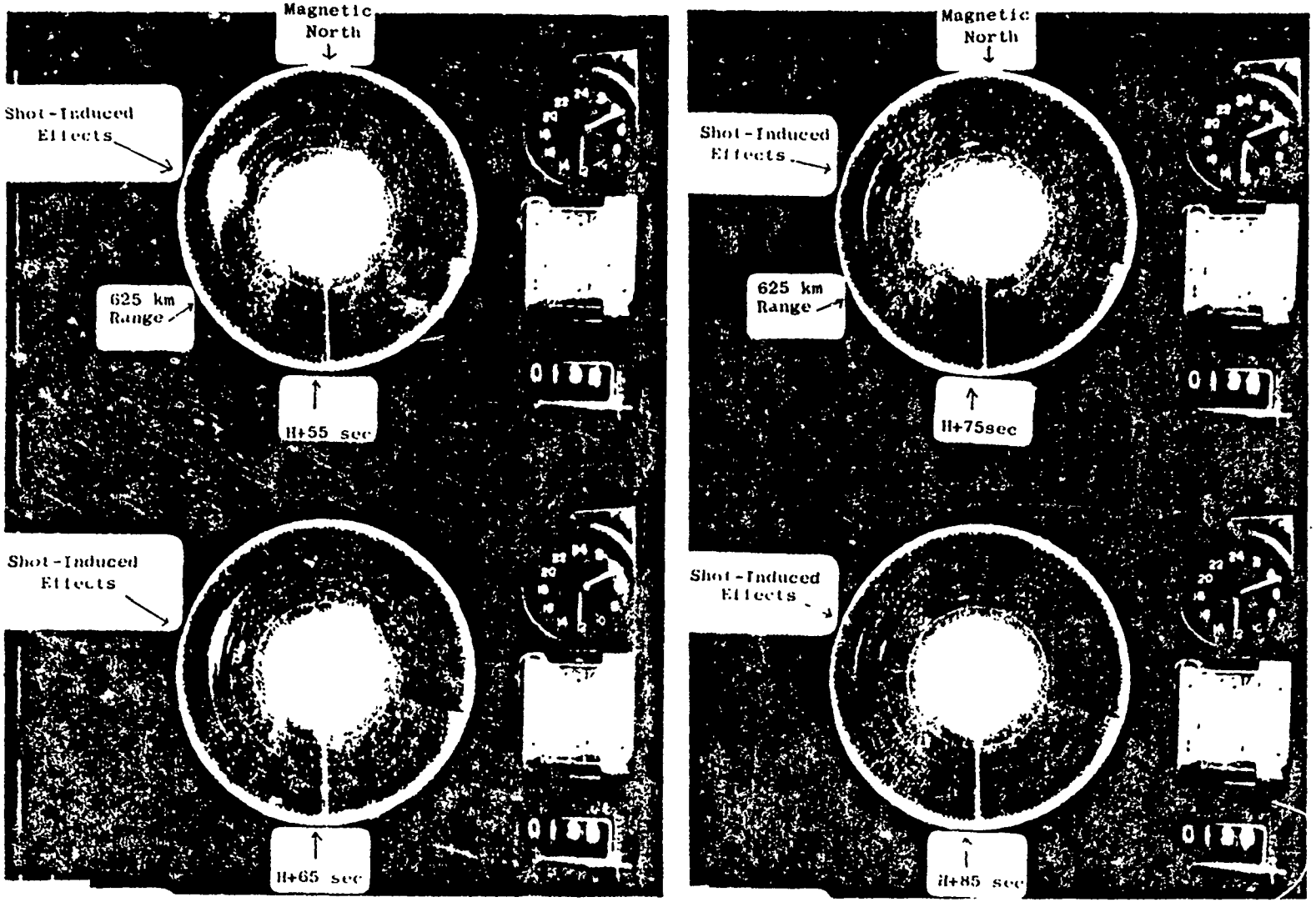

Figure 4.39 AEW aircraft radar PPI for King Fish; Lambkin 1, 55 to 85 seconds.

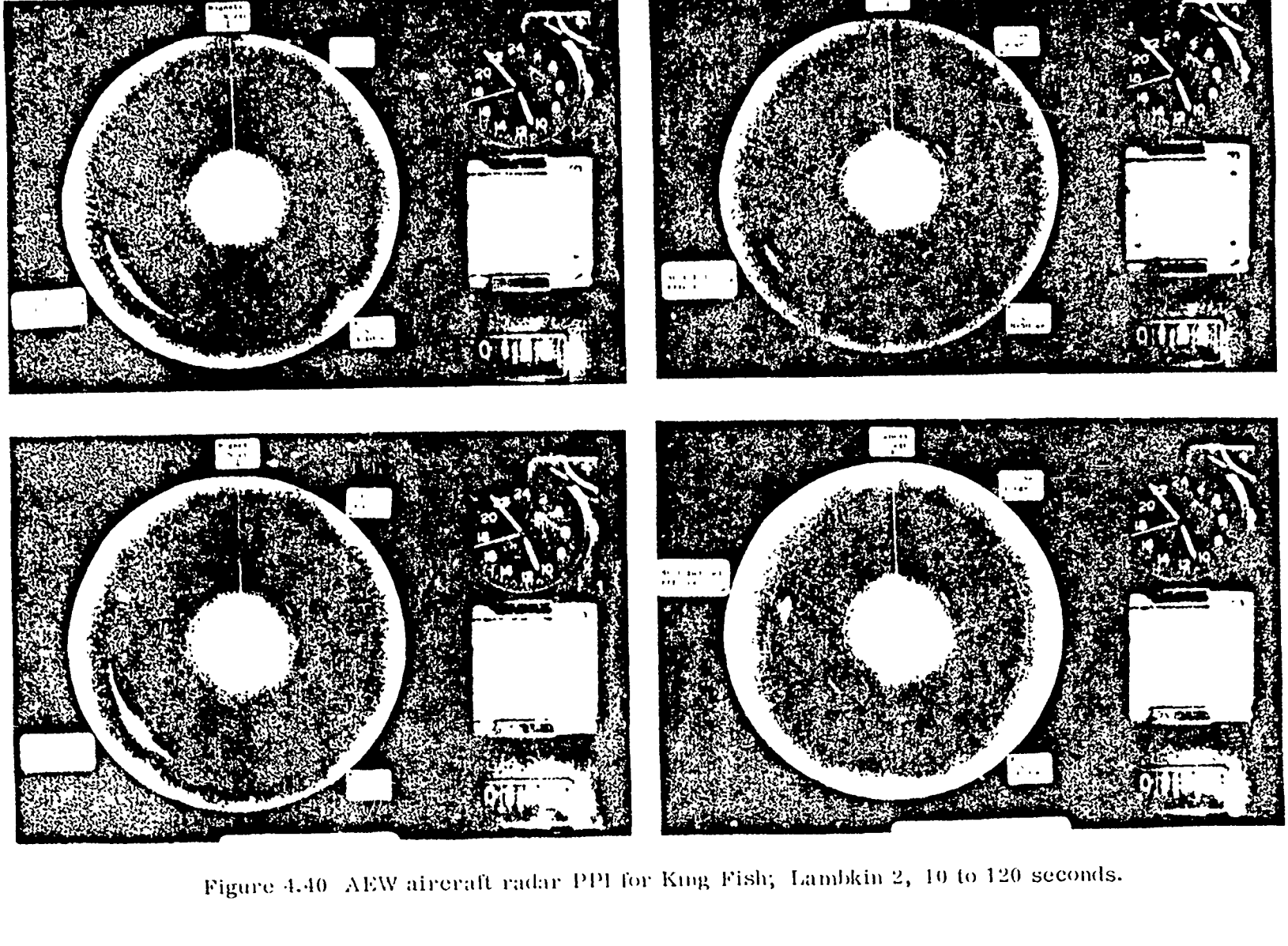

Figure 4.40 AEW aircraft radar PPI for King Fish; Lambkin 2, 10 to 120 seconds.

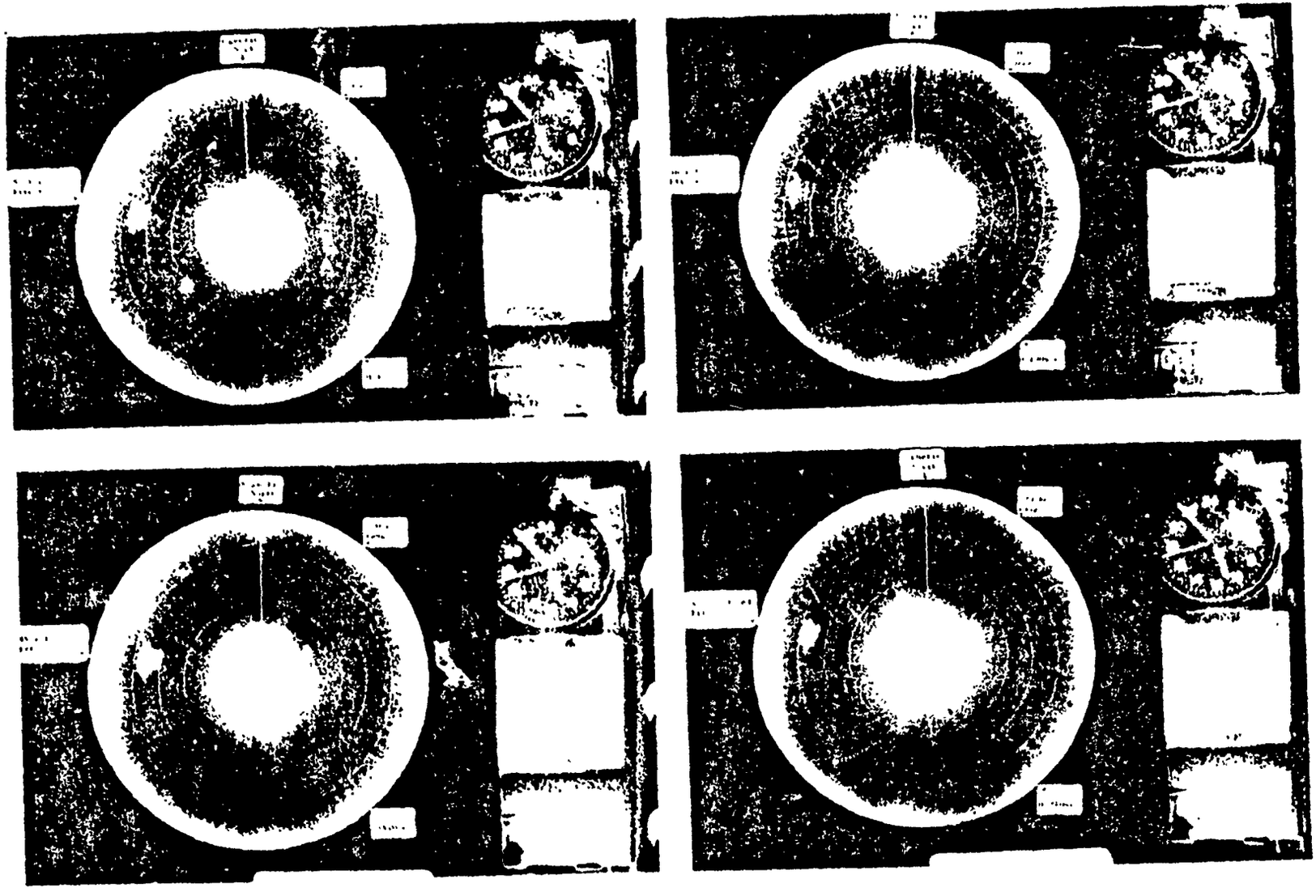

Figure 4.41 AEW aircraft radar PPI for King Fish; Lambkin 2, 150 to 210 seconds.

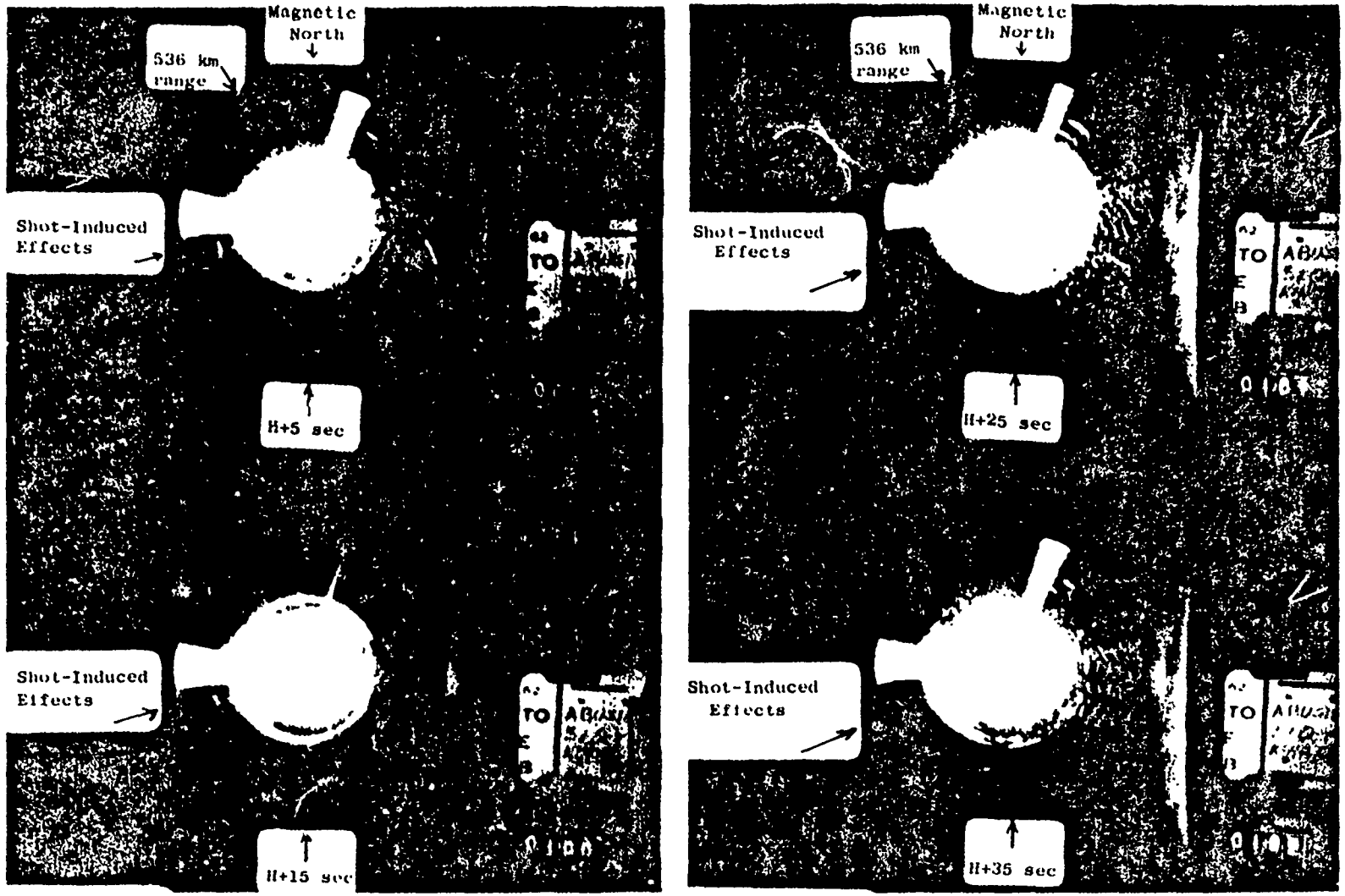

Figure 4.42 AEW aircraft radar PPI for King Fish; Abusive 1, 5 to 35 seconds.

Figure 4.43 AEW aircraft radar PPI for King Fish; Abusive 2, 10 to 40 seconds.

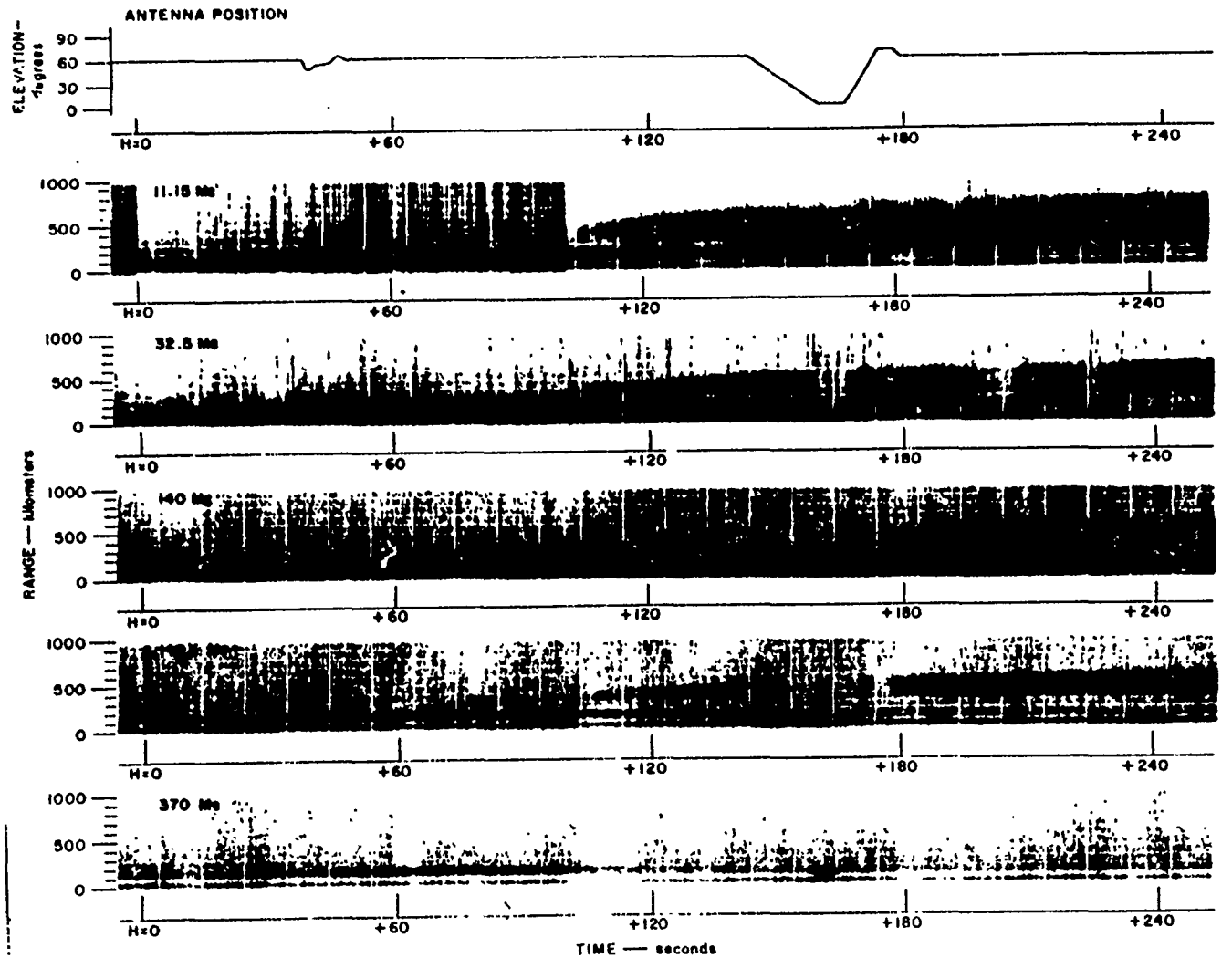

Figure 4.44 M/V ACANIA radar range versus time for King Fish, 0 to 240 seconds.

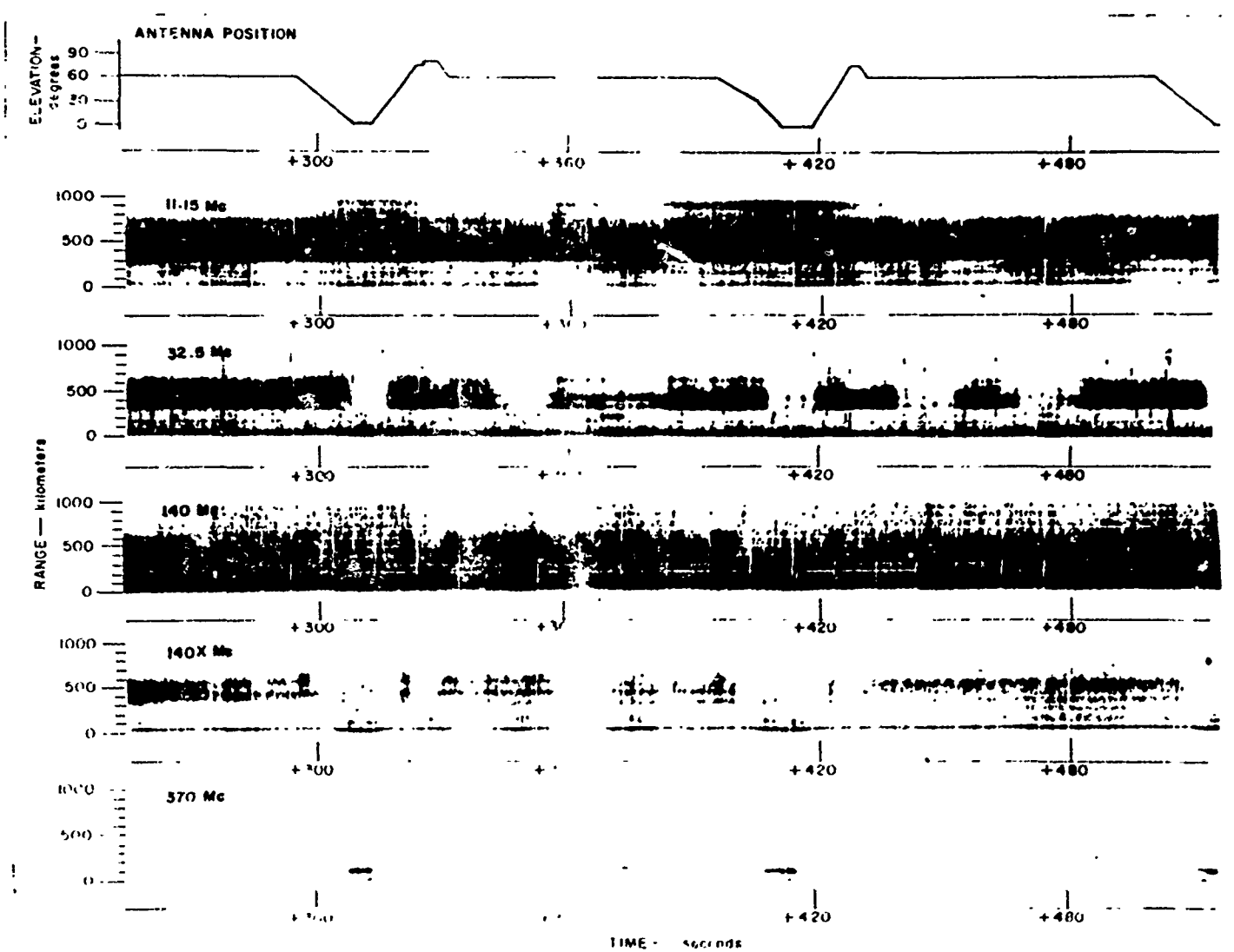

Figure 445 M/V ACANIA radar range versus time for King Fish, 240 to 480 seconds.

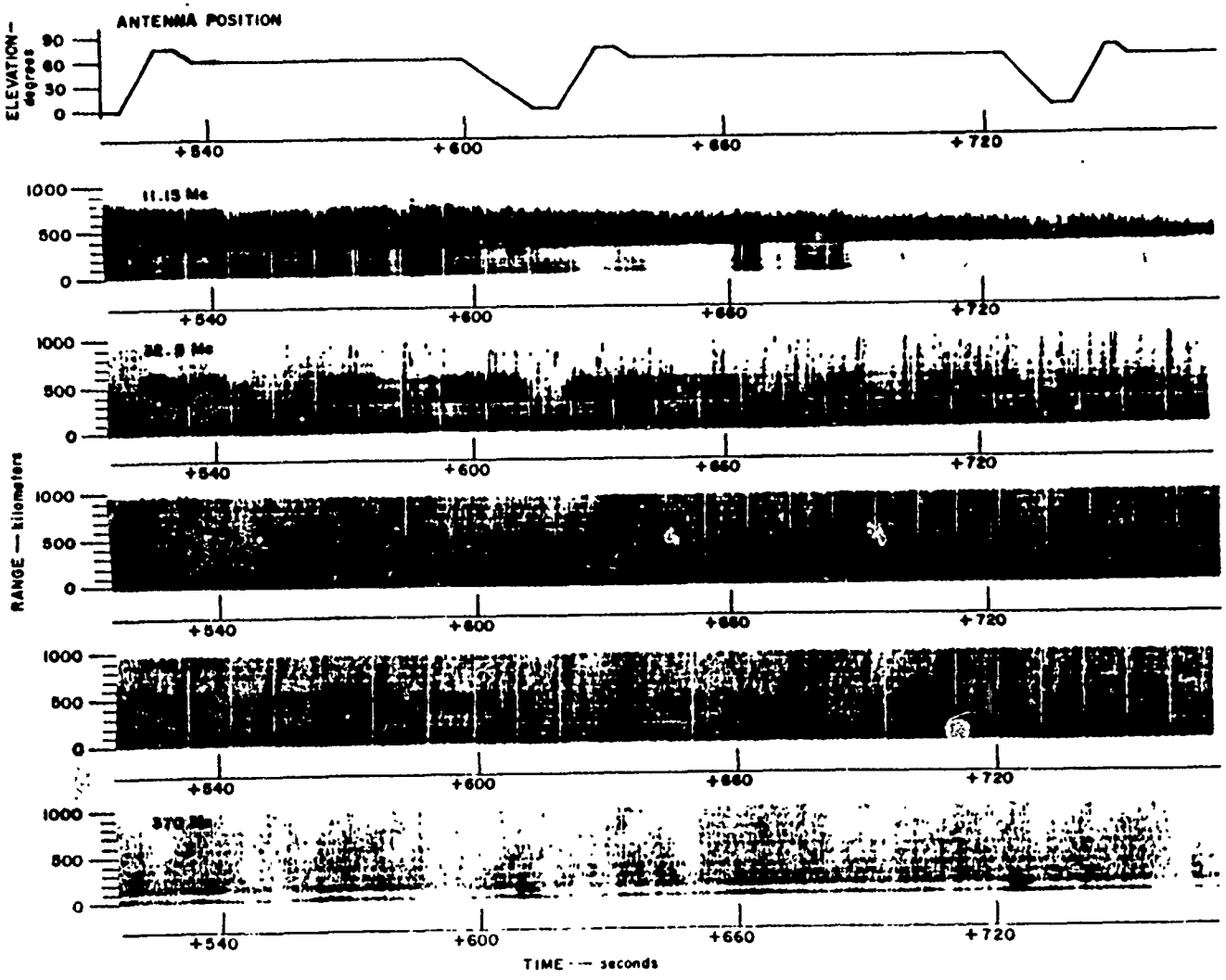

Figure 4.46 M/V ACANIA radar range versus time for King Fish, 480 to 720 seconds.

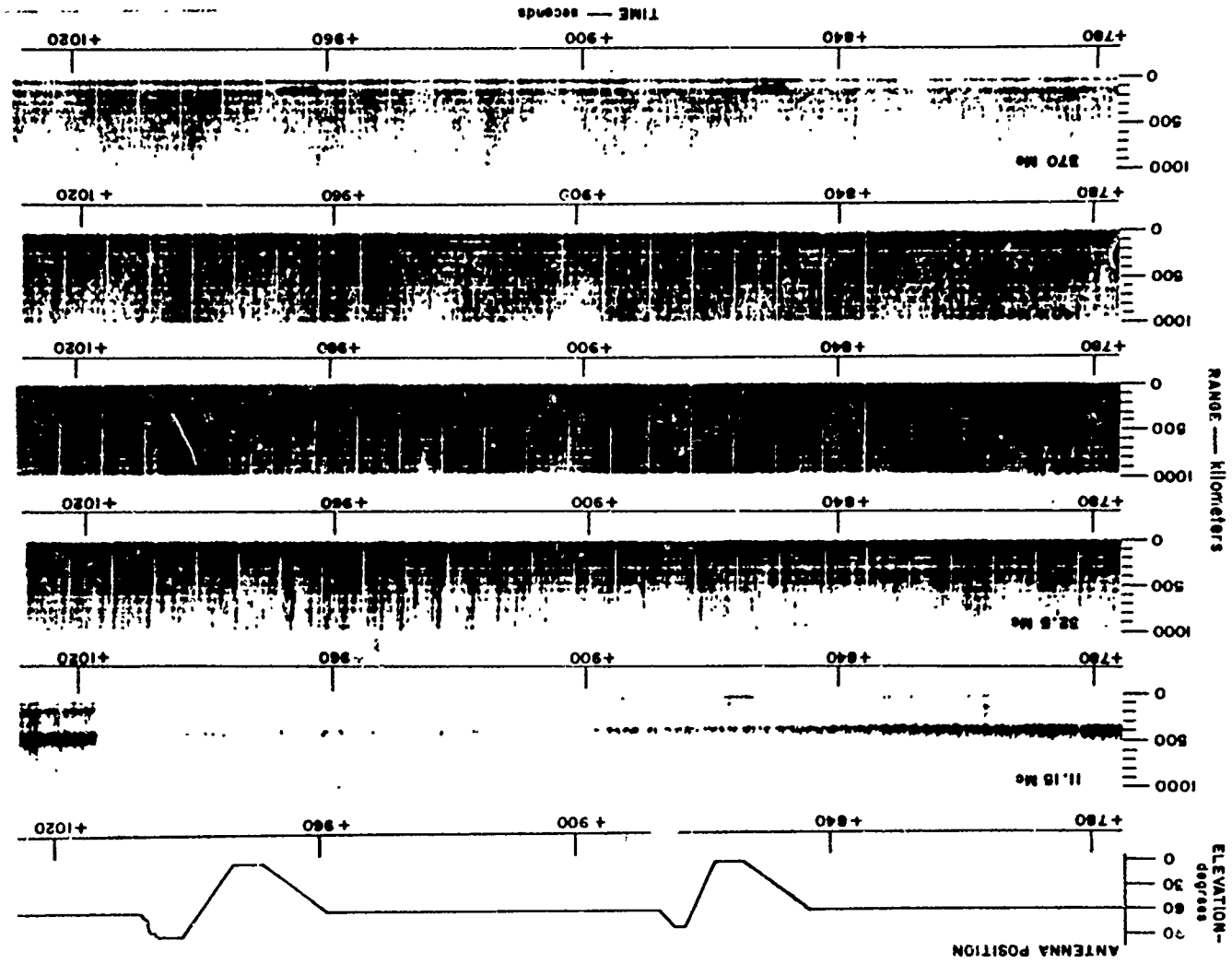

Figure 4.47 M/V ACANIA radar range versus time for King Fish, 780 to 1,020 seconds.

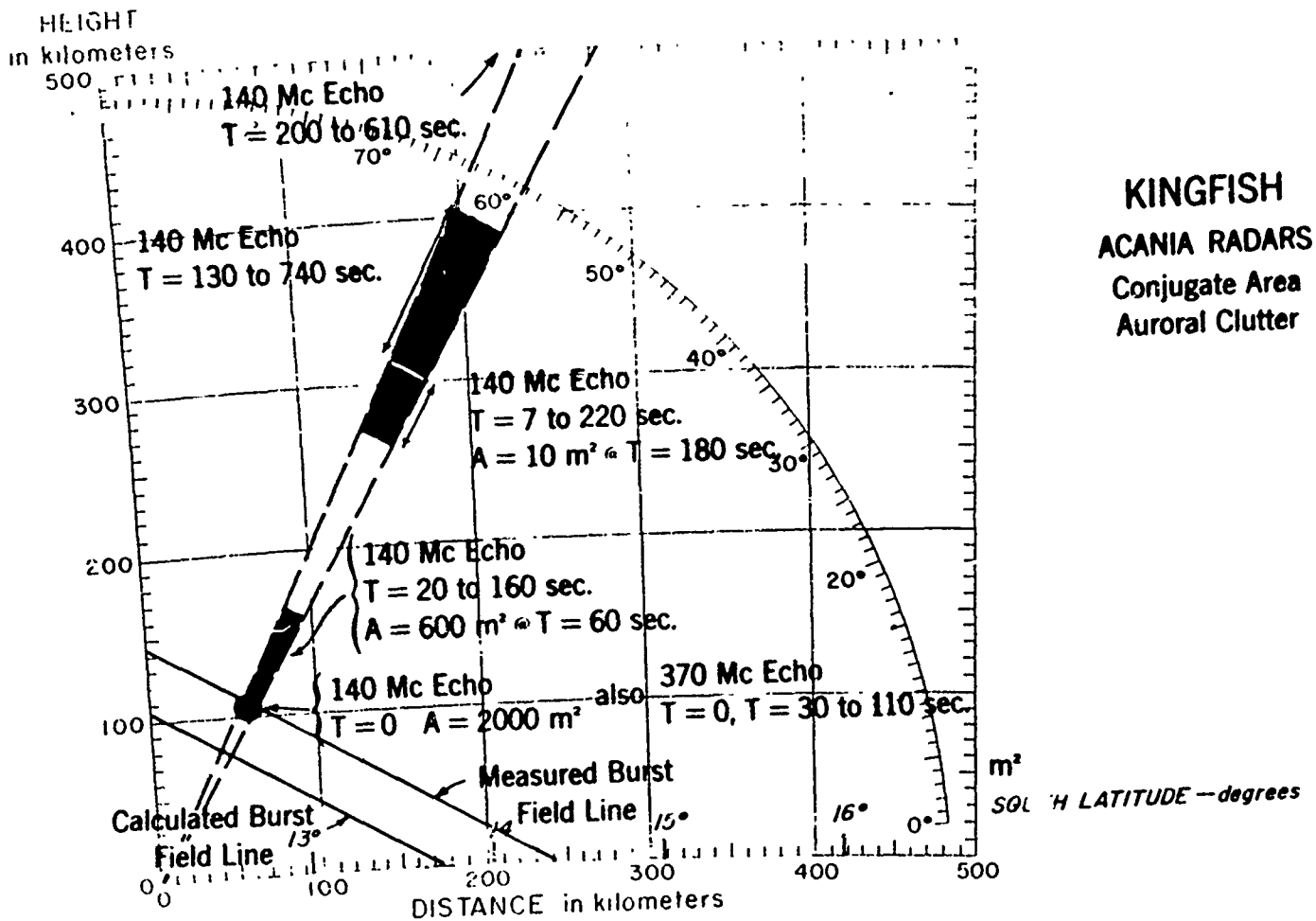

KINGFISH
ACANIA RADARS
Conjugate Area
Auroral Clutter

Figure 4.48 M/V ACANIA radar height versus distance for King Fish.

CHAPTER 5

CHECK MATE

5.1 INTRODUCTION

It was estimated that the Check Mate detonation would develop into a fireball some [redacted] in diameter in the period from H + 0 to H + 7 seconds.[1] This large fireball region would contain the debris and would be of a relatively high electron density. It was also estimated that the fireball region would then rise at about 1 to 2 km/sec until it reached an altitude of some several hundred kilometers.

By the time the formation of the fireball containing the debris had taken place, beta electrons would be streaming down the magnetic field line to the north and up the field lines to the south. These beta electrons would then cause auroral ionization in the vicinity north of the detonation and in the magnetic conjugate area. As the fireball rose and expanded, the beta-produced auroral region would be expected to expand in size and move north and south—in the vicinity of the detonation, and in the magnetic conjugate region, respectively.

Thus, radar returns would be expected from the high electron density of the fireball region and debris. In addition, radar echoes should result when looking at the beta-produced aurorae in the north and in the conjugate area, provided the radar looks at right angles to the earth's magnetic field in this region.

---

[1] See Volume 1 for a more complete discussion of the expected results.

It would also appear possible that an ordinary radar would see increases in the background noise level (equivalent to 500°K), as the temperature of the fireball region should be greater than 1000°K.

At later times it was expected that the debris would disperse and elongate itself along the magnetic field lines, forming auroras.

5.2 PROCEDURE

5.2.1 Johnston Island Radars.

Instrumentation. See Section 2.2.1.

Operating Technique. See Section 2.2.1.

5.2.2 AEW Aircraft Radars.

Instrumentation. See Section 2.2.2.

Operating Technique. Based upon the expected results, the AEW aircraft were positioned (to maximize the results due to the beta aurora) as shown in Figure 5.1. In the north, Lambkin 1 was located so that it was looking at H = 100 km perpendicular to the magnetic field line passing through the detonation. At this location the effects due to the prompt beta electrons from the detonation and any other charged emissions would be best observed. Lambkin 2 was located so that it was looking at H = 100 km perpendicular to the magnetic field line passing through H = 300 km directly above the detonation. In this location it should be possible to measure the rise rate of the debris as long as the debris rose to 300-km altitude.

In the magnetic conjugate area, Lambkin 3 was located conjugate to Lambkin 1, and Lambkin 4 was located conjugate to Lambkin 2, as shown in Figure 5.2. All of the AEW aircraft flew in patterns shown in Figure 2.8 at locations given in Table 5.1. The actual radar operating parameters are shown in Table 5.2.

5.2.3 M/V ACANIA Radars.

Instrumentation. See Section 2.2.3.

Operating Technique. The ACANIA was located in the magnetic conjugate area so that it looked at H = 100 km perpendicular to the magnetic field line passing through the detonation and on the same magnetic meridian as the detonation.

All conjugate locations were based upon calculations of the magnetic field using Finch and Leaton coefficients.

The exact location of the ACANIA is shown in Table 5.1. The radar operating technique is given in Section 2.2.3.

5.3 RESULTS

5.3.1 Johnston Island Radars.

Fireball/Debris Clutter. Prior to the detonation the antenna was positioned at 66° elevation and 191° azimuth. The 398-Mc radar was off until detonation. The actual detonation location was 3.5° lower in elevation. However, the debris cloud expansion was such that it completely filled the radar beam by H + 1 seconds as shown in Figure 5.11. The horizontal time-labeled lines show the debris cloud expansion diameter and rise as a function

of time. A comparison of Figure 5.11 and Figure 5.3 shows that the debris cloud was never out of the radar beam until H + 150 seconds. Comparing this with the distribution of radar echoes shows that visual correlation is good until H + 80 seconds at 398 Mc and only until H + 10 seconds at 850 and 1210 Mc. Following these times the radar echoes are sporadic in time and direction but somewhat correlated in frequency. After H + 3 minutes the antenna was scanned either manually or with the automatic programmer for eight hours following the detonation.

Starting abruptly at H = 0 when the transmitter RF was turned on, 398-Mc echoes at 170-km range saturated the receiver at 50 db S/N. This echo, along with several others also corresponding to direct reflections from the debris cloud, persisted until about H + 80 seconds. The range-versus-time records of the echoes for the first 35 minutes are shown in Figures 5.3 through 5.10. The spatial distribution of all the detonation-area echoes as well as the visual fireball/debris is shown in Figures 5.11 through 5.16. The echo amplitude-versus-time records for the first five minutes are shown in Figures 5.17 through 5.19. The peak echo amplitudes versus time, with antenna-direction-caused fluctuations removed, are shown in Figure 5.20. Starting at H + 1 second, echoes at 330-km range saturated the receiver at 50 db S/N. This echo, which corresponds to a one-hop sea-reflection mode, persisted at a continuously increasing range until about H + 100 seconds. Following H + 90 seconds, the antenna was scanned up and then down in elevation through the detonation

azimuth. Several 40-db S/N echoes were observed at various ranges during this scan. The echoes observed until H + 160 seconds comprise about 90 percent of the total number of echoes seen in the detonation area. No fireball/debris echoes were observed later than H + 5 minutes.

Starting abruptly at H = 0, 850-Mc echoes at 150-km range saturated the receiver at 50 db S/N. This echo persisted only until H + 9 seconds even though the debris cloud was still in the radar beam. Two other saturating echoes appeared somewhat later at H + 50 seconds. Several 40-db S/N echoes were observed at various ranges during the elevation scan following H + 90 seconds. The echoes observed until H + 160 seconds comprise about 95 percent of the total number of echoes seen in the fireball/debris area. No fireball/debris echoes were observed later than H + 5 minutes.

Starting abruptly at H = 0, 1210-Mc echoes at 180-km range saturated the receiver at 50 db S/N. This echo persisted only until H + 6 seconds, even though the debris cloud was still in the radar beam. Two other saturating echoes appeared somewhat later at H + 50 seconds. Several 30-db S/N echoes were observed at various ranges during the elevation scan following H + 90 seconds. The echoes observed until H + 160 seconds comprise about 95 percent of the total number of echoes seen in the detonation area. No fireball/debris echoes were observed later than H + 5 minutes.

Figures 5.21 through 5.23 show the Doppler records for the first five minutes following the detonation at each frequency. The 398-Mc records show both positive and negative shifts and some spread for only the first 60 seconds. The 850- and 1210-Mc records show wide positive-and-negative shifts and spread for only the first 10 seconds.

Auroral Clutter in the Detonation Area. As shown in Figure 5.3, strong auroral echoes were observed the first time a search for them was made at H + 200 seconds. Fifty-db S/N echoes were observed at 200- to 300-km height at 398 Mc. Twenty-db S/N echoes were observed at 275- to 300-km height at 850 Mc, and 3-db S/N echoes were observed at 275- to 300-km height at 1210 Mc.

Figures 5.24 through 5.43 show the spatial distribution of the auroral echoes. Figure 5.44 shows the peak amplitude of the echoes as a function of time, with antenna-direction-caused amplitude fluctuations removed. The 398-Mc echoes persisted until H + 2-1/2 hours with varying amplitudes. The 850-Mc echoes persisted only until H + 35 minutes, but then reappeared briefly at H + 1-1/2 hours. The 1210-Mc echoes faded out permanently at H + 10 minutes.

Figures 5.45 through 5.47 show the correlation of 398-Mc auroral echoes with the visual bomb-produced aurora over three time intervals: 3 to 10 minutes, 10 to 50 minutes, and 50 to 150 minutes.

The Doppler characteristics of the 398-Mc auroral echoes at H + 1,248 seconds are shown in Figure 5.48. This figure shows that the Doppler shift is no greater than ±2 kc, and the Doppler spread is no

greater than the transmitter pulse spectrum 3-db width of approximately 3 kc. Both of these characteristics are consistent with natural aurora-caused radar reflections at this frequency.

Fireball/Debris Noise. Radio noise emission was observed by the 398-, 850-, and 1210-Mc radar looking at the fireball/debris. The noise was most intense on the 1210-Mc radar and was equivalent to about 10,000°K. This amounted to about a 12-db increase in background noise. The increased noise level persisted until H + 140 seconds when the antenna was moved away from the fireball/debris. The noise-level increases are shown in Figure 5.49 for each of the frequencies.

5.3.2 AEW Aircraft Radars.

Fireball/Debris Clutter. Each of the detonation-area AEW aircraft (Lambkin 1 and 2, Abusive 1) observed echoes from air zero in the detonation area as shown in Figures 5.50 through 5.55. The fireball/debris echoes started at about H = 0 and lasted as late as H + 195 seconds. Table 5.3 gives the duration of these fireball/debris echoes and the equivalent radar cross section in m^2 (based upon a point target) and, when applicable, in m^2/m^3 (based upon a volume scatterer).

Auroral Clutter in the Detonation Area. Auroral clutter was observed by Lambkin 1 and Abusive 1 as shown in Figures 5.52 and 5.55. The duration of the auroral clutter observed by Lambkin 1 was H + 170 to H + 240 seconds with a radar cross section of 5 x 10^4 m^2. The duration of the auroral clutter observed by

Abusive 1 was H + 150 to H + 190 seconds with a radar cross section of 10^3 m^2.

Auroral Clutter in the Conjugate Area. No auroral clutter was observed in the conjugate area by the AEW aircraft radars.

5.3.3 M/V ACANIA Radars.

Auroral Clutter in the Conjugate Area. The M/V ACANIA operated its 140- and 370-Mc radars during the detonation and for several hours afterwards. The antenna was positioned magnetically south in azimuth and 60° elevation, and periodically elevation scans were made. Prompt echoes a few pulses in duration were observed at 140 Mc. The range-versus-time records for the first 16 minutes are shown in Figures 5.56 through 5.59. Auroral clutter echoes were observed at 140-Mc again at H + 180 seconds, and between H + 240 and H + 360 seconds. The H + 180-second echoes were at a height of about 200 km as shown in Figure 5.60 and were equivalent to 0.4 m^2. The H + 240 to H + 360-second echoes were at an altitude of 300 km. No 370-Mc echoes were observed.

5.4 DISCUSSION

Interpretation of the Johnston Island radar 50-db S/N ratio echoes in terms of m^2/m^3 (volume cross section) gives a value of about 10^{-11}. Assuming scattering by a point target (a very doubtful interpretation) the equivalent radar cross section is about 10 m^2. If the scattering mechanism is assumed to be incoherent scatter from the electrons in the fireball and debris, the 50-db S/N echoes

yield an electron density of 10^{11} electrons/cc and a plasma frequency of 2500 Mc. As with the events discussed earlier in this volume, the 50-db returns cannot have been produced by this mechanism.

The negative results on the southern AEW aircraft and the 370-Mc ACANIA radar would indicate that the debris associated with yield is not sufficient to produce extensive conjugate-area auroral clutter.

5.5 CONCLUSIONS

A Check Mate event would have a seriously degrading effect on the performance of a ballistic missile defense radar system. To evaluate this effect, a comparison has been made between the radars used during Fish Bowl and the planned BMD radar systems.

The radars used during these tests were, in general, somewhat less sensitive than those being planned for use in BMD activities. The advantage that a particular system radar would have over the test radars is shown for various scattering models in Table 2.6 of Chapter 2. The comparisons were developed by scaling the system radar to its nearest frequency counterpart used during Fish Bowl. For example, the BMEWS radars were compared with the 398-Mc Johnston Island radar and the Nike-Zeus TTR radar was compared to the DAMP FPQ-4 C-band radars.

In order to give the reader a better understanding of the degrading effects of the Check Mate event, an estimate of the effect on the BMEWS tracking radar has been made, ignoring the fact that the

operating pulse length of the BMEWS radar is too long to observe Check Mate fireball/debris clutter at that range. The BMEWS system was picked as an example not to deprecate that particular system, but because that system is operational, field-deployed, and its characteristics are well known. Table 2.7 of Chapter 2 shows the comparison between the BMEWS tracking radar characteristics and the Johnston Island 398-Mc radar. The comparison was made assuming the scattering was from a beam-filling target of range depth of at least one pulse width (300 μsec).

From the comparison, estimates of the strength and time duration of the clutter and noise effects are given below:

Fireball/Debris Clutter

H + 0	S/N = 90 db	Main Beam
	S/N = 40 db	Side Lobes
H + 2 min	S/N = 40 db	Main Beam
	S/N = 0 db	Side Lobes
	S/N = 0 db	Main Beam

Angular Diameter of Affected Region.

1 sec	12^{o}
10 sec	20^{o}
60 sec	33^{o}

Detonation Area Auroral Clutter.

H + 0 to H + 4 hrs.	S/N > 44 db
H + 4 hours to ?	S/N = 44 db

Fireball/Debris Noise.

Maximum 5000°K for 20 seconds duration

7-db increase

Conjugate-Area Auroral Clutter.

H + 0 to H + 1 min	S/N > 54 db
H + 1 min to ?	S/N = 54 db

From the above it is apparent that as much as 1000 square degrees of area would be obscured for a depth of at least one pulse length plus 50 km by the fireball/debris clutter for a period of as much as 2 minutes. In addition, the 1000 square degrees of area would be observed at a 7-db reduction in sensitivity at all ranges at a 50-percent bandwidth for up to 20 seconds because of the fireball/debris noise. Although the Doppler spread of the echoes is not severe, the limited bandwidth of the 20-kc Doppler channel used with the Johnston Island radars does not rule out the possibility of there being Doppler components at a velocity comparable to the radial velocity of an approaching ICBM.

Detonation-area auroral clutter would obscure considerable area at a variety of ranges from 100 km to 500 km for a depth of at least one pulse length for a period of up to 4 hours. However, the Doppler width would be relatively narrow.

Conjugate-area auroral clutter would obscure a relatively small area at a variety of ranges for a depth of at least one pulse length for a period of up to two minutes. The Doppler width would be relatively narrow.

The extended volume of clutter and noise produced by Check Mate would make it difficult to avoid the clutter problem by using spaced radars in a BMD system, and impossible in the case of multiple Check Mate bursts.

TABLE 5.1 LOCATIONS OF AEW AIRCRAFT AND M/V ACANIA DURING CHECK MATE

	Longitude	Latitude
Abusive 1	168°57.5'W	16°00'N
Lambkin 1	166°07'W	16°18'N
Lambkin 2	165°34'W	18°08'N
Lambkin 3	178°22'W	11°41'S
Lambkin 4	178°55'W	14°00'S
ACANIA	174°56'W	12°27'S

TABLE 5.2 OPERATING CHARACTERISTICS OF THE AEW AIRCRAFT RADARS DURING CHECK MATE

L = Lambkin, A = Abusive.

	L1	L2	L3	L4	A1
Frequency, Mc.	428	425	426	443	435
Peak Power, watts x 10^6	1.5	0.9	1.25	1.4	1.4*
Pulse Width, μsec	8.4	9.0	8.0	8.0	8.0*
PRF, cps	239	232	227	248	280
MDS, -dbm	112	115	110	114	114*
Dynamic Range, db	21	21	24	24	18*
σmin at 500 km, m^2	26	22	50	20	.19*

* approximate values

TABLE 5.3 AEW AIRCRAFT RADAR FIREBALL/DEBRIS CLUTTER FOR CHECK MATE

	Time from Burst (Sec)	Radar Cross Section: Point Target (m^2)	Radar Cross Section: Volume Scatterer (m^2/m^3)
Lambkin 1	0-15	8×10^5	1.3×10^{-7}
	45	6×10^4	1×10^{-8}
Lambkin 2	5	2×10^5	0.3×0^{-7}
	25	2.6×10^3	0.4×10^{-9}
	35	5.8×10^2	
	155-195	1.5×10^2	
Abusive 1	1	2.3×10^6	2.1×10^{-6}
	10	1.4×10^6	2.3×10^{-7}
	20	8.6×10^3	1.4×10^{-9}

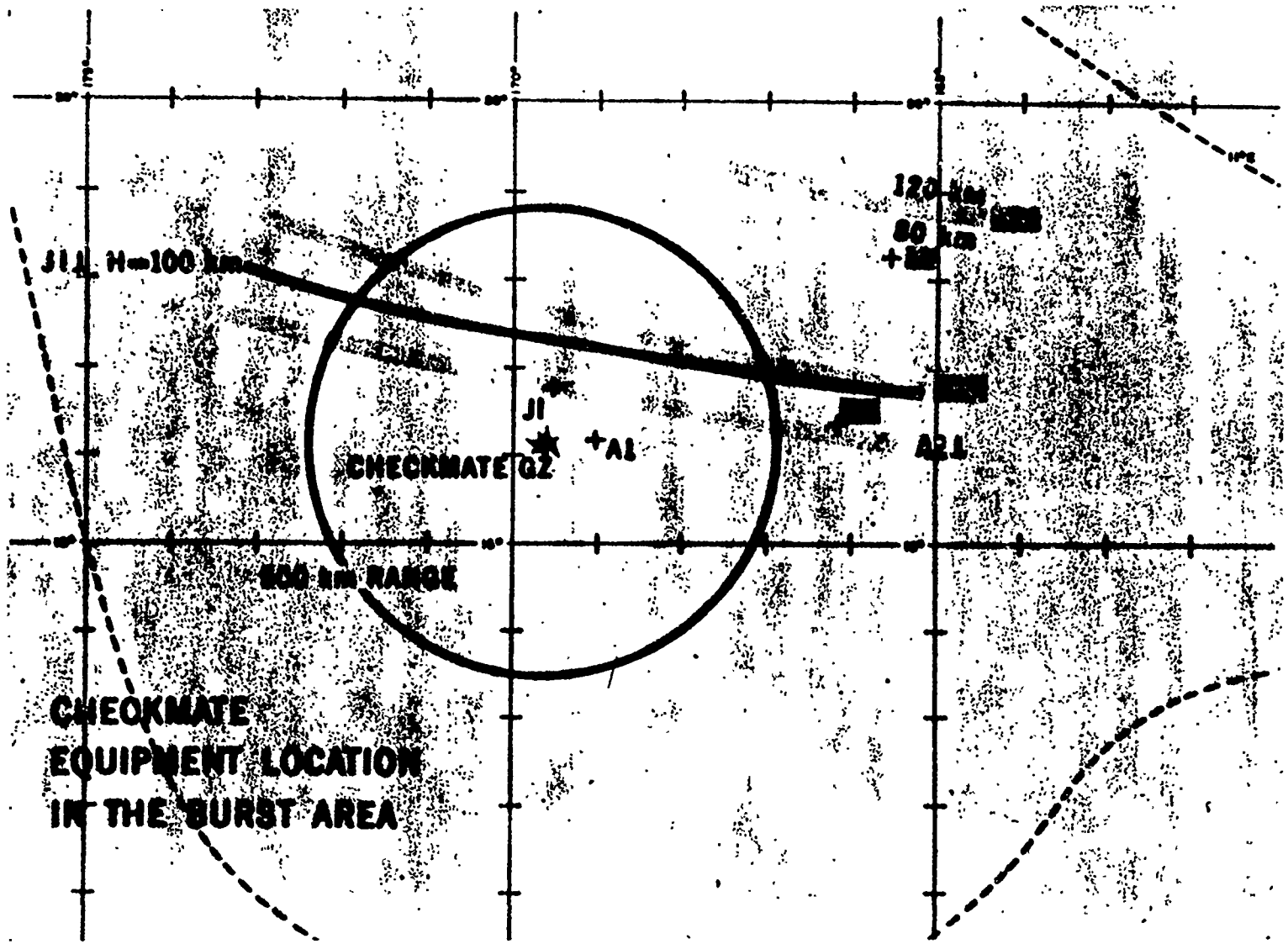

Figure 5.1 Equipment location in the detonation area for Check Mate.

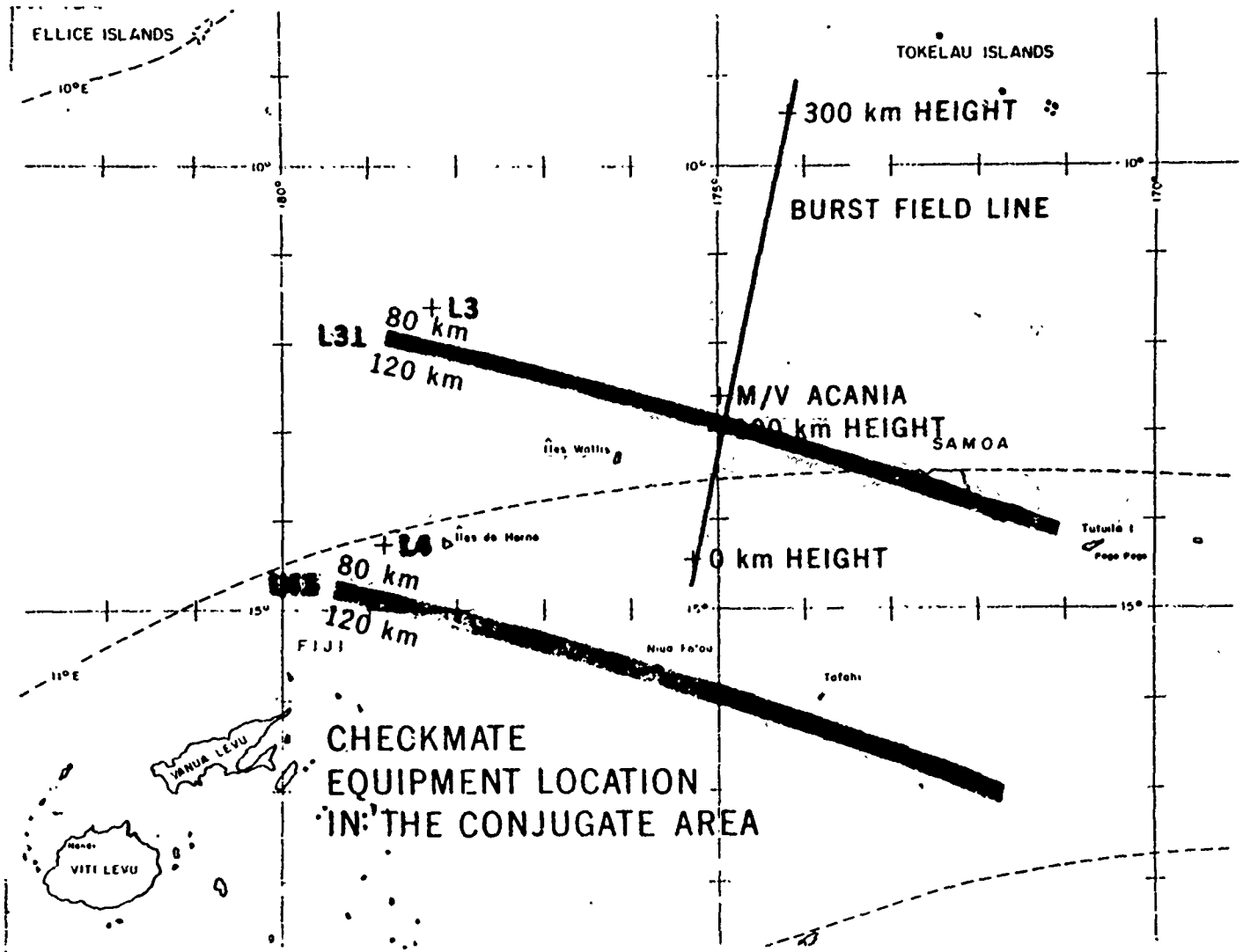

Figure 5.2 Equipment location in the conjugate area for Check Mate.

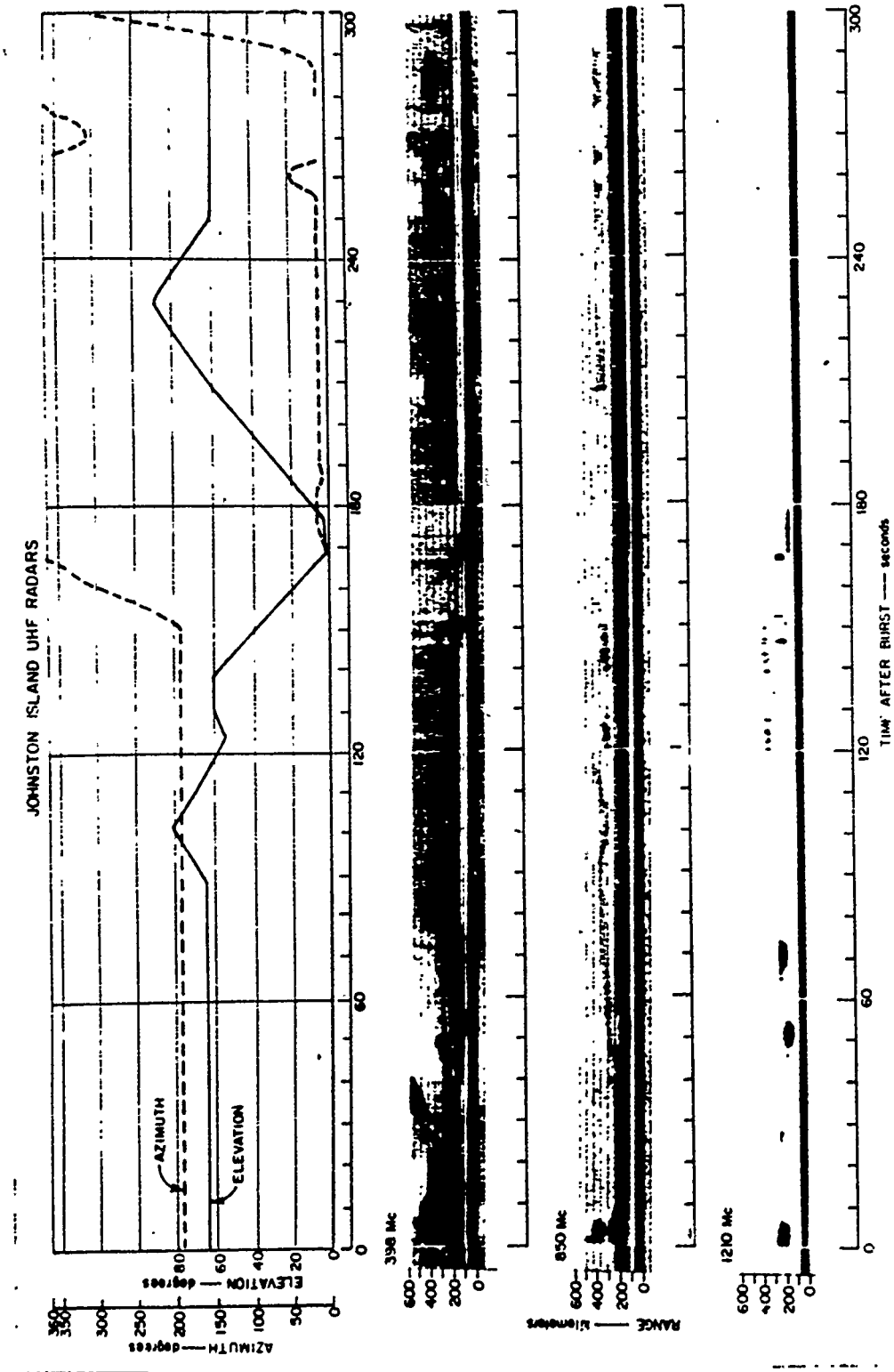

Figure 5.3 Johnston Island radar range versus time for Check Mate; 0 to 600 km, 0 to 300 seconds.

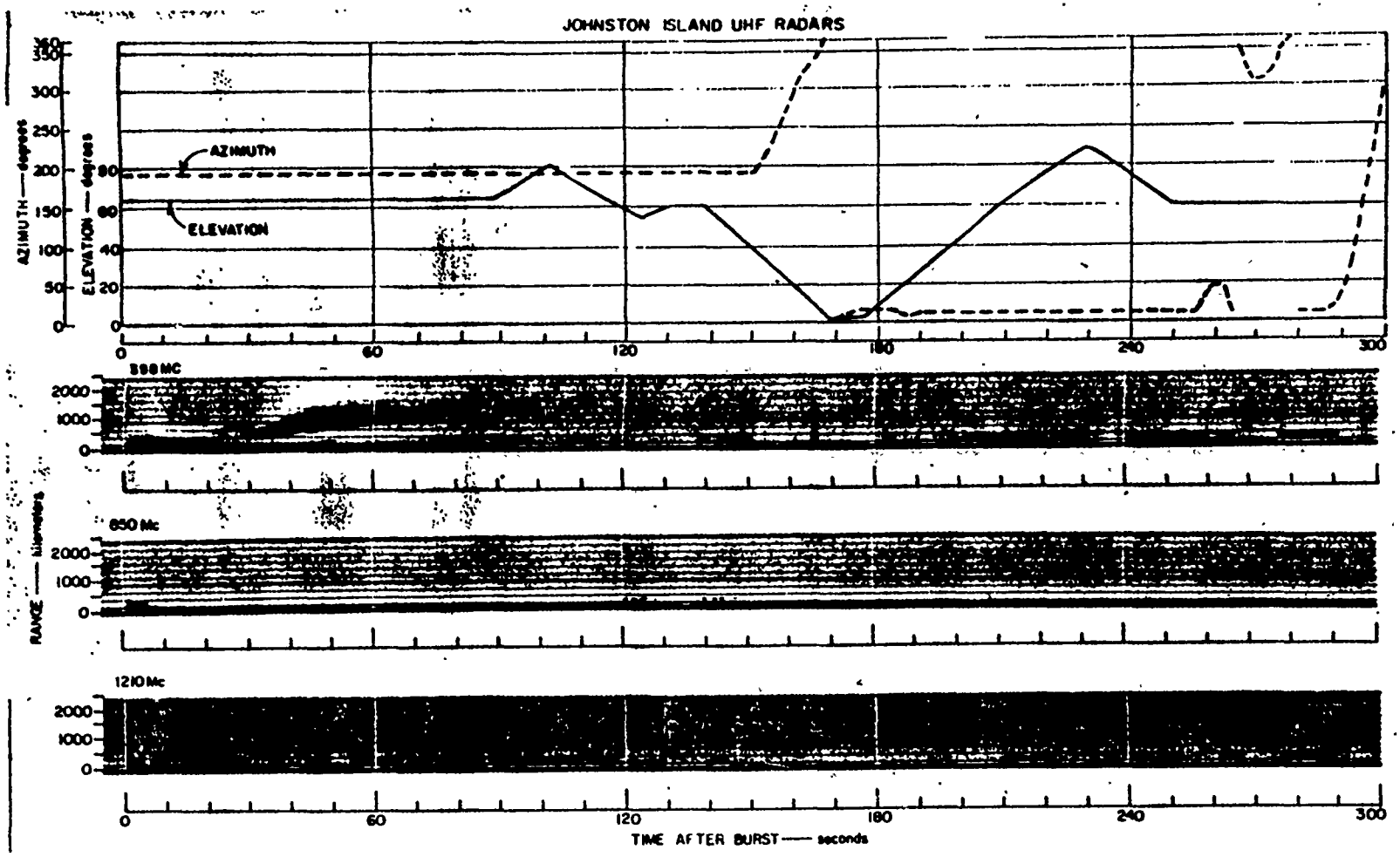

Figure 5.4 Johnston Island radar range versus time for Check Mate; 0 to 2,500 km, 0 to 300 seconds.

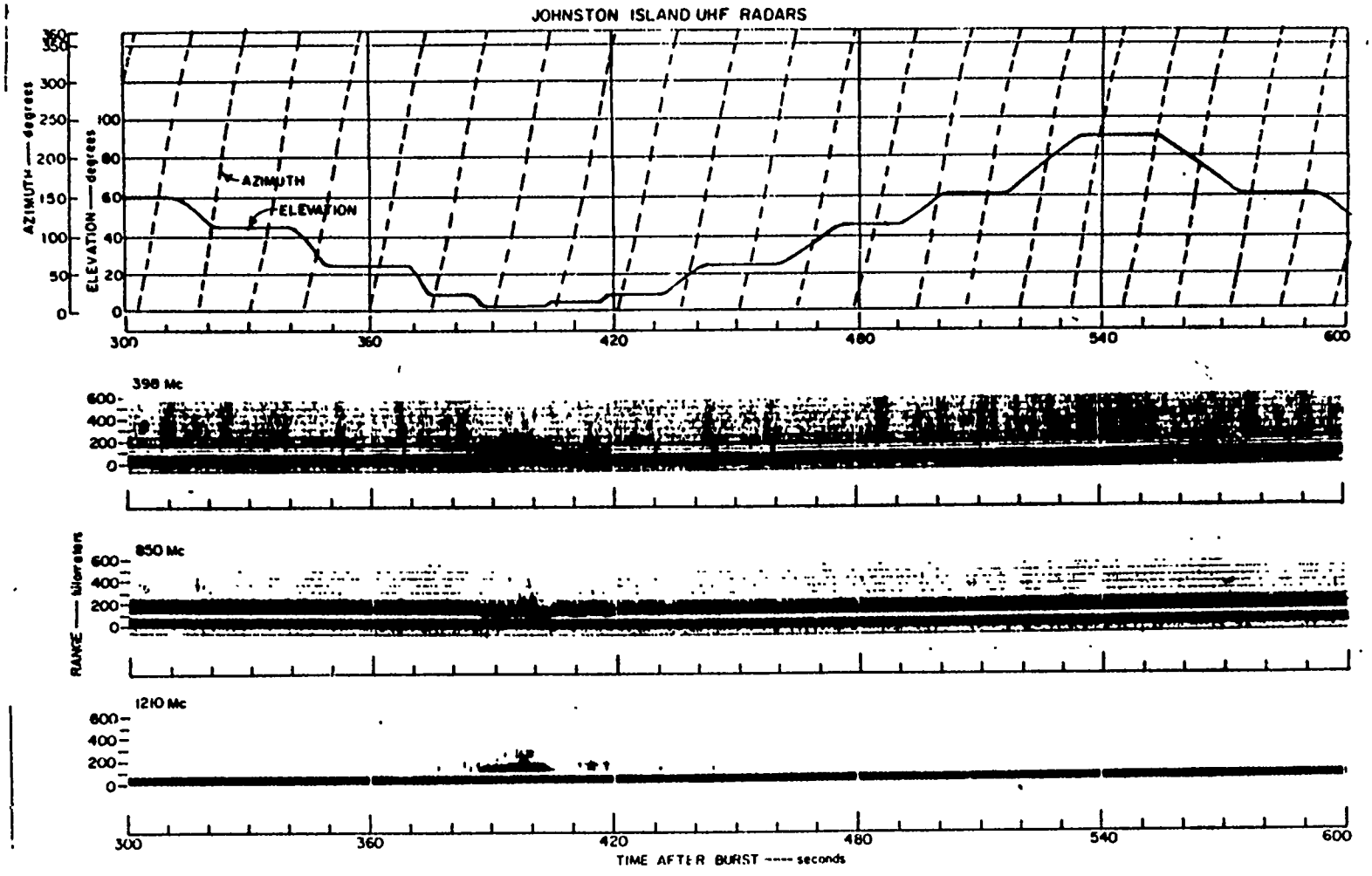

Figure 5.5 Johnston Island radar range versus time for Check Mate; 0 to 600 km, 300 to 600 seconds.

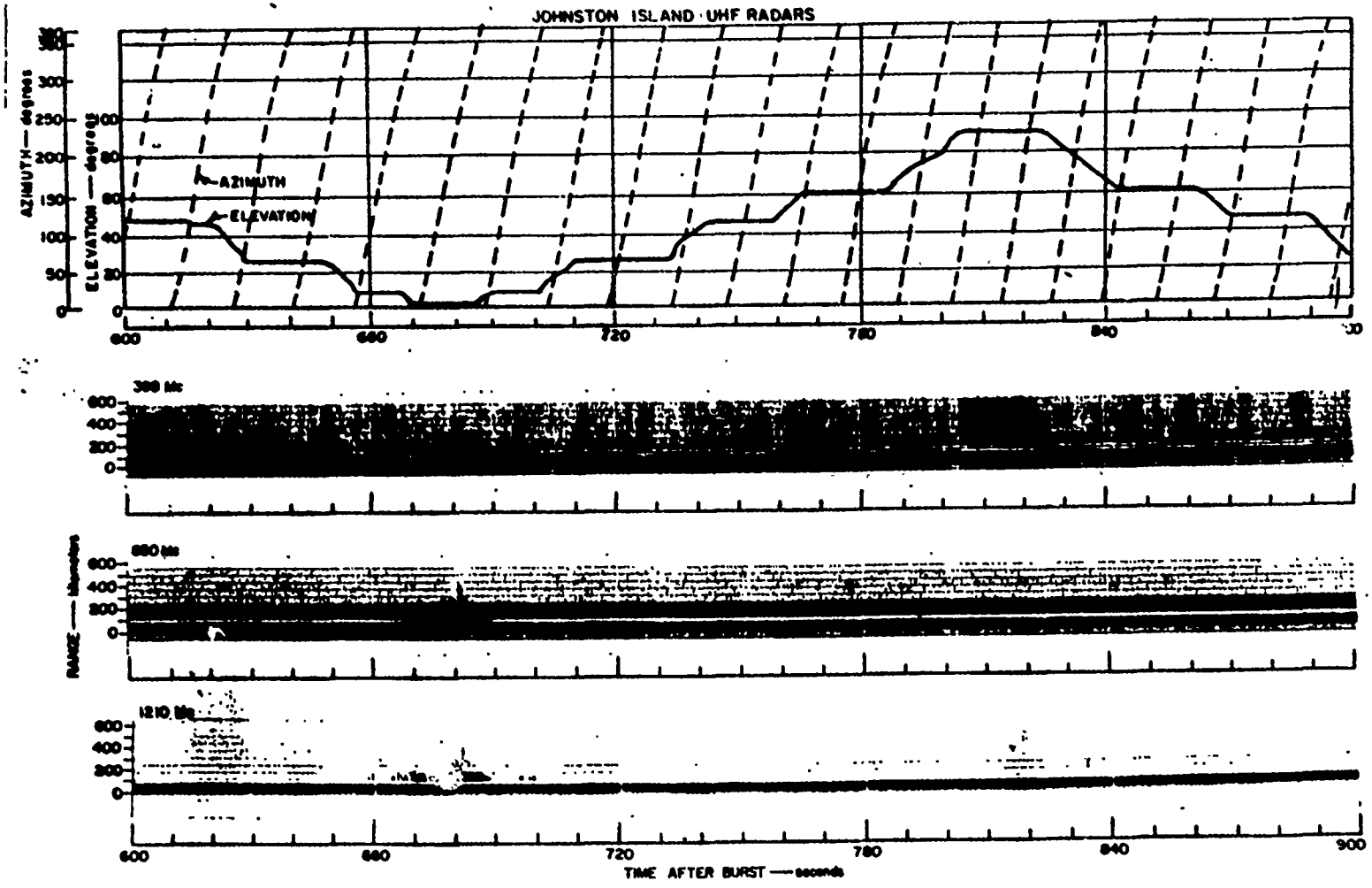

Figure 5.6 Johnston Island radar range versus time for Check Mate; 0 to 600 km, 600 to 900 seconds.

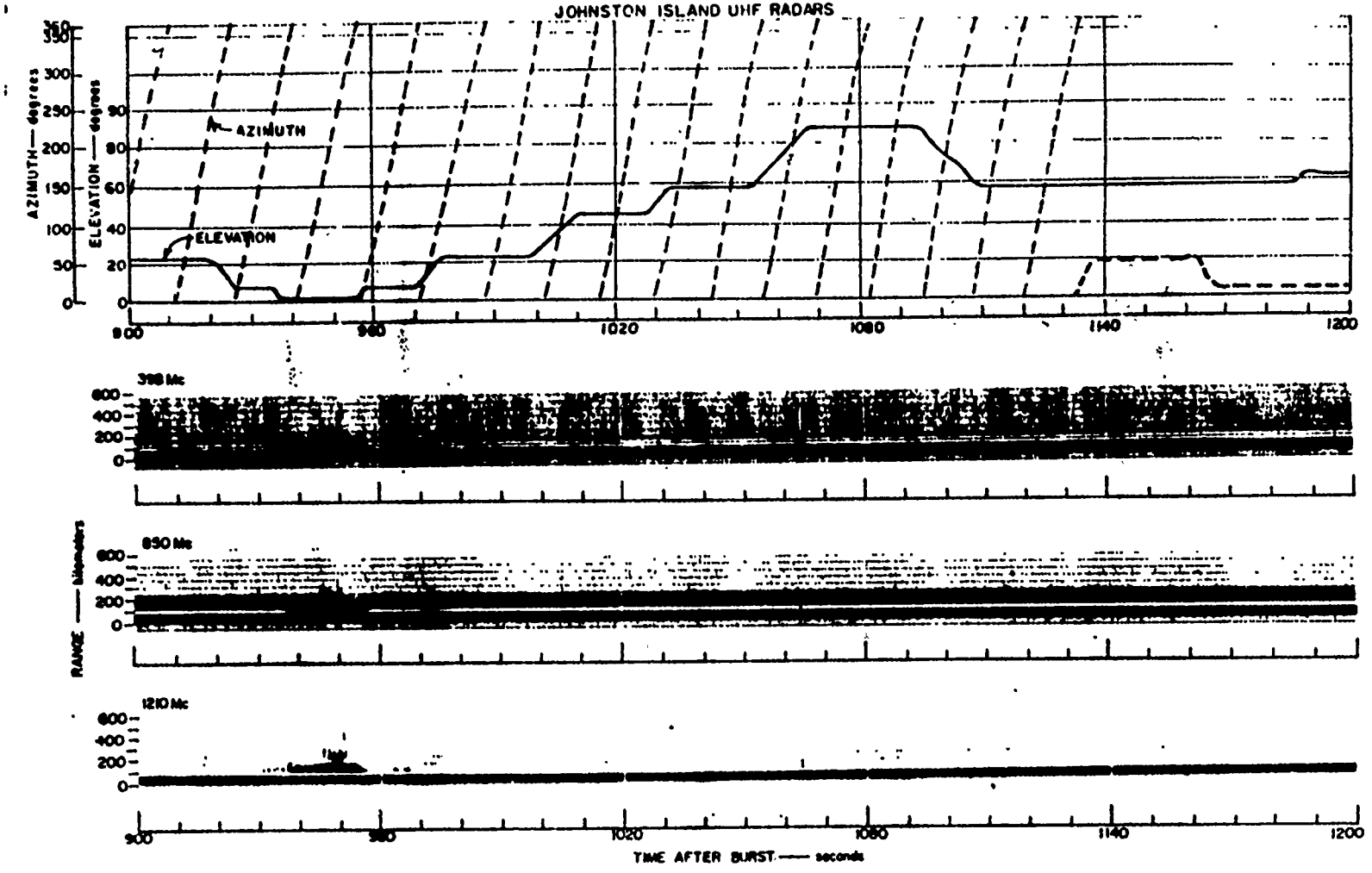

Figure 5.7 Johnston Island radar range versus time for Check Mate; 0 to 600 km, 900 to 1,200 seconds.

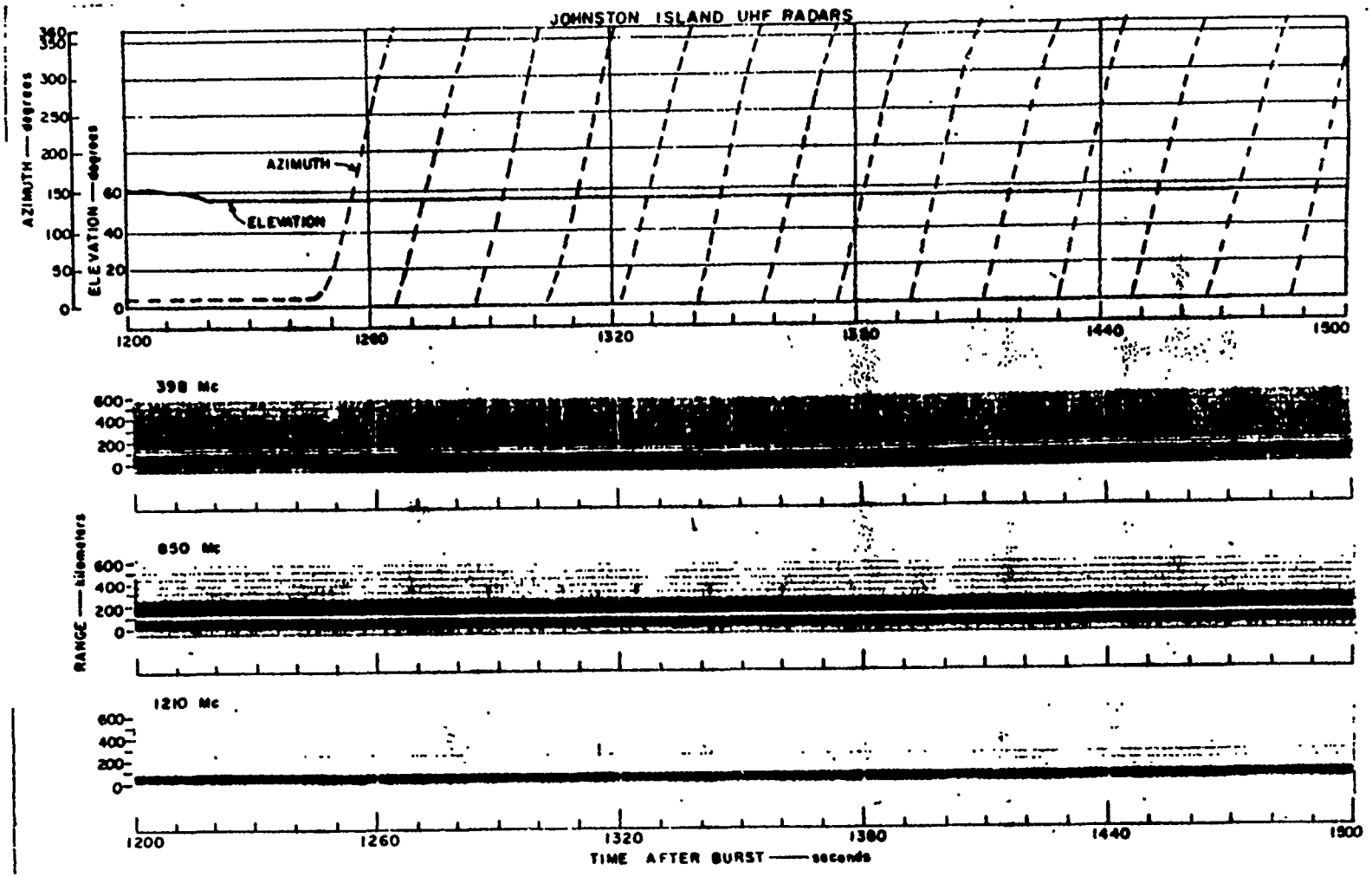

Figure 5.8 Johnston Island radar range versus time for Check Mate; 0 to 600 km, 1,200 to 1,500 seconds.

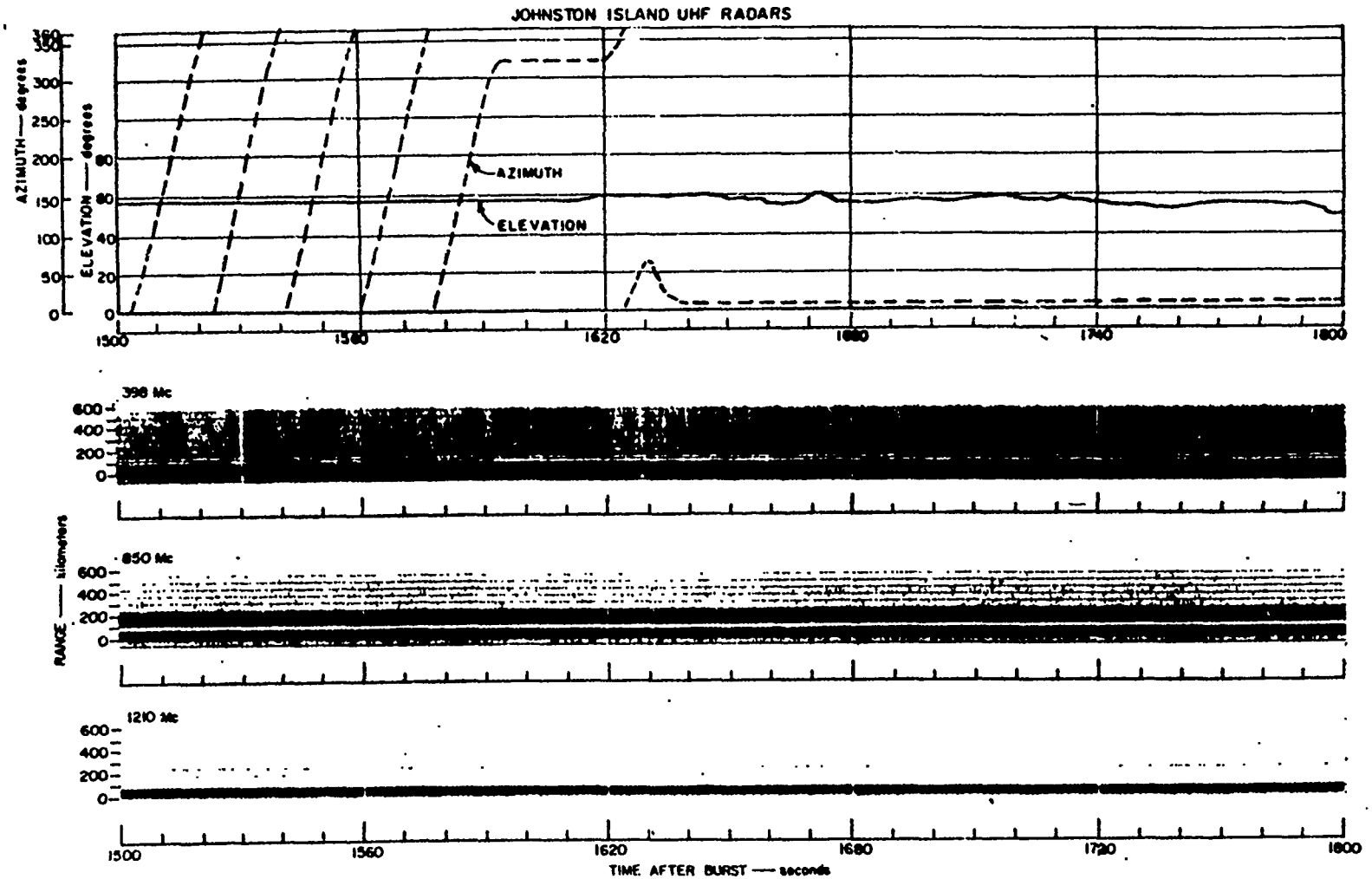

Figure 5.9 Johnston Island radar range versus time for Check Mate; 0 to 600 km, 1,500 to 1,800 seconds.

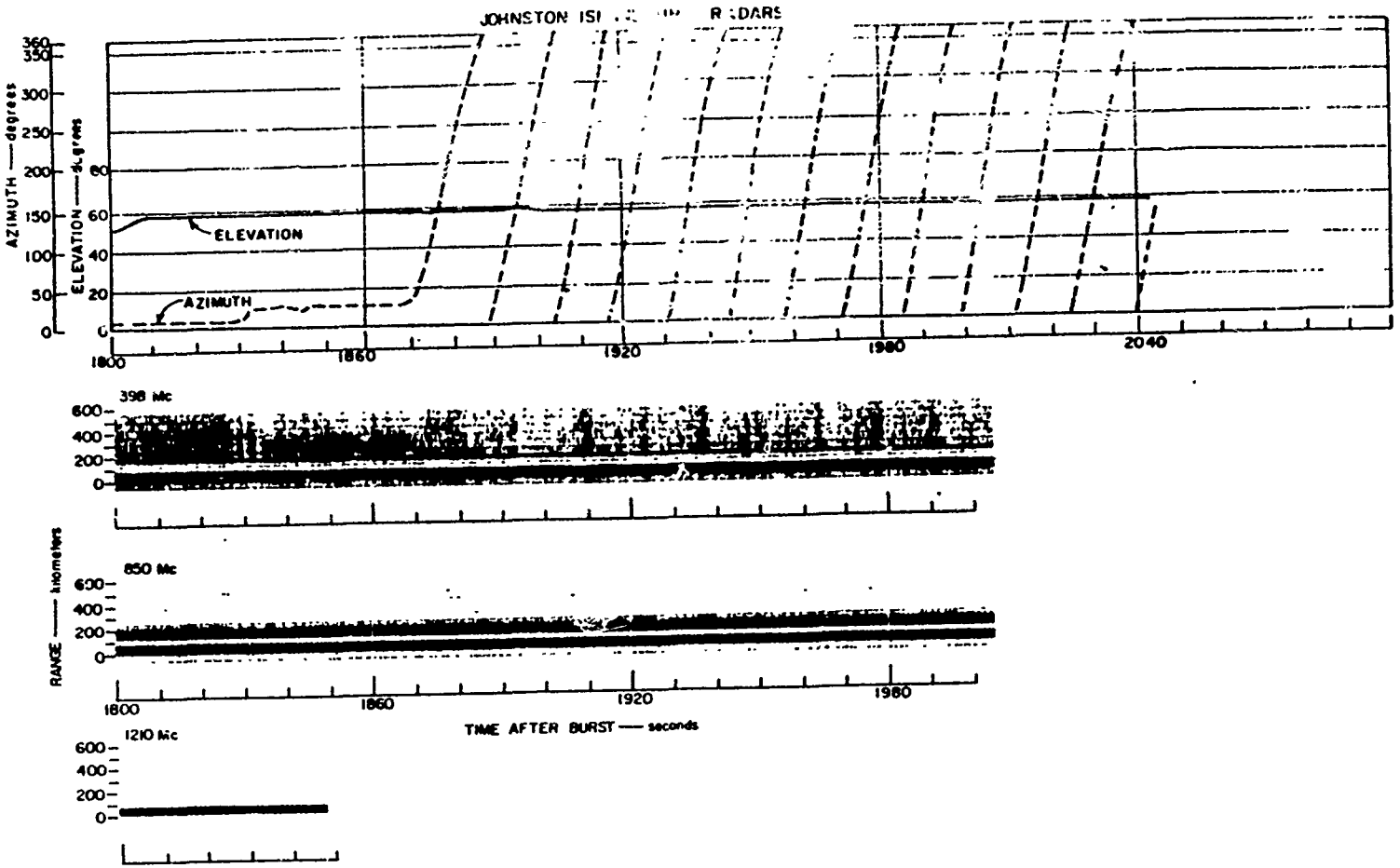

Figure 5.10 Johnston Island radar range versus time for Check Mate; 0 to 600 km, 1,800 to 2,100 seconds.

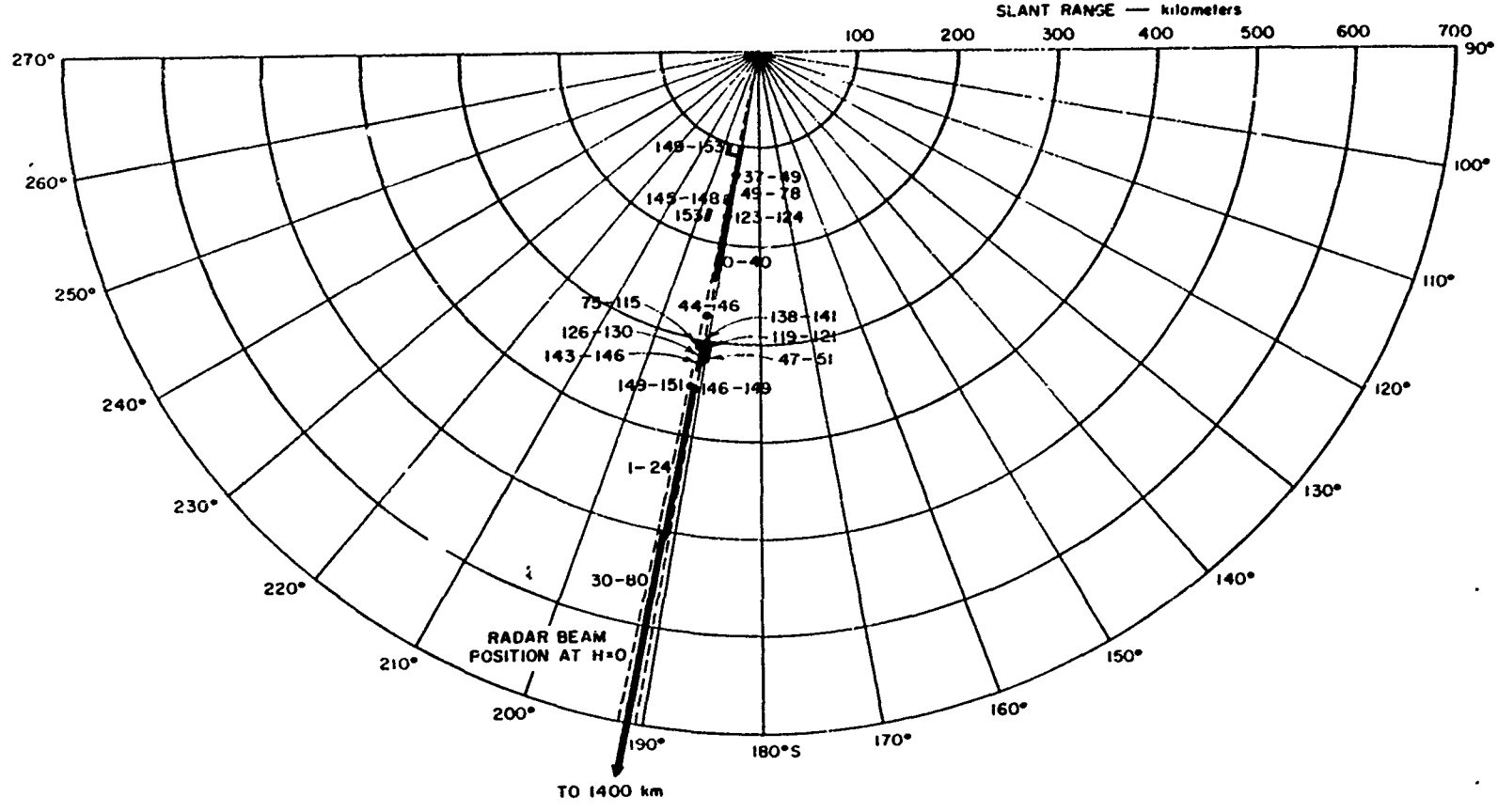

Figure 5.12 Johnston Island radar range versus azimuth for Check Mate; 398-Mc southern echoes, 0 to 300 seconds.

213 (page 214 deleted)

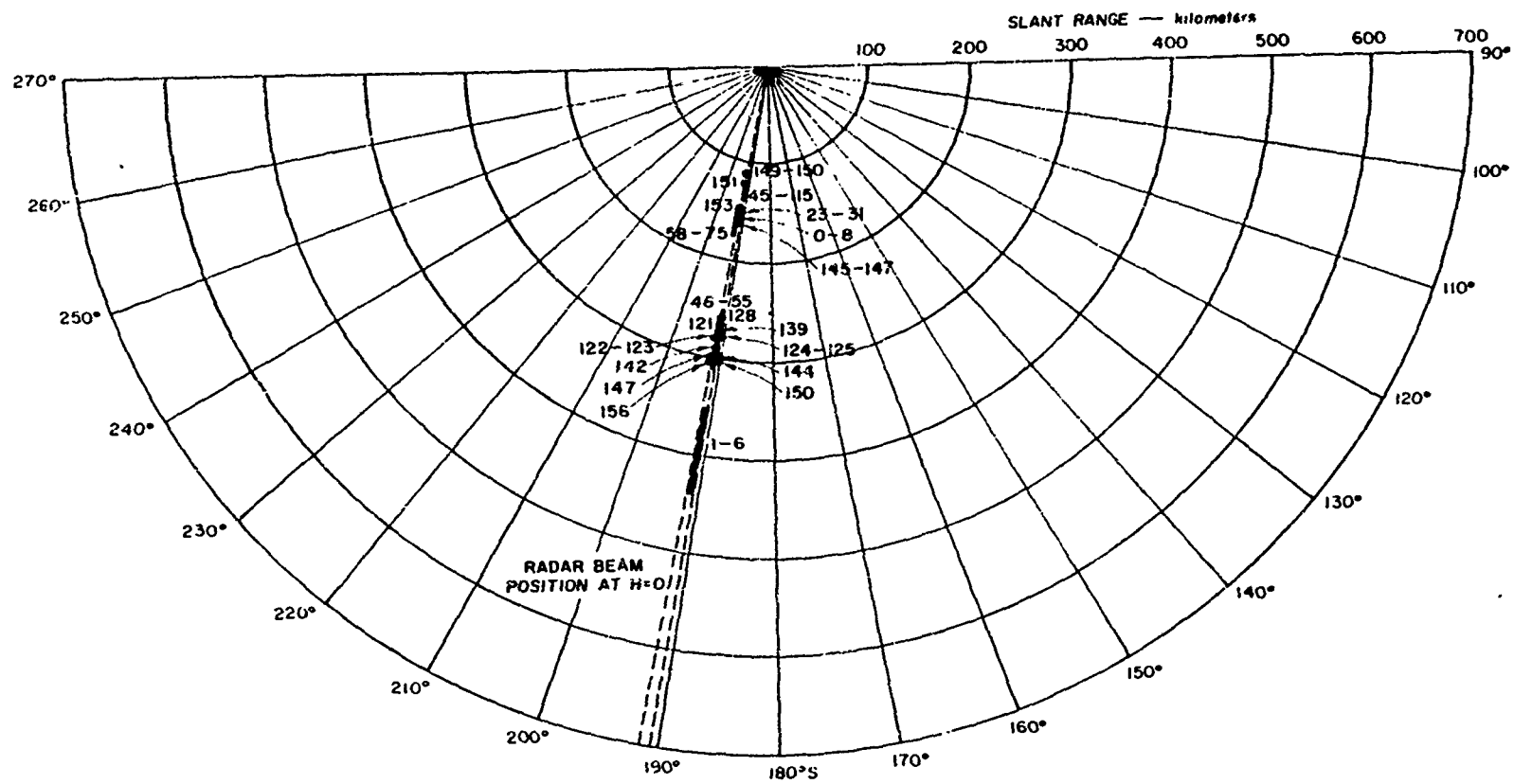

Figure 5.14 Johnston Island radar range versus azimuth for Check Mate; 850-Mc southern echoes, 0 to 300 seconds.

215 (page 216 deleted)

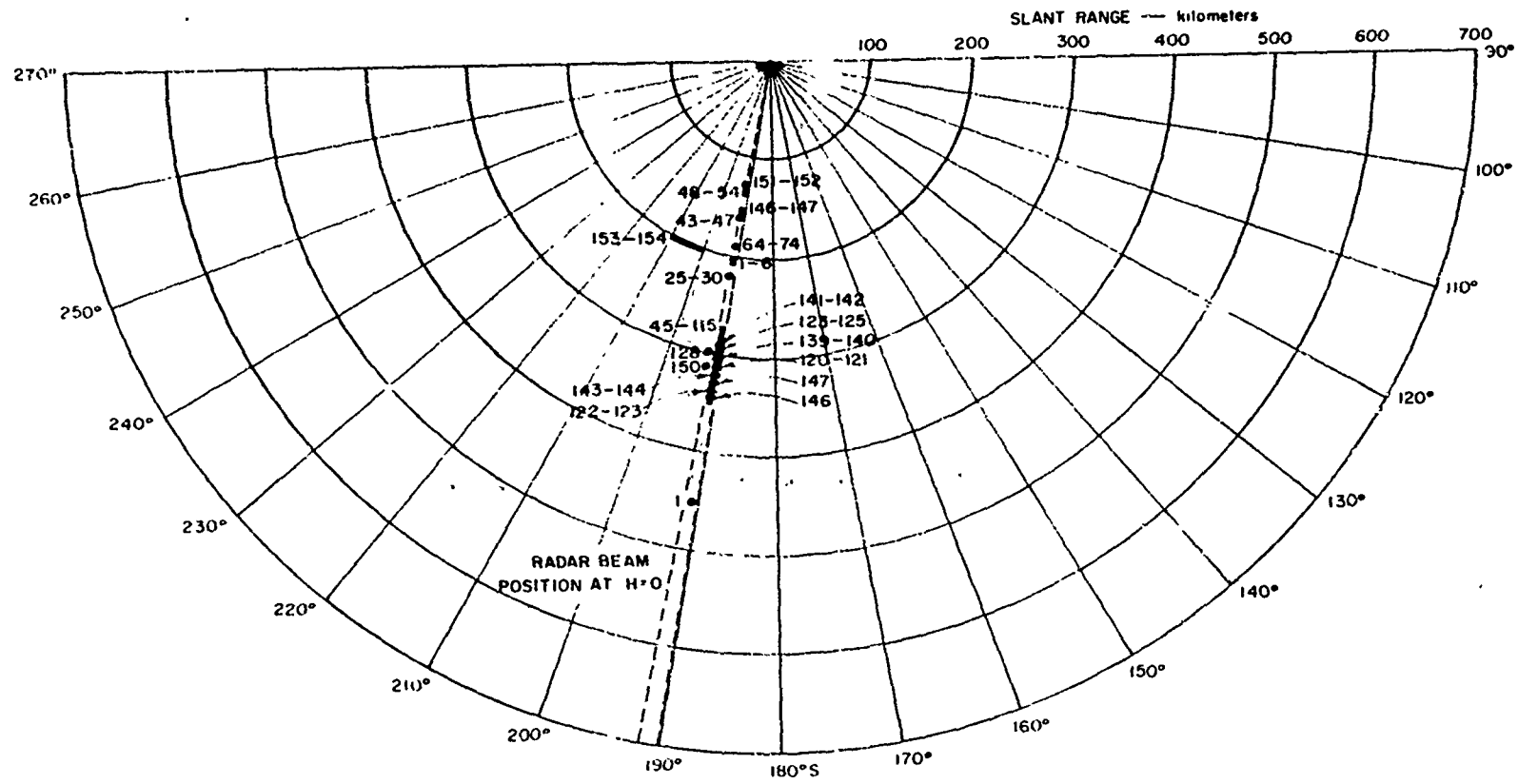

Figure 5.16 Johnston Island radar range versus azimuth for Check Mate; 1210-Mc southern echoes, 0 to 300 seconds.

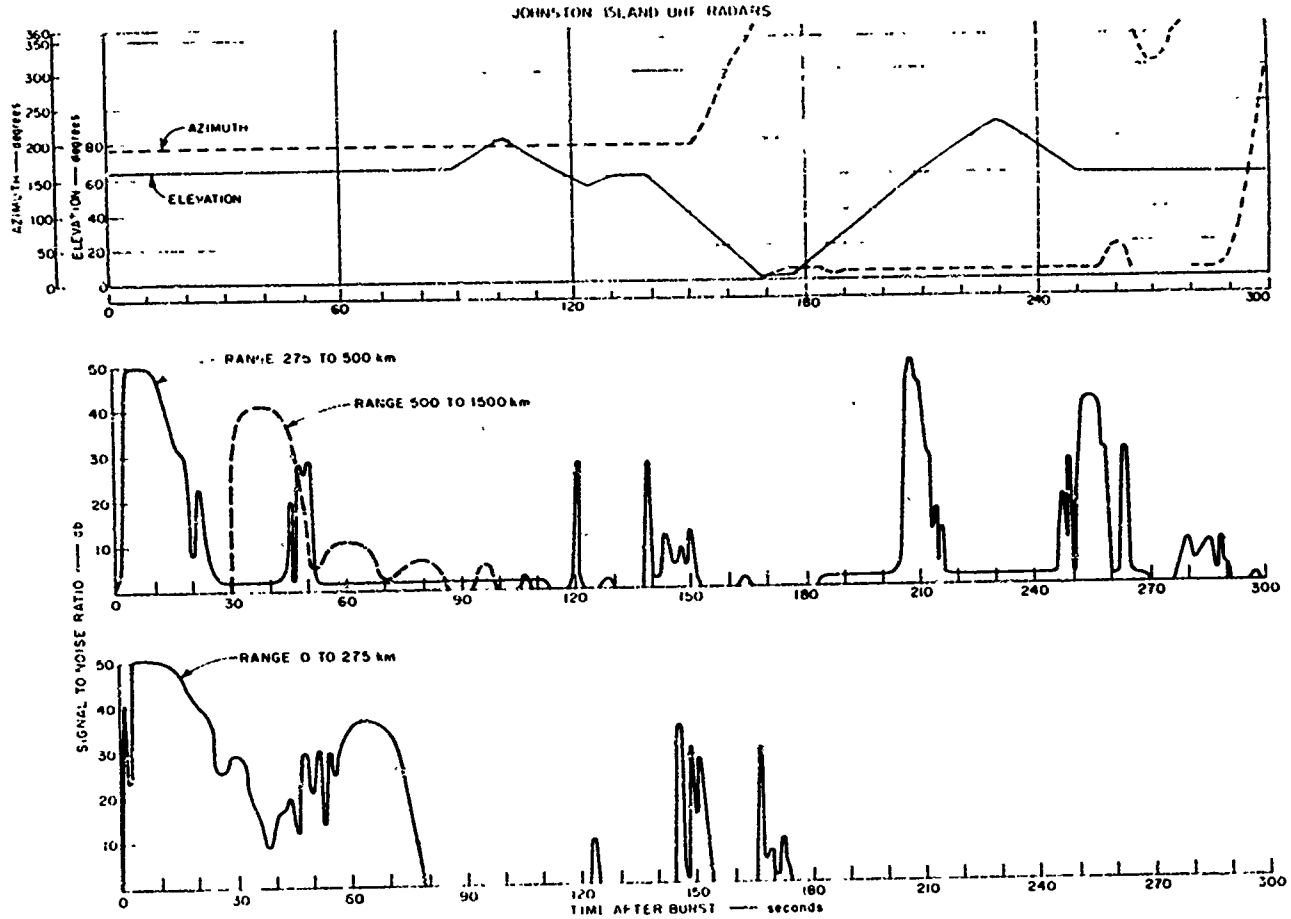

Figure 5.17 Johnston Island radar echo amplitude versus time for Check Mate; 398 Mc, 0 to 300 seconds.

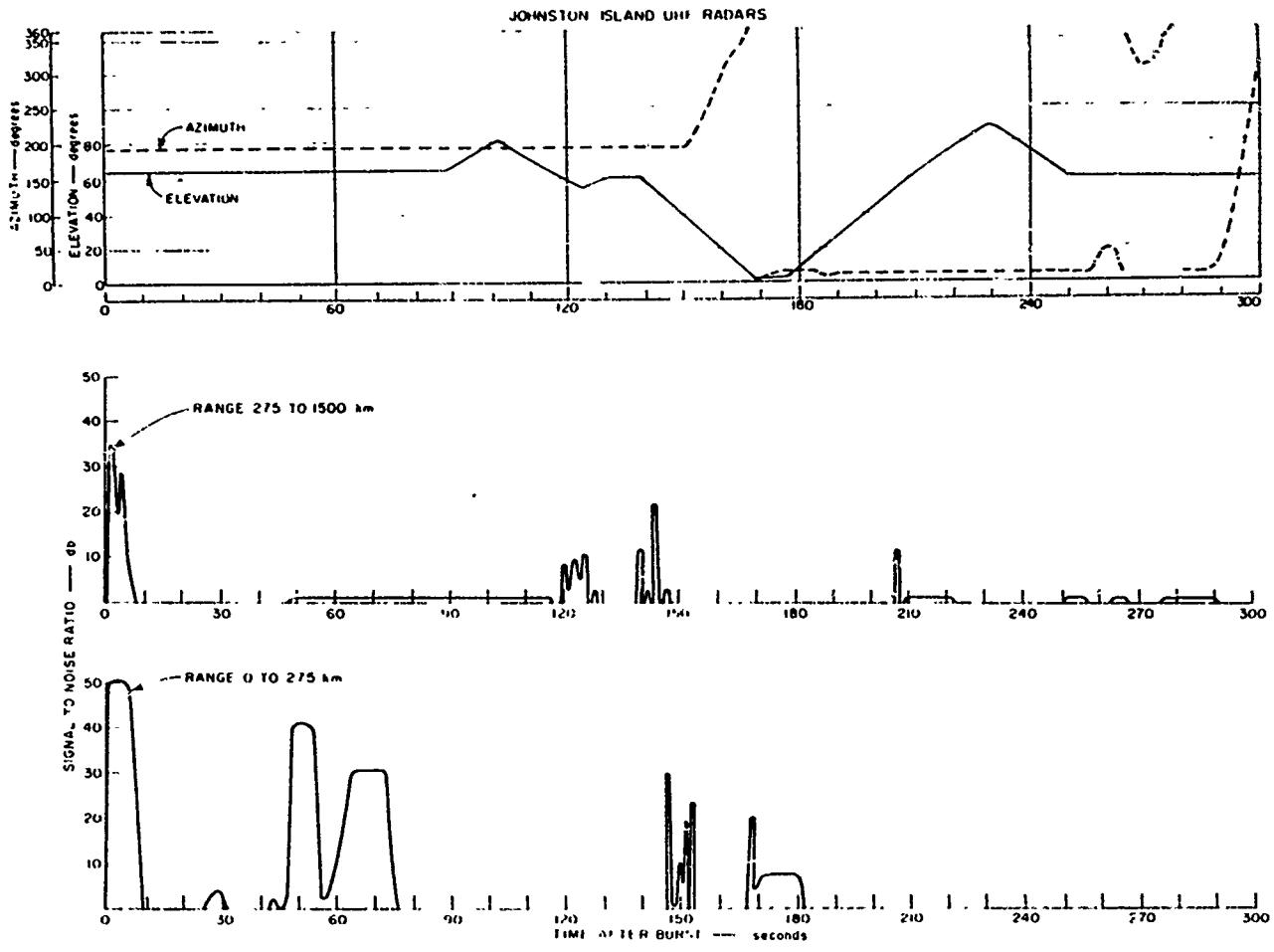

Figure 5.18 Johnston Island radar echo amplitude versus time for Check Mate; 850 Mc, 0 to 300 seconds.

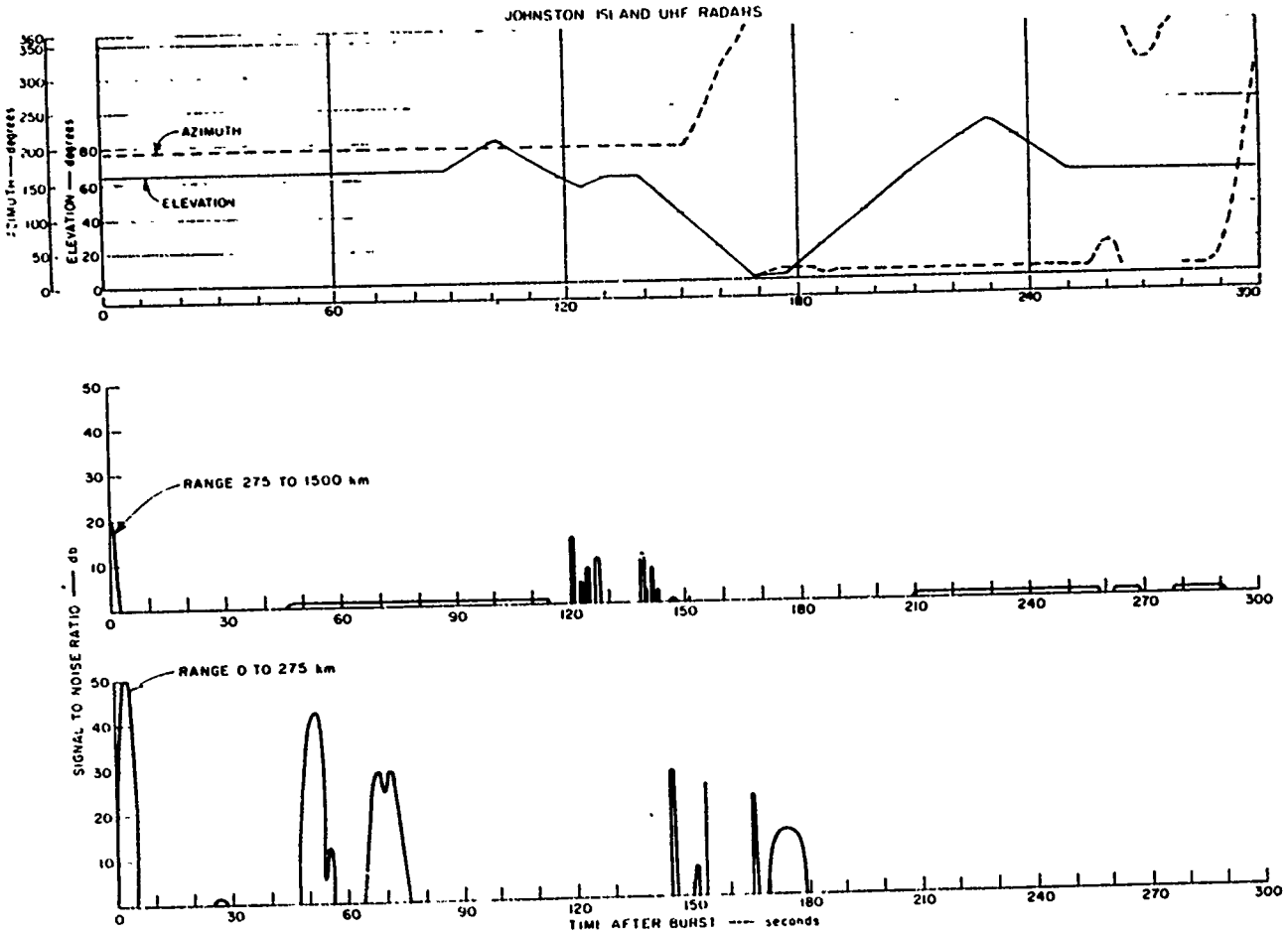

Figure 5.19 Johnston Island radar echo amplitude versus time for Check Mate; 1210 Mc, 0 to 300 seconds.

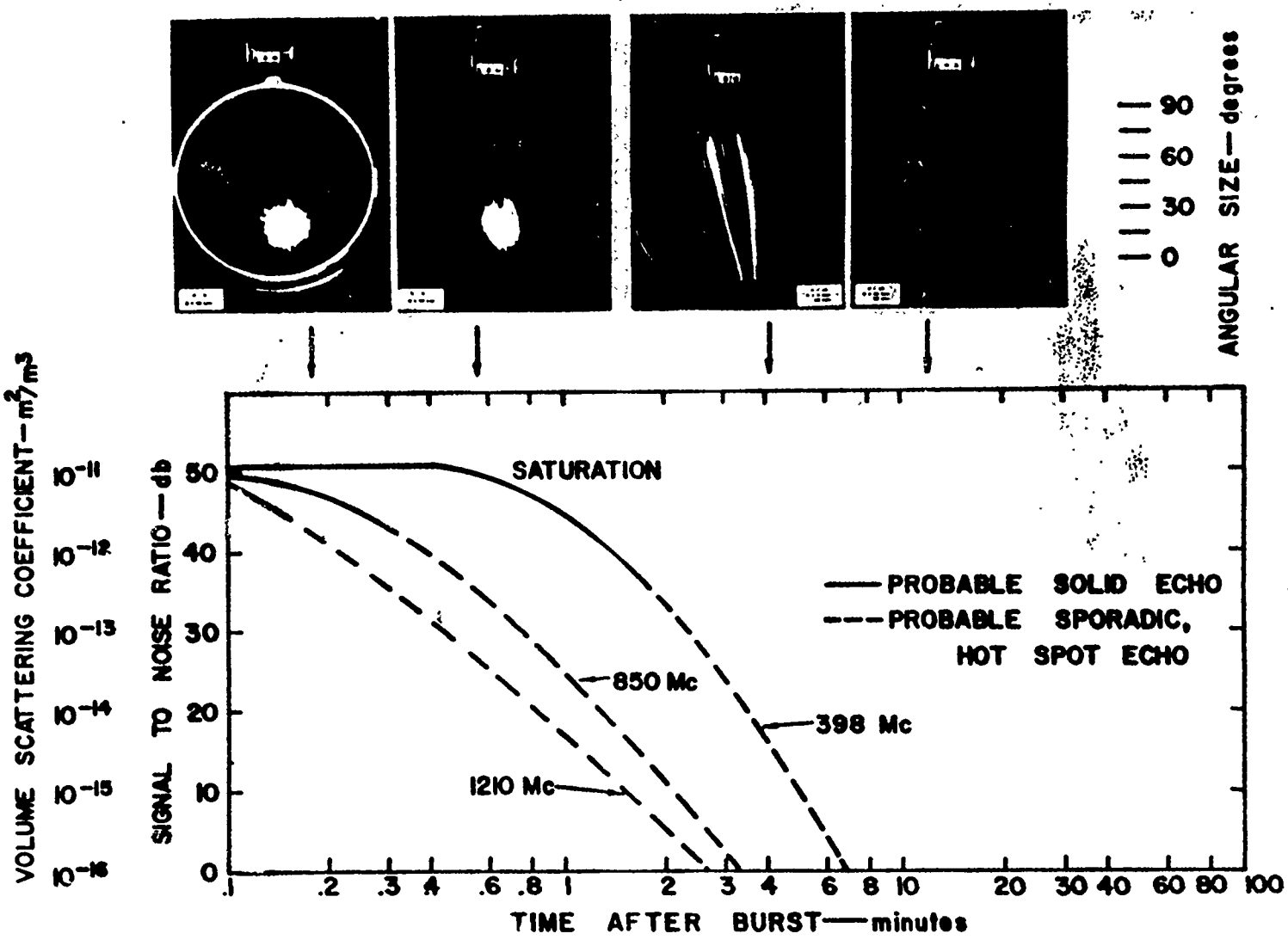

Figure 5.20 Johnston Island radar echo amplitude versus time for Check Mate; 398, 850, and 1210 Mc.

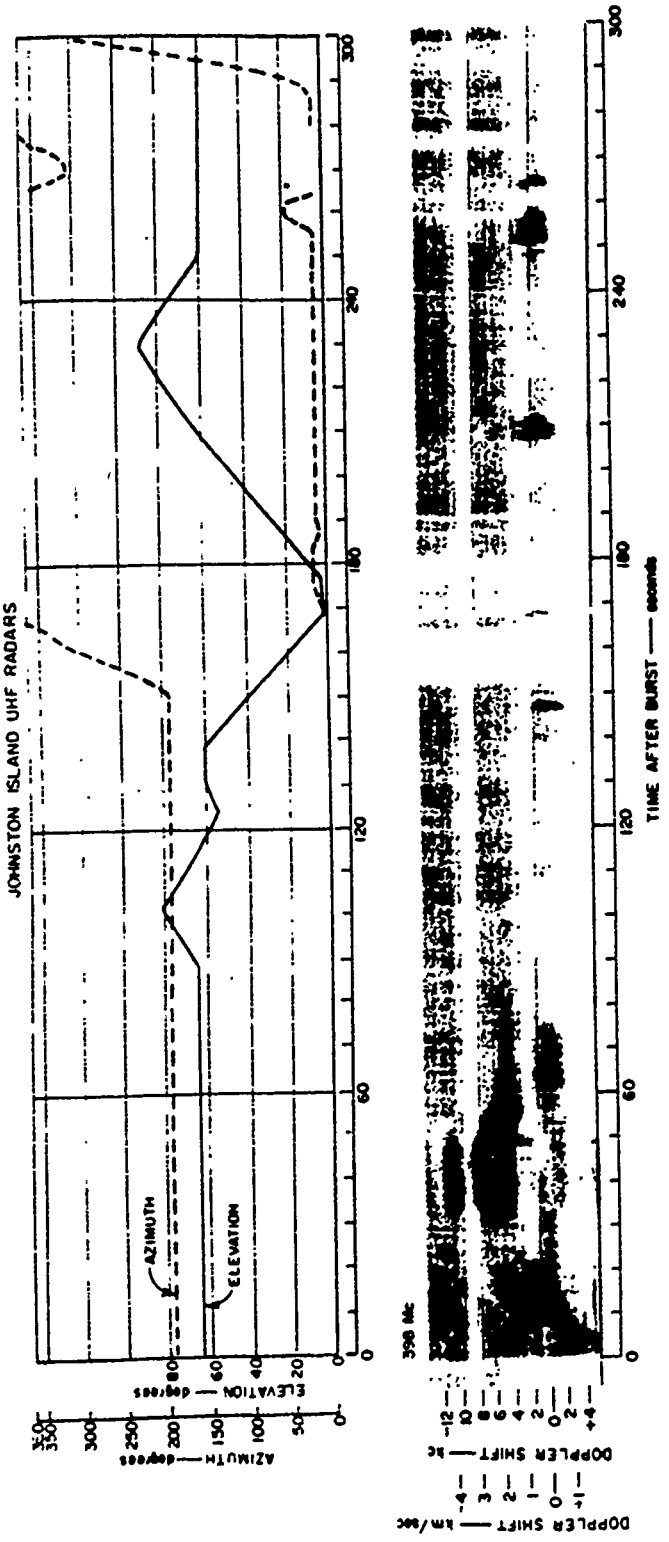

Figure 5.21 Johnston Island radar Doppler versus time for Check Mate; 398 Mc, 0 to 300 seconds.

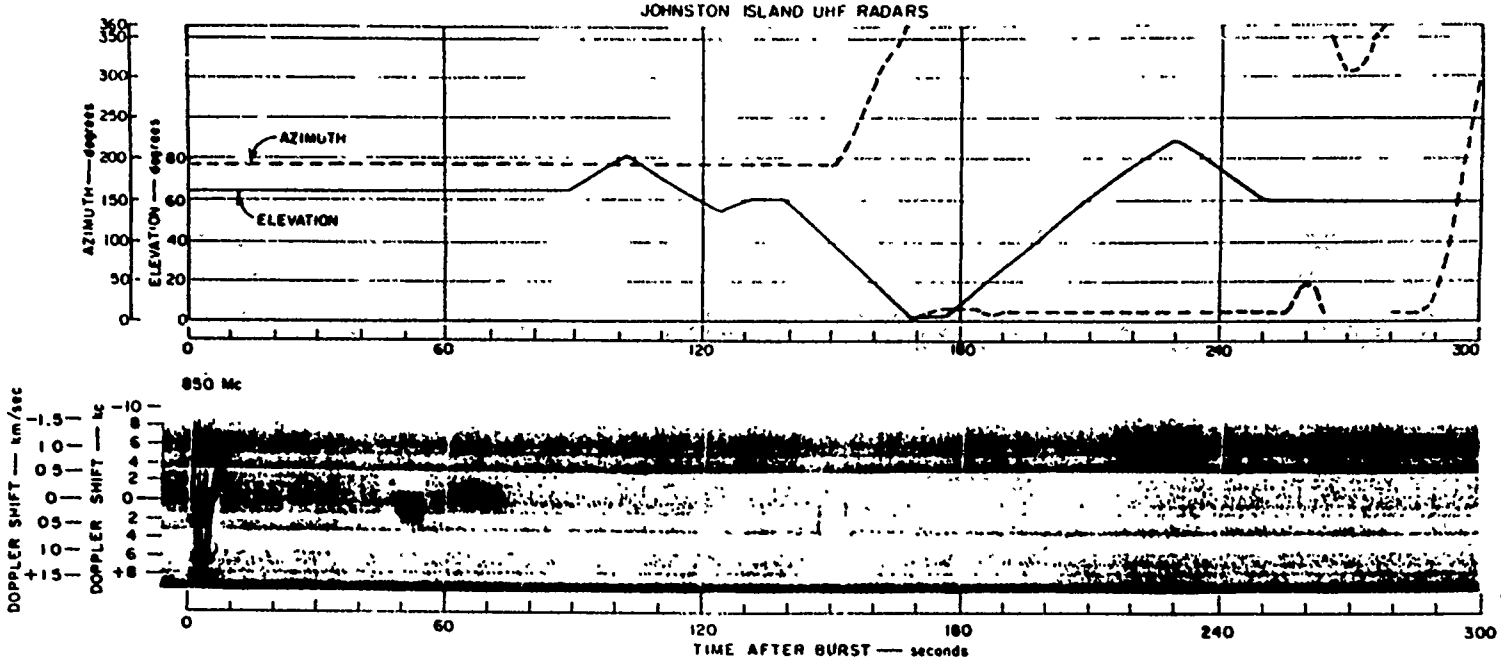

Figure 5.22 Johnston Island radar Doppler versus time for Check Mate; 850 Mc, 0 to 300 seconds.

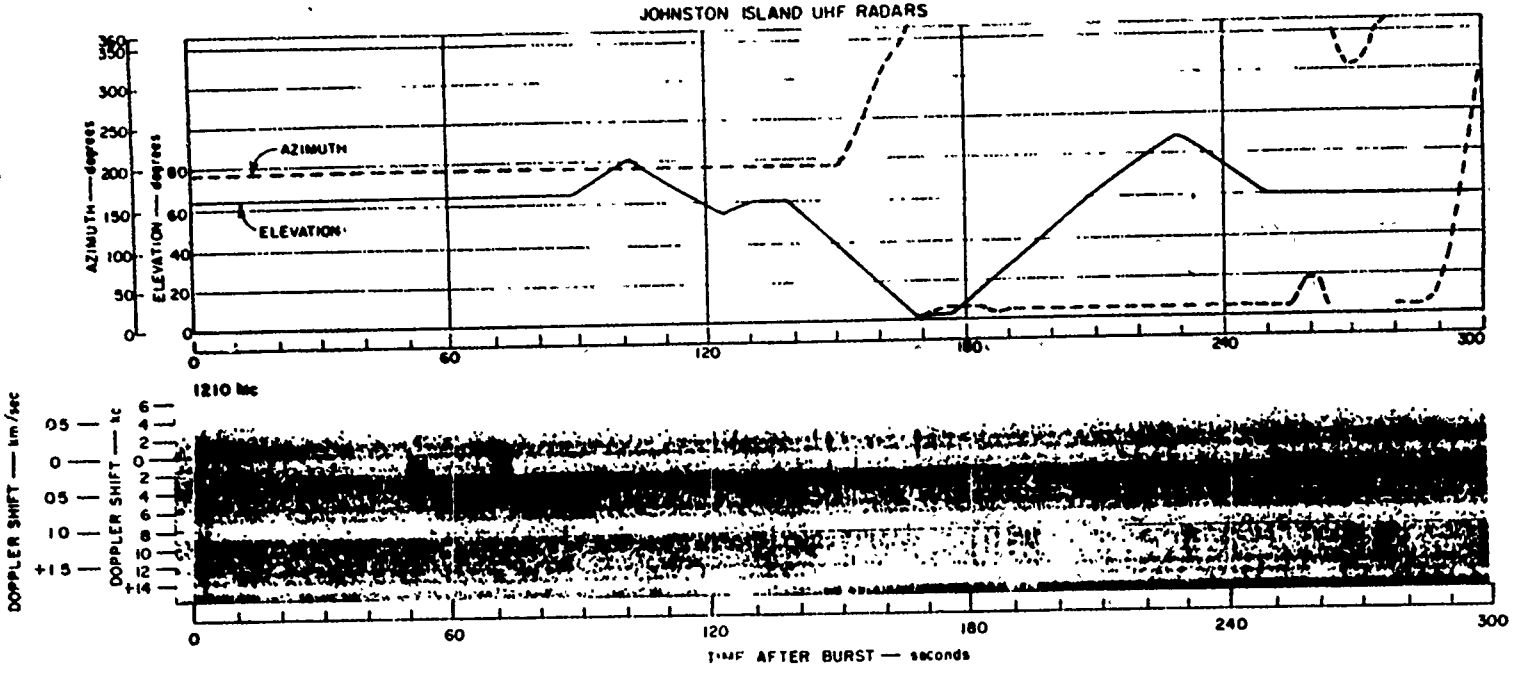

Figure 5.23 Johnston Island radar Doppler versus time for Check Mate; 1210 Mc, 0 to 300 seconds.

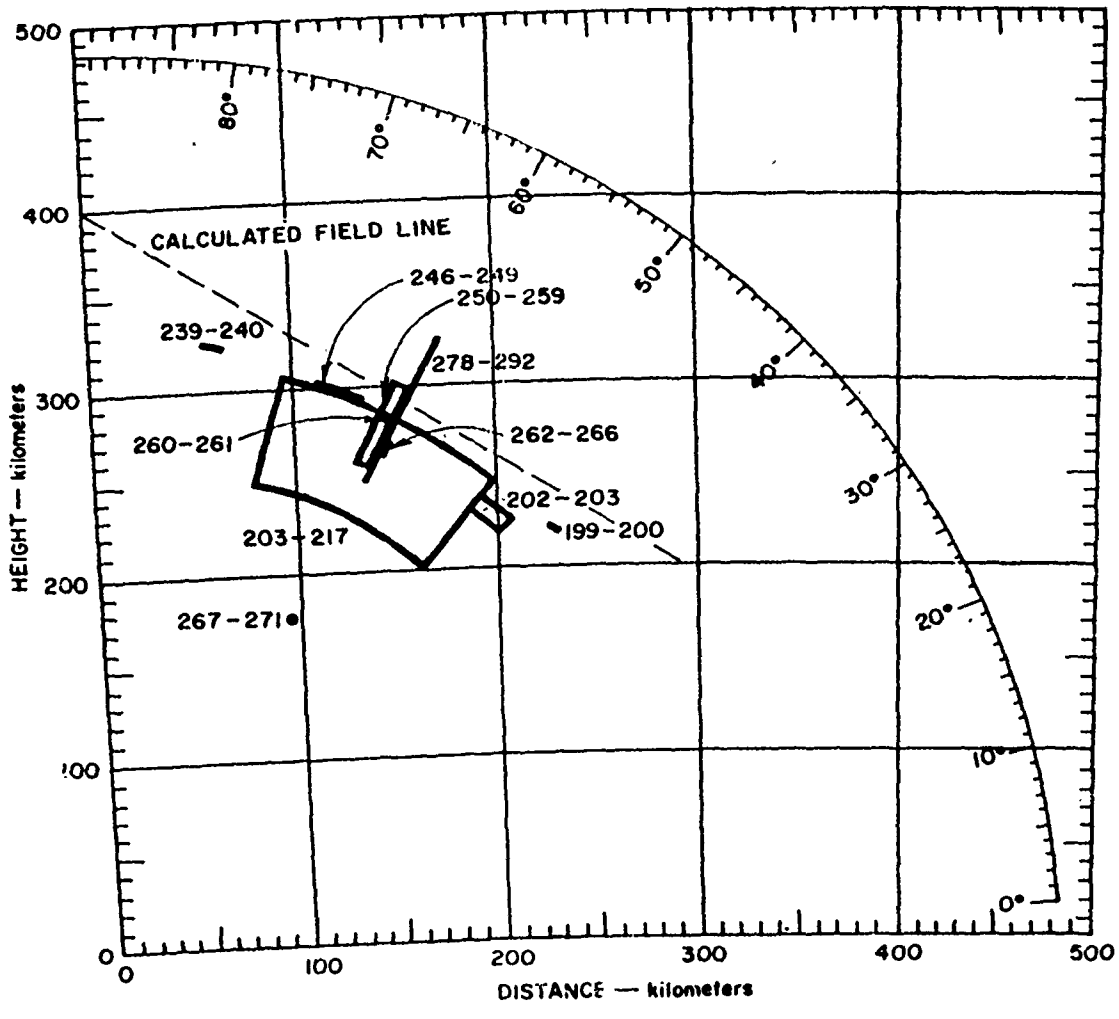

Figure 5.24 Johnston Island radar height versus distance for Check Mate; 398-Mc northern echoes, 0 to 300 seconds.

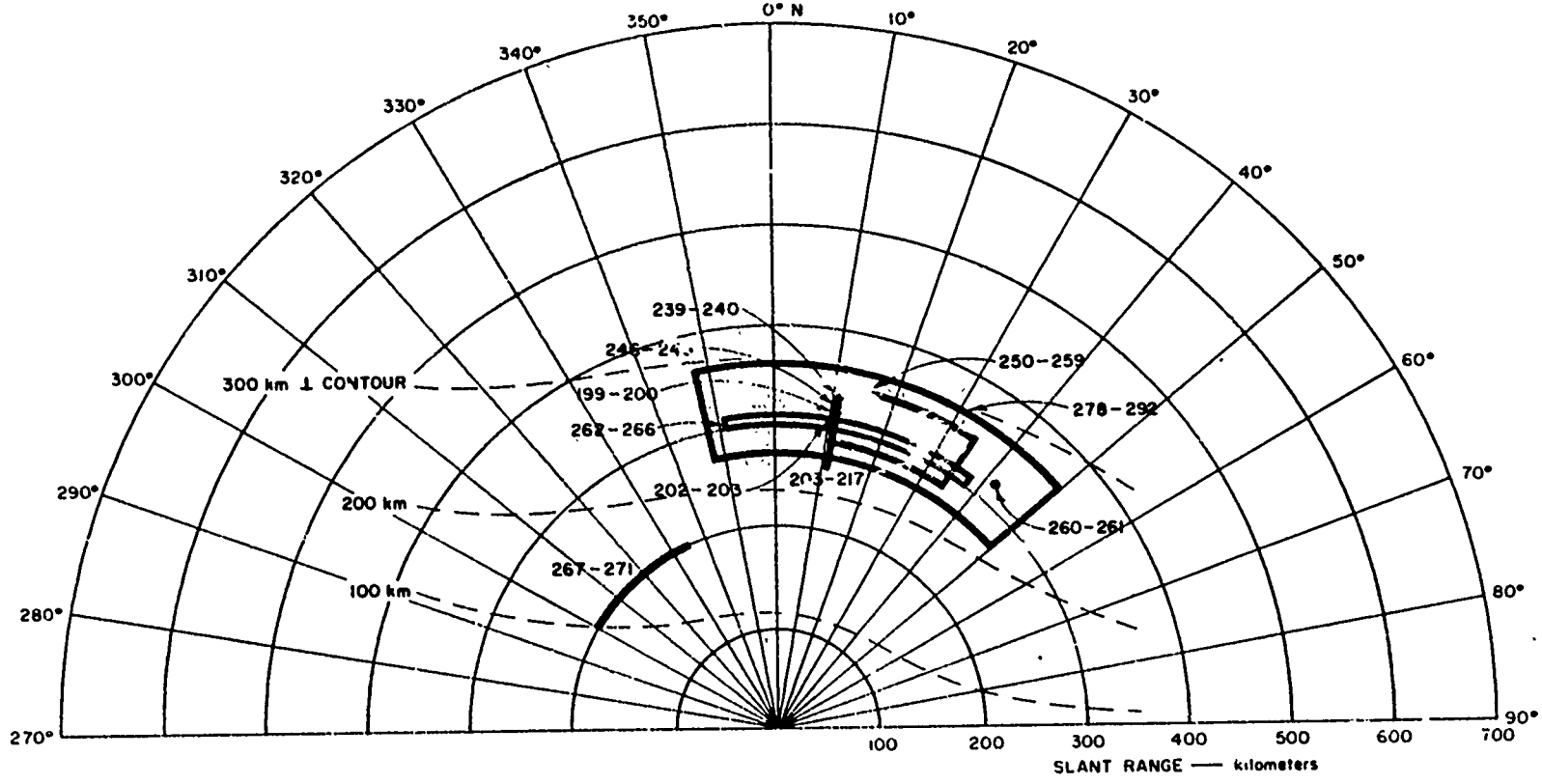

Figure 5.25 Johnston Island radar range versus azimuth for Check Mate; 398-Mc northern echoes, [redacted]00 seconds.

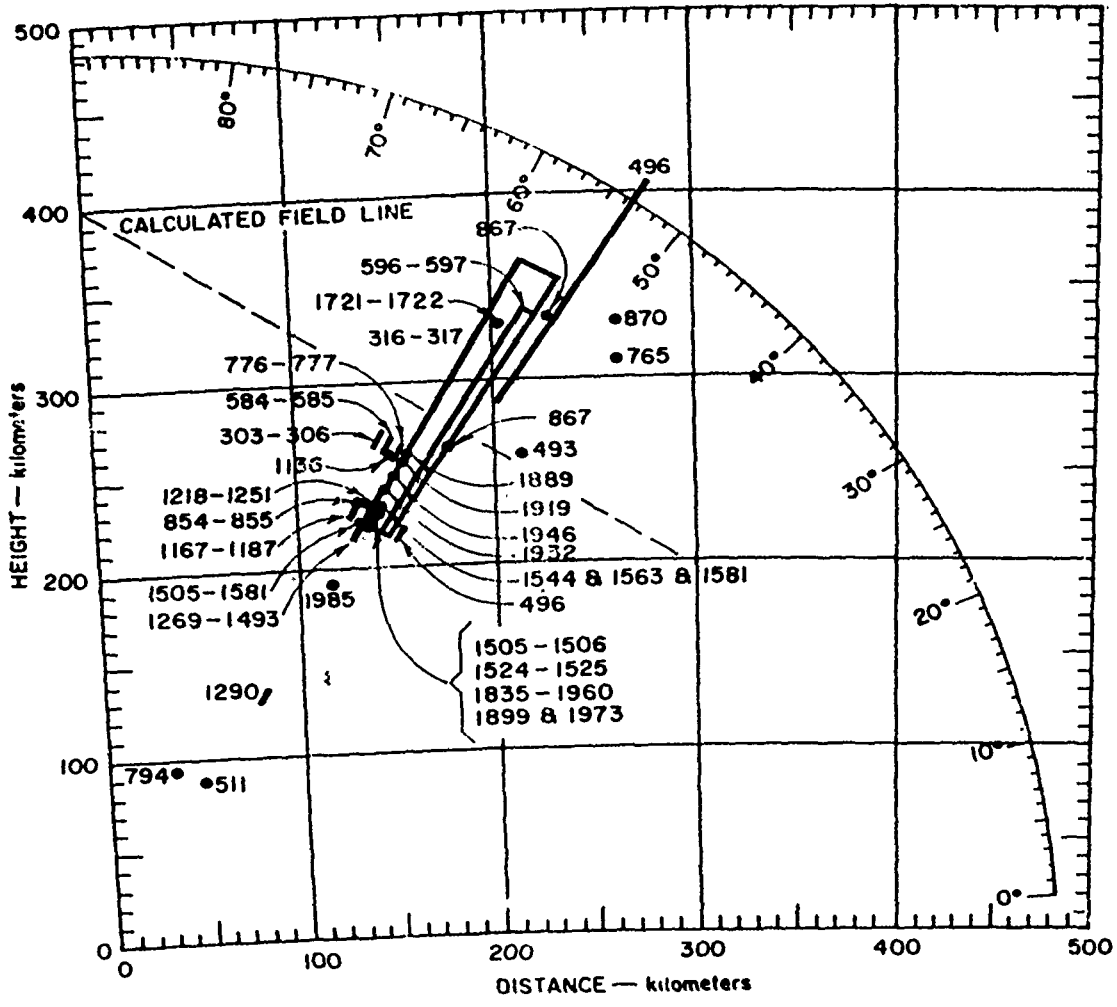

Figure 5.26 Johnston Island radar height versus distance for Check Mate; 398-Mc northern echoes, 300 to 2,100 seconds.

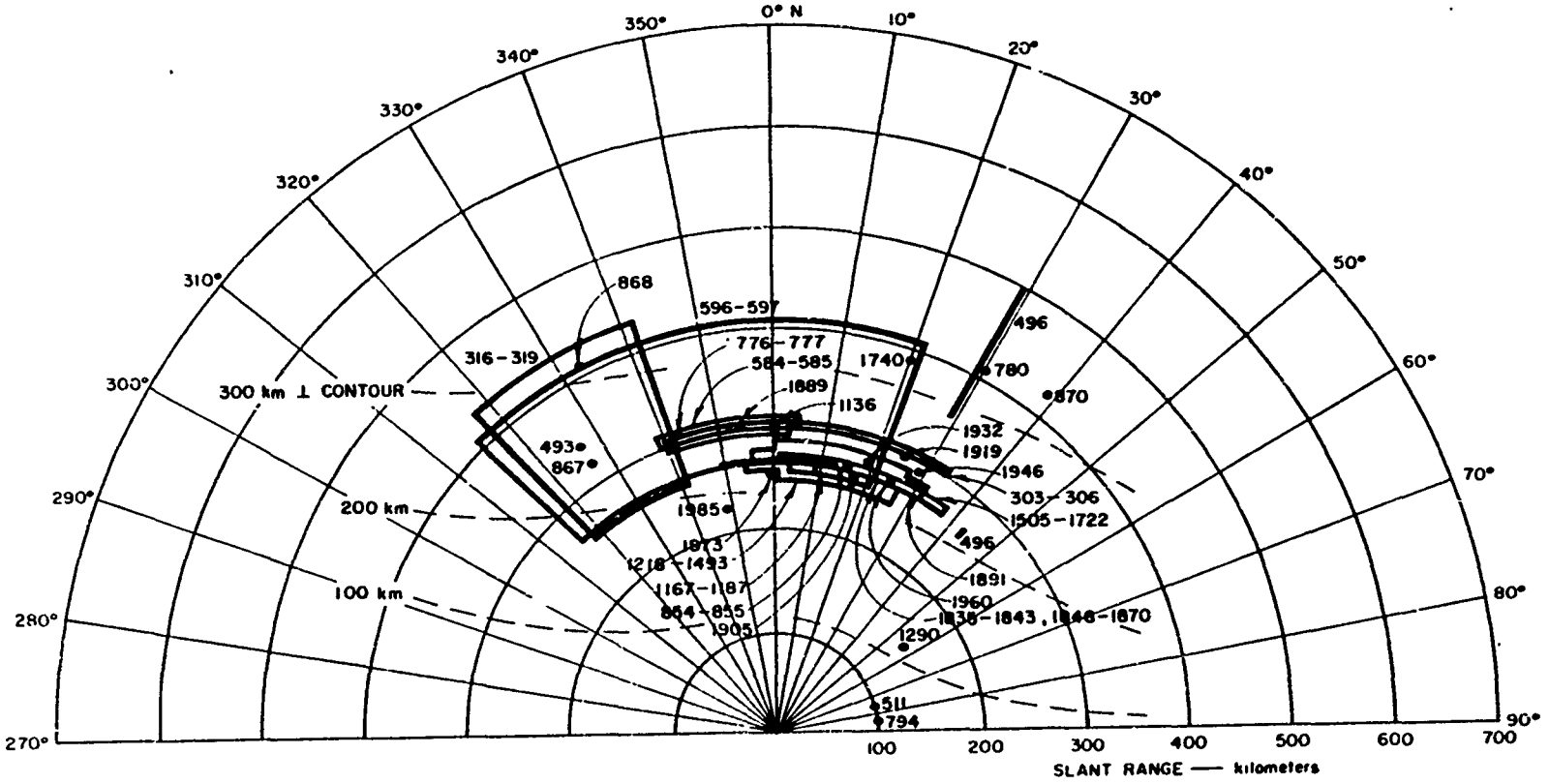

Figure 5.27 Johnston Island radar range versus azimuth for Check Mate; 398-Mc northern echoes, 300 to 2,100 seconds.

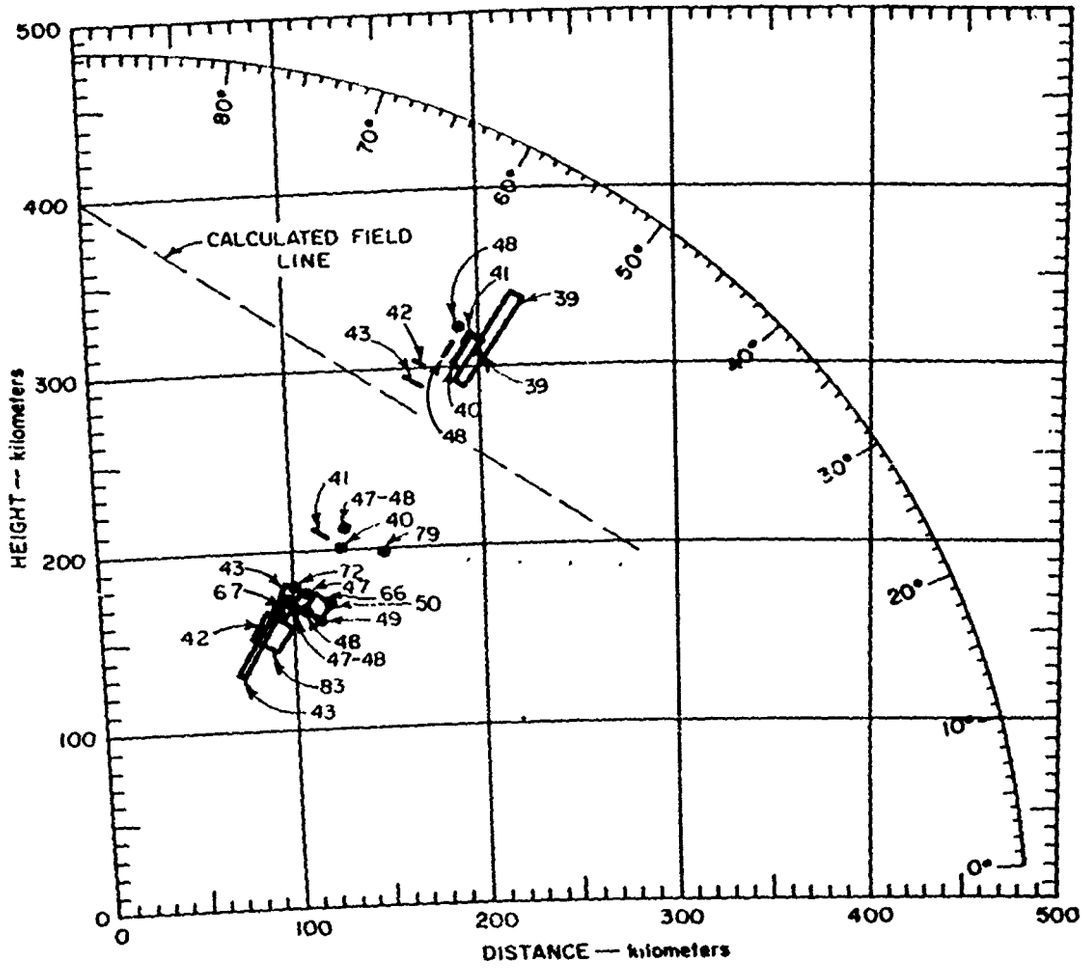

Figure 5.28 Johnston Island radar height versus distance for Check Mate; 398-Mc northern echoes, 36 to 83 minutes.

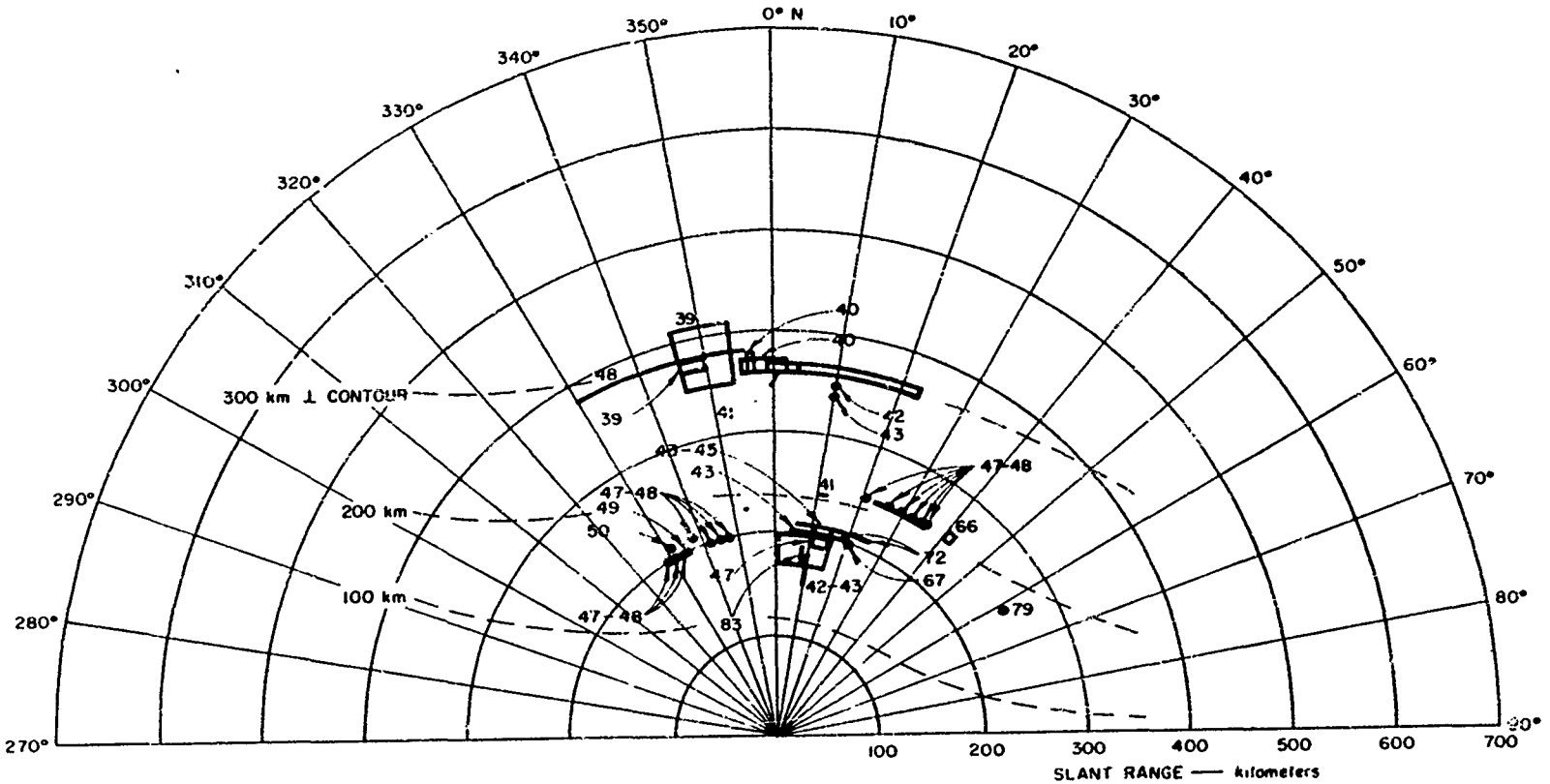

Figure 5.29 Johnston Island radar range versus azimuth for Check Mate; 398-Mc northern echoes, 36 to 83 minutes.

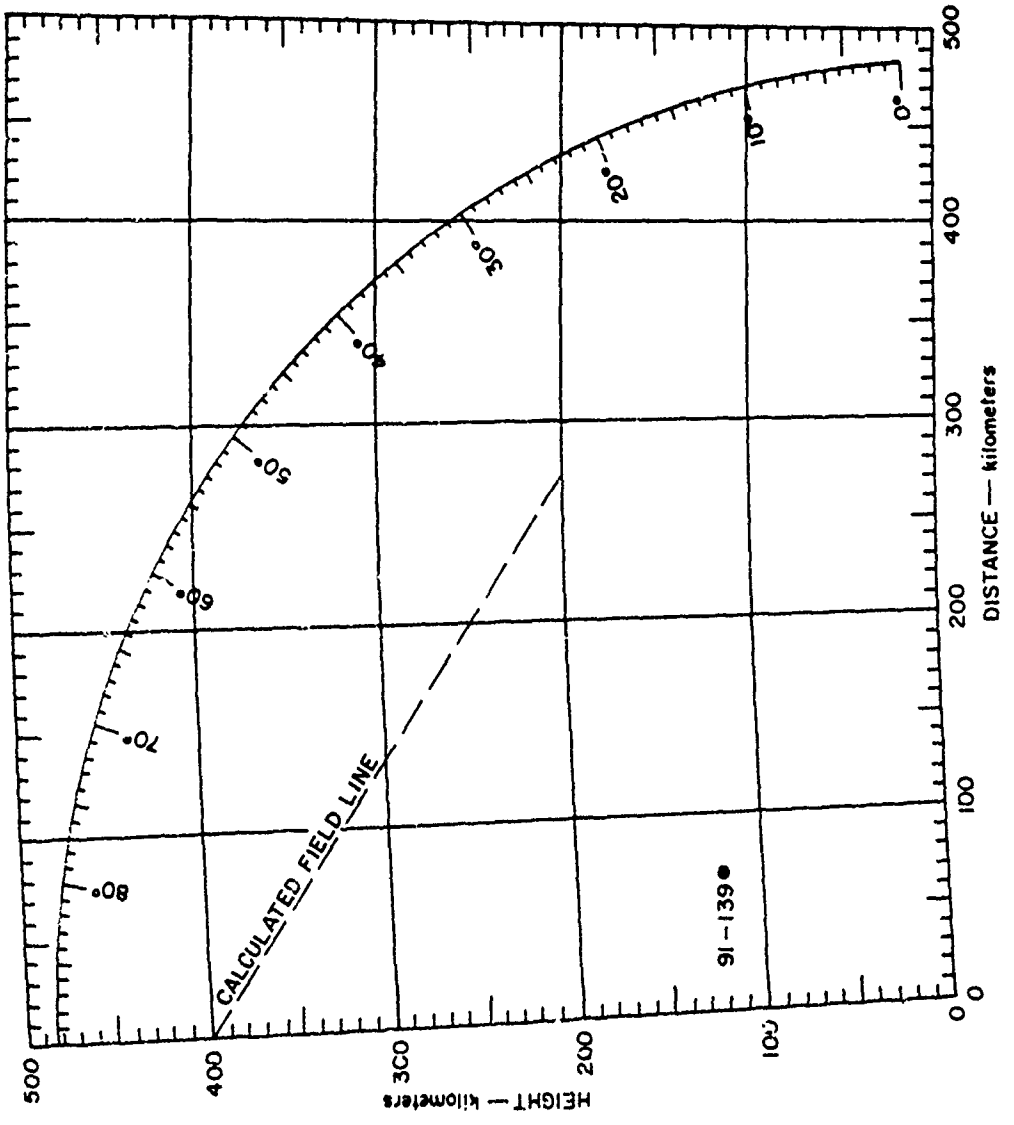

Figure 5.30 Johnston Island radar height versus distance for Check Mate 398-Mc northern echoes, 91 to 139 minutes.

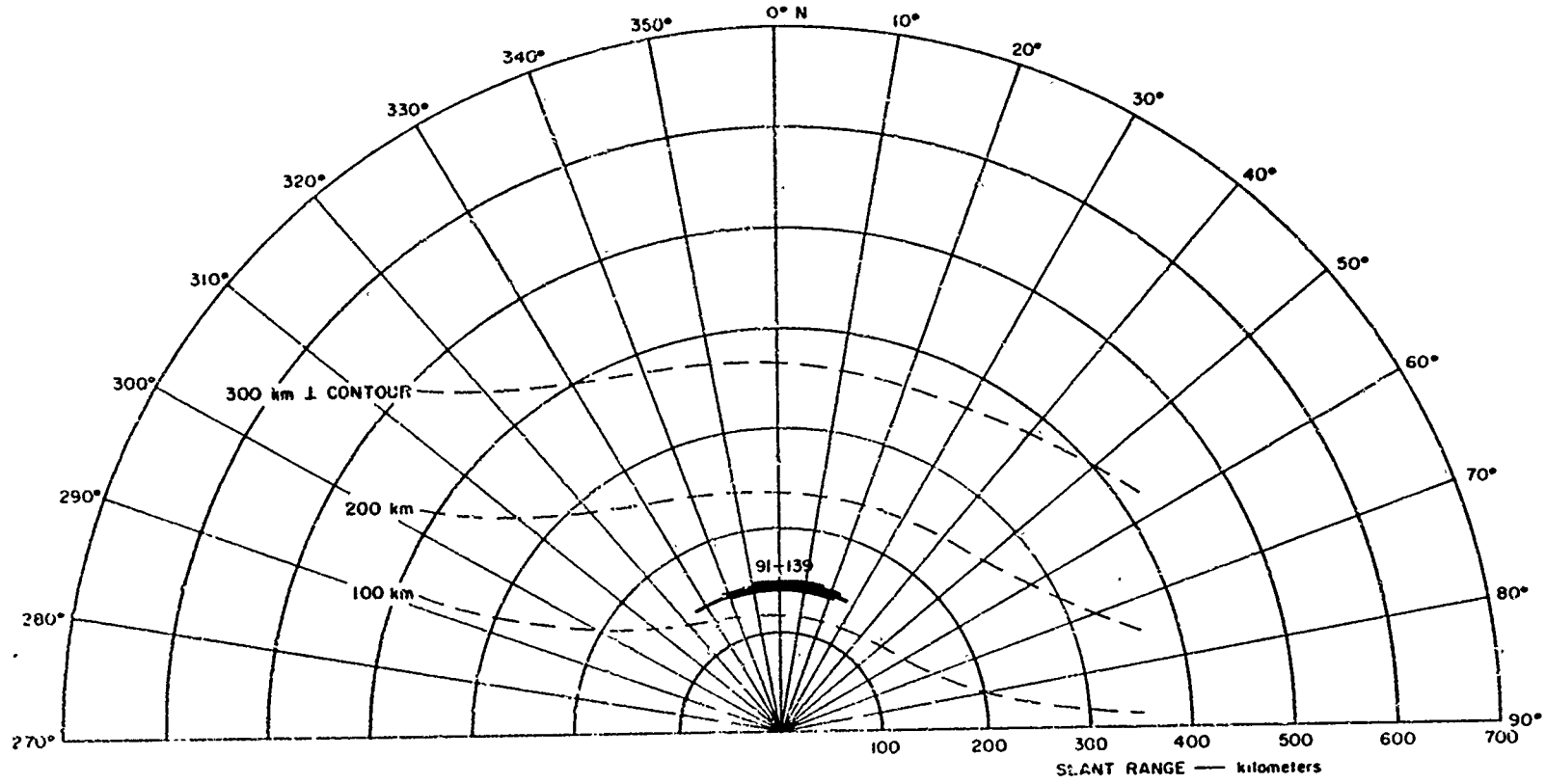

Figure 5.31 Johnston Island radar range versus azimuth for Check Mate; 398-Mc northern echoes, 91 to 139 minutes.

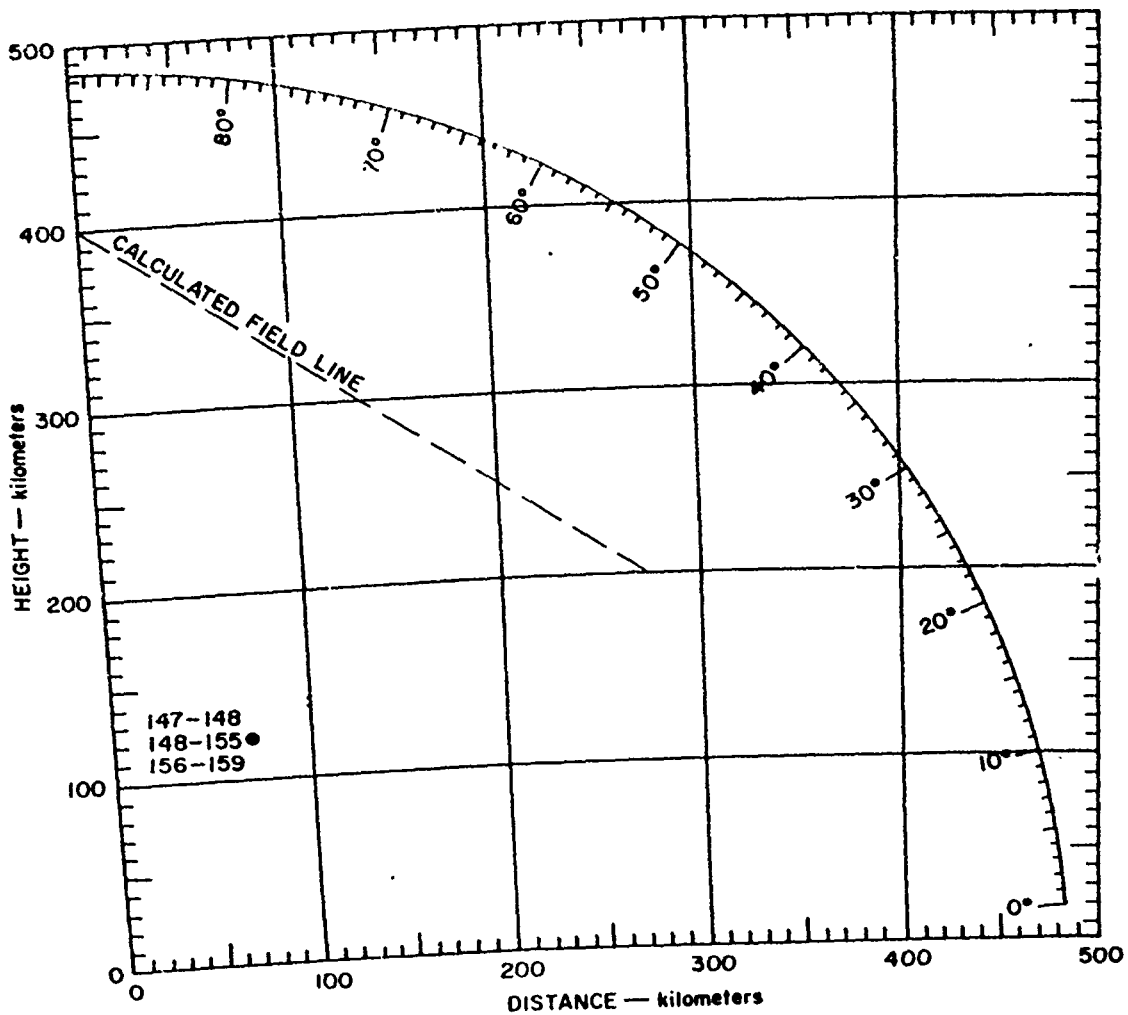

Figure 5.32 Johnston Island radar height versus distance for Check Mate; 398-Mc northern echoes, 140 to 186 minutes.

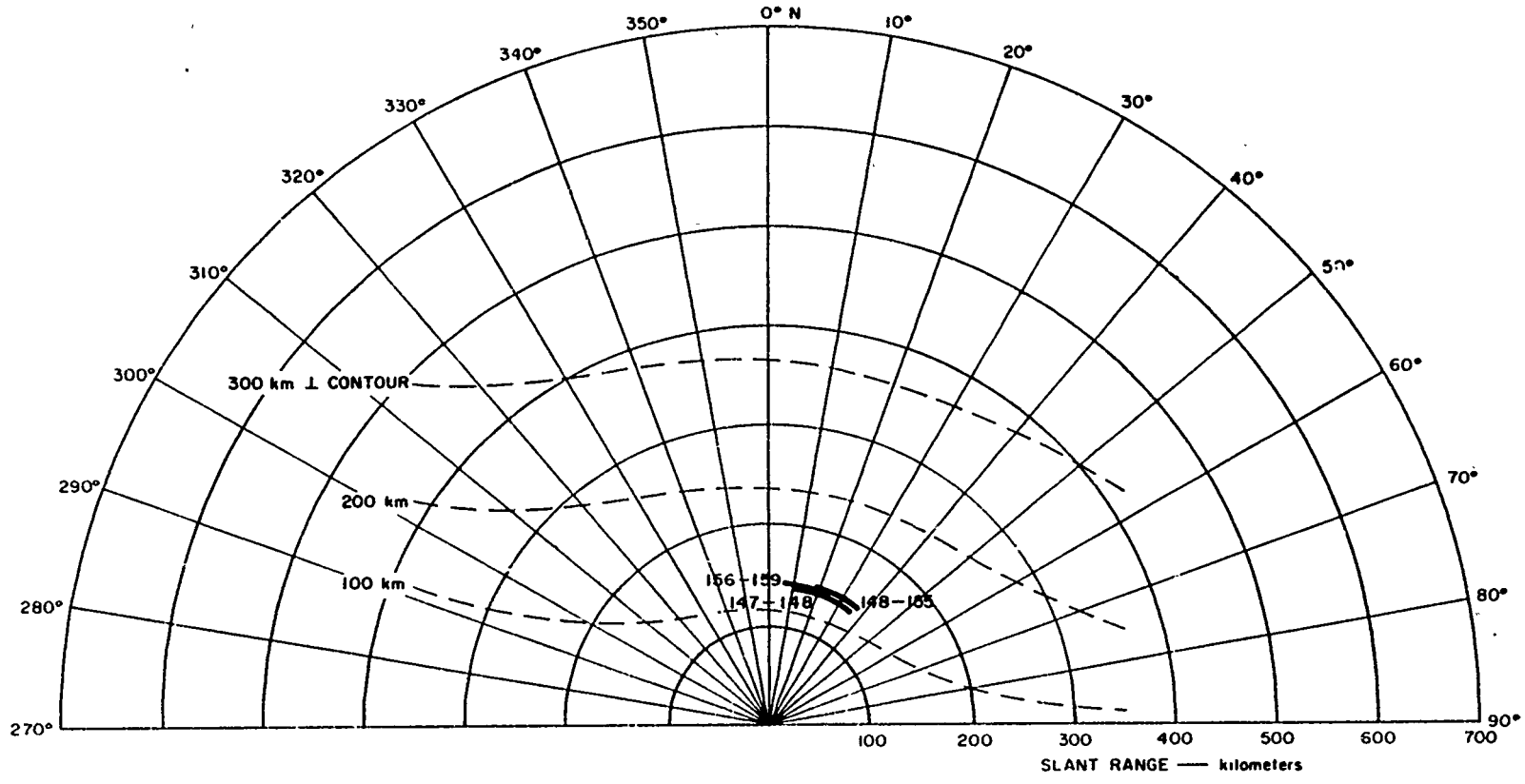

Figure 5.33 Johnston Island radar range versus azimuth for Check Mate; 398-Mc northern echoes, 140 to 186 minutes.

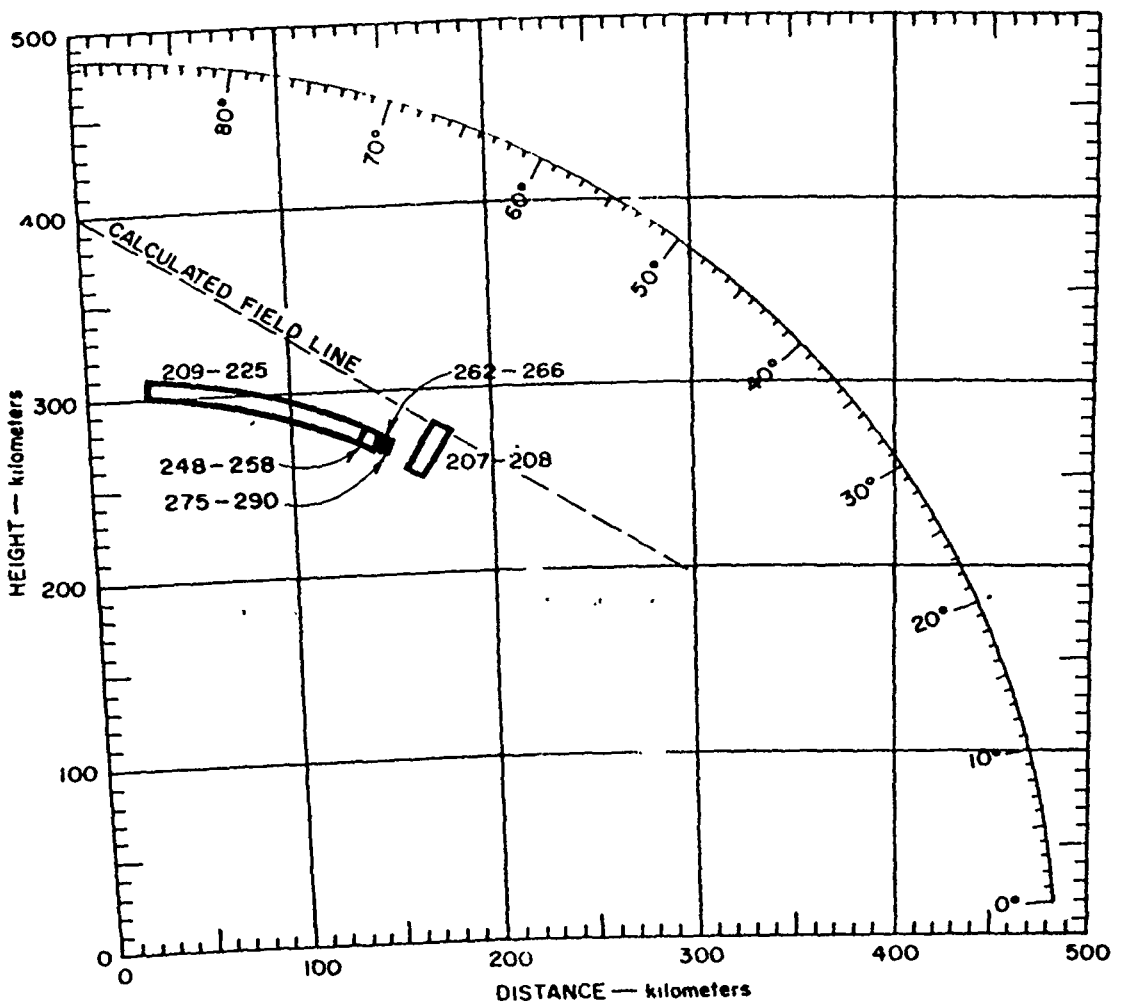

Figure 5.34 Johnston Island radar height versus distance for Check Mate; 850-Mc northern echoes, 0 to 300 seconds.

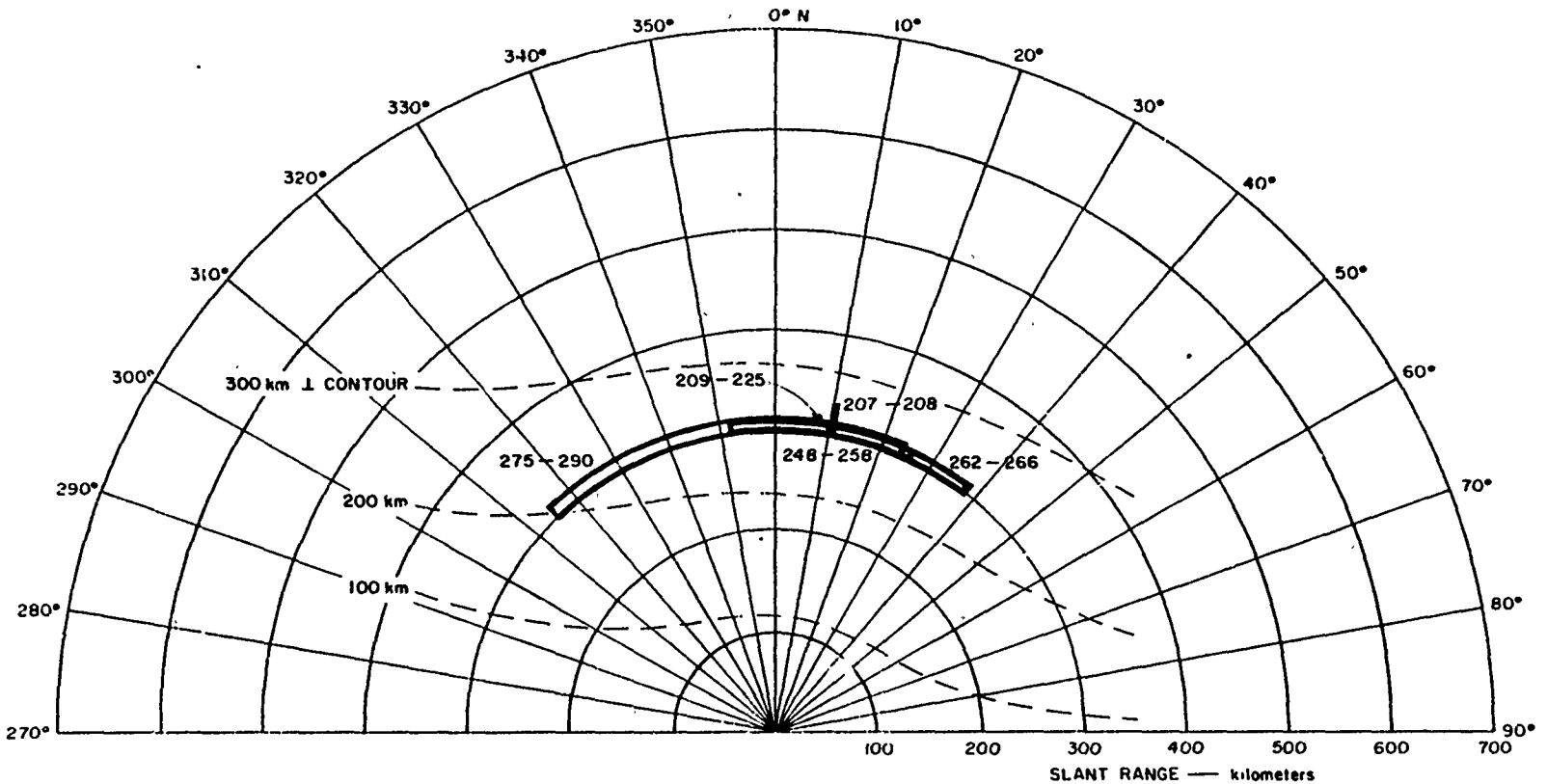

Figure 5.35 Johnston Island radar range versus azimuth for Check Mate; 850-Mc northern echoes, 0 to 300 seconds.

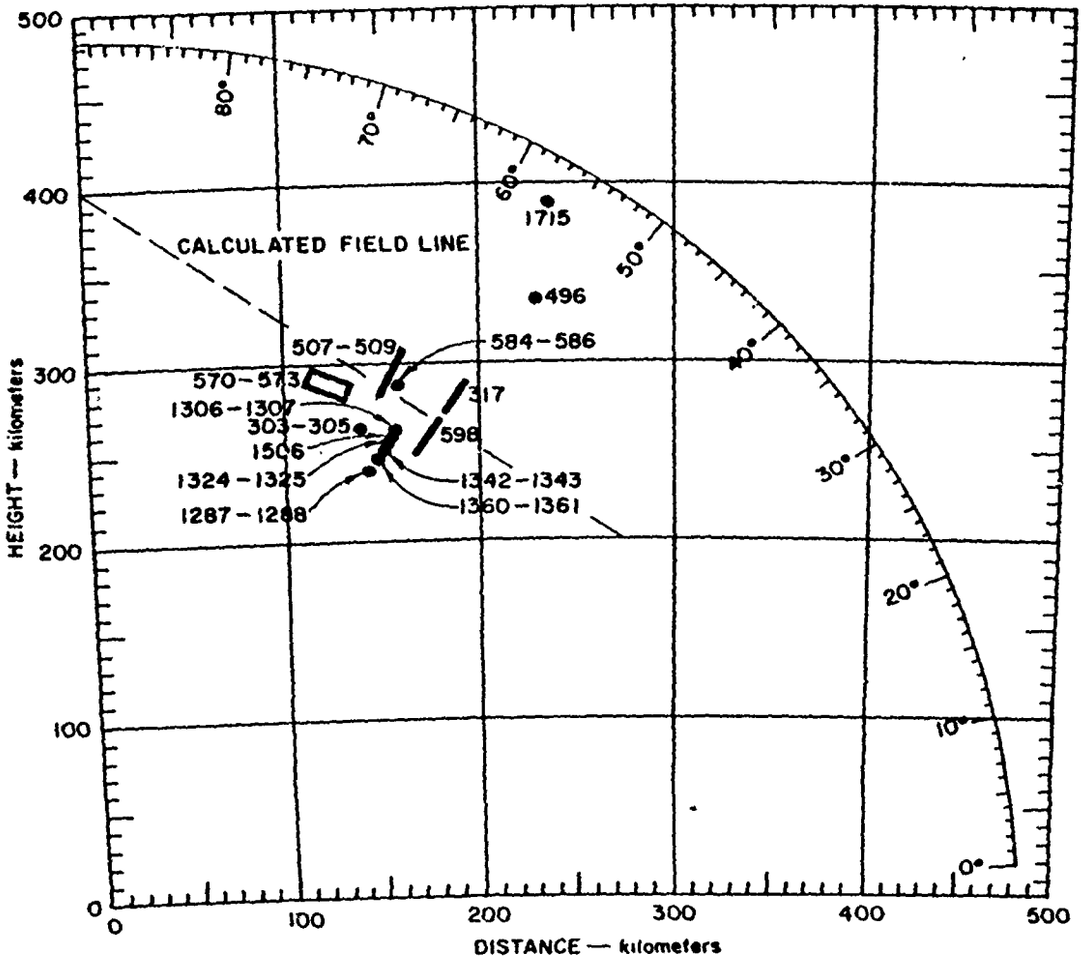

Figure 5.36 Johnston Island radar height versus distance for Check Mate; 850-Mc northern echoes, 300 to 2,100 seconds.

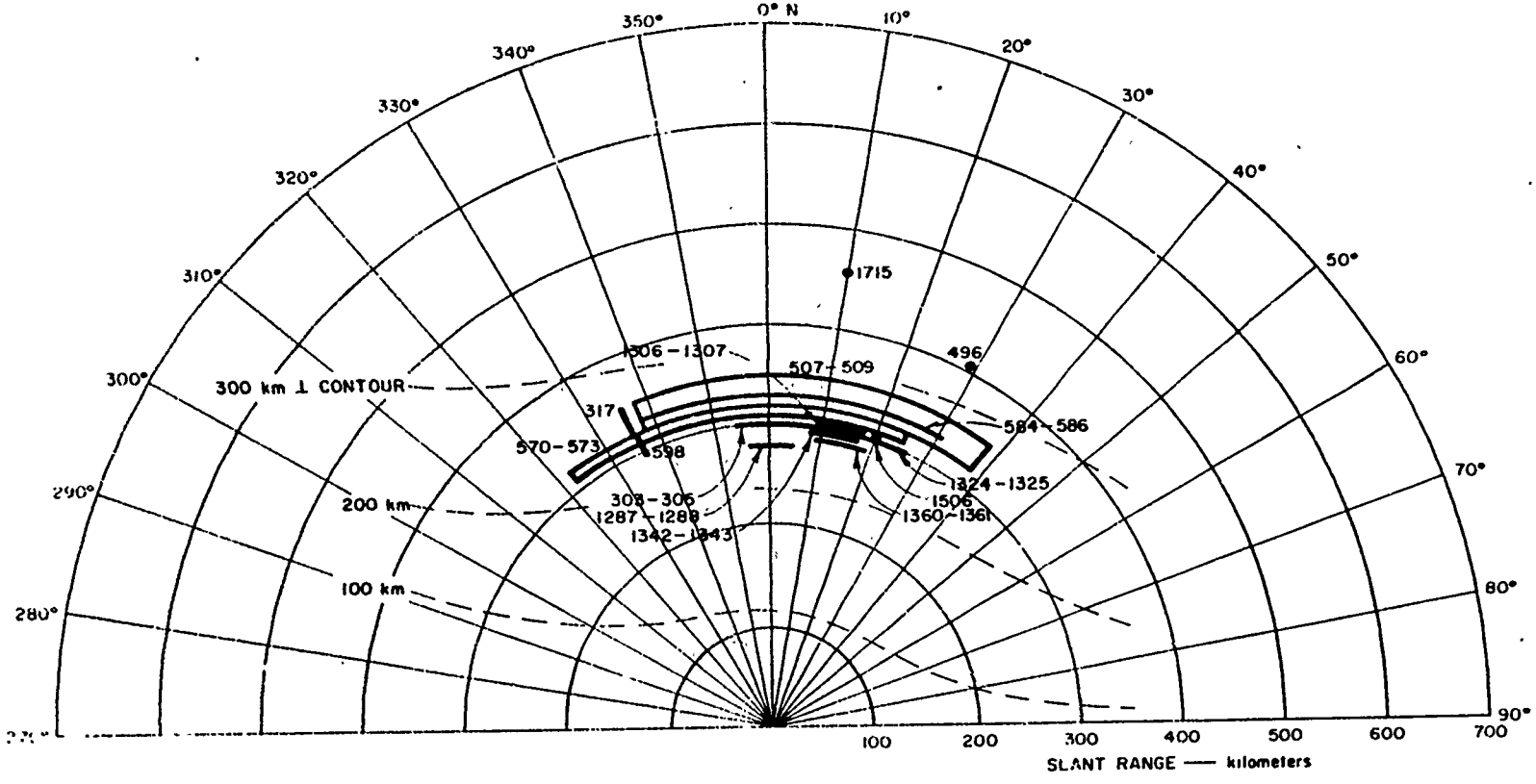

Figure 5.37 Johnston Island radar range versus azimuth for Check Mate; 850-Mc northern echoes, 300 to 2,100 seconds.

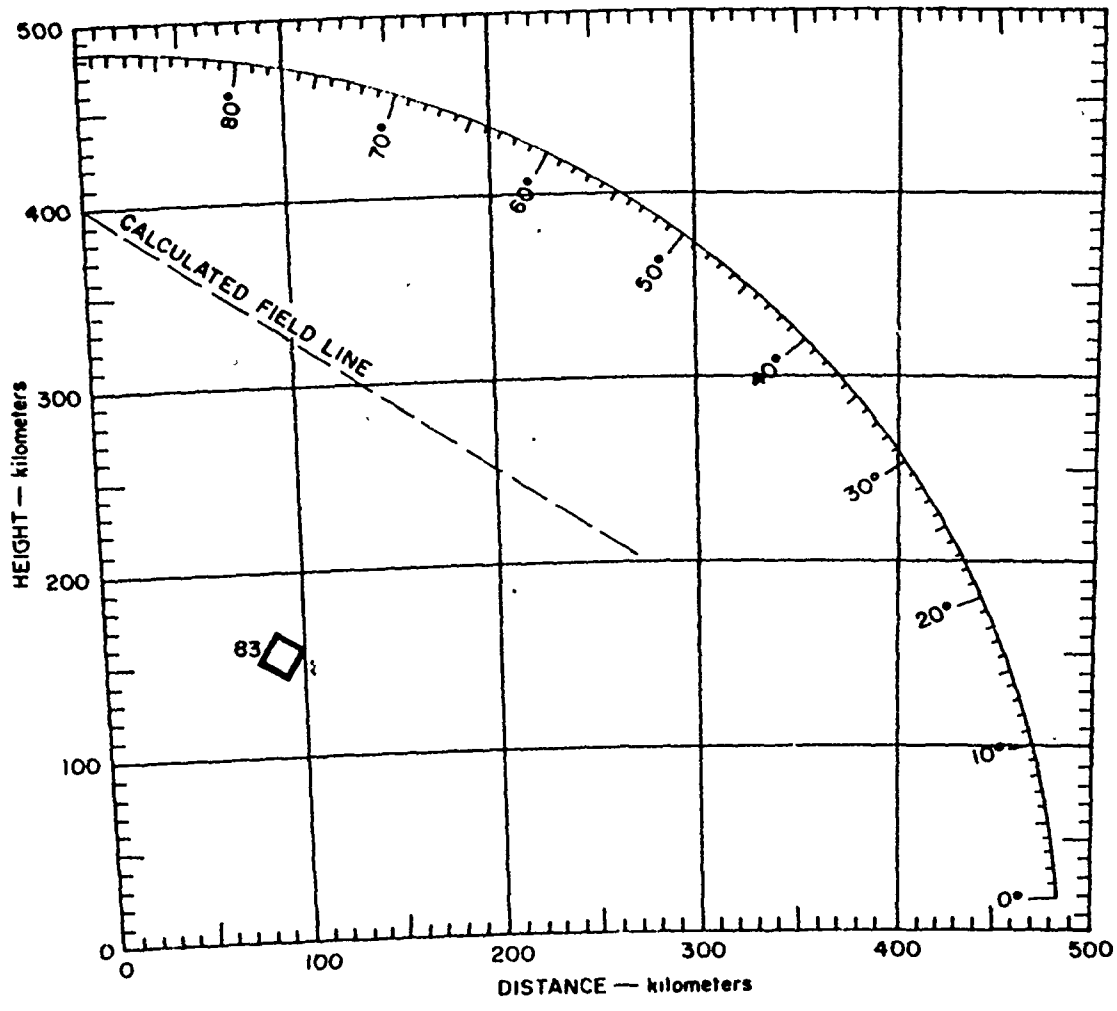

Figure 5.38 Johnston Island radar height versus distance for Check Mate; 850-Mc northern echoes, 36 to 83 minutes.

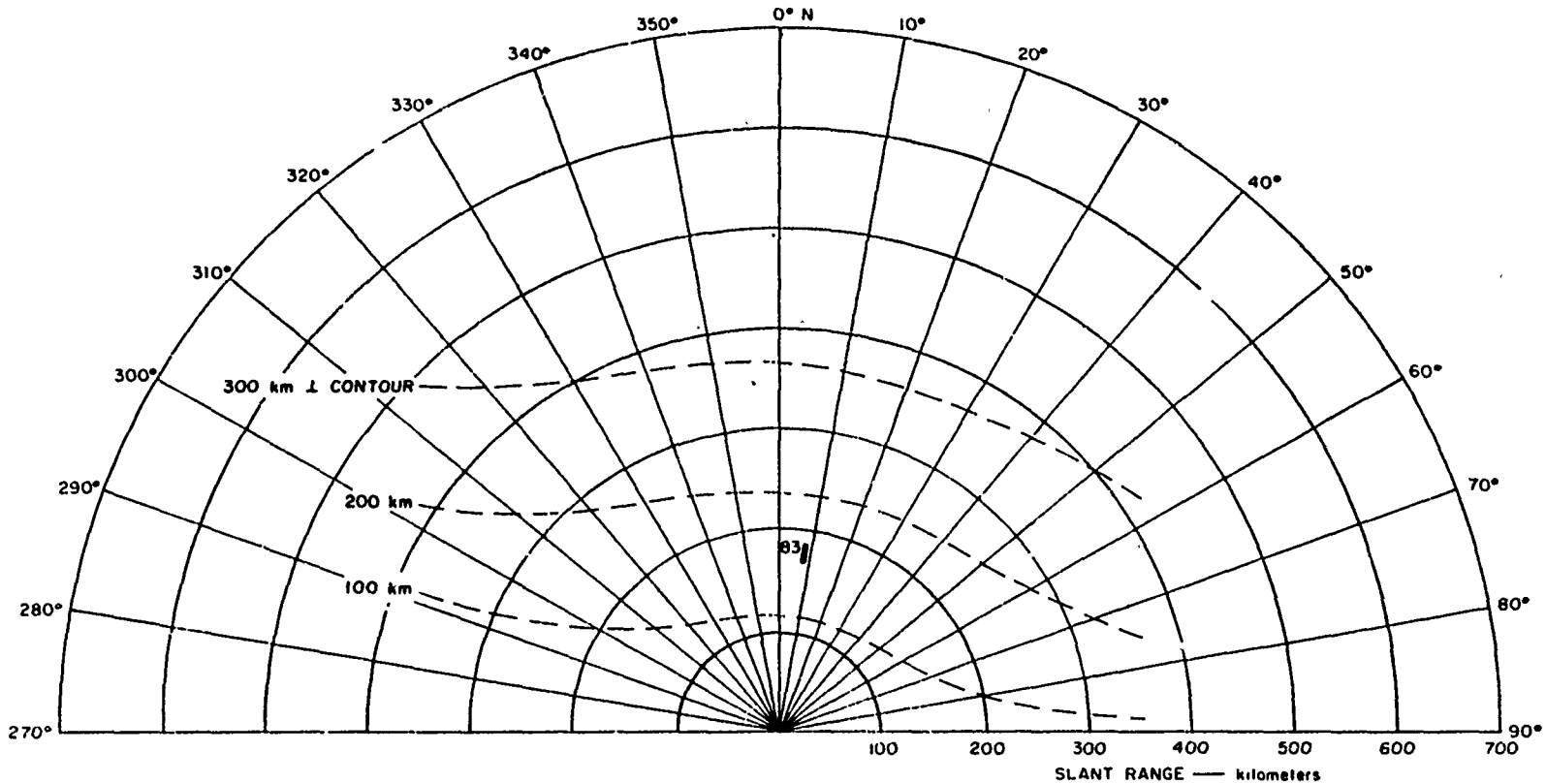

Figure 5.39 Johnston Island radar range versus azimuth for Check Mate; 850-Mc northern echoes, 36 to 83 minutes.

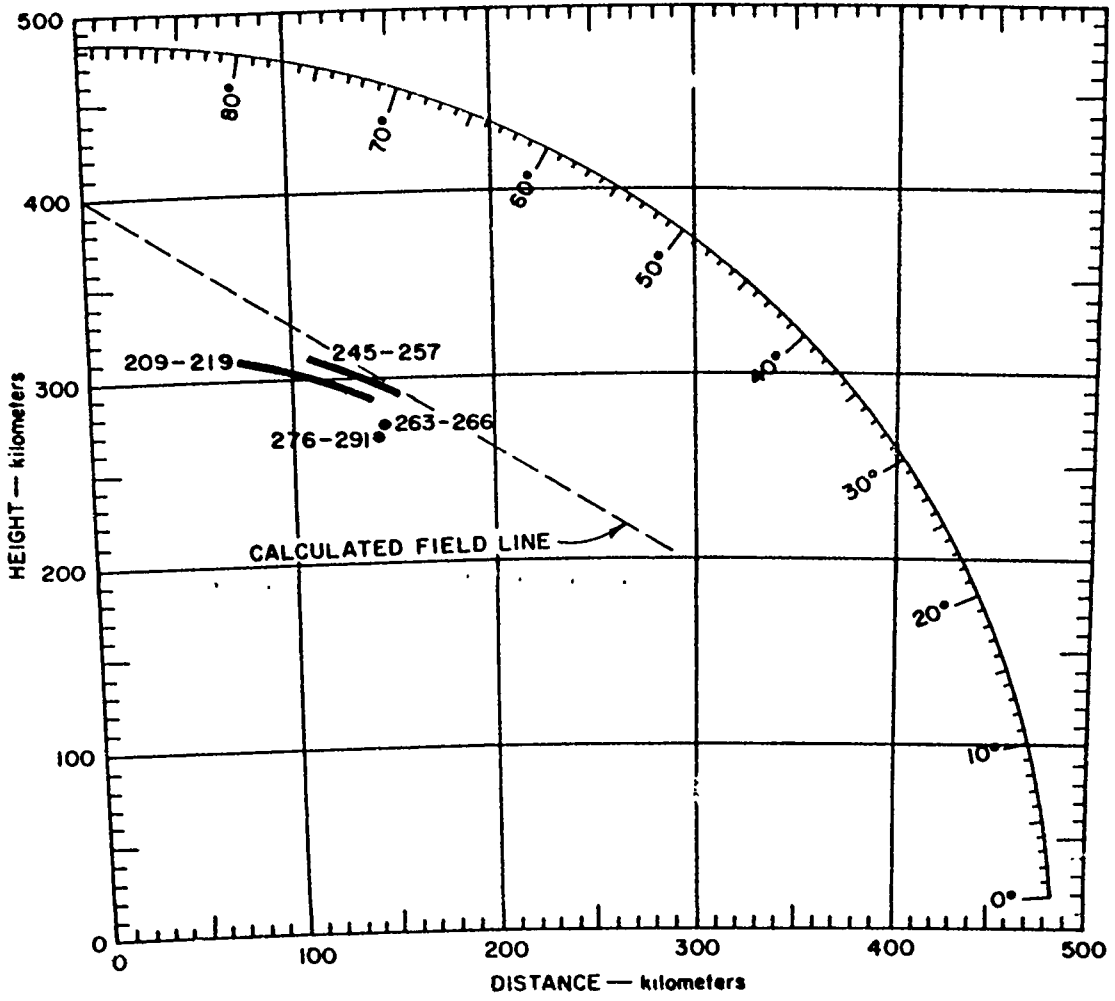

Figure 5.40 Johnston Island radar height versus distance for Check Mate; 1210-Mc northern echoes, 0 to 300 seconds.

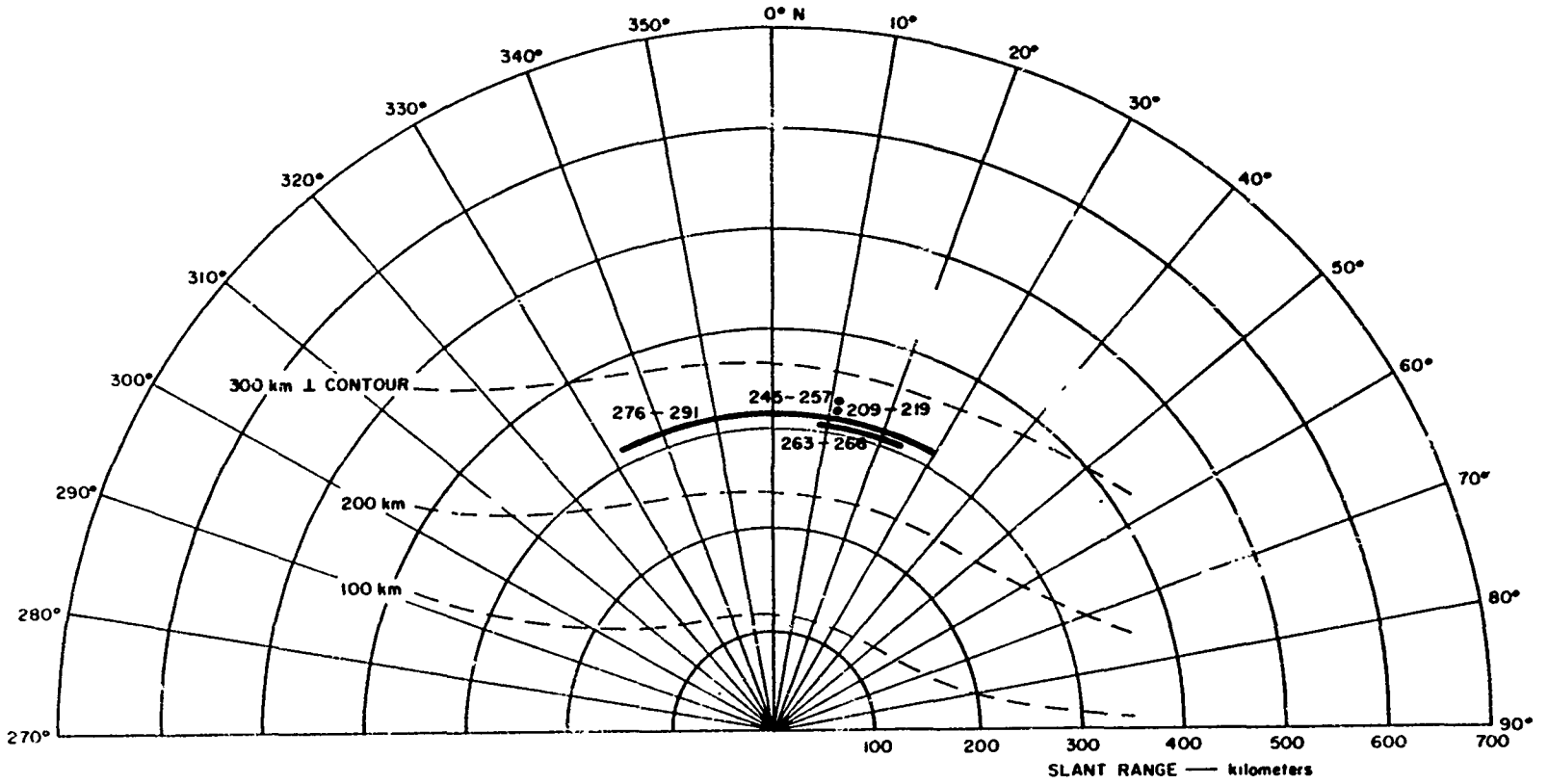

Figure 5.41 Johnston Island radar range versus azimuth for Check Mate; 1210-Mc northern echoes, 0 to 300 seconds.

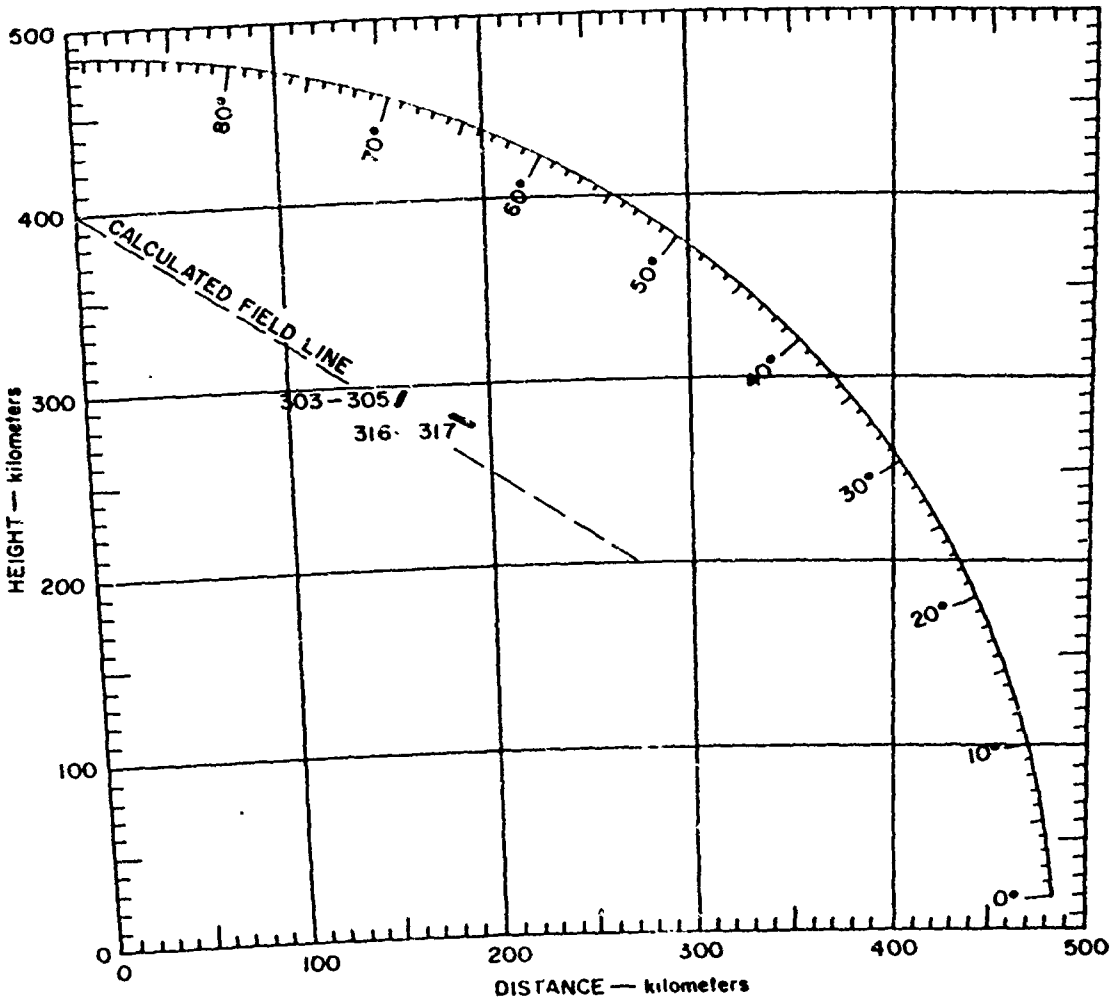

Figure 5.4: Johnston Island radar height versus distance for Check Mate; 1210-Mc northern echoes, 300 to 2,100 seconds.

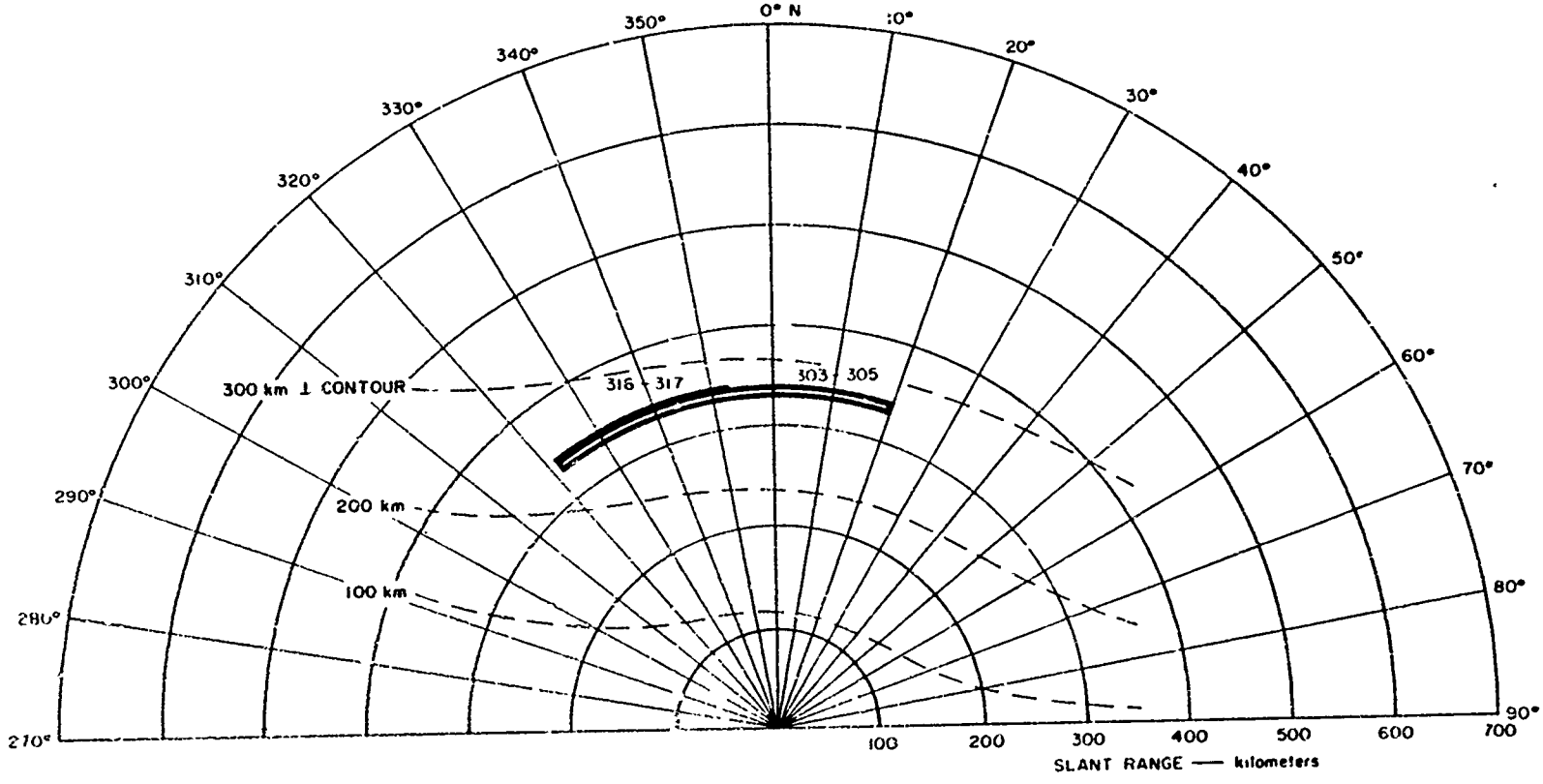

Figure 5.43 Johnston Island radar range versus azimuth for Check Mate: 1210-Mc northern echoes, 360 to 2,100 seconds.

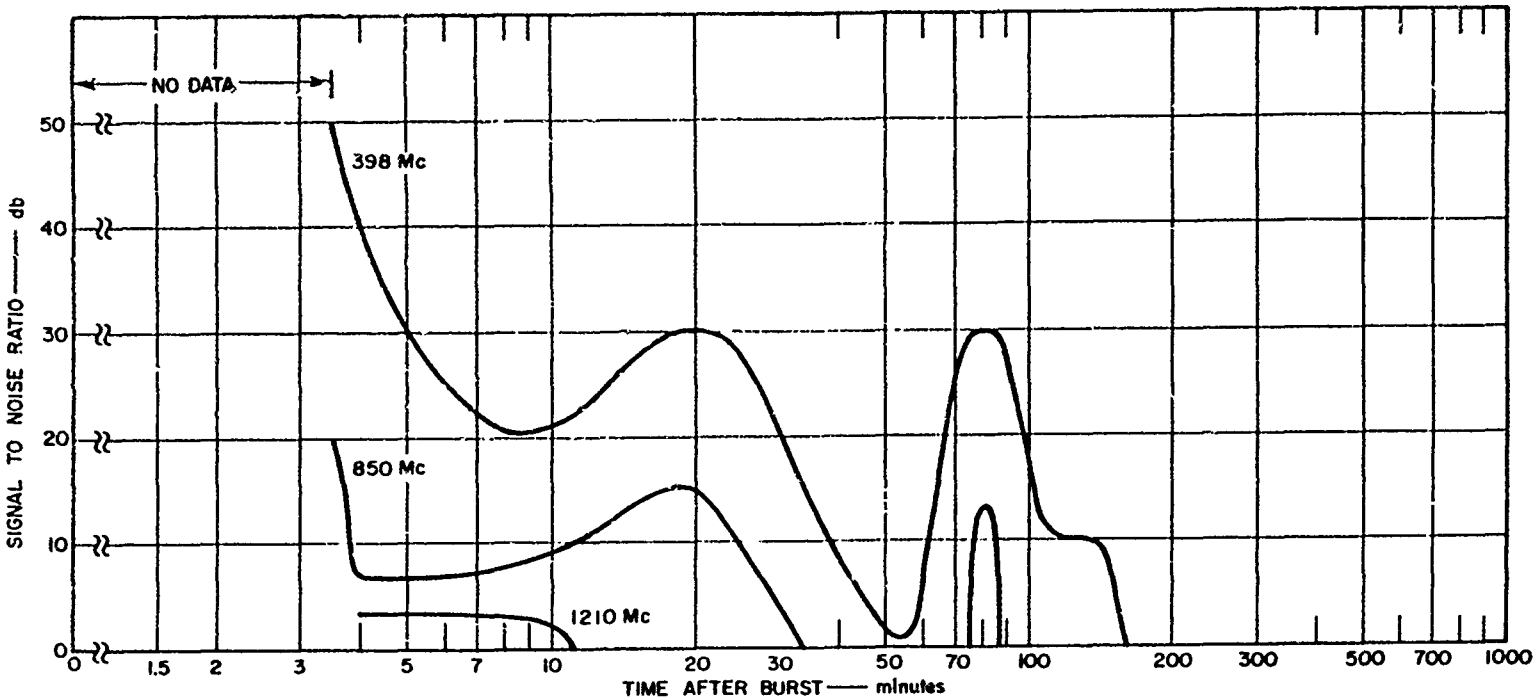

Figure 5.44 Johnston Island radar auroral echo amplitude versus time for Check Mate; 398, 850, and 1210 Mc.

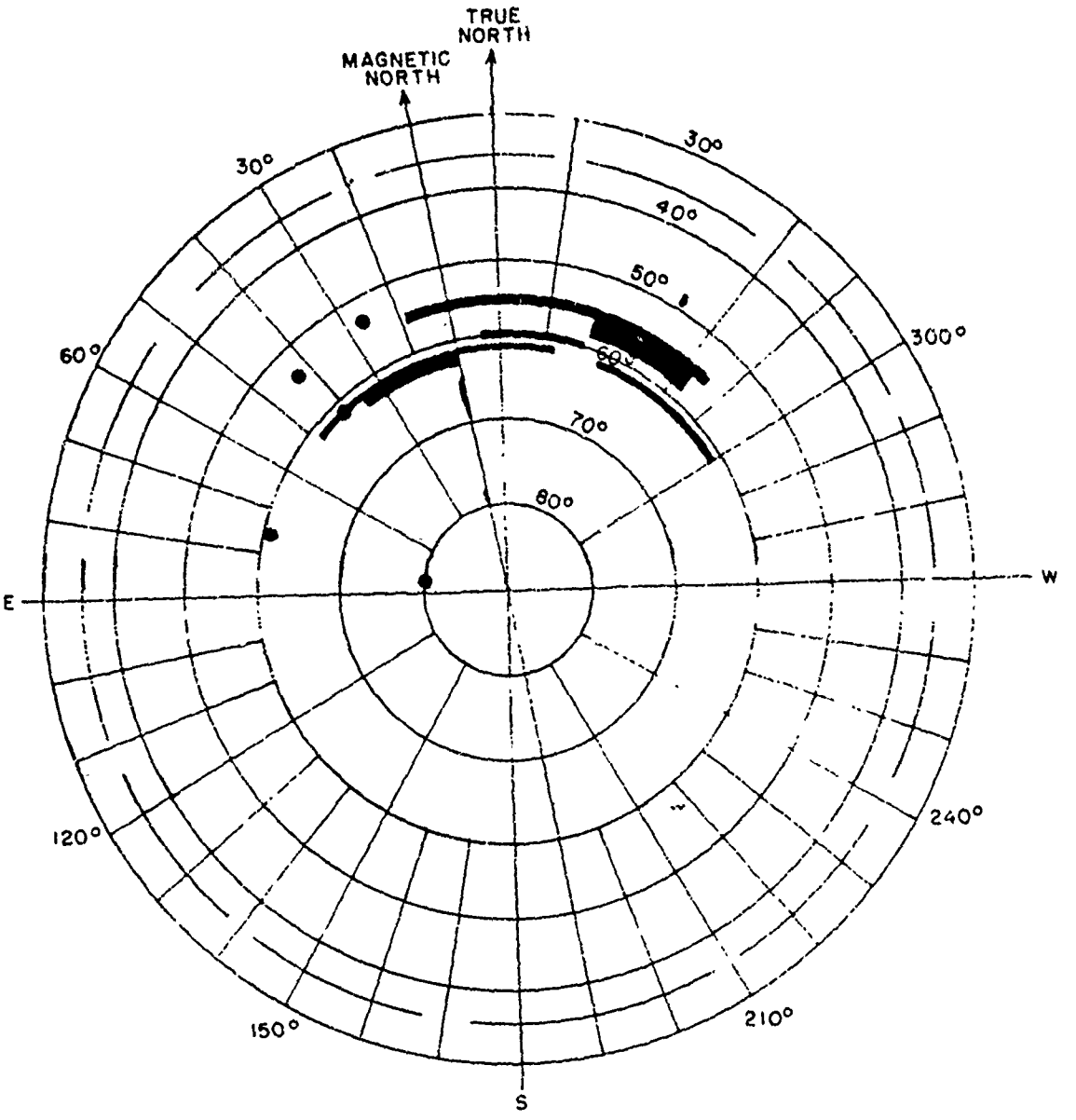

Figure 5.45 Johnston Island radar auroral echoes—visual comparison for Check Mate; 398 Mc, 3 to 10 minutes.

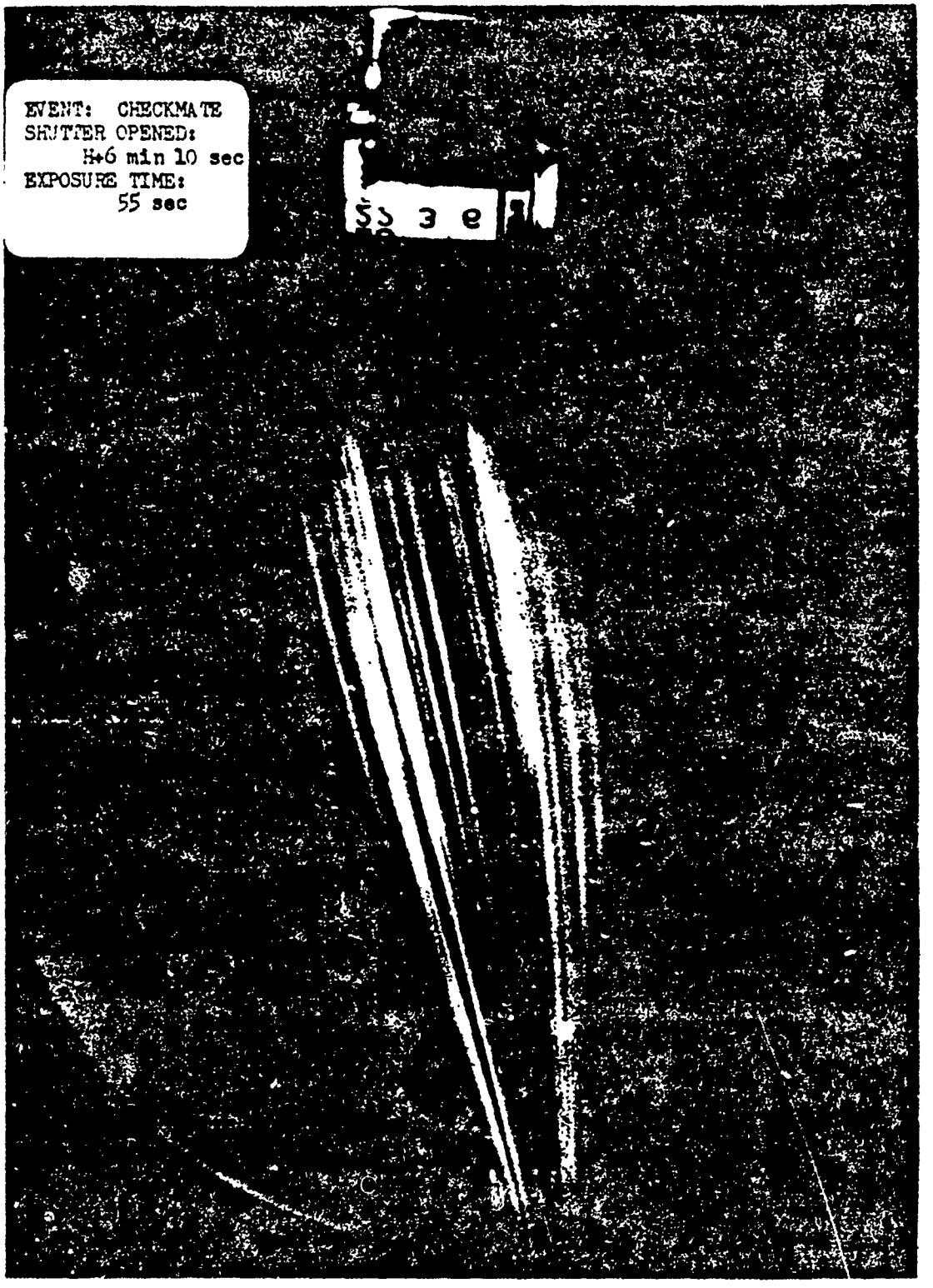

Figure 5.45a Johnston Island all-sky photograph for Check Mate, 6 minutes.

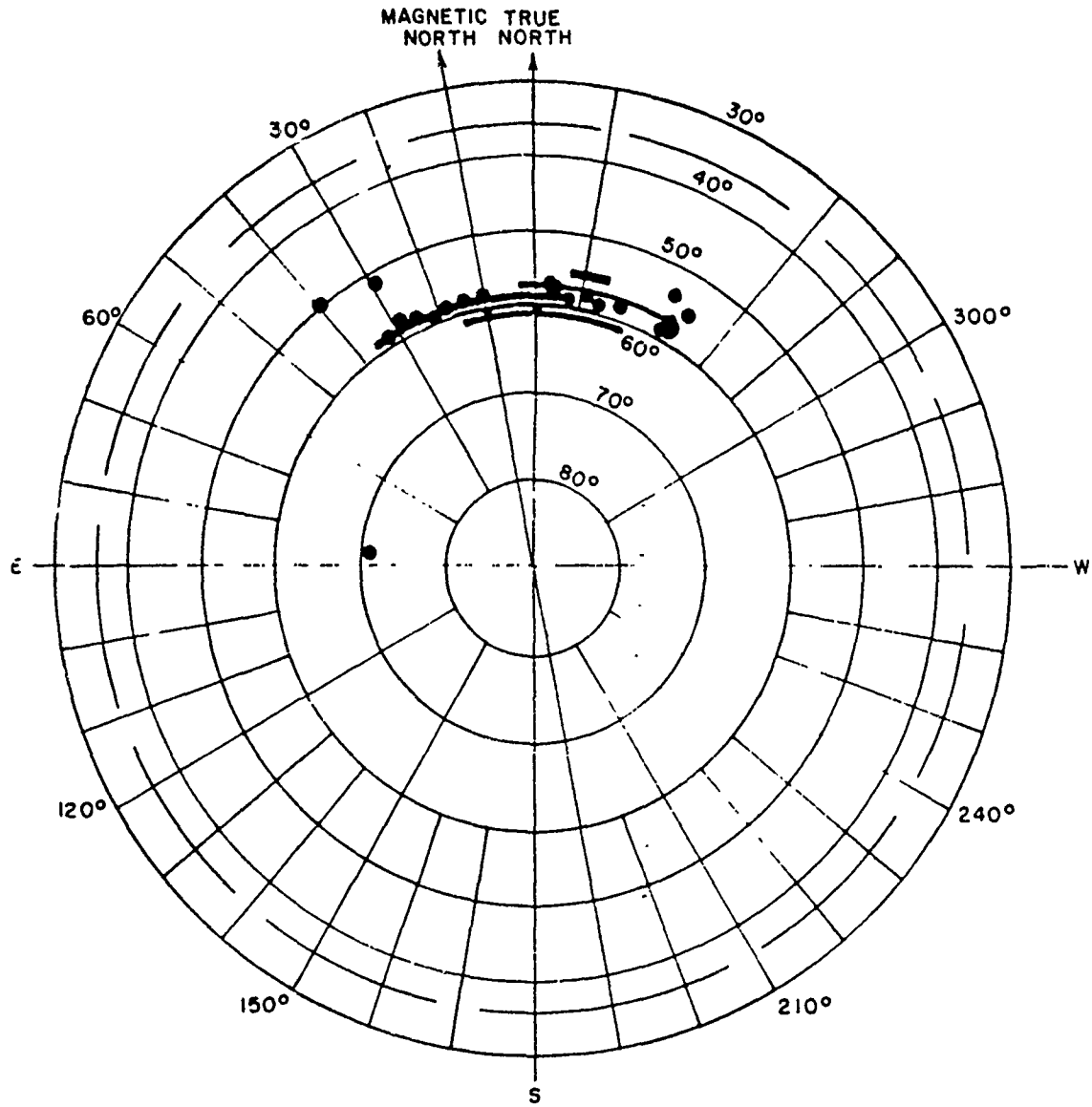

Figure 5.46 Johnston Island radar auroral echoes—visual comparison for Check Mate; 398 Mc, 10 to 50 minutes.

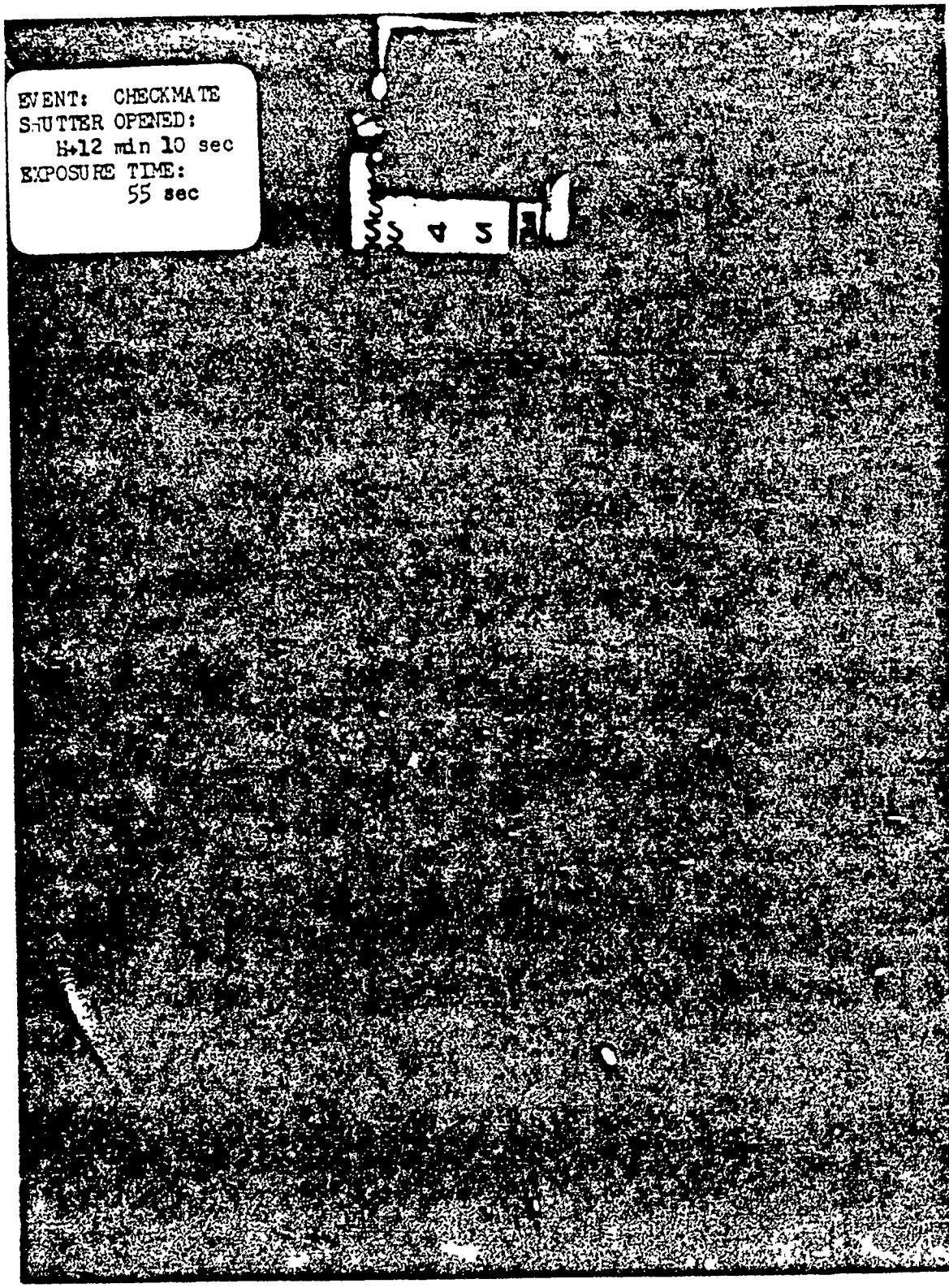

Figure 5.46a Johnston Island all-sky photograph for Check Mate, 12 minutes.

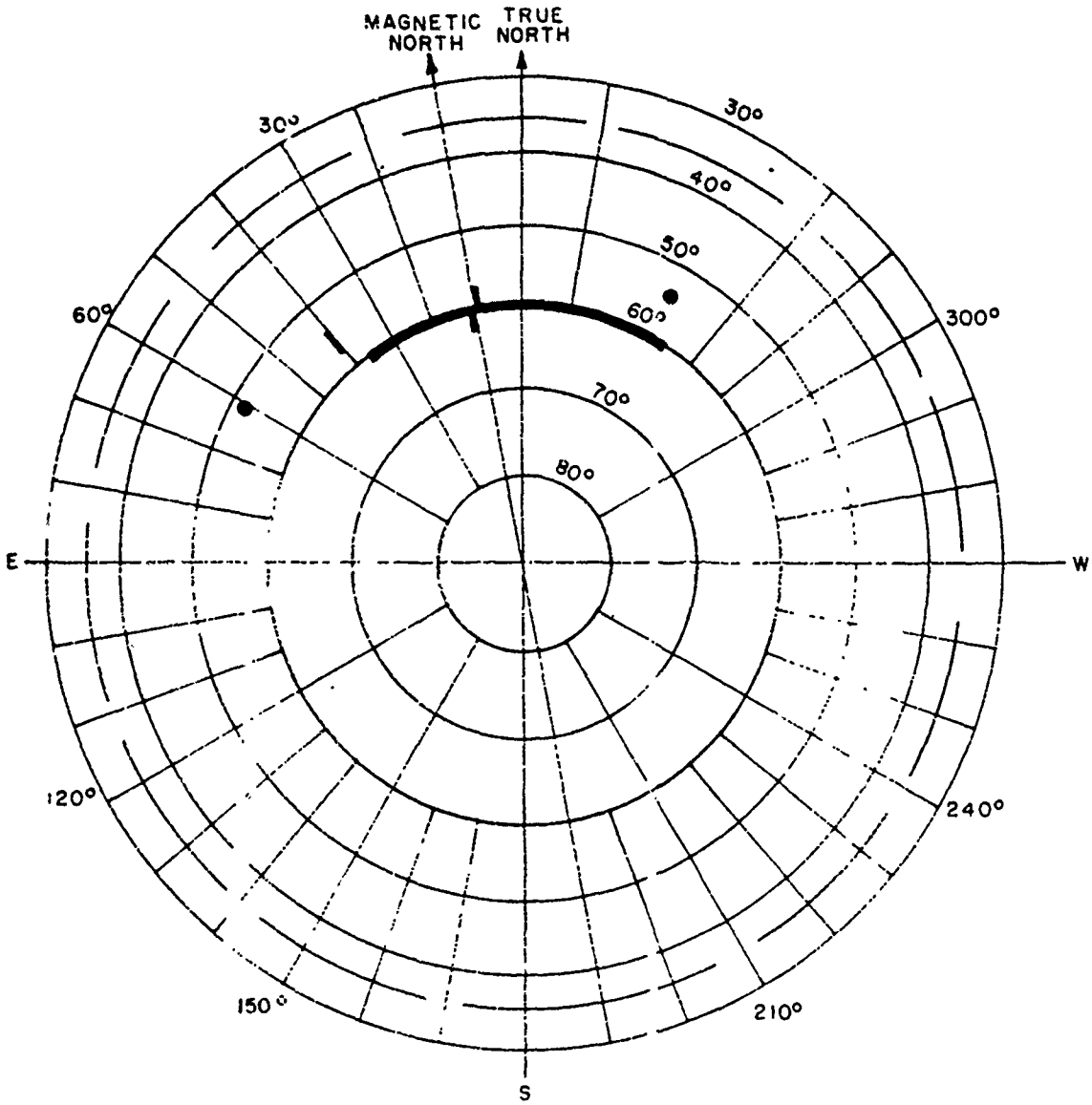

Figure 5.47 Johnston Island radar auroral echoes—visual comparison for Check Mate; 398 Mc, 50 to 150 minutes.

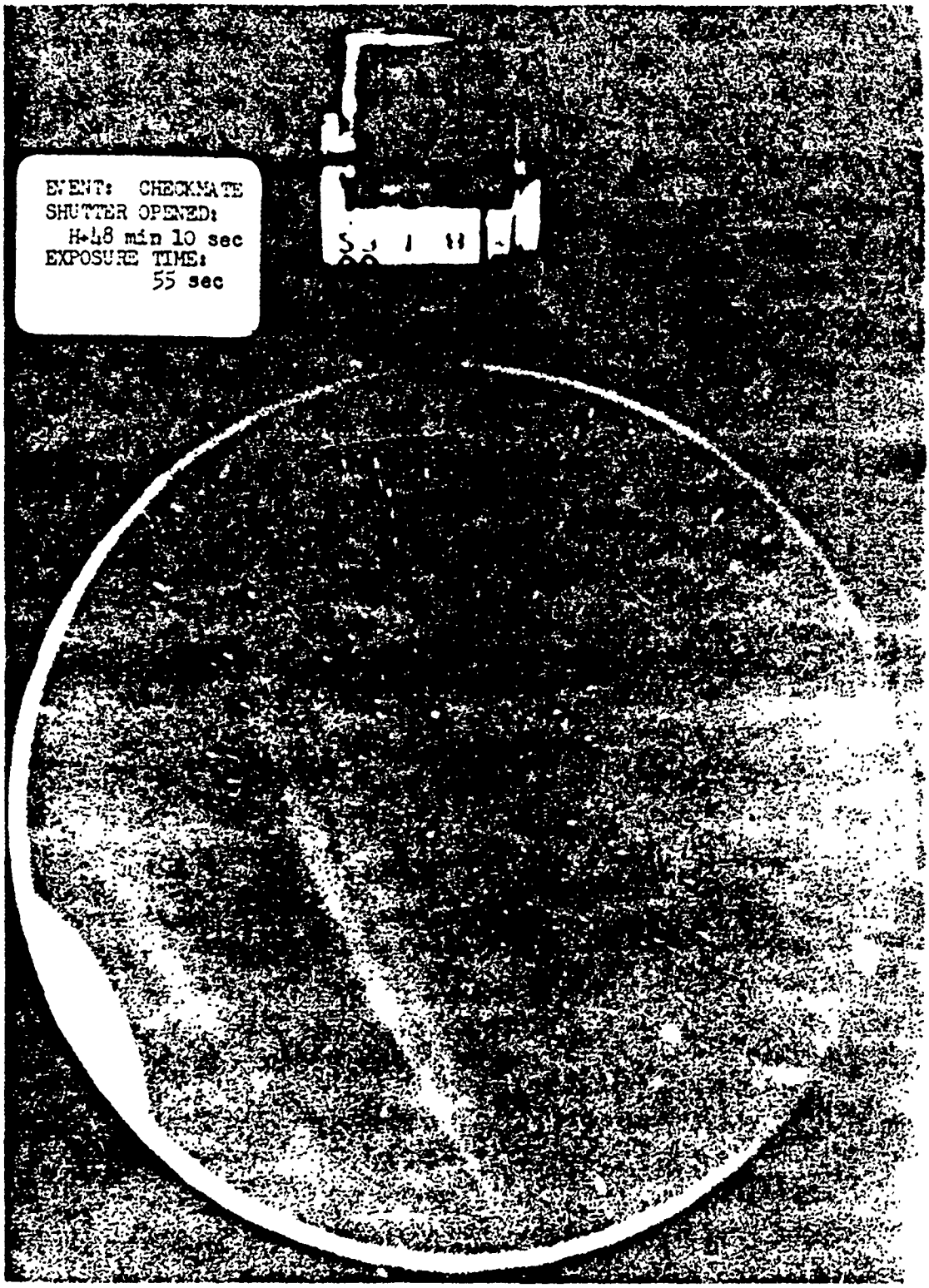

Figure 5.47a Johnston Island all-sky photograph for Check Mate, 48 minutes.

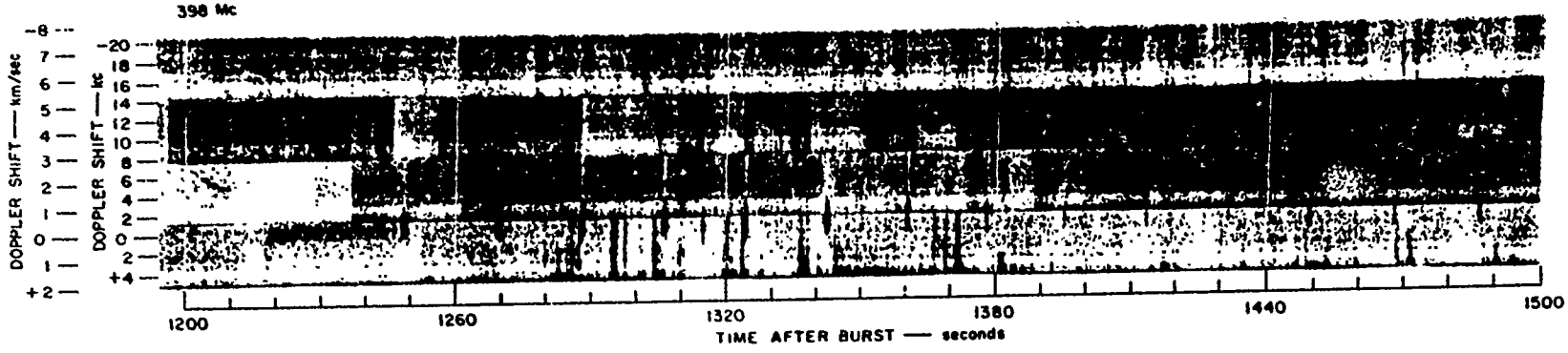

Figure 5.48 Johnston Island radar Doppler versus time for Check Mate; 398 Mc, 1,200 to 1,500 seconds.

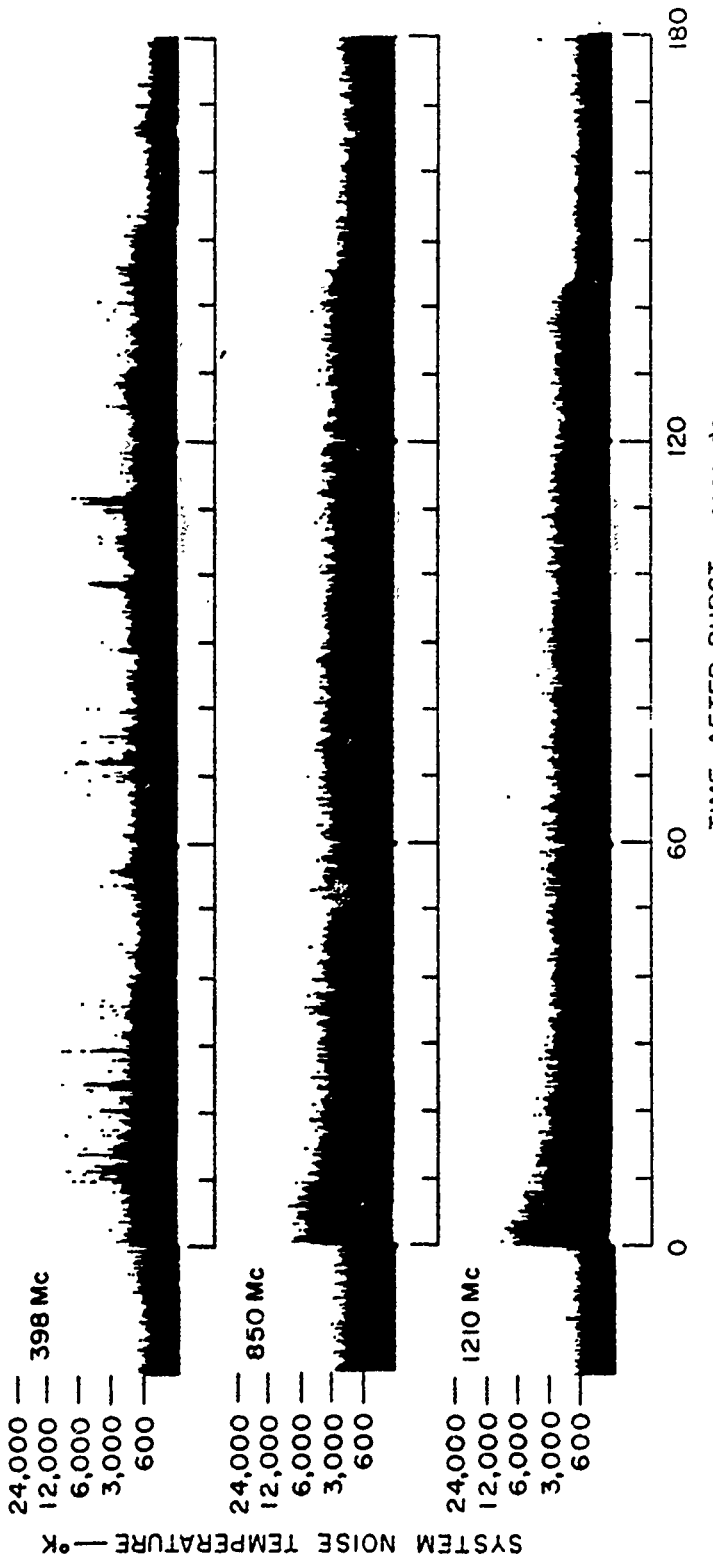

Figure 5.49 Johnston Island radar noise levels for Check Mate.

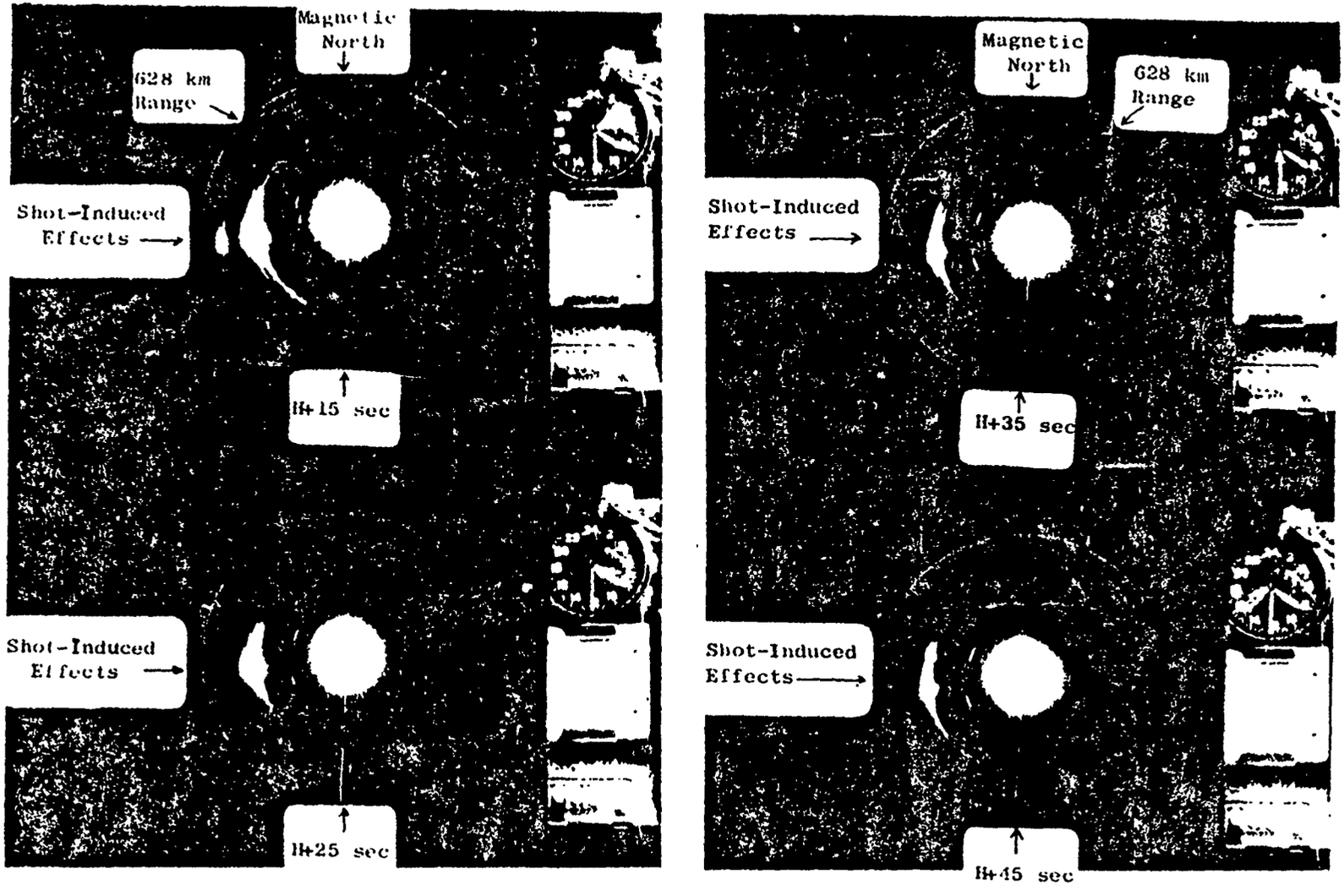

Figure 5.50 AEW aircraft radar PPI for Check Mate; Lambkin 1, 15 to 45 seconds.

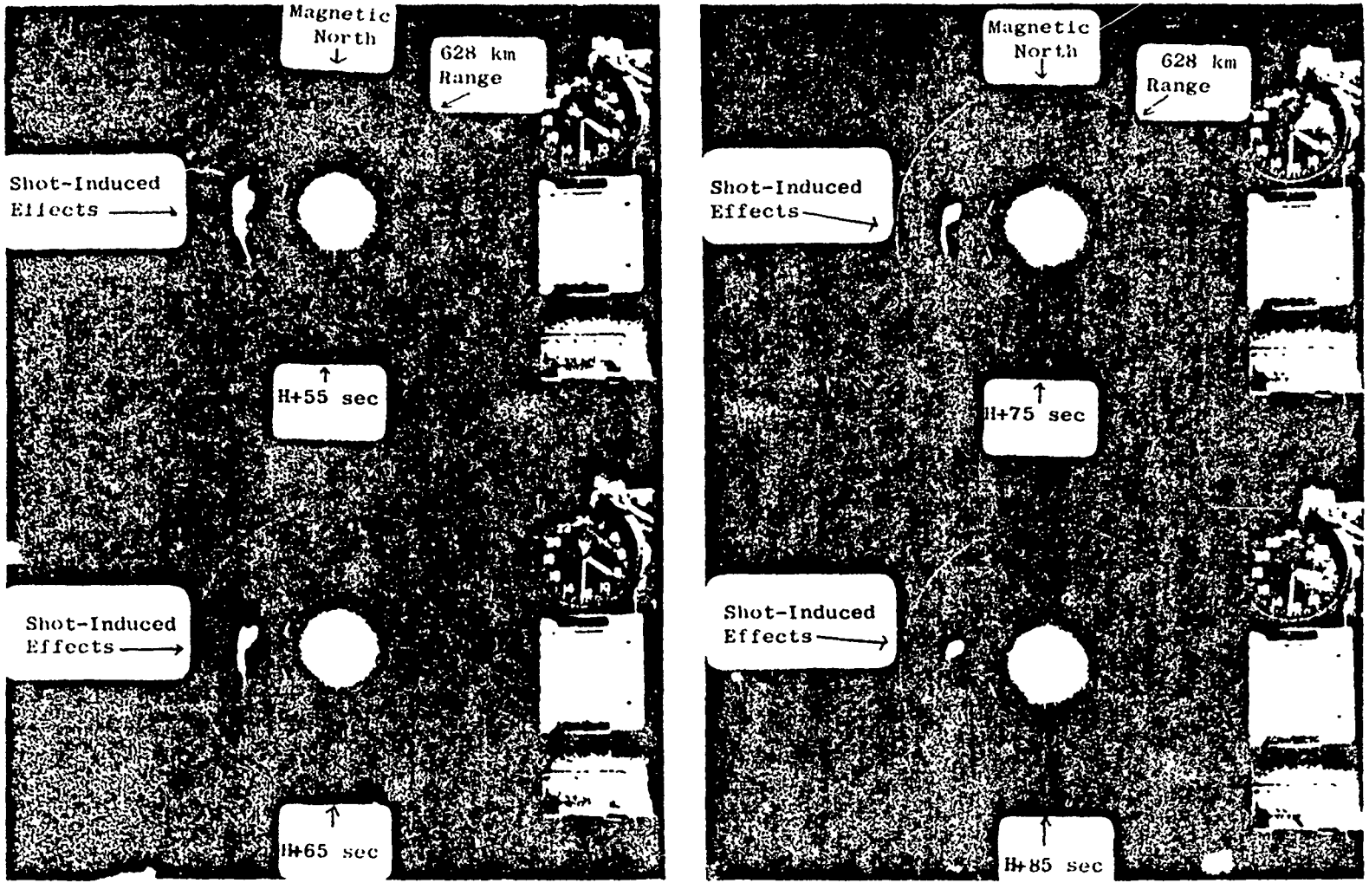

Figure 5.51 AEW aircraft radar PPI for Check Mate; Lambkin 1, 55 to 85 seconds.

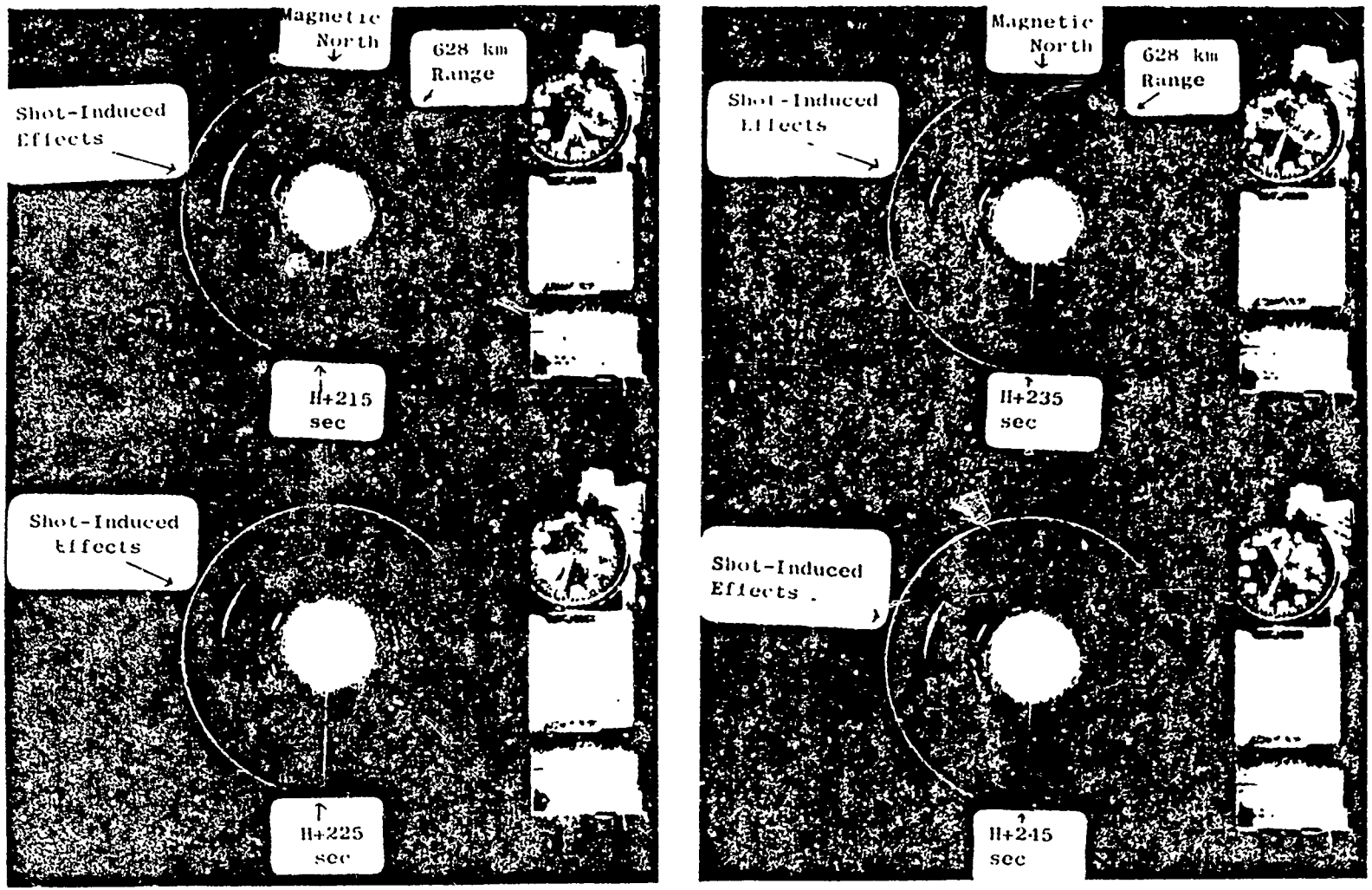

Figure 5.52 AEW aircraft radar PPI for Check Mate; Lambkin 1, 215 to 245 seconds.

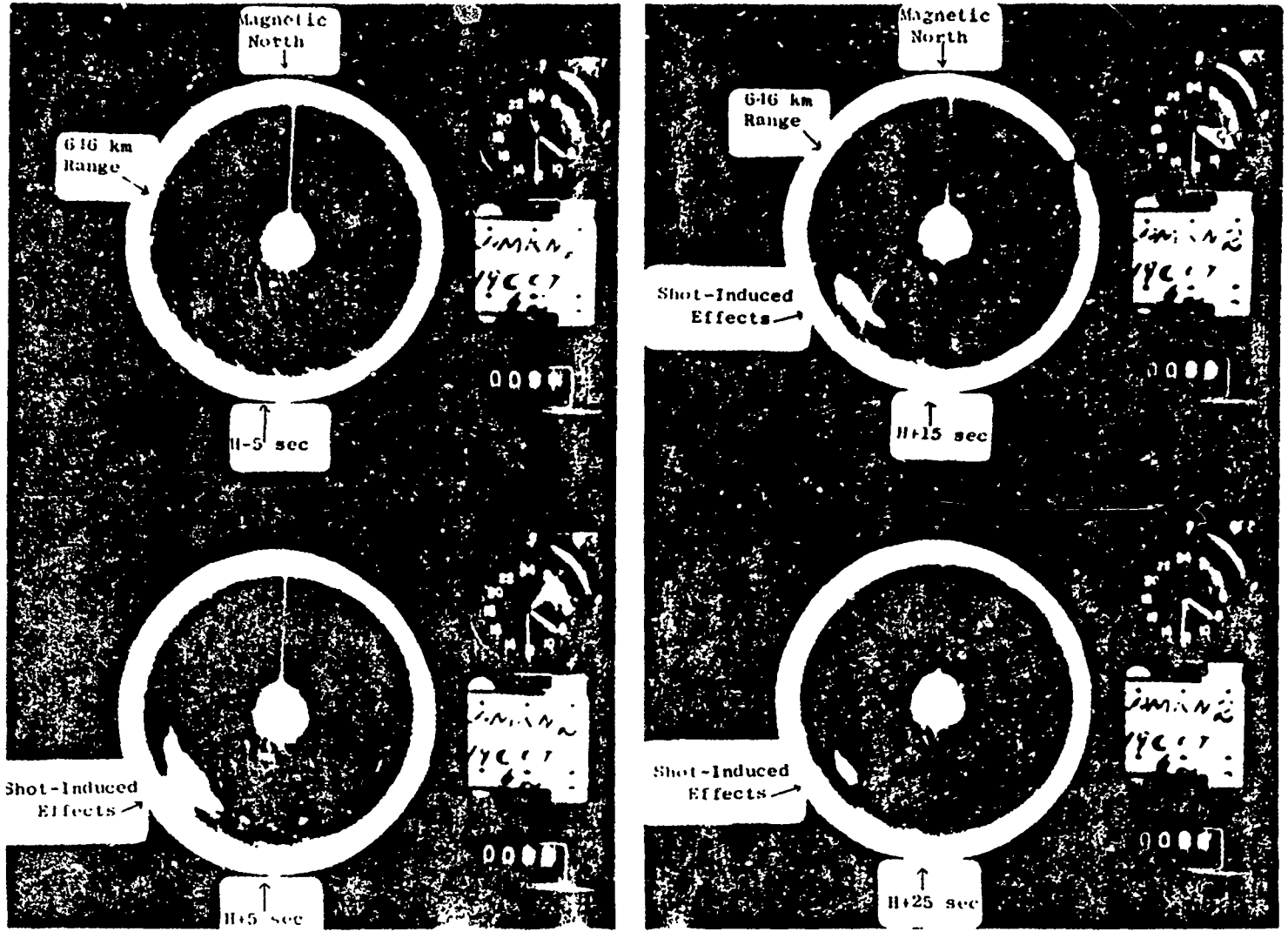

Figure 5.53 AEW aircraft radar PPI for Check Mate; Lambkin 2, 0 to 25 seconds.

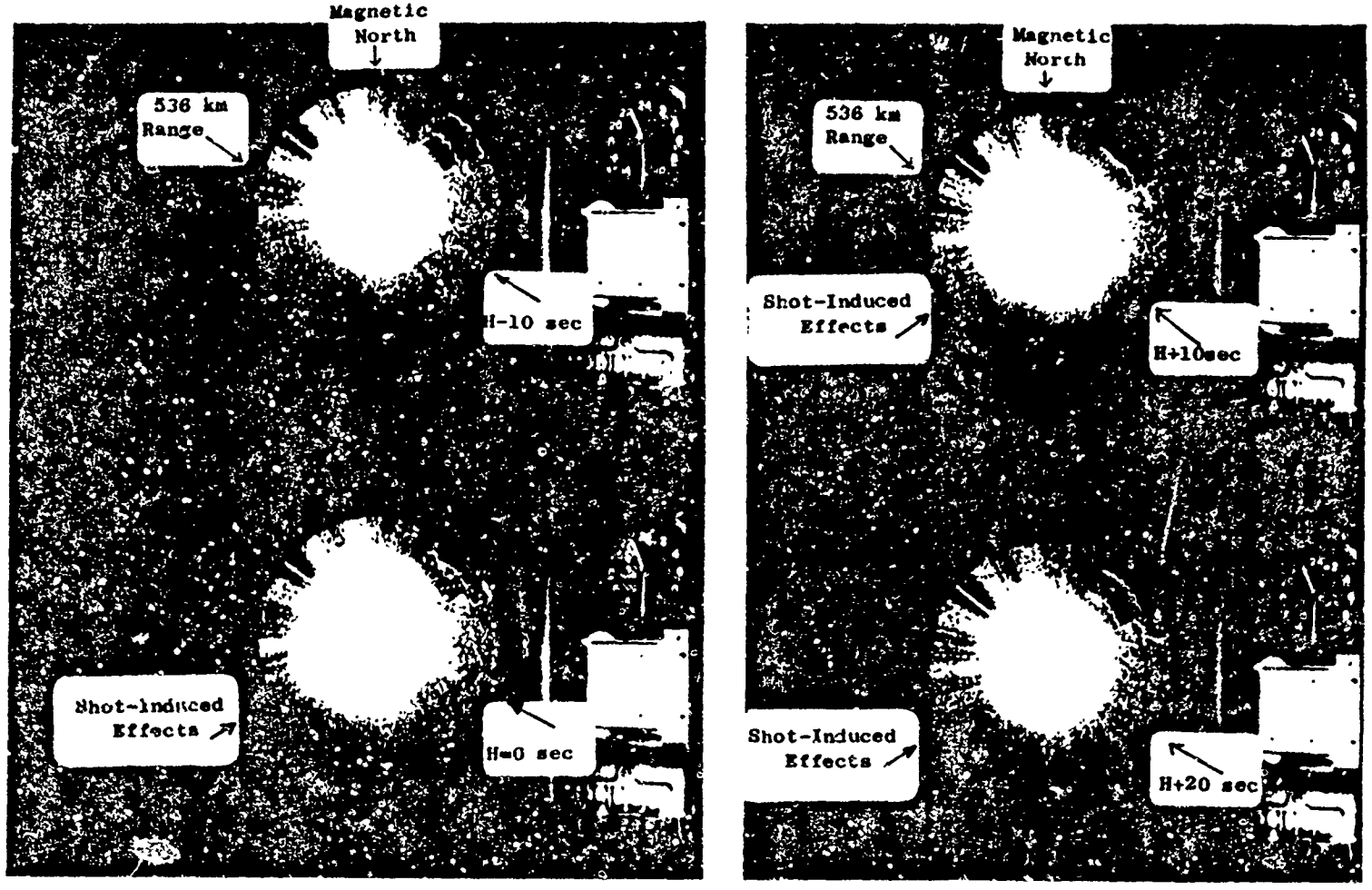

Figure 5.54 AEW aircraft radar PPI for Check Mate; Abusive I, 0 to 20 seconds.

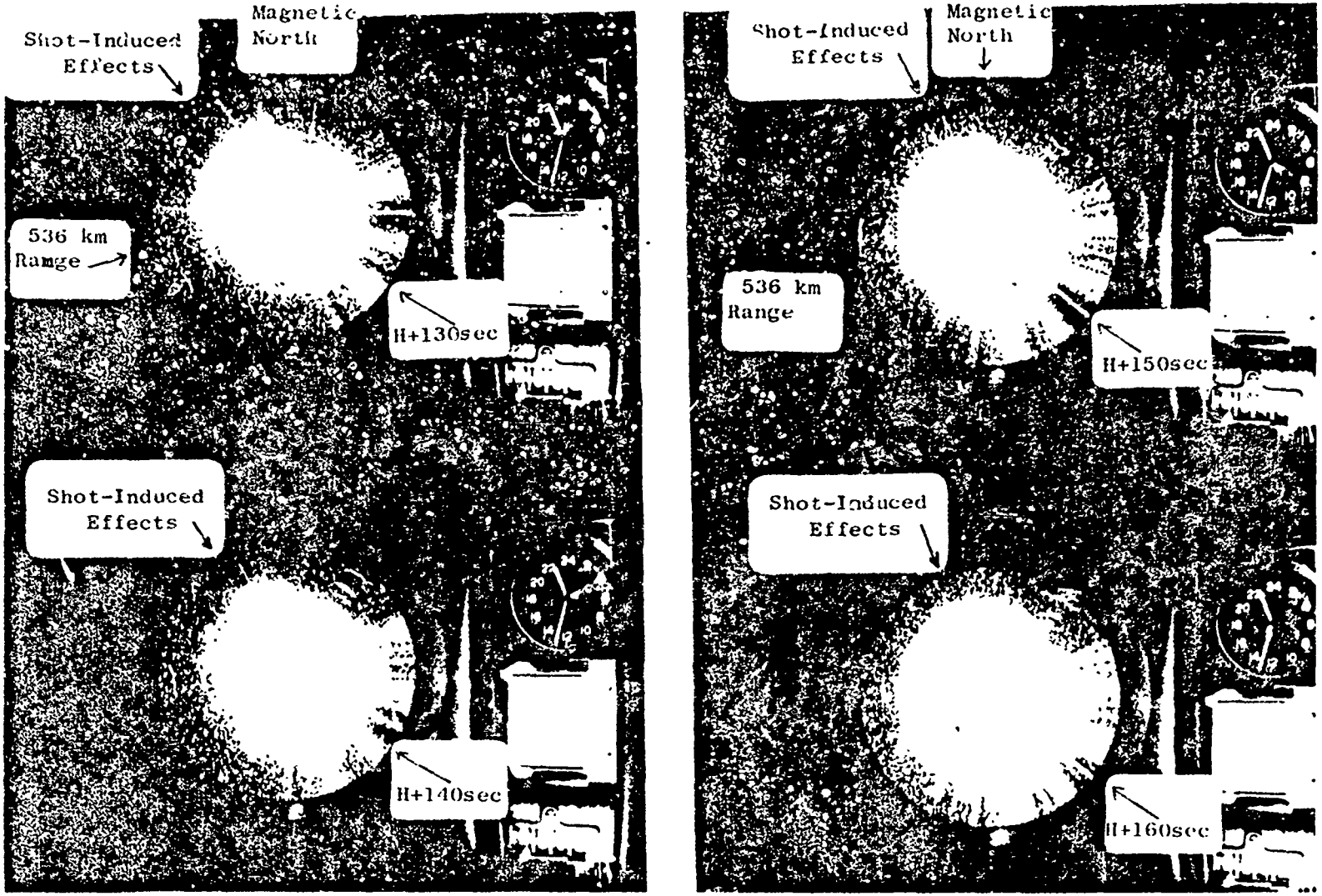

Figure 5.55 AEW aircraft radar PPI for Check Mate; Abusive 1, 130 to 160 seconds.

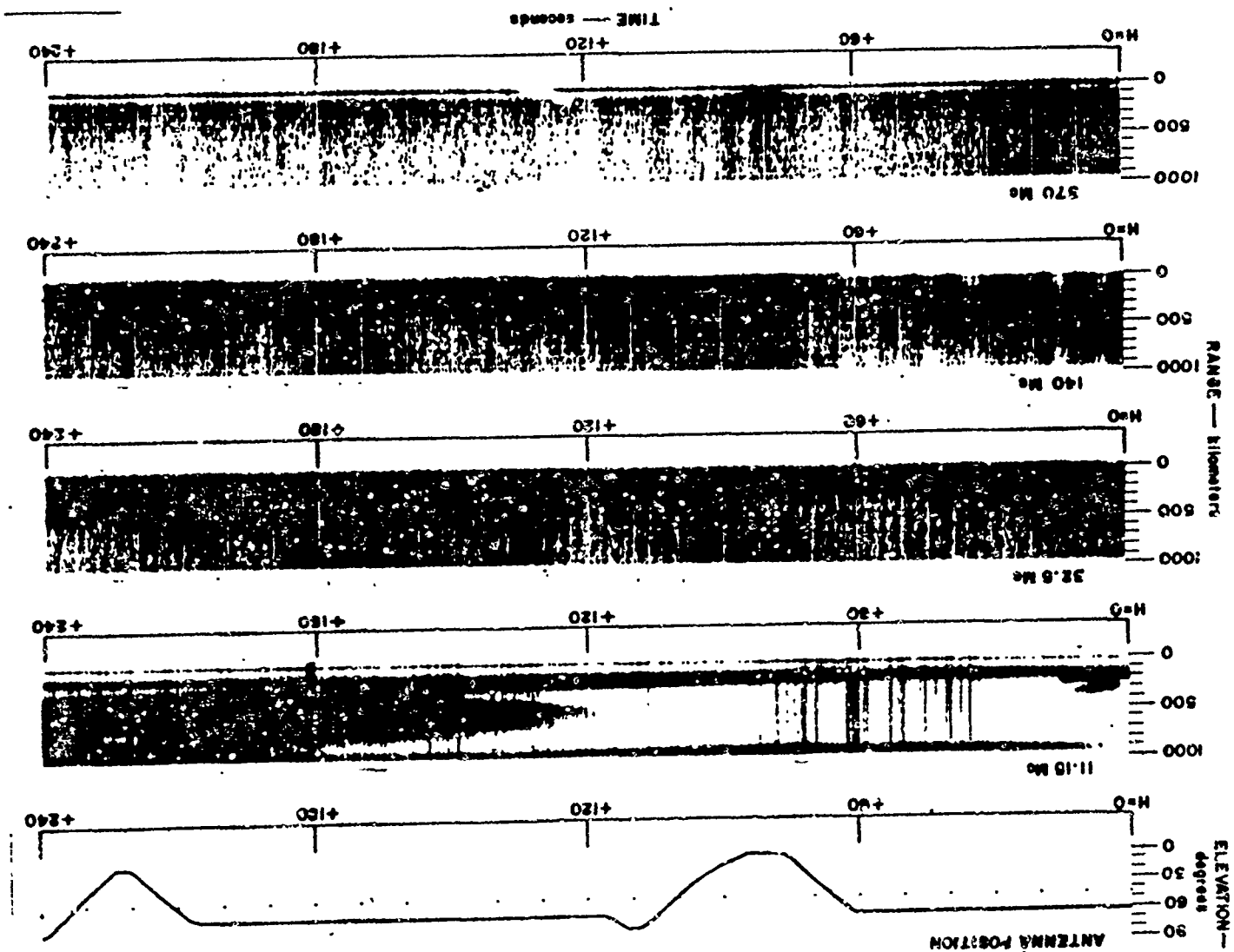

Figure 5.56 M/V ACANIA radar range versus time for Check Mate, 0 to 240 seconds.

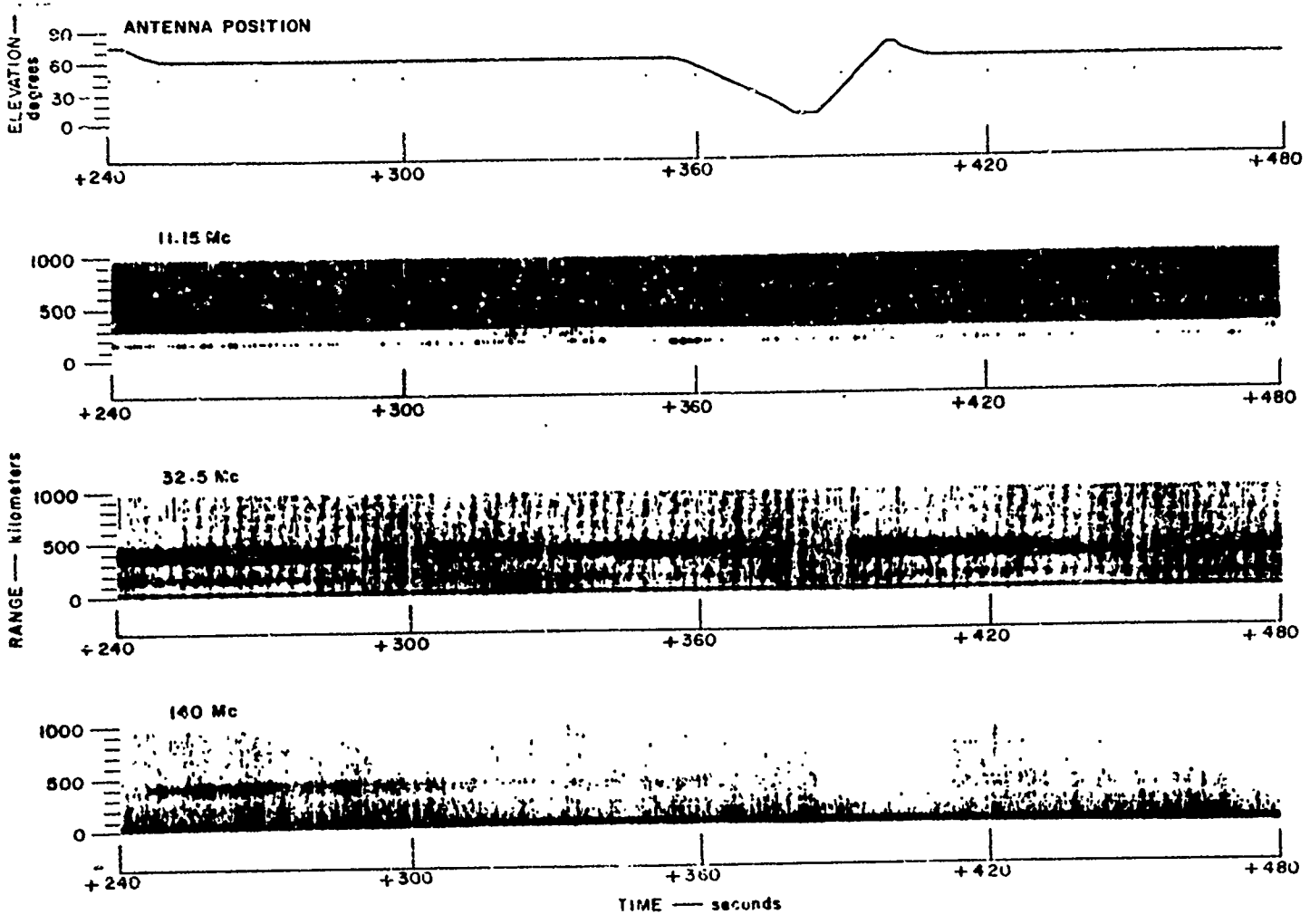

Figure 5.57 M/V ACANIA radar range versus time for Check Mate, 240 to 480 seconds.

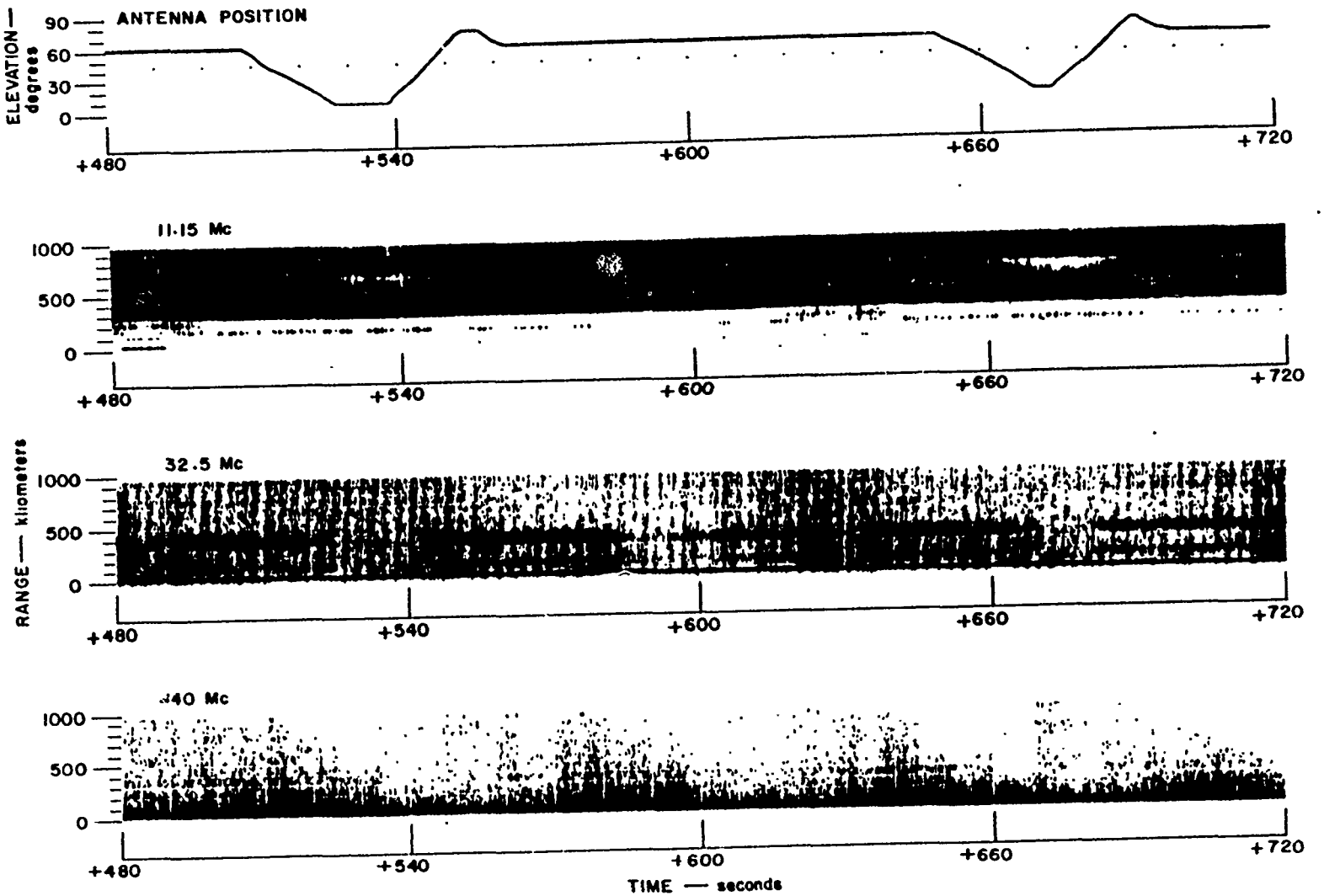

Figure 5.58 M/V ACANIA radar range versus time for Check Mate, 480 to 720 seconds.

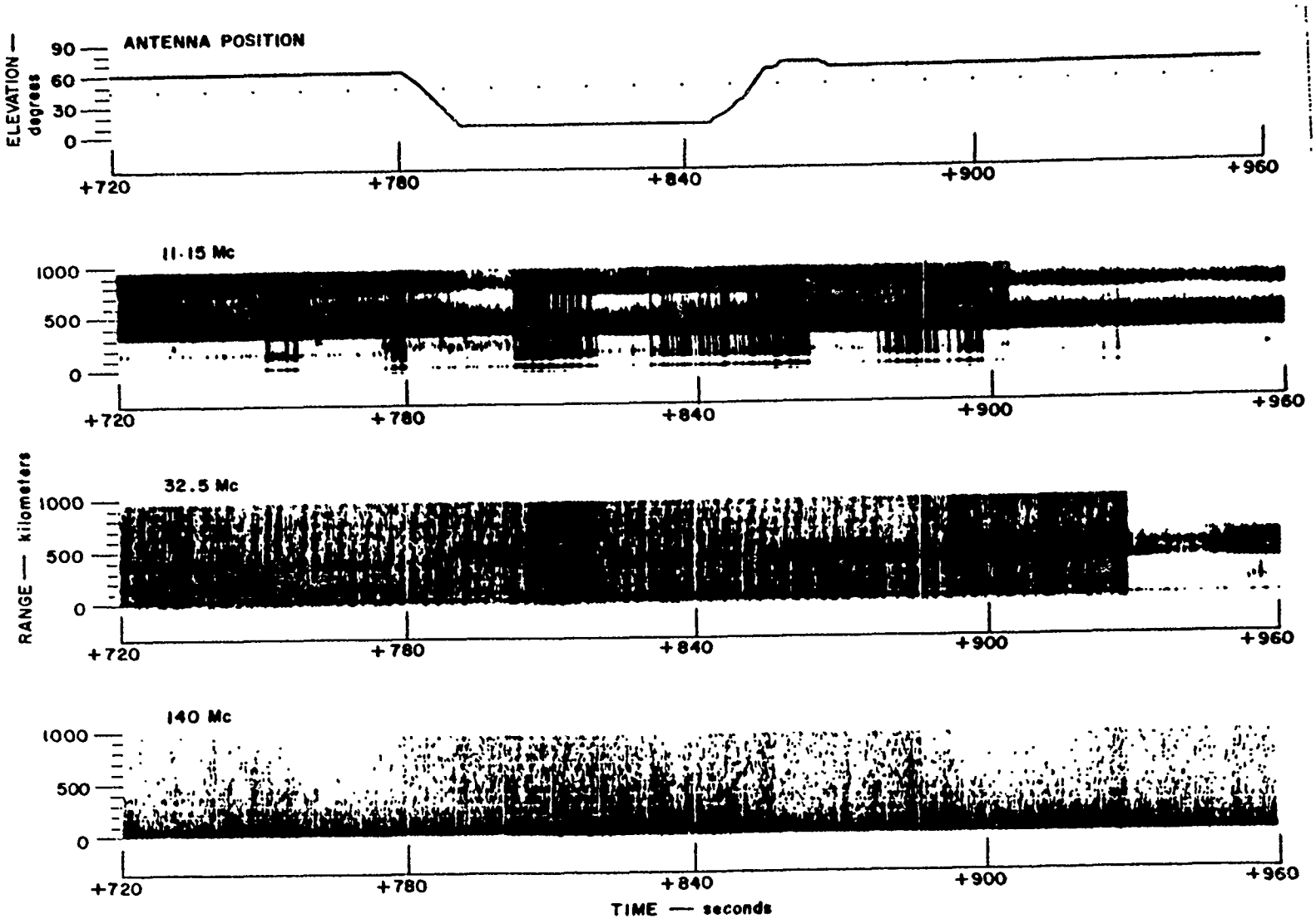

Figure 5.59 M/V ACANIA radar range versus time for Check Mate, 720 to 960 seconds.

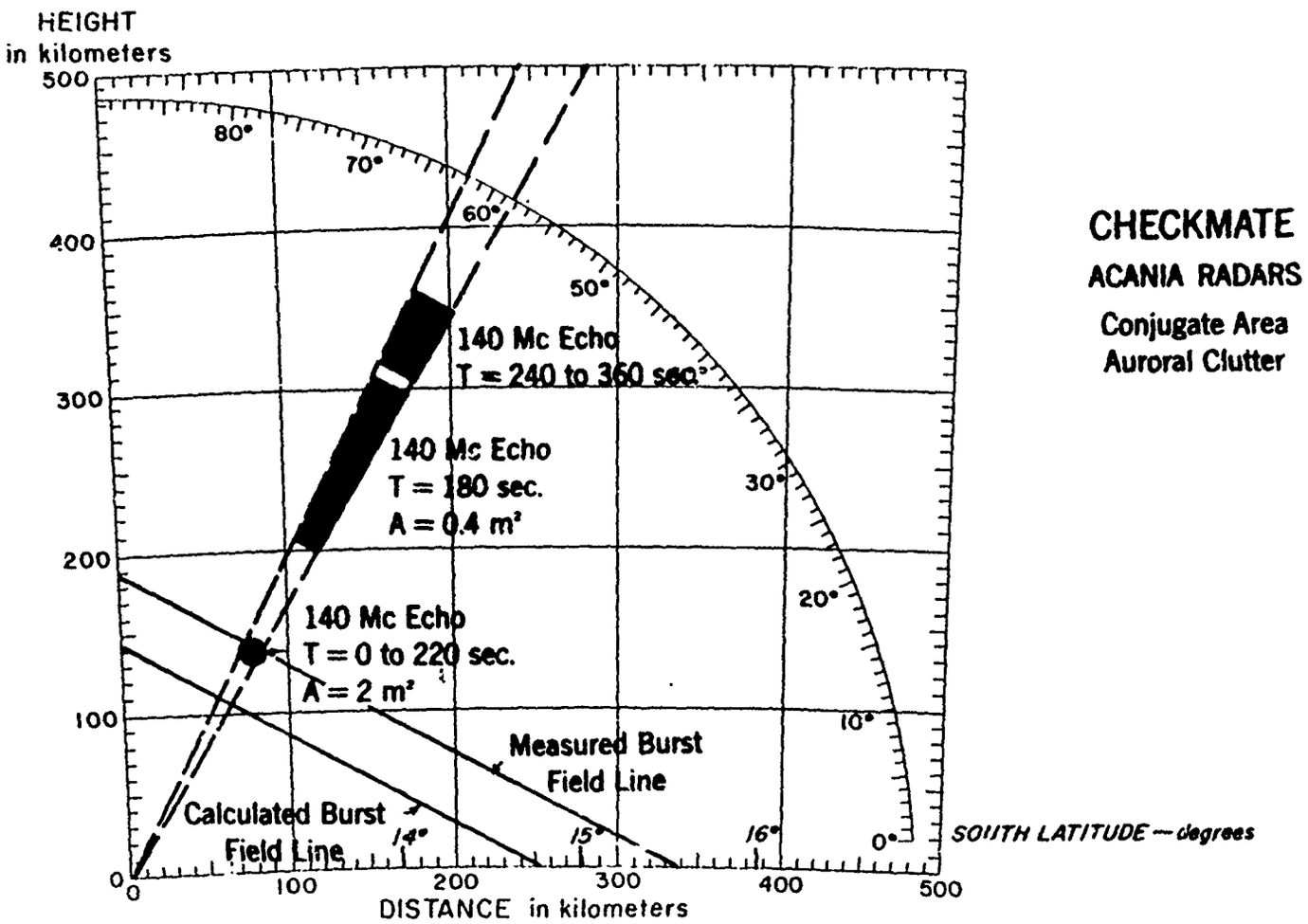

Figure 5.60 M/V ACANIA radar height versus distance for Check Mate.

CHAPTER 6

STAR FISH

6.1 INTRODUCTION

Prior to the Star Fish event, there was considerable uncertainty as to the behavior of the rapidly expanding bomb plasma in the presence of the earth's field.[1] This uncertainty arose because it was not known whether the debris would be ionized, or neutral, after very early times. If the debris fragments were uncharged, the expansion would occur unimpeded in the upward direction, so that approximately one-half of the total fission material would completely escape into outer space. The downward portion, on the other hand, should be stopped by the atmosphere between 150- and 200-km altitude. This pancake model is depicted in Figure 6.1. About one-half of the downward-traveling debris would be expected to be deposited within a 225-km radius of ground zero. All but 10 percent should fall within a 550-km radius.

The debris, however, might not be uncharged. In fact, not only might the debris be heavily ionized, but intense shocks associated with the hydromagnetic expansion might produce still further ionization, maintaining a heavily ionized, expanding plasma bubble. Such a bubble would exclude the magnetic field, compressing the field lines as it expands, until the magnetic pressure due to compressed field lines was equal to the outward plasma pressure.

---

[1] See Volume 1 for a more complete discussion of the expected results.

Parallel to the field lines the plasma encounters no resistance to expansion, however. If such a shock were fully effective and ionized 100 percent of the near-neutral ambient ionosphere, the bubble should be stopped by the field about 0 km [2] radially from the detonation point. This would give rise to a debris distribution shown in Figure 6.2.

The experimental results from Star Fish sketched in Figure 6.3 indicated that neither of the three models discussed here and in Volume 1 were correct. The debris was actually charged, and hence, highly confined by the field; however, the presence of plasma instabilities or a magnetic buoyancy effect permitted the ejection of substantial amounts of debris to very great altitudes. In the downward direction, debris from Star Fish was stopped in the vicinity of 200 to 250 km. A magnetic tube containing substantial debris, and perhaps 100 km across, was formed parallel to the earth's field. Some debris was trapped at very high altitudes to produce absorption and auroral phenomena in Alaska, and to the south of New Zealand. Optical information indicates that bright auroras occurred north of French Frigate Shoals, and south of Samoa—i.e., farther north and farther south of the expected conjugate areas.

---

[2] This estimate was presented at the January 1962 pre-Fish Bowl meeting held at Stanford Research Institute. Using the same technique, we derive a value of the order of 10 times this.

Some 5 percent of the total fission debris is thought to have been trapped at still higher altitudes.

6.2 PROCEDURE

6.2.1 Johnston Island Radars.

Instrumentation. See Section 2.2.1.

Operating Technique. See Section 2.2.1.

6.2.2 AEW Aircraft Radars.

Instrumentation. See Section 2.2.2.

Operating Technique. Based upon the expected results, it was felt that the debris-pancake occurrence was highly probable and that if the debris truly did pancake, a large area of auroral clutter would occur. In addition, it was believed that the auroral clutter in the vicinity of the burst would be mirrored in the magnetic conjugate area. For these reasons, the four AEW radar aircraft that were available to the project were located so that they would cover the extent of the debris spread as seen in the detonation area and as mirrored in the magnetic conjugate area, as shown in Figure 6.4 and Figure 6.5, respectively.

All of the AEW aircraft flew in patterns shown in Figure 2.8 at locations given in Table 6.1. The actual radar operating parameters are shown in Table 6.2.

6.2.3 M/V ACANIA Radars.

Instrumentation. See Section 2.2.3.

Operating Technique. The ACANIA was located at the magnetic conjugate area so that it looked at right angles to the earth's magnetic field line that passed through the detonation. The exact coordinates of the ACANIA are listed in Table 6.1. The radar operating technique was to scan the antenna in a complex fashion shown in Figure 6.6.

6.3 RESULTS

6.3.1 Johnston Island Radars.

Fireball/Debris Clutter. Prior to the detonation, the radar executed a programmed track of the Thor launch, and the 850- and 1210-Mc radars obtained skin echoes during the entire trajectory. The 398-Mc radar was off until detonation. Shortly before the detonation, the antenna was positioned in the direction of 87° elevation and 200° azimuth. The detonation occurred approximately 15 km south of the radar beam, which means that the debris should have expanded through the radar beam completely by H + 15 milliseconds. At H + 30 seconds, the antenna was moved around to the north to scan down the field lines. From H + 120 seconds to about H + 50 minutes, the antenna was positioned at magnetic north and 60° elevation, or was periodically scanned. The radars were operated for seven hours following the detonation. The range-versus-time record of the echoes for the first five minutes are shown in Figure 6.7. The spatial distribution of all echoes is shown in Figures 6.8 through 6.15. Except for the short dura-

tion, fireball/debris echoes on 850 and 1210 Mc and the auroral echoes on 398 and 850 Mc which persisted only for a few seconds, no echoes were observed to correlate with the visual light output which lasted up to H + 15 minutes.

As shown in Figures 6.16 and 6.17, fireball/debris echoes occurred at 350-km range on both 850 and 1210 Mc; these echoes did not occur on 398 Mc, although the 398-Mc radar was up to full power promptly. These echoes started at H + 0.1 sec, and persisted until H + 0.5 sec on 850 Mc and H + 1.0 sec at 1210 Mc. Both echoes reached a peak amplitude of approximately 20 db S/N as shown in Figures 6.18 and 6.19.

Auroral Clutter in the Detonation Area. Strong auroral echoes were observed the first time a search for them was made at H + 70 seconds. Forty-db S/N echoes were observed at 100- to 150-km height at 398 Mc. An unusual echo was observed at heights of 400 to 500 km at the same time. Fifteen-db S/N echoes were observed at 75-to 125-km height at 850 Mc. These echoes disappeared quickly. No other auroral echoes were observed until H + 4 hours when echoes reappeared at 398 Mc at heights of 300 to 400 km with amplitudes up to 15 db S/N. Figure 6.20 shows the peak amplitude of the auroral echoes as a function of time, with the antenna-direction-caused amplitude fluctuations removed.

The Doppler characteristics of the 398-Mc auroral echoes at H + 277 minutes are shown in Figure 6.21. This figure shows that

the Doppler shift is no greater than ±2 kc, and the Doppler spread is no greater than the transmitter pulse-spectrum 3-db width of approximately 3 kc. Both of these characteristics are consistent with natural aurora-caused radar reflections at this frequency.

Fireball/Debris Noise. No noise emission was observed in the detonation area.

6.3.2 AEW Aircraft Radars.

Fireball/Debris Clutter. None of the detonation area AEW aircraft (Abusive 1, Lambkins 1 and 2) observed echoes directly from the fireball/debris.

Auroral Clutter in the Detonation Area. Abusive 1 and Lambkin 2 did not see any auroral echoes. Lambkin 1 saw auroral echoes to the west of the aircraft between H + 46 seconds and H + 76 seconds. These echoes are interpreted as arising from field-aligned ionization located at heights of about 150 km. These results are shown in Figure 6.22.

Auroral Clutter in the Conjugate Area. No auroral clutter was observed in the conjugate area by the AEW aircraft radars.

6.3.3 M/V ACANIA Radars.

Auroral Clutter in the Conjugate Area. The ACANIA was located (according to calculations based upon Finch and Leaton coefficients) on the magnetic meridian of the field line that passed through the detonation, and looking at right angles to the magnetic field line (at H = 100 km) that passed through the

detonation point. The UHF radar antenna was scanned in a complex manner throughout the test. The antenna azimuth and elevation versus time are shown in Figure 6.6. The range-versus-time records for the first 5 minutes are shown in Figure 6.23. The echoes seen by the 140-Mc radar at H + 0 were at approximately 30 km greater range than were predicted. These echoes persisted for less than a second (a few pulses). Visual observations confirmed the location of the ACANIA on the magnetic meridian line passing through the burst. The difference between the observed range of the early-time echoes and the calculated field line was such as to indicate a discrepancy of about $1/2^{\circ}$ of latitude. This discrepancy was also noted on subsequent shots. At H + 50 seconds, the 140-Mc and 370-Mc echoes appeared again and lasted to 240 seconds and 170 seconds at 140 Mc and 370 Mc, respectively. The spatial location of these echoes is shown in Figure 6.24.

6.4 DISCUSSION

The negative results on the majority of the AEW aircraft indicated that the majority of the debris did not pancake as might be expected.

6.5 CONCLUSIONS

A Star Fish event would have some degrading effect on the performance of a ballistic missile defense radar system. To evaluate this effect, a comparison has been made between the radars used during Fish Bowl and the planned BMD radar systems.

The radars used during these tests were, in general, somewhat less sensitive than those being planned for use in BMD activities. The advantage that a particular system radar would have over the test radars is shown for various scattering models in Table 2.6. The comparisons were developed by scaling the system radar to its nearest frequency counterpart used during Fish Bowl. For example, the BMEWS radars were compared with the 398-Mc Johnston Island radar and the Nike-Zeus TTR radar was compared to the DAMP FPQ-4 C-band radars.

In order to give the reader a better understanding of the degrading effects of the Star Fish event, an estimate of the effect on the BMEWS tracking radar has been made. The BMEWS system was picked as an example not to deprecate that particular system, but because that system is operational, field deployed, and its characteristics are well known. Table 2.7 shows the comparison between the BMEWS tracking radar characteristics and the Johnston Island 398-Mc radar. The comparison was made assuming the scattering was from a beam-filling target of range depth of at least one pulse width (300 μsec).

From the comparison, estimates of the strength and time duration of the clutter and noise effects are given below:

Fireball/Debris Clutter.

H + 0 to H + 2-second echoes would be expected with 60 db S/N ratio.

Detonation Area Auroral Clutter.

H + 0 to H + 5 hours > 40 db S/N ratio echoes would be expected. Maximum duration of echoes is not known but would be in excess of H + 5 hours.

Fireball/Debris Noise.

None expected above receiver noise level.

Conjugate-Area Auroral Clutter.

Extensive clutter would be seen with S/N ratios > 60 db.

The most serious effect of a Star Fish event would be the detonation-area auroral clutter. Relatively large areas would be obscured for a depth of at least one pulse length at a variety of ranges for a period of up to 5 hours. The Doppler spread of the auroral echoes would be relatively narrow, however.

Conjugate-area auroral clutter would obscure a smaller area at a variety of ranges for a depth of at least one pulse length for a shorter period. The Doppler width would be relatively narrow.

The extended volume of auroral clutter produced by Star Fish would make it difficult to avoid the clutter problem by using spaced radars in a BMD system, but it could be greatly reduced by using higher (such as L-band) operating frequencies.

TABLE 6.1 LOCATIONS OF AEW AIRCRAFT AND M/V ACANIA DURING STAR FISH

	Longitude	Latitude
Abusive 1	167°57.5'W	17°02'N
Lambkin 1	165°30'W	13°46'N
Lambkin 2	165°36'W	10°54'N
Lambkin 3	169°00'W	8°48'S
Lambkin 4	170°12'W	12°33'S
ACANIA	175°40.3'W	15°35.2'S

TABLE 6.2 OPERATING CHARACTERISTICS OF THE AEW AIRCRAFT RADARS DURING STAR FISH

L = Lambkin, A = Abusive.

	L1	L2	L3	L4	A1
Freq. Mc	425	435	426	443	447
Peak Power, Mw	1.4	1.1	1.9	2.5	1.3
Pulse Width, μsec	9.0	8.0	6.0	8.2	8.5
PRF, cps	243	243	238	240	280
MDS, -dbm	-113	-114	-114	-113	-118
Dynamic Range, db	18	18	21	21	15
σmin at 500 km, m^2	22	24	13	13	9

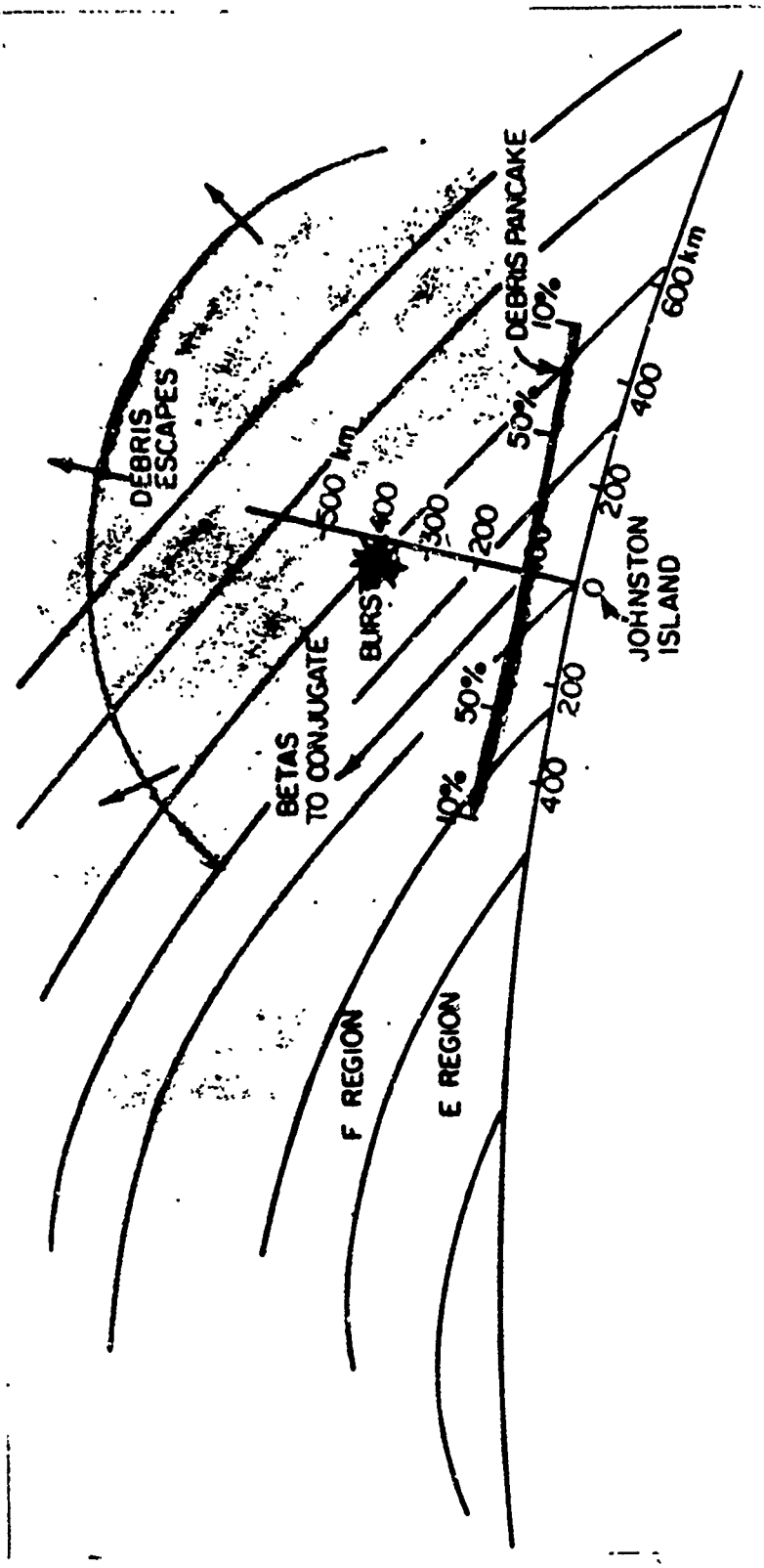

Figure 6.1 Sketch of pancake model for Star Fish.

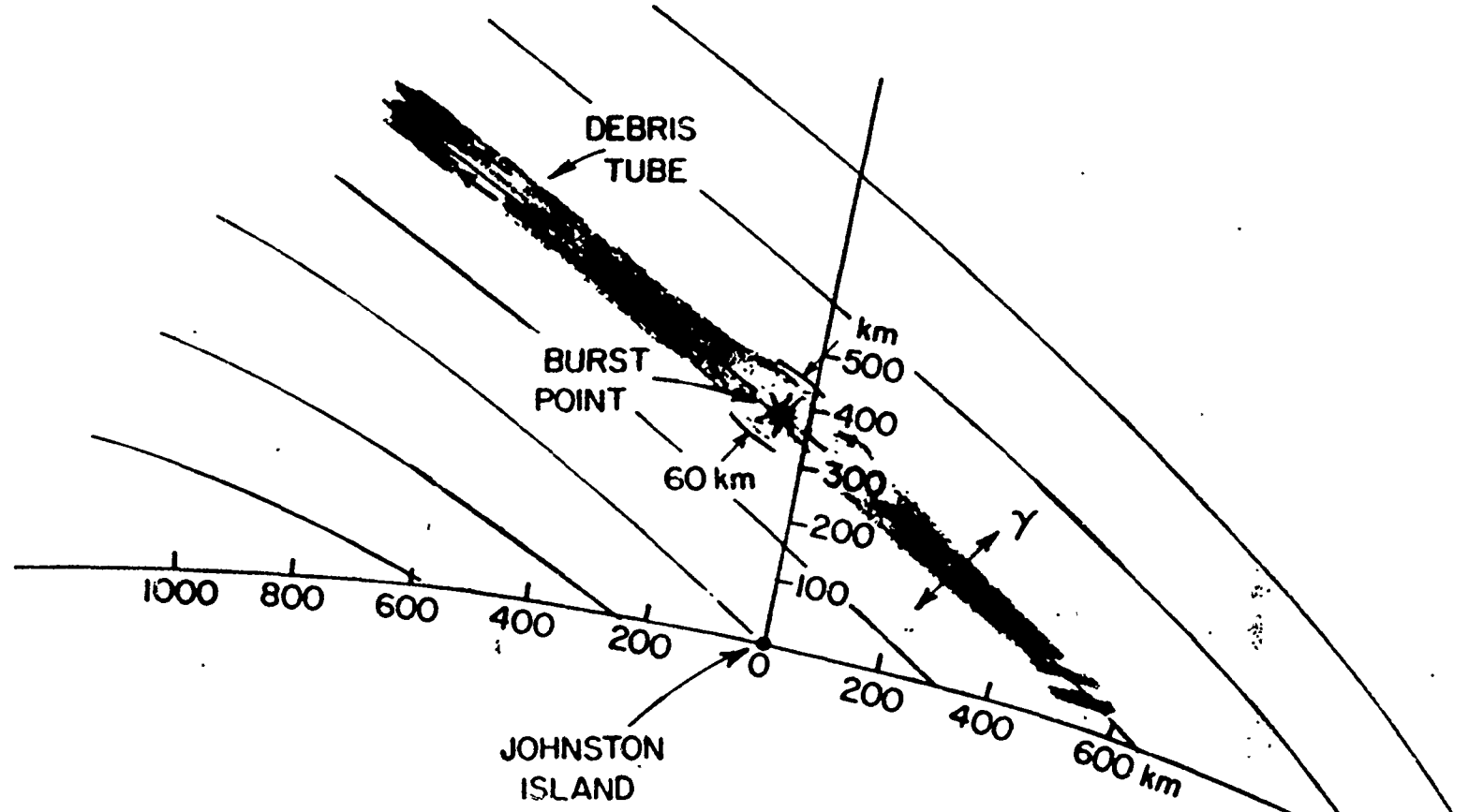

Figure 6.2 Sketch of magnetically contained model for Star Fish.

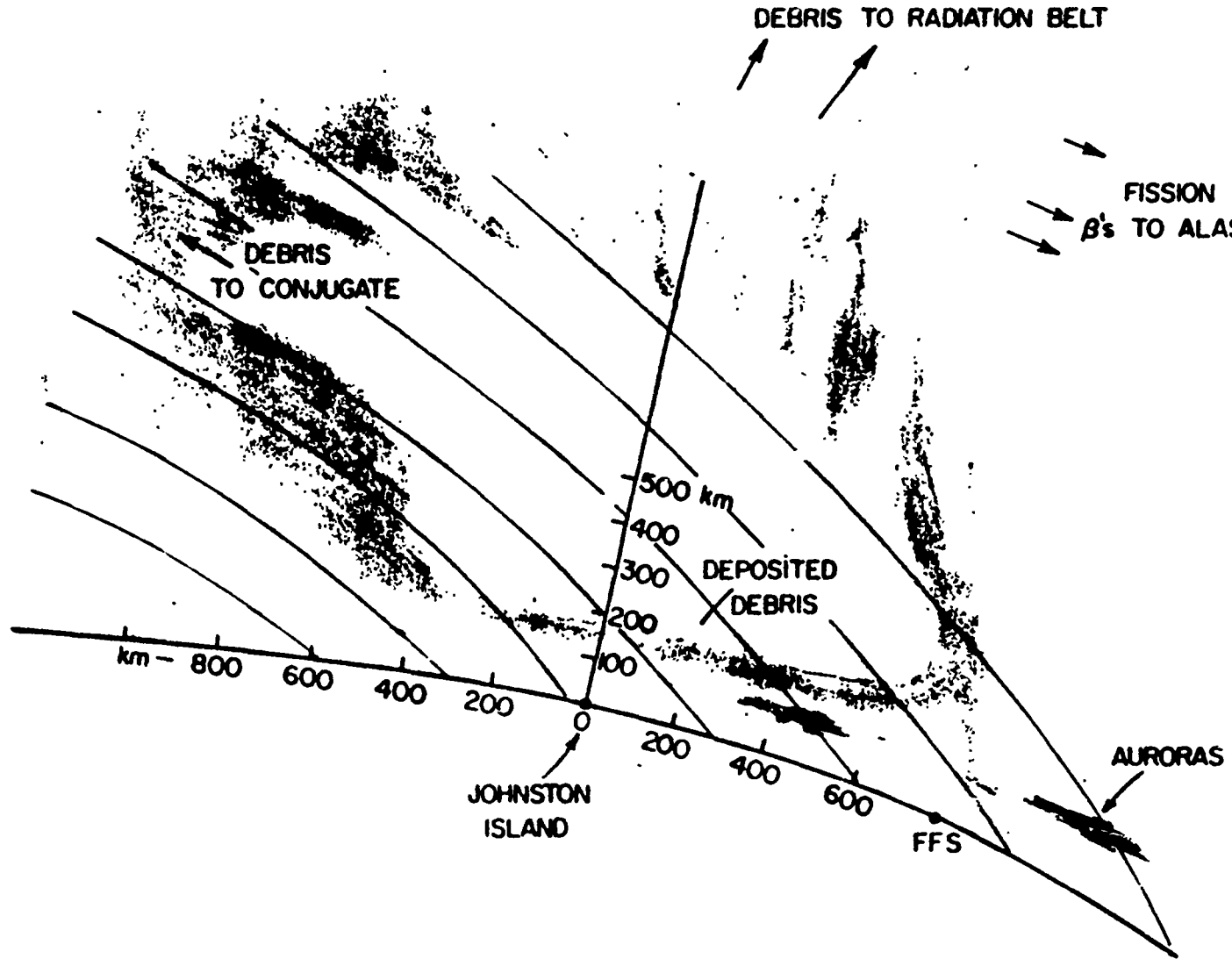

Figure 6.3 Sketch of actual results of Star Fish.

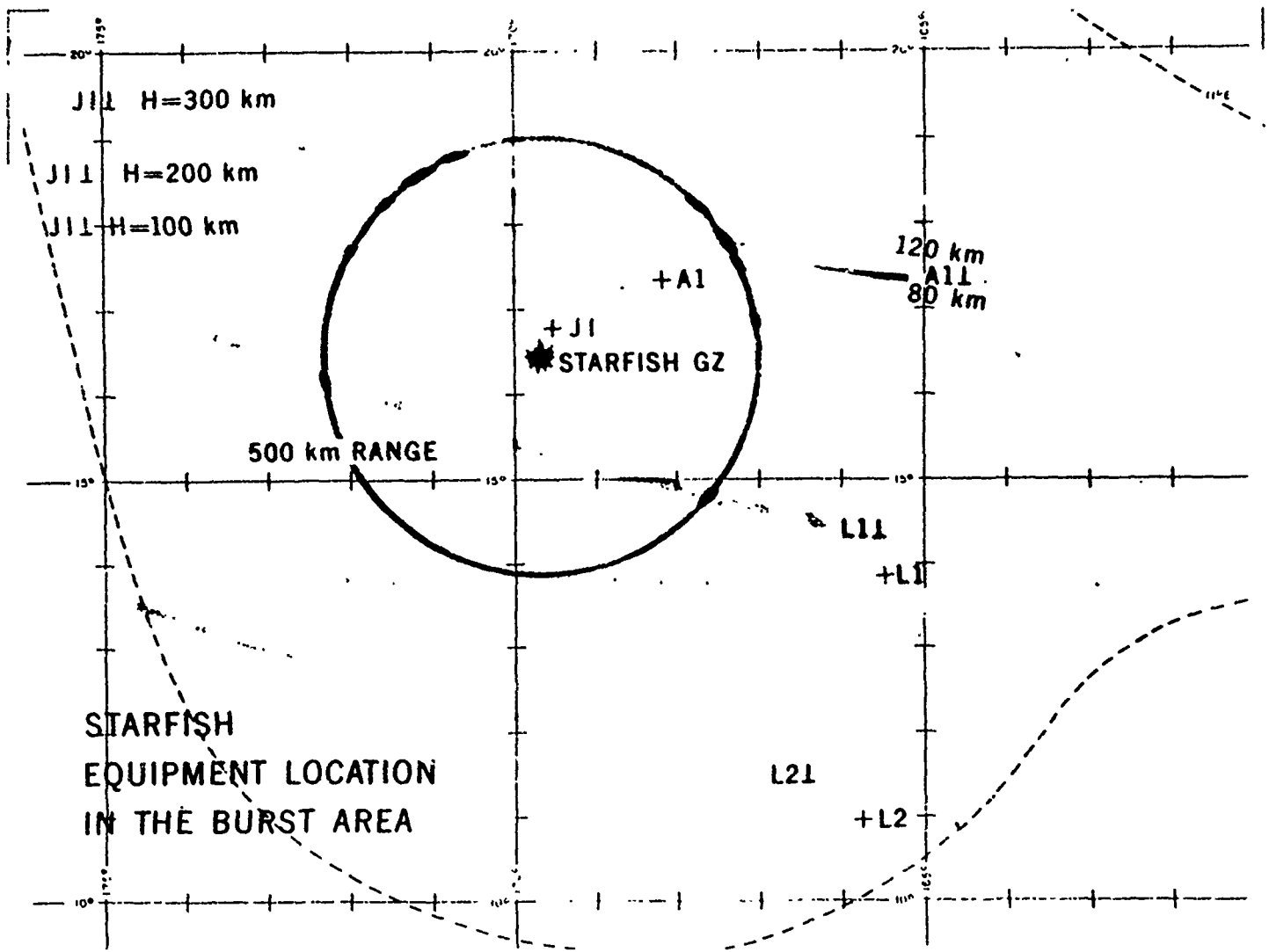

Figure 6.4 Equipment location in the detonation area for Star Fish.

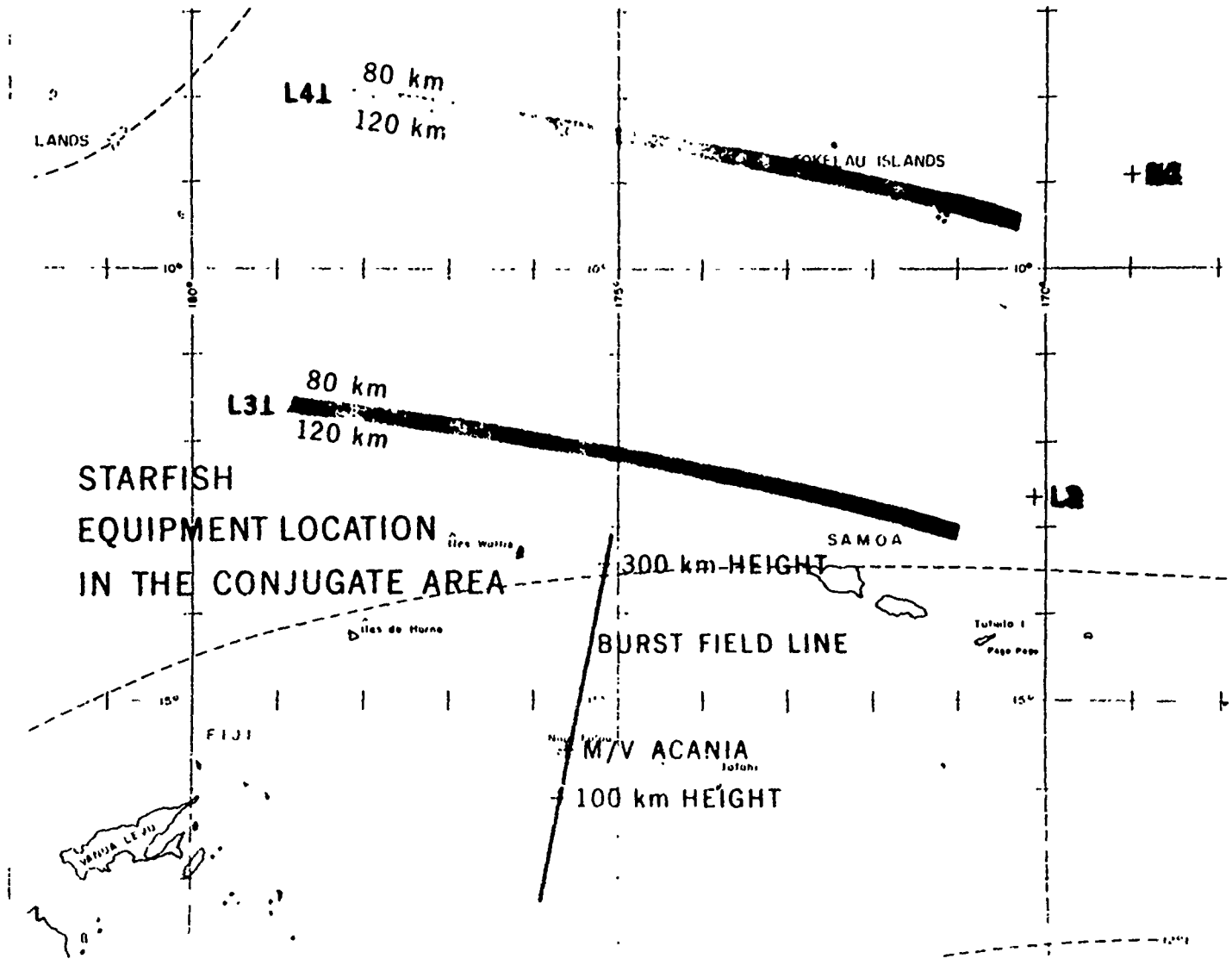

Figure 6.5 Equipment location in the conjugate area for Star Fish.

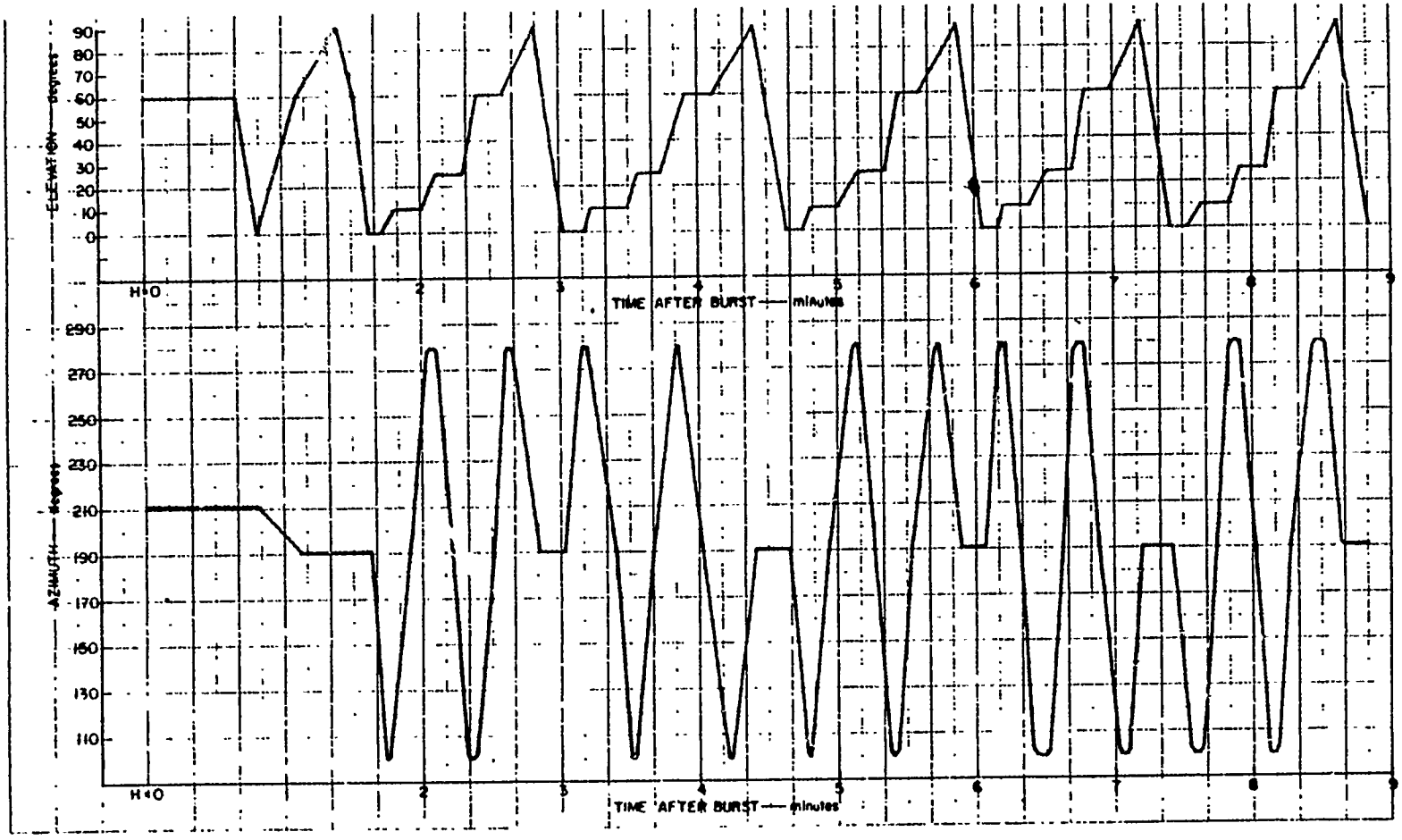

Figure 6.6 M/V ACANIA radar antenna position versus time for Star Fish.

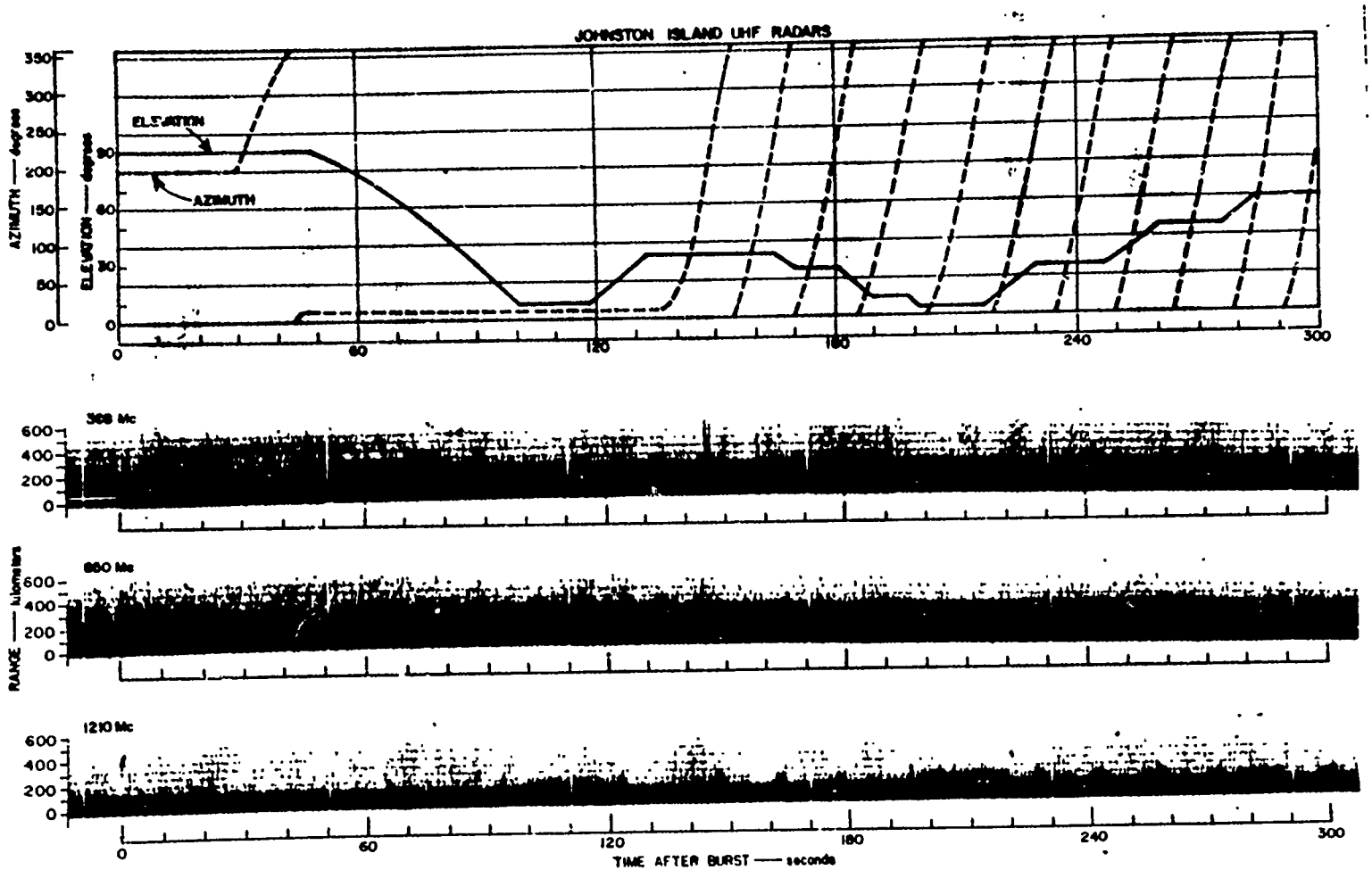

Figure 6.7 Johnston Island radar range versus time for Star Fish; 0 to 600 km, 0 to 300 seconds.

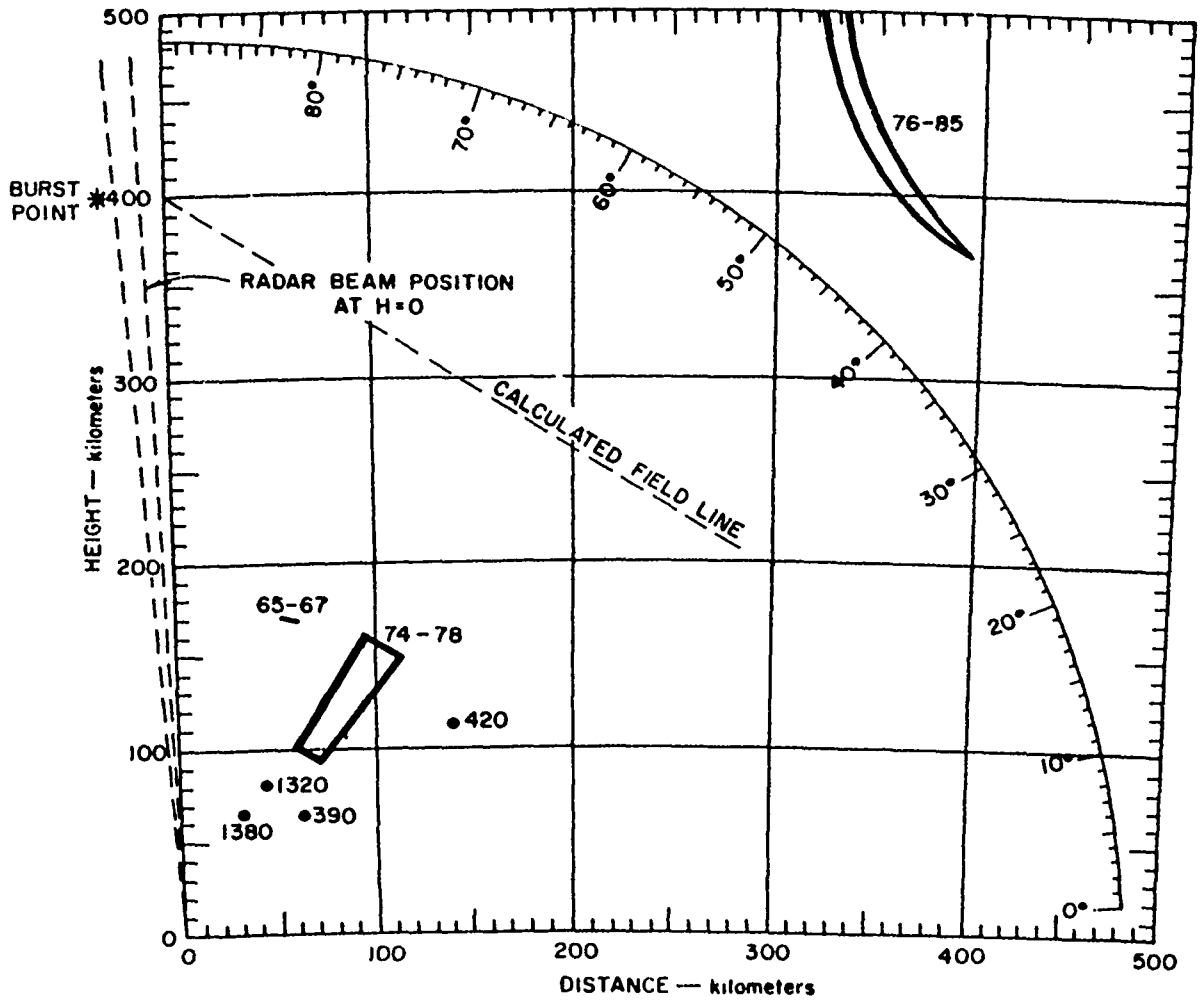

Figure 6.8 Johnston Island radar height versus distance for Star Fish; 398-Mc northern echoes, 0 to 1,400 seconds.

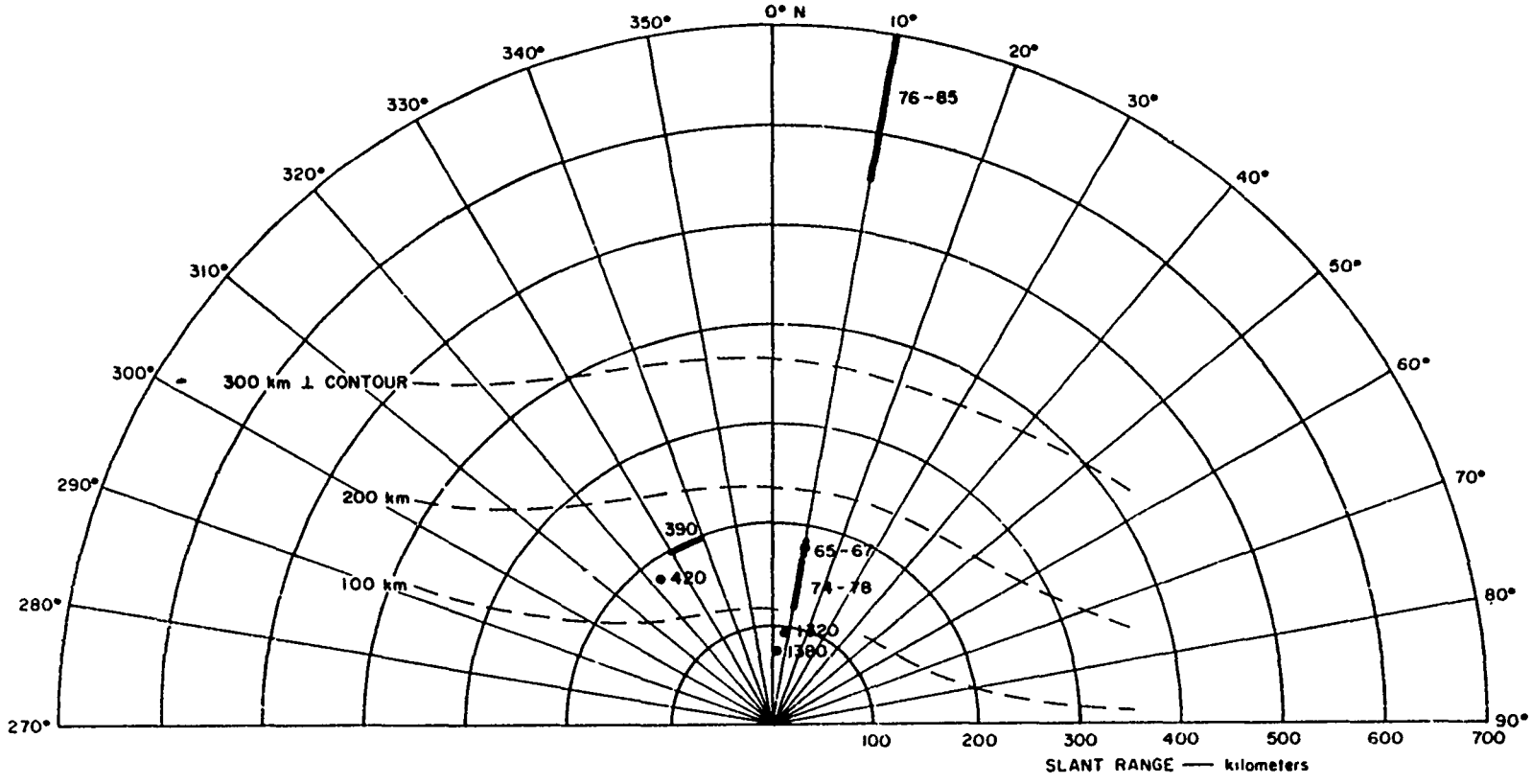

Figure 6.9 Johnston Island radar range versus azimuth for Star Fish; 398-Mc northern echoes, 0 to 1,400 seconds.

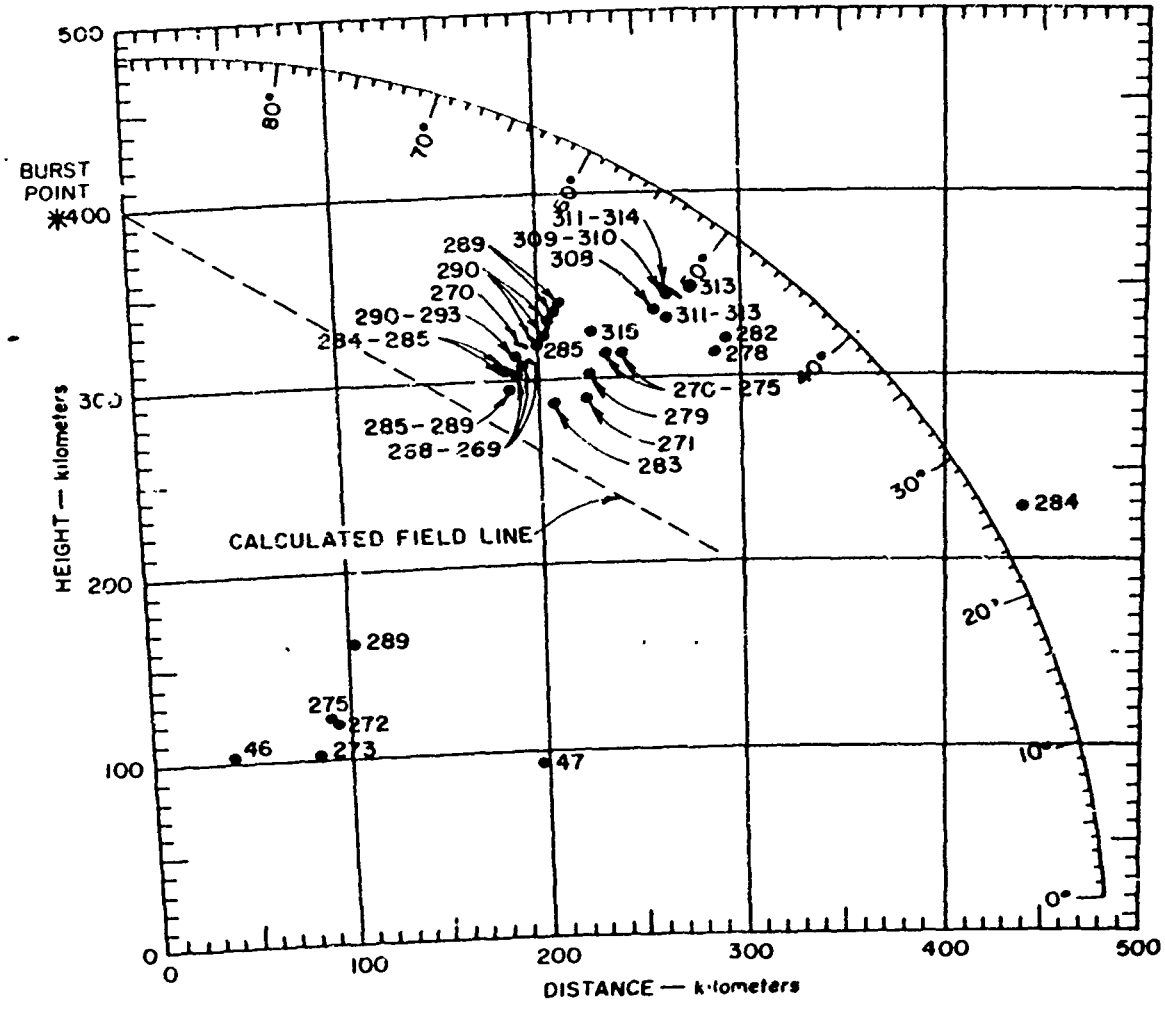

Figure 6.10 Johnston Island radar height versus distance for Star Fish; 398-Mc northern echoes, 29 to 74 and 267 to 315 minutes.

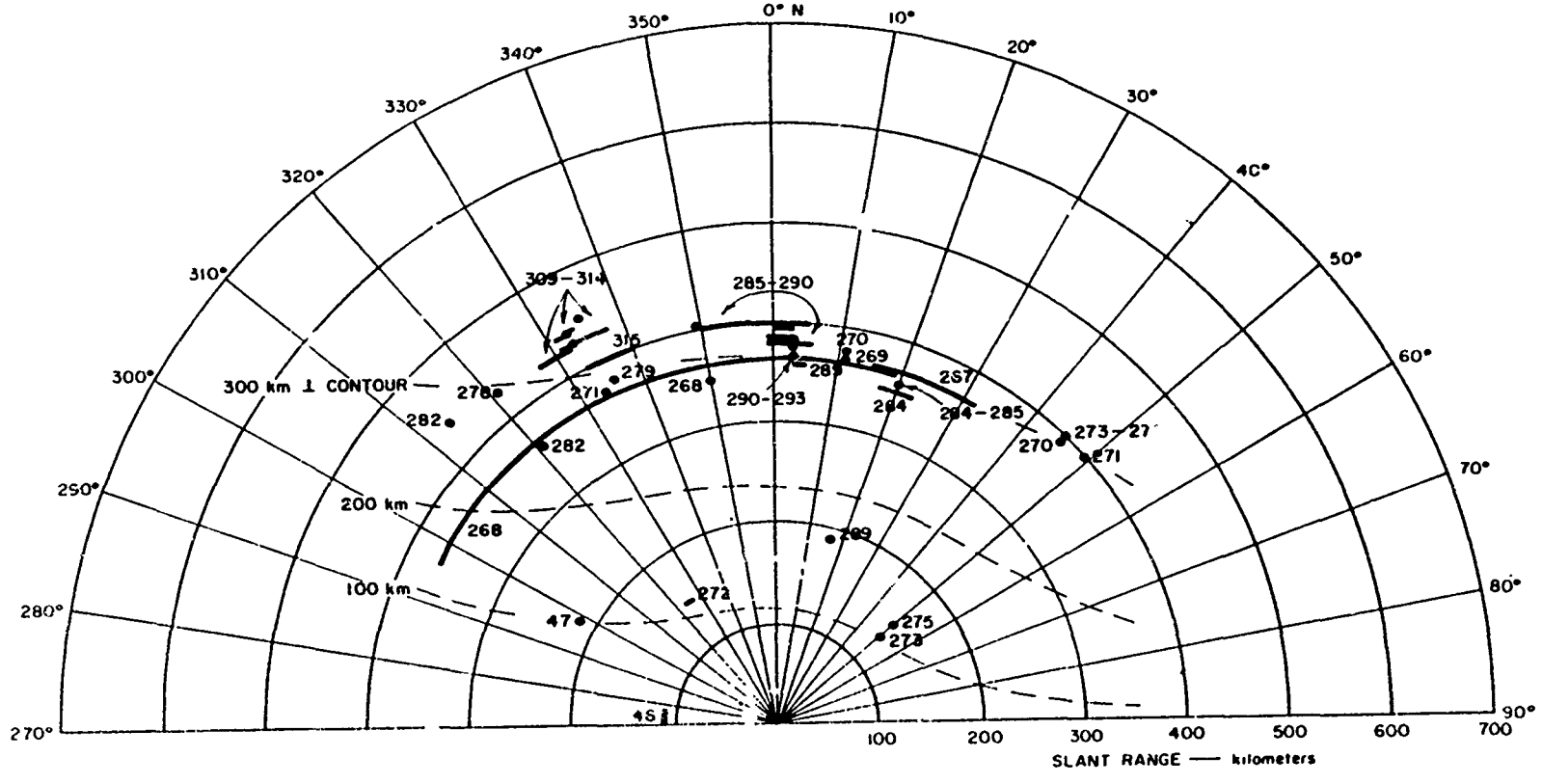

Figure 6.11 Johnston Island radar range versus azimuth for Star Fish; 398-Mc northern echoes, 29 to 74 and 267 to 315 minutes.

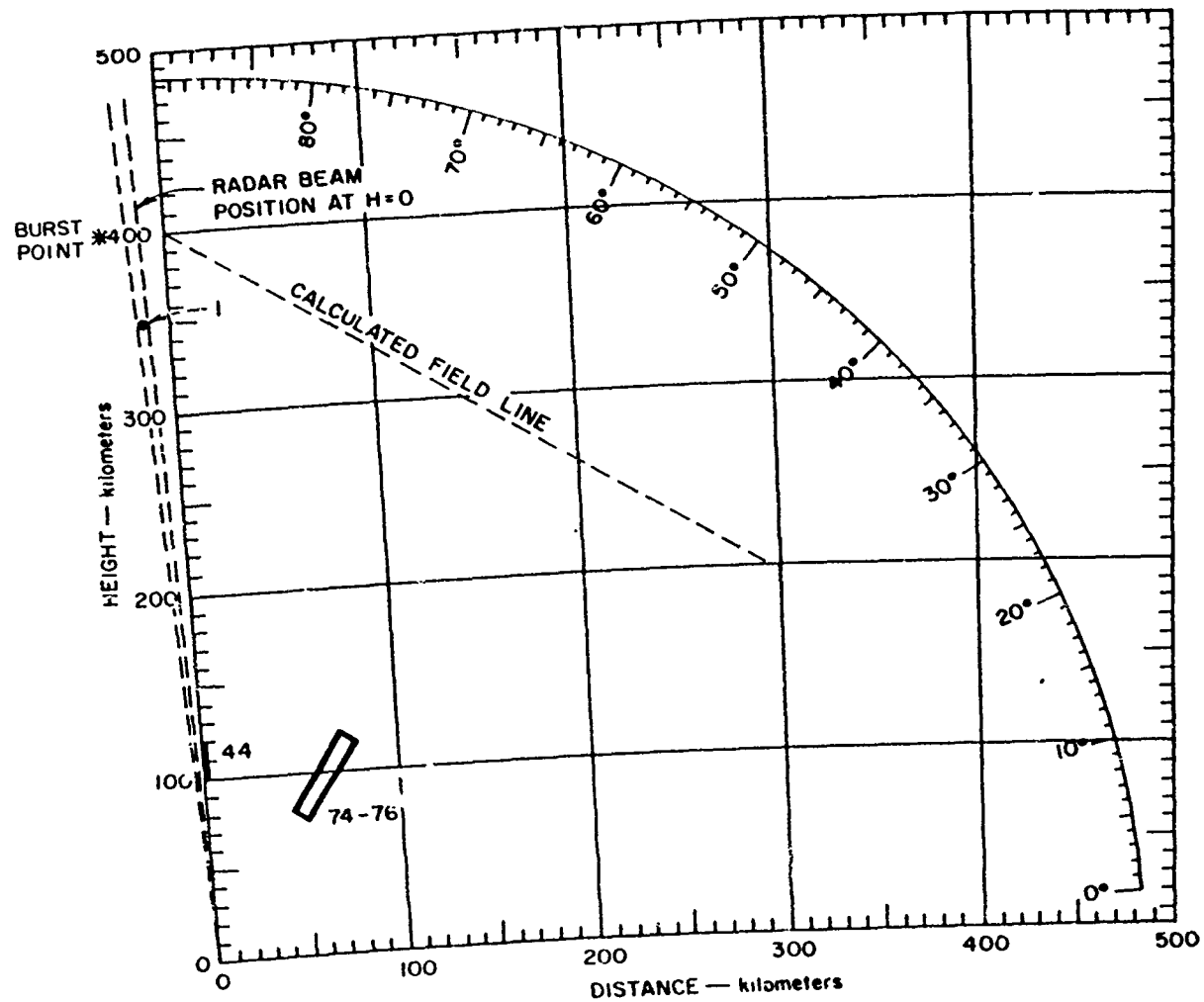

Figure 6.12 Johnston Island radar height versus distance for Star Fish; 850-Mc northern echoes, 0 to 1,400 seconds.

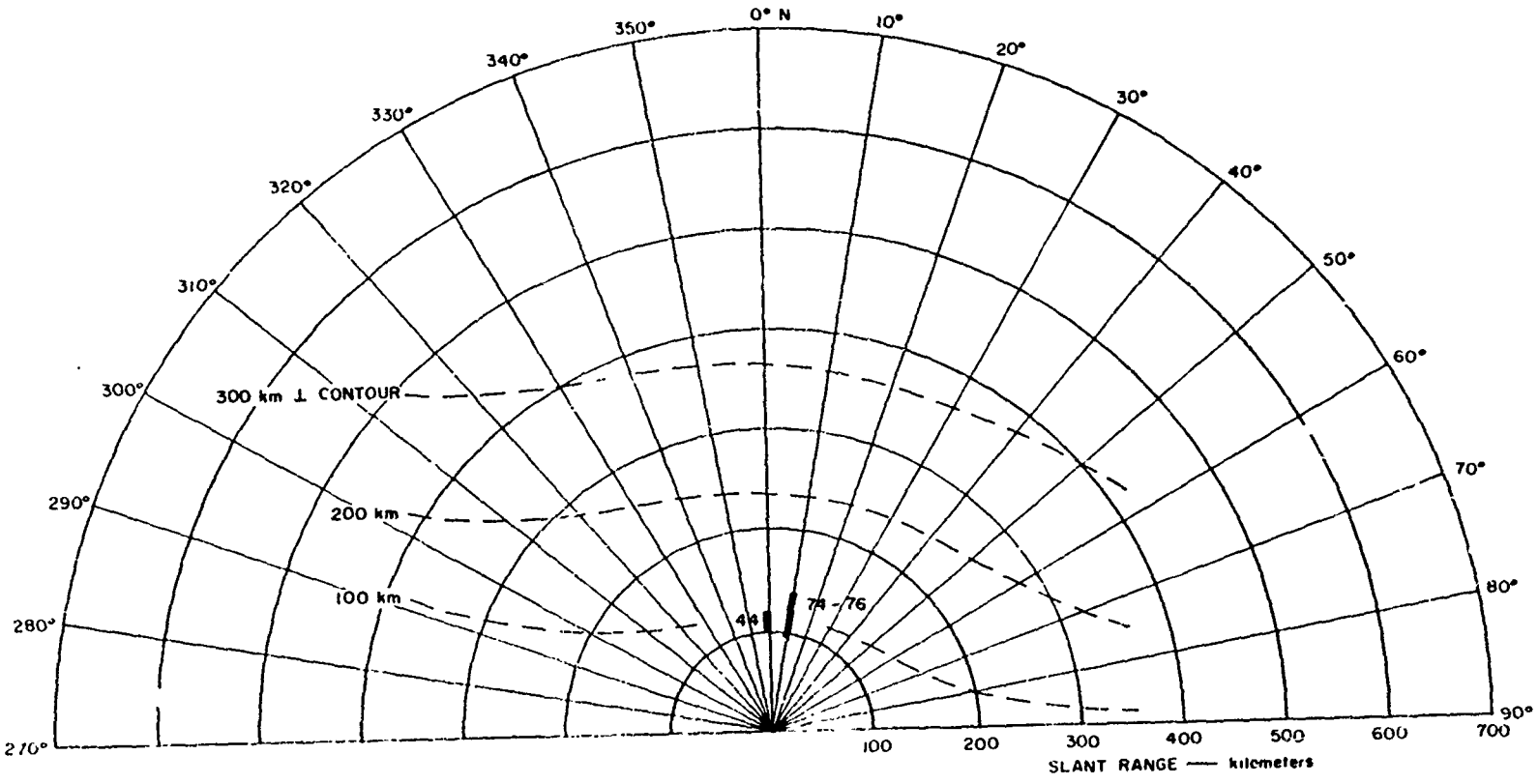

Figure 6.13 Johnston Island radar range versus azimuth for Star Fish; 850-Mc northern echoes, 0 to 1,400 seconds.

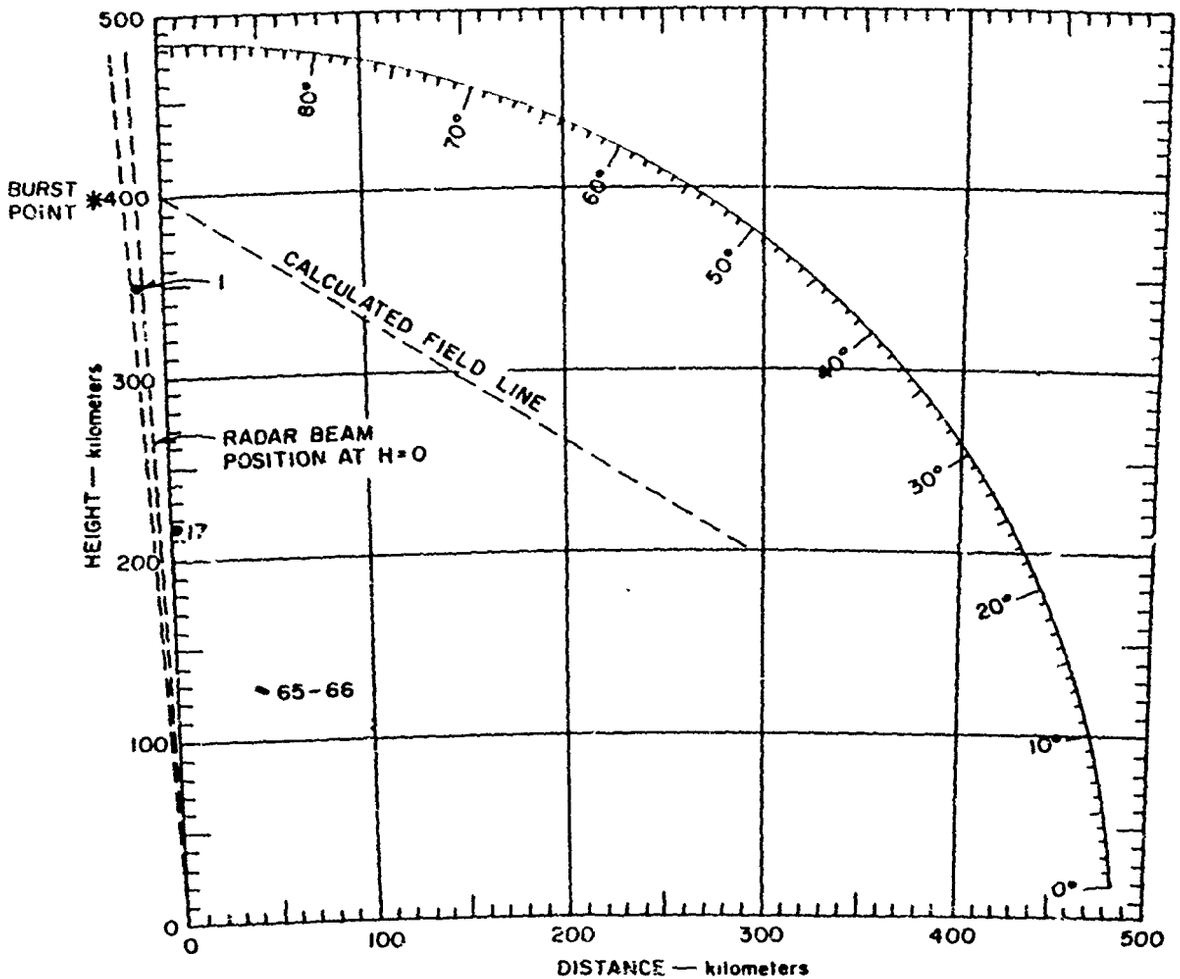

Figure 6.14 Johnston Island radar height versus distance for Star Fish; 1210-Mc northern echoes, 0 to 1,400 seconds.

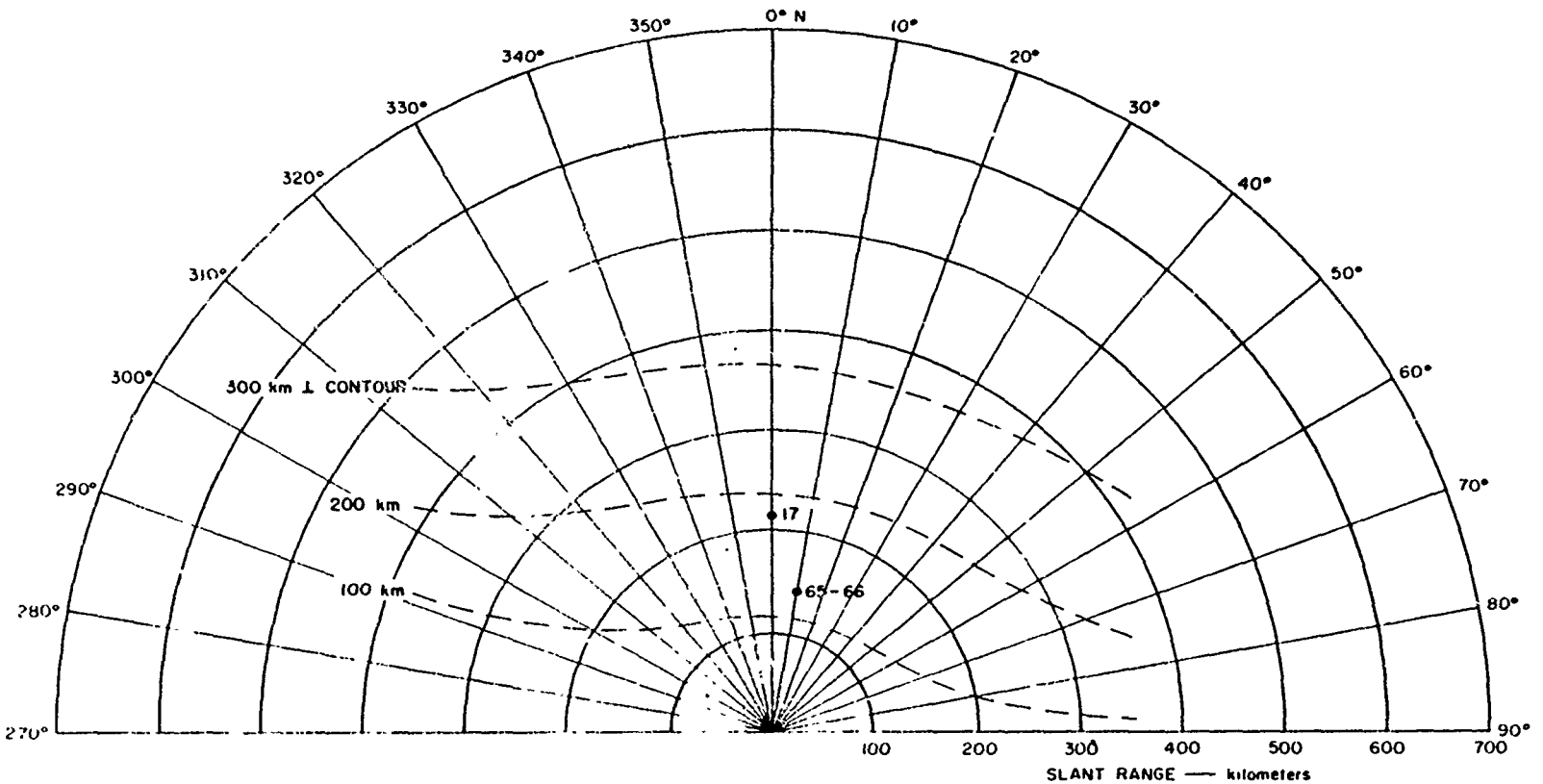

Figure 6.15 Johnston Island radar range versus azimuth for Star Fish; 1210-Mc northern echoes, 0 to 1,400 seconds.

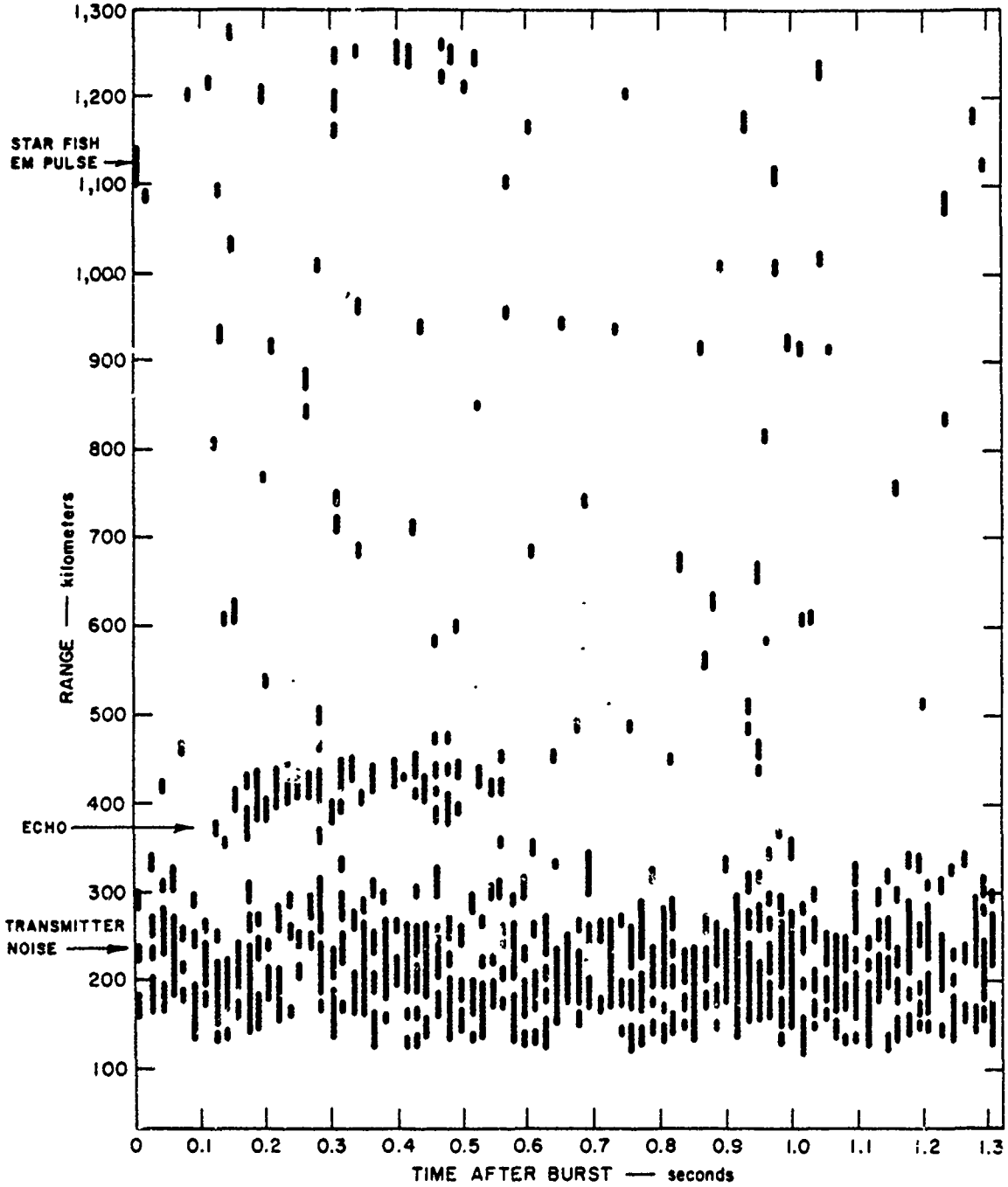

Figure 6.16 Johnston Island radar range versus time for Star Fish; 850 Mc, 0 to 1.3 seconds.

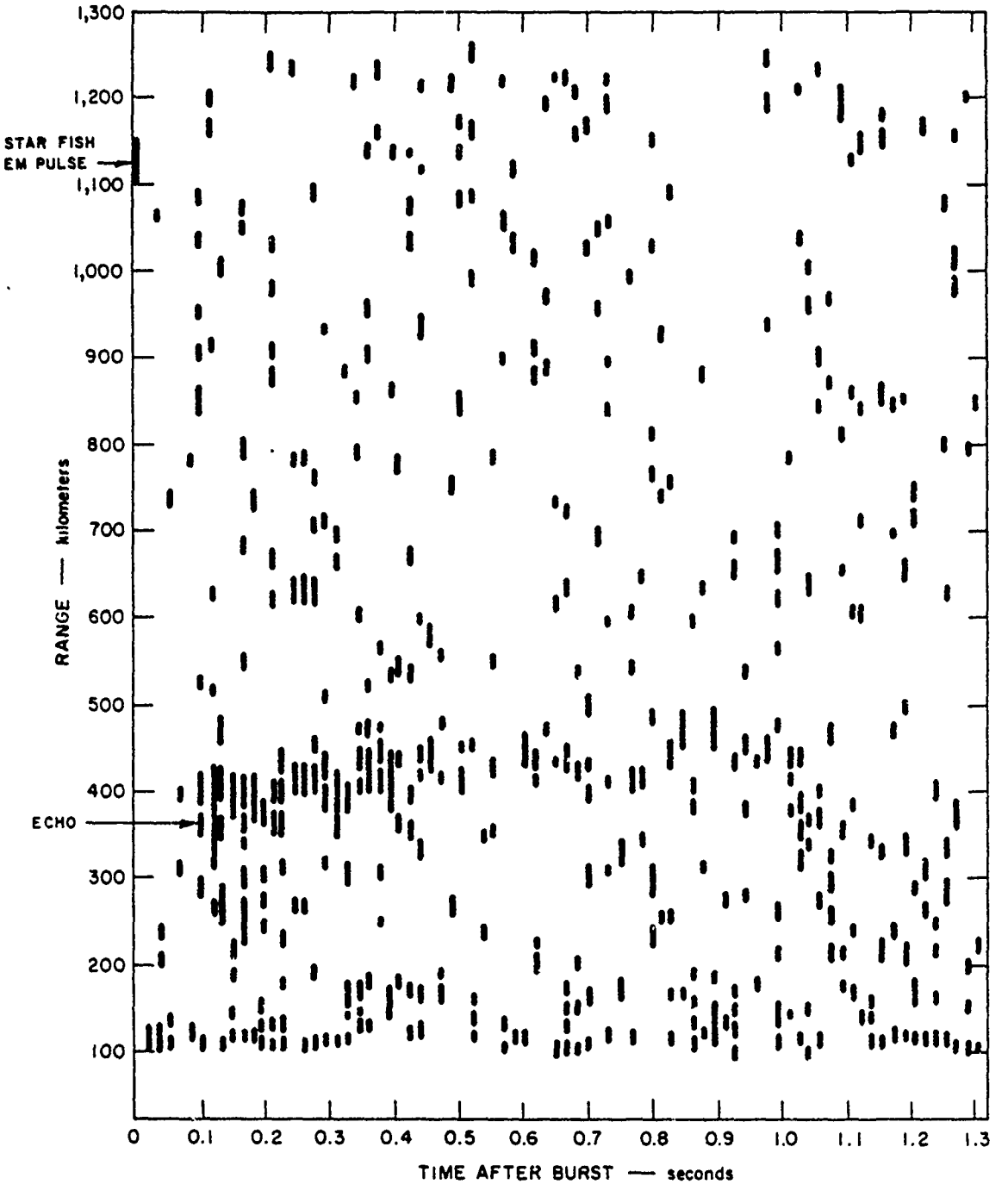

Figure 6.17 Johnston Island radar range versus time for Star Fish; 1210 Mc, 0 to 1.3 seconds.

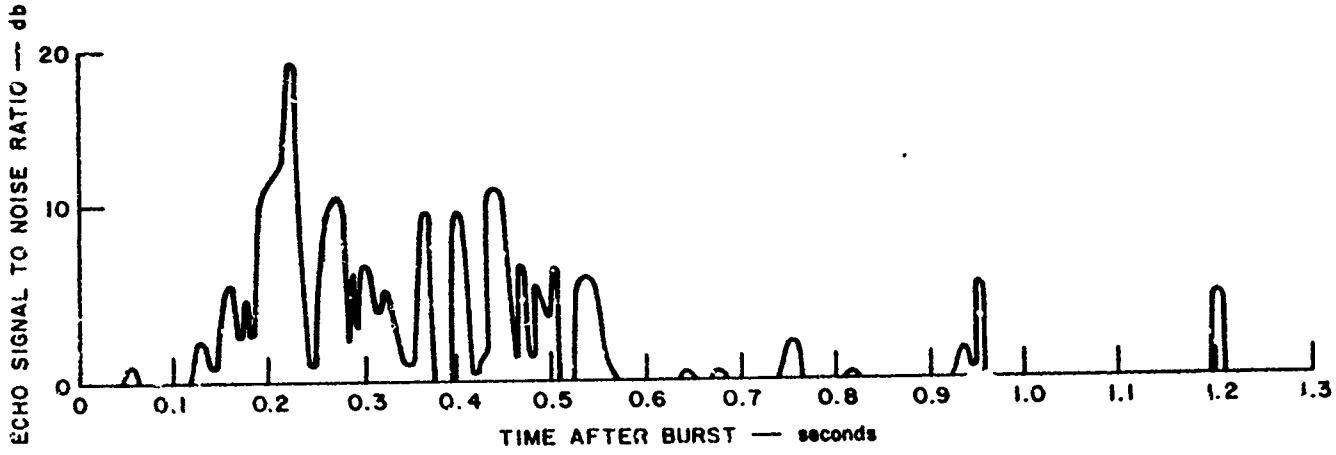

Figure 6.18 Johnston Island radar echo amplitude versus time for Star Fish; 850 Mc, 0 to 1.3 seconds.

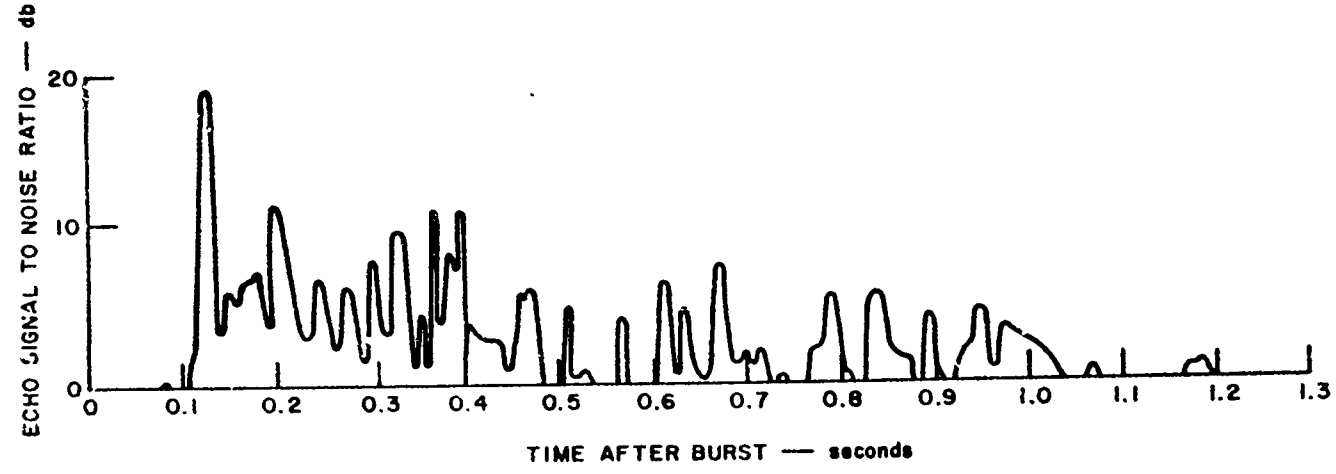

Figure 6.19 Johnston Island radar echo amplitude versus time for Star Fish; 1210 Mc, 0 to 1.3 seconds.

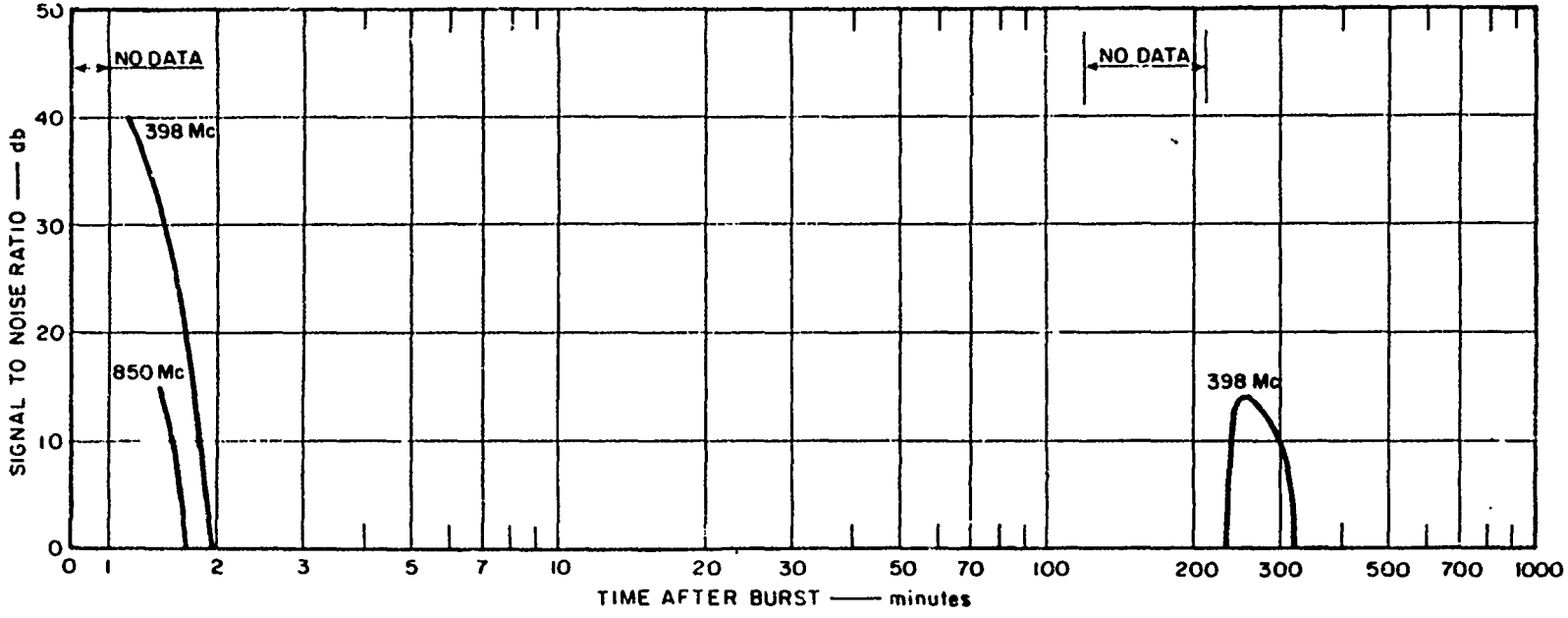

Figure 6.20 Johnston Island radar auroral echo amplitude for Star Fish; 398 and 850 Mc.

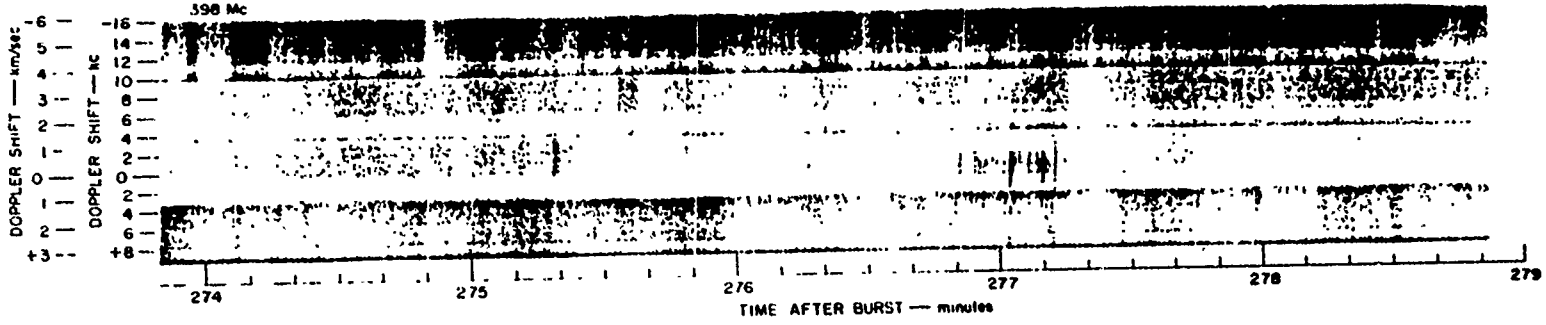

Figure 6.21 Johnston Island radar Doppler versus time for Star Fish; 398 Mc, 274 to 279 minutes.

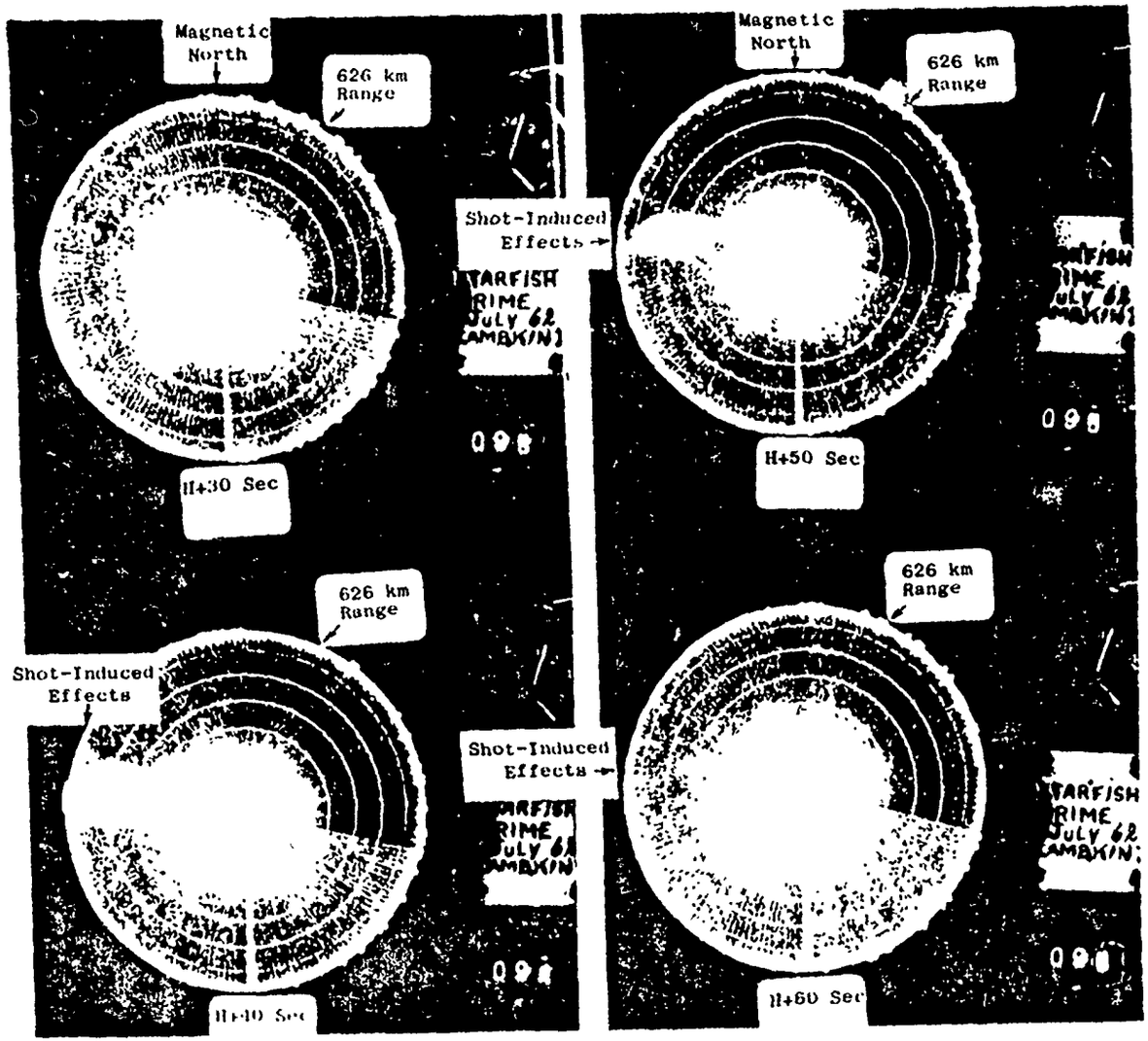

Figure 6.22 AEW aircraft radar PPI for Star Fish; Lambkin 1, 30 to 60 seconds.

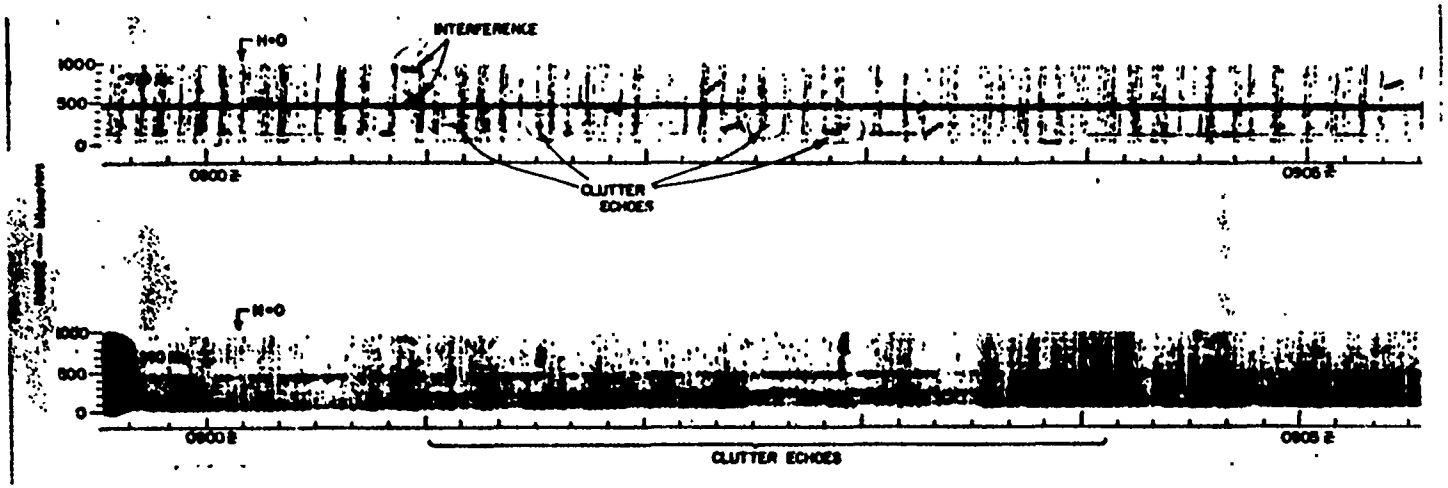

Figure 6.23 M/V ACANIA radar range versus time for Star Fish; 140 and 370 Mc, 0 to 5 minutes.

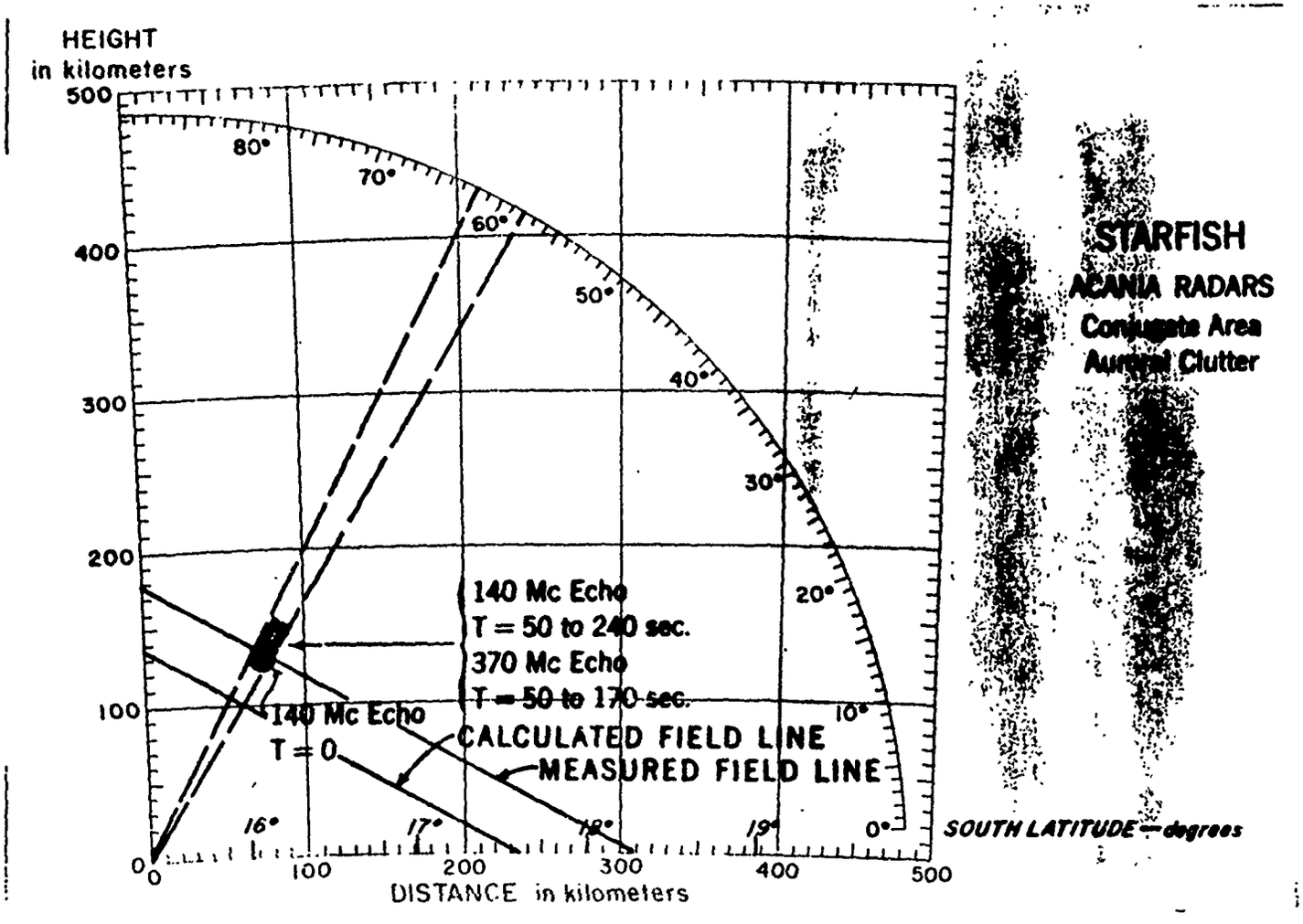

Figure 6.24 M/V ACANIA radar height versus distance for Star Fish.

CHAPTER 7

DISCUSSION OF UHF RADAR RESULTS

Many interesting features have been noticed in the data presented in this report. For example, on both Check Mate and King Fish the long-lasting auroral clutter showed two peaks in amplitude as a function of time. Undoubtedly this is related to the expansion and rise of the debris from these two shots. However, it has not been possible to interpret and analyze these and other interesting results for inclusion in this report. It is hoped that inclusion of such reduced data minus interpretation will be helpful to the reader. Interpretation and analysis of these data by project personnel will be carried out in the future.

7.1 FIREBALL/DEBRIS CLUTTER

The existence of radar clutter from the fireball/debris for each of the events has been established. Previous results and predictions have suggested that such clutter might be seen, but the fact that it was seen at as early a time and for as long a time, even on 1210 Mc, is considered very important to ballistic missile defense radars.

Figures 7.1 through 7.3 are a graphical presentation of the sensitivity of the Johnston Island radars in terms of reflector radar cross section in m^2, m^2/m^3, and electron density, respectively.

The echo-amplitude characteristics for Tight Rope, Blue Gill, King Fish, and Check Mate show that at all three frequencies the fireball/debris echoes saturated or nearly saturated the receivers within the first 60 seconds. Echoes at these levels and at the event ranges give volume-scattering coefficients ranging from 2×10^{-14} m^2/m^3 for Tight Rope to 10^{-11} for Check Mate for beam-filling targets. In all of the events the fireball/debris echoes exhibited negligible dependence upon radar frequency in contradistinction to the auroral returns which were very wavelength-dependent. It is surmised that this result may be due to a fortuitous mixture of reflector strength and path absorption. If incoherent electron scatter could be invoked to explain these echoes (we have shown that it can't for the very early, intense

echoes), then frequency-independent returns might be expected.

An important feature of the fireball/debris echoes for Check Mate and King Fish is the double echo which lasts a few seconds after H = 0. This second echo is a clue to the overall reflection mechanism. If it is assumed that the fireball/debris cloud is ionized but the density is sub-critical, then the following model is possible:

The ionized cloud fills the radar beam and scatters the incident power isotropically as by incoherent scatter with electron density N; the RF power then reflects specularly from the sea, and again scatters isotropically as by incoherent scatter with electron density N from the entire cloud. This model gives the following equation:

$$P_r = \frac{P_t G_t}{4\pi R^2} \cdot \frac{\sigma_m N \pi \alpha^2 R^2 c\tau}{16} \cdot \frac{1}{4\pi 4R^2} \cdot \sigma_m N V_n \cdot \frac{A_e}{4\pi R^2}$$

$$G_t = \frac{4\pi}{\alpha^2}$$

$$\therefore \quad P_r = \frac{P_t \sigma_m^2 N^2 c\tau V_n A_e}{1024\ \pi R^4}$$

$$N = \left(\frac{P_r\ 1024\ \pi R^4}{P_t A_e V_n c\tau \sigma_m^2} \right)^{1/2}$$

P_r = received power

P_t = transmitted power

R = range

A_e = antenna effective aperture

α = antenna beamwidth

V_n = debris cloud volume ($5.6 \times 10^{10} m^3$)

τ = pulse length

σ_m = electron scattering cross section

This equation generates the curves in Figure 7.4. From this figure it is apparent that to support a one-hop sea scatter echo the ionization must be overdense. Indeed, if there were double echoes for Blue Gill and Tight Rope, they would have been overdense also. Unfortunately, the range resolution of the radars does not allow this fact to be determined without doubt. However, the range-versus-time records do show fluctuations in range depth which might be due to a one-hop sea scatter echo appearing and disappearing.

Another significant feature of the fireball/debris echoes is the close correlation of radar echoes and the visual fireball/debris observed on Tight Rope, Blue Gill, King Fish, and Check Mate. The close correlation lasted up to H + 5 minutes for Tight Rope and Blue Gill as shown in Figures 2.9 and 3.3, but only up to H + 1 minute on King Fish and Check Mate.

It has been pointed out [1] that the radar cross-section data previously published by Project 6.9 [2] does not appear to be self-consistent. In particular, the radar cross section of the Blue Gill event as seen by the Johnston Island radar appears to be about seven orders of magnitude lower than the radar cross section observed by the AEW aircraft. About five orders of magnitude difference can be

---

[1] Private communication by John Ise, Defense Research Corporation, Santa Barbara, California.

[2] Symposium Proceedings, Radar Blackout, DASA 1365, DASA Data Center Special Report 11, April 1963 (SRD)

justified by the difference in size of the antenna beams of the Johnston Island radar and the AEW aircraft radar. However, this leaves two orders of magnitude still to be accounted for. At the time of this writing we have not yet reconciled this discrepancy. We have examined our calibrations, calculations, and data-reduction procedures and have found no explanation of the discrepancy there. We have suggested, without opportunity for investigation as yet, that the fireball echoes have an aspect sensitivity depending upon the difference in the viewing angle to the fireball from the two radars. An alternate explanation might be that this discrepancy is a result of absorption. That is, when looking at the fireball from the side, as the AEW radar would do, it might provide less absorption along the radar path than when looking directly up at the fireball, as the Johnston Island radar would do. This discrepancy will be examined in more detail during future analysis work.

7.2 AURORAL CLUTTER IN THE DETONATION AREA

The auroral clutter observed on King Fish, Check Mate, and Star Fish showed very strong wavelength dependence. Figures 4.35, 5.44, and 6.20 show that the echo-amplitude difference between 398 Mc and 850 Mc is usually approximately 15 db. Ignoring other mitigating factors such as aspect sensitivity, this makes the auroral-reflection mechanism proportional to $\lambda^{4.5}$.

Differing from what might have been expected, the auroral reflection did not take place at E-layer heights only. But, as in the case of King Fish, auroral reflections appear to have been obtained from heights up to 750 km.

The relative lack of long-lasting strong auroral clutter observed by the Johnston Island radars and the AEW aircraft radars is assumed to be due to the relative low yields of those events as compared to Teak and Orange. Teak and Orange events of Hardtack (1958) gave rise to very long-lasting returns on airborne radars similar to those carried by the AEW aircraft.

7.3 FIREBALL/DEBRIS NOISE

The radio noise emission observed by the Johnston Island radars is most likely due to black-body radiation from the vicinity of the fireball. The relatively slow buildup of noise is most likely caused by the shielding of the radiating region by absorption. Although on the Johnston Island radars this noise was not extremely strong, it could play a significant role in degrading the capability of ballistic missile defense radars by decreasing their sensitivity.

7.4 AURORAL CLUTTER IN THE CONJUGATE AREA

The ionospheric clutter formed in the conjugate area by the high-altitude nuclear detonations was quite restricted in spatial extent at early times and could produce fake or misleading echoes in an operational radar, provided certain conditions are met. These conditions are that the radar must observe the clutter region at heights of 100 to 400 km, and it must view this clutter region with the line-of-sight very close to perpendicular to the direction of the earth's magnetic field. The clutter area appears to expand after

tens of seconds and can become quite widespread. However, the requirement for viewing this perpendicular to the magnetic field still holds. The second conclusion that can be reached from observations in the conjugate area is that a systematic error appears between the calculated conjugate point and the observed conjugate point. The calculations used were those based on the coefficients derived by Finch and Leaton (loc. cit.). These calculations led to the correct position in longitude, but show a systematic error of approximately 1/2 of a degree of latitude with the true conjugate point located south of the calculated point. The appendix of Volume 1 presents a summary of all the various data which has been used to deduce this systematic shift of the field lines.

7.5 SYSTEM IMPLICATIONS

In order to completely assess the complications that would be caused to a sophisticated radar that is operating in a nuclear burst environment, a complete description of the particular radar and its role is necessary. At the time of this writing, we have no actual ballistic missile defense system designed, and the radars planned for use in proposed systems are having their characteristics and roles changed so often that it is relatively meaningless to try to perform the assessment mentioned above. However, in order to give the reader a general understanding of the radar degradation

that might occur to a radar system as caused by reflections from nuclear bursts, examples were presented at the end of Chapters 2, 3, 4, 5 and 6 for each of the Fish Bowl tests.

Besides the particular examples presented in these previous sections, a few general conclusions may be made.

First, the very strong radar reflections from the fireball regions detected during these tests would appear to be detectable on even the side lobes of radars which are required in ballistic missile defense applications. Such clutter would be seen over large solid angles and range cells and would appear to present serious difficulties to any automatic data-processing techniques being used, if not rendering the radar completely ineffective.

The long-lasting auroral clutter detected by the Johnston Island radars is very geometry-sensitive and may be eliminated from consideration by systems designers when considerations of threat tubes and single bursts are examined. However, when one considers the possibilities of threat tubes that are not well-confined, and multiple bursts, the several hours of auroral clutter would appear to warrant careful consideration in systems studies. The most promising means of eliminating this clutter is by Doppler filtering as is attempted in the natural auroral-clutter environment experienced by BMEWS.

The increases in noise level experienced by a radar looking at a nuclear burst seem to be of sufficient magnitude and of long-enough duration to warrant the consideration that extremely low-noise receiving systems as provided by masers, etc., may not be necessary or warranted.

It would appear that the long-lasting radar effects described in this report are of considerable consequence in the evaluation of ballistic missile defense systems performance. It should be noted that these non-blackout or non-absorption effects must be considered carefully in future systems evaluations if we are to have a realistic picture of radar performance in a nuclear-burst environment.

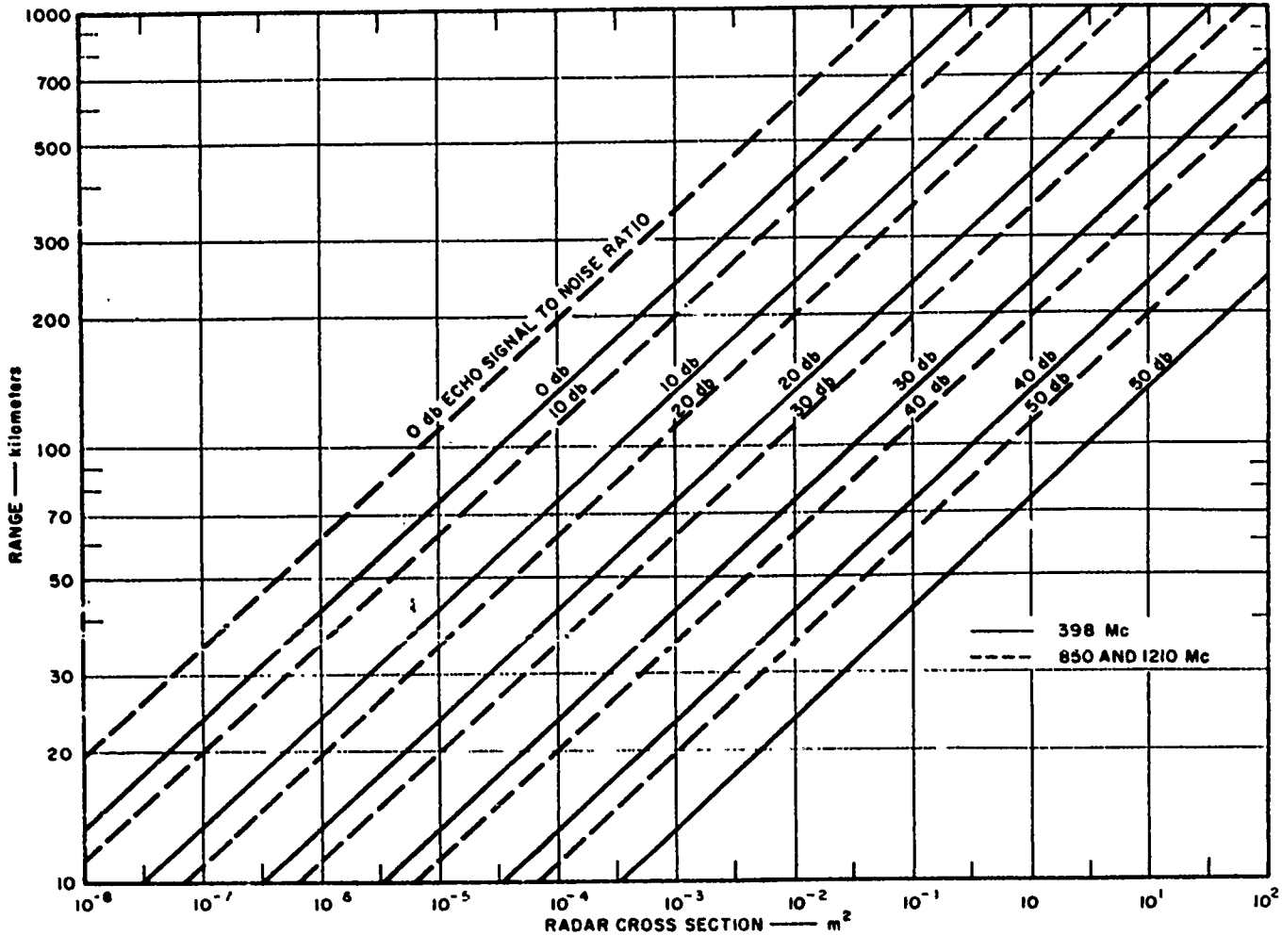

Figure 7.1 Johnston Island radar sensitivity for point targets, in m^2.

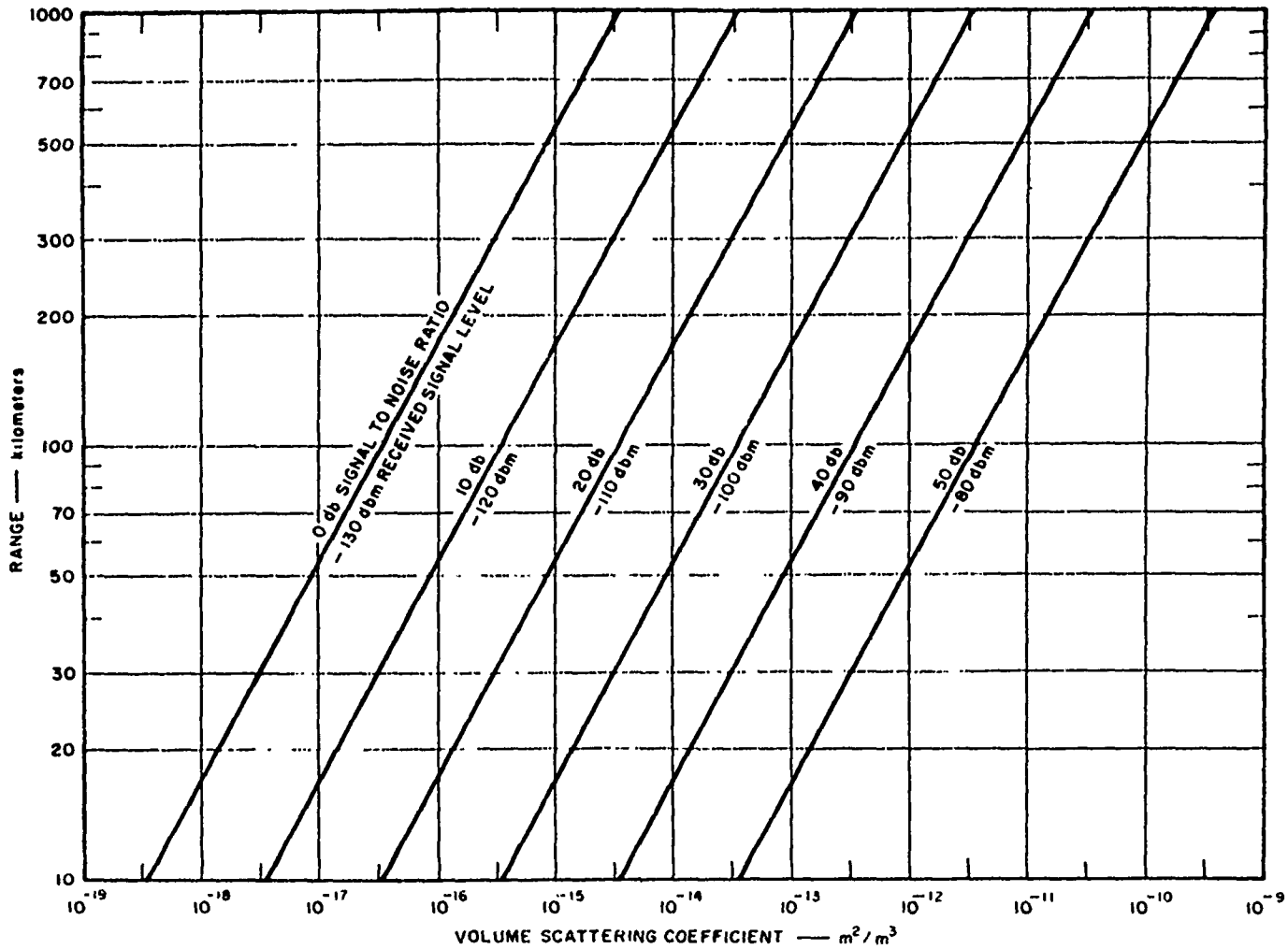

Figure 7.2 Johnston Island radar sensitivity for beam-filling targets, in m^2/m^3.

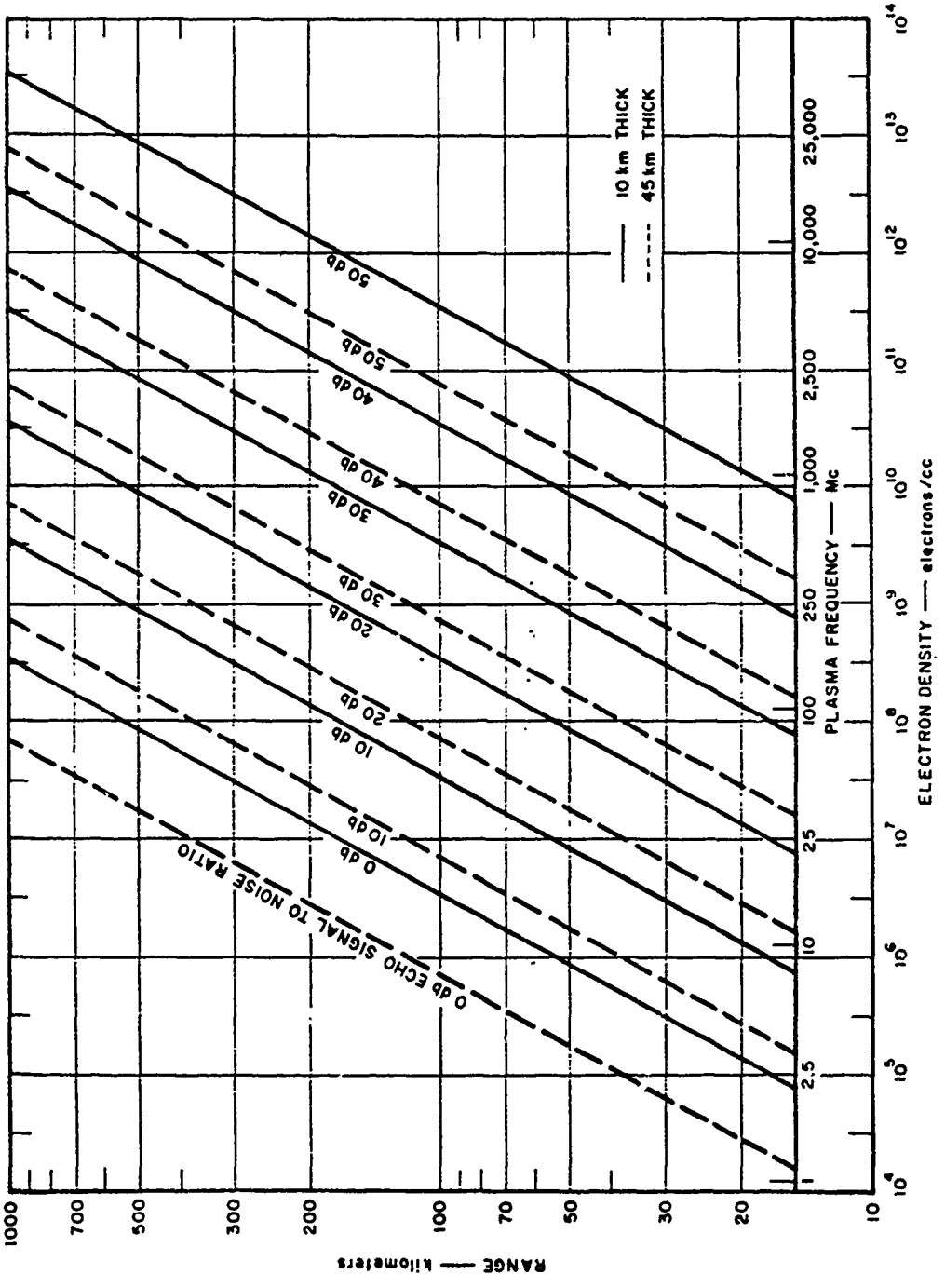

Figure 7.3 Johnston Island radar sensitivity for beam-filling targets, in electron density.

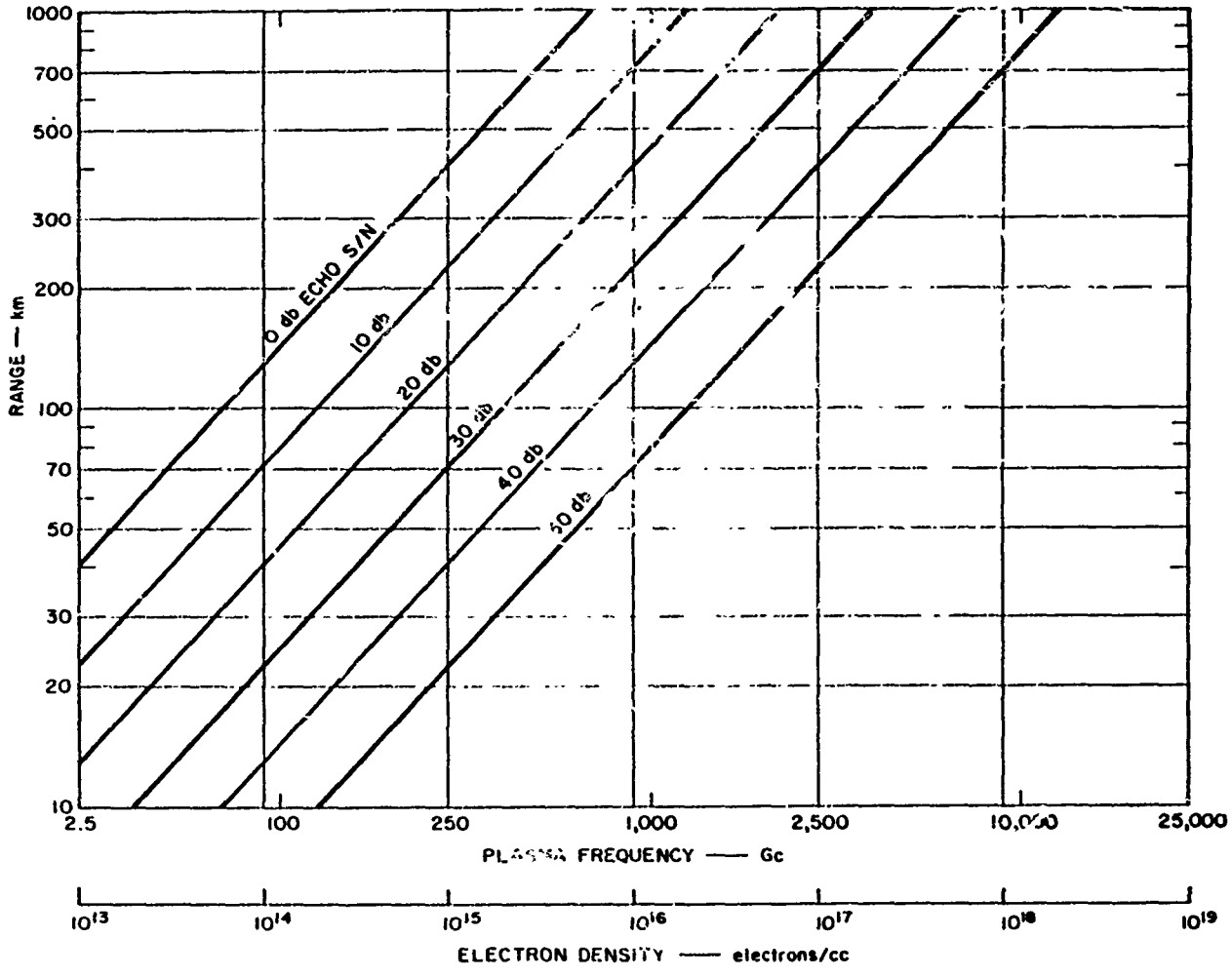

Figure 7.4 Johnston Island radar sensitivity for one-hop sea scatter echo model.

APPENDIX A

RADAR PERFORMANCE

In general the performance of the Project 6.9 radar equipments was very good. Certain deficiencies were noted, however, and during future experiments these deficiencies should be corrected.

A.1 JOHNSTON ISLAND

1. We were very pleased with the 398-, 850-, and 1210-Mc equipment and would recommend their inclusion in any future test plan. However, some modification is necessary to improve the dynamic range, frequency stability, and range resolution of the equipment. Furthermore, the data output of the UHF radars should be digitized on-line to improve the quality of data handling and cut down the data-reduction time.

2. Inasmuch as the UHF radar data was taken to provide information for use in planning anti-ICBM radars, it also seems that the UHF radar receivers should be capable of receiving Doppler shifts which are equivalent to those produced by a radially moving ICBM. This alteration would require 140-kc receiving and recording capability for the 1200-Mc radar. The lower frequency radars would require corresponding smaller bandwidth capability.

3. The only problem with the 85-foot dish is the lack of precise, slow control in elevation and azimuth. The dish should so be modified before further use.

4. The last-minute economics eliminated radar coverage in the 100- to 200-Mc frequency range. The lack was seriously felt on many of the late-time effects, and future test series should include a radar (operating in the 85-foot dish) at about 150 Mc.

5. An incoherent electron scatter experiment would have provided a wealth of data on electron density and temperature and we recommend its inclusion in future test programs. A more complete description of this experiment is included in Appendix C.

6. The low PRF on the 20-, 30-, and 50-Mc sounder (inherent in that particular sounder) should be corrected by the use of separate transmitters at these frequencies. The phase sounder could then be used with all seven frequencies in the HF range.

7. Although higher frequency radars were used to examine the fireball region, (Project 6.13's C-band radars) it has been suggested by systems analysts that future test series should include C- and X-band reflection studies of the burst. For these reasons it is recommended that Project 6.9 should include radar reflection studies at frequencies above L-band (in particular the C- and X-bands during the next test series).

8. It is felt that the number of experiments that Project 6.9 could carry out would be greatly enhanced if the 398-, 850-, and 1210-Mc radars could track. Such tracking ability would

allow absorption studies to be made by observing appropriate targets as well as angular scintillation studies. For these reasons we suggest that the 398-Mc frequency be used with an error-sensing antenna feed to allow tracking experiments to be conducted. It is also recommended that the 1200-Mc incoherent scatter radar proposed in (5) above also have tracking capability for the same reason.

9. We believe that considerably more data could be provided to other experimenters and DASA if automatic data processing equipment for the Project 6.9 radars on Johnston Island and the electron scatter radar recommended in (5) above were used. The reader is referred to Appendix D for a complete description of the automatic-data-processing recommendations.

A.2 AEW AIRCRAFT

The most serious operational problem with these radars involved the data recording method used. Future experiments should use these excellent radars but with the inclusion of magnetic tape recorders sufficient to record the amplitude data completely. It was difficult to position the aircraft by using the theoretical predictions of the effects, but on King Fish we were very successful and on Star Fish very unsuccessful. Future tests should include at least two of these aircraft for radar phenomenology studies.

A.3 M/V ACANIA

This equipment worked out extremely well for these tests. There are many ship improvements which suggest themselves during such extensive tests (such as more adequate air conditioning as well as improvements in the radar equipment). These necessary modifications must be kept in mind before future tests are undertaken.

APPENDIX B

JOHNSTON ISLAND AND M/V ACANIA RADAR DATA REDUCTION

The data reduction process began when the basic radar data was recorded at the field site. The UHF radar data was recorded on magnetic tape in the following manner:

1) Receiver — detected video output and 10-kc IF output
2) Antenna Position — digital antenna position generator output
3) Time — digital time generator output

The next step in the process was to produce a strip print of range versus time with amplitude intensity modulated. The range-versus-time prints were mounted along with the analog presentation of the antenna position and a time scale as shown in Figure 2.10.

From the range-versus-time data, height-versus-distance and range-versus-azimuth plots of the echoes were made over varying time intervals as shown in Figures 3.10 and 3.11. The data presented in the height-versus distance and range-versus-azimuth plots has all of the ground-clutter echoes and some of the extraneous missile echoes subtracted from the original range-versus-time data. The data presented in the height-versus-distance and range-versus-azimuth plots is plotted with the following accuracies: The range is accurate to ±15 km which is a combination of scaling errors and the poor rise time of the receiving system. The angular position is accurate to ±2 degrees, which is a combination of the digital

readout accuracy an the beamwidth of the radar. Time has been scaled to the nearest second or minute depending on the figure. Dots on the plots indicate that the echo was not extended in angular position beyond a beamwidth, or in range beyond a pulse length. Lines on boxes show extension in angular position or range or both.

The Doppler records were produced from the 10-kc IF receiver output recording by range gating out the transmitter leakage and unrelated echoes, and processing the resultant signal with a spectrum analyzer. The records are accurate in Doppler shift to ±1 kc.

The amplitude records were produced from the receiver-detected video output recordings by range gating out the transmitter leakage and unrelated echoes and making an amplitude-versus-time record. The amplitude data was then scaled from this record and replotted as in Figure 2.12. Although the dynamic range of the tape recorders was limited to a little over 30 db, upon careful re-examination of the tape recorder characteristics, it was found that for the pulse lengths used in the Fish Bowl tests, degrees of pulse height saturation could be determined up to 50-db dynamic range. All of the amplitude data presented takes this fact into account. The amplitude records shown in Figure 2.12 are accurate to ±5 db. Figures such as 2.15 are an attempt to reduce some of the confusion caused by the rapid and complex antenna motion. They show what the peak echo amplitude probably would have been if the antenna had been scanning the burst area clutter in a continuous fashion. Similarly, figures such as Figure 5.44 show what the peak echo amplitude probably would have been if the antenna had been scanning the northern auroral clutter in a continuous fashion.

APPENDIX C

A RECOMMENDATION FOR INCOHERENT BACKSCATTER RADAR MEASUREMENTS FOR BLUE ROCK

C.1 SYNOPSIS

Stanford Research Institute recommends that an L-band incoherent electron scatter radar for electron density measurements be used during the next high-altitude nuclear test series.

This radar will, in addition to providing electron density as a function of time and space, also provide estimates of

Electron temperature

Ion temperature

Ionic constituents.

In addition, the use of such a high-power L-Band radar will simulate some of the operational difficulties that will be experienced by L-band ballistic missile defense system radars operating in a nuclear environment.

It also offers the potential for evaluating incoherent electron scatter as a communication mode which is not degraded (but may be improved) by nuclear bursts.

C.2 INTRODUCTION

In the study of nuclear weapon phenomenology, experiments should be designed to satisfy one of at least two requirements. The first

requirement is to provide data of value to military systems designers of a direct simulation nature. Such data would be used directly in system evaluation studies. The other requirement is to obtain data which can be used to evaluate theories of nuclear weapon phenomenology. These theories, fortified by experimental confirmation, could then be used to extrapolate to the effects to be expected for other yields and altitudes of detonation.

It is our purpose to present an experimental technique for measuring many of the physical parameters that theoreticians need to know in their work--namely

Electron density

Electron temperature

Ion temperature

Ionic constituents.

The radio effects of a high-altitude nuclear burst are governed by the density and distribution of free electrons as a function of height and position. Once the electron density distribution is known, many of the radio effects can be predicted. Hence, a prime target for theoretical studies of the output of a nuclear device is the electron density that it produces.

Even for a quiet ionosphere, determination of the electron density as a function of height has been a difficult problem.

While vertical-incidence HF experiments can reveal the approximate nature of a monotonically increasing electron density, it can tell us nothing about the top structure of layers. Furthermore, the method breaks down when there are curvatures of the reflection-ionization distribution. Total dispersion experiments, using rocket-borne transmitters, moon echoes, etc., all suffer from the difficulty of determining the distribution as a function of position when the ionization is also changing with time.

A major research tool has been developed during the past two years which can eliminate most of these objections. With this method, a pencil-beam radar signal at a high frequency penetrates the region of interest with little attenuation. Electrons in the path of this beam weakly scatter energy back to the radar, each electron having a radar cross section of about $10^{-28} m^2$. The number of electrons within a range cell and within an antenna beamwidth is adequate to obtain a measurable echo from the E- and F-region of the normal ionosphere. Hence, it should be readily possible to map the contours of electron density within a few seconds of shot time, despite D-region attenuation. Fortunately, the normal high temperature of the motion-controlling ions in the ionosphere gives a Doppler broadening of the echo that is larger than the echo broadening of auroral clutter. Hence it appears possible to

differentiate between these two types of echoes and record each output separately.

C.3 ELECTRON SCATTERING

In 1958 Gordon (Reference 1) suggested that radar echoes could be obtained from the free electrons in the ionosphere with a sufficiently powerful radar. Total echo power for such incoherent scattering would be proportional to the number of electrons per unit volume times the classical cross section of the electron. The spectrum of such scatter from free electrons should have a Gaussian shape with a characteristic width determined by the thermal motion of the electrons.

That same year Bowles (Reference 2) detected a scatter signal of about the expected intensity but with a much narrower spectrum at 50 Mc. He suggested that this narrower spectrum resulted from the electrons being constrained in their motion by the ions, so that the spectral width should correspond to the ion motion for all observing wavelengths long compared to the Debye shielding distance of the ions. He also argued that the echo spectrum should show amplitude modulation corresponding to the ionic gyro frequencies and their multiples whenever incident and scattered rays make equal

angles with the earth's magnetic field.

Detailed theories of incoherent scattering have recently been developed partially or completely (References 3 through 6). More complete experimental measurements have now been made at 440 Mc by Pineo, Kraft, and Briscoe of Lincoln Laboratory (Reference 7).

While Gordon (Reference 1) gave the name "incoherent electron scattering" to the process being considered here, the detailed theories indicate that the process is best described in terms of the few electrons (in the condensation regions of longitudinal ion acoustic waves) which scatter coherently. The statistical fluctuations are analyzed in terms of such sound waves of all wavelengths going in all directions at all speeds.

The radio waves scatter only from the acoustic waves of one wavelength traveling in one direction with all (plus and minus) speeds. For the wavelengths of interest the total scattered power is one-half the value suggested by Gordon (the factor one-half probably results from the equipartition of kinetic and potential energy of the electrons), the spectrum is approximately flat-topped, and its width corresponds to the thermal motion of the ions, rather than the electrons. The detailed theories indicate that the ion gyro modulation should be present under the proper geometry for

detection (predicted in Reference 2).

For all radio frequencies and heights of practical interest the ratio of received signal power (S) to noise power (N) is given by:

$$\frac{S}{N} = \frac{1}{kTB} \frac{P_T G_T}{4\pi R_1^2} \frac{\sigma n V}{2} \frac{A_R}{4\pi R_2^2} \qquad \text{(C.1)}$$

where

k = $1.38 \times 10^{23}/^{o}K$ (Boltzmann's constant)

T = $T_C + T_R$ where T_C is the antenna temperature (determined primarily by cosmic noise), and T_R is the receiver noise temperature, ^{o}K

B = Receiver bandwidth in cps, assumed equal to, or greater than the bandwidth of the scatter signal

P_T = Transmitter power in watts

G_T = Gain of transmitting antenna

R_1 = Range from transmitter to scattering volume, M

σ = $4\pi r_e^2 \sin^2\alpha \approx 10^{-28} \sin^2\alpha$ m^2, the radar cross section of one electron where r_e = classical electrical radius, 2.8178×10^{-15} meters, and α is the angle at the target between the electric vector of the incident wave and the direction to the receiver

n = Electron density in the scatter volume, electrons/m^3

V = Volume common to transmitting and receiving antenna beams

A_R = Aperture of receiving antenna, m^2

R_2 = Range from scattering volume, M, to receiver.

The approximate bandwidth of the scattered signal, B_S, is

$$B_S = \frac{4 \cos \phi}{\lambda} \sqrt{\frac{2kT_i}{M_i}} \tag{C.2}$$

where

ϕ = Half the included angle between the rays from the scattering volume to the transmitter and receiver

λ = Radio wavelength in meters

T_i = Ion temperature (ion assumed to be in thermal equilibrium with the electrons), ^oK

M_i = Ionic mass.

For the case of backscattering with common transmitting and receiving antennas, Equation C.2 reduces to:

$$\frac{S}{N} = \frac{P_T A \sigma n C \tau}{16 \pi R^2 kTB} \tag{C.3}$$

where

τ = Transmitter pulse length, seconds

C = Velocity of light, 3×10^8 m/sec.

In addition,

$$B_S \sim \frac{4}{\lambda} \sqrt{\frac{2kT_i}{M_i}} \tag{C.4}$$

It is interesting to speculate that some permanent form of natural field-aligned ionization exists at all times. A radar sufficiently sensitive to obtain incoherent-scatter echoes could answer this question by examining incoherently scattered signals in a direction perpendicular to the earth's magnetic field during quiet periods. It would not be surprising to discover a permanent field-aligned component which becomes enhanced during times of auroral disturbance. Thus one would expect to see the transition between auroral scattering and incoherent scattering.

As radar sensitivities are increased, sensitivity will be limited ultimately by incoherent scattering. It is quite possible that clutter will be several orders of magnitude more severe in directions perpendicular to the magnetic field, even during undisturbed periods.

The spectrum of the electron scatter is a function of the ratio of electron to ion temperature (see Figure C.1) as shown by Reference 8. Thus by careful examination of the scattering spectrum it should be possible to deduce the electron and ion temperatures. These curves are for the F-region and the assumption that only O^+ predominates. Other ionic species would give different curves. Hence, in addition to determining electron temperature and ion temperature, the shape of the scattered energy spectrum should also give a clue to the ionic constituents present.

An additional exciting feature of upper atmospheric investigations based on electron scatter is the predicted effect of the magnetic field (References 6 and 9). When electron scatter is obtained at and near the geometry corresponding to specular reflection from the earth's magnetic field, the scattered energy is expected to exhibit a spectrum which is indicative of the kind and amount of ions present in the scattering volume. For example, if only one constituent, say, oxygen, is present, the power intensity-frequency spectrum is expected to show peaks at the ion gyro frequency (about 50 cps for 0^+ at 300-km height) and all of its multiples. The voltage amplitude-time characteristics of the scattered signal should thus show a quasi-periodic feature at 50 cps. If another ionic component is present, its effect on the spectrum or amplitude-time record will be superimposed (Reference 10).

By analyzing the spectrum or noting the periodic components in the amplitude-time record of the scattered energy, it may be possible to deduce the ionic constituents which are present, and their percentage composition in the plasma. Hence, we would have, in effect, a radar mass spectrometer for upper atmospheric studies.

Quite recently the ion gyro frequency of NO^+ has been identified in the normal nighttime E-region field-aligned ionization (Reference 11). Although

this field-aligned scatter is many tens of db more intense than incoherent scatter, the ion control of the electrons when looking at right angles to the earth's magnetic field has been verified for the first time.

C.4 SELECTION OF RADAR PARAMETERS

The choice of radar parameters for the proposed ionospheric radar necessarily involves a careful compromise between specifications set by the scatter mechanism, state-of-the-art of transmitter development, and tolerance of the antenna which could be readily built and installed at the field sites such as Johnston Island.

For the investigation of auroral and electron scatter, frequencies between 100 and 3000 Mc are desirable, as indicated by Figure C.2. Unlike the conventional radar, the sensitivity of the radar for electron scattering varies only as the first power of the antenna-collecting aperture, and is in reality independent of the dish gain. For electron scatter and a given dish size the signal-to-noise ratio is:

$$\left(\frac{S}{N}\right)_i \propto \frac{P_T \tau}{B} \propto P_T \tau^n \qquad (C.5)$$

where

P_T = Transmitted power

B = Receiver bandwidth

τ = Pulse width

n = $\geq$ 2 for pulse widths 100 to 1000 μsec

n = 2 for pulse widths 1 to 100 μsec (see Figure C.2).

For coherent scattering from targets having large range depths compared to the pulse width, τ,

$$\left(\frac{S}{N}\right)_c \text{ oc } \frac{P_T G \tau}{B} \approx P_T \tau^2 G \qquad (C.6)$$

where

G = Dish gain = $\frac{4\pi A}{\lambda^2}$.

For incoherent scattering operations there exists an optimum frequency where maximum signal-to-noise ratio will be obtained if other radar parameters remain unchanged. There is also a marked dependence on pulse width, approaching 20 db per decade of pulse length. Equation C.3 has been plotted, and is shown in Figure C.2 for an assumed receiver noise temperature of 75°K. Relative echo signal-to-noise ratio is plotted versus the logarithm of the radar wavelength for pulse lengths of 1, 10, 100, and 1000 μsec. It will be seen that the maximum signal-to-noise ratio occurs near 400 Mc, but that the fall-off is gradual as a function of wavelength if a long pulse length is used. The existence of a copious coherent clutter at 400 Mc during Fish Bowl would suggest a higher frequency

than 400 Mc. Going to a higher frequency, such as 3000 Mc, would cause serious losses in the signal-to-noise ratio by the bandwidth spread in the electron-scattered energy (the positive ions have less control over the electrons as a higher frequency is used). The availability of good hardware at 1200 Mc and the desirability of making the volume cell as small as possible also makes 1200 Mc a reasonable compromise.

The radar proposed for the incoherent electron scatter experiments during the next test series would be located on Johnston Island for ease of operation. It would be monostatic and would utilize an 85-foot steerable dish similar to the one constructed for Project 6.9 experiments during Fish Bowl. The radar would be mounted in three 40-foot vans except for large transformers, etc. The radar would be phase-coherent, and Doppler spectral examinations could possibly be used to eliminate the other forms of clutter such that only the incoherent electron scatter would be used to measure electron density. The characteristics of the proposed radar are listed below:

Frequency	1200 Mc
Antenna	Steerable 85-foot dish
Gain	56 db
Peak power	5 Mw
Average power	150 kw

Receiver noise figure	2 db
S/N for electron scatter looking directly overhead at normal F-layer ionization.	30 db (assuming a 1-msec pulse)

Automatic data processing would be accomplished in digital form by the use of analog-to-digital conversion equipment and a desk-sized computer, such as a CDC 160-A, with digital magnetic tape recording capability. The radar receiver output would be sampled and digitized at approximately 100 μsec (15 km) intervals with a high-speed analog-to-digital converter under computer control. The computer would be synchronized with the radar PRF to insure that the range to each of the samples remains constant. Along with the sampled amplitude data (which is proportional to electron density), time and antenna position information would be fed into the computer in digital form.

The computer would perform some integration of the sampled data to improve signal-to-noise ratios (about 2 sec) and feed this information, along with the digitized time and antenna position, to digital magnetic tape in a format suitable for computer processing. At the conclusion of the data taking, the digital tapes would be

played back into the computer, and electron density profiles as a function of time and position in space could be computed and plotted automatically.

In addition, analog tape recording of all data would be made and could be used with the computer for additional data processing.

The sensitivity of this radar for electron scatter looking vertically is outlined below:

Pulse Length	Height	Volume Cell Size	S/N
1 msec	300 km	150 km x 3 km x 3 km	30 db
1 msec	1000 km	150 km x 10 km x 10 km	10 db
100 μsec	300 km	15 km x 3 km x 3 km	20 db
100 μsec	1000 km	15 km x 10 km x 10 km	0 db

These results are based upon an F-layer maximum density of 10^6 electrons/cc and a value of 10^5 electrons/cc at 1000-km height. During an actual test, the electron density would be greater than at normal times, and the signal-to-noise ratios would be greater than those listed above. In addition, the use of 1 to 2 seconds integration in the automatic data processing would also increase the S/N ratios shown above by 10 db.

C.5 CONCLUSIONS

It is believed that the incoherent radar scatter technique offers great hope for measurements of physical parameters in nuclear

bomb phenomenology and should be incorporated during future test series.

In particular, radar parameters desirable for these purposes are a compromise but should be of as high a frequency as possible to

(1) Allow ionic control of the electrons to 1000-km altitude

(2) Minimize coherent clutter

(3) Present as simple an interference problem as possible on Johnston Island

(4) Make the sampling volume as small as possible.

It is our opinion that 1200 Mc is an ideal choice.

Additional advantages of incoherent electron scatter radar described above are:

(1) The use of F-region reflections during low-altitude bursts (20 km or so) with the incoherent scatter radar allows accurate absorption measurements to be made on a number of paths surrounding the burst. Approximately 40 db of dynamic range can be obtained (2-way absorption) by this technique.

(2) The radar described above can also be thought to simulate L-band radars planned for use in ballistic missile defense activities. Actually the L-band incoherent radar is 10 db more sensitive than any L-band radar presently being

considered for ballistic missile defense system purposes.

(3) The remote monitoring of the L-band incoherent scatter radar has many implications to communications applications because it is not thought to be affected in a deleterious way by high-altitude nuclear bursts (Reference 12).

(4) It would appear very desirable to use this sensitive radar for tracking of specially provided targets [1] through the nuclear burst environment. Such tracking would result in 1200-Mc angular jitter data as provided by Project 6.13 at C-band during Fish Bowl. In addition, the availability of this tracking radar would allow engineering simulation of the problems encountered by operating a ballistic missile defense system radar in a nuclear bomb environment. The 398-Mc, Project 6.9 radar operating at 1200 Mc, and the C-band tracking radars on the DAMP ship, would provide good frequency coverage for such tracking experiments.

---

[1] It is suggested that 100-foot metalized balloons, similar to the echo balloon satellite, be used as special targets for this and other tracking radars. In addition, the re-entry vehicles planned for some of the test would also serve as excellent targets.

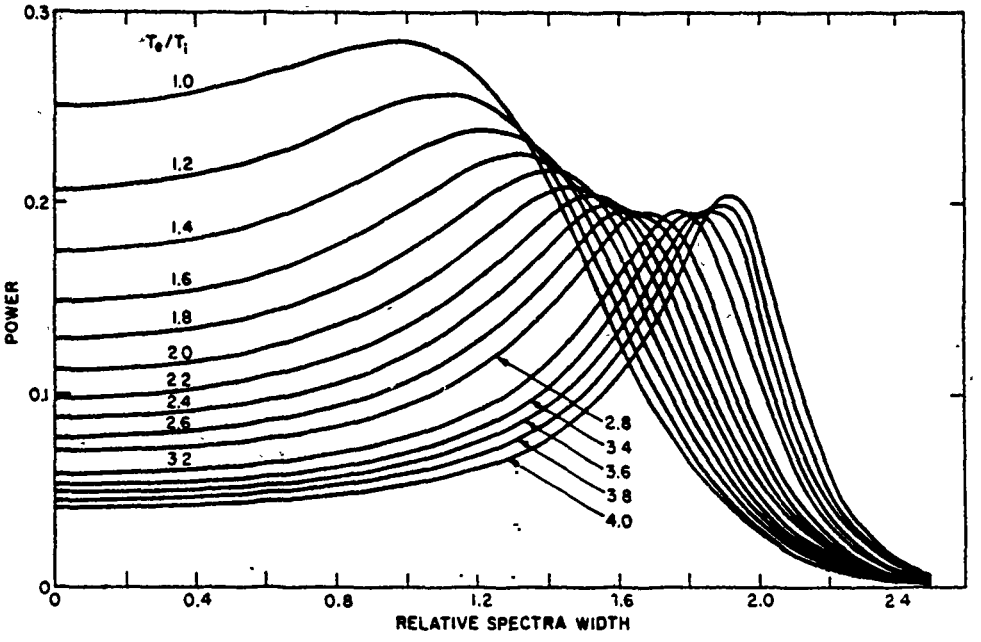

Figure C.1 Backscatter power spectra as a function of T_e/T_i.

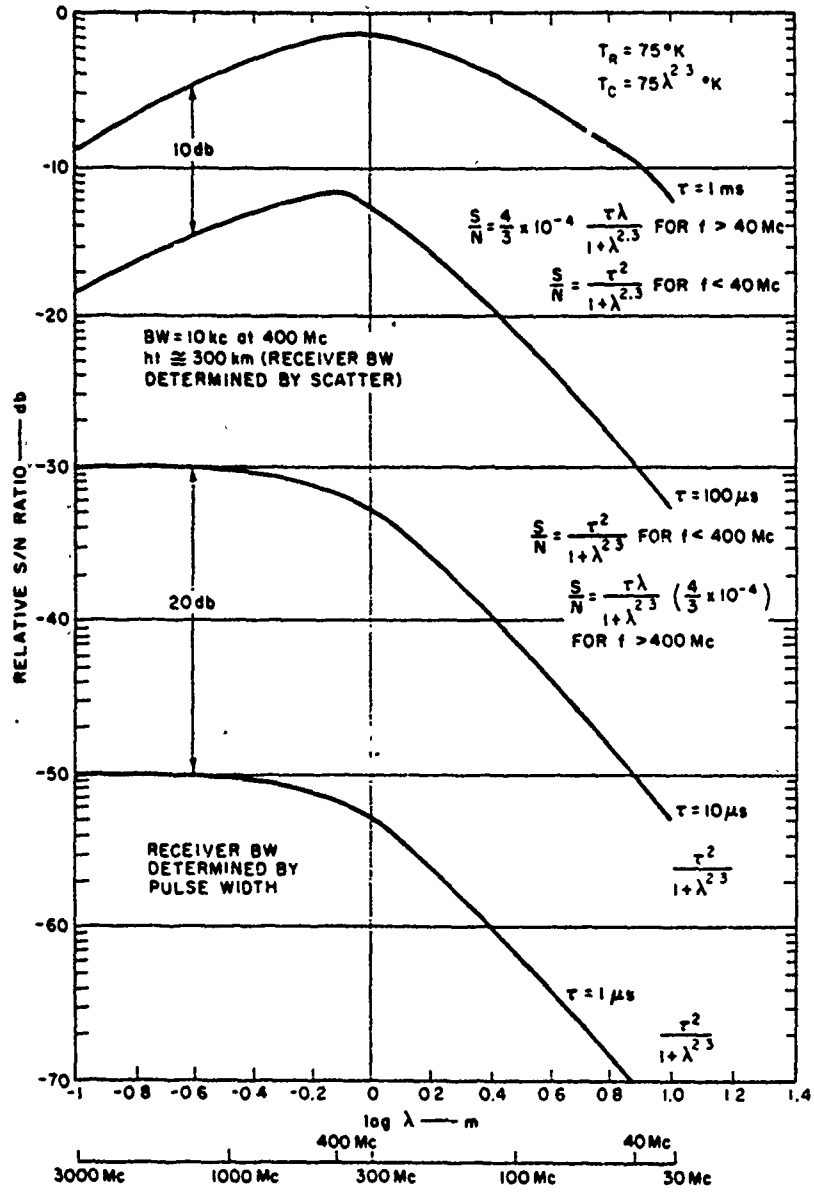

Figure C.2 Radar sensitivity for incoherent scattering.

APPENDIX D

PROJECT 6.9 DATA ACQUISITION AND PROCESSING RECOMMENDATIONS

D.1 INTRODUCTION

Project 6.9's experiments during the last nuclear test series were primarily radar measurements. Our objective was to measure, as functions of time and frequency, the strength and position in space of the reflections associated with the high-altitude nuclear bursts.

The automatic processing of radar information is a fairly complex and difficult task because of the many variables which must be digitized and recorded, and because of the high data rates which must be handled. The variables that need to be measured and recorded in a radar data gathering system are:

(1) The Antenna Position: The azimuth and elevation angles of the antenna must be known and recorded, in general, within an amount less than or equal to the antenna beamwidth. In our case the beamwidth was 0.7 degrees.

(2) Time: The exact time relative to event time must be known to at least one second, a few minutes after burst—probably more accuracy is required closer to zero time.

(3) The Range to the Target: This parameter must be known to at least one pulse width, in our case 300 μsec or 45 km.

(4) The Range Depth of the Target: The transmitted pulse may be stretched or spread in range due to the target characteristics. The range depth should be known in increments of at least the transmitted pulse length.

(5) The Amplitude of the Echo: This parameter is a most important one in determining the size and/or the reflecting characteristics of the target region. The accuracy to which this quantity need be measured depends to a large extent on the radar receiver characteristics. For our case, we would need a dynamic range in the digitizer of approximately 100 quantization increments.

(6) The Doppler Shift of the Returned Energy: The difference in frequency between the transmitted wave and the reflected wave may be a quantity of prime importance.

(7) The Doppler Spread of the Returned Pulse: The characteristics of the target region may cause a spreading in frequency as well as a shifting in frequency of the returned energy as compared to the transmitted energy.

(8) The Polarization of the Returned Energy: The polarization must be measured and the effects of the target upon this parameter deduced.

Considerable simplification of a data-gathering system can be achieved if any of the above-mentioned parameters are not important

to a particular experiment or are not instrumented in the receiving system. In addition, simplifications result if some of the above parameters are constant or vary in a systematic and known way—for example, if the antenna position is fixed, or if it operates in a systematic scanning mode.

During last year's test series, Project 6.9 conducted basically two types of radar experiments: (1) the radar clutter experiment, and (2) the phase path sounder experiment. We had a fixed location on Johnston Island and movable instrumentation platforms in the M/V ACANIA (which operated at sea from a position in the southern conjugate region) and four RC-121 aircraft (two in the north and two in the south conjugate regions). Both the clutter and phase sounder experiments were performed at Johnston and on the ACANIA. The aircraft participated in only the clutter radar study. The following discussion covers the Johnston Island experiments and methods of collecting data; similar techniques were used on the ACANIA.

D.2 RADAR CLUTTER EXPERIMENT

For the radar clutter experiment, a completely steerable azimuth and elevation antenna was used, and it was necessary to record all of the quantities discussed above with the exception of polarization information, which was not instrumented into the

radar system. The experiment was performed at three radar frequencies, tripling the amount of data. The antenna scanning procedure was not in general systematic, but varied at the discretion of the radar operator. Data was recorded on analog magnetic tape and on film at the radar sites and shipped to Menlo Park for analysis. The analysis of the data consisted mainly of making z-axis films from the tapes and hand-scaling the quantities of interest from the film.

By comparing these films with the position information, one can determine the position in space of the radar echoes as a function of time. In addition, amplitude-time films are made from the magnetic tapes. One needs to correlate the amplitude-time plot with antenna position information to determine the positional effect on this data. A large amount of hand scaling from film records such as this was necessary in order to deduce the information such as required for analysis.

Now let us examine the possibility of digitizing the data and letting a computer do the scaling job. The digitizing could be done either on-line at the radar sites or from analog tape recordings at some central facility. First, a consideration of the data rates shows that the digitized data must be stored on digital magnetic tape. Using paper tape or cards would be too slow. The data

rate required to digitize a single frequency of our Johnston Island radar would be of the order of 45,000 bits/sec, or 130,000 bits/sec for the three-frequency system. A block diagram of one possible digitizing and formatting system is shown in Figure D.1.

The commutator switches the analog-to-digital converter input between the three data channels, the converter converts the analog signals to digital numbers in some code compatible with standard computers, the interface unit performs the functions of level shifting and switching the computer input between the various digital outputs; the computer formats the data, controls the timing system, and outputs the digitized data to a digital tape in a standard format. Single-channel systems of this sort have been instrumented at SRI in connection with the reduction of radar auroral data and other radar experiments.

The cost of a three-channel system such as the one previously described would be of the order of $200,000. One system would be required at each radar site.

Such a system would also be applicable to the proposed incoherent electron scatter measurement which has been mentioned at previous meetings, and is discussed in more detail in Appendix C.

D.3 CONCLUSIONS AND RECOMMENDATIONS

During the last test series all of our data was recorded in analog form in the field. There are both advantages and disadvantages

to this method of recording. The advantages are: (1) there is a minimal loss of information in the recording process. Instead of sampling and recording discrete values of the receiver outputs, every bit of data that comes out of the receiver output is retained and can be analyzed over and over. There is only a slight degradation of the data due to the record and play-back process. (2) Unusual phenomena and effects can be more easily interpreted by the experimenter when the data is presented in the form he is more familiar with and has had a great deal of past experience in analyzing. (3) The data gathering and recording system is much less complex, easier to instrument with conventional equipment and techniques, easier to trouble-shoot and repair in case of equipment problems. (4) Less skilled personnel are needed to operate and maintain it. (5) It is considerably less expensive. (6) The analog system in most cases will take less physical space. This is a prime consideration on a ship such as the ACANIA where space is at a premium.

Along with these advantages are the following disadvantages: (1) first and most important—the retrieval of the information is very slow and time-consuming. It may take orders of magnitude more time to hand-reduce the data than it took to generate it.

(2) More people are required to scale the data. (3) The possibility of human error or the systematic weighting of the data by a data clerk is present. (4) Subjective decisions may be required of the data clerk, and different clerks make different decisions. Thus, the hand-scaled data may be non-uniform.

For future test series we would like to make the following recommendations for the handling of our radar data:

(1) The radar clutter experiment should be digitized on-line at Johnston Island.

(2) The electron scatter experiment would require on-line digitization and processing.

(3) The radar clutter experiment on board the ACANIA should not be digitized (primarily due to the limited space available on the ship). Addition of digital equipment would have to be at the expense of experimental equipment.

(4) Digitization on board the RC-121 aircraft is not practical from space and weight considerations, but analog tape records should be on board in addition to the photographic equipment.

(5) Present analog tape recording methods should be retained at all sites, at least as a backup, because of their inherent simplicity, reliability, and ability to preserve all the data and to present it in the form with which the experimenter is most familiar and has the greatest intuitive feelings.

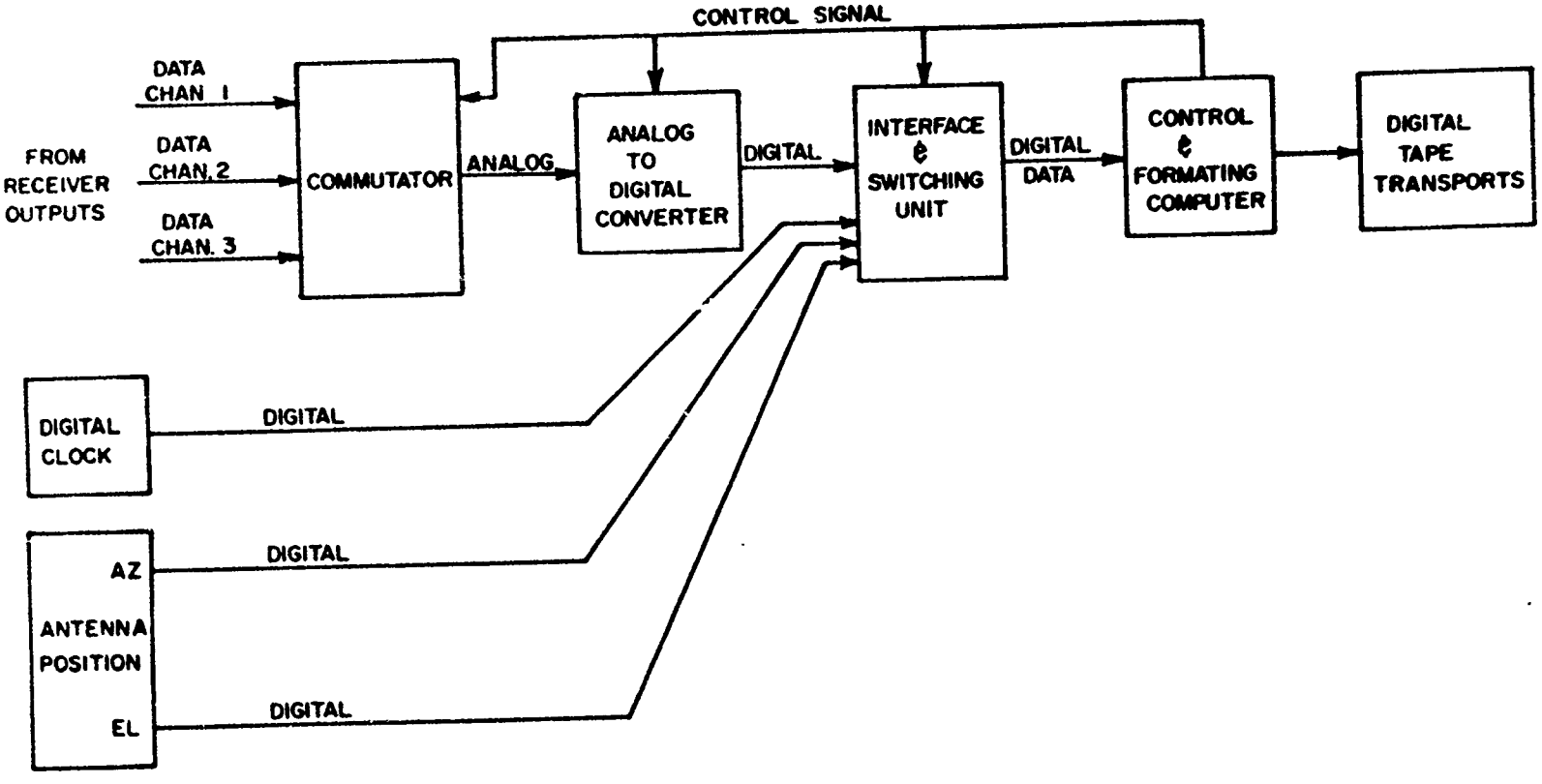

Figure D.1 Radar digital data-collecting system.

REFERENCES

1. W. E. Gordon; "Incoherent Scattering of Radio Waves by Free Electrons with Applications to Space Exploration by Radar;" Proc. IRE 46, 11, pp. 1824-1829 (November 1958); Unclassified.

2. K. L. Bowles; Phys. Rev., Letters, Vol. 1, p. 454 (1958); Unclassified.

3. J. A. Fejer; "Scattering of Radio Waves by an Ionized Gas in Thermal Equilibrium;" Can. J. Phys. 38, 8, pp. 1114-1133 (August 1960); Unclassified.

4. E. E. Salpeter; "Scattering of Radio Waves by Electrons Above the Ionosphere;" J. Geophys. Res., 65, 6, pp. 1851-1852 (June 1960); Unclassified.

5. J. P. Dougherty and D. T. Farley; Proc. Roy. Soc., Vol. 259, p. 79 (1960); Unclassified.

6. T. Hagfors; "Density Fluctuations in a Plasma in a Magnetic Field, with Applications to the Ionosphere;" J. Geophys. Res. 66, 6, pp. 1699-1712 (June 1961); Unclassified.

7. V. L. Pineo, L. G. Kraft and H. N. Briscoe; "Some Characteristics of Ionospheric Backscatter Observed at 440 Mc/s;" J. Geophys. Res. 65, 9, pp. 2629-2633 (September 1960); Unclassified.

8. J. A. Fejer; "Scattering of Radio Waves by an Ionized Gas in Thermal Equilibrium in the Presence of a Uniform Magnetic Field;" Can. J. Phys., Vol. 39, pp. 716-740 (1961); Unclassified.

9. O. Buneman; "Fluctuations in a Multi-component Plasma;" J. Geophys. Res. 66, 6, pp. 1978-1979 (June 1961); Unclassified.

10. T. Hagfors, O. Buneman, D. Westover and V. Eshleman. Presented at the Spring 1961 meeting of URSI-IRE, Washington, D. C.; Unclassified.

11. L. Colin, A. A. Burnes, and V. R. Eshleman; "Radar Detection of Nitric Oxide in the Lower Ionosphere"; Scientific Report 2, Contract AF 19(628)-233, Radio Science Laboratory, Stanford Electronics Laboratory, Stanford University, Stanford, California; Unclassified.

12. A. M. Peterson; "Free Electron Scatter as a Communication Mode;" Presented at 1961 Western Electronic Show and Convention, San Francisco, California; Unclassified.